Universitat Autònoma de Barcelona
Facultat de Filosofia i Lletres
Departament de Prehistòria
Doctorat en arqueologia prehistòrica

FROM MICRO TO MACRO SPATIAL DYNAMICS IN THE VILLAGGIO DELLE MACINE BETWEEN XIX-XVI CENTURY BC

by
Katia Francesca Achino

Thesis submitted for the degree of Doctor in Prehistoric Archaeology

Supervisor: Prof. Juan Antonio Barceló Álvarez, *UAB*
Co-Supervisor: Prof. Alberto Cazzella, *Università degli Studi di Roma"La Sapienza"*

2016

6 MATERIALS AND METHODS: SURFACE SURVEYS

6.1.Introduction: surface surveys

Archaeological surface surveys from the 1970s and throughout recent decades have achieved widespread support (as summarised in Bevan & Connolly 2009), initially particularly in the USA. According to some scholars, it was favoured for being a logistically and economically easier method for obtaining data compared to excavation (cf. Cherry 1983; Dunnell & Dancey 1983; Wandsnider & Camilli 1992) and for its ability to provide a regional perspective on prehistoric activities (for instance, see Cherry 1983, 1984; Dunnell & Dancey 1983). Indeed, *"the archaeological survey, the discovery and documentation of prehistoric and historical cultural remains on modern surfaces, is responsible for a growing portion of the information we have about the prehistoric use of various areas"* (Wandsnider & Camilli 1992: 169, citing Ammerman 1981; Lewarch and O'Brien 1981: 297; Dunnell & Dancey 1983). As Ammerman and Feldman argue (1978: 734 in Johnson 2012: 8), the surface of a site is the one part that an archaeologist has direct and also economical access to. Since archaeologists first employed this method in the 1970s and 1980s, surface artefacts and phenomena have been used to determine where to excavate within sites (Hole & Heizer 1973; Fagan 1978) and have even been applied to research problems that used to be exclusively studied through excavation (Lewarch & O'Brien 1981: 297).

Archaeological survey is considered to be the application of a set of techniques for improving the discovery probability of archaeological materials in an attempt to estimate parameters of the inter- and intra-site archaeological record. Sites, as high density areas, have traditionally been the focus of surveys. A wide variety of survey strategies have developed for answering a variety of research questions, from the site level as well as up to a regional scale and extensive methodological critique is undertaken in specific handbooks (for instance, Bintliff et al. 2001; Banning 2002) and articles (for instance, Wandsnider & Camilli 1992).

A brief summary of the most reliable and suitable techniques for our case study, employed in the analysis at site scale, seems to be enough for the scope of this thesis. Among those techniques, systematic sampling aims to avoid the random sampling pitfall of leaving large areas unexamined (Banning 2002: 117). Adaptive sampling instead takes advantage of the previously gathered surveyed elements, adding further sample elements adjacent to any of those that contain sites, artefacts or features; this addition ends when the most recently surveyed units meet an absence of neighbourhood elements. As a result, a number of clusters of sample elements surrounded by a buffer zone without such elements are analysed (Orton 2000: 34-38; 93-98; Banning 2002: 118). Point sampling, more common in intra-site geophysical survey, are based on the selection of random point samples with x-and-y coordinates within a selected grid-system on the survey area. The resulting sample consists of all the grid intersections (Banning 2002: 121). Finally, prospection or "purposive survey" is the most comparable with the technique adopted in our case study: it can test hypotheses in order to make specific predictions about locations of archaeological materials more efficient, as discussed by Cowgill (1975: 260-251). Prospection makes fruitful use of background research to increase the likelihood of detecting targets and to yield efficient survey designs (Banning 2002: 154)[23].

[23] Regarding these themes see also the journal "Archaeological Prospection" (published since 2015 by Wiley and Sons) and the Proceedings of the International Conference on Archaeological Prospection.

Before a survey starts, some key points have to be determined: in particular, the design of the survey in terms of spatiality (unit size and shape) and intensity. In order to provide a framework for survey, the continuous space which embraces the archaeological evidence has to be partitioned. The most common sampling frame consists of a grid subdivided according to a set of equal geometrical shapes that completely fill a survey area; the most frequently used are rectangles or squares but circles, triangles or hexagons are also attested (Wobst 1983; Orton 2000: 19). Arrangement of point samples in geophysical surveys is obtained using the coordinates of grid corners to define a set of data points and the number of points per unit of space constitutes the resolution (Banning 2002: 86). Frames that consist of a set of long, narrow rectangular strips, i.e. parallel transects, that stretch across a survey area are also fairly common (Banning 2002: 81). Where units are equal in size, this facilitates measurement of observations (material evidence) per unit, i.e. densities.

Traditionally some advantages from a statistical point of view are recognised for a large number of small units compared to a few large units, particularly for site scale analysis. For the same amount of area covered, small units result in a larger sample size and this, in turn, results in a smaller standard error on any estimates of population characteristics and a decrease of variance for many samples (Drennan 1996: 247-253; Banning 2002: 86). Furthermore, smaller units yield improved parameter estimates (Redman 1974: 19; True & Matson 1974: 89; Read 1975: 53; Plog 1976: 151; Plog et al. 1978; Lewarch & O'Brien 1981). However, there is no single best unit size (Thomas 1978) and the choice is influenced by many considerations, including logistics, funding, target parameters and distributions of relevant archaeological materials (Judge et al. 1975: 87). If funds are scarce and the goal is estimation of overall site density, units of intermediate size may be chosen (Read 1975: 58).

As with unit size, even when choosing the unit shape, many considerations may affect the decision. Thus, transects may be optimal for one study, while squares are indispensable for another. Holding constant unit areas, sampling schemes and total surveyed areas, some effects of squares or transects may be identified. For instance, squares may provide better parameter estimates in stratified schemes (Judge et al. 1975: 110; Bettinger 1977: 13-14). In the case of extensive regional studies, the transect sampling unit seems instead to be more applicable for sampling archaeological and environmental variables because of their greater size, but some materials may potentially be overlooked (Hodder & Orton 1976; Cherry et al. 1991; Bintliff 1996; Lock et al. 1996; Wheathley 1996; Shennan 1997; Gillings & Sbonias 1999). Some scholars (such as Shennan 1997; Banning 2002) suggested the use of a combined method of grid squares and transects defined as extensive and intensive in overcoming the limitations of a single method; this strategy would also enhance sampling and parameter estimation precisions (Shennan 1997).

One further basic decision an archaeologist must make in conducting a survey is the degree of intensity of survey. This means the level of detail with which the ground surface of a given sample unit is inspected. Since it is not possible to suggest any particular level of intensity that will always be optimal, a general assumption quite universally accepted is that "*the greater the level of intensity, the higher will be the percentage of all sites (and all artefacts in a micro scale) in an area that will be found*" (Plog et al. 1978: 389; Nance 1988; Wandsnider & Camilli

1992; Orton 2007). However, rather than stating that surveys are complete, archaeologists should specify the level of intensity of survey.

6.1.1 Issues in surface surveys: how to live and work outside a "Garden of Eden"

Problems with surface archaeological deposits and hence with the use of archaeological survey data are manifold. The issues mentioned above, that consist of the choice of best design strategies for surveys in terms of unit size, shape and level of intensity and the quality of results calculated from the analysis, are only among the most widespread. As briefly summarised, the information needed to make a choice can be gathered by different methods in several academic disciplines depending on characteristics of sites and research problems. From the 1970s (among the earlier studies: Krause & Thorne 1971; Schiffer 1972, 1976; Sullivan 1978; Dunnell 1979), the increasing awareness of processes which form and deform the archaeological record highlighted the lack of information about the nature of surface phenomena. This weakness could, however, be corrected by drawing upon a broad knowledge of processes that create surface deposits.

Understanding formation and deformation processes creating artefact assemblages on contemporary surfaces plays an important role for several reasons. This is necessary for obtaining a better understanding of potential biases and factors that must be taken into consideration in order to use surface assemblages for quantitative research. The complexity of all formation and deformation processes creating the contemporary recovery context forces studying sites through a biographical approach which enables recognising and acknowledging each step of their development. This approach can allow archaeologists to overcome the uncertainty of a surface survey's effectiveness when applied to the horizontal overlapping of subsequent occupations: if archaeologists could reconstruct and separate steps which involved the formation of the archaeological record, multi-component sites could also be analysed.

Under these conditions, archaeologists should be able to answer the question "*what do we know about the formation processes that create contemporary surface assemblages?*" (Lewarch & O'Brein 1981: 297) and skip to the next logical questions that must be "*how are contemporary surfaces different from past surfaces, subsurface deposits, or other modern surfaces?*" and "*why are surface assemblages exposed and how has this exposure conditioned their present state?*" (Lewarch & O'Brein 1981: 297-301). Post-depositional processes that are highly documented on modern surfaces have also potentially affected past surfaces and should be considered in an attempt to contextualise the subsurface deposits in the best manner. Natural and cultural post-depositional processes themselves, as well as the kind of exposure and the temporal duration of these effects, influence the preservation of the archaeological record. For instance, different alterations might be expected in contexts where surfaces have not been covered appreciably since entering the archaeological context, as opposed to those covered at varying deposition rates, or which have been covered to be exposed later by natural or cultural processes.

Depending on different types of force and mass and the shape and size of artefacts, various erosional regimes could have differential effects on materials (for more details see Chapter 2, also cf. Isaac 1967; Rick 1976; Flannery 1976; Kirby and Kirby 1976; Yellen 1977; Gifford 1978; Hole 1980). Once exposed on the surface, the longer the temporal duration of exposure, the greater likelihood for the mapping on of additional information and differential subtraction of elements from an assemblage (Clarke 1968; Daniels 1972; Sullivan 1978). Archaeologists are also aware that some classes of more perishable material evidence (e.g. organic finds such as textiles, basketry, bone and shell) suffer drastic changes in preservation, especially if they were

located on the surface. There are clearly severe limitations in using surface materials to deal with these kinds of less durable artefact classes, as proved at the Villaggio delle Macine (Chapter 5), where these observables have been only sporadically retrieved on the surface. Consequently, although this approach may be useful for treating durable kinds of artefacts, there is little doubt that perishable types are not well served by surface study in most environments.

The need to live and work outside the "Garden of Eden" (from Ammerman 2004) particularly refers to the essential awareness of archaeologists of ever-changing features that characterise archaeological landscapes, as long-term processes (Niknami 2007: 102). These changes, understanding the human actions and environmental effects on ancient landscapes (McGlade 1995), should be studied in their own spatio-temporal context. This means that archaeologists should take into account what comes to light on the surface of the landscape in any given year (Ammerman et al. 2013: 291). In other words, it should not be assumed that "*what one saw at a given place on the landscape in 1975 would be the same if the archaeologist went back out to the same place and took a second look in 1985*" (from Ammerman 1981; Ammerman 2013: 291). As highlighted in some case studies, as for instance the Acconia Survey (Ammerman 1981, 1985a, 1985b, 1995, 2004, 2013) and as proved at the Villaggio delle Macine (Chapter 5), the tacit assumption of landscape as a somehow static and stationary place has its problems. Indeed dynamic variation might take place on a landscape during the life of a survey, with visibility, composition and spatial distribution of the site and finds in a state of constant flux. According to this perspective, emphasised during recent decades (Ammerman 1981: 82), surveys have predominantly moved in the direction of becoming smaller in size, more problem-oriented, more practical in the questioning of site visibility and more intensive in their coverage of land (Wandsnider & Ebert 1984; Wandsnider & Larralde 1986; Camilli et al. 1988; Wandsnider 1989; Fish & Kowalewski 1990; Larralde 1990; Bintliff 1992; Wandsnider & Camilli 1992; Peeters 2004; Terrenato 2004; Runnels et al. 2005; Bevan & Connolly 2006; Bevan & Connolly 2009).

Furthermore, the nature of the archaeological record "*as a virtually continuous spatial distribution of material over the landscape"* (Niknami 2007: 103) has to be taken into consideration in reconstructing the full human use of landscape. This process therefore involves the acknowledgment of occurrences of faint scatters that might not qualify as sites but, however, represent significant human activity. From this approach, the concept of "non-site" or "off-site" arose, requiring a special methodology to locate and to record the artefacts found there (Foley 1981; Dunnell & Dancey 1983; Nance 1987; Binford 1992; Dunnell 1992; Banning 2002; Niknami 2007). In an attempt to reconstruct the variability of archaeological sites and their activity areas, effective factors for replacement of artefacts as well as the taphonomic processes in landscapes are indispensable for determining and analysing scatter distribution patterns and reconstructing formation processes.

When a survey surface is organised, archaeologists need to choose the spatial boundaries of the area. They often settle for natural geographical boundaries of some type, in the hope that these had at least some resemblance with past cultural boundaries. However, as mentioned above, landscape has changed over time and boundaries existing today may not have existed during the past or have been in different locations (Banning 2002). In most cases, the boundaries at least reflect some natural geographical units. In some circumstances this could not be defined as a deliberate choice, since it is inevitably influenced by both environmental and human conditions surrounding and characterising the archaeological context. For instance, this is partially the case at the Villaggio delle Macine since the presence of the lake, vegetation and heavily post-depositionally modified areas have imposed defined boundaries and, in some cases, limited the attempt to completely cover the full landscape.

Regardless, the more or less deliberate choice of where to place the boundaries of a survey region involves several "edge effects". These are defined as sources of bias that are caused by the interaction of the distributions that interest the archaeologist and the boundaries that the archaeologist itself imposes on those distributions (from Banning 2002: 80; Wheatley & Gillings 2003; Orton 2004; Conolly & Lake 2006; Ducke 2015). When, as in this case study, estimation of material evidence rather than their detection is the goal, archaeologists need to consider ways to avoid or account for bias that these edge effects would bring to their estimates. The occurrence of observations situated on borders of grid-sampled spatial units, or whose centres actually lie outside sample elements, provoke these effects. A simple count of all the information from the site utilised in estimating the evidence density would lead to bias. How can archaeologists deal with these issues? According to Banning, the fairly easy way to avoid this problem is to exclude these elements from any statistics; their occurrence in edge areas could be described and reported but they should not be allowed to affect estimates of population parameters. Is this the only option or can archaeologists solve this issue in some other way?

Furthermore, one of the major analytical problems in using surface surveys, and one of the main factors working against its analytical potential, is the temporal control (Lewarch & O'Brein 1981: 316-317). In a more general perspective, some authors (Fentress et al. 2004; Johnson 2004; Crema et al. 2010) tackle the issue of temporal domain, highlighting that "*very little effort has been placed on the formal integration of the temporal dimension into practical archaeological spatial analysis*" (Crema et al. 2010: 1119). However, even when this issue is tackled, the archaeological information achieved about time is predominantly uncertain. In the case of surface surveys and unstratified assemblages, archaeologists typically work with relative dates based on the style of surface artefacts, when they are preserved (Bevan et al. 2013: 312).

A recent proposal for overcoming this issue (Bevan et al. 2013) takes into account the uncertainty in a different way, by considering the possibility of identifying *n* time spans traditionally recognised in a particular geographical region and which are chronologically well-defined. For this method, specialists assert the correspondence of artefacts to a defined period. In cases of initial disagreement, a consensus view is eventually reached and also a residual "other" category is introduced in cases when this condition is not available. When the whole assemblage has been treated in this way, the frequencies of different assigned confidences by period are plotted (Bevan et al. 2013: 316, figure 1). Such plots constitute an important first stage in interrogating patterns of chronological uncertainty in the artefact record. The incorporation of these data with the spatial distribution of material and the analysis of uncertainty, even throughout the application of simulations, proved its advantages in order to explore regional patterns profiling and its variability. However, this is a lucky case study, since archaeologists could also have to deal with stylistic elements insufficient for precisely determining the age of a cluster of surface portable artefacts: in this case, the determination of surface age deposits is one of the greatest liabilities in the current application of survey technique.

Lastly, some issues could derive from the applied classification system and the data quality. As discussed by Orton (2004: 300), archaeologists have to take into consideration four main sources of error from minor, referring to the measurement of locations, to major, ascribable to transposition of digits or of x and y coordinates for instance. These problems are related to potential differences in the strategy of measurement used during data collections carried out over a period and/or by different individuals or organizations. In this case, similar objects may be recorded in different categories "*depending on when or by whom they were recorded*" (Orton 2004: 300) and according to different scales of precision. For instance, while locations of some

artefact types may be recorded "exactly" in specific x and y coordinates, others may be collected in bulk from grid units or sub-units. In order to take full advantage of the available datasets, archaeologists are forced to align the classification system, opting for the largest common sample grid unit or sub-unit. Although this condition involves a loss of resolution, this is the only option for making the entire dataset available for spatial and archaeological analysis.
Another source of problems is represented by missing data. Different issues may be included in this group. Indeed, the data absence could be attributable to failures in recording the objects' locations, even though they exist. However, the missing data could be also the result of "destroyed" evidence, that no longer exist at their location, for instance due to the potential effects of post-depositional disturbances. Finally, the occurrence of missing data could be induced by natural boundaries which characterise the sampling area or that resulted from the initial choice of the area. In the next section, the analysis of the case study will introduce an example of this issue.
This brief summary of the main general strengths and weaknesses of surface surveys provides the background to a required premise introducing the concrete application of surface survey to this case study. Its design in terms of intensity, shape and size, and reporting a detailed analysis of the adopted classification system (including a brief description of all archaeological categories involved in this research) will be discussed. Issues encountered concerning the creation, elaboration and analysis of the entire area will be also tackled.

6.1.2 Surface survey design at the Villaggio delle Macine: premise

Excavation of the site started[24] in 2001, when a lake water drop had occurred (as discussed in Chapter 5), with a regression of the current shoreline of about 25 m. The field procedure was based on a contiguous grid system of 1.50 squared metres, in accordance with the previous grid size and shape previously employed in underwater excavation. Each 1.50 m grid square has been divided into 0.50 squared metres sub-units and internally into 4 quadrants. This procedure adopted for the excavation was successively maintained during surveys in order to standardise the scale of analysis.
During the excavation, the spatial location of each find from the sub-surficial stratigraphic units was georeferenced, with x- y- and z- coordinates and levels, and hand-drawn on plots on a scale of 1:10. All wooden posts and the most important finds were also recorded through a total station. However, due to the haste of recovery needed and the surrounding environmental conditions, for upper layers (surficial level) some very fragmented categories of finds, such as pottery, were spatially defined according to their presence in quadrants of the grid.
During 2001, 9 macro-areas of various size were defined, subdivided into the aforementioned 1.5 squared metres cells into a total of 28 to 42 cells (which were subsequently subdivided as described). Each macro-area was assigned an identifying letter, from A to M (Figure 132). Each was surveyed taking into account the spatial distribution of artefacts and ecofacts, identifying the following categories of material evidence:posts, beams, wooden structures; grindstones and millstones; faunal remains; Bronze age pottery; Roman pottery; lithic industry; stones; bronze artefacts; concotto slabs and fragments; clay fishing weights; spindle-whorls.

[24] Previous short underwater excavations have taken place during previous years (for more details see Chapter 5, and also Angle et al. 2002).

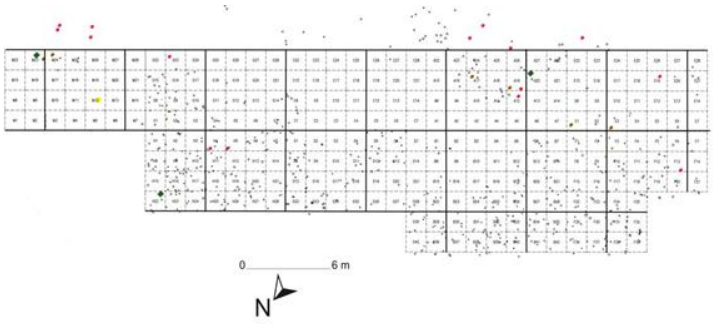

Figure 132 Example of sector surveyed during 2001 (courtesy of Federica Micarelli and Micaela Angle).

Among all these categories, bronze objects have been excluded from this analysis since they have predominantly been retrieved during occasional surface collections, without any specific indication of their provenance. Furthermore, these objects have not been recovered during successive surveys (in particular during those carried out in 2009 and 2012), thus they are not taken into account in this research. Similarly, the Roman pottery, georeferenced during the survey of 2009, has not been taken into consideration during previous campaigns forcing exclusion of this evidence in the study. Stones, numerous on the surface of areas surveyed in 2001 and 2003, are equally not considered, as their specific primary spatial location is not available. Furthermore, their widespread presence in these firstly surveyed sectors did not seem to be consistent in all areas successively investigated.

During 2003 a further water drop, with a subsequent regression of the shoreline a further 15-20 m, increased the width of the available archaeological area. Consequently, surveys were carried out following the same methodological procedure mentioned above. In 2009, a successive regression episode enabled undertaking further analyses. The first survey was fulfilled in May - June 2009, covering an area of 576 m^2 divided into broad sectors labelled alphabetically from A to L, each subdivided into 16 1.5 squared metres cells. Between September - November 2009 the second survey was performed and an area of 648 m^2 was covered. Again it was divided into broad sectors assigned alphabet letters from M to W, each one sub-divided into 16 1.5 squared metres cells, until reaching the lake's edge (Figure 133).

Figure 132 Distribution of macro areas of 1.5 squared metres identified by letter, from A to W (surveys 2009).

In summer 2012 (July - August), simultaneous with the excavation of a small sector of the site (around 30 m^2) (Angle et al. 2014), a further survey was carried out in the areas surrounding those already explored in 2009, reaching the lake's edge and a region until that time partially covered by flora consisting of both reeds and small or medium bushes. The same field procedure was used, covering an area of around 504 m^2, divided into broad areas defined

according the categorisation applied during previous years (Figure 133). This strategy enabled directly linking these new archaeological data into the previous grid system without loss of resolution. Furthermore, in order to collect as many data as possible through the total station, a beach located on the right side of this area was also surveyed and archaeological finds were recovered and drawn in a georeferenced map; sectors overlooking the water have also been surveyed according to this method.

B 297	D 304	D 293	D 292	D 291	D 289	D 288	H 294	H 293	H 292	H 291	H 290	H 289	H 288
B 290	D 297	D 286	D 285	D 284	D 282	D 281	H 287	H 286	H 285	H 284	H 283	H 282	H 281
B 283	D 290	D 279	D 278	D 277	D 275	D 274	H 280	H 279	H 278	H 277	H 276	H 275	H 274
B 276	D 283	D 272	D 271	D 270	D 268	D 267	H 273	H 272	H 271	H 270	H 269	H 268	H 267
B 269	D 276	D 265	D 264	D 263	D 261	D 260	H 266	H 265	H 264	H 263	H 262	H 261	H 260
B 263	D 269	D 258	D 257	D 256	D 254	D 253	H 259	H 258	H 257	H 256	H 255	H 254	H 253
B 256	D 262	D 251	D 250	D 249	D 247	D 246	H 252	H 251	H 250	H 249	H 248	H 247	H 246
B 249	D 255	D 244	D 243	D 242	D 240	D 239	H 245	H 244	H 243	H 242	H 241	H 240	H 239
B 242	D 248	D 237	D 236	D 235	D 234	D 233	H 238	H 237	H 236	H 235	H 234	H 233	H 232
B 235	D 241	D 229	D 228	D 227	D 226	D 225	H 231	H 230	H 229	H 228	H 227	H 226	H 225
B 228	D 238	D 222	D 221	D 220	D 219	D 218	H 224	H 223	H 222	H 221	H 220	H 219	H 218
B 221	D 230	D 215	D 214	D 213	D 212	D 211	H 217	H 216	H 215	H 214	H 213	H 212	H 211
B 214	D 202	D 208	D 207	D 206	D 205	D 204	H 210	H 209	H 208	H 207	H 206	H 205	H 204
B 197	D 195	D 201	D 200	D 199	D 198	D 197	H 203	H 202	H 201	H 200	H 199	H 198	H 197
190	D 196	D 194	D 193	D 192	D 191	D 190	H 196	H 195	H 194	H 193	H 192	H 191	H 190
	D 189	D 187	D 186	D 181	D 182	D 183	H 189	H 188	H 187	H 186	H 185	H 184	H 183

Figure 133 Example of sector surveyed during 2012 (Zone 1).

6.1.3 Surface survey design at the Villaggio delle Macine: strategy versus sampling issues

The set of prospections carried out over recent years generated a broad variety of information, the majority being hand-drawn maps as well as distributional maps created through the total station; the latter are usable in different formats and graphic programs such as AutoCAD and CorelDraw, as a unique layer of all archaeological evidence or as multilayers (each category corresponding to a specific layer). This diversity forced designing a procedure to manage all these archaeological data together, homogenising them. A new grid system which could join all the surveyed areas was created in an attempt to take full advantage of this complex data system. The previous grid arrangement of 1.5 squared metres was followed as the main structural unit of reference; however, a smaller unit was chosen, the 0.5 squared metres subdivided into quadrants, in an attempt to suitably undertake intra-site spatial analyses. From both the hand-drawn and digitised distributional maps it is possible to recover the exact x-y coordinate of each piece of material evidence, except for the pottery as mentioned above. This condition led to choosing an alternative system which would allow recording the spatial location of all evidence, still in the most accurate way. Since pottery was spatially located in specific quadrants within each 1.5 squared metres, the use of a centroid-system seemed to fit our archaeological data best. Thus, each 1.5 square metres was initially subdivided in 0.5 squared metres and for each subunit the x-y centroid coordinates (0.25 squared metres)[25] were calculated. For each x-y sampling unity the total frequency of occurrence of each material category was calculated.In the next section, the definition and deeper analysis of each category will shed some light on issues

[25] From now "sampling unit"

affecting this quantification, because of the strong fragmentation which characterised the archaeological observables.
The region studied here includes the total amount of surveyed area and in the process of integrating all the available data some issues came to light. First of all, the main difficulty was associated with the nature of the studied region that could not be defined as continuous. Indeed, some natural boundaries such as variations of lake shoreline occurred during these years, as well as the growth of natural vegetation, limited the possibility of covering the entire region. This condition leads to some "missing data": the absence of specific x-y sampling unit is ascribable to this impossibility to survey concrete spatial sectors. Instead, a recorded presence of 0 for each category of material evidence in concrete sampling unit means that, in surveyed areas, these archaeological finds were not retrieved.
A further "empty area", located between the sector surveyed in 2001 and the sector surveyed in 2009 (see figure 1 chapter 5), is associated with the spatial portion of the area surveyed in 2003; since archaeological finds and data retrieved in this occasion are not yet analysed in detail, they were not included in the database. However, among aims of this research is a predictive study, through the archaeological information provided by the available areas, of these empty zones. Throughout the interpolation, these missing data will be obtained and taken into account in the analysis. The results of these predictions will be tested through a comparison with the available archaeological data (the analysis of each category) (see Chapters 7,8 and 9).
In an attempt to partially fill the gap of the missing archaeological data related to the portion of region surrounding the main sectors, the surveys of 2012 took place and provided interesting results. However, the internal discontinuities of the broader area and the high occurrence of missing data are among central issues concerning the intra-site spatial analysis encountered during this research. Operative strategies and potential ways to overcome both edge effect issues and the overabundance of zeros will be proposed in next chapters.

6.1.4 The database: contents and data structure

The database is currently composed of 4396 data entries, corresponding each to an x-y centroid coordinate, associated with a 0.5 squared metres cell, including the entire region covered by surveys. The first columns are related to the x and y centroid coordinates, whereas successive ones are devoted to different categories of archaeological evidence. Initially, categories are strictly subdivided into a wider sub-categorisation that will be specifically discussed in each devoted paragraph: however, this data division was not suitable for the analysis since it is generating a higher presence of zero for the majority of this sub-category. Thus, they were internally reassembled. Categories considered in the database are: posts, horizontal (wooden) poles and wooden fragments; saddle querns (grindstones and handstones), faunal remains, pottery, lithic artefacts, concotto slabs and fragments, clay fishing weights and spindle-whorls. The categories considered in the

Each category was assessed according to its occurrence, in terms of frequency, in the relative sampling unit. In general terms, the choice of analysing the frequency of material evidence in concrete spatial location is related to the manifold aims of the research: as already mentioned in Chapter 1, the count of frequency enables archaeologists to reconstruct the most likely activities that could take place during the past in certain spatial regions. Indeed, the higher the frequency of certain material observables in such location, the higher the likelihood that the action that produced such evidence was carried out there or in the local surroundings. Thus, if frequencies

of different material evidence unequally changed in correspondence to certain sub-regions, as archaeologists we could explore events that have produced these differences. If a homogenisation of frequencies is attested in all the spatial locations and for all categories of evidence, according to our null hypothesis, deformation processes have totally re-arranged the original observables in an obliterating manner that prevents even a probabilistic reconstruction of the past. In order to support or confute the null hypothesis through this intra-site spatial analysis of specific categories, the starting point of the research is represented by the specific definition of such categories to be explored.

6.1.4.1 The dataset of categories: a methodological premise

As already mentioned, eight categories are introduced as part of the dataset for this intra-site analysis. The main issue faced during this research and affecting all the categories is the fragmentation of material evidence. Although this condition affects certain classes of finds more than others, such as pottery, in general terms the entirety of the sample suffered this widespread archaeological issue. In each section devoted to the analysis of a single category, the problem of fragmentation will be introduced in order to display how this issue has been overcome in defining the subcategories of the sample.

6.2 *Posts: discovery and meaning*

As very often happens, posts were the first evidence unearthed when the water level drop took place. At the Villaggio delle Macine the first occurrence of this phenomenon, during 2001, exposed around one thousand posts and their number rose during 2003, reaching around five thousand. They are predominantly derived from the deciduous oak (*Quercus sp.*) (Figure 134). This great availability of wooden poles enabled undertaking dendrochronological preliminary analyses in 2003 on a limited sample (six poles). In 2009, the further emergence of a portion of the site revealed a large succession of poles (around five hundred**).** Thus, around seventy poles ascribable to both the deciduous oak (*Quercus sp.*) (section Robur) and evergreen oak (*Quercus sp*.) were sampled in three different areas across the lakeshore. Five groups of contemporary poles were identified and they allowed developing a chronology of about 95 years for the site, which includes a ring series of twenty-two poles and the six previously sampled. The presence of the sapwood on the samples enabled the identification of at least three different felling phases: the first one is dated to years 49 to 56 of the relative chronology, while the second in the years 63 to 76 and the third in the years 85 to 96 (Martinelli, personal communication; Angle et al. in press). The recently sampled new area contains poles ascribable to the three different phases of felling and currently a chronological model for the spatial distribution of structures has not been recognised. Furthermore, this analysis does not shed light on the presence of specific pole alignments or spatial arrangements strictly associated with lakeside settlement structures. Four different typological elements have been identified and categorised accordingly:

1) Fully circular-shaped posts,
2) Pointed posts,
3) Three-quarter circular-shaped posts,
4) Quarter circular-shaped posts.

Figure 134 Wooden poles preserved in the surface of the site; some, as in this case, showed evidence of bark.

6.2.1 Posts recovered during the surveys of 2001

A total amount of 531 posts were retrieved on the site's surface in 2001. Of the four typological elements already mentioned, pointed posts seemed to be absent[26] in this area. Two half and four three-quarter circular-shaped posts have been identified. Posts not considered in this list were located outside of these macro-areas (Table 1).

	Circular-shaped posts	pointed posts	3/4 of circular-shaped posts	1/2 of circular-shaped posts
Macro Area A	24	0	0	0
Macro Area B	130	0	1	1
Macro Area D	72	0	2	0
Macro Area E	14	0	0	0
Macro Area F	114	0	0	0
Macro Area G	48	0	0	0
Macro Area H	117	0	1	1
Macro Area M	6	0	0	0

Table 1 Spatial distribution of different kinds of posts recovered during 2001.

6.2.2 Posts recovered during the surveys of 2009

A total amount of 444 posts were recovered on the surface of the site in 2009. Posts that were not included in specific macro-areas, being located in peripheral areas (as is visible in the map), have not been included.

[26] the data referred to this type of posts is absent, although we do not know if they were identified and were not reported in the available documentation or if they are actually absent

	Circular-shaped posts	pointed posts	3/4 of circular-shaped posts	1/4 of circular-shaped posts
macro area A	5	0	0	0
macro area B	9	0	0	0
macro area C	29	0	0	0
macro area D	59	0	0	0
macro area E	2	0	0	0
macro area F	16	0	0	0
macro area G	5	0	0	0
macro area H	15	0	0	0
macro area K	13	4	1	1
macro area J	14	3	4	0
macro area -J	5	0	0	4
macro area I	9	0	0	0
macro area L	35	0	0	0
macro area N	4	4	0	0
macro area O	6	13	0	0
macro area P	12	6	0	0
macro area R	8	4	0	0
macro area Q	7	4	0	1
macro area S	17	1	1	0
macro area T	24	0	2	3
macro area U	24	1	5	2
macro area V	22	0	7	3
macro area -V	0	0	0	0
macro area Z	23	0	0	0
macro area W	3	1	0	0
macro area -Z	3	0	0	0

Table 2 Spatial distribution of different kinds of posts recovered during 2009.

6.2.3 Posts recovered during the surveys of 2012

A total amount of 357 posts were retrieved on the site's surface in 2012. Among four typological elements only entire circular-shaped posts were attested. They were identified predominantly in areas reported by total station, with twenty-five being located in the macro-area D.

6.2.4 The creation of the unitary dataset

Posts collected during the recent surveys were grouped together in the database by spatial distribution, by equating 0.5 squared metres cell coverage to corresponding to sampling units. They were attested in 1238 sampling units within a total sample of 4396 records. For each cell the frequency of this category, that spans from one to four finds, was calculated. In some cases posts were located at the intersection between two square cells which forced the inclusion of those finds in two cells. For this reason, a wider number of posts is attested in the dataset

compared to the amount previously listed (595 posts for the survey of 2001, 519 for the survey of 2009 and 359 for the survey of 2012).

6.3 Grindstones and millstones: old data and new perspectives

Both these terms, grindstones and millstones, are used to define grinding tools; however, currently the most general and widely used term is millstone. In 1993, Wiliams-Thorpe and Thorpe, in describing early millstones in the Eastern Mediterranean, were among the first to differentiate between these two categories in highlighting that grindstones meant a non-rotary milling stone (Wiliams-Thorpe & Thorpe 1993: 265). In contrast, according to their article, the term millstones corresponded to four types of finds: saddle querns, hopper-rubbers, rotary querns and Pompeian-style mills (Figure 135).

Figure 135 Example of saddle querns which mirrors our remains (from Wiliams-Thorpe & Thorpe 1993:266, figure 1a). In particular this image is referred to saddle querns and rubbing stones at Kourion, Cyprus.

Saddle querns were the only form of mill known during the prehistoric period "*prior to the invention of the hopper-rubbers of the Classical Greek and Hellenistic periods, and are ubiquitous in the east Mediterranean*" (Wiliams-Thorpe & Thorpe 1993: 265; Antonelli et al. 2004). The term meant a concave, generally ovate or rectangular stone base (Wiliams-Thorpe & Thorpe 1993: 265), grinding slab or grindstone (Curwen 1937; Storck & Teague 1952; Roux 1986; De Beaune 1989; Antonelli et al. 2004: 537) paired with a rounded, oval or elongated rubbing stone, an active implement usually called the handstone. They were produced without a standardised purpose, since they showed a wide variation in size and in the raw materials that composed them. However, most millstones for grinding practices from the Mediterranean area are made of volcanic stone (Williams-Thorpe 1988; Williams-Thorpe & Thorpe 1991, 1993; Renzulli et al. 2002; Antonelli & Lazzarini 2010; Santi et al. 2013; Santi et al. 2015: 804). This choice is probably favoured by the easy-workability of volcanic rocks, characterised by wear resistance and a good grinding capacity, because of their abrasive properties and rough vesicular surface (Peacock 1980; Williams-Thorpe 1988; Renzulli et al. 2002: 175; Santi et al. 2004, 2015: 804). However, the selective criteria for the choice of raw materials used for stone artefacts also took into account the accessibility of rock outcroppings and the existence of an adequate transportation network.

In the last two decades, in an attempt to shed further light on this topic, technomorphological studies (Delgado Raack et al. 2008, 2009), often based on ethnographic data (Hayden 1987; Adams 1993, 1994; Baudais & Lundström-Baudais 2002), functional studies (Dubreuil 2001; Hamon et al. 2008; Adams et al. 2009; Delgado-Raack & Risch 2009; Šajnerová-Dušková et al. 2009), and use wear analysis (Clemente et al. 2002; Portillo et al. 2013; more references in Dubreuil et al. 2015), were married with archaeometric, petrographic and geochemical studies of volcanic rocks (e.g. Thorpe-Williams 1988; Thorpe-Williams & Thorpe 1988, 1990, 1993; Schoumacker 1993; Schneider 2002; Antonelli et al. 2004; Buonasera 2007, 2012; Antonelli & Lazzarini 2010), in order to unravel the ancient communication routes and trade networks. Such studies have been carried out in different regions of Italy (e.g. Cattani et al. 1997; Antonelli et al. 2000, 2001, 2004, 2014; Capedri et al. 2000; Lorenzoni et al. 2000 a,b; Renzulli et al. 2002; Santi et al. 2004, 2013, 2014).

6.3.1 Millstones of the Villaggio delle Macine

The millstones retrieved on the surface of the Villaggio delle Macine fall into the first type listed by Thorpe and Thorpe, as they are saddle querns (Figure 136). Both the components of this type, i.e. the grindstones and the handstones, have been recovered. Their local provenience is certain since they are made of volcanic porous rocks (i.e. grey, scoriaceous, leucithic lavas) which outcrop in the surrounding area (Angle et al. 2001: 54, inventory number XI, 4-5; Angle et al. 2011: 232); original rock slabs are still visible nearby the site. Chiarucci has even considered these slabs as formal quarries of blocks (Chiarucci 1995-96**:** 180). During underwater surveys divers pinpointed the presence of springs where different-sized porous volcanic rocks of various thicknesses emerged in vertical positions (Chiarucci 1986-88: 416).

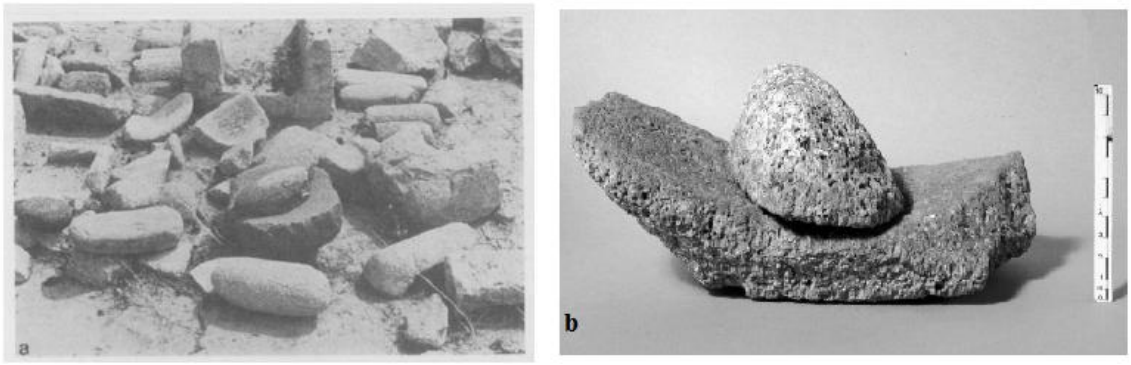

Figure 136 a)see figure 134, b)grindstones and handstones from Villaggio delle Macine (Angle et al. 2001: 54, inventory number XI, 4-5).

The occurrence of these tools, quantitatively incomparable to coeval settlements in Lazio, enabled Chiarucci to preliminarily hypothesise that they have not only been used in situ but may also have been "exported" as, for instance, exchange objects (Chiarucci 1986-88: 414-6, 1995-96:180-1). In the light of their high occurrence at the site, he suggested that their manufacturing might have had a certain economic relevance, since their production required a total devotion of some community members (Chiarucci 1985: 180-1).
Contrary to other material categories, grindstones have not been strongly affected by post-depositional processes. Indeed, in most cases they seem to maintain the original rectangular shape, without traces of strong fissures or superficial and/or internal damage. In the chapter devoted to the results of intra-site spatial analysis (Chapters 7, 8 and 9) it will be proved if they

were affected by a spatial rearrangement caused by these processes. Clearly, this relocation could particularly affect the smaller and more easily transported handstones. However, the presence of some beach properties and commercial activities (such as restaurants) might have caused a recent reclamation phenomenon that, regardless, should affect only a short number of artefacts due to their weight (grindstones) and their shape (handstones).

6.3.1.1 Saddle querns recovered in 2001

A significant amount of saddle querns were retrieved on the site's surface during surveys carried out in 2001: about 1221 saddle querns were identified and reported in the hand-drawn map (Table 3). A variable number of 42 cells were surveyed for the macro-area B, while 27 for macro-area C, 30 for macro-area D, 28 for macro-area E, 33 for macro-area F, 28 for macro-area G, 27 for macro-area H and 2 for macro-ares 2. In contrast with the distinction drawn between grindstones and handstones within the general category of saddle querns as directly applied during surveys in 2009, the available data reported for 2001 are provided by hand-drawn maps carried out by a different team and lacking this information. Although their manual characterisation could enable their probable identification according to the stone's shape and dimension, these two categories, in an attempt to avoid further approximations and loss of accuracy, are listed together among the more general "saddle quern" category.

	saddle querns
macro area A	37
macro area B	227
macro area C	60
macro area D	144
macro area E	272
macro area F	94
macro area G	217
macro area H	158
macro area M	11

Table 3 spatial distribution within the area surveyed in 2001 of saddle querns.

6.3.1.2 Saddle querns recovered in 2009and 2012

During surveys carried out in 2009, 182 grindstones and 30 handstones were identified (Table 4). Conversely, 55 grindstones and 12 handstones were recovered during surveys carried out in 2012 (Table 4), both in areas reported through hand-drawn maps and in the sector only reported through the total station. For some macro-areas, again, a variable number of 1.5 m^2 cells were surveyed: for instance, for the area Z, a total amount of 56 cells, for H 98 cells and finally for the area D 84 cells.

	grindstone	handstone
macro area C	4	0
macro area D	1	0
macro area I	3	0
macro area K	1	0
macro area J	10	1
macro area -J	7	3
macro area L	2	0
macro area N	15	2
macro area O	25	5
macro area P	30	6
macro area Q	15	2
macro area R	9	1
macro area S	9	0
macro area T	10	2
macro area U	10	2
macro area V	10	3
macro area -V	1	0
macro area Z	5	2
macro area -Z	10	1
macro area W	5	0

Table 4 spatial distribution within the area surveyed in 2009 of grindstones and handstones.

	grindstone	handstone
Macro area D	16	2
Macro area H	15	5
Macro Area Z	24	5

Table 5 spatial distribution within the area surveyed in 2012 of grindstones and handstones.

6.3.1.3 The creation of the unitary dataset

All saddle querns collected during the recent surveys were grouped together in the database by spatial distribution, by equating 0.5 squared metres cell coverage to their corresponding to sampling units. They were attested in 846 sampling units within the total sample of 4396 records. For each cell the frequency of handstones and grindstones was calculated with values that span from a minimum of 1 to a maximum of 12 within each cell. In sectors surveyed in 2009, the large dimensions of particular grindstones forced inclusion, in some cases, of the same finds in at least two sampling units since they occupied two of them. For this reason wider numbers of grindstones are attested in the dataset, compared with the amount previously listed. Counting the frequency of this evidence recovered from the site surface for each cell it was highlighted that their occurrence did not achieve, with handstones and grindstones separated, a

reliable statistically relevant sample. If forced to consider both sub-classes of finds, the unitary category of saddle querns was applied.

6.4 Faunal remains recovered during surveys at the site

Faunal remains retrieved in last few years during surveys were classified anatomically and taxonomically, and they were also divided for classes of age[27]. In general terms, bones were characterised by a medium/mediocre state of preservation. The rates and trajectory of their decay are products of a complex interaction between many variables that range from pre-depositional agents of destruction, to post-depositional events, and specifics of burial environment (Behrensmeyer 1978; Nicholson 1991, 1996, 2001; Robinson et al. 2003). The sedimentation rate and the action of atmospheric agents determine the dynamics of the burial processes.

Although bone remains are generally vulnerable when subjected to many physical, chemical and biological agents, which might affect their mineral matrix, collagen content and structure (histology, porosity) (Thomas et al. 2012; Saña et al. 2014: 73), very wet environments are anoxic which at least inhibits microbiological attack (Lyman & Fox 1989; Hedge 2002: 325; Armstrong 2010). This condition can assure that the faunal assemblage, if buried reasonably quickly, does not lose its integrity in physical terms, as attested, for instance, at the site of La Draga, sector B (Saña et al. 2014). These faunal remains were characterised by homogeneous and dark surfaces, with edges that were generally polished (Saña et al. 2014: 76-77, figure 5). These same patina marked faunal remains recovered at the Villaggio delle Macine. They are particularly evident on bones retrieved during the surveys of 2009. However, in sector B of La Draga, traces of abrasions are practically absent on bones, while these strongly characterised faunal remains retrieved at the Villaggio delle Macine (Figure 137). Indeed most bones displayed small fissures and such surficial exfoliation that in a small number of cases was penetrating (Figure 138). This physical state mirrors the original underwater, peaty conditions of provenance but may also be produced by the bones' movement (Gaudzinski-Windheuser et al. 2010; Saña et al. 2014).

Figure 137 Faunal remains from surveys of 2009. Evident traces of abrasion.

[27] The anatomical and taxonomical definition was obtained according to Barone 1976; Schmid 1972; Wilkens 2003 and ages were estimated according to Brown et al. 1960; Silver 1969; Bull & Payne 1982; Grant 1982; Amorosi 1989

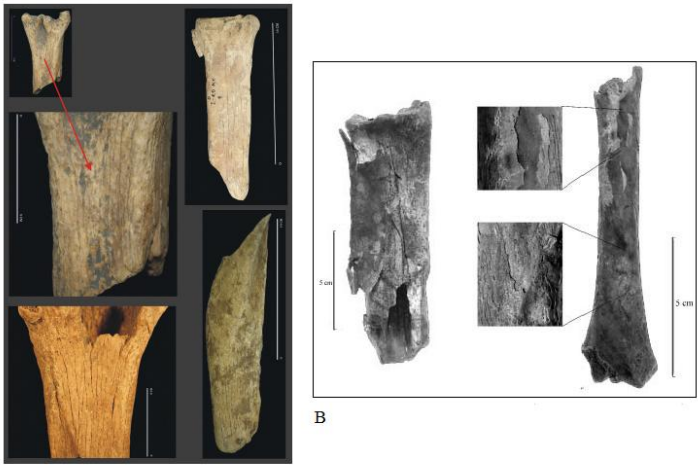

Figure 138 A) Examples of hair-line cracks on the bone surface and flaking of the cortical surface (La Draga, Sector A) (from Saña et al. 2014: 76, figure 4); B) examples of fissures and surficial exfoliation (Villaggio delle Macine, excavation) (from Tagliacozzo et al. 2012: 146, figure 1).

When the site emerged during recent years, the passage to an aerial environment even involved, in cases largely exposed to the atmospheric conditions, a reduction of bone volumes. Some of the affected faunal remains displayed hairline cracks comparable to those highlighted on the surface of bones recovered in sector A at La Draga. These alterations have compromised the possibility of identifying some anthropic as well as natural modifications on such bones (Tagliacozzo et al. 2012: 146); however, the sample has still provided some useful data.

Since this research started with material from the 2009 surveys and the other material evidence (recovered in 2001 and in 2012) was analysed later, this summary starts from results of the first study, originally presented in the author's Master's thesis.

6.4.1 Faunal remains retrieved in 2001

The analysis of faunal remains from the 2001 surveys yielded an Excel database with 184 records (ascribable to 430 finds)[28]. The spatial location is recorded through both macro-areas (each macro-area of variable number of surveyed 1.5 squared metres cells, defined alphabetically as A, B, C, D, E, F, G, H and M) as well as micro-areas (the specific square cells within the macro-areas).

The sample consisted of a total amount of 430 finds. In general, 242 undetermined fragments, four macrofaunal fragments, and 17 cranial fragments and 54 axial fragments of undetermined species have been identified as well as 160 fragments ascribable to specific other species and body part. The differentiation by body part and species is summarised in Figure 139. During the analysis of faunal remains, where it was possible considering the limited sample size, age attribution was carried out.
The majority of *Bos taurus* fragments are ascribable to adult individuals. For the 33 *Cervus elaphus* fragments, adults as well as young individuals are attested, and there are even a few ascribable as intermediate juvenile adults. Two of the three fragments of *Canis familiaris*

[28] The work was realised in co-operation with the archaeozoological team of the University of Tor Vergata, Lecturer of Palentologia, particularly with the help of Letizia Silvestri and Leonardo Salari.

belong to adult individuals, as well as the two fragments of *Lepus sp*. The finds of *Ovis vel Capra sp.* are equally representative of young and adult individuals, although the sample is very small. On the contrary, a clear age pattern is identifiable for *Sus domesticus* remains: indeed, among a sample of 12 finds, only one is attributable to a full-grown adult individual while the others are distributed between the younger ages and juvenile adults.
The total amount of domestic fauna is predominant (59 fragments, compared to the 36 wild faunal fragments) although the aforementioned pattern of *Cervus elaphus* predominance is confirmed (33 finds), compared to the small presence of domestic faunal remains for each taxon (for instance only four *Bos taurus* fragments have been recovered, 29 of *Ovis vel Capra sp.* and 23 of a domestic variant of *Sus scrofa*).
Furthermore, cut marks have been identified on some bones. Markers associated with butchery are identified on seven vertebrae, on one macro-cranial fragment, on one rib and on two fragments of *Ovis vel Capra sp.* and a *Canis familiaris* femur. The majority of finds were characterised by a strong reddening and some were blackened by fire, probably in association with food practices (a total amount of 25 finds). Five finds were even calcinated.

	Cranial					Axial				Appendicular																
BODY PART	SK	TT	MAND	MAX	UND	Tot	RIB	VER.	UND	Tot	SC.	HM.	RD.	UL	Tot	PL.	FM.	TB.	FB.	TOT	ANK	CA.	C-T	MC	MT	MTP	PL	UND	TOT	TOT
Ovis aries vel Capra hircus		10	1			11		1		1		2	2	2	6	2	2	1		5		1			1	1	3		6	29
Sus scrofa var. domesticus		8	2			10					1	1	1	1	4	2	2			4	1	1					3		5	34
Bos taurus																		1		1	1						2		3	4
Canis familiaris														1	1		1			1						1			1	3
capreolus capreolus																									1				1	1
Cervus elaphus		3		1		4						3	1	1	5		3	3		6	1	1	2	1	1	6	6		18	33
Lepus sp.													1		1												1		1	2
macro fauna		3				3																						1	1	4
Meso fauna																														
Undetermined size						17	17	29	25		54																	7	7	78
Undet																														242

Figure 139 Distribution for species and anatomical body part of faunal remains retrieved during 2001 at the site (Cranial (SK:Skull, TT:teeth, MAND:mandible, MAX:Maxillary, UND:undetermined cranial fragments); Axial (RIB:Ribs, VER:vertebrae, UND: undetermined axial fragments), Appendicular (SC:Scapula, HM:Humerus, RD:Radius, UL:Ulna, PL:Pelvis, FM:Femur, TB:Tibia, FB:Fibula, ANK:Anklebone, CA:Calcaneus, C-T:Carpal-Tarsal, M-C:Metacarpal, M-T:Metatarsal, MTP:Metapodial bones, PL:phalanxes).

6.4.2 Faunal remains retrieved in 2009

The analysis of the faunal evidence from surveys carried out in 2009 (a total amount of 2164 fragments) yielded[29] an Excel database with 387 records (ascribable to 426 finds). This preliminary dataset included information about the spatial location of recovery, in terms of macro-area (the macro-area of 16 1.5 squared metres cells, labelled alphabetically, such as Sector A, B….) as well as the specific micro-area (specific square cells within this macro-area) and the number of finds assigned within the field.

The sample consisted of 1769 undetermined fragments, 158 macro-faunal (*Bos taurus* and *Cervus elaphus*) fragments, 53 meso-faunal (*Ovis vel Capra sp.* and *Sus sp.*) fragments have been identified by body part where possible. The differentiation by body part and species is summarised in Figure 140.

[29] The remains were first analysed and subdivided by Beatriz Pino Úria and Antonio Tagliacozzo, (Soprintendenza al Museo Nazionale Preistorico Etnografico "L. Pigorini", Sezione Paleontologia del Quaternario e Archeozoologia.

Nine *Bos taurus* fragments are identifiable as adult, while only one belong to a young individual. For the 30 *Cervus elaphus* fragments as well as for the 12 *Sus sp.* fragments a predominance of adult individuals is attested (26 and 11 fragments respectively), while few fragments (respectively 4 and 1) belong to young individuals. The same pattern is identifiable for *Ovis vel Capra sp.*, since nine fragments are ascribable to adult individuals, while only one to young. The only four *Capreolus capreolus* fragments are ascribable to adult individuals, as is the case of the one *Sus domesticus*. Finally, one fragment of meso-appendicular is ascribable to a young individual and one unique fragment ascribable as an old individual belongs to *Sus scrofa*. Although the total amount of domestic fauna (163 finds ascribable to *Bos taurus, Sus sp., Ovis sp., Canis familiaris*) is higher than the wild fauna (99 finds ascribable to *Cervus elaphus, Capreolus capreolus,* undetermined carnivorous taxa, *Meles meles, Vulpes vulpes*), the pattern already mentioned is confirmed since the highest value of presence is ascribable to *Cervus elaphus.*

Furthermore, cut marks[30] have been identified on some bones. In particular, markers associated with butchery are identified on eight vertebrae (predominantly attributable to *Cervus elaphus* and, in one sample, to *Ovis vel Capra*), and in three macro-appendix fragments (a tibia, a *Bos taurus* metatarsal and a fragment of pelvis). Furthermore, one *Cervus elaphus* fragmented tibia displayed gnawing marks. The majority of finds were characterised by a strong reddening and blackish patina (a total amount of 147 finds) while some were blackened by fire (such as an ankle bone of *Cervus elaphus* and macro-cranial (teeth) fragments).

	Cranial					Axial				Appendicular																
BODY PAR	SK	TT	MAND	MAX	UND	TOT	RIB	VER.	UND	TOT	SC.	HM.	RD.	UL	TOT	PL.	FM.	TB	FB	TOT	ANK	CA	C-T	MC	MT	MTP	PL	UND	TOT	TOT
Ovis aries va	Capra	40				39		1		1	1	1			2			2		2	2	1					1	4	44
sus sp.		5				5						1		1	2			1		1					1			1	9
Sus scrofa var. dome		14	7	3		24						2			2	1				1	4	2				1	1	8	35
Bos taurus		54				54							3	1	4						1		1	1	3		4	10	68
Canis familiaris								1		1				1	1		1			1									3
capreolus capreolus												1			1		1	1		2									3
Cervus elaphus		30				30		3		3		1	2	1	4	4	4	9		17	9	5	2	3	4	4	9	36	90
Meles meles			1			1																							1
Vulpes vulpes		1	1			2											2			2									4
Lepus sp.																													
turtle shells																													19
Unidentified carnivorous			2			2																							2
Macro fauna		2			8	10	1	8	2	11						1				1			1					40	41	63
Meso fauna		1	2		1	4	2		2	4		1			1			2		2								19	19	30
bird																													1
Undet																												54		54

Figure 140 Distribution for species and anatomical body part of faunal remains retrieved during 2009 at the site (Cranial (SK:Skull, TT:teeth, MAND:mandible, MAX:Maxillary, UND:undetermined cranial fragments); Axial (RIB:Ribs, VER:vertebrae, UND: undetermined axial fragments), Appendicular (SC:Scapula, HM:Humerus, RD:Radius, UL:Ulna, PL:Pelvis, FM:Femur, TB:Tibia, FB:Fibula, ANK:Anklebone, CA:Calcaneus, C-T:Carpal-Tarsal, M-C:Metacarpal, M-T:Metatarsal, MTP:Metapodial bones, PL:phalanxes).

6.4.3 Faunal remains retrieved in 2012

Among the remains recovered during the 2012 surveys, the sample taken into account for this research exclusively included finds which were spatially well-defined, within a concrete cell-grid system, whereas the majority of archaeological data that were excluded derived from the

[30] Such analyses have been carried out according to Guilday et al. 1962; Shipman 1981; Shipman et al. 1984; Noe-Nygaard 1989; Higgins 1999; McCutcheon 1992; Nicholson 1995.

sample manually retrieved on the beach for a range of 10 meters. This dataset will be reanalysed in future work in order to take full advantage of this available source of interesting data.

The Excel database included a total amount of 122 finds distributed in 36 records[31]. For these data, the exact spatial location of each find was available. This small sample is composed of 124 fragments, 101 undetermined fragments and few differentiation according to body part and species, as summarised in Figure 141.
The few *Ovis vel Capra sp.* finds are ascribable to adult individuals as is the only evidence of *Bos Taurus*. In contrast, the *Sus domesticus* are from young or young/adult individuals as even the *Cervus elaphus* remains with available kill-pattern data are ascribable to the class of adult.
The scarcity of faunal remains attributable to specific taxa did not provide a large sample size. However, the amount of domestic faunal fragments is slightly higher with nine in contrast to five wild faunal fragments (*Cervus elaphus*).
A limited number of cut marks, probably associated with butchery, are identified in two fragments of *Canis familiaris* atlans, in a macro-appendicular fragment (a fragment of radius longitudinally cut) and in some vertebrae (one belonging to *Ovis vel Capra sp.*, one of *Bos taurus*, one ascribable to a macrofaunal species and two related to animals of undetermined size).

	Cranial				Axial				Appendicular																
BODY PAR	SK	TT	MAX	TOT	RIB	VER	UND	TOT	SC.	HM.	RD.	UL	TOT	PL.	FM.	TB.	FB.	TOT	ANK	CA	MC	MT	MTP	PL	UND	TOT	TOT
Ovis aries vel Capra		1		1		1		1	1				1														3
Sus scrofa var. domesticus												1	1										2	1		3	4
Bos taurus						1		1																			1
Canis familiaris						1		1																			1
Cervus elaphus																			1					4		5	5
Meles meles																											
Vulpes vulpes																											
Lepus sp.																											
turtles shells																											
Unidentified carnivorous																											
Macro fauna		1		1		1		1			2		2							1						1	5
Meso fauna	1			1																2						2	3
Undet						1		1																			1

Figure 141 Distribution for species and anatomical body part of faunal remains retrieved during 2012 at the site (Cranial (SK:Skull, TT:teeth, MAND:mandible, MAX:Maxillary, UND:undetermined cranial fragments); Axial (RIB:Ribs, VER:vertebrae, UND: undetermined axial fragments), Appendicular (SC:Scapula, HM:Humerus, RD:Radius, UL:Ulna, PL:Pelvis, FM:Femur, TB:Tibia, FB:Fibula, ANK:Anklebone, CA:Calcaneus, C-T:Carpal-Tarsal, M-C:Metacarpal, M-T:Metatarsal, MTP:Metapodial bones, PL:phalanxes).

6.4.4 "Catalogue raisonné" of faunal remains: the creation of the database

All archaeozoological data collected in the surveys during these years were rearranged together in the database into sets of 0.5 squared metres cells that, as mentioned above, correspond to x-y centroid coordinates. Faunal remains were attested in 1028 centroid sampling units within a total sample of 4396 records. For each centroid coordinate, the frequency of faunal remains identified was calculated and the frequency values span from a minimum of 1 occurrence to a maximum of 23, with each centroid coordinate. Initially, faunal remains were divided according to the previously mentioned subcategories, relating to their attribution to specific taxa and anatomical part. However, in the concrete case study, rather than providing further detail on the

[31] Cf. previous note.

dataset, this subdivision was generating "noise" and preventing reaching a statistically relevant sample size. Indeed, zero values were highly attested because of the strong fragmentation of remains which prevented many samples from being attributed to specific anatomical parts or taxa, as in the case of finds retrieved during the 2012 survey.

Furthermore, the occurrence of only low numbers of fragments of specific secondary species (for instance, *Meles meles*, carnivorous taxa, *Vulpes vulpes*) and even the presence of one fragment of a particular anatomical part complicated the situation. In order to obtain a suitable categorisation, various systems were trialled. Faunal remains were finally divided according to their attribution to more general categories (such as appendicular, axial and cranial fragments subdivided into macro- or mesofauna where possible) or by their meat yield.

Traditionally, this count has taken into consideration, among other data, the kill-off patterns of faunal remains (White 1953; Casteel 1978; Lyman 1989; Madrigal & Zimmermann Holt 2002). In this case study, this is unknown for faunal remains retrieved during 2009. As such, this forced adopting a different approach that calculates the contribution towards meat production (i.e. meat yield) associated with different faunal anatomical body parts. As a methodological contribution (Bietti Sestieri et al. 2002), this distinction has been extended, taking into account assumptions supported by Barker (1982) regarding this theme[32]. Four categories of meat yield have been identified:

1) primary cut: scapula, pelvis, humerus, femur, vertebra and rib
2) secondary cut: radius, tibia, ulna and fibula
3) cut with scarce meat yield: mandible, teeth, cranium, jaw and maxilla
4) cut with very scarce meat yield: metapodial, carpal, tarsal, phalanx

This approach has been applied to this case study in published analyses (Achino et al. 2011, Achino et al. 2013) that took into account the visual distribution of these different faunal remains in particular macro-areas recovered during the surveys of 2001 and 2009. The results of these preliminary visual analyses enabled identifying sectors differentially devoted to the treatment of faunal remains: some waste areas were identified, where lesser meat yield elements were widespread, in contrast with others where the processing of faunal remains seemed to be attested due to the presence of elements of all meat yield categories. This suggests that certain macro-mesofaunal remains were brought into the settlement whole. This preliminary analysis and interpretation was carried out before the completion of the database analysed in this research and will be further argued specifically in chapters of analysis and, if it will provided interesting resultsstressed in the discussion (Chapter 10).

This approach based both on meat yield and the division into different macrocategories of anatomical body regions (axial, cranial and appendicular) to categorise the available database will be analysed in more depth and tested, in order to verify the suitability for its application to the intra-site spatial analysis. If it is revealed to be irrelevant, archaeozoological data will be gathered in the more general category of "fauna" in carrying out these analyses, also taking into consideration the breadth of the spatial sample under analysis.

[32] A similar scheme, which includes in the last class all the extremities, is listed in Saña et al. 2014, p. 75.

6.5 Pottery

The potsherds recovered at the Villaggio delle Macine were firstly analysed and published by Chiarucci in 1985, who identified a majority of fragments of big bowls and bowls, mugs, jars, *dolia* and cups (Chiarucci 1985). The preliminary analysis of finds suggested their attribution mainly to the Grotta Nuova facies, dated to the Middle Bronze Age; shards attributable to the Protoappenninic B facies have also been identified (Chiarucci 1986-88: 409, 1995-96: 177). These preliminary considerations have been confirmed during the more recent site investigations and related publications (Angle et al. 2002; Angle et al. 2007; Angle 2008; Angle et al. 2011; Angle et al. 2012; Angle et al. in press). The Grotta Nuova facies, largely analysed in the chrono-typological research carried out in recent years (particularly at the conference of Viareggio in 1998; Cocchi Genick et al. 1995; Cocchi Genick 2001) is the most common on the site, represented by the numerous band-handled bowls with upright neck and rim, carinated cups and carinated bowls with inside-flattened rim. Furthermore, shards of the coeval Protoappenninic phase, such as cups with a surmounted band-handle or with a handle on the rim, are also attested. The majority of finds retrieved during the most recent surveys are attributable to the Grotta Nuova archaeological facies and some examples of specific vessel forms will be provided.

6.5.1 Pottery from surveys: a required methodological premise

This category seems to have been affected by post-depositional processes more than others, showing a higher fragmentation rate. This might be due to the fact that their damage might have occurred not only during and after the abandonment phase of the settlement, but also during its last occupation phase. Their intrinsic nature, as material broken objects involved in everyday activities, might partially justify the highest fragmentation rates (as already mentioned in Chapter 2). However, manifold effects of anthropic as well as natural actions which took place after voluntary or accidental pottery deposition are more likely responsible for their preservation status.

The direct contact of pottery with water left evident traces, such as strong washing away of their surfaces, with the emersion of smaller inclusions. Furthermore, shards showed irregular, mostly rounded shapes, damage and breakage which caused their high occurrence in centimetric dimensions. No intact vessels have been retrieved and the attribution of finds to specific shapes, classes and typologies has been, in some cases, very difficult.

Such issues, formerly stressed in the Master's thesis of the author, led to seeking for an alternative strategy of research in this work. Taking into account the archaeological context and the intra-site spatial analysis carried out[33], functional studies seemed to be the most suitable working approach with regards to pottery. In Italian prehistoric scholarship, this research field was first developed by Peroni (1994, chap.4), Bietti Sestieri (1992:223), Ruby (1995) and Cazzella (1999), followed by G. Recchia (1996-1997, PhD dissertation; Recchia 1997)[34] who recently tackled the topic in depth (only as an example and with an ethno-archaeological perspective, Recchia 2000; Cazzella & Recchia 2008). Taking into consideration methods applied to different chronological time spans and geographical settings (for instance Braun 1983; Henrickson-McDonald 1983; Steponaitis 1984; Smith 1985; Hally 1986; Rice 1987; Mill

[33] In my Master's thesis, the intra-site spatial analysis was carried out according to a visual perspective, which was improved by the use of a geostatistical approach in this PhD thesis.
[34] For more details about the early state of the art of such research see Recchia 1997:207-218.

1989; Henrickson 1990; Sinopoli 1991, Skibo 1992; Juhl 1995, for more details Recchia 1996-97; Recchia 1997), she proposed a series of 54 classes of pottery retrieved in southern Italian Bronze Age contexts. She considered variables such as morphological features of vessels (the mouth, the belly's maximum width, the total and partial height, among others), which are required to perform specific "practical actions" (such as pouring, or manipulating the content of vessels, and as such these features could suggest the potential activities that were carried out with the different forms of pottery). Furthermore, relationships between the values of these variables enabled identifying the volume of liquid that the vessel could potentially contain (firstly in Recchia 1997: 219). These data enabled assessing the potential multi-functionality of pottery: the case-by-case analysis of both the archaeological context of provenience and the spatial location of finds, in association with technological aspects (surface treatment, differentiated selection of raw materials, clay textures and contents' analysis) could represent a manifold strategy of action (Recchia 1997: 297-99). The frequency of this type of research has increased during recent years, leading to two different approaches: a taxonomic and typological one (Peroni 1994: 28; Cocchi Genick 1999; Cocchi Genick 2001; Cocchi Genick 2009: 48-51; Vidale 2007 chapter 5; Cattani et al. 2015: 21) is matched by the analysis of archaeometric and technological aspects (Santoro & Bianchi 1997; Recchia & Levi 1999; Levi & Jones 2014 for theoretical contributions), taking into consideration functional research (Aldi et al. 1997; Recchia 2001; associated with content residues analysis in Evans and Recchia 2001; Recchia 2004; Magrì et al 2015; Cattani et al 2015). Among all these methodological contributions, the analysis of those functionally-oriented has been based on the possibility of exploring and measuring some minimum parameters (Recchia 1997: 224-29; Cocchi Genick 2009:43-44) such as the already mentioned proportional relations/absolute dimensions, the profile, rim and bottom shapes (and width), the presence/absence of handles, the vessel capacity[35].

However, in the case of archaeological contexts which displayed highly fragmented pottery shards, the data listed above are frequently unavailable to archaeologists. This condition, observed for the majority of pot shards retrieved during surveys of 2009, lead to experimenting with other strategies of analysis, such as the measurement of shard thickness.

6.5.2 Fragment thickness experiment: preliminary results

This analysis has been carried out with the majority of pot shards recovered during surveys of 2009 (around 24,000 fragments) identifying some selected reference categories related to their thickness:

1) Thickness between 0 and 0.5 cm

2) Thickness between 0.6 and 1 cm

2) Thickness between 1.1 and 2 cm

3) Thickness between 2.1 and 3 cm

4) Thickness between 3.1 and 4 cm

5) Thickness between 4.1 and 5 cm

[35] For a complete list see Cattani et al. 2015: 22.

6) Thickness greater than 5 cm

Throughout the comparison with thicknesses of a few pot shards ascribable to specific categories, these thickness classes have been associated with particular functional tasks: for instance, and according to this provisional and first categorisation, shards between 0 and 1 cm thick may be associated with forms involved in activities of consumption and food preparation (bowls, cups and mugs). Fragments with thicknesses between 1.1 and 2 cm may be ascribable to small-medium sized jars and bigger shallow bowls, also related to consumption and food preparation. Bigger jars, big bowls and large trays, generally less than 2 cm thick may be attributable to food preparation, while shards over 2 cm thick may be associated with storing tasks (such as *dolia*). The first class of shards, i.e. those of thickness between 0 and 1 cm, are the most widespread in surveyed areas, without particularly visually-interpretable distributions. Shards of 1-3 cm thickness are present in a proportional manner in all areas, although they are overall less frequently attested. The thickest fragments (3-5 cm) are instead limited to only five macro-areas (B, Q, T, V and Z) with very low percentages (0.25-1%). They visually appeared almost absent and were spatially concentrated in small areas.

These assumptions have been re-analysed in light of the available data referring to sectors surveyed in 2001 and published in a more general analysis of the visual spatial distribution of several categories of material evidence (Achino et al. 2012). According to the result of a statistical analysis carried out in order to identify the most representative thickness interval for the sample (pot shards retrieved both in 2001 and 2009), three functional categories have been established:

1) Thickness between 0.1 and 0.7 cm: ascribable to consumption practices (cups, mugs, small or medium-sized bowls)

2) Thickness between 0.8 and 1 cm: ascribable to food processing activities (medium-sized bowls, jars, big bowls and different large pans)

3) Thickness between 1.1 and 4 cm: ascribable to storage functions (big containers such as *dolia*).

Pot shards attested in the sector surveyed in 2001 were predominantly ascribable to consumption and preparation vessel shapes, but in a few macro-areas storage forms, such as big *dolia*, were also strongly attested. These interesting preliminary results would require validation through comparison with entire vessels; the current absence of pottery in a good state of preservation prevented undertaking such validation, which could potentially be applied in the future, should new material become available.

6.5.3 Fragments of pottery ascribable to specific functional and/or typological categories: preliminary considerations

The adopted methodology aims to identify useful indicators to assess both a chrono-typological placement and a functional interpretation of the most highly retrieved classes of pottery. However, most archaeologists are aware that one of the most common issues faced in building reference categories of vessel shards is the mediocre preservation rate of pottery. Due to their strong fragmentation index, finds are often ascribable to only two ceramic classes, with their typological attribution uncertain or even undefinable. In designing the classifications, this

condition forced the creation of mixed categories that included the dubiously interpretable shards (Cattani et al. 2015: 23-24), as further developed in this case study. Ceramic vessels are made in response to practical needs but a functional interpretation can only be considered reliable if various factors are evaluated simultaneously, such as morphological vessel features, the recovery context, and physical and chemical properties highlighted by the archaeometric analysis. This must be done without underestimating the multifunctional character of such ceramics and their interchangeability (Cattani et al. 2015: 26). The available data that inform on such factors have been all taken into account in the elaboration of this set of categories.

Three general functional categories have been created, in keeping with the methodological constraints

1) Pottery with a storage function: classes devoted to the conservation and storage of foodstuffs, or liquid and solid substances. They are used to preserve contents from external agents, over potentially long timespans, or to facilitate their arrangement in a particular structure or space. This category includes big containers such as *dolia* and some types of medium-sized multifunctional jars.

2) Pottery suitable for cooking: which includes items devoted specifically to cooking, such as pans.

3) Tableware pottery: this class includes a variety of vessel forms devoted to the distribution and consumption of substances, as well as multiple processing activities of dry and liquid food. Mugs, cups, ladle-like cups, and bowls are included in this category.

For the discussion, a distinction is drawn between main vessel parts and main vessel categories, with reference to their spatial location. Each main vessel part and category ascribable to specific forms will then be analysed in detail in the section devoted to the specific context of recovery.

6.5.4 The main vessel parts

A. Bases

Three sub-types of base have been identified:

1) Flat bottom: this type of base could be associated with pans or shallow bowls[36] ((pan) Cocchi Genick 2001: 317, figure 453, p. 321, figure 458; related to shallow bowls Cocchi Genick 2001: 260, figure 359). This shape is often related to troncoconical bowls, cups and large shallow bowls.

2) Concave bottom: this type of base is likely predominantly ascribable to pans (Cocchi Genick 2001: 321, figure 457).

3) Bases with *omphalos.*

Vessel bases preserved in small portions (and not attributable to specific shapes) could sometimes be ascribed to specific vessels based on the preservation of other diagnostic vessel parts.

[36] For specific graphic reference see quoted specific handbooks.

B. Rims

Six main sub-categories of rim have been identified:

a) Detached rim (not associated with specific vessel forms).

b) Brimmed rim (not associated with specific vessel forms).

c) Curved rim (not associated with specific vessel forms).

d) Rounded rim (not associated with specific vessel forms).

e) Neck-like rim**:** in this archaeological context, such rims are associated with small cups (Cocchi Genick 2001: 139, figure 139).

f) Inwards curved rim: such rims are mostly associated with both closed (jar) and open (such as bowl) forms in this context.

g) Flared rim: predominant vessels that have shown examples of such rims were both closed (mug and jar) and open (such as bowl and ladle) forms.

C. Handles

Among this category, Italian typologists have identified three subgroups that could be defined within the more general term of handles (Figure 142). Their main difference lies in the association with some differentiated vessel shapes (and their uses) (Peroni 1994; Cocchi Genick 1995; 2001). Handles are the most diversified vessel part due to being modelled in response to specific functional requests. Among the main types, differentiated by their section and morphological features, are band, ring, *a maniglia*, tongue-shaped, and *canaliculata* type handles and handles with vertical expansion. Both band and ring handles are predominantly associated with vessels devoted to storage functions, while both *a maniglia* and tongue-shaped handles are related to vessels suitable to processing and consumption practices. Further functional attributions have been preliminarily suggested by Recchia (1997: 238), such as hanging functions for band handles if they were used in connection with supports inserted in their holes.

1) Grips (“*prese”)*: generally these are not found connected to their vessels, since the point of connection was extremely fragile and easily broken. Among the variety of shapes found in this archaeological context are semicircular-shaped and tongue-shaped grips, band-shaped grips (*appendice nastriforme*) and some examples with one or more holes.

2) Type 1 Handles (“*manico*”): different types of band-shaped handles have been recovered, although their severe fragmentation did not allow association with specific vessel forms.

3) Type 2 Handles (“*maniglia*”): this category includes two main types, namely the simple and the tongue-shaped *maniglia*. As in the previous case, these artefacts are not ascribable to specific vessel forms.

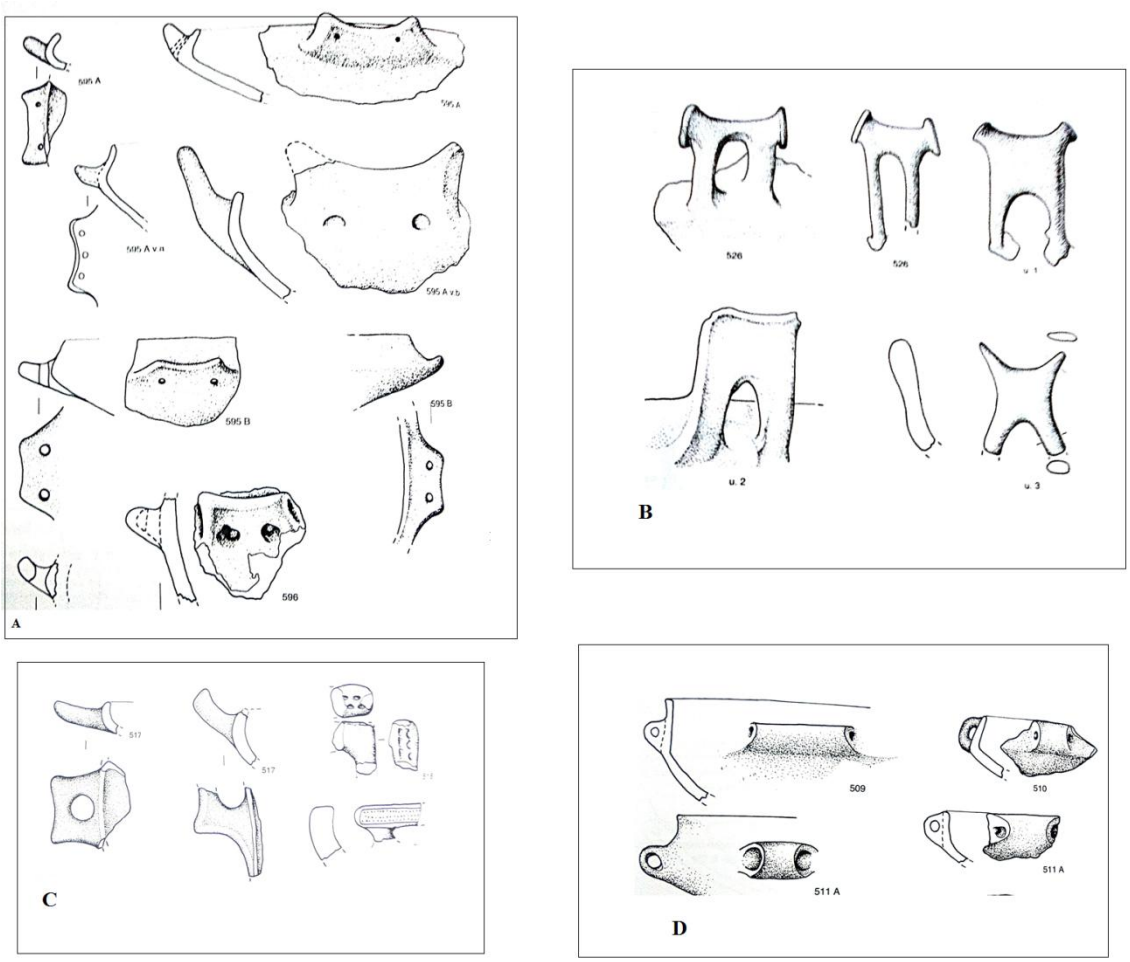

Figure 142 Different types of handles: A) prese; B)manico; C)maniglia; D)ansa canaliculata (from Cocchi Genick 2001).

6.5.5 The main vessel forms

Some categories of vessel forms were identified during the surveys at the Villaggio delle Macine. They are predominantly attributable to two more general groups: open and closed forms. Among the former category are included different types of deep bowls, cups, shallow and large shallow bowls and ladles, while in the latter are jars, mugs and *dolia*. Because of the severe fragmentation that characterised such artefacts in most cases it was difficult to attribute every fragment to a specific vessel shape within these more general categories as shards were indistinguishable and potentially associated with different subtypes. This condition led to creating "mixed categories" that included two or three sub-types of the same macrocategory. This occurred especially for the general category of "bowl/cup/shallow bowl", as well as for the "jar/*dolia*" type.

A. The closed forms (Figure 143)

Dolia are deep, big, generally immovable containers devoted to the storage of dry and liquid substances. They are usually characterised by a wide mouth that facilitates access to the contents, thick walls and continuous or articulated profiles (Cattani et al. 2015: 29). Their severe fragmentation often limited the possibility of reconstructing the total diameter and thus their

defined attribution. Their presence is often inferred based on the presence of coarse, very thick walls. However, close comparisons with the recovered artefacts is not possible due to their fragmentation.

The category of jars includes an abundant dataset consisting of a heterogeneous set of samples. The high morphological variability in essential and secondary attributes and dimensions suggests different potential functions for various containers. In general terms, they often showed handles and decorative elements such as plastic cords under the rim, studs and decorative fingerprint impressions. In contrast to the unmovable *dolia*, this category is portable and easily carried thanks to the solid handles. Among the attested subtypes within this category, ovoid-shaped jars are most common (Cocchi Genick 2001: 107, types 89, 92, 102 b, 135, 136), as well as cylindrical-ovoid-shaped jars with flared, protruding and inwardly curved rims.

The category of mugs includes types of vessels specifically aimed at the individual processing and consumption of beverages and semi-liquid substances. Mugs, morphologically defined, showed an articulated profile with flared or neck-shaped rims (Cocchi Genick 2001: type 130).

Lastly, a "mixed" category is necessary which includes all vessel parts which may belong to jars as well as to *dolia*, lacking features for certain attribution.

B. The open forms (Figure 143)

The macrocategory of open forms includes a range of subclasses. Generally such shapes are associated with the preparation, treatment, processing and consumption of liquid and dry substances, such as tableware ceramics. Among the most widespread forms are bowls, shallow bowls and cups. Within these subtypes are included carinated shapes with flared or inwardly curved rims (for the bowls, Cocchi Genick 2001: 180, type 230, p. 201, type 268 b and type 241, Cocchi Genick 2001; while for the shallow bowls cf. Cocchi Genick 2001: 175 (example of comparison in Angle et al. 2007: 175, figure 59.4; for the cups, Cocchi Genick 2001: 139, type 161, 170, 175, p. 139, Cocchi Genick 2001: 173, figure 56.1).

The category of ladle is defined by carinated walls, handles with vertical expansion and flared rims that favour their function, to collect and pour particularly fluid substances. The samples attested at the Villaggio delle Macine are comparable with type 160, u.1.d. 203, Cocchi Genick 2001.

The subtype of large shallow bowls is devoted to individual or perhaps collective consumption, taking into consideration their high capacity. However, their potential use in the treatment, preparation, manipulation and/or cooking of foods is not excluded since they are often associated with combustion structures (as noted by Cattani et al. 2015: 36). They are predominantly defined by particular vessel parts (such as different types of handle).

This macro-category furthermore includes a more generic category into which shards not ascribable to any specific subtype (namely bowls, shallow bowls and cups) were grouped.

CLOSED FORMS

OPEN FORMS

Figure 143 Examples of closed and open forms from the site of Villaggio delle Macine (courtesy of Micaela Angle, Soprintendenza per i Beni Archeologici del Lazio e dell'Etruria Meridionale).

6.5.6 The ceramic artefacts recovered in 2001

During surveys carried out in 2001, 2846 total ceramic shards were identified. In the framework of the macro-areas (each macro-area of variable number of surveyed 1.5 squared metres cells, labelled alphabetically as A, B, C, D, E, F, G, H and M) and micro-area (the specific square cells within the macro-areas), finds were distributed as summarised in Table 6. 46 shards are from bases, 28 fragments from rims and 106 from different types of handle. 95 fragments are ascribable to jars, one to a *dolium*, 89 to the mixed category of jar/*dolium*, two to mugs, 95 to shallow bowls, 35 to shallow bowls/bowls/cups and 11 to bowls.

	Bases	Rims	Handles	Grips ("prese")	Handle ("appendice")	Handle ("manico")
Macro area A	13	8	4	5	2	1
Macro Area B	6	0	4	1	2	0
Macro Area C	2	2	1	2	0	0
Macro Area D	1	1	2	2	2	0
Macro Area E	7	5	2	6	1	0
Macro Area F	4	1	10	15	1	1
Macro Area G	4	0	1	1	1	0
Macro Area H	6	8	7	4	4	3
Macro Area M	3	3	8	4	1	1
Macro Area N	0	0	5	1	1	0

Table 6 Spatial distribution of pottery (divided according to main vessel parts) (surveys 2001).

6.5.7 The ceramic artefacts recovered in 2009

During surveys carried out in 2009, 22599 ceramic fragments were identified. In the framework of the macro-areas (each macro-area of 16 1.5 squared metres cells, labelled alphabetically from A to W, as well as -Z, -J and - V) finds are distributed as summarised in Table 7. 112 shards belong to bases, 104 fragments to rims, and 121 to the different types of handle. 38 fragments are ascribable to jars, two to *dolia*, 66 to the mixed category of jar/*dolium*, one to pan, two to mugs, one to ladle, six to shallow bowls, 13 to the mixed category of shallow bowl/bowl, seven to bowl/cup, 18 to shallow bowl/bowl/cup, six to large shallow bowls, 58 to bowls, 19 to cups and two to lids or covers.

Area	Bases	Rims	Handles	Grips ("prese")	Handles ("maniglia")	Handles ("manico")
A	2	2	1	2		
B	4	2	2	1		
C						1
D	23	4		4	1	
E						
F						
G	7	17	2	7	4	
H	3	6			1	
I						
J	8	9	9	3		
-J	2	7	2			
K	2	6		1		
L		4				
N	2	2	2	1		
O	3	5	3	2		
P	9	3	4	4		2
Q	10	7	5	2	1	1
R	5	2	1			2
S	6	7	1	3		3
T	4	6	5	1	1	
U	5	8	6	7		1
V	6	1	1		1	
-V						
Z	5	5	6	5	1	3
-Z	6	1	1	2		
W			2			

Table 7 Spatial distribution of pottery (divided according to main vessel parts) (surveys 2009).

6.5.8 The ceramic artefacts recovered in 2012

During surveys carried out in 2012, 1361 ceramic shards were identified. Finds are attributable to identified vessel parts (bottoms, rims and different types of handles) and vessel original shapes (as jars, dolia, jars/dolia, bowls, shallow bowls, cups, bowl/shallow bowl/cup, large shallow bowls, mugs and ladles 2 shards are from bases, one fragment from a rim and four are from different handles. Two fragments are ascribable to jars, five to the mixed category of jar/*dolium* and five to the mixed category of shallow bowl/bowl/cup.

6.5.9 *The creation of the unitary dataset*

All pot shards collected during surveys in recent years were collated together in the database by spatial distribution into 0.5 squared metres cells corresponding to centroid sampling units. They were attested in 1629 cells within a total sample of 4396 records. For each centroid, the frequency of fragments was calculated with values that span from a minimum of 1 to a maximum of 194 within each centroid sampling unit.

6.6 The lithic industry recovered at the Villaggio delle Macine: early collection and excavations

Among the lithic industry retrieved during the most recent years at the site[37], some foliate flint arrowheads with tangs and flint harpoons on triangular flakes, probably used in fishing activities, are listed (recovery 1999, Inv. 112713, Angle et al. 2001: 56) as well as a few flint flakes, cores and tools (especially scrapers) strictly comparable with those retrieved in northern lakeside settlements with pile-dwelling and *terramare* contexts. The broad spread of this evidence was confirmed during surveys and various categories of finds were identified.

Generally, the lithic industry retrieved from the Villaggio delle Macine displayed the marks of some post-depositional processes, such as chemical, thermal and physical alterations. Such mechanisms that disturbed the archaeological record produced distinctive combinations of wear features on the surface of the artefacts. Many retrieved pieces were eventually defined as natural, because they resulted directly from interactions with the sediments and are often the indirect result of environmental processes (e.g. bioturbation), not human activities (e.g. tool-use) (Burroni et al. 2002: 1277). The effects are predominantly witnessed in the emergence of different patinas on the artefacts' surfaces. Accidental thermal alteration as well as the soil chemistry could produce these in this context. The patinas could vary in chromatic scales and strength (Arzarello et al. 2011: 101-106) and at the Villaggio delle Macine they assumed predominantly both shiny and opaque aspects and a further black coloration.

6.6.1 Lithics retrieved during surveys in 2001 and 2012

Both the 2001 and 2012 surveys did not recover a significant amount of lithic material; indeed, lithics were scarce and could not be associated with specific typological groups. For 2001, a partially chipped pebble was recovered in macro-area C and an undetermined flake has been identified in macro-area A. Even the excavation of the covered sector has confirmed this absence since, at least so far, only arrowheads and harpoons have been retrieved.
The same pattern was seen during surveys carried out in 2012, since only small pebbles were retrieved. Their smaller dimensions and scarce presence (they did not exceed a total around 15) did not enable using this artefact category in a statistically relevant manner. They were distributed across the two areas surveyed, without any particular aggregation since only one find per grid square was retrieved in macro-areas D, H and Z.

6.6.2 Lithics recovered during surveys of 2009

The 2009 surveys provided the greatest and most diversified assemblage of lithics. 95 finds were identified including pebbles, chopper/chopping tools**,** flint débitage, tools, cores, core residuals and core retouching[38]. In general, flints were attested in all areas, except sectors E, F, H, I, O, -V and W. They were most widespread in the sector Z (11 finds), T and U (9 finds)Some finds were marked by traces of more or less direct contact with fire (Figure 144). Others were characterised by different patinas: the black colour of one of them most likely

[37] both in the framework of the early surficial collections and the excavations
[38] their analysis is carried out at the Laboratory of Palentologia, at the University of Roma Tor Vergata, with the help of Professor M. F. Rolfo and their typological definition follows Débenant & Dibble 1993 and Inizan et al. 1995; Arzarello et al. 2011

resulted from the chemical impact of the soil whereas both shiny and opaque pieces derived from water contact.

6.6.2.1 Pebbles and chopping tools/choppers

Pebbles recovered at the site were probably collected from fossil beaches located in a coastal area (for instance Ardea, Nettuno and Lavinio) (as quoted by Ansuini et al. 1990-91), since source outcrops in the Alban Hills are absent. The data referring to the raw provenience were gathered through the analysis of the available cortex which, in this specific case, was smoothened by fluvial transport. They appeared in a total amount of five distributed as one find in macro-areas -J, K, P, R and Z, and two finds in the macro-area G. Only one pebble displayed traces of cryoturbation. One flint chopping tool/chopper is also identified in macro-area R. In these macro-areas, 18 small pebbles were also retrieved, four with traces of cryoturbation.

6.6.2.2 Lithic tools

A small number of lithic tools were retrieved (five finds) on the site's surface. The assemblage included one notched piece, one scraper, one fragment of a backed knife and a side scraper. These tools were predominantly distributed in the central zone of the survey (3 artefacts), while two were located in the northern sector.

6.6.2.3 Debitage

The debitage assemblage included different categories:

- Forty-one flakes (which included micro-flints and extra-micro-flints)
- Four bladelets with triangular section (which included micro-bladelets)
- Two bladelets with trapezoidal section (which also included micro-bladelets)
- A single blade.

The typometric classes proposed by Laplace (1964-6) were followed, i.e. dividing the categories according to the following criteria:

- Micro-bladelet: small dimensions ranging from two to four centimetres
- Bladelet: medium dimensions ranging from four to six centimetres
- Blade: larger dimensions, greater than six centimetres.

Such categorisation is required to identify different phases of flint manufacture: for instance, bladelets with triangular and trapezoidal sections reflected two different steps of manufacturing, as the former were associated with the first stage of core work, while the latter marked their full utilization. Two flakes belonging to this group showed a black shiny patina and five displayed traces of cryoturbation. They were absent in areas A, B, E, F, H, I, N, O, P, -V and W.

6.6.2.4 Cores, fragments and core retouching

One prismatic core was retrieved from each of following macro-areas: A, D, G and Q. The find N. 2601, from macro-area Q displayed a platform rejuvenated through percussion that was not re-used, probably due to the large availability of raw material. Six core fragments were found, one of which in macro-area B and five (among those one polyhedric, one prismatic and one with

traces of cryoturbation) in the macro-area Z. The core with retouch, with traces of cryoturbation, was recovered in the macro-area T. Furthermore, one percussion hammer is attested at the site (in macro-area N). These are usually, as in this case, pebbles with variable dimensions and weights, used for chipping and hammering platforms.

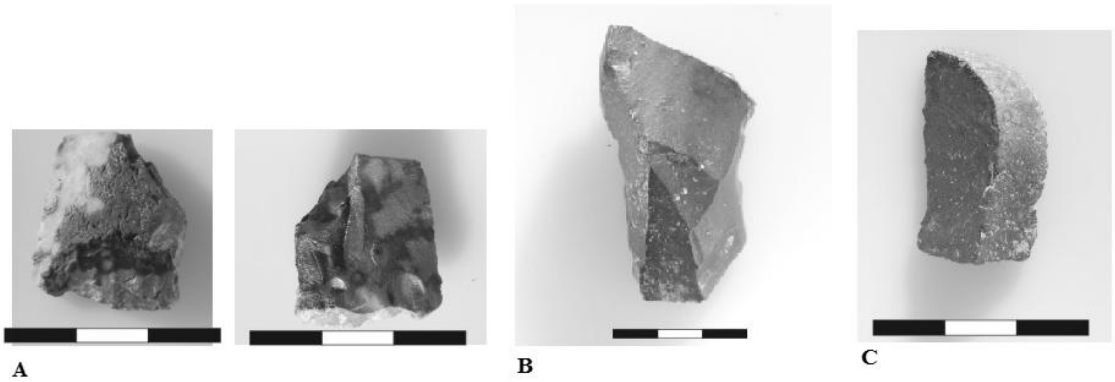

Figure 144 Lithic industry recovered during surveys of 2009: A)traces of cryoturbation; B-C)example of lithic tools (in particular C is the above mentioned backed knife).

6.6.2.5 The creation of the unitary dataset

All lithic finds collected during the recent surveys were collated together in the database, grouped by their 0.5 squared metres cells converted to corresponding centroid sampling units. They were attested in 107 cells within the total sample of 4396 records. For each units, the frequency of the general category of lithic industry represented was calculated, since the occurrence of evidence ascribable to specific typologies is limited to the sector surveyed in 2009. Values of frequency span only from a minimum of 1 to a maximum of 2. The scarceness of lithic finds in areas surveyed in 2001 and 2012 caused the unreliability of both samples from a statistical point of view. For this reason, the intra-site spatial analysis will take into account the entirety of the available archaeological data and, separately, only finds retrieved in 2009.

6.7 Wooden evidence: wooden structures and debris

The majority of the wooden evidence retrieved on the surface of the Villaggio delle Macine was characterised by small dimensions. A small number of remains ascribable to collapsed wooden structures were recognised. Although they are not attributable to specific structural portions, it is most likely that they could be referred to wooden flooring and/or crossbeams. Their severe fragmentation does not enable comparison with better preserved remains retrieved in the more widespread prehistoric lakeside settlement contexts.

6.7.1 *Wooden remains recovered during surveys of 2001*

146 wooden fragments were retrieved in the area surveyed during 2001, while partial preserved horizontal wooden structures were attested by 35 remains.

6.7.2 *Wooden remains recovered during the surveys of 2009*

A total amount of 316 wooden fragments was recovered in this area in 2009. Only macro-areas A and G yielded the remains (a total amount of 141 fragments) for horizontal posts that, being strictly related to each other, constituted the material evidence of a potential collapsed structure (Figure 145).

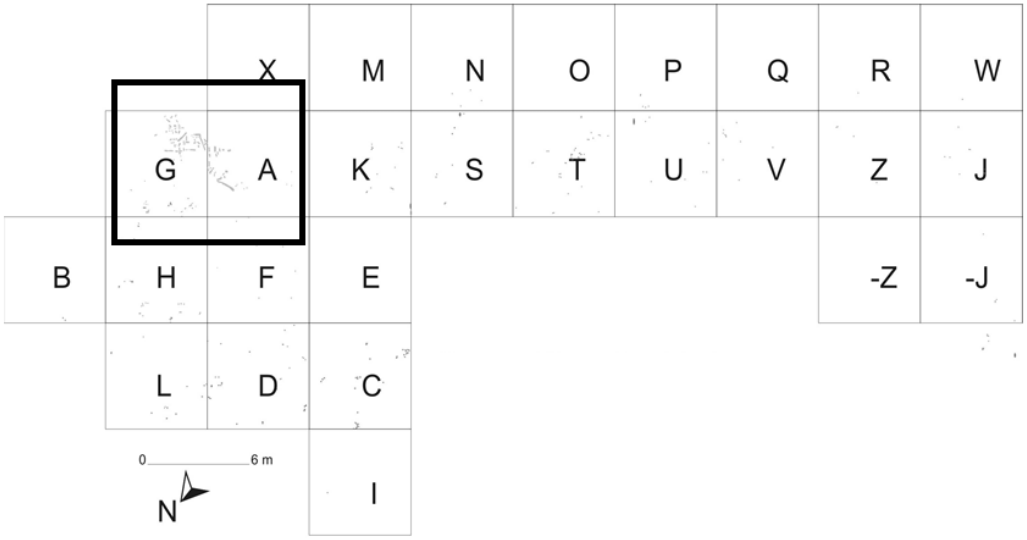

Figure 145 map of the sampling units surveyed during 2009 with highlighted the two macro-areas where have been recovered remains of horizontal posts.

6.7.3 The creation of the unitary dataset

Wooden artefacts collected during the recent surveys were grouped together in the database by spatial distribution, by equating 0.5 squared metres cell coverage to the corresponding to centroid sampling units. The total frequencies of artefacts for each centroid was calculated spanning from 1 to 11 finds (11 for wooden debris, while 8 for horizontal posts). As already mentioned for grindstones and posts, in some cases horizontal portions of structures which suggested original structures were located in more than one single quadrant-cell; thus, they are included in two or more neighbouring centroid coordinate cells. For this reason, a greater number of remains ascribable to this class is attested in the dataset compared with the amount previously listed.

6.8 Concotto slabs and fragments at the Villaggio delle Macine

As introduced in Chapter 5 during excavations carried out at the site in the most recent years, some sub-quadrangular or sub-circular concotto slabs, in some cases associated with wooden and vegetal elements, were identified. Differences in their shapes might be associated with different cooking practices.

6.8.1 Concotto slabs and fragments from 2001 and 2012

During the surveys carried out in 2001, 12 concotto fragments and 5 slabs were recovered. In addition, during the 2012 surveys, 25 concotto shards and 27 fragmented concotto slabs have been recovered and both reported manually and via total station; the former were predominantly distributed in macro-area D (with 8 finds).

6.8.2 Concotto slabs and fragments retrieved during surveys of 2009

During surveys carried out in 2009, concotto slabs as well as shards of concotto were recovered. The 6 slabs are predominantly characterised by rectangular shapes and show thicknesses between 1 to 3 cm; one of these showed the negative impression of a spike (see Chapter 5). Small or medium concotto fragments, with rectangular or rounded shapes, were strongly affected by post-depositional effects that only partially guaranteed their preservation; they are attested as 15 fragments.

6.8.3 The creation of the unitary dataset

Both concotto slabs and shards collected during the recent surveys were grouped together in the database by spatial distribution, by equating 0.5 squared metres cells coverage to their corresponding to centroid sampling unit. They were attested in 76 centroid coordinate records within the total sample of 4396 records. For each centroid, the frequency of these categories did not exceed one find.

6.9 Clay fishing weights and spindle-whorls recovered at the site: early collection

Clay fishing weights and spindle-whorls were first recovered during the earliest collections, without record of their exact spatial locations. The majority of them consisted of prehistoric as well as Roman clay fishing weights. They appear to have been widespread across the entire area as during surveys carried out in 2009, local villagers delivered a large quantity of these finds to the author.
In general terms, due to the intrinsic clay composition of these artefacts, they strongly suffered under post-depositional processes, including a progressive washing away of their surfaces causing the emersion of smaller inclusions and irregular shaping. Because of their small dimensions and lower weight, it is reasonable that they had been subject to rearrangement during the past by the water, although as a lake, very powerful wave effects are not attested.

6.9.1 Clay fishing weights and spindles retrieved during the 2001, 2009 and2012 surveys

During surveys carried out in 2001, three spindle-whorls were recovered in the macro-area F (2) and M (1). During 2009 2 spindle-whorls were observed in macro-area Z, 1 in J, 1 in P, 1 in T and 1 in O. In addition, two clay fishing weights were recovered in the macro-area P and T. During surveys of 2012 further two were identified in the sector near the beach, surveyed through the total station.

6.9.2 Discussion

This summary of the main features characterising the categories taken into consideration for this research project enables a better understanding of the strengths and weaknesses of the analysed sample. Becoming conscious of these issues will make it easier to overcome them in order to carry out the intra-site spatial analysis, reconstructing the most important formation and deformation processes which created the archaeological record of the Villaggio delle Macine.

7 GEOSTATISTIC INTRA-SITE SPATIAL ANALYSIS

The site of Villaggio delle Macine: the area surveyed in 2001

7.1. Introduction

This chapter is devoted to the analysis and results of intra-site spatial analyses of the areas surveyed in 2001 at Villaggio delle Macine. We begin by analyzing the absolute counts of archaeological observations, by mixed all identified materials together in the way of a palimpsest. It is used as null hypothesis for the separated analysis of each archaeological category, according to the discussion in Chapter 4. For a spatial correlation perspective, multidimensional analysis integrates all selected categories. The step-by-step procedure is the following one:

1) Plot of Locations where some elements have been detected (x, y coordinates of grid centroids)

2) Density Analysis of Single Presences (Kernel Density Estimate) and Statistical Relevance of the Null Hypothesis of Spatial Randomness

4) Statistical Description of the Spatial Distribution. Measures of Central Tendency

5) Plot of Spatial Frequencies (Lorenz curve, 3D Histogram). Weighted Measures of Central Tendency. Statistical Relevance of the Null Hypothesis of Spatial Randomness

6) Semivariance Modeling and Spatial Interpolation. Kriging

7) Spatial Correlation

7.1.1 The area surveyed in 2001

An area of 1280 sq. meters was surveyed in 2001. Given the impossibility of individually geo-referencing all archaeological observations (in particular pottery), we have divided the surveyed area using a regular grid of 50 cm (0.25 squared meters), and calculated the spatial frequencies per cell (for more details see chapter 6). We have 1460 cells, which should be understood as sampling units, summing up to 365 square meters (Convex Hull=885.88 meters), that is more than 1/2 of the total area. Both North-West and South-East quadrants were unsurveyed for different reasons: the first one was occupied by recent constructions and a local road in its proximity, while the latter was considered outward of the initial plan of excavation, which included only a sector parallel to the ancient estimated lake shoreline.

7.2 Absolute count of archaeological observations (palimpsest)

5342 archaeological observations (ascribable to all the categories recovered during survey of 2001) were identified and counted in the 1460 surveyed cells. In 6 cases the surveyed cell was empty. In one case, a single cell of 0.25 squared meters presented a total of 42 items. A frequency mean of 3.65 observations per sampling unit and a standard deviation of 3.87 have been calculated for this sample. Mean distance between the centroid of surveyed cells is 1.6413. The spatial distribution of only those sampling units with material evidence is showed in Figure 146.

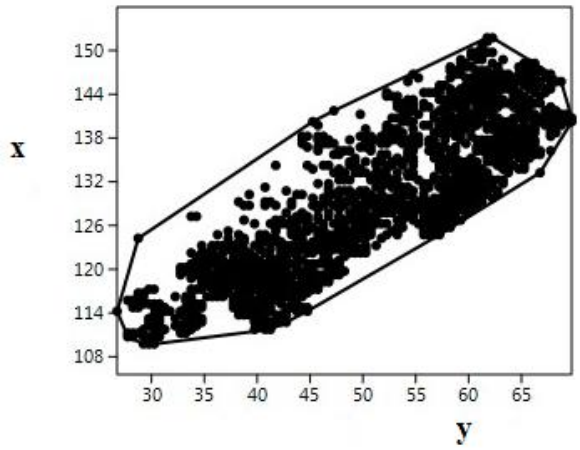

Figure 146 spatial distribution of sampling units centroids where any kind of archaeological evidence has been recorded in surveys of 2001 (Past).

Ripley's *k* analysis on the distance between sampling units with all material evidence gives support to the hypothesis of some spatial clustering in the reference area (1280 squared meters), for distances beyond 2.5 meters (Figure 147).

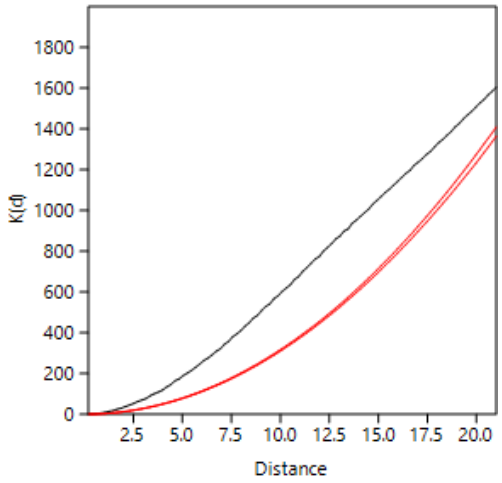

Figure 147 Ripley's *k* analysis on the distance between sampling units with all material evidence recorded in surveys of 2001 (Past).

Within the convex hull defined by the effectively surveyed cells, the Kernel Density Estimation of non-empty cells (cells where a minimum of 1 archaeological observation has been recorded) shows the possible accumulation of archaeological observations in two differentiated concentrations of higher density, separated by a central area of lower density, respectively at the South-West and North-East corners of the surveyed area (Figure 148).

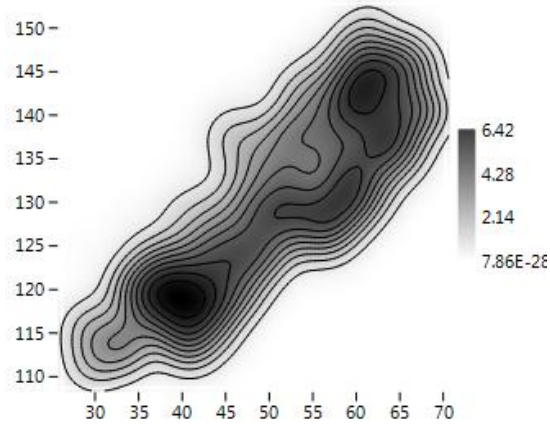

Figure 148 KDE of non-empty sampling units (surveys 2001) (Past).

When considering the raw quantity of archaeological observations at each cell, the probability density distribution of spatial frequencies clearly follows a J-shaped distribution. A majority of sampling units have raw counts of archaeological observations of less than 5 elements (global mean = 3.75 observations per sampling unit). Two cells distinguish from the majority, with 34 and 42 observations (interpretable as outliers). Zero values appear to be quite absent (attested only in 6 sampling units): this condition is expected in the case of palimpsest, since it sums up all categories of material evidence. We have signaled an apparent discontinuity at the number of 10 observations as if, beyond this threshold, frequencies exceed what the theoretical exponential model predicts (Figure 149).

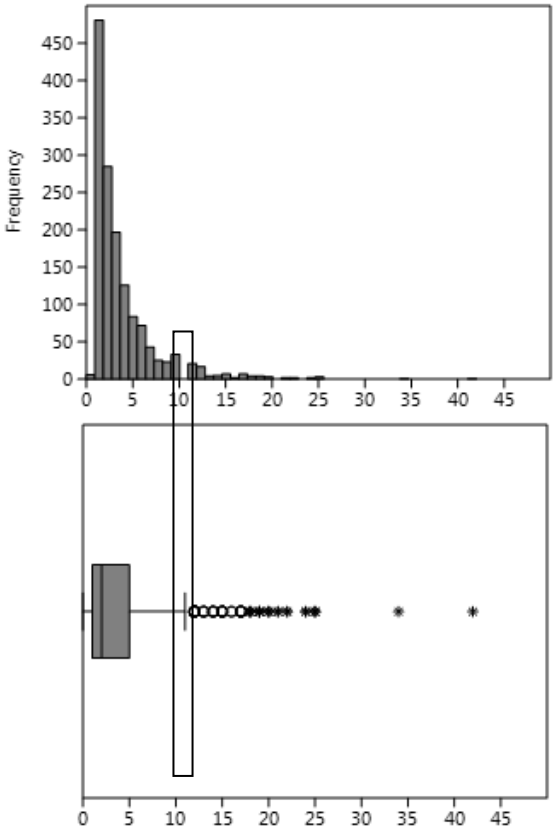

Figure 149 Histogram and box plot of frequencies observed for all material evidence summed up (Past).

A Lorenz curve (Figure 150) gives a Gini coefficient of 0.4727, with a 95% bootstrap confidence interval between 0.459 and 0.486. The Coefficient of asymmetry is 0.9702, with a 95% Bootstrap confidence interval between 0.928, and 1.016. In general, we can see that 47% of all archaeological observations have been found at 80% of sampling units and the remaining 20% sampling units concentrate more than half of the count data (53%). This result do not follow the standard geometrical (exponential) accumulation model, but reveals less accumulative behavior than expected, or, in any case, different accumulations all mixed together.

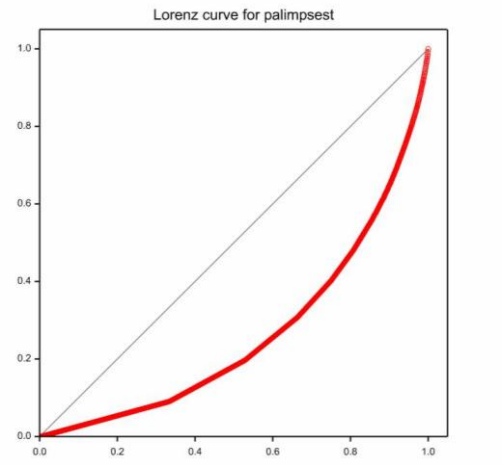

Figure 150 Lorenz Curve for all material evidence recovered during surveys of 2001 (Genstat).

In this sense, the 3D histogram also shows an irregular and non-homogeneous distribution characterized my outliers and strong multimodality (Figure 151), which does not fit with an exponential theoretical model of intentional discard at a fixed center (tested using Kolmogorov-Smirnov tests, $p<0$ in all cases).

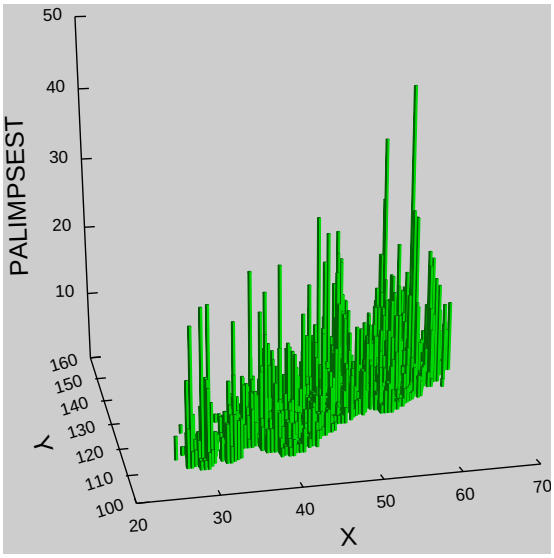

Figure 151 3D Histogram of all material evidence recovered during surveys of 2001 (Systat 13).

The spatial distribution of count data per sampling unit shows a Global Moran's *I* of -0.000605. The theoretical (expected) value assuming spatial autocorrelation (lack of spatial independence) is -0.000685 and the standard error of *I* is 0.000685. The test of significance using the normality

assumption gave a *z* value of 0.116898, a highly non-significant value. Consequently, we can accept that the spatial distribution of accumulations of undifferentiated material elements is not significantly different than the expected value under a random distribution. This is what would be expected when a mixture of too much different intentionality is mixed and summed up. Such results are comparable with those of the Geary statistic (for this case *C*=0.999885) and Getis-Ord general G (*G*=1.000000).

The Moran's *I* Correlogram (Figure 152) has been calculated for uniform class distance intervals of 1 meter and taking into account a 10 meters active lag distance. *I* value at the starting point of the function (less than 2 meter between sampling units) are significantly above the expected value for randomness, but it decreases quickly to the level of randomness at a radius of a mere 3 meters. Given that the absolute minimum for the spatial continuity of human behaviour at a micro-scale is a circumference of 1.5 meters of radius (the extension of the open human arms), we can conclude a general pattern of spatial independence at a global scale, and some spatial continuity between immediate adjacent cells (one squared meters implies four adjacent sampling units).

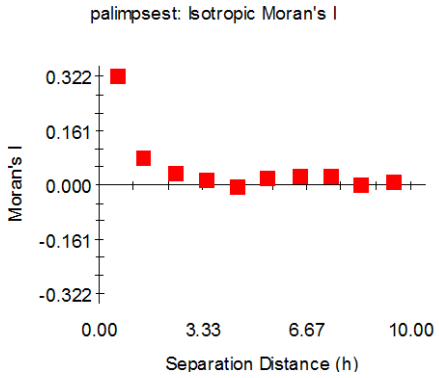

Figure 152 Moran's I Correlogram for all evidence recovered during surveys of 2001 (GS+).

These data suggest that we cannot signal concentrated accumulations of archaeological observations that extend beyond 3 meters. Local indicators of spatial association (see at the end of the chapter) coincide with the histogram of frequencies, indicating that those cells with more than 10 items are significantly different from their neighbours. Only 118 sampling units have more than 10 observations and, among them, only 11 cells have more than 20 items (Figure 153).

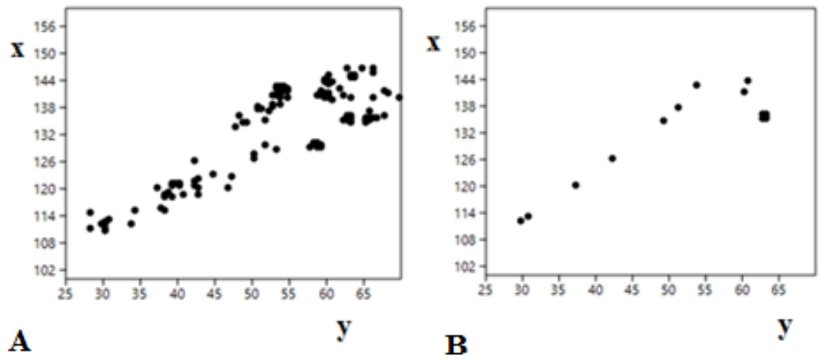

Figure 153 A) Location of sampling units with more than 10 items B) Location of cells with more than 20 items (Past).

At first sight it may seem that there is some spatial patterning. Clark and Evans test gives a significant result of spatial clustering (p=0.003). Moran's I Correlogram (Figure 154) of cells with more than 20 items fits with a random model at small distances, and some possible clustering between 3 and 6 meters. That is, one main concentration zone (whose center for minimum distances is around x= 65 and y= 135) and other dispersed and independent accumulations.

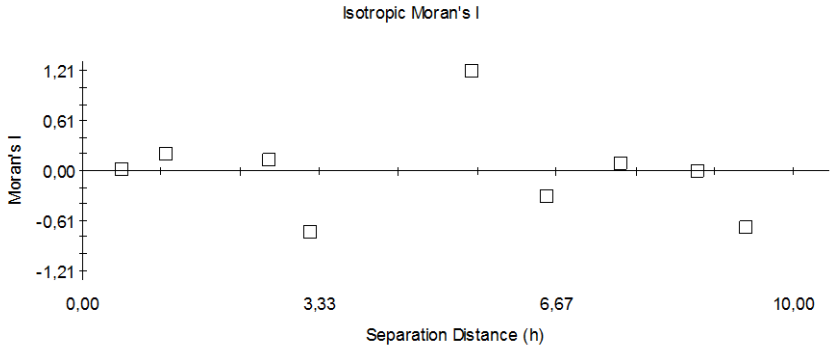

Figure 154 Moran's I Correlogram of cells with more than 20 items (GS+).

A Kernel density estimate model of cells with more than 10 items provides a clearer image (Figure 155).

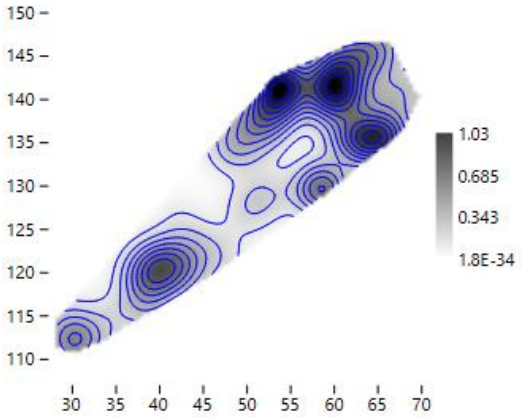

Figure 155 KDE model of cells with more than 10 items (Past).

It is easy to see the presence of four higher density points in the North-East corner of the surveyed area, delimiting a less dense area. Following the South-West direction, there are two differentiated areas, where high density of material concentrations is observed.

It is obvious that anisotropy is present in the main direction North-East-South-West, that is, parallel to the ancient estimated lake shoreline. We have calculated anisotropic variograms at different directions (Figure 156).

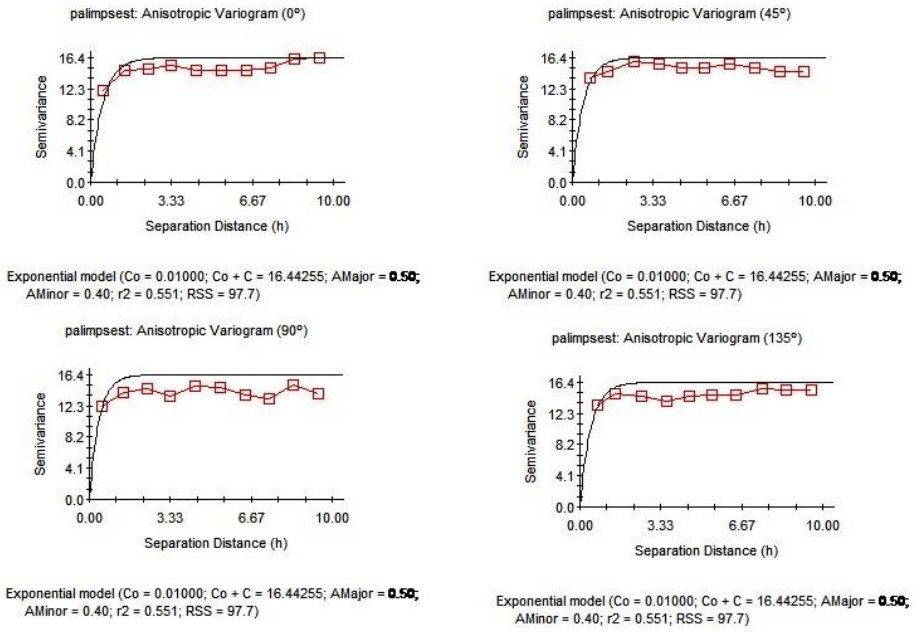

Figure 156 Anisotropic Variogram of all material evidence recovered during surveys of 2001 (GS+).

Semivariance is very high in all directions and it is fairly constant in the different directories. The very steady slope of initial curve suggests the lack of spatial continuity, even at small distances. The Semivariance Surface or Variogram Map (Figure 157) shows the strong North-East-South-West deformation of semivariance, following the ancient estimated lake shoreline, and the main axis of the survey area. Spatial continuity is higher in this direction than in any other. It is also interesting to remark the lack of spatial continuity – perpendicular to the ancient estimated lake shore line - generated by a concentration of cell with higher frequencies in the upper band of the North-East-south-West main axis. This pattern is exactly the opposite of what would be expected in case of post-depositional alteration caused by the rolling materials downhill towards the shoreline. In the surveyed area, a majority of archaeological observations are the farthest possible from the ancient shoreline.

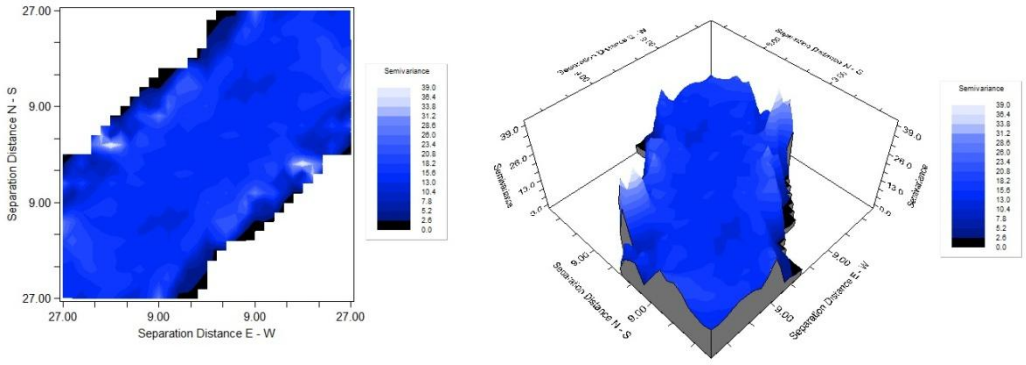

Figure 157 Variogram Map of all material evidence recovered during surveys of 2001 (GS+).

In this graph, the centre of the map corresponds to the origin of the variogram $\gamma(h) = 0$ for every direction. We can see that semivariance is constant at small distances, and higher at longer distances, most notably, in the East-West direction than in the North-South. We can conclude then that the low influence of anisotropy at small distances, and the existence of an East-West

pattern of differentiation, would be compatible with a distinction in two areas, one at the South-East and another at the North-East.

An Exponential Isotropic Variogram model has been fitted to the empirical variogram. Given the relatively flat anisotropic variogram, we have fitted an exponential model with a very short range and a high random factor (nugget) (Figure 158). C_0 (nugget variance) =1.53, C_0+C (sill) = 14.91 and A_0 (Range) = 0.32, characteristic of spatial independence even at small distances.

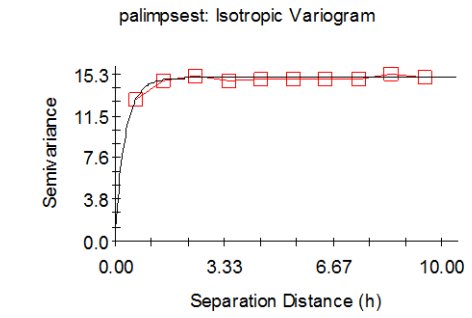

Exponential model (Co = 1.53000; Co + C = 14.91000; Ao = 0.32; r2 = 0.929; RSS = 0.284)

Figure 158 Exponential Isotropic Variogram for all material evidence recovered during surveys of 2001 (GS+).

This model explains 92.9% of sample variance and offers the best fit possible for the data at hand. Lags are showed at 1 meter intervals. With this particular variogram, we have estimated the global variation of the total number of archaeological observations, using an Inverse Distance Weighting (Figure 159).

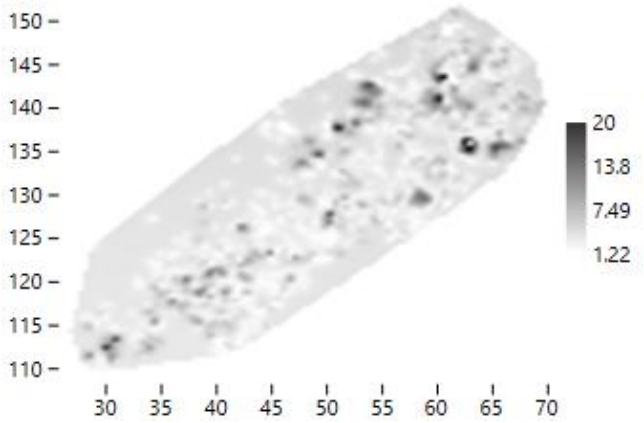

Figure 159 Graphic results of Inverse Distance Weighting calculated for all material evidence recovered during surveys of 2001 (Past).

This visualization shows the spatial independence of cells with the highest frequencies, and the abundance of outliers and multimodality. The model do not predict conveniently outliers (cells with more than 30 observations), although it gives correct estimates for all sampling units with less than 10 observations. Not a single well defined accumulation can be interpreted, but a deformed pattern. After all, we are here analyzing archaeological materials that come from very different activities associated to different discard behaviours. In any case, anisotropy can be decomposed into two differentiated directions, a strong North-East-South-West axis at the South-Western corner of the surveyed area, and isotropy at the North-Eastern corner. This result

would be compatible with two differentiated accumulations, the first one more deformed post-depositionally that the other. It is important to remark the high resemblance between the interpolated model of abundance data and the Kernel Density Estimation of cells with more than 10 identified items (above).

7.3 *Vertical Posts*

595 posts (or part of it) were identified and counted in this area. Instead of their individual *xy* coordinates, we have recorded the coordinates of the centroid of the cell in which they have been surveyed (Figure 160). There are more empty cells (977) than cells with a post, but this fact cannot be interpreted as evidence of spatial irregularity, because the global mean is 1.23 posts per sampling unit, and a standard deviation of 0.49. Here, the lack of resolution in the spatial coordinates of posts is a problem.

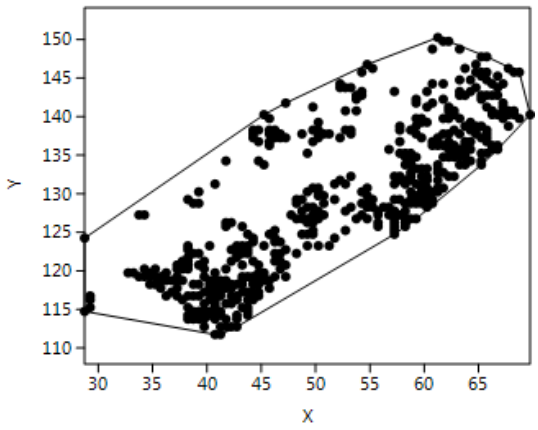

Figure 160 Spatial distribution of sampling units where posts have been recorded during surveys of 2001 (Past).

Ripley's *k* analysis for all the reference area suggests the possibility of some degree of spatial clustering, at any distance (Figure 161).

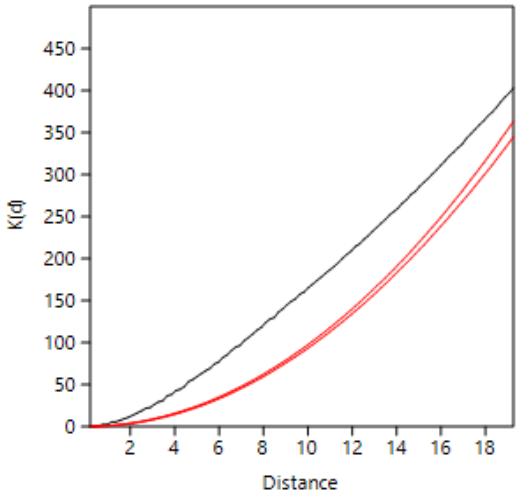

Figure 161 Ripley's *k* analysis on the distance between sampling units with posts recorded in surveys of 2001 (Past).

However, within the convex hull –greater than the effectively surveyed area, given the existence of some outlying sampling units- the null hypothesis of a random pattern (a Poisson process) cannot be rejected at $p<0.05$ (Clark and Evans test of nearest neighbourhood). This may indicate

the possibility that, if we do not take into account false zero, equidistant cells have the same probability of counting one or more posts. In the same way, those cells where no evidence of post was observed are significantly overdispersed (Clark and Evans test $p<1$)

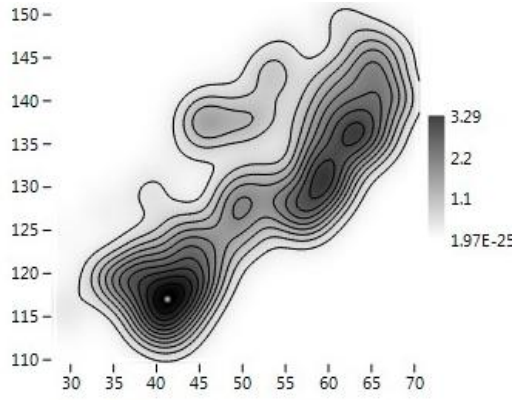

Figure 162 KDE of sampling units where posts have been recorded during surveys of 2001 (Past).

This hypothesis of randomness should be remarked when are explained the results of the KDE graphs (Figure 162). It allows identifying two areas of greater density, at the North-East and at the South-West of the surveyed areas, separated by a region of lower density. The discrepancy between the assumption of randomness according to Clark and Evans test and the traces of clustering in KDE is based probably on the low gradient of density.

Given that the majority of cells have only one or none, we have not considered here the probability density distribution of spatial frequencies.

The spatial centroid of the area with posts, calculated using an abundance weighted mean spatial center is x= 51.792017 y=129.297899, with 10.18 m of standard deviation along the *x* axis, and 9.55 m along the *y* axis. A standard deviation ellipse with a long axis of 37.59 m and a short one of 12.24 m delimits an area of 361.25 square meters, where most data count appears. It has been estimated an average density of 0.33 posts per square meter.

The spatial distribution of the abundance of posts per sampling unit gives a Global Moran's *I* result of -0.000655**.** The theoretical (expected) value assuming spatial autocorrelation (lack of spatial independence) is -0.000685 and the standard error of I is -0.000685. The test of significance using the normality assumption gave a *z* value of 0.043930, a non-significant value. Consequently, we can accept that the probability of detecting a post at some sampling unit is independent of the observation of other one in the neighbourhood. These results are comparable with those of the Geary statistic (for this case C=1.000067) and Getis-Ord general G (G=0.007645).

The Moran's *I* Correlogram (Figure 163) has been calculated for uniform class distance intervals of 1 meter, and taking into account a 10 meters active lag distance. *I* value between adjacent sampling units is a mere 0.170, above expected value for randomness. As the distance between sampling units increases, *I* value drops off quite gently reaching values corresponding to spatial randomness at 6.67 meters. From this threshold and beyond, randomness is the rule. That means the actual distribution of posts configures homogenous areas of positive correlation of around 12 squared meters.

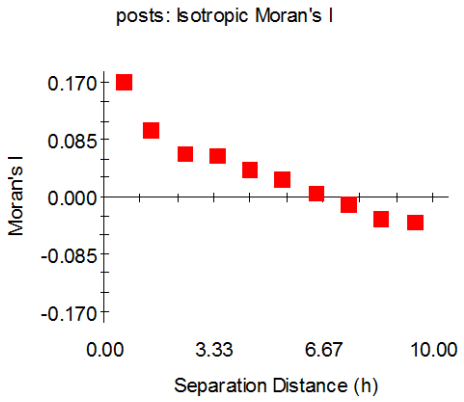

Figure 163 Moran's I Correlogram for posts recovered during surveys of 2001 (GS+).

The spatial distribution of empty cells gives no result of positive autocorrelation, what can be interpreted as the lack of significant empty areas between the main concentrations of vertical posts. Empty cells seem to be overdispersed (as showed by the Clark Evans test, $p<1$). However, those 386 cells with one post are statistically significantly clustered (as showed by the Clark Evans test) (Figure 164A). These constitute 26% of all posts and are located in 92% of the effectively surveyed area. Only 97 cells show more than 1 post (Figure165B). For such cells, the Clark Evans test suggests that the null hypothesis of a random pattern (Poisson process) cannot be rejected at $p<0.05$.

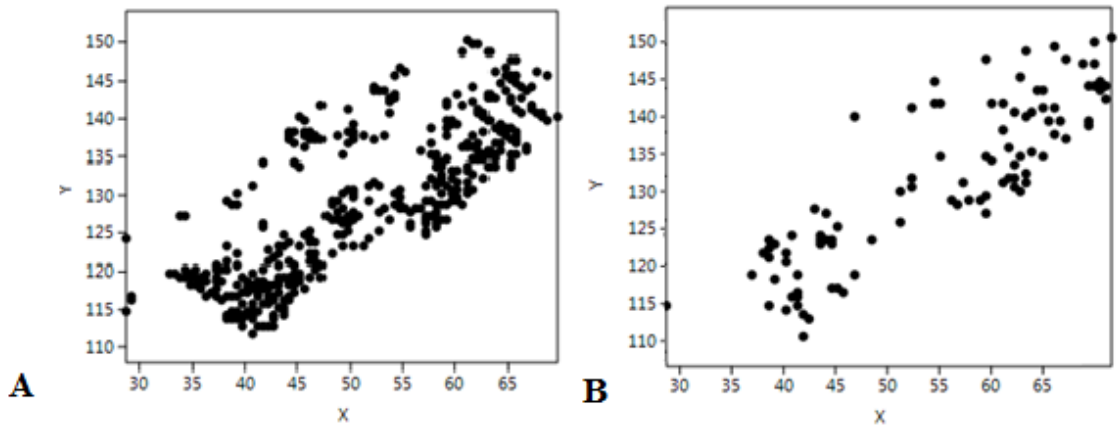

Figures 165 A)Location of sampling units with 1 post (surveys 2001) B)Location with more than 1 post (surveys 2001) (Past).

Kernel Density estimate model of cells with 1 posts provides a clearer image (Figure 166). It is easy to see in the North-East corner of the surveyed area higher density points delimiting a less dense area. Following the South-West direction there is another area of high density of posts. The same spatial distribution is attested for cells with 2 or more presences of post, attesting a continuity and linearity in posts occurrence.

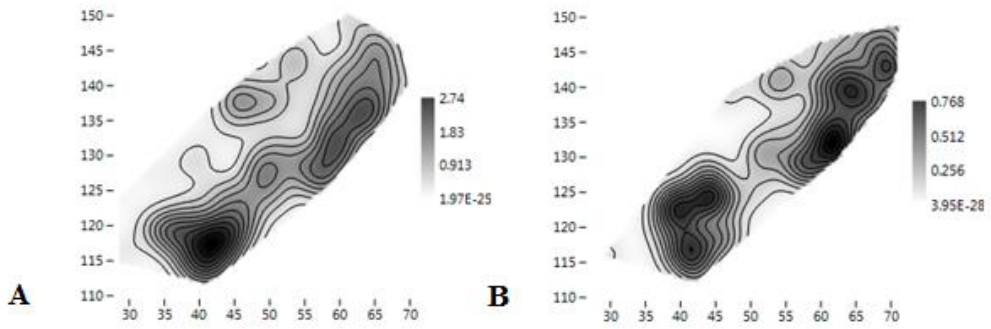

Figure 166 A) KDE of cells with 1 post (surveys 2001) (Past). B)KDE of cells with more than 1 post (surveys of 2001) (Past).

We have explored the possible presence of anisotropic variation studying the empirical variogram at different directions (Figure 167).

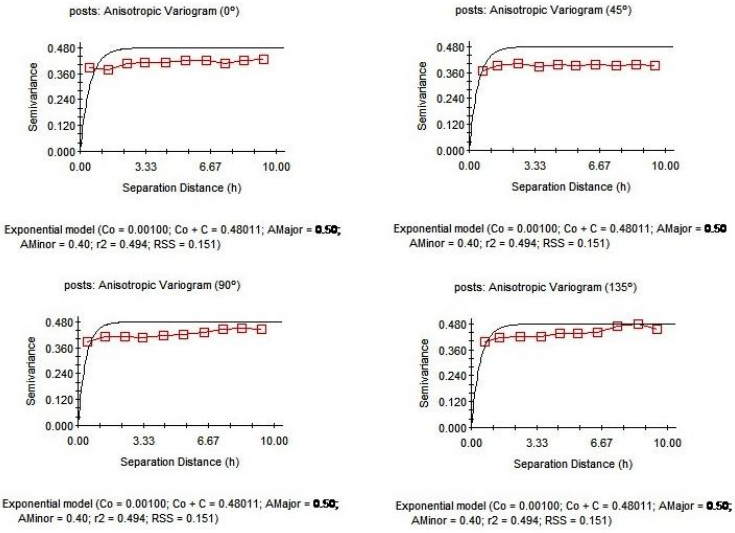

Figure 167 Anisotropic Variogram of posts recovered during surveys of 2001 (GS+).

Resulting variograms are characteristically flat, indicating that no autocorrelation seems to exist between the units, even at the lowest *h*'s. We expect this pattern to appear when there is no accumulation, but a random or uniform distribution. In general, these results confirm those of Isotropic Moran Correlogram, showing statistical independence of the presence/absence of posts at any distances, with some hints of continuity in medium sized areas (below 10 meters). Semivariance does not vary at 0º and 45º (particularly between 1 and 6 meters), at 90º and 135º (that are particularly similar at the same distance interval, between 1 and 6 meters). In the graph of anisotropic Semivariance Surface or Variogram Map (Figure 168), the centre of the map corresponds to the origin of the variogram $\gamma(h) = 0$ for every direction. We can see that semivariance is only constant at a very narrow fringe folowing the main axis of the surveyed area (paralel to the estimated ancient lake shoreline). Anisotropy seems to be stronger in the opposite Northwest-Southeast direction. This is mainly an effect of the unsurveyed areas at the Northwest and southwest corners of the surveyed area, where the hypothesis of statistical independence cannot be proved.

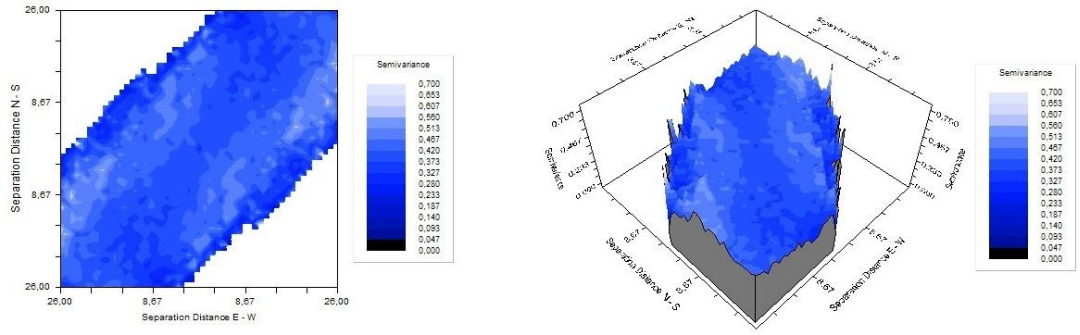

Figure 168 Variogram Map of posts recovered during surveys of 2001 (GS+).

An exponential model with very low random noise (Nugget Variance, $C_0 = 0.049$) and stressing continuity (Sill, $C_0+C = 0.417$) at the level only of single cells (Range, $A_0 = 0.25$) is the best we can fit to the data (Figure 169). However, it gives a very poor goodness of fit ($r^2 = 0.588$), that is, it explains just 58.8% of the spatial differences between the frequency of posts per sample unit.

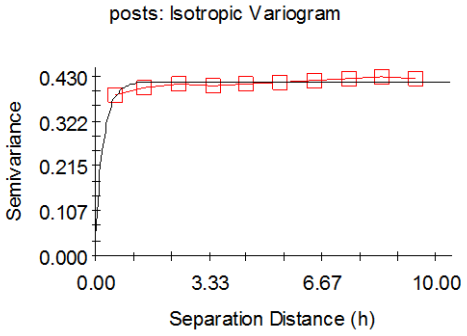

Exponential model (Co = 0.04900; Co + C = 0.41700; Ao = 0.25; **r2 = 0.588;** RSS = 6.319E-04)

Figure 169 Exponential Isotropic Variogram for posts recovered during surveys of 2001 (GS+).

The related Inverse Distance Weighting interpolated model (Figure 170) has very low explanatory power, but it stresses the alignment of a majority of vertical posts along the estimated ancient lake shoreline. Two differentiated areas can also be tentatively suggested, separated by a central area rather homogenous in its emptiness.

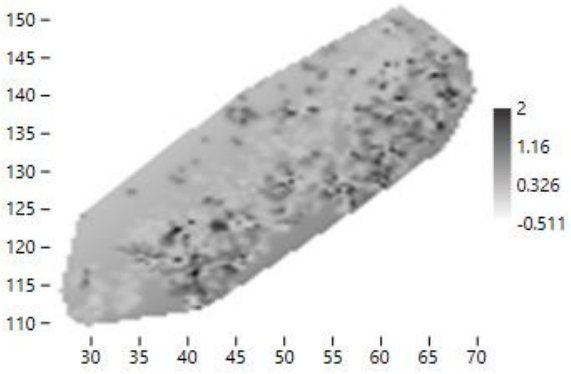

Figure 170 Graphic results of Inverse Distance Weighting calculated for posts recovered during surveys of 2001 (Past).

7.4. Saddle Querns

1221 saddle querns (grindstones and handstones integrated into this single category (see Chapter 6 were identified and counted. A lot of empty cells have been identified (859), giving a frequency mean of 2.03 saddle querns per sampling unit and a standard deviation of 1.49. A single cell with 12 saddle querns should be remarked. Figure 171 shows the spatial distribution of cells with saddle querns.

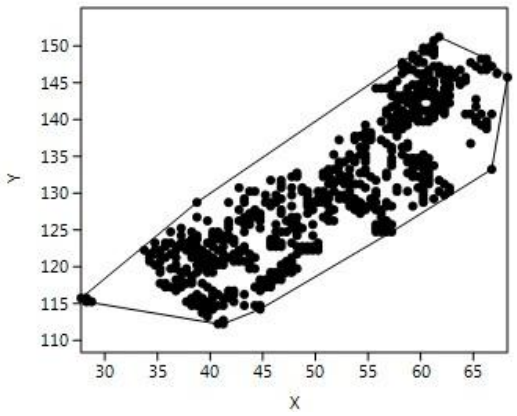

Figure 171 Spatial distribution of sampling units where saddle querns have been recorded during surveys 2001 (Past).

Ripley's *k* analysis of the distance between sampling units with saddle querns (Figure 172) suggests the possibility of clustering at the global scale of the reference area

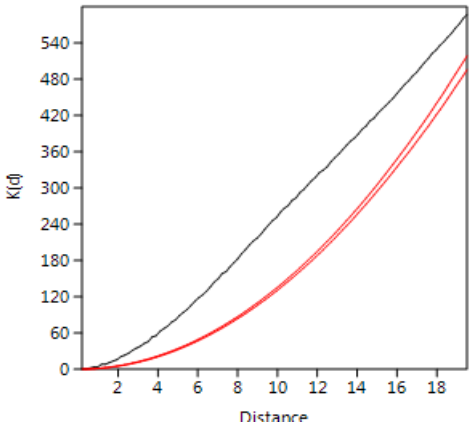

Figure 172 Ripley's *k* analysis on the distance between sampling units with saddle querns recorded in surveys of 2001 (Past).

However, within the convex hull defined by the effectively surveyed sampling units (cells), there is overdispersion, according to the Clark and Evans test ($p<1$).

A Kernel Density Estimation (Figure 173) shows a relatively regular distribution with three main focus or subareas of stronger density. At the level of the total reference area –including the non effectively surveyed corners-, there are some hints of spatial clustering, as suggested by Ripley's k analysis.

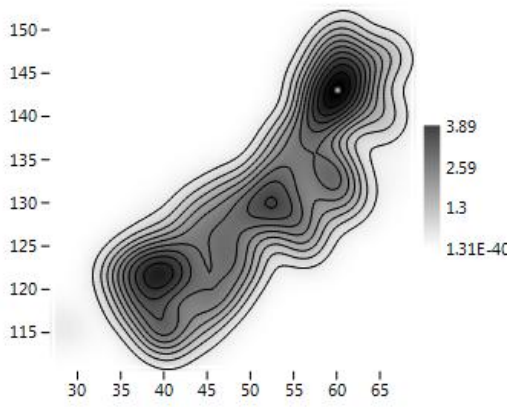

Figure 173 KDE of sampling units where saddle querns have been recorded during surveys of 2001 (Past).

When considering the raw quantity of saddle querns at each cell, the probability density distribution of spatial frequencies clearly follows a J-shaped distribution. A majority of sampling units have raw counts of saddle querns of less than 3 elements (global mean = 2.03 saddle querns per sampling unit). Three cells are distinguished from the majority (interpretable as outliers), with 10, 11 and 12 saddle querns. 92% of saddle querns are located in 40% of the effectively surveyed area. According to both histogram and boxplot, there is a clear break point in the frequency of occurrence of saddle querns in relation to the value 6 (as showed in Figure 174).

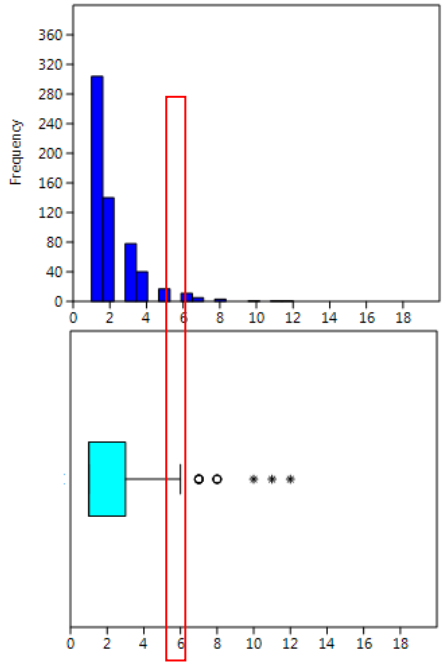

Figure 174 Histogram and box plot of frequencies observed for saddle querns (Past).

The spatial distribution of saddle querns frequencies fits with a Negative Binomial distribution with a k=0.630 and p=0.430 with the Kolmogorov Smirnov test=1. This condition suggests randomness and overdispersion in the spatial distribution of the saddle querns frequency per sampling unit (Figure 175).

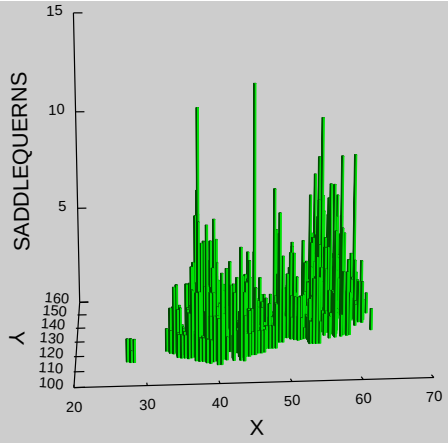

Figure 175 3D Histogram of saddle querns recovered during surveys of 2001 (Systat 13).

Obviously, saddle querns are not concentrated in an easily predictable way. We can design an ellipse along the north-East-South-West main axis of the surveyed area (parallel to the estimated ancient lake shoreline), with a long axis of 38.37 m and a short one of 9.87 m, delimiting an area of 297.49 square meters, where most data count appear. The elongated and possibly deformed shape of such an ellipse, gives poor explanatory value to the abundance weighted mean spatial center, at x=51.654177 and y=131.630016. Within this area, it has been estimated an average density of 0.67 saddle querns per square meter.

The spatial distribution of the abundance of saddle querns per sampling unit shows a Global Moran's *I* of -0.000631**.** The theoretical (expected) value assuming spatial autocorrelation (lack of spatial independence) is -0.000685 and the standard error of *I* is -0.000685. The test of significance using the normality assumption gives an undetermined *z* value. Consequently, we can accept that the spatial distribution of saddle querns is not significantly different than the expected value under a random distribution. This is what would be expected in the case of quite same frequency of evidence in every spatial location. These results are comparable with those of the Geary statistic (for this case *C*=0.999717) and Getis-Ord general G (*G*=0.010086).

However, as it was suggested in chapter 4, global measures of autocorrelation are misleading in the case of aggregated behaviour resulting in an accumulation of things. The Moran's *I* Correlogram (Figure 176) has been calculated for uniform class distance intervals of 1 meter, and taking into account a 10 meters active lag distance. *I* value at the starting point of the function is 0.256, above the expected value for randomness. As the distance between sampling point increases, the hypothesis of spatial continuity drops off gently until a threshold of 4 meter, beyond which overdispersion reigns. Some evidence of negative autocorrelation at around 7-9 meters suggests the possibilities of differentiated continuous areas in origin, around 3-4 meters, that have been unified towards randomness, as a consequence of post-depositional scattering of evidence.

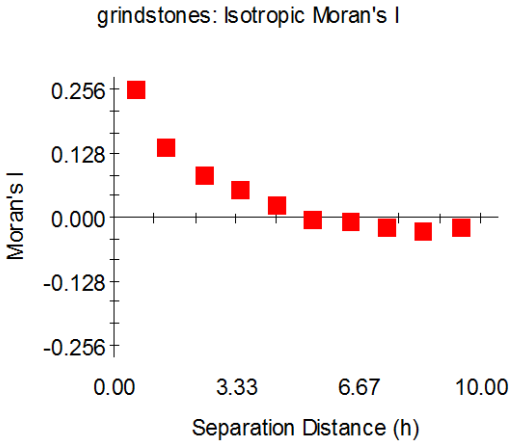

Figure 176 Moran's I Correlogram for saddle querns recovered during surveys of 2001 (GS+).

Using local indicators of spatial association (see at the end of the chapter), we have considered only those cells in which the frequency of saddle querns exceed, what would be expected according to a random model, that is the eleven cells with 6 or more items. These sampling units appear to be overdispersed according to the Clark and Evans test (p<1). Despite the absence of spatial clustering within such data it is interesting to note that they are predominantly distributed according to the North-East-South-West alignement, parallel to the estimated ancient lake shoreline (Figure 177A), and more homogenously distributed in the northeast corner than in its opposite southwest one (Figure 177B).

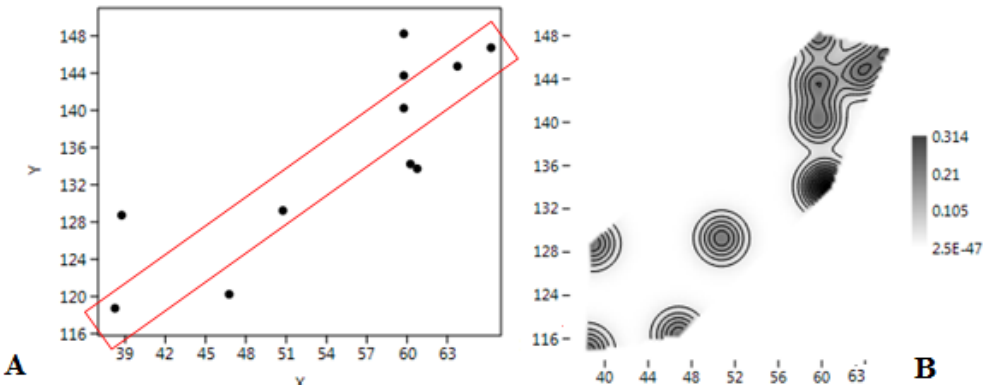

Figure 177 A)Spatial distribution of cells with more than 6 saddle querns (surveys 2001) (Past). B)KDE of such cells (surveys of 2001) (Past).

We have investigated the obvious presence of anisotropic variation, exploring the empirical anisotropic variogram at different directions (Figure 178).

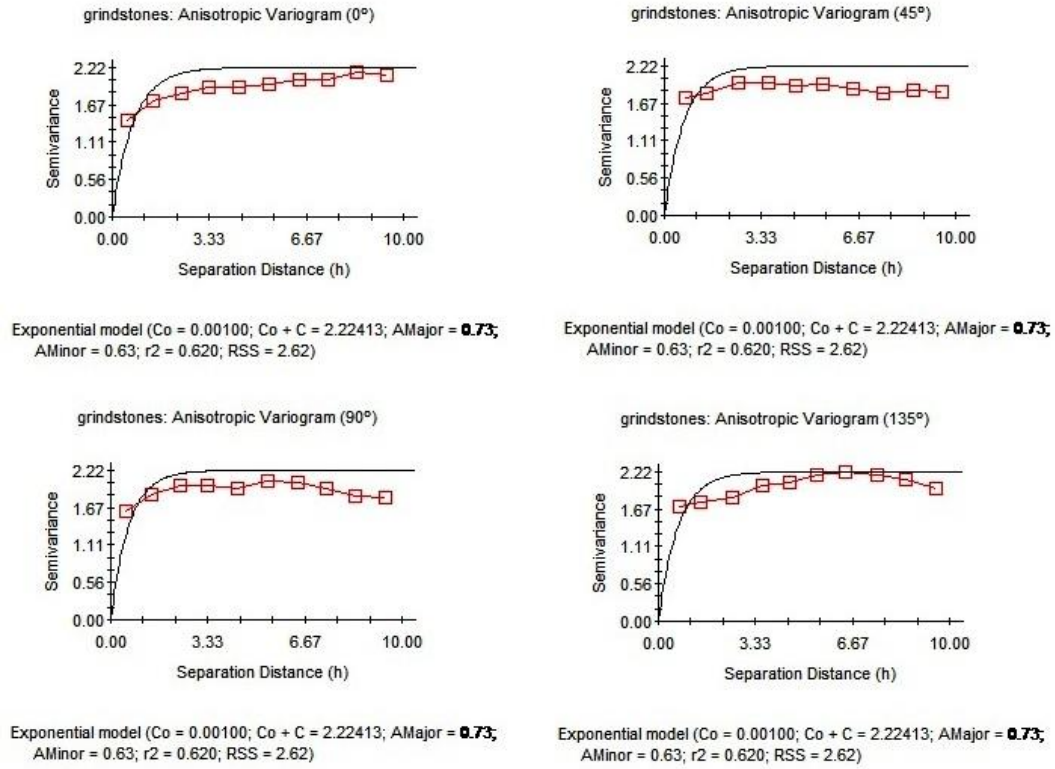

Figure 178 Anisotropic Variogram of saddle querns recovered during surveys of 2001 (GS+).

In general, anisotropic variograms appear to be comparatively flat, signaling the lack of statistical dependence even between near sampling units. The Semivariance Surface or Variogram Map (Figure 179) suggests that the maximum anisotropy is in the North-South direction, that is perpendicular to the orientation of the estimated ancient lake shoreline. The hypothesis of positive autocorrelation and spatial continuity can only be suggested for immediate cells, and not far beyond the 1 m threshold.

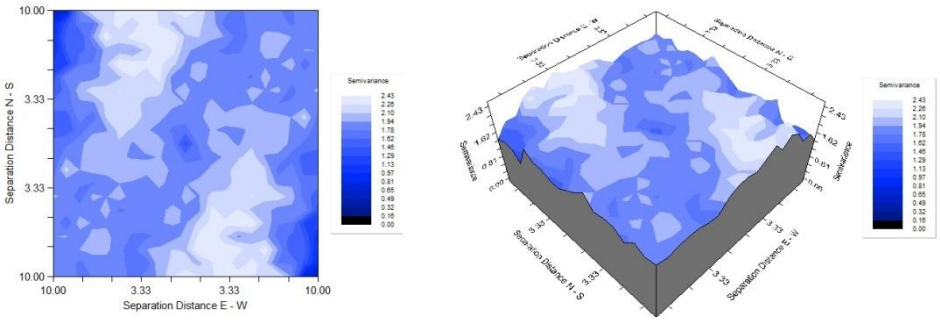

Figure 179 Variogram Map of saddle querns recovered during surveys of 2001 (GS+).

An exponential variogram model (Figure 180) has been fitted to the empirical variogram, using very low random noise (Nugget Variance, C_0 = 0.27700), very small hypothetical high continuity areas (Range = 0.40), and fairly high semivariance (Sill, C_0+C =1.96300). This model explains only 79.5% of spatial variance.

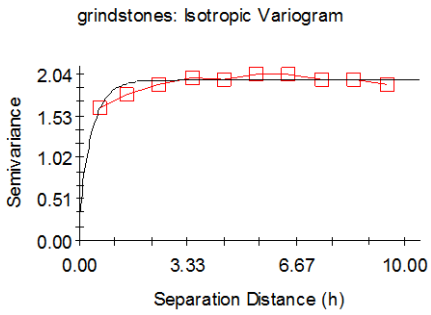

Exponential model (Co = 0.27700; Co + C = 1.96300; Ao = 0.40; r2 = 0.795; RSS = 0.0295)

Figure 180 Exponential Isotropic Variogram for saddle querns recovered during surveys of 2001 (GS+).

Although not entirely trustworthy because of the low non-linear fit, the inverse distance weighting corresponding to the above exponential model (Figure 181) shows some differences with the spatial distribution of posts. The general alignment (anisotropy) North-East-South-West is maintained, but now the differentiated areas in the South-West and North-East corners are more clearly remarked. For this category, the anisotropic deformation seems to affect in higher degree the concentration at North-East, whereas the South-Western accumulation would have maintained better its original organization. There are some very relevant empty areas in between, more remarked at Centre-North and at the South of the most relevant North-East concentration.

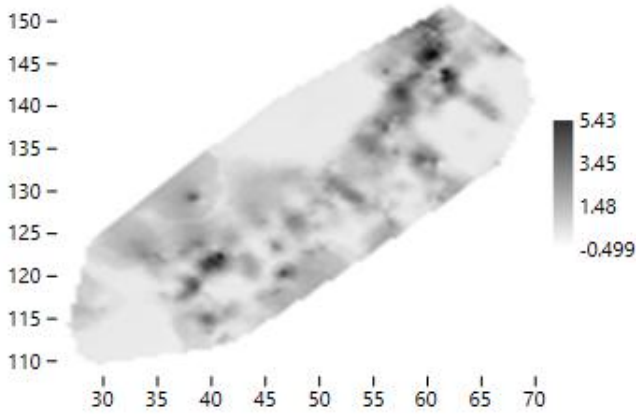

Figure 181 Graphic results of Inverse Distance Weighting calculated for saddle querns recovered during surveys of 2001 (Past).

It is important to take into account that this interpolated model has some relevant limits: it does not predict well the outliers, but gives a sufficiently good prediction of more frequent abundance values.

In general, saddle querns seem to be distributed according to a quite regular spatial pattern in two distinct sub-sectors (South-West and North-East) with a further concentration in the middle of the surveyed area. Allignements in the distribution of saddle querns can be detected and suggest some working hypothesis: the pattern of uniformity with quite everywhere the same number of items located in closer sampling units (attesting some kind of positive spatial autocorrelation) seems to be the most expected result, hypothesising that such evidence was

used in performing some, and the same, specific activities, that the comparison with the spatial distribution of other categories of observables could help to clarify.

7.5. Faunal remains (all taxa and all skeletal parts mixed together)

430 faunal remains of different animal species and from different skeletal parts were identified and counted. They are concentrated in a low number of sampling units, in such a way that 1304 cells were empty of faunal bones. Sampling units where faunal remains have been recorded are showed in Figure 182.

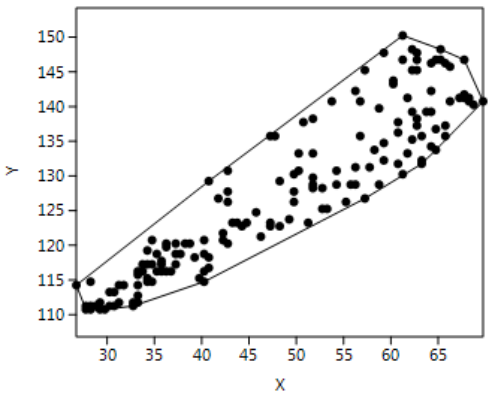

Figure 182 Spatial distribution of sampling units where faunal remains have been recorded during surveys of 2001 (Past).

Ripley's *k* analysis on the distance between sampling units with faunal remains evidence, suggests the possibility of some degree of spatial clustering, at the scale of the total reference area (Figure 183).

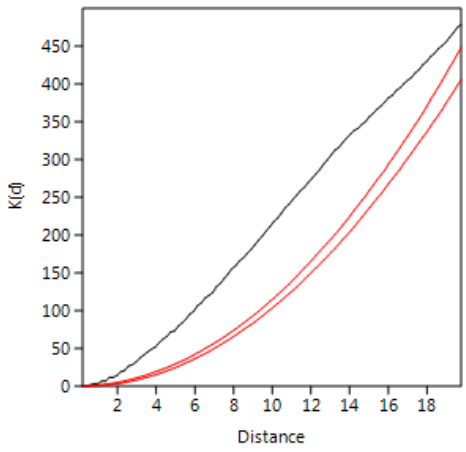

Figure 183 Ripley's *k* analysis on the distance between sampling units with faunal remains, recorded in surveys of 2001 (Past).

Within the convex hull defined by the effectively surveyed sampling units, however, the null hypothesis of a random pattern cannot be rejected. Empty cells seem to be statistically overdispersed (according to Clark and Evans test ($p<1$). KDE (Figure 184) gives equivalent results, although it suggests the occurrence of a main concentration of higher density locations, with higher inter-distance following the direction of the estimated ancient lake shoreline, until a

secondary concentration at the opposite North-East corner. A Kernel Density Estimation of cells with faunal evidence shows a quite irregular distribution of locations.

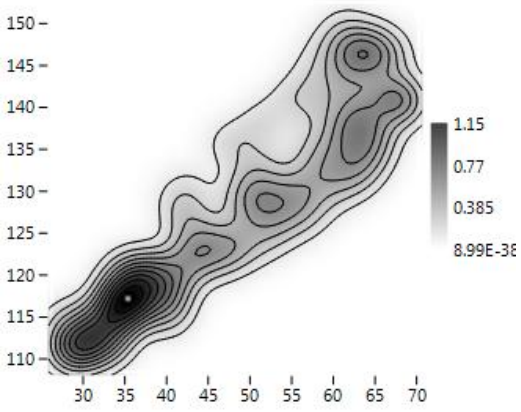

Figure 184 KDE of sampling units where faunal remains have been recovered during surveys of 2001 (Past).

When considering the raw quantity of faunal remains at each cell, the probability density distribution of spatial frequencies follows a *J*-shaped distribution. A majority of sampling units have raw counts of fauna of less than 3 elements (global mean = 2.75 faunal remains per sampling unit), but with a high standard deviation (3.0), suggesting a very irregular dispersion. Four cells are distinguished from the majority (interpretable as outliers) with 15, 16 and 20 faunal remains. According to both histogram and box plot is evident a break point in the frequency of occurrence of faunal remains in relation to the value 6 (as showed in Figure 185). 69% of faunal remains is located in 10% of the effectively surveyed area.

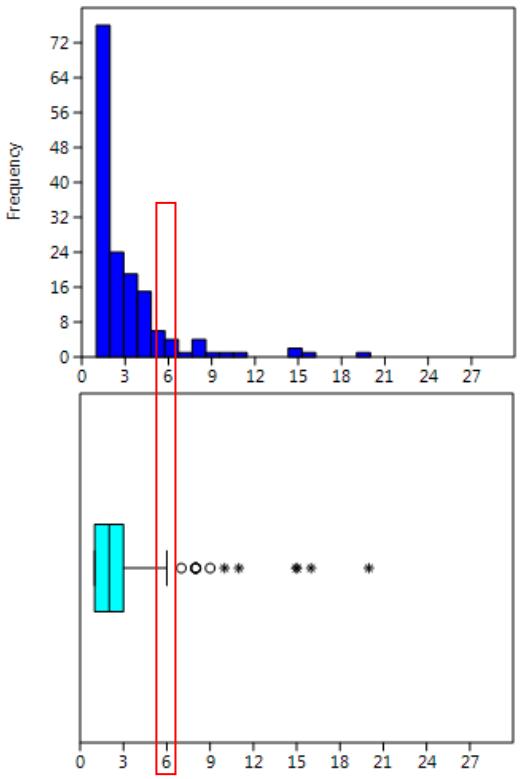

Figure 185 Histogram and box plot of frequencies observed for faunal remains (Past).

The spatial distribution of faunal remains frequencies fits with a Negative Binomial distribution with a k=0.067 and p=0.185 and the Kolmogorov Smirnov test=1. This condition suggests scarce differences in the spatial frequencies between sampling units. It is noted, however, a strong effect of outliers (Figure 186).

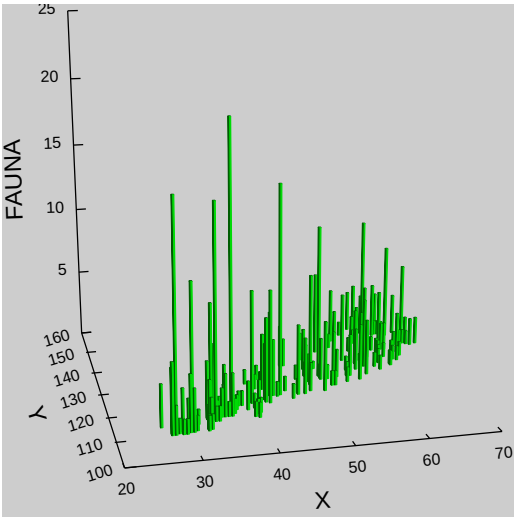

Figure 186 3D Histogram of faunal remains recovered during surveys of 2001 (Systat 13).

Again, we observe a very complex spatial pattern, which does not fit with the theoretical simple model of a single accumulation. Data are spread along an ellipse with a long axis of 47.65 m and a short one of 8.66 m, delimiting an area of 324.24 square meters, where most data count appears. The spatial centroid of this ellipse has very poor relevance, because it is not the point of maximum frequency (x=46.825581, y=126.659302). Within this area, we have estimated an average density of 0.24 faunal remains per square meter.

The spatial distribution of abundance of faunal remains per sampling unit shows a Global Moran's *I* of -0.000646**.** The theoretical (expected) value assuming spatial autocorrelation (lack of spatial independence) is -0.000685 and the standard error of I is -0.000685. The test of significance using the normality assumption gave a *z* value of 0.057354. Consequently, we can accept that the spatial distribution of faunal remains is not significantly different than the expected value under a random distribution. This is what would be expected in the case of predominance of the same frequencies of faunal remains in the majority of spatial location. Such results are comparable with those of the Geary statistic (for this case *C*=0.998537) and Getis-Ord general G (*G*=0.008590).

Obviously, we cannot trust on these global results given the strong heterogeneity and the evidences of outliers and multimodality in the distribution of faunal remains. The Moran's *I* Correlogram (Figure 187) has been calculated for uniform class distance intervals of 1 meter and taking into account a 10 meters active lag distance. *I* value at the starting point of the function is extremely low, 0.0352, and drops off quite fast to the level expected for randomness beyond the 3 meters threshold. Beyond that, a quite cyclical pattern is observed; at 5, 7 and 9 meter *I* value is on the line (corresponding to spatial randomness) followed by *I* value located above the expected value for randomness. In any case, those differences do not exceed the confidence level of 0.05 and are hence of very low relevance.

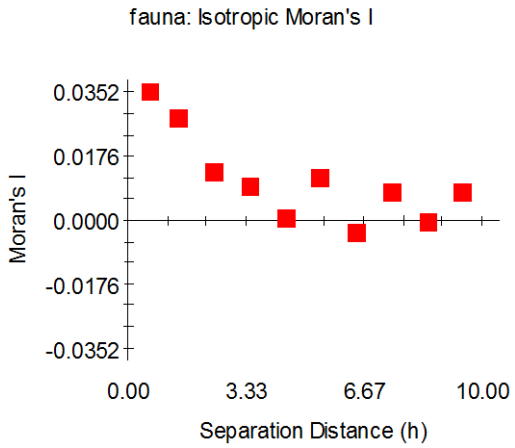

Figure 187 Moran's I Correlogram for faunal remains recovered during surveys of 2001 (GS+).

Then, spatial continuity in the first 4 meters is scarce, but there is some evidence of continuity, although very low, at higher distances, even at the scale of 10 meters. This is a characteristically irregular pattern affected by the presence of outliers and multimodality. Taking into consideration this assumption and the scarce difference, in terms of values, that characterizes *I* values and those expected for randomness (equal to 0), it is possible to suggest potential spatially continuous areas of 4 meters of radius, that may coincide with ancient activity areas.

Local indicator of spatial association suggests that 12 cells with 6 or more fragments of animal bone distinguish from their neighbours items. These differentiated sampling units show an overdispersed pattern (according to the Clark and Evans test (p<1). Despite the absence of spatial clustering within such data, it is interesting to note that they are predominantly distributed according to the North-East-South-West line of concentrations (Figure 188A), with more continuous and spatially dependent areas in the southwestern corner than further to the northeast, as showed even by the Kernel Density Estimation (Figure 188B).

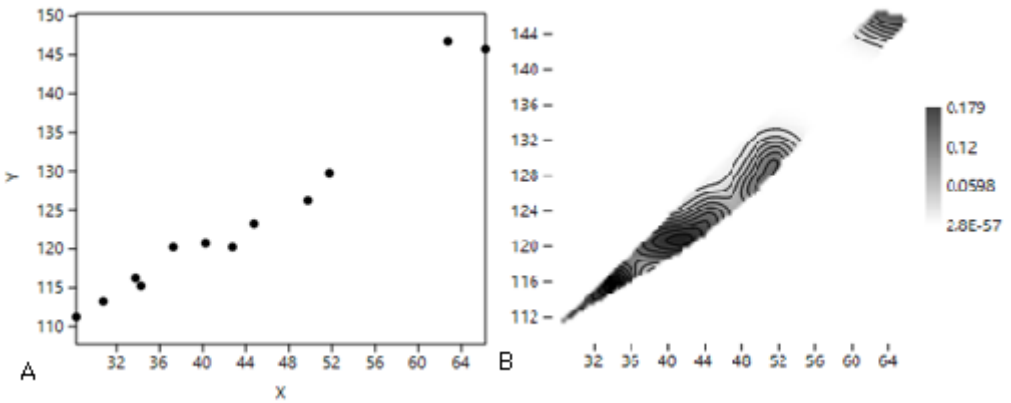

Figure 188 A) Spatial distribution of cells with more than 6 faunal remains (surveys 2001) (Past). B) KDE of such cells (surveys 2001) (Past).

We have explored the possible presence of anisotropic variation fitting a theoretical variogram at different directions (Figure 189).

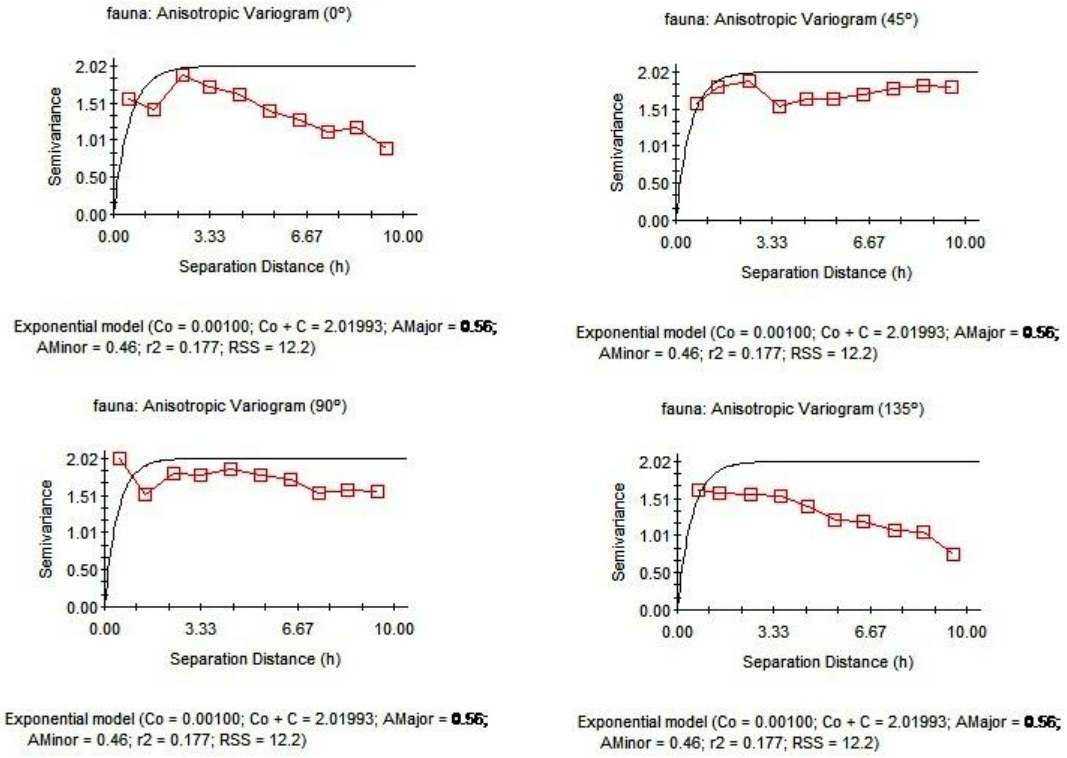

Figure 189 Anisotropic Variogram of faunal remains recovered during surveys of 2001 (GS+).

Semivariance is very high, and it diminishes with distance, suggesting that spatial continuity increases with distance, but always below what would be expected in a random model. This can be explained in terms of an intentional pattern at higher scales, probably configuring differentiated activity areas, and randomness within each area. Semivariance varies in strongly different ways at 0º, 45º, 90º and 135º. Only in the second part of the function (between 3 and 6 meter) some similarities in semivariance values are attested, respectively at 0º and 135º and at 45º and 90º. The graph of anisotropic Semivariance Surface or Variogram Map (Figure 190) reveals strong anisotropy which affects the pattern of similarity at small distances (the centre of the 3D diagram). Spatial continuity seems to be very scarce there and a strong irregularity of overabundant cells. The strong North-East-South-West trend in this anisotropy map reinforces the working hypothesis of a main concentration of faunal remains at the South-West corner, and a probably post-depositional deformation, parallel to the estimated ancient lake shoreline.

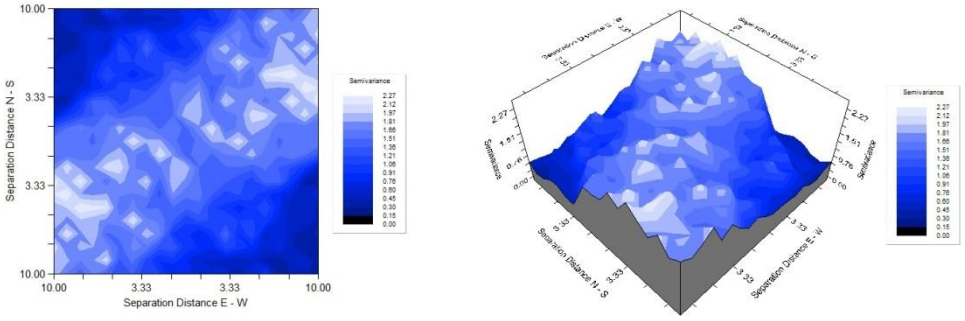

Figure 190 Variogram Map of faunal remains recovered during surveys of 2001 (GS+).

The strong anisotropy makes misleading any effort to model spatial distribution using kriging or any other similar interpolation method. An isotropic variogram, with C_0 (nugget variance)= 0.107000, C_0+C (sill)= 1.578000 and range (A)= 0.0300, explains only 17.70% of variance (Figure 191).

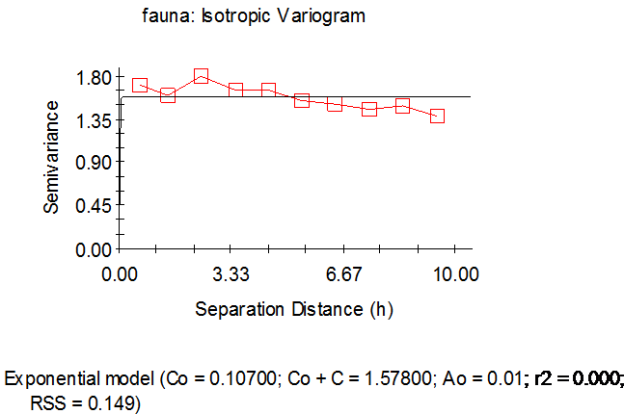

Figure 191 Exponential Isotropic Variogram for saddle querns recovered during surveys of 2001 (GS+).

This is a flat variogram where no autocorrelation exists between the units even at the lowest *h*'s.

Consequently, we used the Kernel Density Estimation of non-empty cells items (above) to predict the spatial distribution of faunal remains: they seem to be distributed along a marked North-East-South-West orientation and are predominantly concentrated in the South-West corner with continuity until the middle of the area under study. Small concentration is attested in the North-East corner with lower faunal remains presences.

7.5.1.1 Sub-categories of faunal remains

We have explored the spatial distribution of different skeletal parts. Nevertheless, frequencies are low in quantitative terms, and we have limited the analysis to an exploration of presence/absence in the surveyed area.

7.5.1.2 Cranial faunal remains

45 cranial remains from all taxa have been identified and counted; they are spatially distributed in 30 sampling units (Figure 192).

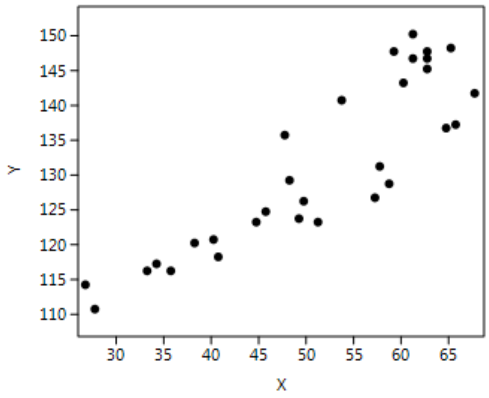

Figure 192 Spatial Distribution of sampling units where cranial faunal remains have been recorded in surveys of 2001 (Past).

Ripley's *k* analysis on the distance between sampling units with cranial remains suggests, as proved by the KDE, the possibility of some degree of spatial clustering, although the tendency towards clustering seems less relevant than in the case of all skeletal parts mixed together, specially at greater areas, beyond 16 meters (Figure 193).

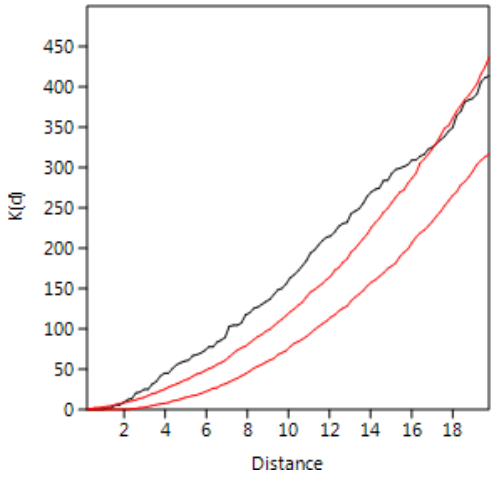

Figure 193 Ripley's *k* analysis on the distance between sampling units with cranial faunal remains, recorded in surveys of 2001 (Past).

Within the convex hull defined by the effectively explored sampling units, there are traces of overdispersion, according to Clark and Evans test ($p<1$). However, a Kernel Density Estimation (Figure 194) shows the occurrence of two possible concentrations (the North-Eastern more dense than the South-Western one), located between x=26-60 and y=110-135 and between x=50-65 and y=135-150, within the complex hull defined by the effectively surveyed area.

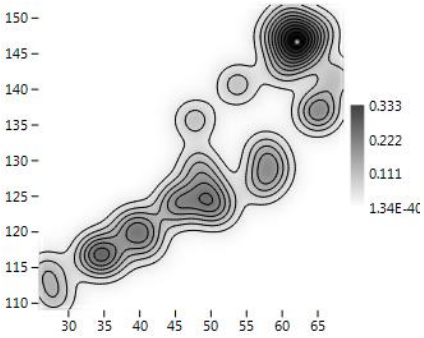

Figure 194 KDE of sampling units where cranial faunal remains have been recovered during surveys of 2001 (Past).

When considering the raw quantity of cranial remain at each cell, the probability density distribution of spatial frequencies follows a *J*-shaped distribution. Sampling units where cranial remains have been recovered show raw counts of less than 2 elements (global mean = 1.53 observables per sampling unit). Both histogram and box plot identified a break point in the distribution of frequencies in correspondence to the value 3. Furthermore, three cells are distinguished from the majority (interpretable as outliers), with 4 and 5 cranial fragments (Figure 195).

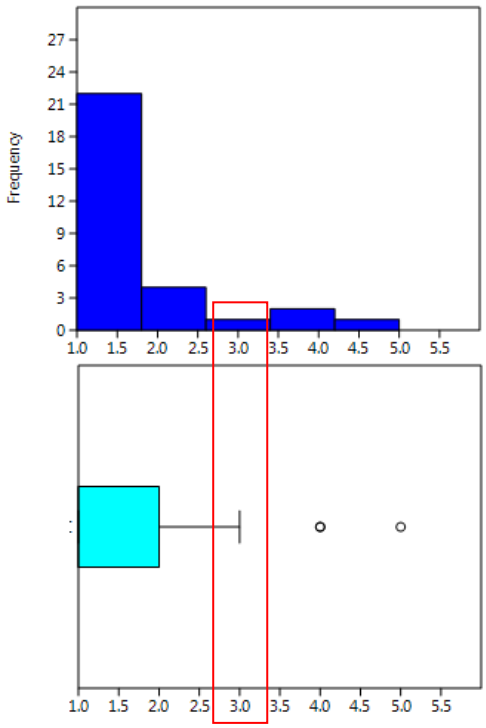

Figure 195 Histogram and box plot of frequencies observed for cranial faunal remains (Past).

65% of cranial fragments are located in 87% of the effectively surveyed area. Only 4 cells, spatially overdispersed, show more than 3 items (representing, this limit, the break point).

The spatial distribution of cranial fragments is fitted with a Negative Binomial distribution with k=0.026 and p=0.456 and Kolmogorov Smirnov Test=1. This condition suggests randomness in the spatial distribution of the abundance of cranial fragments per sampling unit. It is important to remark the fact that, although there are more sampling units with cranial remains at the North-East, while there are more frequencies per cell in the South-East (Figure 196).

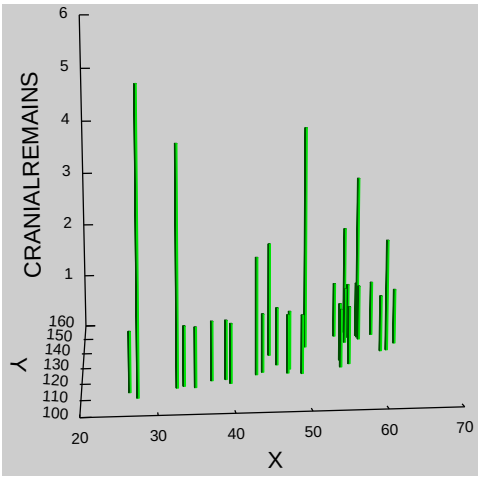

Figure 196 3D Histogram of cranial faunal remains recovered during surveys of 2001 (Systat 13).

The spatial distribution of count data per sampling unit for cranial fragments shows a Global Moran's I of -0.000685. The theoretical (expected) value assuming spatial autocorrelation (lack of spatial Independence) is -0.000685 and the standard error of I is 0.000685. The test of significance using the normality assumption gave a z value of 0.001055, a highly non-

significant value. Such results are comparable with those of the Geary statistics (C=0.997410) and Getis-Ord general G (G=0.002982). Consequently, it is evident that the spatial distribution of cranial fragments corresponds to the expected value under a random distribution. This is what would be expected in the case of predominant similar frequency of items within every spatial location.

Moran's *I* Correlogram (Figure 197) has been calculated for uniform class distance interval of 1 meter, and taking into account a 10 meters active lag distance. *I* values are very low, since they are arriving to the threshold of 0.05. Although characteristically cyclic, the ups and downs of the Correlogram around the line of autocorrelation are hardly relevant as expected when is observed a rather erratic pattern, with randomness.

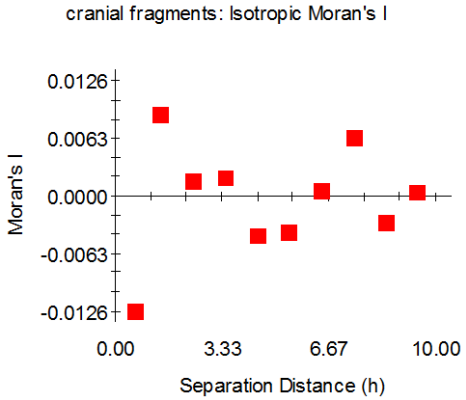

Figure 197 Moran's I Correlogram for cranial faunal remains recovered during surveys of 2001 (GS+).

We have explored the possible presence of anisotropic variation fitting a theoretical variogram at different directions (Figures 198 and 199). Anisotropy is higher in the 0º and 90º, showing a spatial distribution that seems to be different from the global pattern of faunal remains. It can be relevant the general North-West-South-East pattern, perpendicular to the main axis of the surveyed area, parallel to the shoreline of the lake.

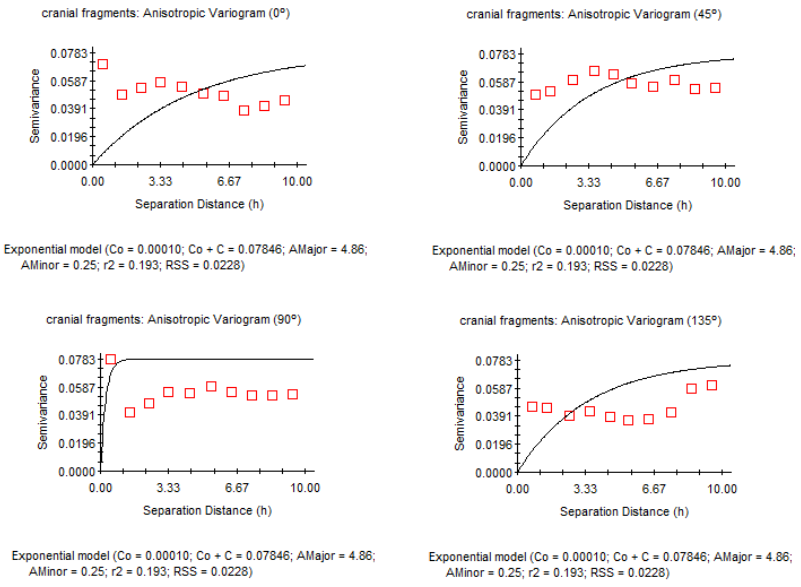

Figure 198 Anisotropic Variogram of cranial faunal remains recovered during surveys of 2001 (GS+).

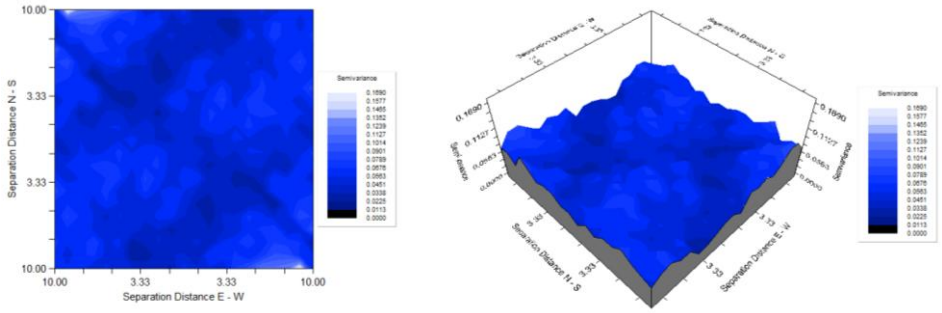

Figure 199 Variogram Map of cranial faunal remains recovered during surveys of 2001 (GS+).

Again, spatial semivariance is not quite relevant to calculate a reliable interpolated model of spatial frequencies. An isotropic model would explain a tiny 19.30% of global variance.

7.5.1.3 Axial faunal remains

55 axial faunal remains were identified and counted; they were distributed in 37 sampling units. The spatial distribution of sampling units, where axial remains have been identified, is showed in Figure 200.

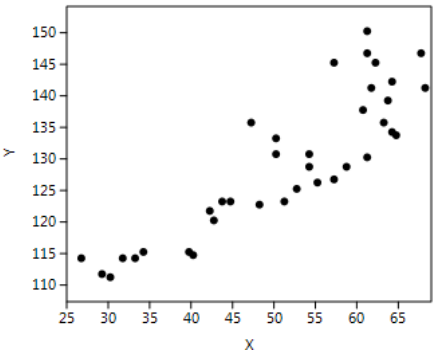

Figure 200 Spatial distribution of cells where axial remains have been recovered during surveys of 2001 (Past).

Ripley's *k* analysis on the distance between sampling units with axial remains suggests the possibility of low degree of spatial clustering, particularly concentrated between 4 and 18 meters, with the probability of randomness at very small distances (Figure 201).

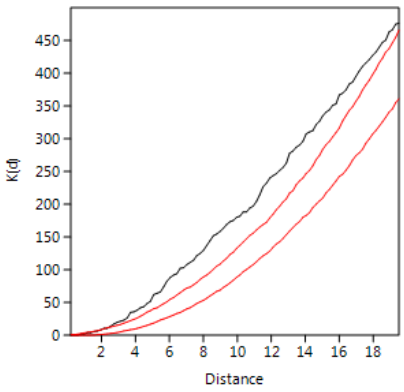

Figure 201 Ripley's *k* analysis on the distance between sampling units with axial faunal remains, recorded in surveys of 2001 (Past).

Within the convex hull defined by the 37 sampling units where axial fragments have been recovered, the null hypothesis of random pattern (Poisson process) cannot be rejected at $p<0.05$ (according to Clark and Evans test). A Kernel Density Estimation (Figure 202) suggests the occurrence of small concentrations of evidence located respectively between x=30-35 and y=112-115 y, between x=40-45 and y=120-125, between x=52-57 and y=125-130 and between x=60-62 and y=132-135. This is what would be expected when the majority of sampling units shows the same frequency of remains.

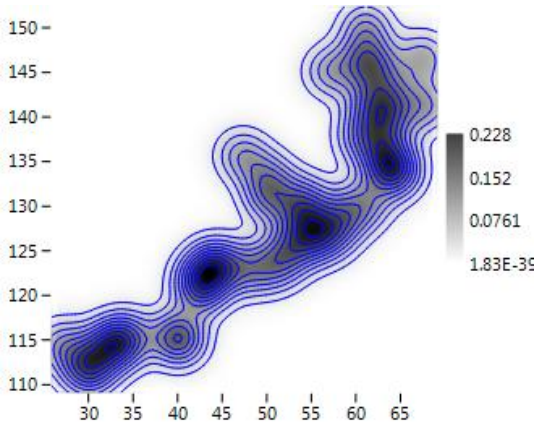

Figure 202 KDE of sampling units where axial faunal remains have been recovered during surveys of 2001 (Past).

When considering the raw quantity of axial remains at each cell, the probability density distribution of spatial frequencies follows a *J*-shaped distribution. A majority of sampling units have raw counts of such faunal remains of less than 2 elements (global mean = 1.48 observables per sampling unit). Both histogram and box plot identified a break point in the distribution of frequencies in correspondence with the value 3. Furthermore, one cell is distinguished from the majority (interpretable as outlier) with 7 axial remains (Figure 203).

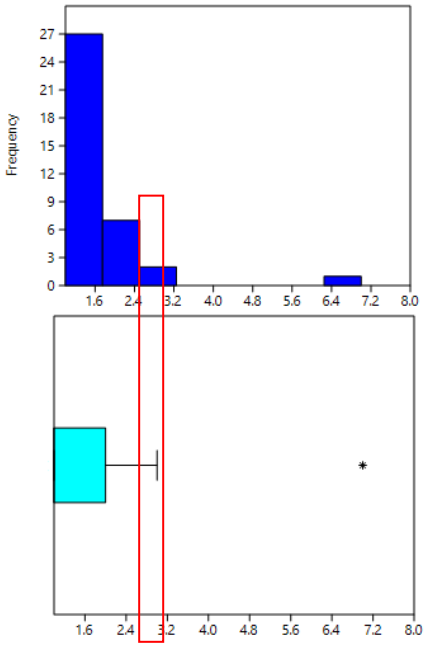

Figure 203 Histogram and box plot of frequencies observed for axial faunal remains (Past).

A frequency mean of 1.48 axial faunal remains per sampling unit and a standard deviation of 1.12 were counted. The spatial distribution of axial fragments is fitted with a Negative Binomial distribution, with k=0.035 and p=0.484, and Kolmogorov Smirnov Test=1. This condition suggests randomness in the spatial distribution of the abundance of axial fragments per sampling unit (Figure 204).

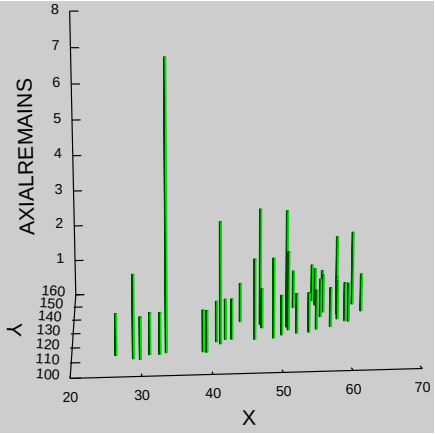

Figure 204 3D Histogram of axial faunal remains recovered during surveys of 2001 (Systat 13).

The spatial distribution of count data per sampling unit for axial fragments shows a Global Moran's *I* of -0.000687. The theoretical (expected) value assuming spatial autocorrelation (lack of spatial Independence) is -0.000685 and the standard error of *I* is 0.000685. The test of significance using the normality assumption gave a *z* value of -0.002296, a highly non-significant value. Such results are comparable with those of the Geary statistics (C=0.998834) and Getis-Ord general G (G=0.002070). Consequently, we can accept that the spatial distribution of axial fragments could not be significantly different than the expected value under a random distribution. This is what would be expected in the case of predominant similar frequency of occurrence, within quite every spatial location.

Moran's *I* Correlogram (Figure 205) has been calculated for uniform class distance interval of 1 meter, and taking into account a 10 meters active lag distance. *I* values are always beyond the probabilistic relevance threshold (0.05), and therefore we should conclude the randomness in the distribution. This is a characteristic pattern of overdispersion, where all measures seem to be below what is expected by a random autocorrelation model. In this overdispersed distribution, some outliers seem to differentiate from others.

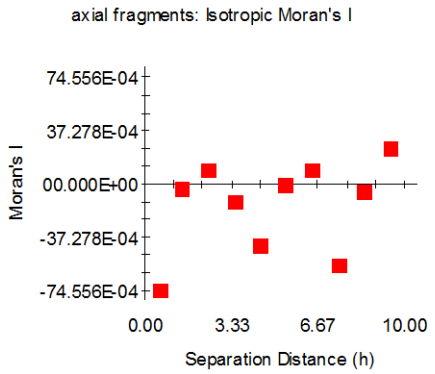

Figure 205 Moran's I Correlogram for axial faunal remains recovered during surveys of 2001 (GS+).

Taking into consideration the scarce frequencies of axial fragments within the surveyed area (ranging from 1 to 7), it is interesting to verify if are attested differential spatial distributions between sampling units with more frequencies. However, 87% of axial fragments are located in 97% of the effectively surveyed area, in such a way that only 1 cell shows more than 3 items (representing, this limit, the break point, highlighted by both histogram and box plot).

We have explored the possible presence of anisotropic variation, fitting a theoretical variogram at different directions (Figure 206). It is strongest in the 135º degrees, that is, in the general North-West-South-East direction, perpendicular to the ancient estimated shoreline of the lake.

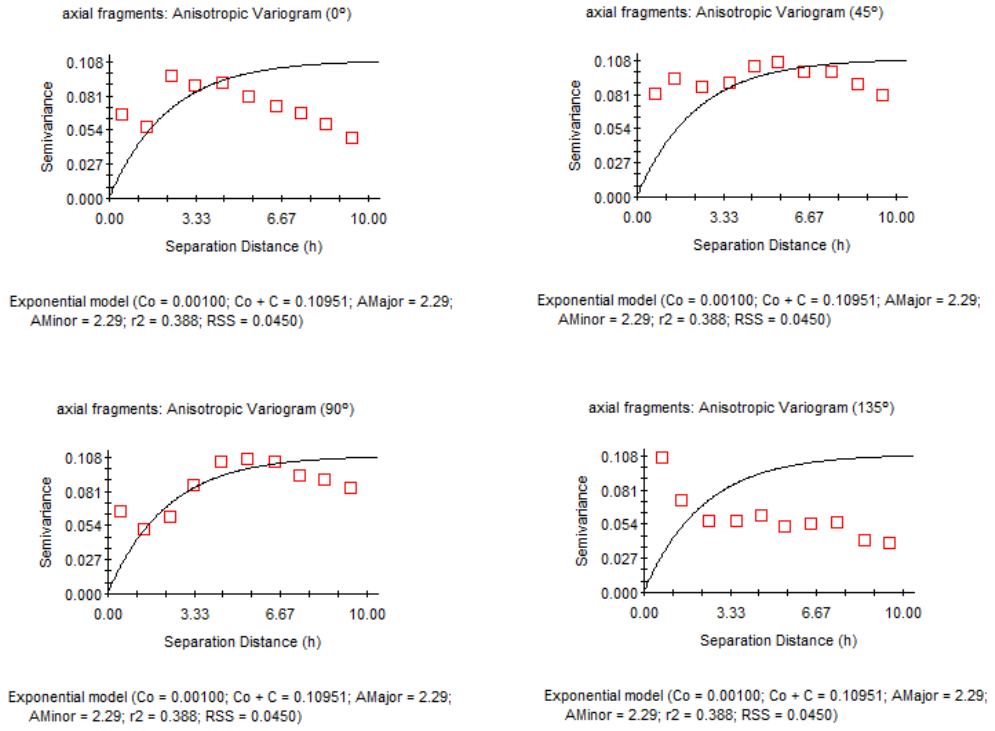

Figure 206 Anisotropic Variogram of axial faunal remains recovered during surveys of 2001 (GS+).

The graph of anisotropic Semivariance Surface or Variogram Map (Figure 207) would suggest the existence of two minor deformed high gradient areas, one at the west and another at the east, separated by a low frequency, more continuous region.

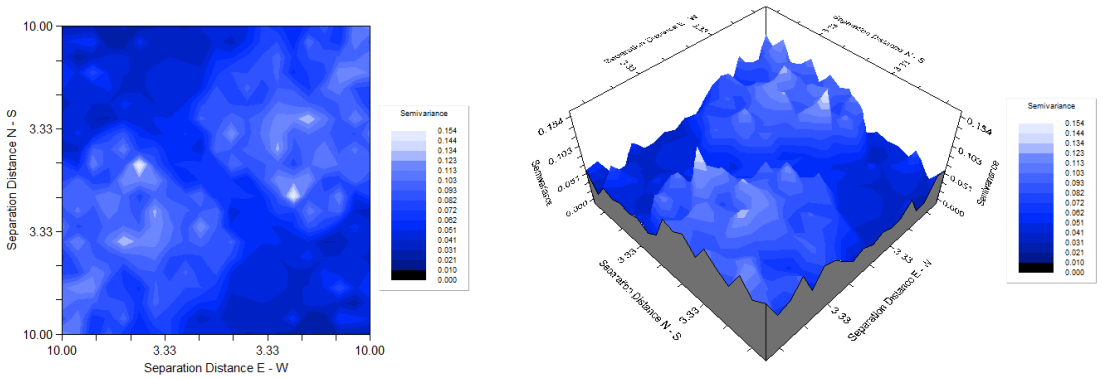

Figure 207 Variogram Map of axial faunal remains recovered during surveys of 2001 (GS+).

An exponential model fits the empirical variance better in this case than in the other faunal categories (C_0 (nugget variance) =0.00420, C_0+C (sill) = 0.07990 and A_0 (Range) = 0.01 (Figure 208). It explains 38.80% of predicted spatial differences. We should remark that it is a flat variogram, where similarity between some individual outliers (multimodality) gives an appearance of spatial trend; however, it is more relevant the presence of such outliers than the similarity in frequency between them.

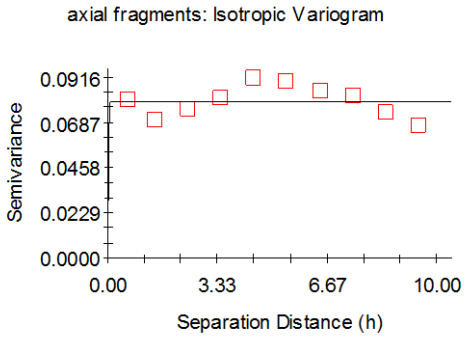

Exponential model (Co = 0.00420; Co + C = 0.07990; Ao = 0.01; **r2 = 0.000;**
RSS = 5.496E-04)

Figure 208 Exponential Isotropic Variogram for axial faunal remains recovered during surveys of 2001 (GS+).

7.5.1.4 Appendicular Faunal Remains

79 appendicular remains were identified and counted; they are spatially distributed in 57 sampling units and their spatial distribution is showed in Figure 209.

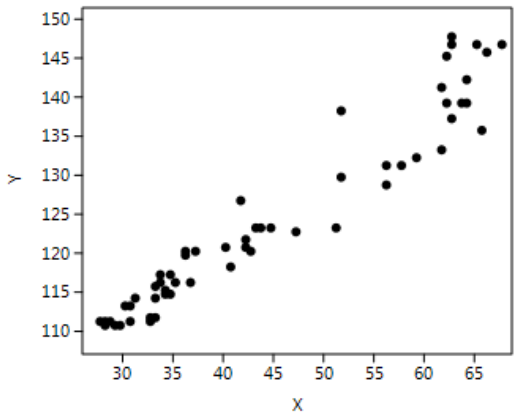

Figure 209 Spatial distribution of sampling units where appendicular faunal remains have been recorded (surveys of 2001) (Past).

Ripley's *k* analysis on the distance between sampling units with appendicular fragments suggests the possibility of some degree of spatial clustering, for all the reference area (Figure 210).

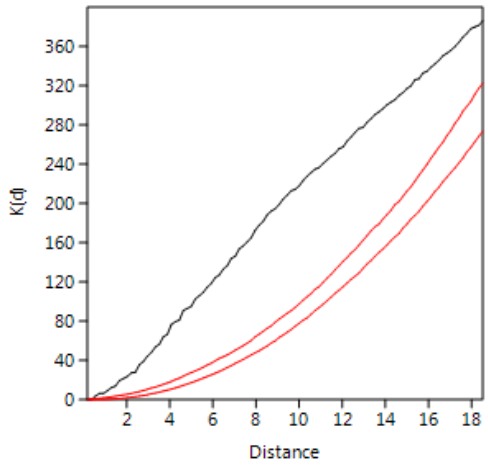

Figure 210 Ripley's k analysis on the distance between sampling units with appendicular faunal remains, recorded in surveys of 2001 (Past).

Within the convex hull, configured by sampling units with appendicular faunal remains, the null hypothesis of a random pattern (Poisson process) cannot be rejected at $p<0.05$. This condition suggests that equidistant cells have the same probability of counting one or more appendicular remains. However, there are some hints of clustering, as suggested by Kernel Density Estimation (Figure 211), which shows the occurrence of two predominant concentrations located between x=26-46 and y=110-126 and between x=50-67 and y=127-147. A further low dense point is observed at x=54 y=137.

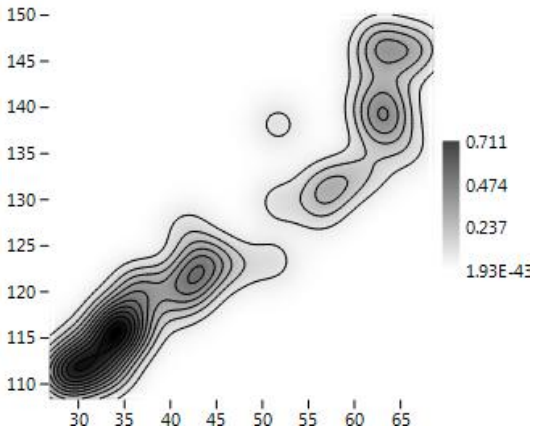

Figure 211 KDE of sampling units where appendicular faunal remains have been recovered during surveys of 2001 (Past).

When considering the raw quantity of appendicular remain at each cell, the probability density distribution of spatial frequencies follows a *J*-shaped distribution. A majority of sampling units have raw counts of such faunal remains of less than 2 elements (global mean = 1.38 observables per sampling unit). Both histogram and box plot identified a break point in the distribution of frequencies in correspondence to the value 3. Furthermore, one cell is distinguished from the majority (interpretable as outlier), with 5 appendicular fragments (Figure 212).

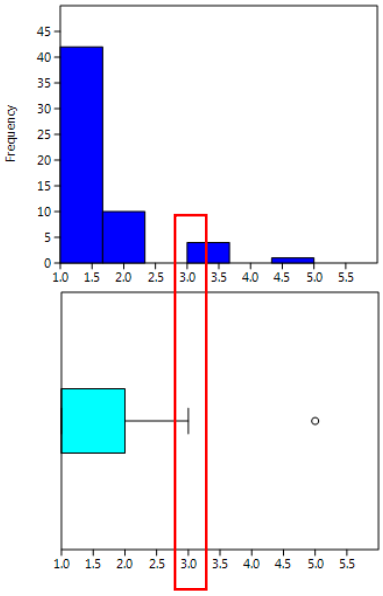

Figure 212 Histogram and box plot of frequencies observed for appendicular faunal remains (Past).

94% of appendicular fragments is located in 98% of the effectively surveyed area, in such a way that only 1 cell show more than 3 items (representing, this limit, the break point).

The spatial distribution of appendicular fragments is fitted with a Negative Binomial distribution with k=0.068 and p=0.558 and Kolmogorov Smirnov Test=1. This condition suggests randomness in the spatial distribution of the abundance of appendicular fragments per sampling unit (Figure 213).

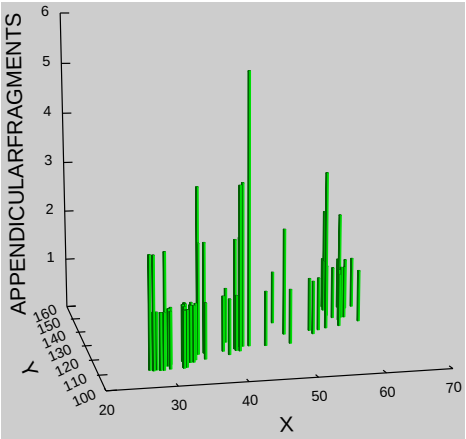

Figure 213 3D Histogram of appendicular faunal remains recovered during surveys of 2001 (Systat 13).

The spatial distribution of count data per sampling unit for appendicular fragments shows a Global Moran's I of -0.000625. The theoretical (expected) value assuming spatial autocorrelation (lack of spatial independence) is -0.000685 and the standard error of I is 0.000685. The test of significance using the normality assumption gave a z value of 0.087905, highly non-significant value. Such results are comparable with those of the Geary statistics (C=0.999248) and Getis-Ord general G (G=0.022630). Consequently, we can accept that the spatial distribution of appendicular fragments could not be significantly different than the expected value under a random distribution. This is what would be expected in the case of similar frequency of occurrence within every spatial location.

Moran's *I* Correlogram (Figure 214) has been calculated for uniform class distance interval of 1 meter, and taking into account a 10 meters active lag distance. *I* value at the starting point of the function is about 0.0810, a very few above the expected value for randomness. As the distance between sampling units increases, *I* value drops off quite gently and reaches values less above the expected value for randomness until 3 meter where they are located predominantly on the line (corresponding to spatial randomness). Scarce positive spatial autocorrelation is attested in the first 3 meters of the function, giving the possibility of finding spatially dependent area of 3 meters of radius, what is suggestive working hypothesis for locating individual activity area; however, it is notable that all *I* values are around 0.

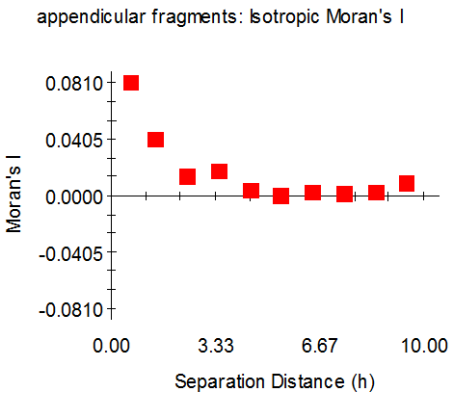

Figure 214 Moran's I Correlogram for appendicular faunal remains recovered during surveys of 2001 (GS+).

We have explored the possible presence of anisotropic variation, fitting a theoretical variogram at different directions (Figure 215). Anisotropy is higher in the 45º degrees (North-East-South-West) than in any other direction but, in most cases, semivariance is very low, suggesting the general lack of spatial continuity.

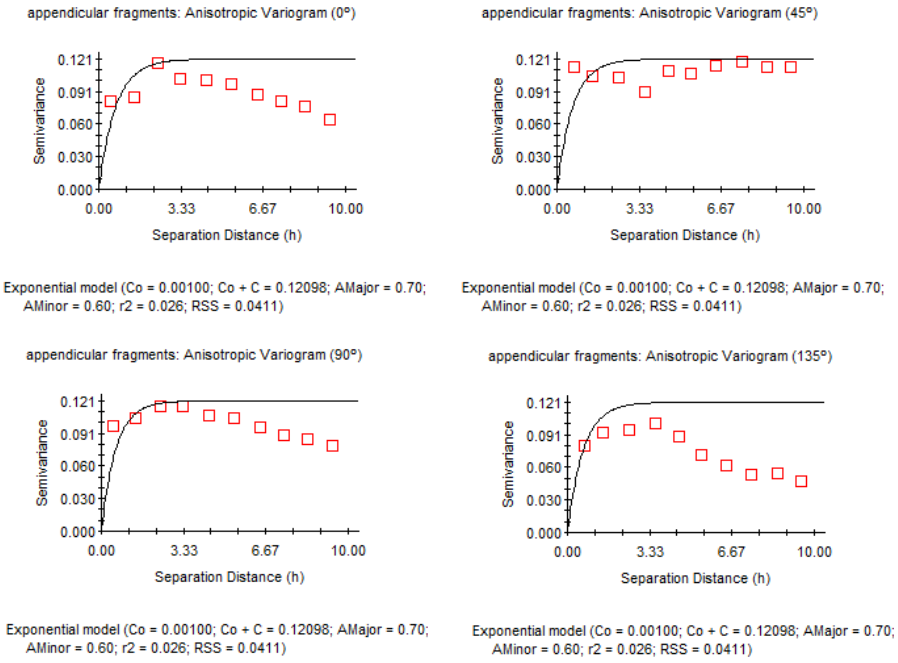

Figure 215 Anisotropic Variogram of appendicular faunal remains recovered during surveys of 2001 (GS+).

As suggested by the graph of anisotropic Semivariance Surface or Variogram Map (Figure 216), anisotropy and the lack of spatial contiguity is a very remarkable effect, as observed for other categories of faunal remains. However, an exponential model could not be fitted to the empirical variogram.

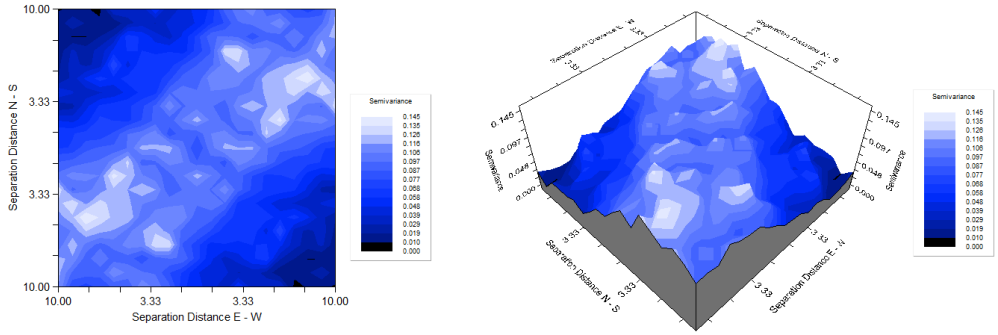

Figure 216 Variogram Map of appendicular faunal remains recovered during surveys of 2001 (GS+).

7.5.1.5 Faunal Remains ascribable to Ovis Vel Capra

29 faunal remains of *ovis vel capra* species were identified and counted; they were spatially distributed in 26 sampling units, while 1434 cells were empty. Sampling units where *ovis vel capra* remains have been identified are spatially distributed as showed in Figure 217.

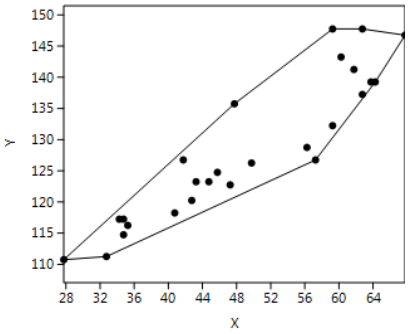

Figure 217 spatial distribution of cells with *ovis vel capra* faunal remains (surveys of 2001) (Past).

Ripley's *k* analysis on the distance between sampling units with *ovis vel capra* remains suggests the possibility of low degree of spatial clustering at the scale of the reference area (Figure 218).

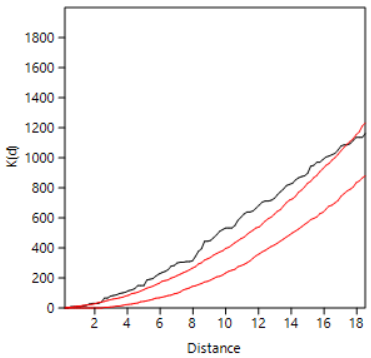

Figure 218 Ripley's *k* analysis on the distance between sampling units with *ovis vel capra* remains, recorded in surveys of 2001 (Past).

Within the convex hull configured by those sampling units with some positive frequency of these remains, there is overdispersion (according to the Clark and Evans test). A Kernel Density Estimation (Figure 219) shows a random distribution of small concentrations, along the main axis of the surveyed area, parallel to the ancient estimated lake shoreline.

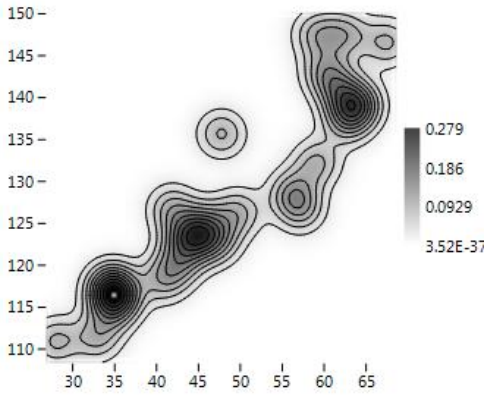

Figure 219 KDE of sampling units where *ovis vel capra* remains have been recovered during surveys of 2001 (Past).

When considering the raw quantity of *ovis vel capra* remains at each cell, the probability density distribution of spatial frequencies does not follow a *J*-shaped distribution. A majority of sampling units have raw counts of such fauna of less than 2 elements (global mean = 1.11 *ovis vel capra* fragment per sampling unit). Three cells are distinguished from the majority (interpretable as outliers), with 2 observables (Figure 220).

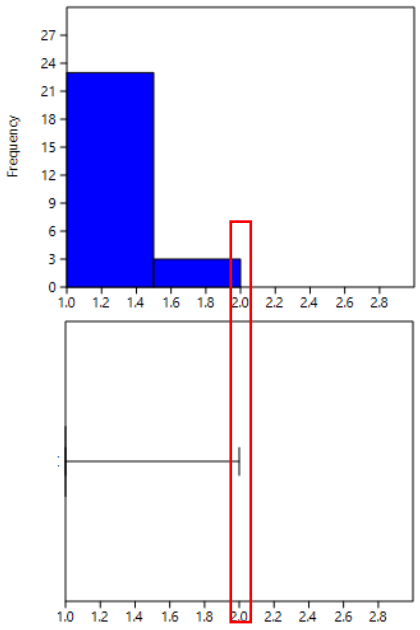

Figure 220 Histogram and box plot of frequencies observed for *ovis vel capra* remains, surveys 2001 (Past).

79% of *ovis vel capra* fragments is located in 88% of the effectively surveyed area, in such a way that only 3 cells show more than 1 item.

The spatial distribution of *ovis vel capra* remains can be fitted both with a Negative Binomial distribution, with k=0.092 and p=0.822, and a geometric distribution, with p=0.981 and Kolmogorov Smirnov Test=1. This is what is expected when, as in this case, the sample consists

in predominant empty sampling units, and similar frequencies values are observed in all non-empty cells, obtaining randomness (as also showed in Figure 221).

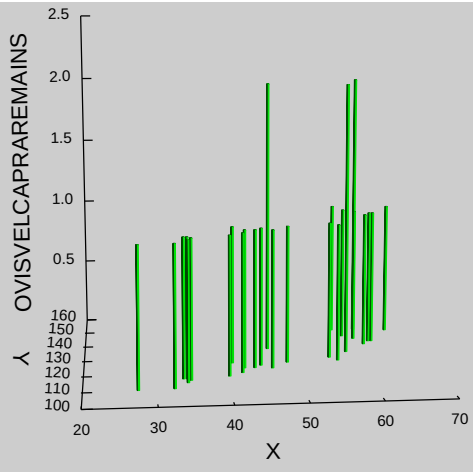

Figure 221 3D Histogram of *ovis vel capra* remains recovered during surveys of 2001 (Systat 13).

The spatial distribution of count data per sampling unit for *ovis vel capra* remains shows a Global Moran's *I* of -0.000690. The theoretical (expected) value assuming spatial autocorrelation (lack of spatial Independence) is -0.000685 and the standard error of *I* is 0.000685. The test of significance using the normality assumption gave a *z* value of 0.006657, a highly non-significant value. Such results are comparable with those of the Geary statistics (*C*=0.999623) and Getis-Ord general G (*G*=0.004963). Consequently, we can accept that the spatial distribution of *ovis vel capra* fragments could not be significantly different than the expected value under a random distribution. This is what would be expected in the case of similar frequency of occurrence within every spatial location.

Moran's *I* Correlogram (Figure 222) has been calculated for uniform class distance interval of 1 meter, and taking into account a 10 meters active lag distance. *I* value at the starting point of the function is about 0.0123, below the threshold. The result suggests, then, randomness.

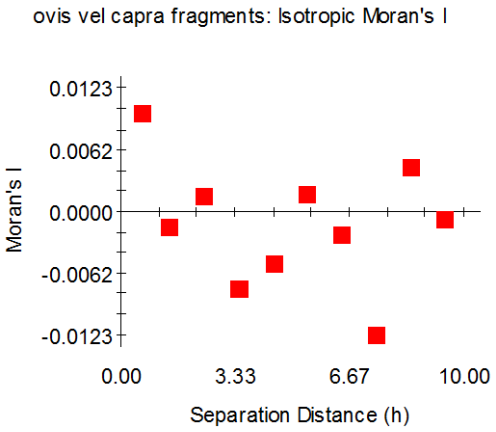

Figure 222 Moran's I Correlogram for *ovis vel capra* remains recovered during surveys of 2001 (GS+).

We have explored the presence of anisotropic variation comparing the anisotropic variogram for different directions (Figure 223). Anisotropy is higher in the 45º-90º than in any other direction.

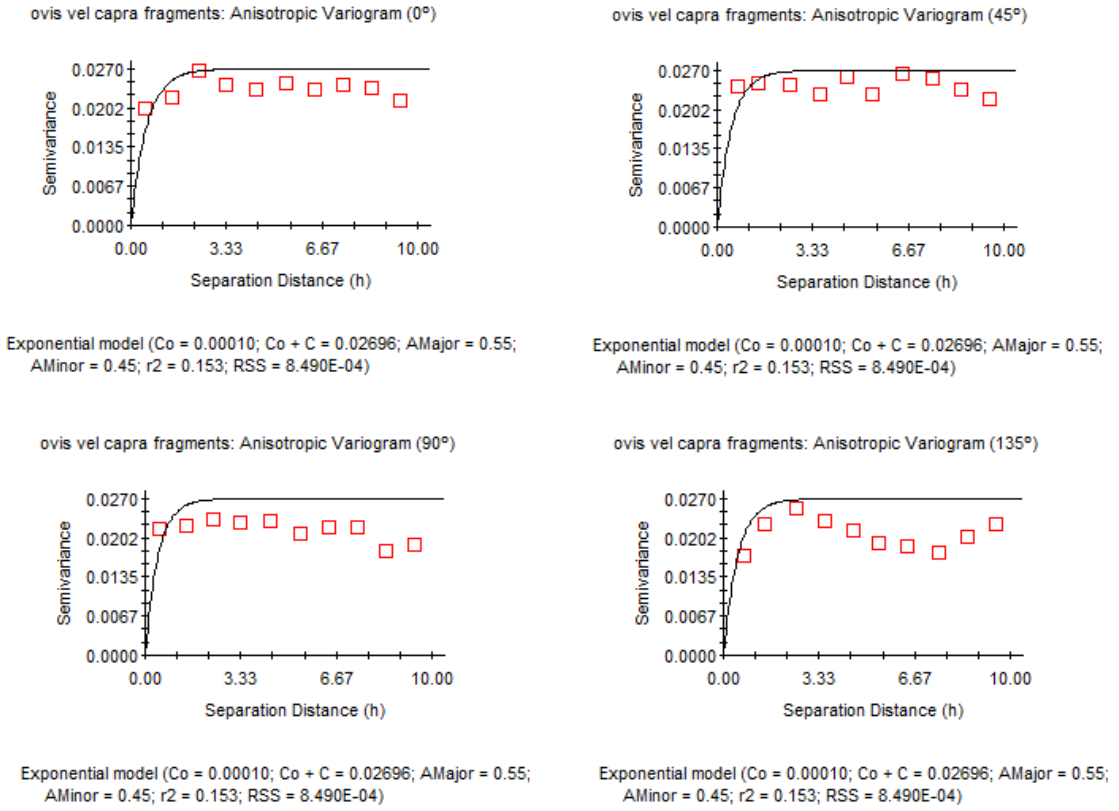

Figure 223 Anisotropic Variogram of *ovis vel capra* remains recovered during surveys of 2001 (GS+).

The graph of anisotropic Semivariance Surface or Variogram Map, suggests however, that semivariance variation is also very low, and that anisotropy probably does not affect seriously spatial variation, except along the main axis of the surveyed area. (Figure 224).

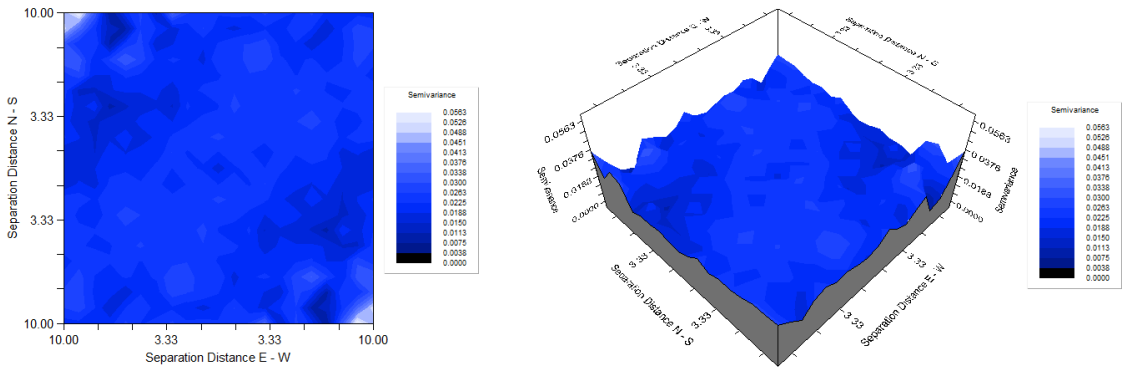

Figure 224 Variogram Map of *ovis vel capra* remains recovered during surveys of 2001 (GS+).

An exponential isotropic variogram model fitted to the empirical variogram - Nugget Variance, C_0=0.00194, Sill, C_0+C = 0.02288 and and Range, A_0 =0.26- explains 27.9% of sample variance (Figure 225). It is rather flat, insisting on the hypothesis of randomness. A Kriging interpolated surface, although it fits poorly observed data (Figure 226), gives the same image of random variation and some outlier exceptions.

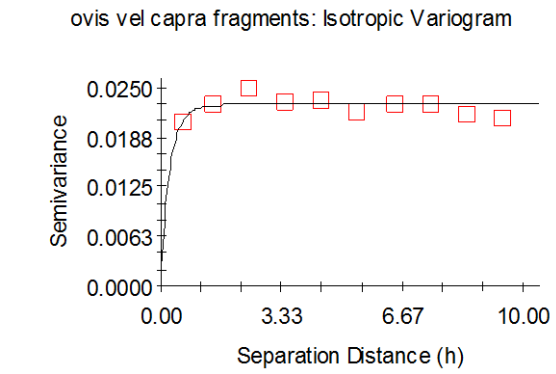

Exponential model (Co = 0.00194; Co + C = 0.02288; Ao = 0.26; **r2 = 0.279;** RSS = 1.022E-05)

Figure 225 Exponential Isotropic Variogram for *ovis vel capra* remains recovered during surveys of 2001 (GS+).

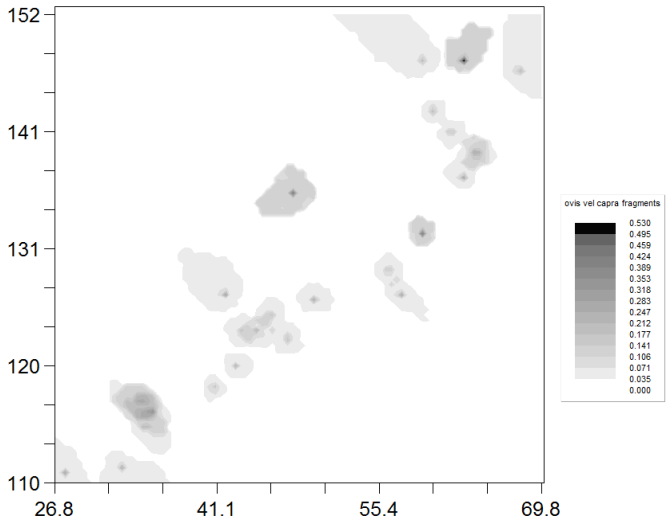

Figure 226 Graphic results of Kriging calculated for *ovis vel capra* remains recovered during surveys of 2001 (Past).

The model predicts emptiness in the North-West and South-East corners of the surveyed region and overdispersed concentrations following the main axis of the surveyed area.

7.5.1.6 Faunal Remains ascribable to Sus Domesticus

23 faunal remains of *sus domesticus* species were identified and counted; they were spatially distributed in 17 sampling units, while 1443 cells were empty. Cells where faunal remains ascribable to *sus domesticus* have been identified are spatially distributed as showed in Figure 227.

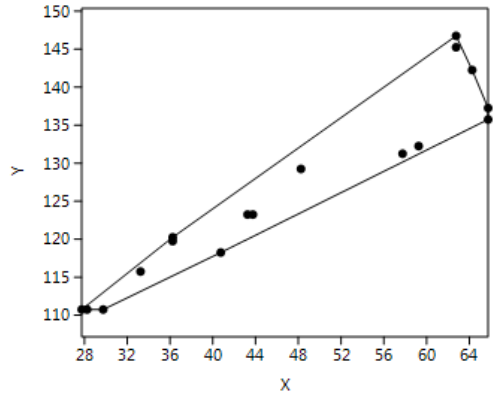

Figure 227 Spatial distribution of sampling units where *sus domesticus* remains have been recovered (surveys 2001) (Past).

Ripley's *k* analysis suggests the possibility of some low degree of spatial clustering at the scale of the global reference area, which at some particular spatial distance tends to randomness (as at 2, 5 and 17 meter). Beyond 18 meter randomness seems to be dominant in the spatial distribution of data.

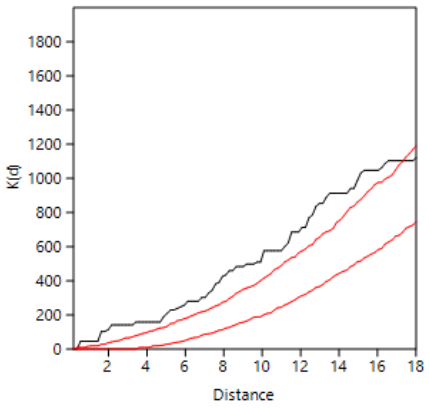

Figure 228 Ripley's *k* analysis on the distance between sampling units with *sus domesticus* remains, recorded in surveys of 2001 (Past).

Within the convex hull configured by those sampling units where *sus domesticus* have been identified, the null hypothesis of a random pattern (Poisson process) cannot be rejected at $p<0.05$. This result suggests that randomness characterizes the spatial distribution of *sus domesticus* fragments; this is what would be expected when the majority of the scarce sampling units show the same frequency of remains. A Kernel Density Estimation (Figure 229) shows, however, a more irregular pattern than expected. Some small concentrations (ranging from 1 to a maximum of 4 presences) are identified between x=27-32 and y=110-112, between x=33-40 and y=116-123, between x=42-46 and y=120-127, between x=46-48 and y=126-132, between

x=54-62 and y=128-134, between x=62-64 and y=133-137 and between x=60-64 and y=140-147.

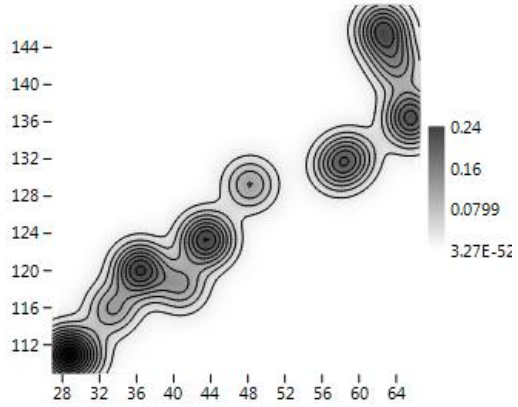

Figure 229 KDE of sampling units where *sus domesticus* remains have been recovered during surveys of 2001 (Past).

When considering the raw quantity of *sus domesticus* remains at each cell, the probability density distribution of spatial frequencies does not follow a *J*-shaped distribution. A majority of sampling units have raw counts, of such fauna, of less than 2 elements (global mean = 1.35 *sus domesticus* fragment per sampling unit). One cell is distinguished from the majority (interpretable as outlier), with 4 observables (Figure 230).

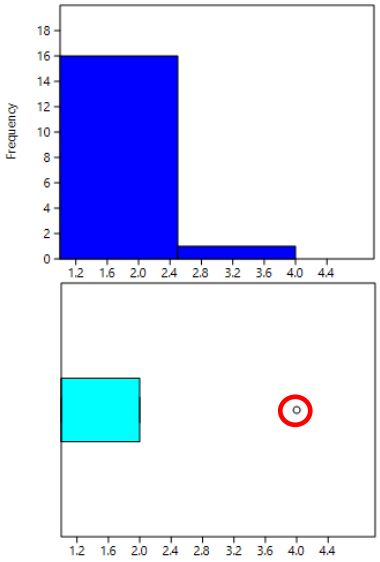

Figure 230 Histogram and box plot of frequencies observed for *sus domesticus* remains (Past).

83% of *sus domesticus* fragments are located in 94% of the effectively surveyed area, in such a way that only 1 cell shows more than 2 items (the outlier which has showed 4 fragments).

The spatial distribution of *sus domesticus* remains is fitted both with a Negative Binomial distribution, with k=0.021 and p=0.568, and a Geometric distribution, with p=0.984, and a Kolmogorov Smirnov Test=1. This is what is expected when, as in this case, the sample consists in predominant empty sampling units, and similar frequencies values in all non-empty cells are observed, obtaining randomness (as also showed in Figure 231).

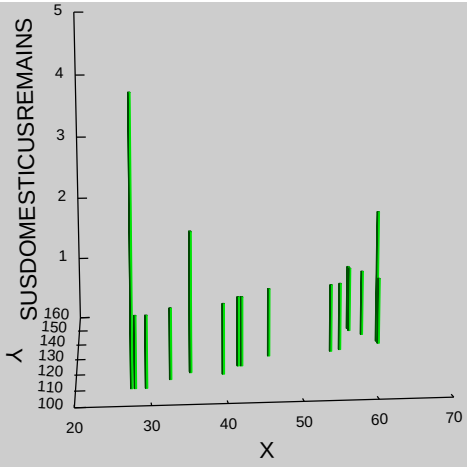

Figure 231 3D Histogram of *sus domesticus* remains recovered during surveys of 2001 (Systat 13).

The spatial distribution of count data per sampling unit for *sus domesticus* remains shows a Global Moran's *I* of -0.000672. The theoretical (expected) value assuming spatial autocorrelation (lack of spatial Independence) is -0.000685 and the standard error of *I* is 0.000685. The test of significance using the normality assumption gave a *z* value of 0.019822, highly non-significant value. Such results are comparable with those of the Geary statistics (C=0.996336) and Getis-Ord general G (=0.036885). Consequently, we can accept that the spatial distribution of *sus domesticus* fragments could not be significantly different than the expected value under a random distribution. This is what would be expected in the case of similar frequency of occurrence within every spatial location.

Moran's *I* Correlogram (Figure 232) has been calculated for uniform class distance interval of 1 meter, and taking into account a 10 meters active lag distance. *I* value at the starting point of the function is about 0.0802, a few above the expected value for randomness. As the distance between sampling units increases, *I* values drop off abruptly, and in quite all spatial distance they are located on the line (corresponding to spatial randomness). A spatial independence in *I* values quite everywhere is confirmed and it is notable that all such values are around 0.

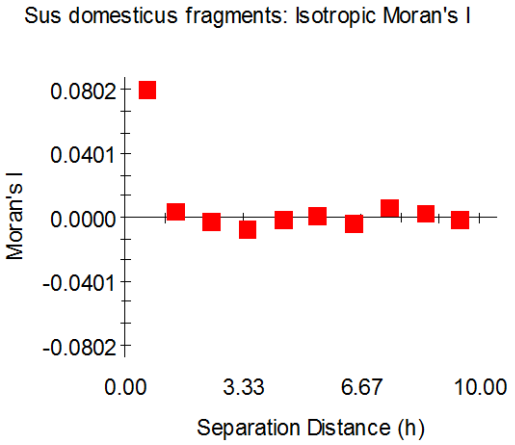

Figure 232 Moran's I Correlogram for *sus domesticus* remains recovered during surveys of 2001 (GS+).

Characteristically, there is spatial continuity only at very small distances, and a random distribution beyond. We have explored the possible presence of anisotropic variation,

comparing the variogram for different directions (Figure 233). Anisotropy is higher in the 45º than in any other direction, that is, parallel to the main axis of the surveyed area.

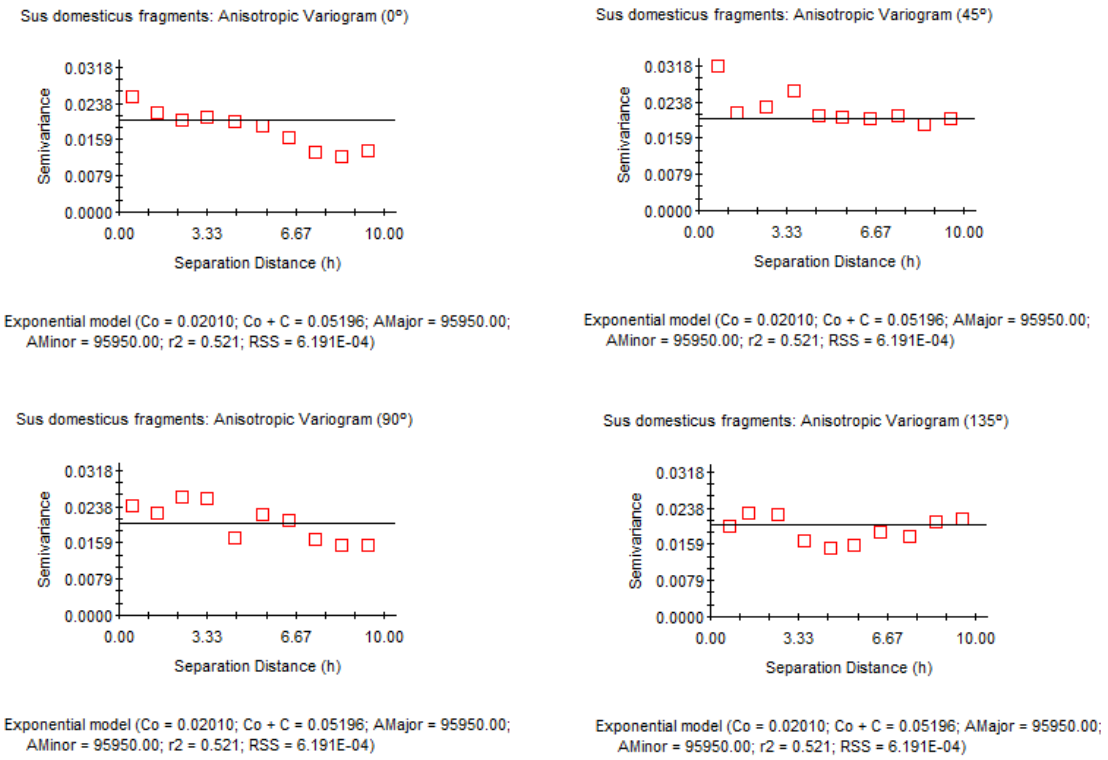

Figure 233 Anisotropic Variogram of *sus domesticus* remains recovered during surveys of 2001 (GS+).

The graph of anisotropic Semivariance Surface or Variogram Map gives a similar result and gives more strong support to the hypothesis of lack of spatial continuity (Figure 234).

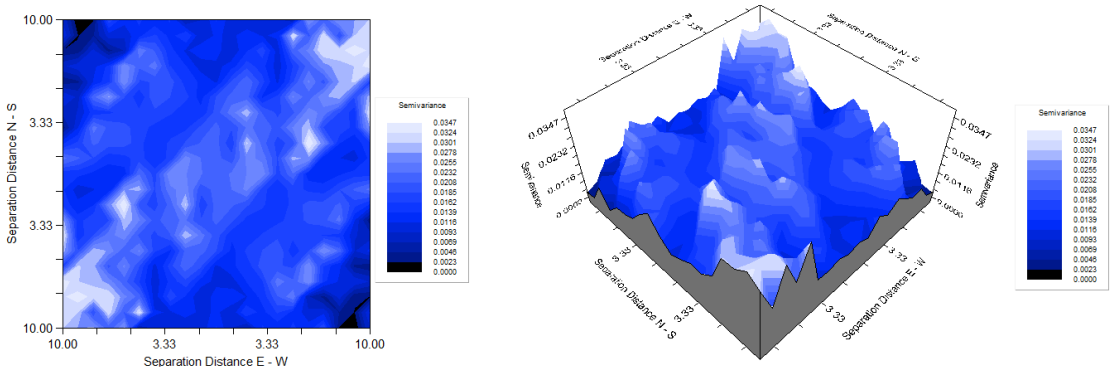

Figure 234 Variogram Map of *sus domesticus* remains recovered during surveys of 2001 (GS+).

As it is typical of a random distribution, anisotropy is more relevant at smaller distances (the center of the 3D graph) than at higher distances, what can be used to suggest potential differentiation in sectors, and a random variation within them.

An exponential model fitted to the empirical variogram - Nugget Variance, C_0 =0.00001, Sill, C_0+C = 0.02022 and Range, A_0 = 0.01- (Figure 235), gives a surprising high fitting, explaining 52.10% of differences in semivariance.

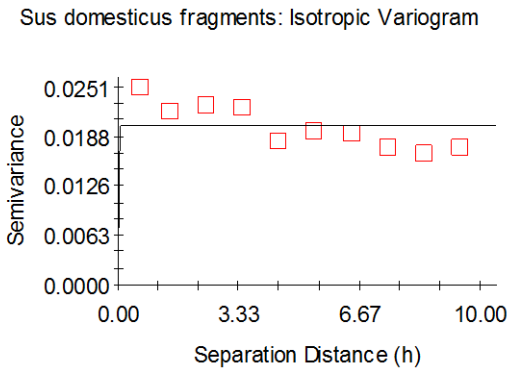

Exponential model (Co = 0.00001; Co + C = 0.02022; Ao = 0.01; **r2 = 0.000;** RSS = 7.151E-05)

Figure 235 Exponential Isotropic Variogram for *sus domesticus* remains recovered during surveys of 2001 (GS+).

A kriging interpolated scalar field (Figure 236) coincides with the other faunal categories, signaling overdispersed concentrations of fragments following the direction of the main axis of the surveyed area, and a secondary dispersion, perpendicular to the ancient estimated lake shoreline, at the North-East corner.

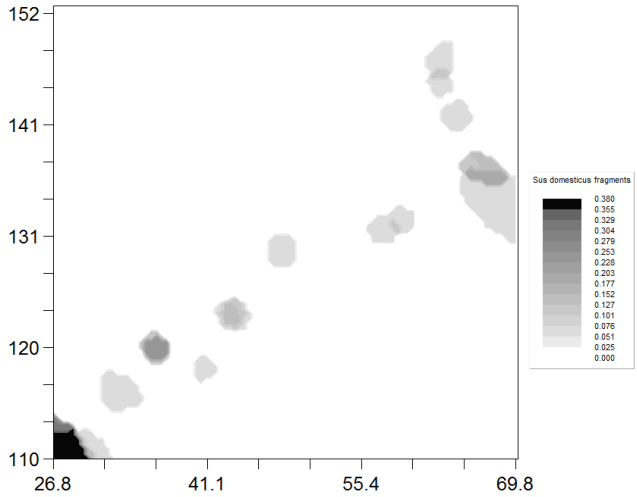

Figure 236 Graphic results of Kriging calculated for *sus domesticus* remains recovered during surveys of 2001 (Past).

7.5.1.7 Faunal Remains ascribable to Cervus Elaphus

33 *cervus elaphus* faunal remains were identified and counted; they are spatially distributed in 27 sampling units, while 1433 squares were empty. Cells where *cervus elaphus* fragments have been identified are spatially distributed as showed in Figure 237.

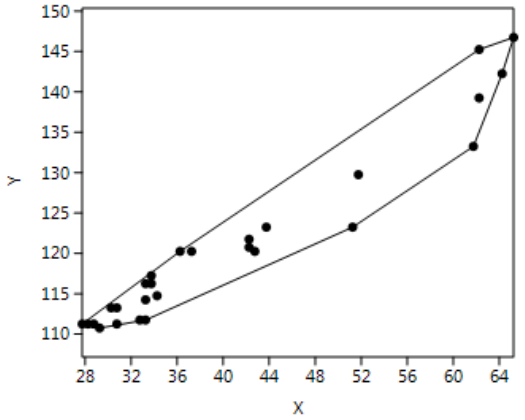

Figure 237 spatial distribution of sampling units where *cervus elaphus* faunal remains have identified (surveys 2001) (Past).

Ripley's *k* analysis on the distance between sampling units with *cervus elaphus* evidence suggests the possibility of some degree of spatial clustering, at the scale of the global reference area (Figure 238).

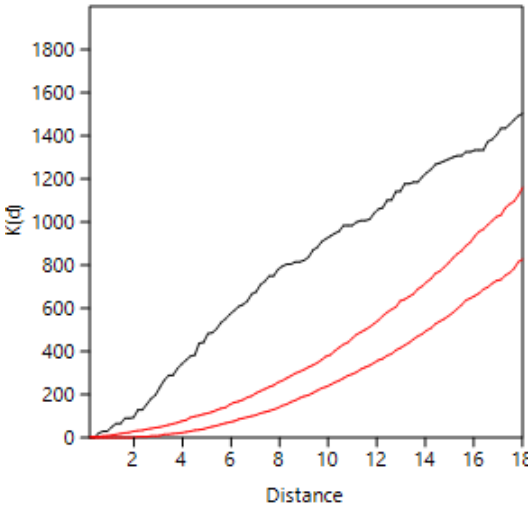

Figure 238 Ripley's *k* analysis on the distance between sampling units with *cervus elaphus* remains, recorded in surveys of 2001 (Past).

Within the convex hull configured by 27 sampling units where *cervus elaphus* remains have been identified, the null hypothesis of a random pattern (Poisson process) cannot be rejected with $p<0.05$ (Clark and Evans test). Thus, randomness characterizes the spatial distribution of *cervus elaphus* fragments; this is what would be expected when the majority of the scarce sampling units show the same frequency of remains. However, as in the case of other faunal categories, Kernel Density Estimation (Figure 239) shows some degree of irregularity, by detecting two predominant small concentrations, respectively observed between x=27-36 and y=109-118 and between x=42-46 and y=118-124.

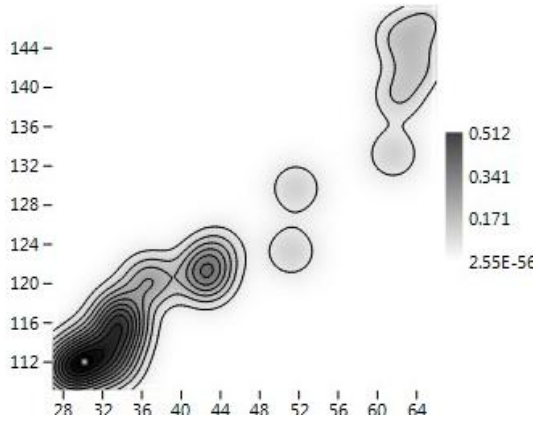

Figure 239 KDE of sampling units where *cervus elaphus* remains have been recovered during surveys of 2001 (Past).

When considering the raw quantity of *cervus elaphus* remains at each cell, the probability density distribution of spatial frequencies does not follow a *J*-shaped distribution. A majority of sampling units have raw counts, of such fauna, of less than 2 elements (global mean = 1.35 *cervus elaphus* fragment per sampling unit). One cell is distinguished from the majority (interpretable as outlier), with 4 observables (Figure 240).

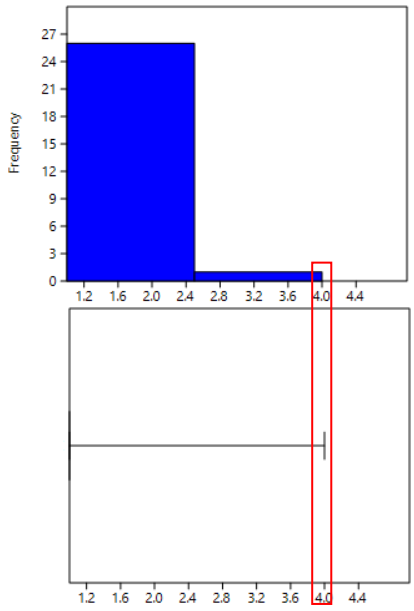

Figure 240 Histogram and box plot of frequencies observed for *cervus elaphus* remains (Past).

88% of *cervus elaphus* fragments are located in 96% of the effectively surveyed area, in such a way that only 1 cell show more than 4 items.

The spatial distribution of *cervus elaphus* fragments is fitted both with a Negative Binomial distribution, with k=0.050 and p=0.689, and a Geometric distribution with Kolmogorov Smirnov Test=1. This is what is expected when, as in this case, the sample consists in predominant empty sampling units and similar frequencies values in all non-empty cells, obtaining randomness (as also showed in Figure 241).

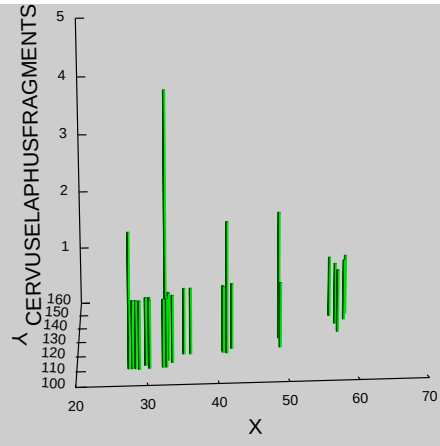

Figure 241 3D Histogram of *cervus elaphus* remains recovered during surveys of 2001 (Systat 13).

The spatial distribution of count data per sampling unit for *cervus elaphus* fragments shows a Global Moran's *I* of -0.000606. The theoretical (expected) value assuming spatial autocorrelation (lack of spatial Independence) is -0.000685 and the standard error of I is 0.000685. The test of significance using the normality assumption gave a *z* value of 0.115778, non-significant value. Such results are comparable with those of the Geary statistics (*C*=0.997335) and Getis-Ord general G (*G*=0.032755). Consequently, we can accept that the spatial distribution of *cervus elaphus* fragments could not be significantly different than the expected value under a random distribution. This is what would be expected in the case of similar frequency of occurrence within every spatial location.

Moran's *I* Correlogram (Figure 242) has been calculated for uniform class distance interval of 1 meter, and taking into account a 10 meters active lag distance. *I* value at the starting point of the function is about 0.0863, a few above the expected value for randomness. As the distance between sampling units increases, *I* value drops off quite gently and reaches values above the expected for randomness until 4-5 meter, where it is located predominantly on the line (corresponding to spatial randomness). Scarce positive spatial autocorrelation is observed in the first 4-5 meters of the function, giving the possibility of finding spatially dependent area of 4-5 meters of radius, what suggests working hypothesis for locating individual activity area; however, it is notable that all *I* values are around 0.

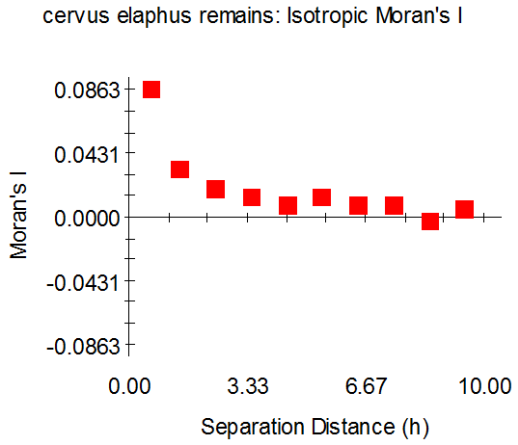

Figure 242 Moran's I Correlogram for *cervus elaphus* remains recovered during surveys of 2001 (GS+).

We have explored the possible presence of anisotropic variation, fitting a theoretical variogram at different directions (Figure 243). Anisotropy is clearly present, most notably at 0º and 135º.

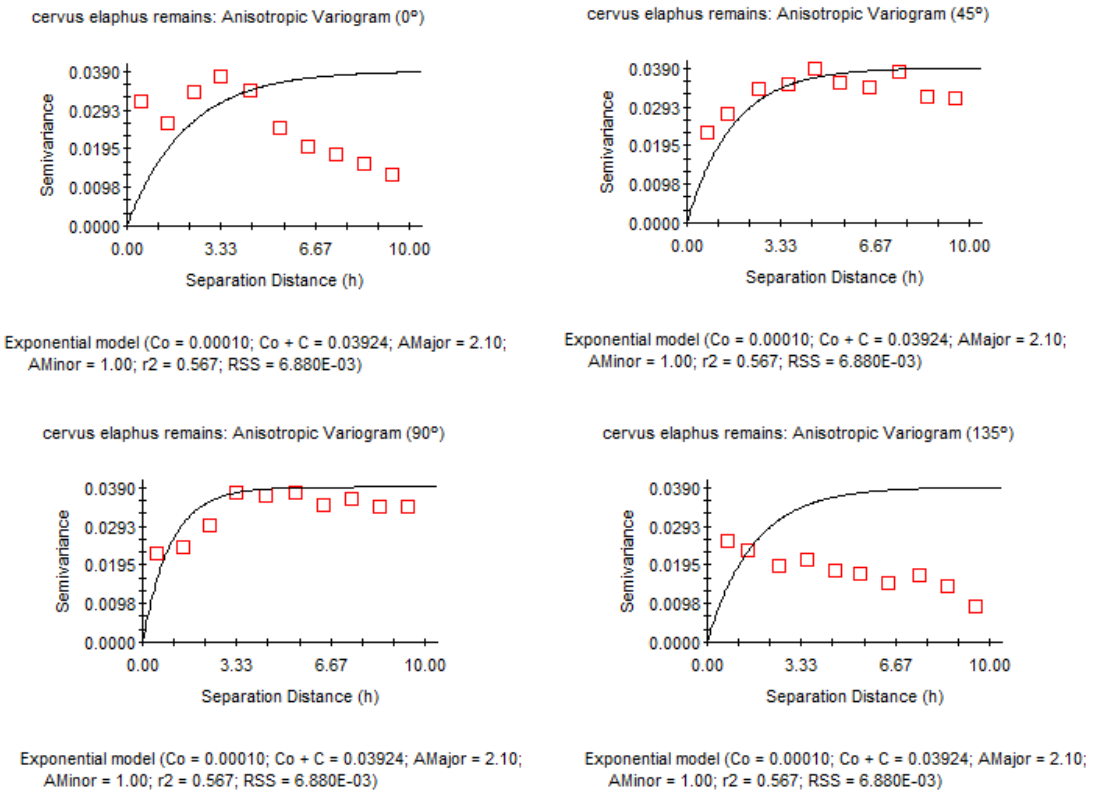

Figure243 Anisotropic Variogram of *cervus elaphus* remains recovered during surveys of 2001 (GS+).

The graph of anisotropic Semivariance Surface or Variogram Map insists on the lack of spatial continuity, even at very small distances, although it allows the hypothesis of two main differentiated sectors, with random distribution within each one (Figure 244).

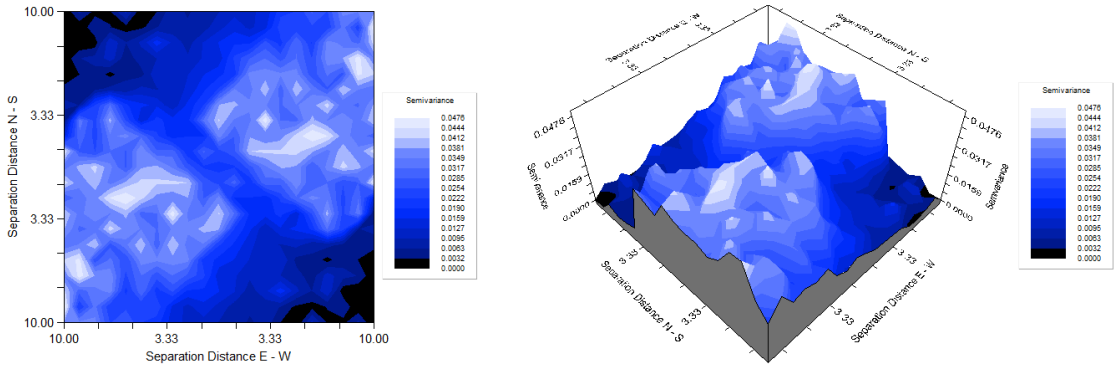

Figure 244 Variogram Map of *cervus elaphus* remains recovered during surveys of 2001 (GS+).

An exponential variogram model, fitted to the empirical variogram, has too low values of goodness of fit, and therefore cannot be used to obtain an interpolated model by kriging.

7.6 Pottery

2893 fragments were identified and counted. 682 were the surveyed empty cells, while the sampling unit with more presence gave 40 items. The spatial distribution of sampling units with pottery evidence is showed in Figure 245.

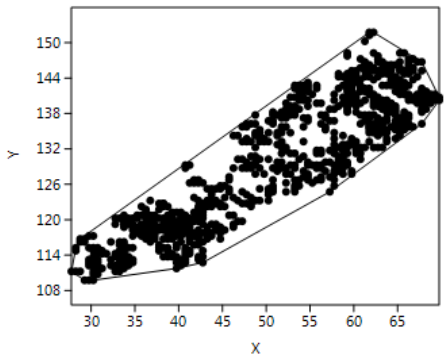

Figure 245 Spatial distribution of sampling units where pottery has been recorded in surveys of 2001 (Past).

Ripley's *k* analysis on the distance between sampling units with pottery evidence suggests the possibility of some degree of spatial clustering, at the scale of the reference area (Figure 246).

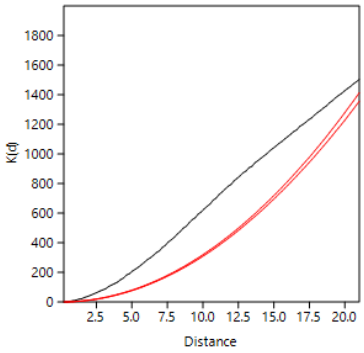

Figure 246 Ripley's K analysis on the distance between sampling units with pottery, recorded in surveys of 2001 (Past).

Within the convex hull configured by those sampling units with some positive frequency of pottery, Clark and Evans test suggests overdispersion. KDE of such cells (Figure 247) shows a relatively homogenous area with two possible concentrations of higher density, at both extremes of the surveyed area.

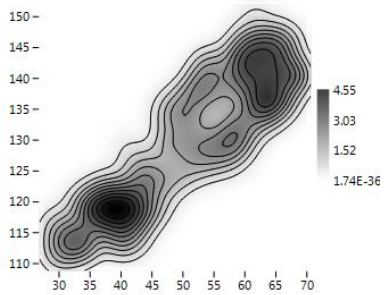

Figure 247 KDE of sampling units where pottery has been recovered during surveys of 2001 (Past).

When considering the raw quantity of pottery at each cell, the probability density distribution of spatial frequencies follows a *J*-shaped distribution. Where pottery is present, it appears in relatively high frequency (global mean = 3.71 potsherds per sampling unit). A standard deviation of 4.04 suggests the extreme irregularity and variance of such an estimate. Furthermore, two cells are distinguished from the majority (interpretable as outliers), with 30 and 40 pottery fragments. According to both histogram and box plot, it is evident a break point in the frequency of pottery occurrence, beyond 10 fragments (as showed in Figure 248).

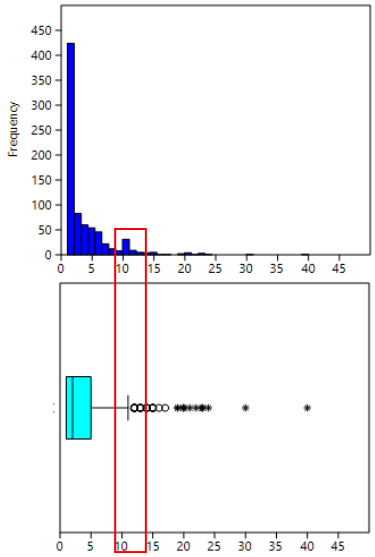

Figure 248 Histogram and box plot of frequencies observed for pottery (Past).

The spatial distribution of pottery frequencies fits with the Negative Binomial distribution with a *k*=0.349 and *p*=0.166 and with Kolmogorov Smirnov Test=0.911. This condition suggests randomness in the spatial distribution of the abundance of pottery per sampling unit (Figure 249).

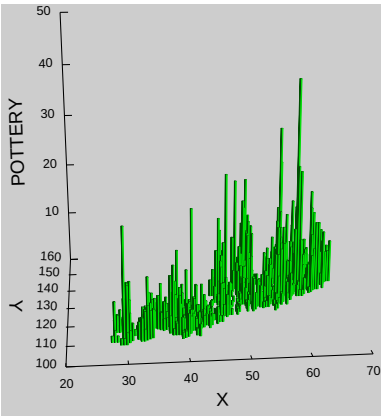

Figure 249 3D Histogram of pottery recovered during surveys of 2001 (Systat 13).

74% of pottery is located in 50% of the effectively surveyed area, in such a way that only 48 cells show more than 10 fragments.

The spatial centroid of the area with pottery, calculated using an abundance weighted mean spatial center is x=52.505099 and y=131.621241, with 11.34 m of standard deviation along the x axis and 10.45 m along the y axis. A standard deviation ellipse with a long axis of 42.23 m

and a short one of 11.04 m delimits an area of 366.17 square meters, where most data count appears. Within such an area, it has been estimated an average density of 1.60 pottery fragments per square meter.

The spatial distribution of the abundance of pottery per sampling unit shows a Global Moran's *I* of -0.000572**.** The theoretical (expected) value assuming spatial autocorrelation (lack of spatial independence) is -0.000685 and the standard error of *I* is -0.000685. The test of significance using the normality assumption gave a *z* value of 0.165562, non-significant value. Consequently, we can accept that the spatial distribution of pottery is not significantly different than the expected value under a random distribution. This is what would be expected in the case of quite same frequency of pottery in every spatial location. Such results are comparable with those of the Geary statistic (for this case *C*=0.999971) and Getis-Ord general G (*G*=0.012146).

The Moran's *I* Correlogram (Figure 250) has been calculated for uniform class distance intervals of 1 meter and taking into account a 10 meters active lag distance. *I* value at the starting point of the function is 0.458, and drops quite abruptly above the expected value for randomness until the 4 meter, where the *I* value is located on the line (corresponding to spatial randomness). Between 5 and 7 values are a little bit above the expected value for randomness, while at 8 and 9 meter they are located on the line (randomness).

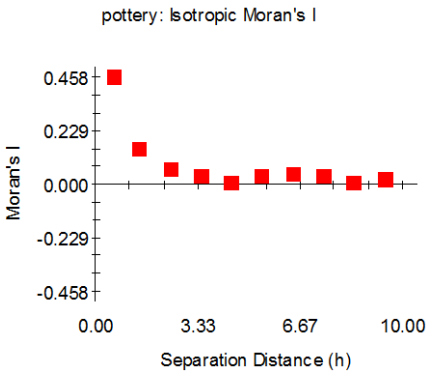

Figure 250 Moran's I Correlogram for pottery recovered during surveys of 2001 (GS+).

A continuous regular spatial pattern characterizes the initial slope of the values (between the starting point of the function and 4 meter), suggesting the presence of positive spatial autocorrelation, and spatial continuity in very small areas of less than 4 meters of radius.

Using sampling units selected by local indicators of spatial association, as overabundant in respect to others, we obtain a spatial distribution of concentrations (more than 10 fragments of pottery). Within the convex hull defined by this selected locations, there is statistically significant degree of clustering. KDE shows how concentrations in the North-East corner generate spatial continuity in this area, and contribute to differentiate it from the rest of the surveyed area (Figures 251A and B).

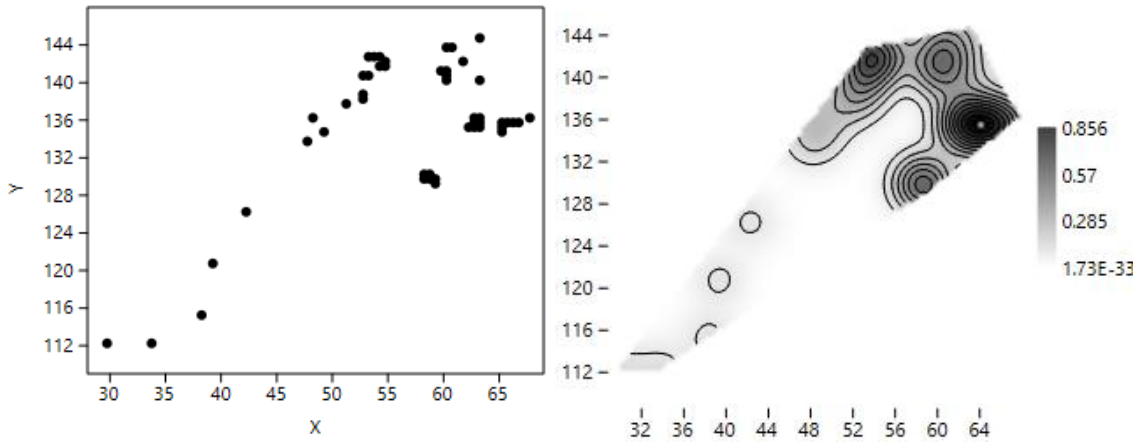

Figure 251 A)Spatial distribution of cells with more than 10 fragments of pottery (surveys 2001) (Past). B)KDE of such cells (surveys of 2001) (Past).

We have explored the possible presence of anisotropic variation (Figure 252). 45º and 135º directions concentrate the evidence of anisotropy, what would coincide with an apparent deformation of the main concentration, in the direction of the estimated ancient lake shoreline, directed towards South-West.

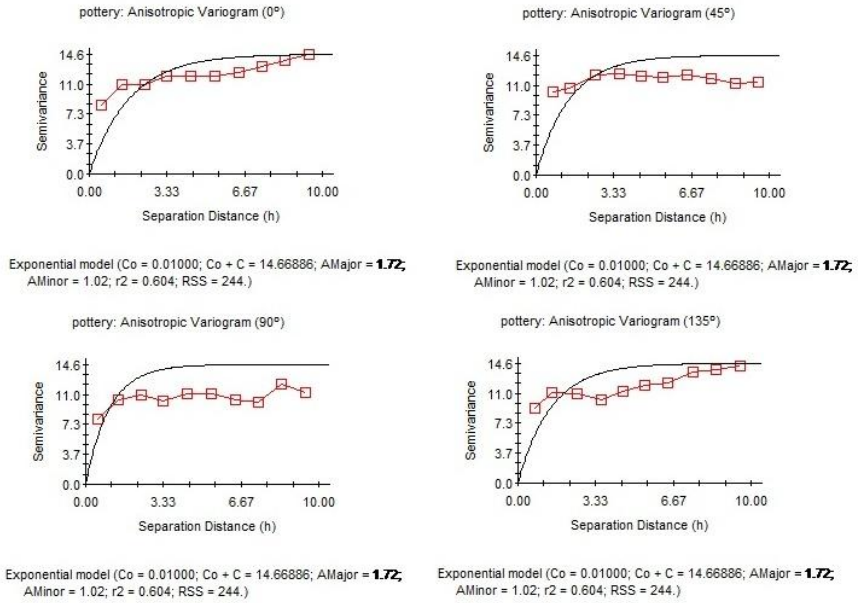

Figure 252 Anisotropic Variogram of pottery recovered during surveys of 2001 (GS+).

The graph of anisotropic Semivariance Surface or Variogram Map (Figure 253) shows the relatively low impact of anisotropy and the relatively high area of spatial continuity in all directions. The effects of anisotropy are only relevant beyond 9 meters of radius.

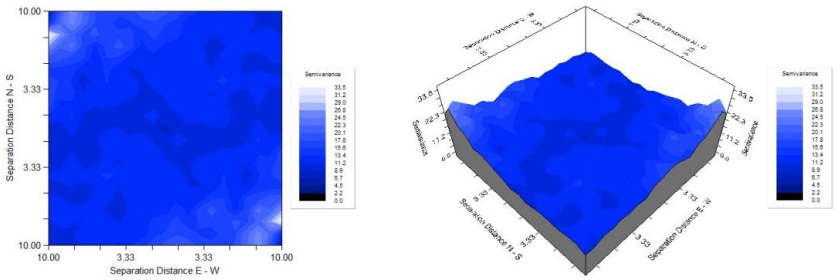

Figure 253 Variogram Map of pottery recovered during surveys of 2001 (GS+).

The scarce differences in the Variogram Map are distributed in each sectors of the surveyed area; however, a higher effect is observable on the North-West and South-East corners, confirming that it could be caused by the unsurveyed areas, beyond the surveyed region.

An exponential model (Figure 254) has been fitted to the empirical variogram; in this case, Nugget Variance, C_0 =1.15000, Sill, C_0+C = 11.87000 and Range, A_0= 0.50, showing a global fit of 81.3%.

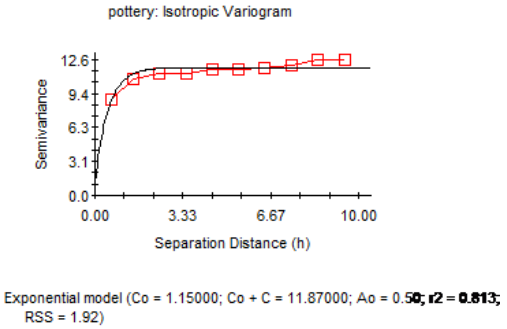

Figure 254 Exponential Isotropic Variogram for pottery recovered during surveys of 2001 (GS+).

Using this model, an inverse distance weighting algorithm has allowed building a spatial predictive model of pottery in this reference area (Figure 255). Such category seems to be distributed irregularly, with very small continuity at medium distances. Points of maximum concentration, however, are not random nor overdispersed, but they offer a significant trend, concentrated on the North-East corner of the surveyed area. It is relevant the fact that anisotropy, at the sector of maximum concentration of pottery, follows a different direction: East-West, instead of the strong orientation North-East-South-West for the areas with less accumulation.

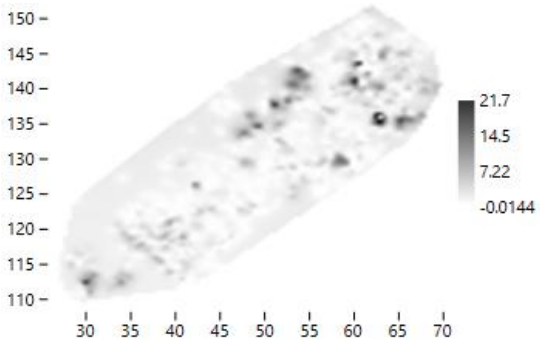

Figure 255 Graphic results of Inverse Distance Weighting calculated for pottery recovered during surveys of 2001 (Past).

7.6.1.1 Sub-categories of pottery

We have explored the spatial distribution of different pottery functional categories. Nevertheless, frequencies are low in quantitative terms, and we have limited the analysis to an exploration of presence/absence in the surveyed area.

7.6.1.2 Jars

95 fragments ascribable to this category were identified and counted; they are spatially distributed in 79 sampling units, while 1381 cells were empty. Sampling units with jars are spatially distributed according to Figure 256.

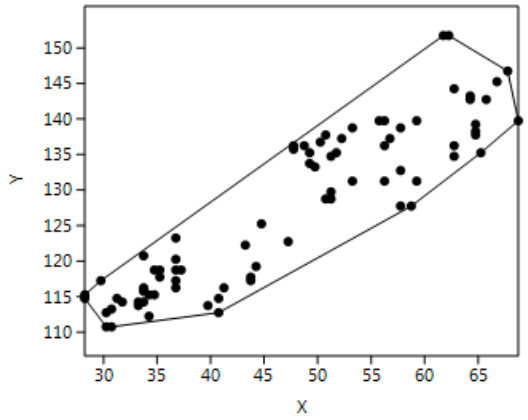

Figure 256 Spatial distribution of sampling units where jars fragments have been recovered during surveys of 2001 (Past).

Ripley's *k* analysis on the distance between sampling units with jars evidence suggests the possibility of some degree of spatial clustering below 18 meter, at the scale of all the reference area (Figure 257).

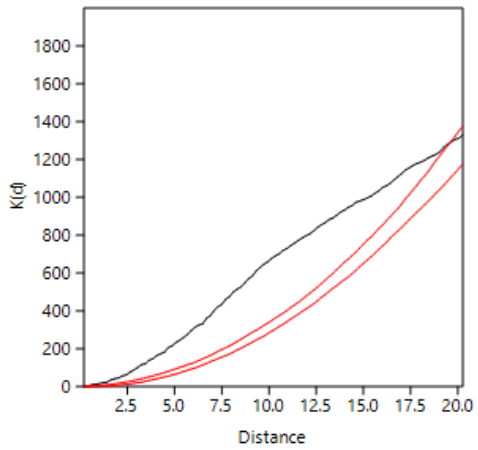

Figure 257 Ripley's *k* analysis on the distance between sampling units with jars, recorded in surveys of 2001 (Past).

Such clustering is also relevant, within the convex hull defined by those sampling units where pottery has been recovered (Clark and Evans test). A KDE (Figure 258) shows the relevant presence of two predominant concentrations located respectively between x=26-40 and y=109-123 and between x=47-55 and y=132-140.

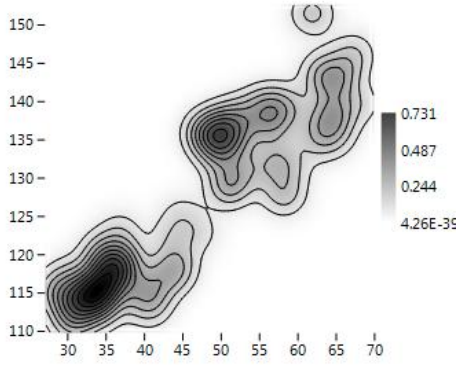

Figure 258 KDE of sampling units where jars have been recovered during surveys of 2001 (Past).

When considering the raw quantity of jars at each cell, the probability density distribution of spatial frequencies does not follow a J-shaped distribution. A majority of sampling units have raw counts of jars of less than 2 elements (global mean = 1.20 jar per sampling unit, with a comparatively small standard deviation, 0.46). 14 cells are distinguished from the majority (interpretable as outliers), with 2 and 3 fragments of jars (as showed in Figure 259).

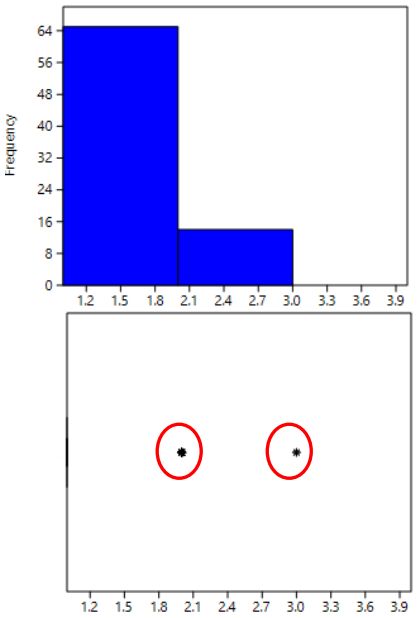

Figure 259 Histogram and box plot of frequencies observed for jars (Past).

The spatial distribution of jars is fitted both with a Negative Binomial distribution, with k=0.184 and p=0.739, and a Geometric distribution with p=0.939 and a Kolmogorov Smirnov Test=1. This is what is expected when, as in this case, the sample consists in predominant empty sampling units and similar frequencies values in all non-empty cells (Figure 260).

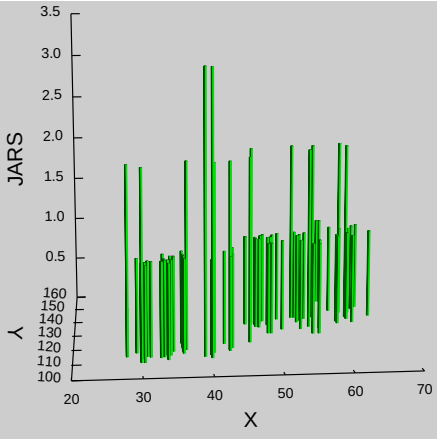

Figure 260 3D Histogram of jars recovered during surveys of 2001 (Systat 13).

82% of jars is located in 68% of the effectively surveyed area, in such a way that 18% of cells show more than 1 item, and they are located in 32% of the effectively surveyed area (representing, the value>1 outliers).

The spatial distribution of count data per sampling unit for jars shows a Global Moran's *I* of -0.000656. The theoretical (expected) value assuming spatial autocorrelation (lack of spatial Independence) is -0.000685 and the standard error of *I* is 0.000685. The test of significance using the normality assumption gave a *z* value of 0.043362, highly non-significant value. Such results are comparable with those of the Geary statistics (*C*=0.998997) and Getis-Ord general G (*G*=0.007870). Consequently, we can accept that the spatial distribution of jars could not be significantly different than the expected value under a random distribution. This is what would be expected in the case of similar frequency of occurrence within every spatial location.

Moran's *I* Correlogram (Figure 261) shows very low values of autocorrelation, but always with the 10 meter radius range over the level of positive autocorrelation. The quantity of jar fragments per sampling unit is very low, and therefore spatial continuity is more a question of the number of non-empty cells than a question of relevant peaks in spatial frequency.

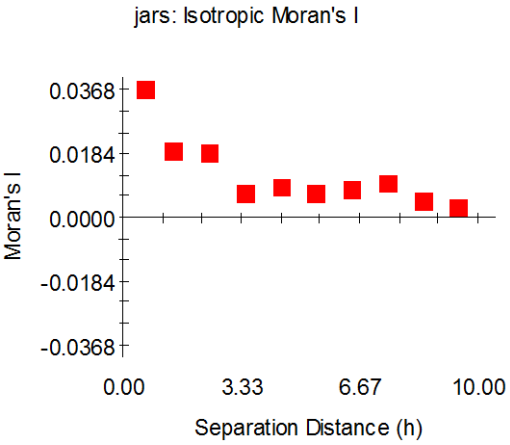

Figure 261 Moran's I Correlogram for jars recovered during surveys of 2001 (GS+).

Using sampling units selected by local indicators of spatial association, as overabundant in respect to others, we obtain a spatial distribution of concentrations or more than 2 fragments of

jars. Within the convex hull defined by this selected locations, the Clark and Evans test (p<0) confirms their overdispersion (Figure 262).

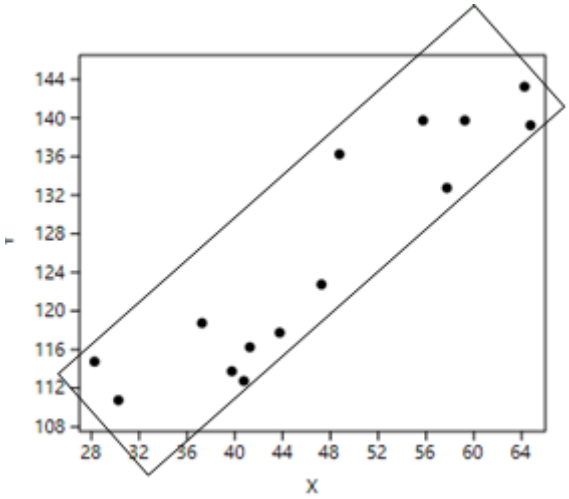

Figure 262 Spatial distribution of sampling units where more than 2 fragments of jars have been recorded during surveys of 2001 (Past).

We have explored the possible presence of anisotropic variation in the spatial distribution of jars (Figure 263). All semivariograms are flat, with extremely reduced ranges, insisting on the idea of randomness in spatial frequency differences.

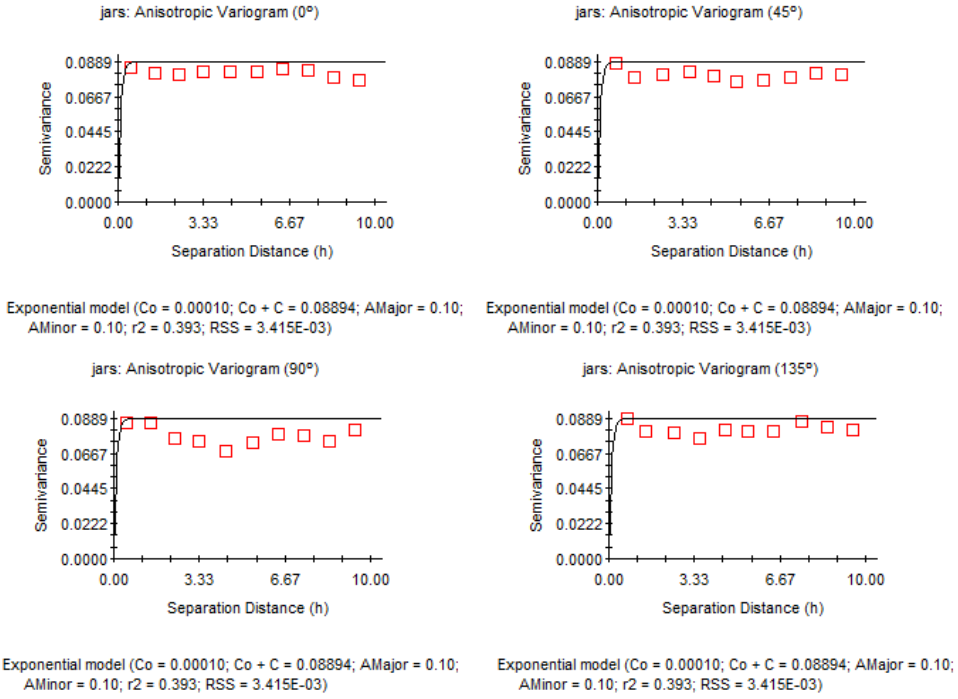

Figure 263 Anisotropic Variogram of jars recovered during surveys of 2001 (GS+).

The graph of anisotropic Semivariance Surface or Variogram Map (Figure 264) shows extreme anisotropy and the lacks of spatial continuity in frequency, even at small distances.

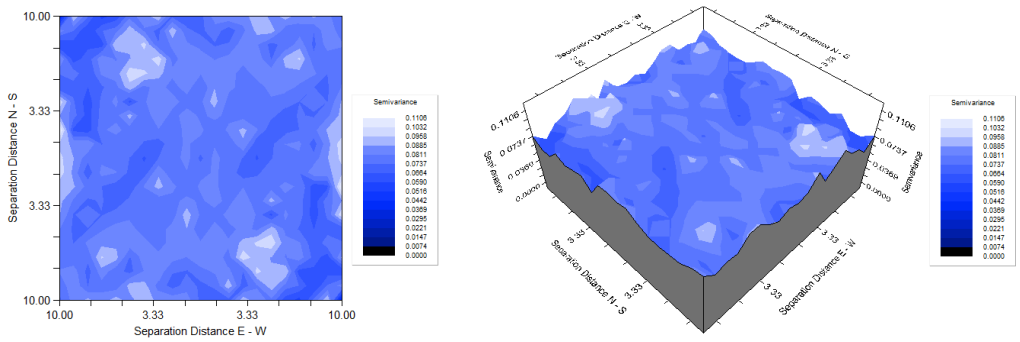

Figure 264 Variogram Map of jars recovered during surveys of 2001 (GS+).

The exponential model that best fits the data -C_0 (nugget variance) =0.000480, C_0+C (sill) = 0.08050 and A_0 (Range) = 0.013 (Figure 265) explains only 39.30%.

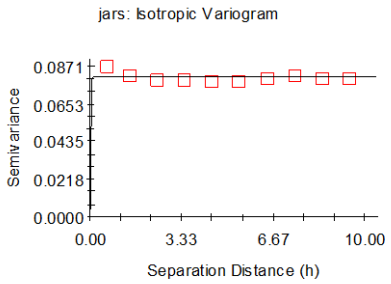

Exponential model (Co = 0.00480; Co + C = 0.08050; Ao = 0.01; **r2 = 0.000**; RSS = 5.934E-05)

Figure 265 Exponential Isotropic Variogram for jars recovered during surveys of 2001 (GS+).

A prediction model obtained by Kriging interpolation (Figure 266), although not very reliable, gives an image of heterogeneity based on two differentiated sectors, one in the centre of the graph, and another one in the South-Western extreme corner. There are interesting minor concentrations (outliers) following the main axis of the surveyed area, parallel to the ancient estimated lake shoreline.

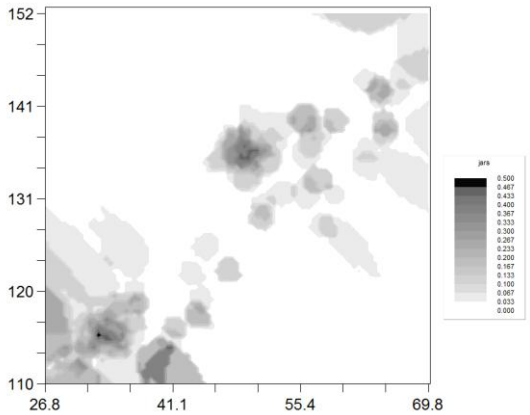

Figure 266 Graphic results of Kriging calculated for jars recovered during surveys of 2001 (Past).

7.6.1.3 Closed Forms

Taking into account the above results for jars –a typical example of closed form-, we have added all other evidence for this category (jars, dolia and mugs). We have identified 187 fragments ascribable to closed forms; they are spatially distributed in 140 sampling units. Cells where fragments of ceramic closed forms have been identified are spatially distributed according to Figure 267.

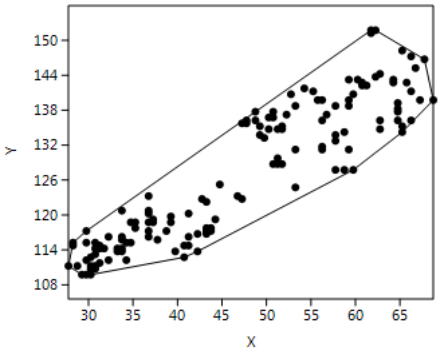

Figure 267 Spatial distribution of sampling units where ceramic closed forms have been recovered during surveys of 2001 (Past).

Ripley's *k* analysis on the distance between sampling units with fragments of ceramic closed forms suggests the possibility of some degree of spatial clustering below 18 meter, at the scale of all the reference area (Figure 268).

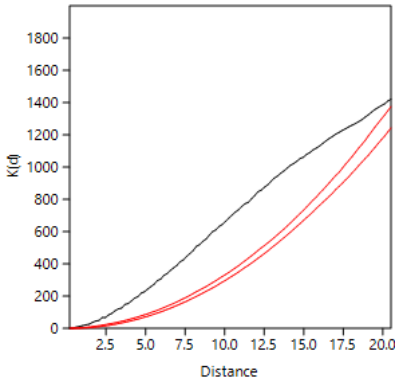

Figure 268 Ripley's *k* analysis on the distance between sampling units with closed forms, recorded in surveys of 2001 (Past).

Such clustering is also relevant within the convex hull defined by those sampling units where closed forms have been recovered (Clark and Evans test). A KDE (Figure 269) shows the relevant presence of two predominant concentrations located respectively between 27-45 x 109-120 y and between 47-67 x 130-143 y.

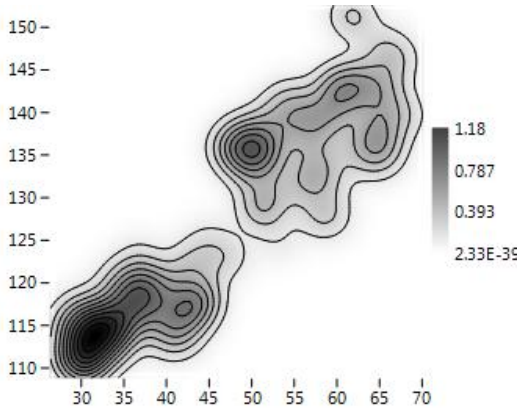

Figure 269 KDE of sampling units where closed forms have been recovered during surveys of 2001 (Past).

A majority of sampling units have raw counts of such pottery of less than 2 elements (global mean = 1.33 closed forms fragment per sampling unit). One cell is distinguished from the majority (interpretable as outlier), with 5 observables (Figure 270).

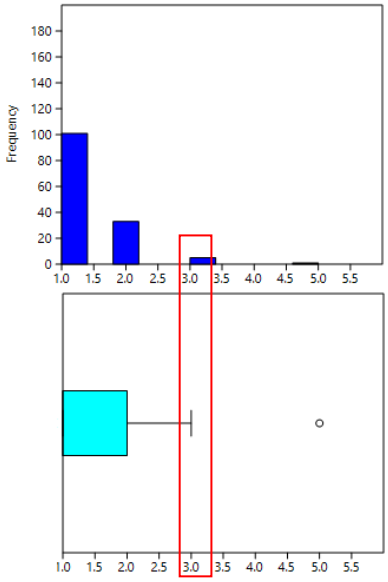

Figure 270 Histogram and box plot of frequencies observed for closed forms (Past).

The spatial distribution of ceramic closed forms is fitted with a Negative Binomial distribution with k=0.224 and p=0.636 with Kolmogorov Smirnov Test=1. This condition suggests randomness in the spatial distribution of the abundance of ceramic closed forms per sampling unit (Figure 271).

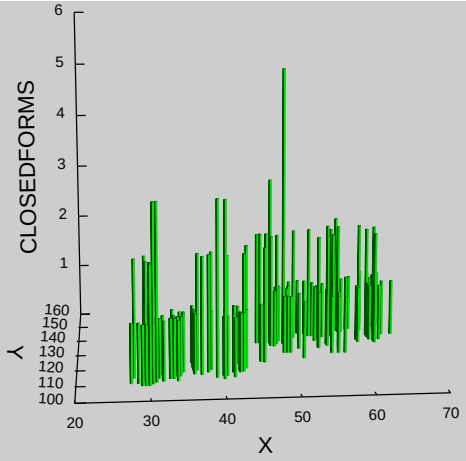

Figure 271 3D Histogram of closed forms recovered during surveys of 2001 (Systat 13).

97% of closed forms fragments are located in 99% of the effectively surveyed area, in such a way that only 1 cell shows more than 3 items (representing, this limit, the break point highlighted by both histogram and box plot).

The spatial distribution of count data per sampling unit for ceramic closed forms shows a Global Moran's *I* of -0.000625. The theoretical (expected) value assuming spatial autocorrelation (lack of spatial Independence) is -0.000685 and the standard error of *I* is 0.000685. The test of significance using the normality assumption gave a *z* value of 0.087822, highly non-significant value. Those results are comparable with those of the Geary statistics (*C*=0.999051) and Getis-Ord general G (*G*=0.009808). Consequently, we can accept that the spatial distribution of ceramic closed forms could not be significantly different than the expected value under a random distribution. This is what would be expected in the case of similar frequency of occurrence within every spatial location.

Moran's *I* Correlogram (Figure 272) shows very low values of autocorrelation, but always with the 10 metre radius ranging over the level of positive autocorrelation. The quantity of closed forms fragments per sampling unit is very low, and therefore spatial continuity is more a question of the number of non-empty cells, than a question of relevant peaks in spatial frequency.

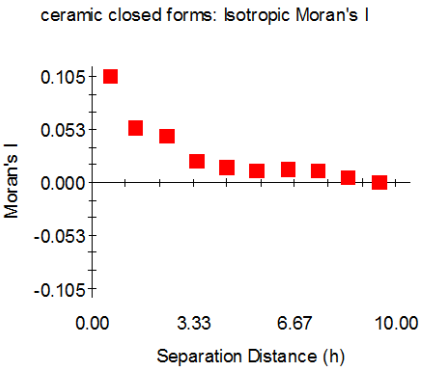

Figure 272 Moran's I Correlogram for closed forms recovered during surveys of 2001 (GS+).

We have explored the possible presence of anisotropy (Figure 273). Differences in the range are very scarce in the four variograms, and therefore we can conclude lack of anisotropy. It is interesting the fact that once we have increased the number of observations, by making more

general the pottery type, the degree of spatial continuity in all directions and ranges also increases.

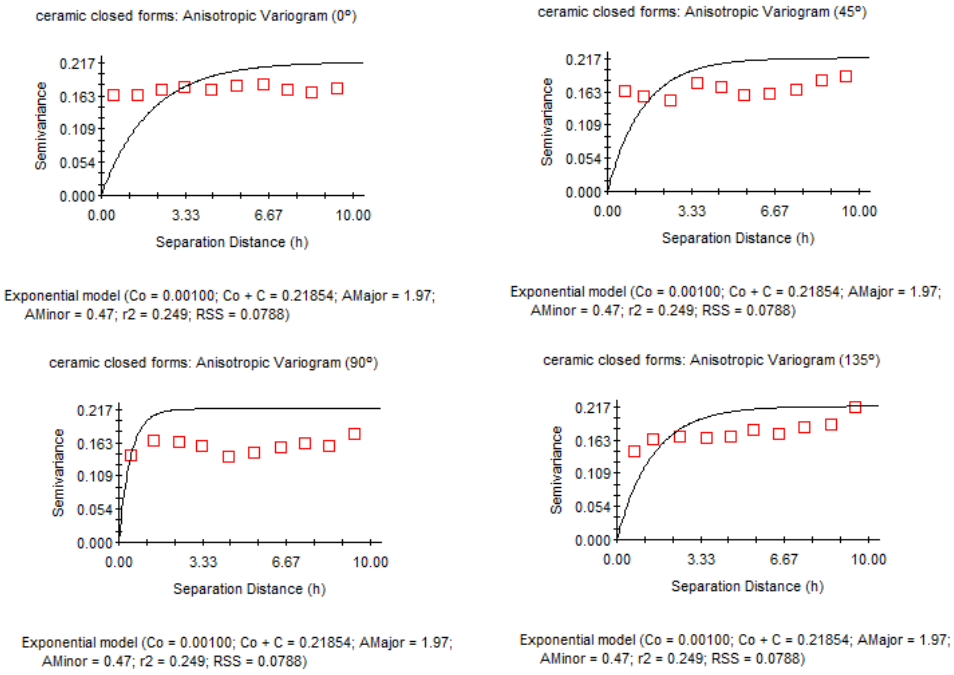

Figure 273 Anisotropic Variogram of closed forms recovered during surveys of 2001 (GS+).

The graph of anisotropic Semivariance Surface or Variogram Map, confirms the less anisotropy than in the case of the spatial frequency of jars alone (Figure 274).

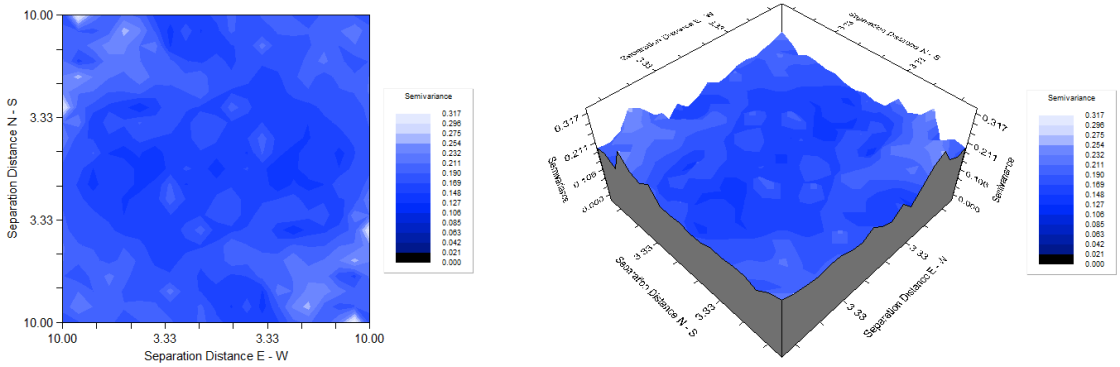

Figure 274 Variogram Map of closed forms recovered during surveys of 2001 (GS+).

The best fitted exponential model - C_0 (nugget variance) =0.00010, C_0+C (sill) = 0.16920 and A_0 (Range) = 0.25- explains a mere 31.9% (Figure 275). It is flat around the line for randomness, indicating the lack of spatial continuity, even at small distances.

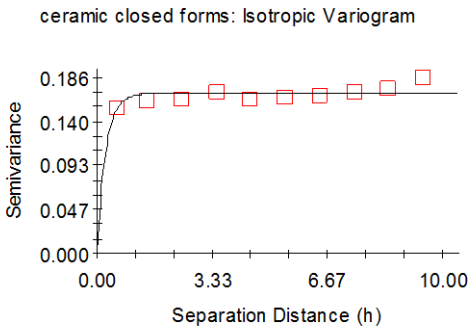

Exponential model (Co = 0.00010; Co + C = 0.16920; Ao = 0.25; **r2 = 0.319;** RSS = 4.365E-04)

Figure 275 Exponential Isotropic Variogram for closed forms recovered during surveys of 2001 (GS+).

An unreliable but interesting interpolated model by kriging (Figure 276) gives a result similar to that obtained in the case of jars alone, with two main concentrations at ca. x=26-45 and y=109-120 and between ca. x=47-67 and y=130-143. Notice the differently oriented anisotropy in the South-West and in the North-Eastern corners.

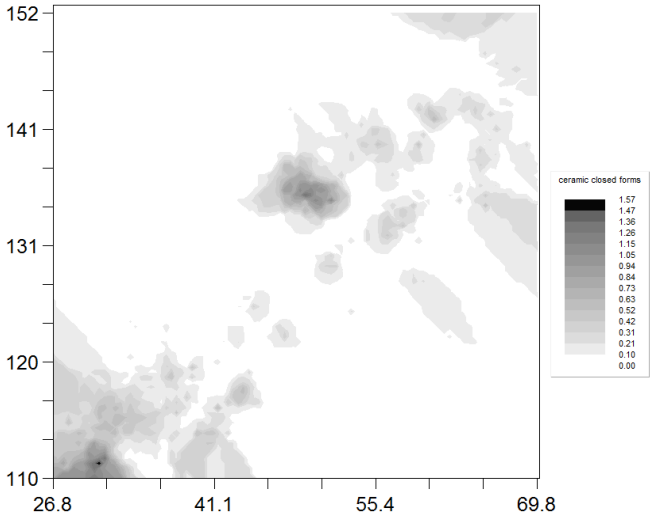

Figure 276 Graphic results of Kriging calculated for closed forms recovered during surveys of 2001 (Past).

7.6.1.4 Shallow Bowls

95 fragments ascribable to shallow bowls were identified and counted; they are spatially distributed in 78 sampling units. Cells where shallow bowls have been identified are spatially distributed according to Figure 277.

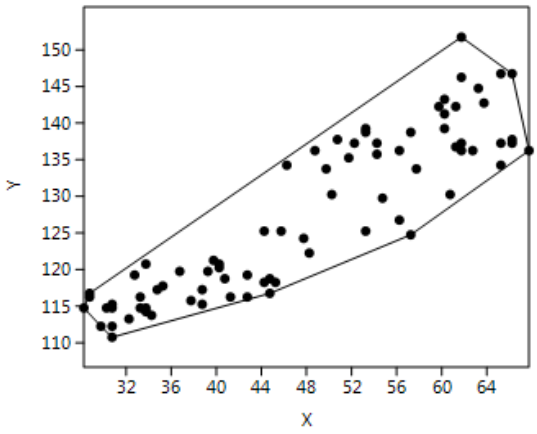

Figure 277 Spatial distribution of sampling units where shallow bowls have been recovered during surveys of 2001 (Past).

Ripley's *k* analysis on the distance between sampling units with shallow bowls evidence suggests the possibility of some degree of spatial clustering, at the scale of the global reference area (Figure 278).

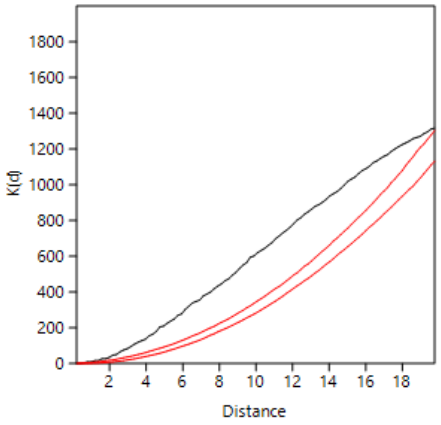

Figure 278 Ripley's *k* analysis on the distance between sampling units with shallow bowls, recorded in surveys of 2001 (Past).

Within the convex hull defined by those sample units with a presence of shalow bowls, the null hypothesis of a random pattern cannot be rejected (Clark and Evans Test (p=0.13), what indicates the possibility that equidistant cells have the same probability of counting one or more fragments of shallow bowls. However, a Kernel Density Estimation (Figure 279) shows a configuration that appears to be very similar to the clustered distribution of jars, in two predominant concentrations located respectively between x=27-45 and y=109-120 and between 4x=7-70 and y=130-147. Some minor concentrations (outliers) are also distinguished, in such a way that the apparent global randomness can be a consequence of the random distribution of cells with highest frequency.

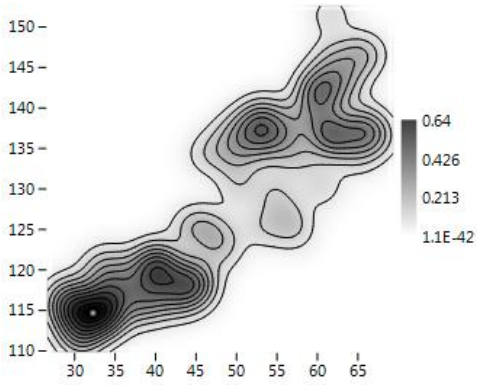

Figure 279 KDE of sampling units where shallow bowls have been recovered during surveys of 2001 (Past).

When considering the raw quantity of shallow bowls fragments at each cell, the probability density distribution of spatial frequencies does not follow a J-shaped distribution. A majority of sampling units have raw counts of such pottery of less than 2 elements (global mean = 1.21 shallow bowl fragment per sampling unit, and a standard deviation of 0.63). 11 cells are distinguished from the majority (interpretable as outliers), with 2, 3 and 4 observables (Figure 280).

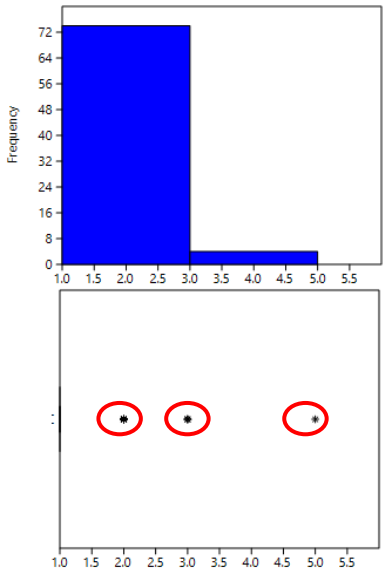

Figure 280 Histogram and box plot of frequencies observed for shallow bowls (Past).

The spatial distribution of shallow bowls fragments fits both a Negative Binomial distribution, with k=0.163 and p=0715, and a Geometric distribution, with p=0.939, with Kolmogorov Smirnov Test=1. This is what is expected when, as in this case, the sample consists in predominant empty sampling units and similar frequencies values in all non-empty cells are observed, obtaining randomness (as also showed in Figure 281).

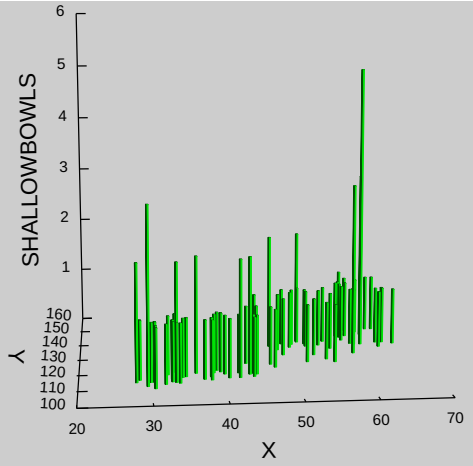

Figure 281 3D Histogram of shallow bowls recovered during surveys of 2001 (Systat 13).

71% of shallow bowls fragments are located in 86% of the effectively surveyed area, in such a way that 29% of cells show more than 1 item (representing, this limit, the break point highlighted by both histogram and box plot), and they are located in 14% of the effectively surveyed area.

The spatial distribution of count data per sampling unit for shallow bowls fragments shows a Global Moran's *I* of -0.000671. The theoretical (expected) value assuming spatial autocorrelation (lack of spatial independence) is -0.000685 and the standard error of *I* is 0.000685. The test of significance using the normality assumption gave a *z* value of 0.020337 highly non-significant value. Such results are comparable with those of the Geary statistics (*C*=0.999204) and Getis-Ord general G (*G*=0.007659). Consequently, we can accept that the spatial distribution of shallow bowls fragments could not be significantly different than the expected value under a random distribution. This is what would be expected in the case of predominant similar frequency of occurrence within quite every spatial location.

Moran's *I* Correlogram (Figure 282) shows extremely low values at the starting point of the function (0.0146), what gives a signal of randomness. The changes in positive and negative autocorrelation are not significant at such low values.

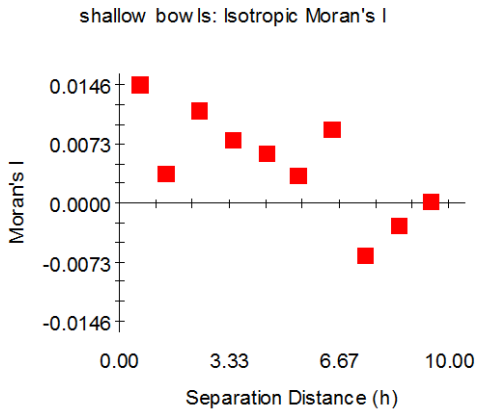

Figure 282 Moran's I Correlogram for shallow bowls recovered during surveys of 2001 (GS+).

Using sampling units selected by local indicators of spatial association as overabundant in respect to others, we obtain a spatial distribution of concentrations of more than 2 fragments of shallow bowls. Within the convex hull defined by this selected locations, there is overdispersion, according to the Clark Evans test (p<1) (Figure 283).

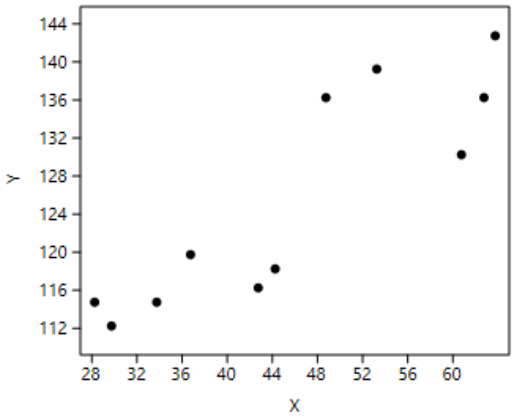

Figure 283 Spatial distribution of sampling units where more than 2 fragments of shallow bowls have been recovered during surveys of 2001 (Past).

We have explored the possible presence of anisotropic variation (Figure 284). The North-South direction (0º) seems to have less anisotropy than all other directions.

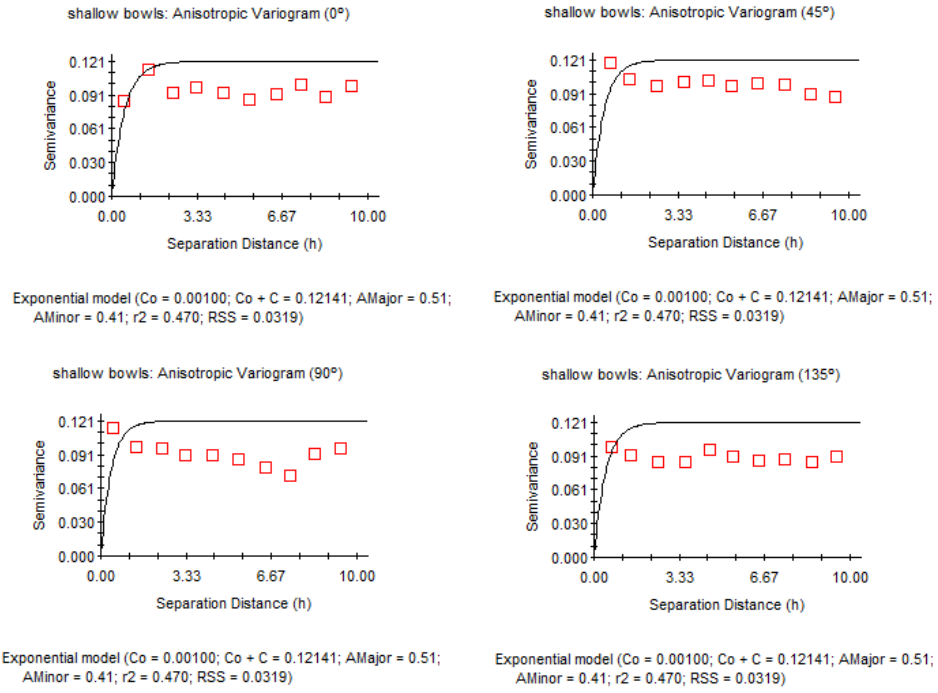

Figure 284 Anisotropic Variogram of shallow bowls recovered during surveys of 2001 (GS+).

The graph of anisotropic Semivariance Surface or Variogram Map (Figure 285) suggests a relatively low impact of anisotropy, and a general pattern of spatial continuity in areas of 3 meters of radius in all directions, with higher continuity along the main axis of the surveyed area than in any other direction.

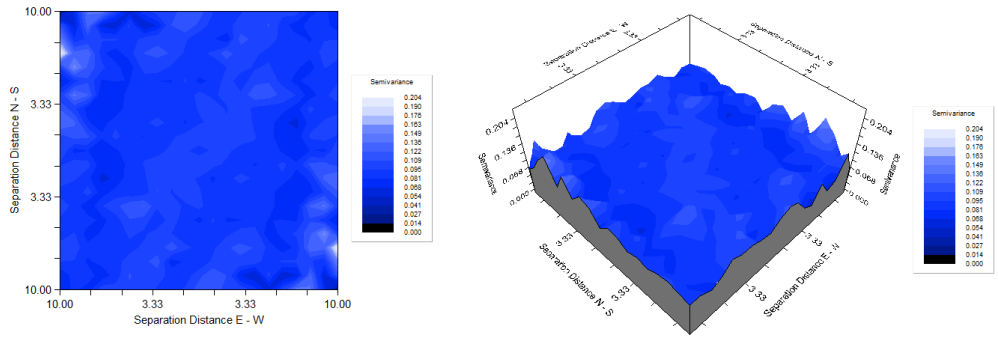

Figure 285 Exponential Isotropic Variogram for shallow bowls recovered during surveys of 2001 (GS+).

The best exponential model - C_0 (nugget variance) =0.00960, C_0+C (sill) = 0.09420 and A_0 (Range) = 0.01 (Figure 286) explains 47%. The variogram is fairly flat, suggesting the random nature of the spatial differences in the frequency of shallow bowls.

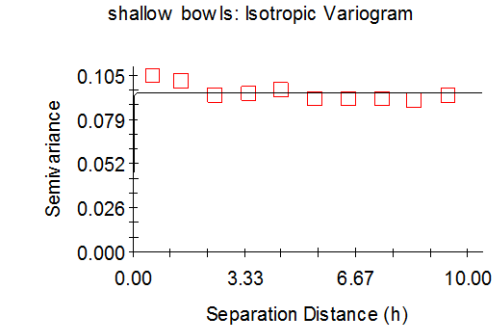

Exponential model (Co = 0.00960; Co + C = 0.09420; Ao = 0.01; **r2 = 0.000;**
RSS = 2.249E-04)

Figure 286 Exponential Isotropic Variogram for shallow bowls recovered during surveys of 2001 (GS+).

Although not entirely reliable, a predictive model for the frequency of shallow bowls fragments distribution (Figure 287) shows a pattern that it is not dissimilar for the equivalent model for other categories of pottery.

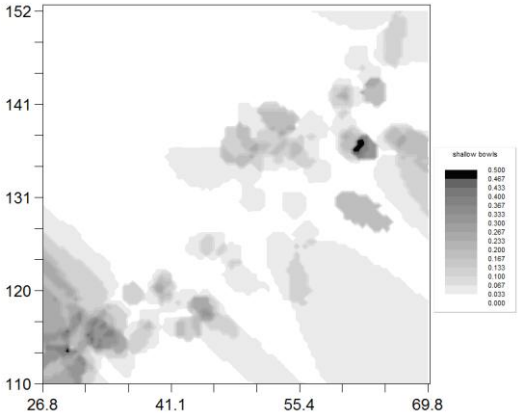

Figure 287 Graphic results of Kriging calculated for shallow bowls recovered during surveys of 2001 (Past).

7.6.1.5 Open forms

Taking into account the above results for shallow bowls –a typical example of open form-, we have added all other evidence for this category (bowls, cups and the mixture category of bowls/shallow bowls and cups). 140 fragments ascribable to open forms were identified and counted; they are spatially distributed in 105 sampling units. Sampling units where ceramic opened forms have been identified are spatially distributed according to Figure 288.

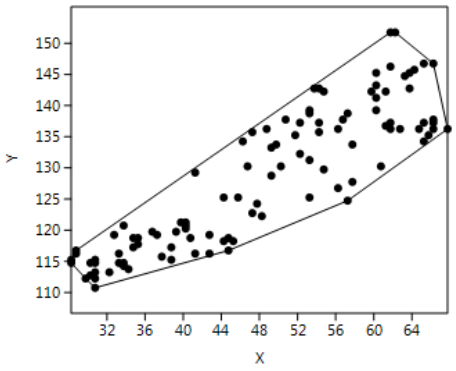

Figure 288 Spatial distribution of cells where ceramic open forms fragments have been recovered (Past).

Ripley's *k* analysis on the distance between sampling units with open forms evidence suggests the possibility of some degree of spatial clustering, at the scale of global reference area (Figure 289).

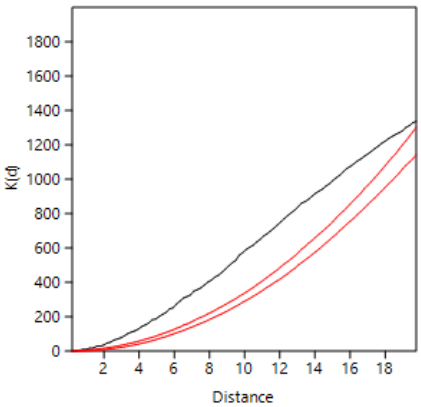

Figure 289 Ripley's *k* analysis on the distance between sampling units with open forms, recorded in surveys of 2001 (Past).

Within the convex hull defined by those sampling units with a presence of open forms, the null hypothesis of a random pattern cannot be rejected (Clark and Evans Test). A Kernel Density Estimation (Figure 290) shows, however, two differentiated sectors located respectively between 27-45 x 109-124 y and between 50-70 x 130-147 y.

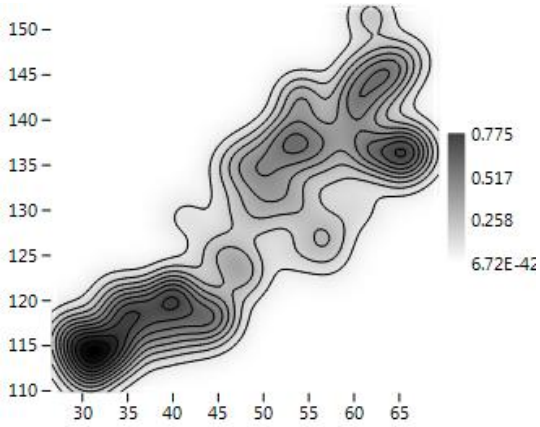

Figure 290 KDE of sampling units where open forms have been recovered during surveys of 2001 (Past).

When considering the raw quantity of open forms fragments at each cell, the probability density distribution of spatial frequencies does not follow a J-shaped distribution. A majority of sampling units have raw counts of ceramic open forms of less than 2 elements (global mean = 1.33). 25 cells are distinguished from the majority (interpretable as outliers), with 2, 3 and 5 observables (Figure 291).

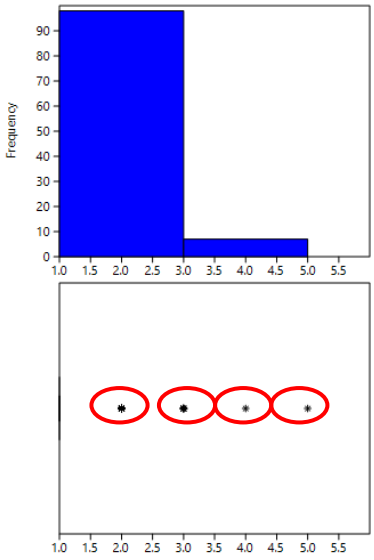

Figure 291 Histogram and box plot of frequencies observed for open forms (Past).

The spatial distribution of open forms fragments is fitted with a Negative Binomial distribution, with k=0.155 and p=0.618 and with Kolmogorov Smirnov Test=1. This condition suggests randomness in the spatial distribution of the abundance of open forms fragments per sampling unit (Figure 292).

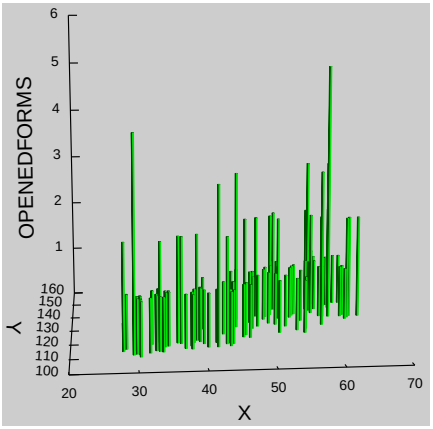

Figure 292 3D Histogram of open forms recovered during surveys of 2001 (Systat 13).

57% of open forms fragments are located in 76% of the effectively surveyed area, in such a way that 43% of cells show more than 1 item (representing, this limit, the break point highlighted by both histogram and boxplot), and they are located in 43% of the effectively surveyed area.

The spatial distribution of count data per sampling unit for open forms fragments shows a Global Moran's *I* of -0.000679. The theoretical (expected) value assuming spatial autocorrelation (lack of spatial independence) is -0.000685 and the standard error of *I* is 0.000685. The test of significance using the normality assumption gave a *z* value of 0.008830, highly non-significant value. Such results are comparable with those of the Geary statistics (C=0.999320) and Getis-Ord general G (=0.007024). Consequently, we can accept that the spatial distribution of open forms fragments could not be significantly different than the expected value under a random distribution. This is what would be expected in the case of predominant similar frequency of occurrence, within quite every spatial location.

Moran's *I* Correlogram (Figure 293) shows extremely low values at the starting point of the function (0.0233), what gives a signal of randomness. The changes in positive and negative autocorrelation are not significant at such low values.

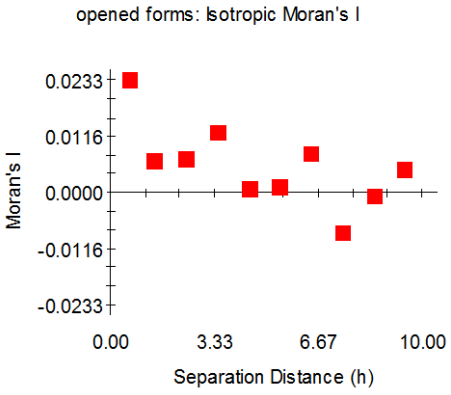

Figure 293 Moran's I Correlogram for open forms recovered during surveys of 2001 (GS+).

Using sampling units selected by local indicators of spatial association, as overabundant in respect to others, we obtain a spatial distribution of concentrations of more than 2 fragments of open forms. Within the convex hull defined by this selected locations, there is overdispersion, according to the Clark Evans test ($p<1$) (Figure 294).

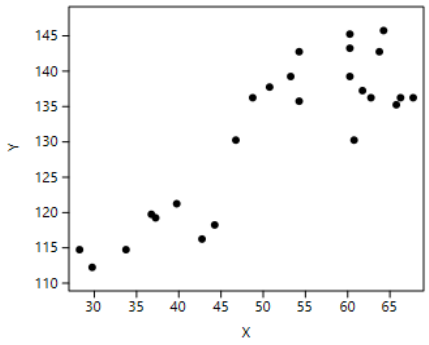

Figure 294 Spatial distribution of sampling units with more than 2 fragments of open forms (surveys of 2001) (Past).

We have explored the possible presence of anisotropic variation (Figure 295). The North-East-South-West direction (45º) and East-West (90º) seem to have less anisotropy than all other directions.

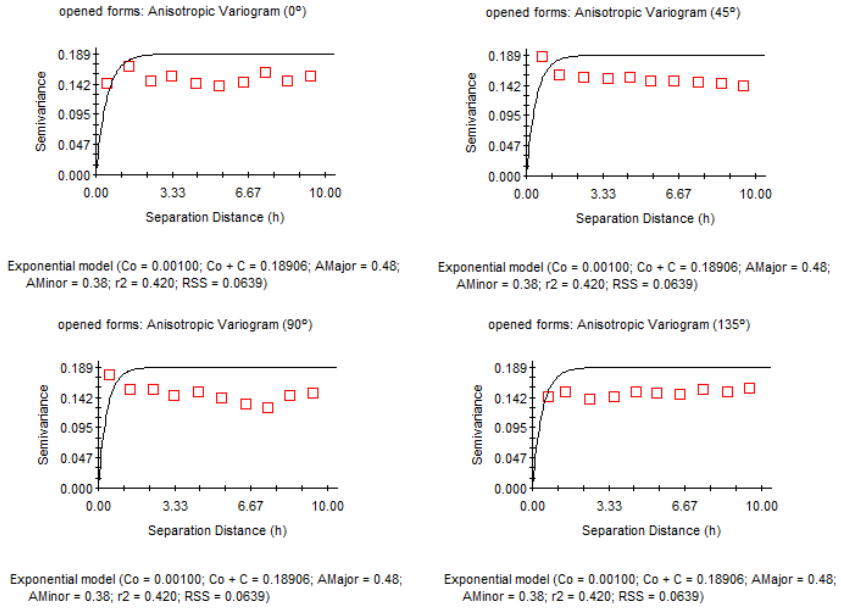

Figure 295 Anisotropic Variogram of open forms recovered during surveys of 2001 (GS+).

The graph of anisotropic Semivariance Surface or Variogram Map (Figure 296) suggests a slightly higher impact of anisotropy, still maintaining a general pattern of spatial continuity in very small areas of less than 3 meters of radius in all directions.

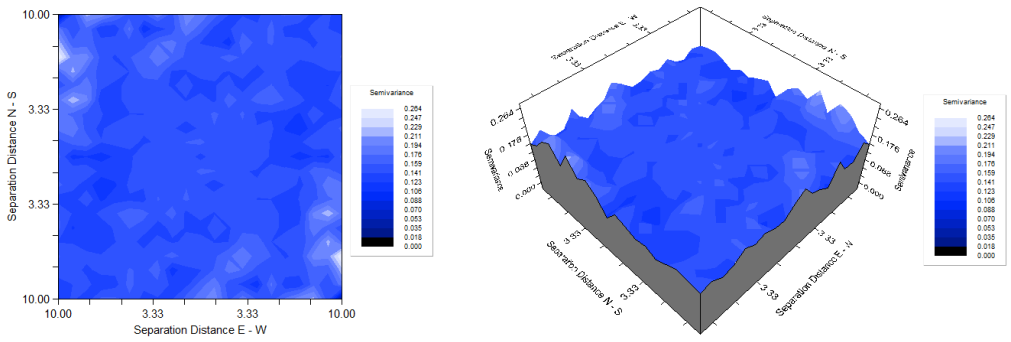

Figure 296 Variogram Map of open forms recovered during surveys of 2001 (GS+).

The best fitted exponential model - C_0 (nugget variance) =0.01460, C_0+C (sill) = 0.15020 and A_0 (Range) = 0.01 (Figure 297) explains 42% of spatial variance. As in the majority of cases in the sector, it is flat, what suggests the strong randomness in the spatial frequencies difference.

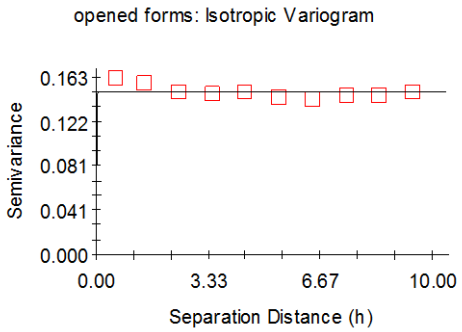

Exponential model (Co = 0.01460; Co + C = 0.15020; Ao = 0.01; **r2 = 0.000;**
RSS = 3.282E-04)

Figure 297 Exponential Isotropic Variogram for open forms recovered during surveys of 2001 (GS+).

Although not entirely reliable, a predictive model for the frequency of open forms fragments distribution (Figure 298) shows a pattern that it is not dissimilar for the equivalent model for other categories of pottery.

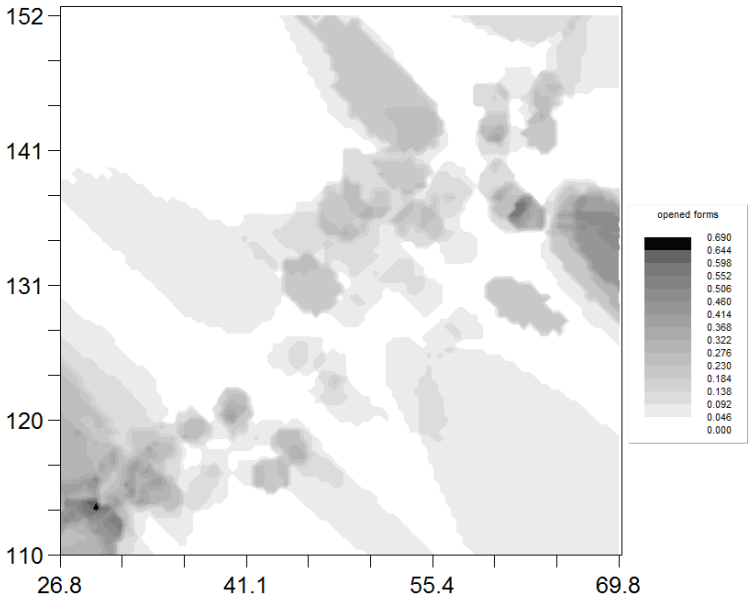

Figure 298 Graphic results of Kriging calculated for open forms recovered during surveys of 2001 (Past).

7.7 Wooden remains

As above mentioned in chapter 6, this more general category includes two sub-classes (wooden fragments and wooden horizontal posts) and the intra-site spatial analysis was performed separately for each one of them.

7.7.1 General Wooden Remains (excluding vertical posts)

146 wooden fragments were identified and counted; they are spatially distributed in 73 sampling units. Cells where wooden fragments have been identified are distributed according to the Figure 299.

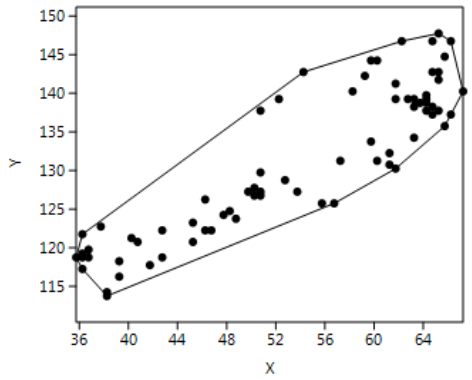

Figure 299 spatial distribution of sampling units where wooden remains have been recorded during surveys of 2001 (Past).

Ripley's *k* analysis on the distance between sampling units with wooden fragments evidence suggests the possibility of some degree of spatial clustering, at the scale of global reference area (Figure 300).

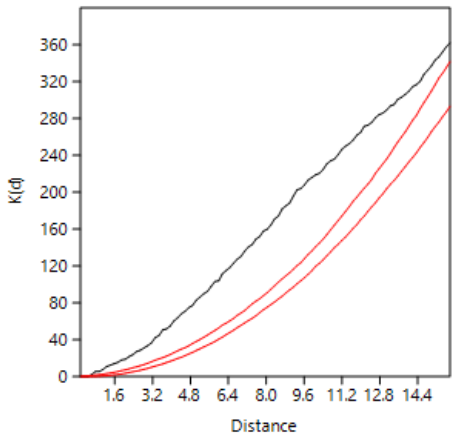

Figure 300 Ripley's *k* analysis on the distance between sampling units with wooden fragments, recorded in surveys of 2001 (Past).

Within the convex hull defined by those sampling units with a presence of wooden fragments, the null hypothesis of a random pattern cannot be rejected (according to Clark and Evans Test (p=0.99). A Kernel Density Estimation (Figure 301) shows, however, three areas of higher density, spatially located between x=30-40 and y=116-122, between x=45-55 and y=120-130 and between x=60-68 and y=133-142.

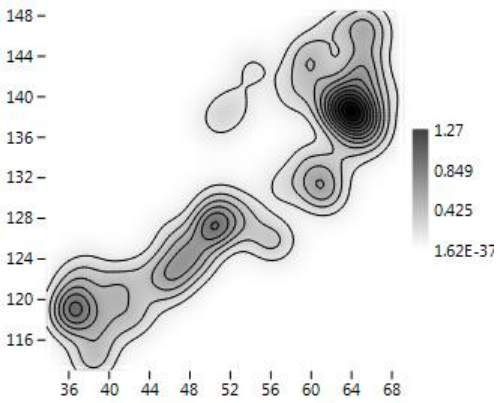

Figure 301 KDE of sampling units where wooden fragments have been recovered during surveys of 2001 (Past).

When considering the raw quantity of wooden fragments at each cell, the probability density distribution of spatial frequencies follows a J-shaped distribution. A majority of sampling units have raw counts of wooden fragments of less than 3 elements (global mean = 2 wooden fragments per sampling unit). Because of the scarce presence of sampling units with more than 3 wooden fragments, the box plot shows values of 4, 7, 9, 10, 12 and 15 occurrences as outliers (Figure 302).

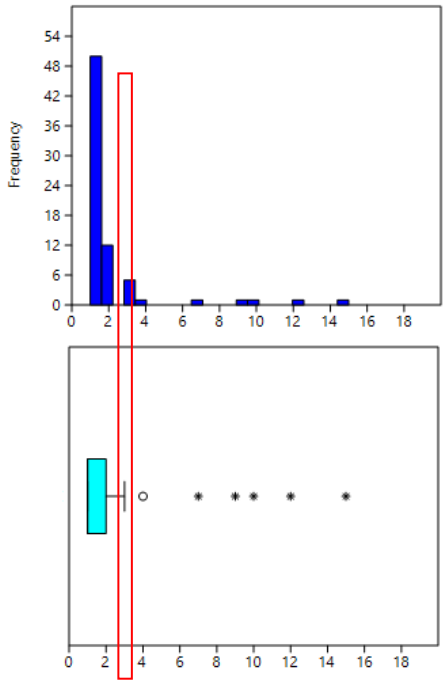

Figure 302 Histogram and box plot of frequencies observed for wooden fragments (Past).

The spatial distribution of wooden fragments can be fitted to a Negative Binomial distribution with k=0.042 and p=0.294 and Kolmogorov Smirnov Test=1. This condition suggests randomness in the spatial distribution of the abundance of wooden fragments per sampling unit (Figure 303).

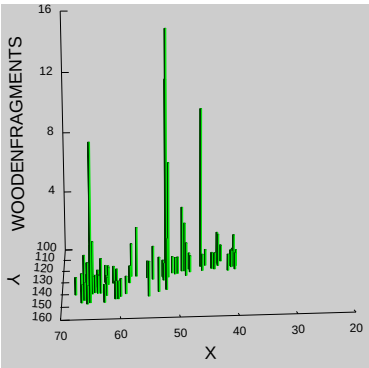

Figure 303 3D Histogram of wooden fragments recovered during surveys of 2001 (Systat 13).

61% of wooden fragments are located in the 4,5% of the effectively surveyed area, in such a way that only 6 cells show more than 3 items (representing, this limit, the break point highlighted by both histogram and box plot).

The spatial centroid of the area with wooden fragments, calculated using an abundance weighted mean spatial center is x=52.839041 and y=130.390411, with 9.15 m of standard deviation along the x axis and 9.23 m along the y axis. A standard deviation ellipse with a long axis of 35.96 m and a short one of 8.30 m delimits an area of 234.44 square meters, where most data count appears. It has been estimated an average density of 0.24 wooden fragments per square meter.

The spatial distribution of the abundance of wooden fragments per sampling unit shows a Global Moran's *I* of -0.000685, which corresponds with the theoretical (expected) value assuming absence of spatial autocorrelation (lack of spatial independence) and the standard error of *I* is -0.000685. The test of significance using the normality assumption gave an *z* value of -0.000018, a highly non-significant value. Consequently, the spatial distribution of wooden fragments is not significantly different than the expected value under a random distribution. This is what would be expected in case of predominant same frequency of wooden fragments in quite every spatial location. Such results are comparable with those of the Geary statistic (for this case *C*=1.001232) and Getis-Ord general G (*G*=0.047865).

The Moran's *I* Correlogram (Figure 304) shows extremely low values at the starting point of the function (0.0132), what gives a signal of randomness. The changes in positive and negative autocorrelation are not significant at such low values.

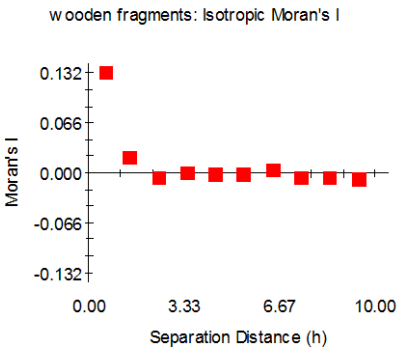

Figure 304 Moran's I Correlogram for wooden fragments recovered during surveys of 2001 (GS+).

This result suggests the presence of small dependent areas of 2-3 meters of radius and randomness beyond that threshold.

Using sampling units selected by local indicators of spatial association as overabundant in respect to others, we obtain a spatial distribution of concentrations of more than 3 wooden remains (Figure 305A**)**. Within the convex hull defined by this selected locations, the spatial distribution of these sampling units shows a random pattern since, according to the Clark and Evans Test, the null hypothesis of a random pattern cannot be rejected at $p<0.05$. Despite the absence of spatial clustering within such data, it is interesting to note that they are distributed according to the North-East-South-West line of concentration, as showed by the Kernel Density Estimation (Figure 305B).

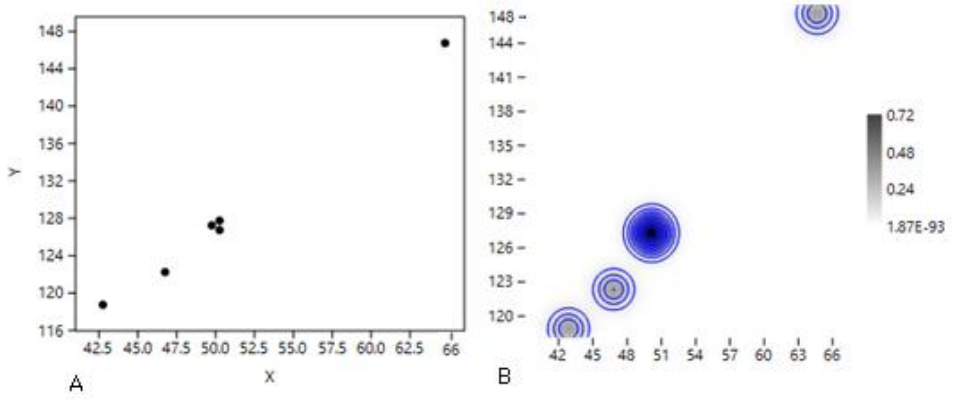

Figure 305 A) Spatial distribution of cells with more than 4wooden fragments (surveys of 2001) (Past). B) KDE of such cells (surveys of 2001) (Past).

We have explored the possible presence of anisotropic variation (Figure 306). The North-East-South-West (45º) and North-West-South-East (135º) direction seem to have less anisotropy than all other directions.

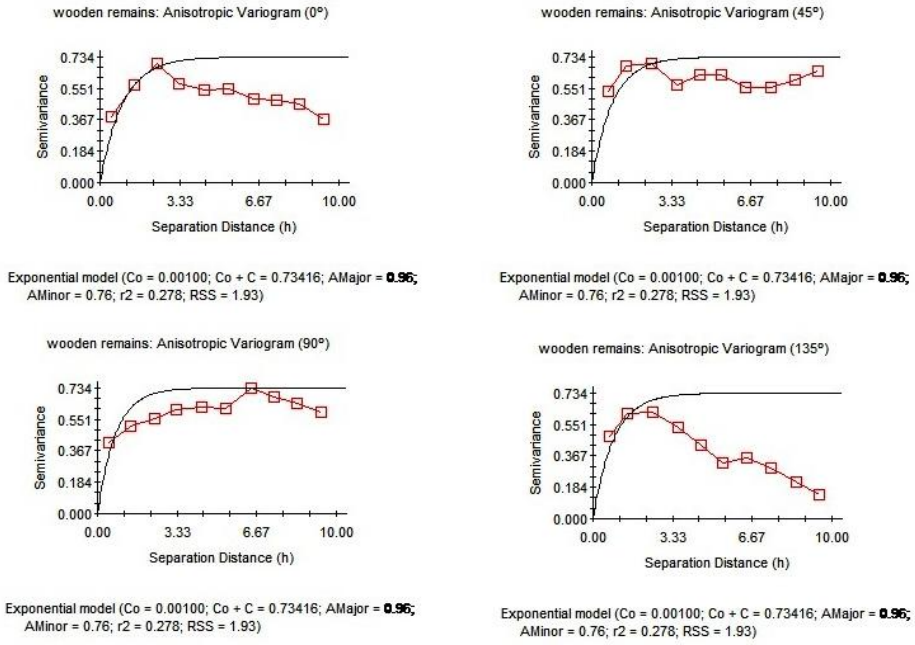

Figure 306 Anisotropic Variogram of wooden fragments recovered during surveys of 2001 (GS+).

The graph of anisotropic Semivariance Surface or Variogram Map (Figure 307) suggests a higher impact of anisotropy, even at small distances, what can be interpreted in terms of statistical independency in the spatial difference of wooden remains frequency.

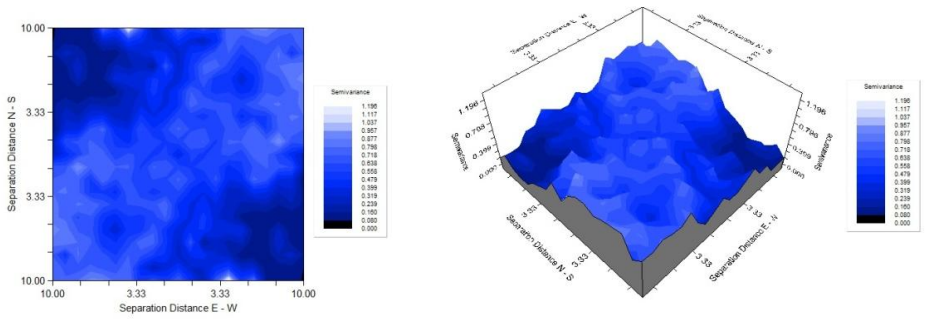

Figure 307 Variogram Map of wooden fragments recovered during surveys of 2001 (GS+).

The best fitted exponential model - C_0 (nugget variance)= 0.10100, C_0+C (sill)= 0.55400 and range (A)= 0.36. (Figure 308) explains 42% of spatial variance.

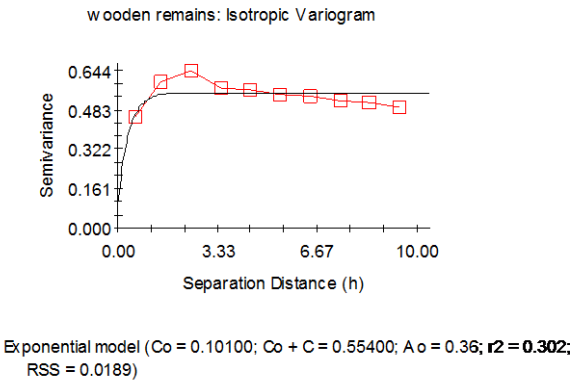

Figure 308 Exponential Isotropic Variogram for wooden fragments recovered during surveys of 2001 (GS+).

Although not entirely reliable, a predictive model for the frequency of wooden fragments distribution (Figure 309) shows a pattern where outlier/overabundant cells seem to be following the ancient estimated lake shoreline. It is important to note that the point of predicted higher concentration seems to be equidistant to the South-West and North-East corners, where most of all observations of other categories accumulated.

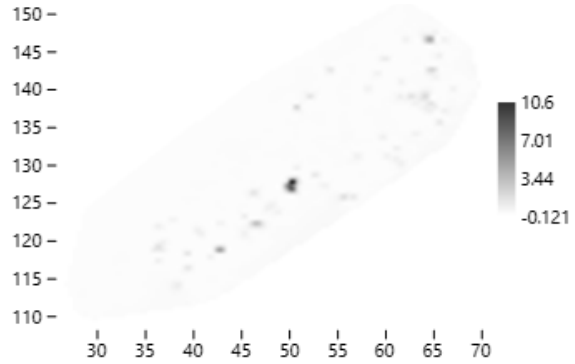

Figure 309 Graphic results of Kriging calculated for wooden fragments recovered during surveys of 2001 (Past).

7.7.2 Remains of horizontal posts

35 fragments related to horizontal posts were identified and counted; they are spatially distributed in 30 sampling units. Cells where remains of horizontal posts have been recovered are spatially distributed according to Figure 310**.**

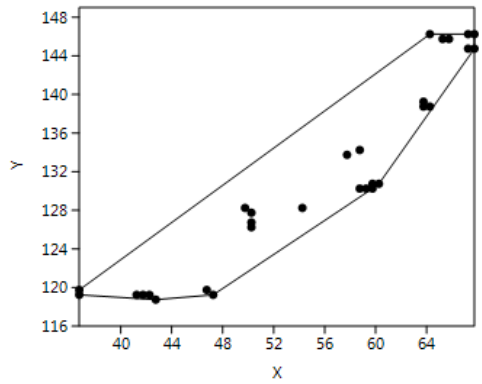

Figure 310 spatial distribution of sampling units where horizontal posts remains have been recorded during surveys of 2001 (Past).

Ripley's *k* analysis on the distance between sampling units with horizontal posts suggests the possibility of some degree of spatial clustering, at the scale of global reference area (Figure 311). At the distance of 12.8 meter is observed some kind of randomness.

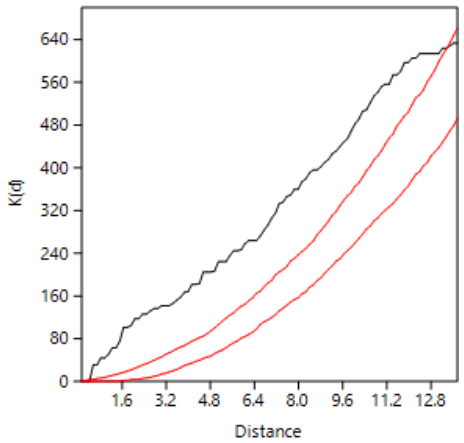

Figure 311 Ripley's *k* analysis on the distance between sampling units with horizontal posts remains, recorded in surveys of 2001 (Past).

Within the convex hull defined by the sampling units where horizontal posts have been recovered, such cells are statistically significantly clustered, according to Clark and Evans test. A Kernel Density Estimation (Figure 312) shows different small concentrations located respectively between x=40-44 and y=118-122, between x=48.52 and y=125-130, between x=58-62 and y=128-136, between x=62-66 x and y=136-142 and finally between x=62-68 and y=142-148 y.

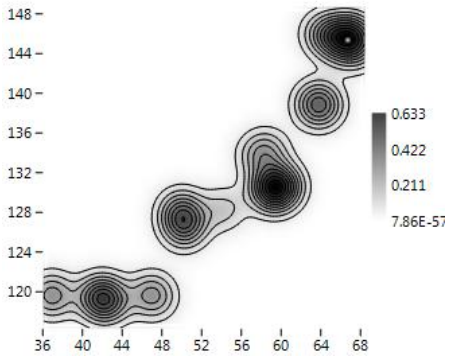

Figure 312 KDE of sampling units where horizontal posts remains have been recovered during surveys of 2001 (Past).

When considering the raw quantity of horizontal posts at each cell, the probability density distribution of spatial frequencies does not follow a J-shaped distribution. A majority of sampling units have raw counts of horizontal posts of less than 2 elements (global mean= 1.16). Three cells are distinguished from the majority (interpretable as outliers) with 2 and 3 observables (Figure 313).

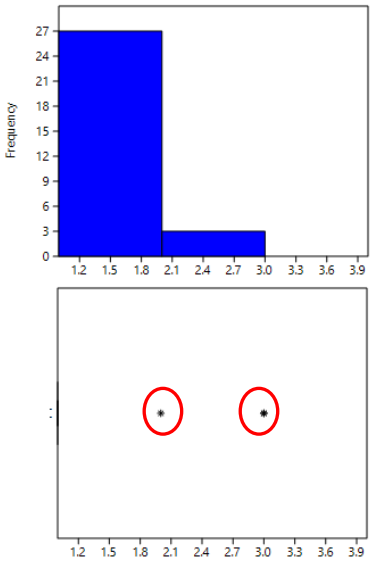

Figure 313 Histogram and box plot of frequencies observed for horizontal posts remains (Past).

The spatial distribution of horizontal posts remains is fitted both with a Negative Binomial distribution, with k=0.073 and p=0.75, and a Geometric distribution, with p=0.977, and with Kolmogorov Smirnov Test=1. This is what is expected when, as in this case, the sample consists in predominant empty sampling units and similar frequencies values in all non-empty cells, obtaining randomness (as also showed in Figure 314).

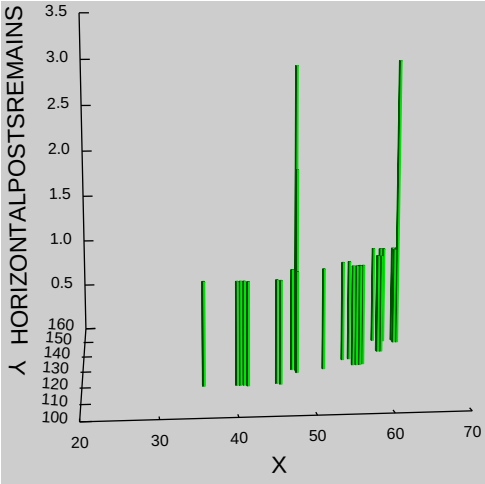

Figure 314 3D Histogram of horizontal posts remains recovered during surveys of 2001 (Systat 13).

77% of horizontal posts remains are located in 90% of the effectively surveyed area, in such a way that only 3 cells show more than 1 item (representing, this value, the break point highlighted by both box plot and histogram).

The spatial distribution of count data per sampling unit for horizontal posts remains shows a Global Moran's *I* of -0.000397. The theoretical (expected) value assuming spatial autocorrelation (lack of spatial independence) is -0.000515 and the standard error of *I* is 0.000515. The test of significance using the normality assumption gave a *z* value of 0.230379, quite significant. Such results are comparable with those of the Geary statistics (*C*=10.999683) and Getis-Ord general G (*G*=0.015518). Consequently, we can accept that the spatial distribution of horizontal posts could not be significantly different than the expected value under a random distribution. This is what would be expected in the case of predominant similar frequency of occurrence within quite every spatial location.

Moran's *I* Correlogram (Figure 315) has been calculated for uniform class distance interval of 1 meter, and taking into account a 10 meters active lag distance. *I* value at the starting point of the function is about 0.180, a bit above the expected value for randomness. As the distance between sampling units increases, *I* value drop off abruptly and reaches values less above the expected value for randomness until 3 meter where they are located on the line (corresponding to spatial randomness).

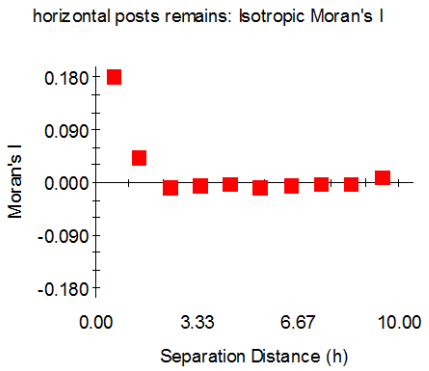

Figure 315 Moran's I Correlogram for horizontal posts remains recovered during surveys of 2001 (GS+).

Scarce positive spatial autocorrelation is observed in the first 2 metresof the function; however, it is notable that all *I* values are quite around 0.

We have explored the possible presence of anisotropic variation (Figure 316). Anisotropy is strongly concentrated in the North-East and South-West corners (and in the middle between them), as previously observed for faunal remains and wooden fragments.

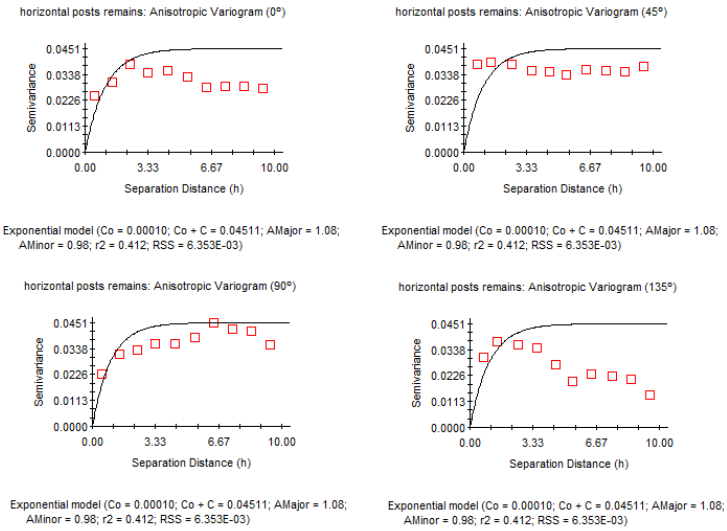

Figure 316 Anisotropic Variogram horizontal posts remains recovered during surveys of 2001 (GS+).

The graph of anisotropic Semivariance Surface or Variogram Map (Figure 317) suggests a higher impact of anisotropy, even at small distances, what can be interpreted in terms of statistical independency in the spatial difference of horizontal posts frequency.

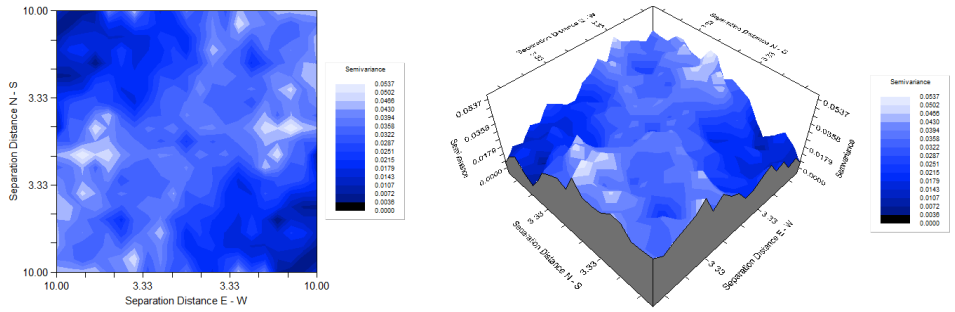

Figure 317 Variogram Map of horizontal posts remains recovered during surveys of 2001 (GS+).

The best fitted exponential model - C_0 (nugget variance) =0.00435, C_0+C (sill) = 0.03370 and A_0 (Range) = 0.32 - explains 47.2% of spatial variance (Figure 318).

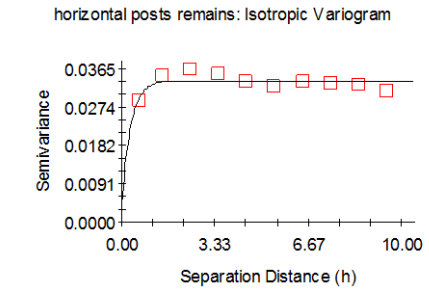

Exponential model (Co = 0.00435; Co + C = 0.03370; Ao = 0.32; **r2 = 0.472**; RSS = 2.168E-05)

Figure 318 Exponential Isotropic Variogram for horizontal posts remains recovered during surveys of 2001 (GS+).

Although not entirely reliable, a predictive model for the frequency of horizontal posts remains distribution (Figure 319) shows a pattern where outlier/overabundant cells seem to be following the ancient estimated lake shoreline.

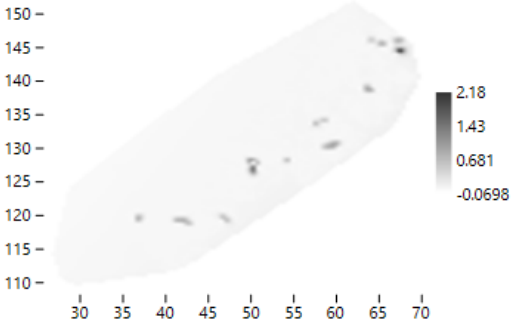

Figure 319 Graphic results of Inverse Distance Weighting calculated for horizontal posts remains recovered during surveys of 2001 (Past).

7.8 Concotto Remains

In Chapter 5 two different sub-categories of concotto have been identified; however, their scarce occurrence does not allow us to consider them separately. Then, 17 remains were identified and counted; they were spatially distributed in 14 cells and 1447 squares were empty. Sampling units where concotto remains have been identified are spatially distributed according to Figure 320.

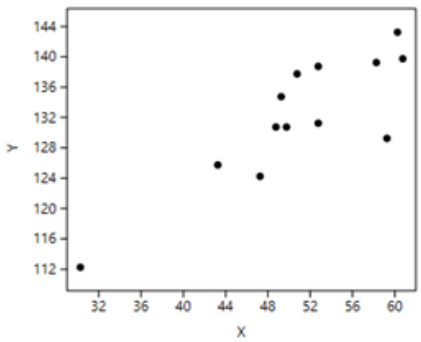

Figure 320 spatial distribution of sampling units where concotto remains have been recorded during surveys of 2001 (Past).

Ripley's *k* analysis on the distance between sampling units with concotto evidence, at the scale of global reference area, suggests the presence of spatial randomness between 1 to 3.3 metre and at 6.4 metre. Other distances show some kind of spatial clustering which, in the majority of cases, tend, however, to the randomness (Figure 321).

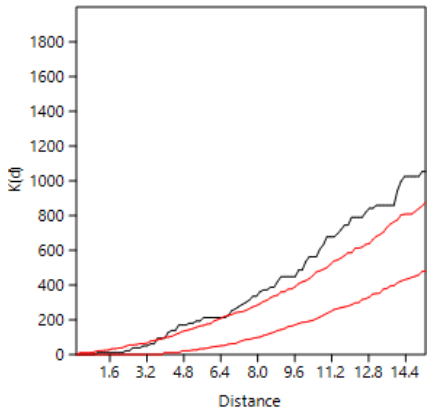

Figure 321 Ripley's *k* analysis on the distance between sampling units with concotto remains, recorded in surveys of 2001 (Past).

A Kernel Density Estimation (Figure 322) shows an irregular distribution of remains concentrated particularly in the North-East corner in different sub-concentrations. A further small accumulation is located in the South-West corner. 1447 surveyed empty cells were overdispersed, according to Clark and Evans test ($p<1$). For 13 non-empty surveyed cells Clark and Evans test highlights that the null hypothesis of random pattern cannot be rejected, what indicates the possibility that equidistant cells have the same probability of counting one or more concotto remains.

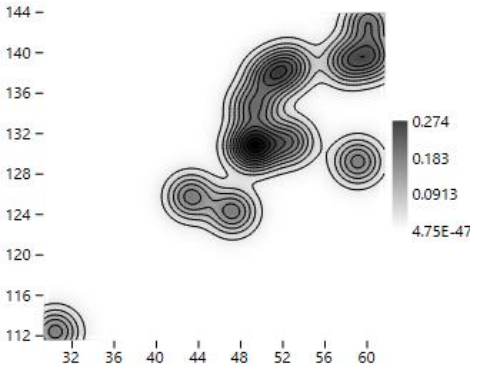

Figure 322 KDE of sampling units where concotto remains have been recovered during surveys of 2001 (Past).

When considering the raw quantity of concotto remains at each cell, the probability density distribution of spatial frequencies does not follow a J-shaped distribution. A majority of sampling units have raw counts of concotto remains of less than 2 elements (global mean=1.30). Three cells are distinguished from the majority (interpretable as outliers) with 2 and 3 observables (Figure 323).

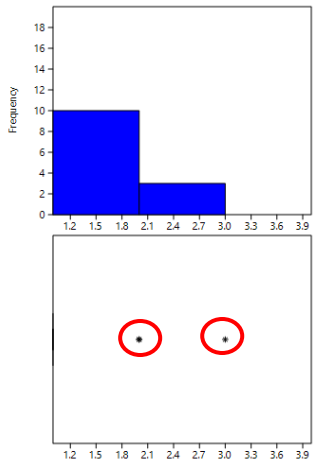

Figure 323 Histogram and box plot of frequencies observed for concotto remains (Past).

The spatial distribution of concotto fragments is fitted both with a Negative Binomial distribution, with k=0.018 and p=0.602, and a Geometric distribution, with p=0.988, with Kolmogorov Smirnov Test=1**.** This condition suggests randomness in the spatial distribution of the abundance of concotto fragments per sampling unit (Figure 324).

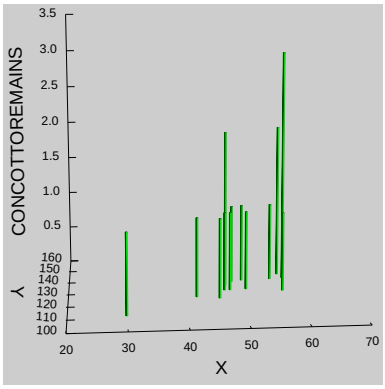

Figure 324 3D Histogram of concotto fragments recovered during surveys of 2001 (Systat 13).

The spatial distribution of count data per sampling unit for concotto remains shows a Global Moran's *I* of -0.000683. The theoretical (expected) value assuming spatial autocorrelation (lack of spatial Independence) is -0.000685 and the standard error of *I* is 0.000685. The test of significance using the normality assumption gave a *z* value of 0.004094, highly non-significant value. Such results are comparable with those of the Geary statistics (*C*=1.000844) and Getis-Ord general G (*G*=0.007634). Consequently, we can accept that the spatial distribution of concotto remains could not be significantly different than the expected value under a random distribution. This is what would be expected in the case of similar frequency of occurrence within every spatial location.

Moran's *I* Correlogram (Figure 325) has been calculated for uniform class distance interval of 1 metre, and taking into account a 10 metres active lag distance. *I* value are in all cases below the expected value for randomness indicating a quite predominant random pattern.

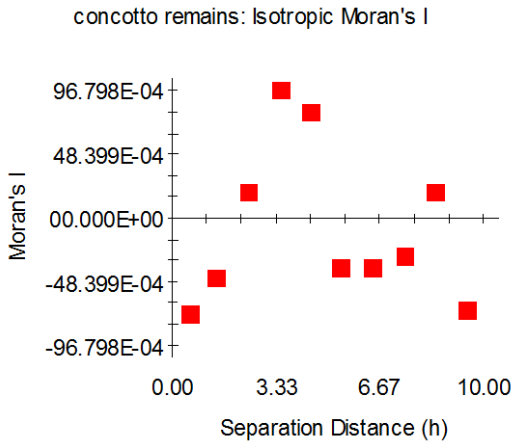

Figure 325 Moran's I Correlogram for concotto fragments recovered during surveys of 2001 (GS+).

7.9 MULTIDIMENSIONALITY OF SPATIAL RELATIONSHIPS

7.9.1 Introduction

The results of geostatistic intra-site analyses suggest the existence of two differentiated zones. To know better the spatial organization of them, the spatial correlation of main variables is analysed. The purpose here is to define 'clusters of artefact categories' which occur together on occupation floors, as a consequence of having been used together in certain activities, as suggested by Whallon (1973) and presented in detail in Chapter 4.

7.9.2 Selecting the most relevant areas (cells with the highest frequencies)

As it has been already mentioned in this chapter, the high amount of sampling units with very low counts of data may alter the correlation structure. Therefore, we have selected cells with the highest counts of each archaeological functional category. "Highest" means here what has been considered "outlier" in preceding analysis, that is those sampling units clearly beyond the interquartile range. Local indicators of spatial association have also been taken into account to select locations with higher relevance.

The following figures (Figure 326) depict the localization of cells with higher measures of positive autocorrelation, using Local Moran one dimensional analysis. The Local Moran statistic $I_{i,t}$ is positive when values at neighbouring locations are similar, and negative if they are dissimilar. Given a Null Hypothesis of no association between the value observed at a location and values observed at nearby sites, that is where values of Moran *I* are close to zero, we have selected those cells for which this hypothesis was below the 0.05 threshold of statistical relevance. Monte Carlo randomizations, using conditional randomization, have been used for evaluating the significance of Local Moran statistic values (Jacquez et al. 2014).

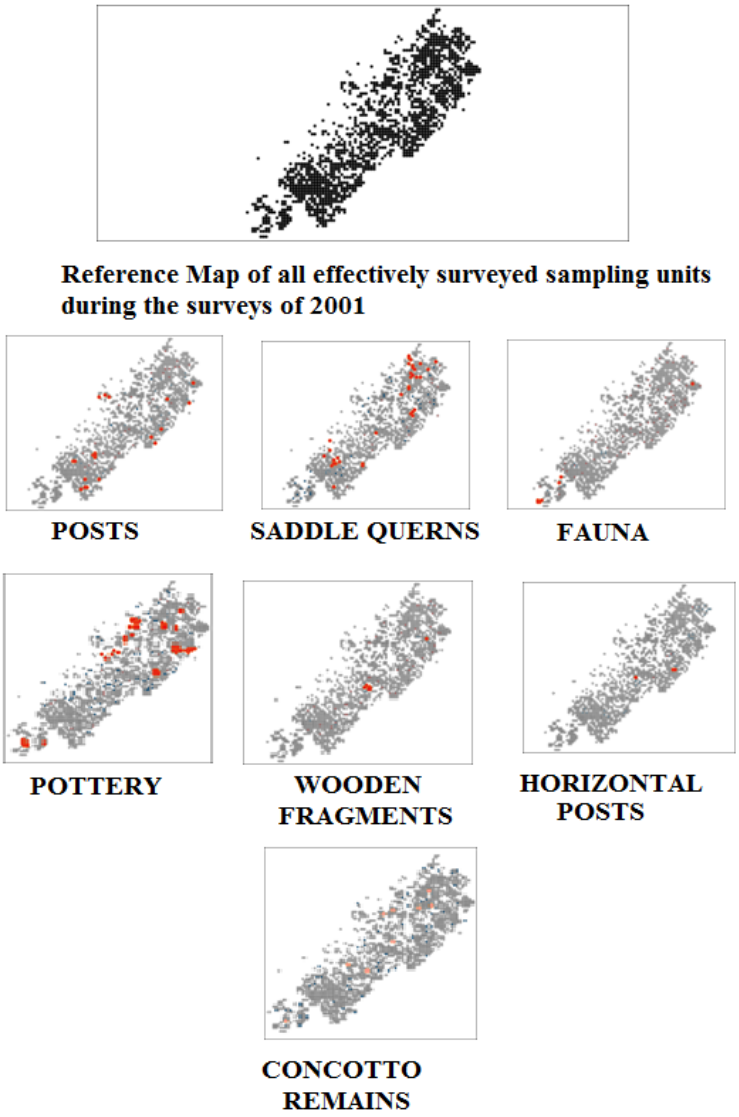

Figure 326 Localization of cells with higher measures of positive autocorrelation for each category of evidence, using Local Moran one dimensional analysis (SpaceStat 4).

VERTICAL POSTS: Positive Correlation is observed between cells with significant higher frequency, surrounded by neighbour sampling units with also high frequencies; they are concentrated in both extremes of the distribution but they are overdispersed. There is a significant empty area (cells with low frequency surrounded by sampling units with also low frequency) at the South-West corner; some other empty areas are observed near some positive correlated ones. Negative autocorrelation is observed between cells with high frequency, surrounded by areas of low frequency, which are overdispersed, without significant alignment. Areas negatively autocorrelated seem to be related with empty areas.

SADDLE QUERNS: Positive Correlation is observed between cells with significant higher frequency, surrounded by neighbour sampling units, with also high frequencies; they are concentrated in both extremes of the distribution. Empty areas are surrounded by cells with low frequency and they are overdispersed. Negative autocorrelation is observed between cells with

high frequency, surrounded by areas of low frequencies; they are overdispersed, without evidence of significant alignment. Negative autocorrelation is attested between empty areas.

FAUNA: Cells with significant higher frequency, surrounded by neighbour sampling units with also high frequencies (Positive Correlation), are concentrated in both extremes of the distribution. In particular, at the South-West corner, are observed four differentiated concentrations. At the center of the distribution, an area of significant low frequency is surrounded by empty areas. Negative autocorrelation is observed between sampling units with high frequency, surrounded by cells of low frequency (overdispersion).

POTTERY: cells with significant higher frequency, surrounded by neighbour cells with also high frequencies, are concentrated in both extremes of the distribution; they are positively correlated. There are no areas of significant low frequency surrounded by cells with low frequency (empty areas). Cells with high frequency, surrounded by areas of low frequency, are overdispersed, without significant alignment; they are negatively autocorrelated.

WOODEN FRAGMENTS*:* cells with significant higher frequency, surrounded by neighbour cells with also high frequencies, are concentrated at the center of the distribution and are positively autocorrelated. There are no areas of significant low frequency surrounded by cells with low frequency (empty areas). Negative autocorrelation is observed between sampling units with high frequency, surrounded by cells of low frequency; they are randomly distributed.

HORIZONTAL POSTS: cells with significant higher frequency, surrounded by neighbour cells with also high frequencies, are concentrated at the centre of the distribution and are positively autocorrelated. There are no areas of significant low frequency surrounded by cells with low frequency (empty areas). Cells with high frequency, surrounded by sampling units with low frequency, are concentrated in the North-East corner and aligned (concentration of outliers). They are negatively autocorrelated.

CONCOTTO: There are no areas of significant higher concentration; positive correlation is observed between cells with significant low frequency, surrounded by neighbour cells with also low frequencies (empty areas). Negative correlation is observed between areas with higher frequencies (outliers), surrounded by cells with lower frequency; they are overdispersed but aligned.

7.9.3 Looking for correlations

7.9.3.1 Correlation between general categories within the entire dataset

The entire database (1460 entries) has been used to calculate potential ordinal correlations between general categories (that is posts, saddle querns, faunal remains, pottery, concotto, wood fragments and horizontal posts remains). Spearman's Correlation Coefficient has significant positive values in very few cases. In the majority of crossing pairs, the rank correlation adopts negative values. For instance, saddle querns are negatively correlated with pottery, fauna, posts and horizontal posts remains. Positive correlation relates instead pottery with fauna and concotto, as well as horizontal posts remains and wood fragments.

	fauna	posts	horizontal posts	saddle querns	concotto remains
saddle querns	2.65E-09	3.93E-26	0.02983		
wooden fragments			8.79E-05		
pottery	4.23E-05			1.68E-47	0.0012024
	fauna	posts	horizontal posts	saddle querns	concotto remains
saddle querns	-0.15495	-0.27174	-0.056855		
wooden fragments			0.10246		
pottery	0.10695			-0.36599	0.084671

Table 8 Spearman's Correlation Coefficient of the ranks for general categories (values of p(uncorrect) (above) and p(uncorrect)-statistic (below).

7.9.3.2 Correlation between salient locations (Local Moran significant cells)

We have selected those cells that are beyond the 0.05 level in the local Moran analysis. Rank order correlation between dependent variables has been recalculated for those 90 sampling units. Results are different from what obtained in the case of all surveyed sampling units, with a significant zero inflation. The positive correlation between wood fragments and horizontal posts is the most relevant coincidence. Pottery and saddle querns are correlated negatively –where there is overabundance of pottery there are lesser saddle querns-. The same is true for faunal remains and horizontal posts.

	posts	saddle querns	horizontal posts	wooden fragments
fauna	0.029908			
pottery		0.0041544	0.022193	0.0099431
wooden fragments			1.76E-05	
	posts	saddle querns	horizontal posts	wooden fragments
fauna	-0.22903			
pottery		-0.29935	-0.24088	-0.27042
wooden fragments			0.43581	

Table 9 Spearman's Correlation Coefficient of the ranks for salient locations (values of p(uncorrect) (above) and p(uncorrect)-statistic (below).

7.9.3.3 Correlation between sub-categories: wild and domestic fauna versus ceramic open and closed forms

In some cases, global categories like "fauna" or "pottery" can be subdivided into more coherent functional categories, like wild and domestic fauna on one hand, and open and closed pottery forms. Using the results of the above Local indicators of spatial association, 121 cells have been selected, according to the frequency of such subcategories at those locations, higher than expected assuming the null hypothesis. Rank order correlations are predominantly positive, relating subcategories within the same global category. Negative correlation is observed between wild fauna and both saddle querns and posts.

	domestic fauna	saddle querns	posts	horizontal posts	ceramic closed forms
wild fauna	0.038734	0.035065	0.023148		
wooden fragments				4.48E-08	
ceramic open forms					0.0060915
	domestic fauna	saddle querns	posts	horizontal posts	ceramic closed forms
wild fauna	0.18818	-0.19181	-0.20637		
wooden fragments				0.47243	
ceramic open forms					0.24801

Table 10 Spearman's Correlation Coefficient of the ranks for sub-categories (wild and domestic fauna as well as open and closed ceramic forms) (values of p(uncorrect) (above) and p(uncorrect)-statistic (below).

7.9.3.4 Correlation between sub-categories: skeletal faunal anatomical parts versus ceramic open and closed forms

When specifying taxa and skeletal part, instead of a global and undifferentiated "faunal remains" category, and restricting rank order correlation to salient points in Local Moran analysis, it is again obtained a pattern of positive relationship between subcategories of the same global category. Neither different skeletal parts, nor distinct remains from different taxa, are distributed at different locations, but a similar frequency of each subcategory appears at the same locations. Specific subcategories –skeletal and taxonomic- of fauna are also positively

correlated with specific functional subcategories of pottery. Negative correlation can be detected between saddle querns and appendicular faunal fragments.

	cranial fragments	appendicular fragments	horizontal posts	ceramic open forms
axial fragments	0.03642	2.49E-05		
saddle querns		0.090282		
posts		0.041636		
ceramic closed forms		0.092115		0.0028835
wooden fragments			2.52E-07	
	cranial fragments	appendicular fragments	horizontal posts	ceramic open forms
axial fragments	0.20067	0.39204		
saddle querns		-0.16304		
posts		-0.19549		
ceramic closed forms		0.16213		0.28283
wooden fragments			0.47003	

Table 11 Spearman's Correlation Coefficient of the ranks for sub-categories (cranial, axial and appendicular faunal remains as well as open and closed ceramic forms) values of p(uncorrect) (above) and p(uncorrect)-statistic (below).

7.9.4 Correspondence Analysis between general categories: higher frequencies

Considering the low value of correlations observed between sub-categories of pottery and faunal remains with other categories, Detrended Correspondence Analysis (Figure 327) is only performed for higher frequencies of general categories. Posts are excluded because of their frequency uniformity. First two axes explain a cumulative 80%. The first one explains the 44%, proving the negative correspondence between wooden fragments, associated to horizontal posts and pottery (associated to concotto remains).

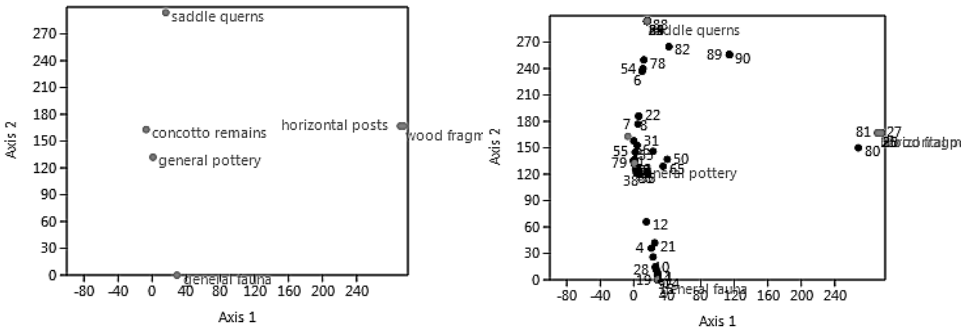

Figure 327 Graphic results of Correspondence Analysis calculated using higher frequencies of general categories (Detrended Correspondence Analysis) (surveys 2001) (Past).

The graphic result of the inverse distance weighting for Axis 1 (Figure 328) shows the spatial distribution of cells with horizontal posts remains and wooden fragments (corresponding to black values) negatively correlated to pottery and concotto remains (corresponding to clear values). Main concentrations of wooden fragments (associated to horizontal posts) are predominantly observed in the middle of the area, in low density points in the North-East corner and around x=40-45 and y=115. Pottery and concotto remains are instead predominantly observed in the North-East corner and with some low density points around the South-West corner. As proved by Figure 181, where pottery and concotto remains are observed, horizontal posts remains as well as wooden fragments are absent.

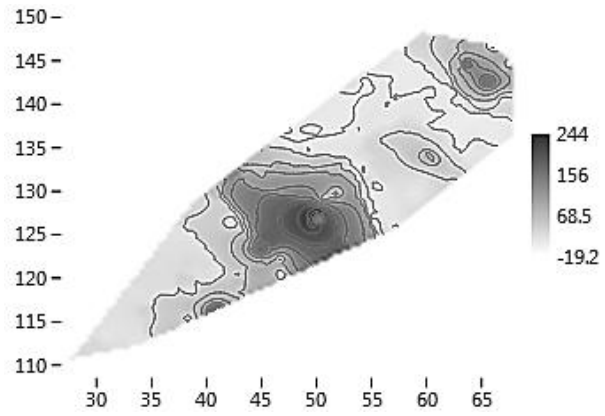

Figure 328 Graphic result of inverse distance weighting for Axis 1 (higher frequencies of general categories) (surveys 2001) (Detrended Correspondence Analysis) (Past).

The second axis explains 36%, proving the negative correspondence between faunal remains and saddle querns. The graphic result of the inverse distance weighting shows a spatial distribution of saddle querns (corresponding to black values) in some isolated high density points located around the North-East corner, in the centre of distribution and around the South-West corner. In contrast, faunal remains (corresponding to clear values) are predominantly accumulated in the South-West corner and in lower density points distributed in the centre of the area (Figure 329). As already mentioned, the result of correspondence is suggesting that where saddle querns are observed, faunal remains are predominantly absent.

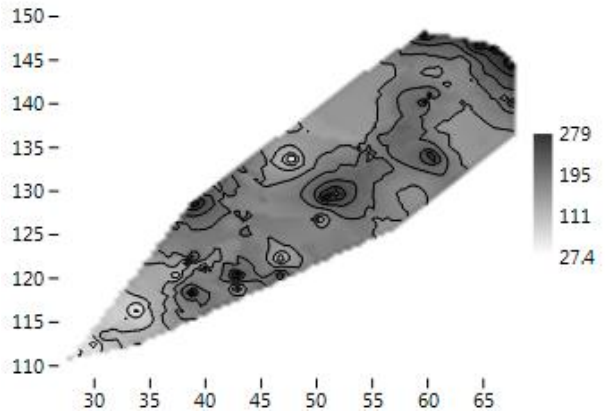

Figure 329 Graphic result of inverse distance weighting for Axis 2 (higher frequencies of general categories) (surveys 2001) (Detrended Correspondence Analysis) (Past).

Instead of analyzing the second axis in depth, which can be affected by the classical "horse-shoe" deformation effect (it is partially correlated with the first axis) the analysis has been repeated without the scarcest categories, that is those observations that appear in very low frequencies in the studied area: wooden fragments and horizontal posts. The first axis of the resulting analysis explains 40%, what suggests that, by deleting these categories, spatial variation does not significantly change. The analysis shows the high contribution of pottery (darkest values) and faunal remains (clear values) as the leading opposition: where there are more faunal remains (clear values) there are fewer potsherds. In contrast, where the pottery is absent the faunal remains neither are observed. A spatial view of first axis row scores appears in Figure 330.

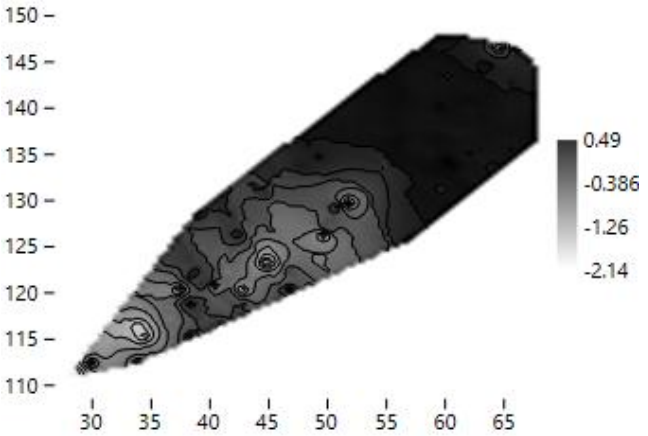

Figure 330 Graphic result of inverse distance weighting for Axis 1 (higher frequencies of general categories) (Correspondence Analysis) (surveys 2001) (Past).

8 GEOSTATISTIC INTRA-SITE SPATIAL ANALYSIS

The site of Villaggio delle Macine: the area surveyed in 2009

8.1 Introduction

This chapter is devoted to the analysis and results of intra-site spatial analyses of the areas surveyed in 2009 at the Villaggio delle Macine. We begin by analysing the absolute counts of archaeological observations, by mixed all identified materials together in the way of a palimpsest. It is used as null-hypothesis for the separated analysis of each archaeological category, according to the discussion in Chapter 6 and Chapter 7. For a spatial correlation perspective, multidimensional analysis integrates all selected categories. The step-by-step procedure is the following one:

1) Plot of locations where some element has been detected (x, y coordinates of grid centroids)

2) Density analysis of single presences (Kernel Density Estimate) and Statistical Relevance of the null hypothesis of Spatial Randomness

4) Statistical Description of the Spatial Distribution. Measures of Central Tendency.

5) Plot of Spatial Frequencies (Lorenz curve, 3D Histogram). Weighted Measures of Central Tendency. Statistical Relevance of the Null Hypothesis of Spatial Randomness

6) Semivariance Modeling and Spatial Interpolation. Kriging

7) Spatial Correlation

8.1.1 The area surveyed in 2009

An area of 2400 sq. meters was surveyed in 2009. Only 920.5 sq. meters provided reliable data. In agreement with what has been done for 2001, spatial frequencies per squared sampling unit of 0.25 squared meters have been taken into account. The effectively surveyed area was divided in 1941 cells, summing up to 485.25 square meters (Convex Hull=1232.8). Both North-West and South-East quadrants were unsurveyed for different reasons: the former was occupied by spontaneous vegetation, while the latter was occupied by the shoreline that, in some spatial locations, was directly connected with the surveyed area.

8.2 Absolute count of archaeological observations (palimpsest)

26142 archaeological observations (ascribable to all the categories recovered during survey of 2009) were identified and counted in 1941 surveyed cells. In 72 cases the surveyed cell was empty. In one case, a single cell of 0.25 squared meters presented a total of 194 items. A frequency mean of 13.98 observations per sampling unit and a standard deviation of 16 have been calculated for this sample. The spatial distribution of only those sampling units with material evidence is showed in Figure 331.

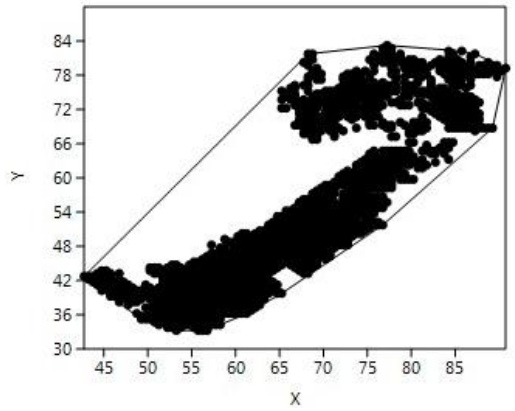

Figure 331 spatial distribution of sampling units centroids where any kind of archaeological evidence has been recorded in surveys of 2009 (Past).

Ripley's *k* analysis on the distance between sampling units with all material evidence gives support to the hypothesis of spatial clustering in the reference area (2400 squared meters) for distances beyond 2.5 meters (Figure 332).

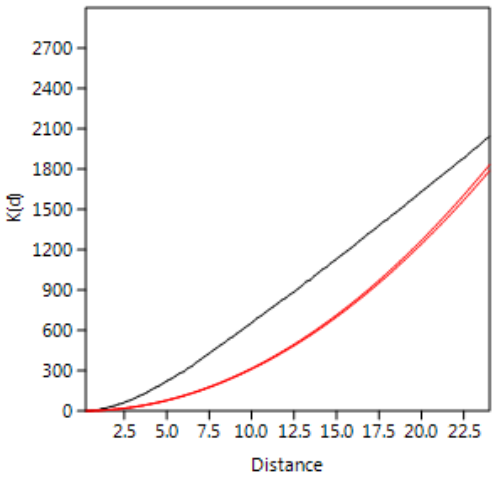

Figure 332 Ripley's *k* analysis on the distance between sampling units with all material evidence recorded in surveys of 2009 (Past).

Within the convex hull defined by the effectively surveyed cells, the Kernel Density Estimation of non-empty cells (cells where a minimum of 1 archaeological observation has been recorded) shows the possible accumulation of archaeological observations in two differentiated sectors, separated by some clustered empty cells, respectively at the South-West and North-East corners of the surveyed area (Figure 333).

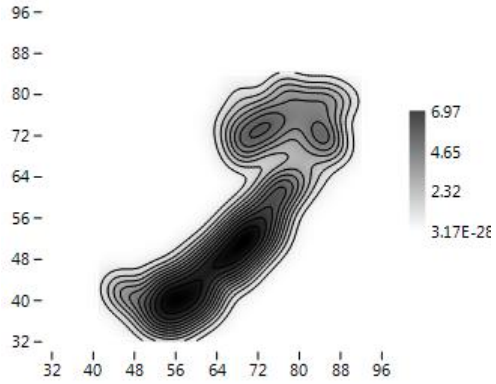

Figure 333 KDE of non-empty sampling units where any kind of archaeological evidence has been recorded in surveys of 2009 (Past).

When considering the raw quantity of archaeological observations at each cell, the probability density distribution of spatial frequencies clearly follows a J-shaped distribution. A majority of sampling units have raw counts of archaeological observations of less than 15 elements (global mean=13.98 observations per sampling unit). One cell distinguishes from the majority, with 194 observations (interpretable as outlier). Zero values are scarcely attested (attested in 72 sampling units): this condition is expected in the case of palimpsest, since it sums up all categories of material evidence. We have signaled an apparent discontinuity at the number of 40 observations as if, beyond this threshold, frequencies exceed what the theoretical exponential model predicts (Figure 334).

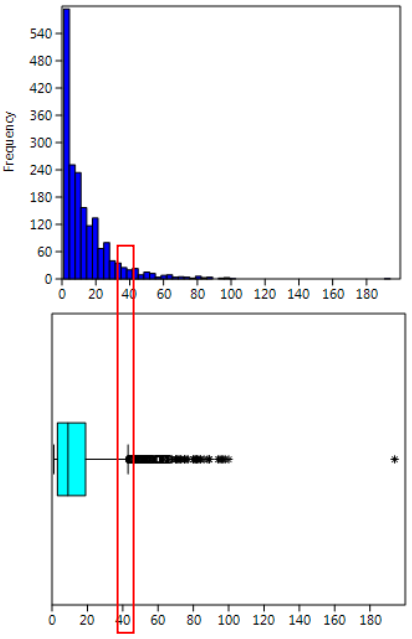

Figure 334 Histogram and box plot of frequencies observed for all material evidence summed up (Past).

A Lorenz Curve (Figure 335) gives a Gini Coefficient of 0.534, with a 95% Bootstrap confidence interval between 0.534 and 0.570. The Coefficient of asymmetry is 0.8954, with a 95% Bootstrap confidence interval between 0.847 and 0.922. In general, we can see that 53% of all archaeological observations have been found at 80% of sampling units and the remaining 20% sampling units concentrate around a half of the count data (47%). This result does not follow the standard geometrical (exponential) accumulation model, but reveals less

accumulative behaviour than expected, or, in any case, different accumulations all mixed together.

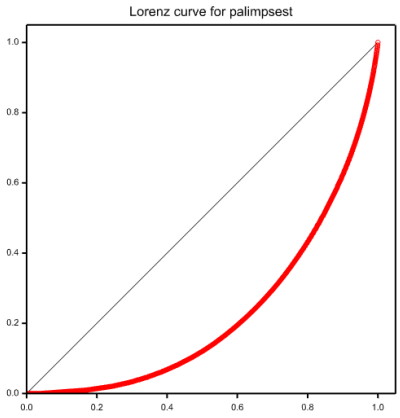

Figure 335 Lorenz Curve for all material evidence recovered during surveys of 2009 (Genstat).

In this sense, the 3D histogram also shows an irregular and non-homogeneous distribution characterized by outliers and strong multimodality (Figure 336), which does not fit with an exponential theoretical model of intentional discard at a fixed center (tested using K-S tests, $p<0$ in all cases).

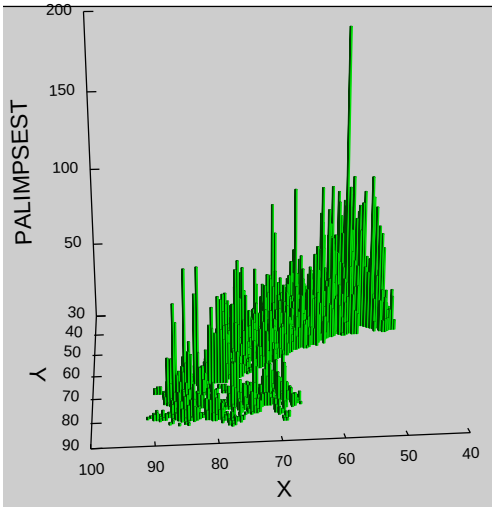

Figure 336 3D Histogram of all material evidence recovered during surveys of 2009 (Systat 13).

The spatial distribution of count data per sampling unit shows a Global Moran's *I* of 0.000811. The theoretical (expected) value assuming spatial autocorrelation (lack of spatial independence) is -0.000515 and the standard error of *I* is 0.000515. The test of significance using the normality assumption gave a *z* value of 2.57, a significant value. Consequently, we can accept that the spatial distribution of accumulations of undifferentiated material elements is partially different than the expected value under a random distribution. However, a mixture of too much different intentionality, mixed and summed up, could have produced such pattern. Such results are comparable with those of the Geary statistics (C=0.998069) and Getis-Ord general G (G=0.008078).

The Moran's *I* Correlogram (Figure 337) has been calculated for uniform class distance intervals of 1 meter and taking into account a 10 meters active lag distance. *I* value at the

starting point of the function is at 0.464, above the expected value for randomness. Such condition is followed within the entire sample, since *I* value drops off quite gently and continuosly along all the function.

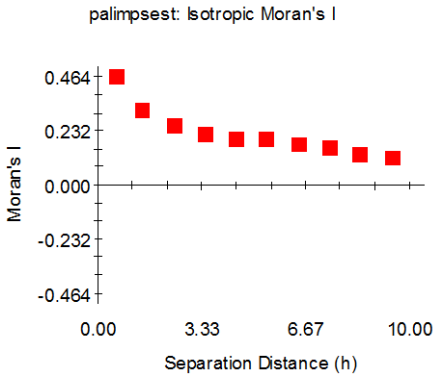

Figure 337 Moran's I Correlogram for all evidence recovered during surveys of 2009 (GS+).

These data suggest that signal of concentrated accumulations are observed for, at least, 10 meters. Local indicators of spatial association (see at the end of the chapter) coincide with the histogram of frequencies, indicating that those 123 cells with more than 40 items are significantly different from the neighbours (Figure 338).

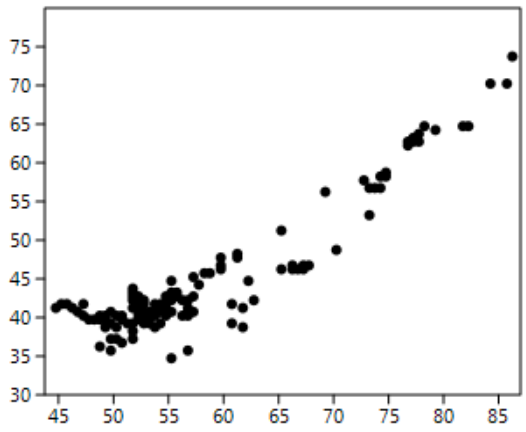

Figure 338 Location of cells with more than 40 items (Past).

At first sight it may seem that there is some spatial patterning. Clark and Evans test gives a significant result of spatial clustering (p=0.0001). Moran's *I* correlogram (Figure 339) of cells with more than 40 items fits with a random model at small distances, and some possible clustering between 0 and 1 meters and between 5 and 8 meters (in this last case as negative spatial autocorrelation). That is, two main concentration zone (between x=49-55 and y=35-40).

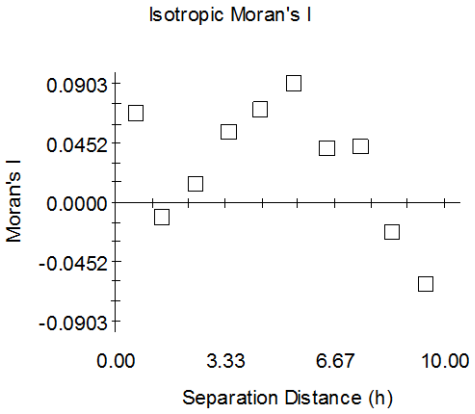

Figure 339 Moran's I Correlogram of cells with more than 40 items (GS+).

A Kernel density estimate model of cells with more than 40 items provides a clearer image (Figure 340).

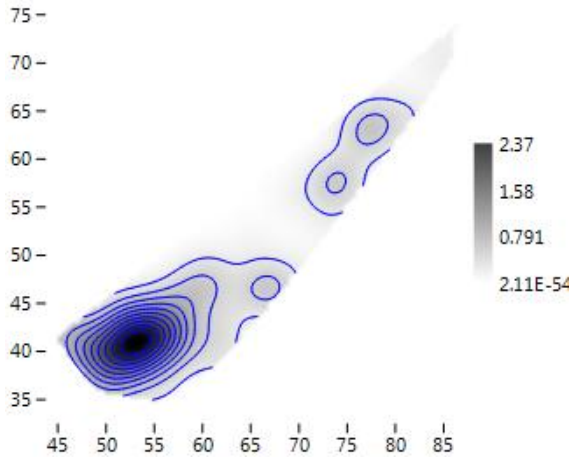

Figure 340 KDE model of cells with more than 40 items (Past).

It is easy to see in the South-West corner of the surveyed area a higher density concentration delimiting a less dense area. Following the North-East direction, there is a small concentration of material evidence with lower frequencies.

It is obvious that anisotropy is present in the main direction North-East-South-West, that is, parallel to the ancient estimated lake shoreline. We have calculated anisotropic variograms at different directions (Figure 341).

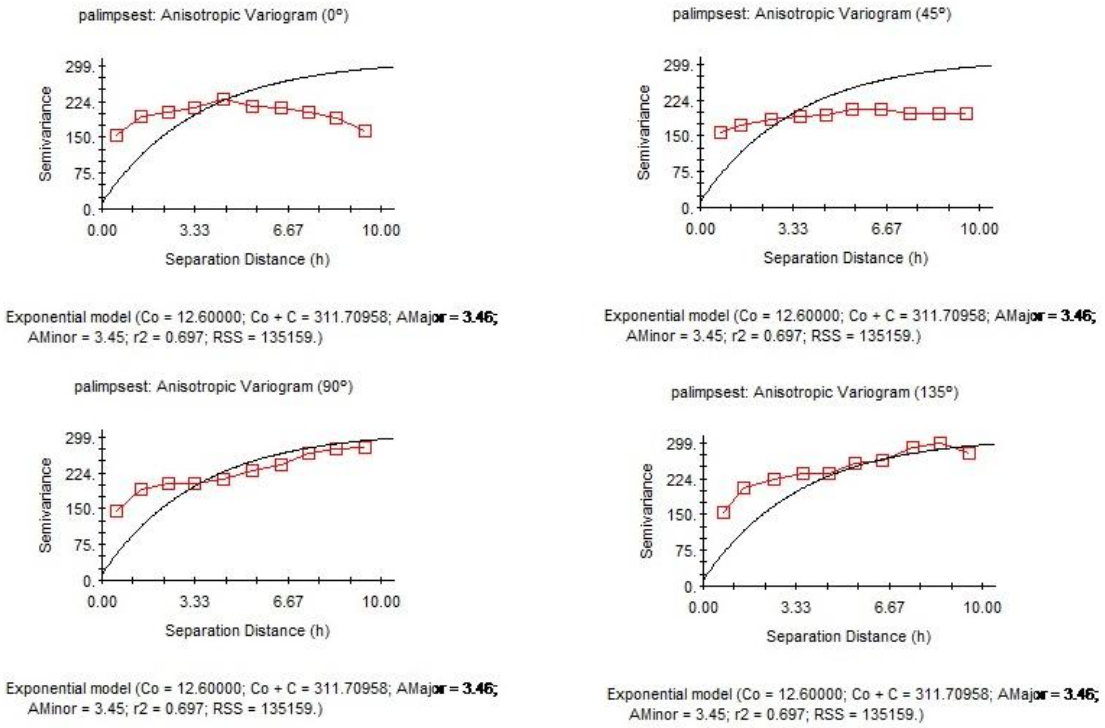

Figure 341 Anisotropic Variogram of all material evidence recovered during surveys of 2009 (GS+).

Semivariance is very high in all directions and it varies in quite same way respectively in 0º and 45º (particularly in the first part of the function), and in 90º and 135º. The slope of curve suggests a quite regular spatial pattern, with continuity in medium-large area. The Semivariance Surface or Variogram Map (Figure 342) shows spatial continuity in North-East-South-West direction, following the ancient estimated lake shoreline and the main axis of the surveyed area.

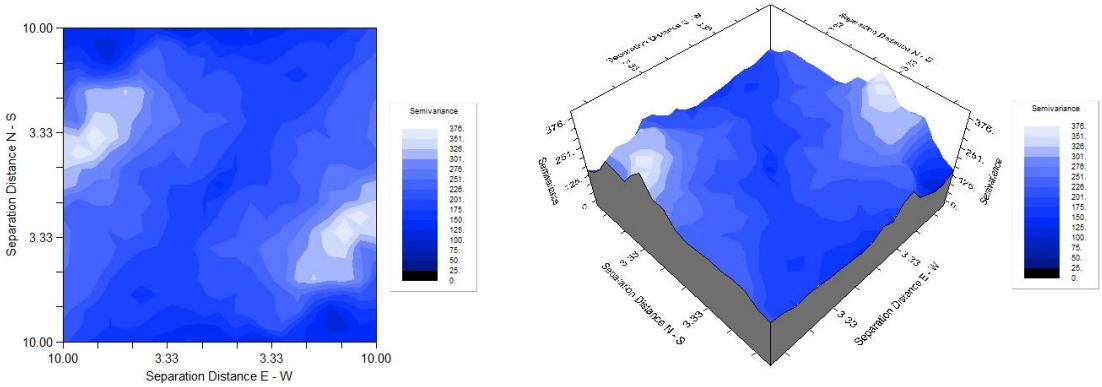

Figure 342 Variogram Map of all material evidence recovered during surveys of 2009 (GS+).

North-West and South-East sides (around the corners) are the strongly affected by anisotropy; as the raw data clearly indicates, there is no reliable information for such quadrants of the area submittend to surveying. The South-East quadrant was underwater at the time of surveying. In this graph, the centre of the map corresponds to the origin of the variogram □(h) = 0 for every direction. We can see that semivariance is quite constant at small distances and higher at longer ones, in the centre of the surveyed area.

An Exponential Isotropic Variogram model (Figure 343) has been fitted to the empirical variogram. In this case C_0 (nugget variance) = 63.30, C_0+C (sill) = 221.50 and A_0 (Range) = 0.84.

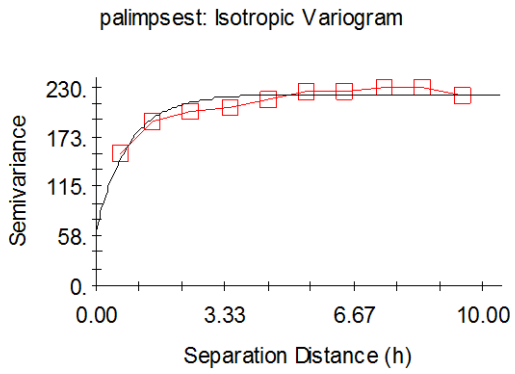

Exponential model (Co = 63.30000; Co + C = 221.50000; Ao = **0.84**; **r2 = 0.910**; RSS = 493.)

Figure 343 Exponential Isotropic Variogram for all material evidence recovered during surveys of 2009 (GS+).

This model explains 91% of sample variance and offers the best fit possible for the available data. Lags are shown at 1 meter intervals. With this particular variogram, we have estimated the global variation of the total number of archaeological observations, using an Inverse Distance Weighting (Figure 344).

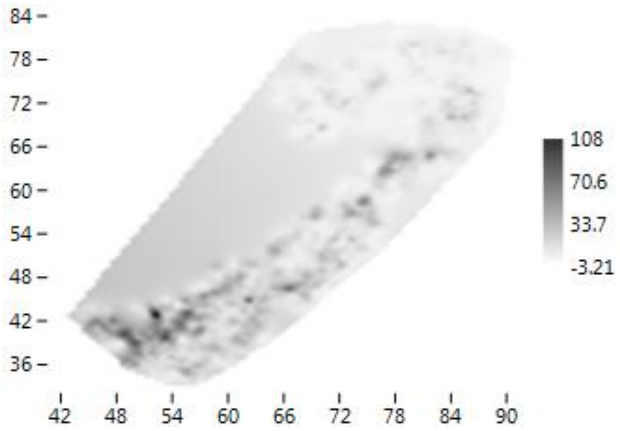

Figure 344 Graphic results of Inverse Distance Weighting calculated for all material evidence recovered during surveys of 2009 (Past).

This visualization shows the spatial dependence of cells with highest frequencies, concentrated especially in the South-West corner and in the centre of the surveyed area, distributed according to a general predominant North-East-South-West orientation. In addition, other small concentrations, with less material evidence, are observed between x=75-85 and y=64-67. Not a single well defined accumulation can be interpreted, but a quite deformed pattern. After all we are analyzing archaeological materials that come from very different activities associated to different discard behaviours. In any case, anisotropy is distributed according to the predominant North-East-South-West orientation around the North-West and South-East corners. This result would be compatible with two differentiated accumulations (within Zone 1 and Zone 2). It is important to remark the high resemblance between the interpolated model of abundance data and the Kernel Density Estimation of cells with more than 40 identified items (above).

8.2.1 Absolute count of archaeological observations (palimpsest) within Zone 1 and Zone 2

As above mentioned, two zones can be identified within the sector surveyed in 2009.

We use the y< 65 as the threshold to divide both hypothetical subareas, since it is the point of minimum frequency in the histogram of *y* values. In this way such sub-areas are obtained: Zone 1 with *y*<65 and Zone 2 with *y*>65 (Figure 345).

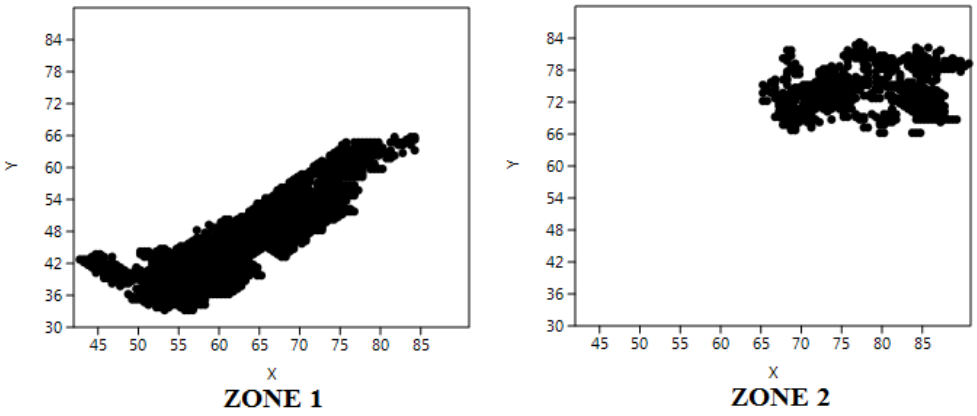

Figure 345 Spatial distribution of non-empty sampling units in Zone 1 and Zone 2.

Ripley's *k* analyses on the distance between sampling units with all material evidence for both areas give support to the hypothesis of spatial clustering in two main zones, beyond 2.5 meters (Figure 346); for Zone 2 such spatial pattern is however more restricted.

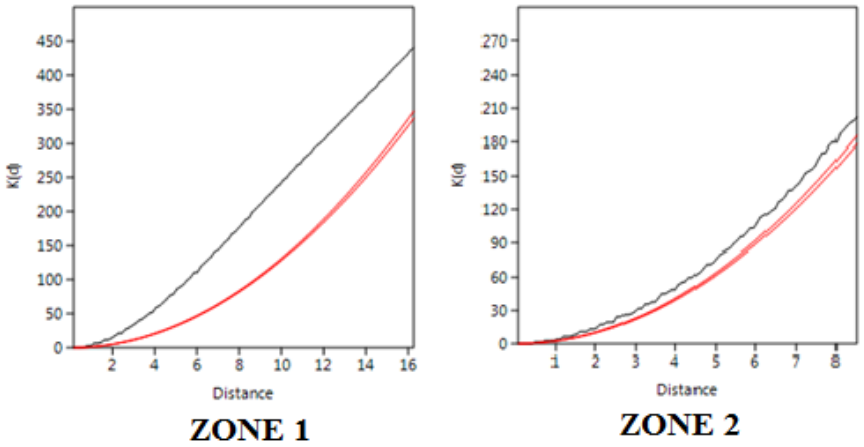

Figure 346 Ripley's *k* analysis on the distance between sampling units with all material evidence recorded in Zone 1 and Zone 2 during surveys of 2009 (Past).

Within the convex hull defined by the effectively surveyed cells, the Kernel Density Estimation of non-empty cells (cells where a minimum of 1 archaeological observation has been recorded) shows for Zone 1 the occurrence of a wider central area which is extended between x=50-60 and y=35 y and x=67-73 and y=56, while within Zone 2 two sub-sectors emerge (one between x=67-72 and y=69 and x=72-78 and y=78 and the other between x=85-88 and y=67 and x=82-88 and y=75). Within Zone 1 are observed 1301 surveyed non-empty cells, while within Zone 2 are attested 562 surveyed non-empty cells. For both zones Clark and Evans Test (p<0) gives a

result of significant overdispersion. We can conclude that the spatial distribution in both zones is not significatively different, despite the different directionality in the spatial distribution of observations (Figure 347).

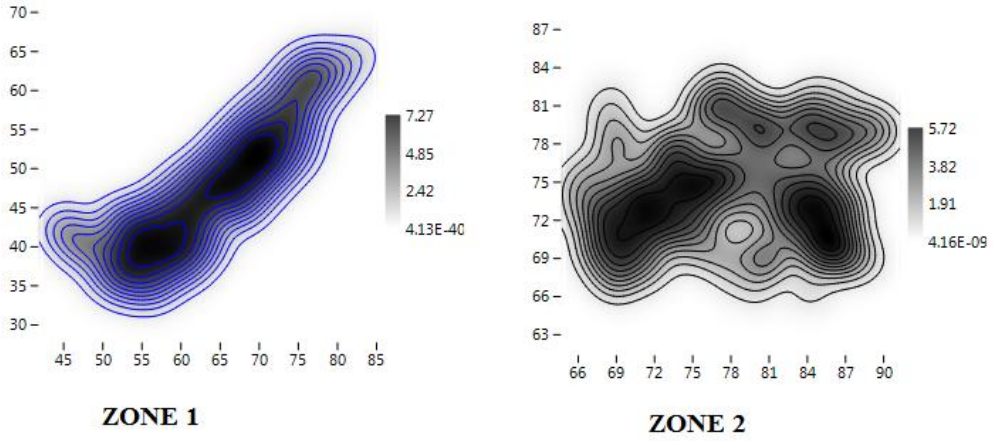

Figure 347 KDE of non-empty sampling units where any kind of archaeological evidence has been recorded in Zone 1 and Zone 2 during surveys of 2009 (Past).

There are relevant differences in the spatial location of palimpsest frequencies within these two zones (Figure 348). Zone 1 concentrates the majority of observations (n=23145) with raw counts of evidence of less than 18 elements (global mean= 17.79 observations per sampling unit). One cell is distinguished from the majority, with 194 observations (interpretable as outlier). An apparent discontinuity is signaled at the number of 41 observations, as if beyond this threshold, frequencies exceed what the theoretical exponential model predicts.

In Zone 2 there are only 2997 observations, with raw counts of evidence of less than 6 (global mean=5.27 observations per sampling unit). An apparent discontinuity is signaled at the number of 16 observations, as if beyond this threshold, frequencies exceed what the theoretical exponential model predicts. In addition, three cells distinguish from the majority, with 44, 59 and 75 observations (interpretable as outliers).

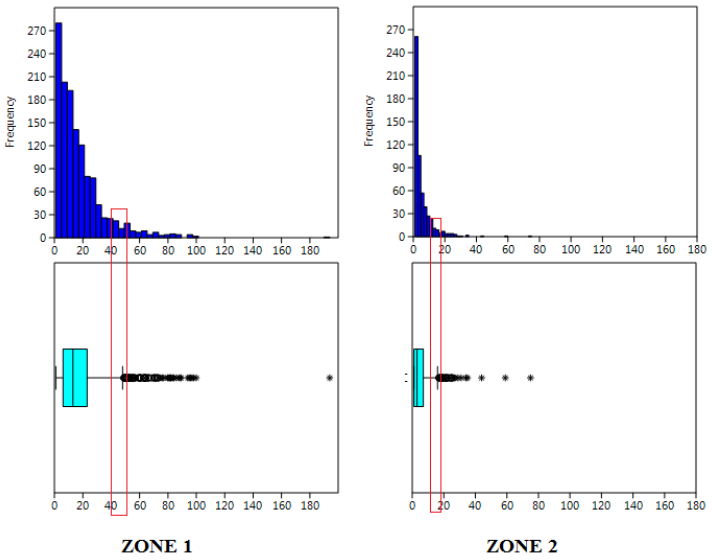

Figure 348 Histogram and box plot of frequencies observed for all material evidence summed up separately for Zone 1 and Zone 2 (surveys 2009) (Past).

In both cases, Lorenz Curve is quite similar (Figure 349), as well as the Gini coefficient (0.4750 for Zone 1 and 0.54 for Zone 2 and even the deformation of the curve is similar (curve asymmetry for Zone 1 0.9181 and for Zone 2 1.007). In general we can see that 47% (for Zone 1) and 54% (for Zone 2) of all archaeological observations have been found at 80% of sampling units, and the remaining 20% sampling units concentrate around and half of the count data (53% for Zone 1 and 46% for Zone 2). These results do not follow the standard geometric (exponential) accumulation model, but reveals less accumulative behaviour than expected, or, in any case, different accumulations all mixed together.

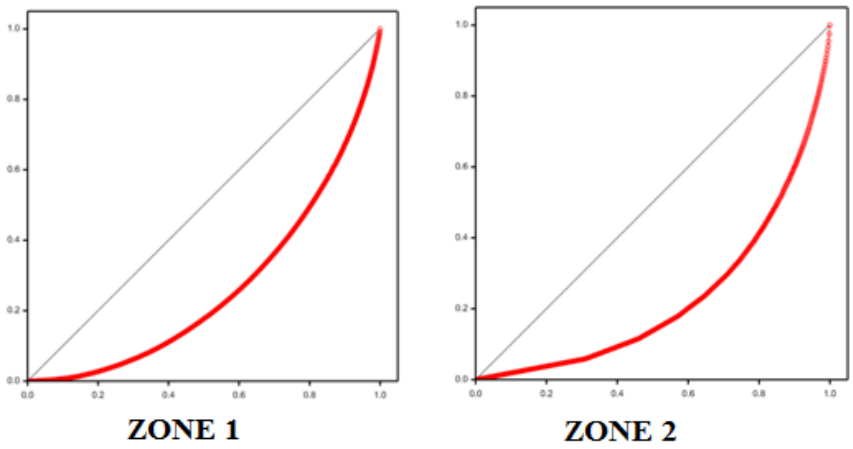

Figure 349 Lorenz Curve for all material evidence recovered during surveys of 2009 for Zone 1 and Zone 2 (Genstat).

In this sense, the 3D histograms also show irregular and non-homogeneous distributions characterized by outliers and strong multimodality (Figure 350), which do not fit with an exponential theoretical model of intentional discard at a fixed center (tested using Kolmogorov Smirnov tests, $p<0$ in all cases).

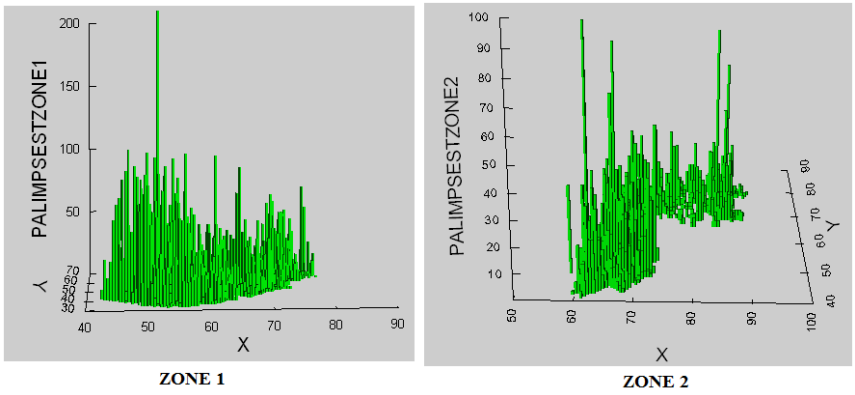

Figure 350 3D Histogram of all material evidence recovered during surveys of 2009 in Zone 1 and Zone 2 (Systat 13).

In Zone 1, the spatial distribution of count data per sampling unit shows a Global Moran's *I* of -0.000357. The theoretical (expected) value assuming spatial autocorrelation (lack of spatial independence) is -0.000756, and the standard error of *I* is 0.000756. The test of significance using the normality assumption gave a *z* value of 0.523439, a significant value. Such results are comparable with those of the Geary statistic for this case (*C* = 0.999216) and Getis-Ord general G (*G*= 0.010006).

In Zone 2, the spatial distribution of count data per sampling unit shows a Global Moran's *I* of -0.001479. The theoretical (expected) value assuming spatial autocorrelation (lack of spatial independence) is -0.001621, and the standard error of *I,* is 0.001618. The test of significance using the normality assumption gave a *z* value of 0.087776, a highly non-significant value.

Consequently, we can accept that the spatial distribution of accumulations of undifferentiated material elements is not significantly different than the expected value under a random distribution[39]. This is what would be expected when a mixture of too much different intentionality is mixed and summed up.

The Moran's *I* Correlogram for both areas (Figure 351) has been calculated for uniform class distance intervals of 1 meter and taking into account 10 meters active lag distance. For Zone 1 at the starting point of the function *I* value is at 0.377. When the distance between sampling units increases, *I* value drops off quite gently and continuously above the expected value for randomness; only between 9 and 10 meters *I* values are distributed on the line (corresponding to spatial randomness). Thus, for the first 6-7 meters it is attested positive spatial autocorrelation.

A Moran's *I* correlogram for Zone 2 (Figure 351) shows a more irregular spatial pattern. At the starting point of the function *I* value is 0.169 and at 1 meter is around the same value. When the distance between sampling units increases, *I* value drops off abruptly between 1-2 meters and from 5 meters it reaches values below those expected for randomness. Between 0-3/4 meters positive spatial autocorrelation is attested.

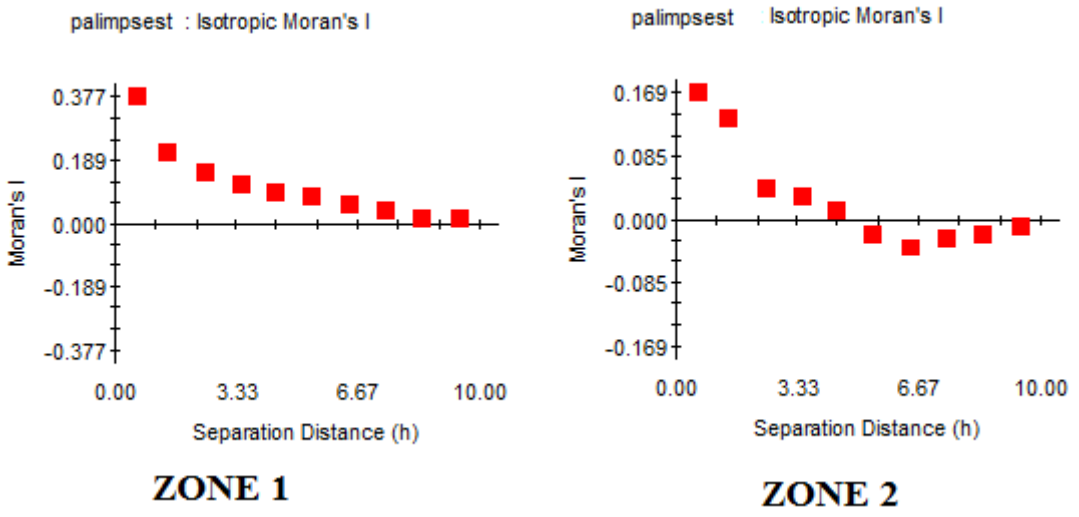

Figure 351 Moran's I Correlograms for all evidence recovered during surveys of 2009 in Zone 1 and Zone 2 (GS+).

These data that the amount of archaeological evidence appear to be spatially positively autocorrelated for distance of at least 6-7 meters of radius, within Zone 1. For Zone 2 such spatial dependence is limited to 3-4 meters of radius, associable to individual activity.

Local indicators of spatial association (see at the end of the chapter) coincide with the histogram of frequencies, indicating that those cells with more than 41 items (for Zone 1) and 16

[39] within Zone 1 it could be only low significantly different

fragments (for Zone 2) are significantly different from their neighbours. Within Zone 1 only 114 cells have more than 41 items (Figure 352).

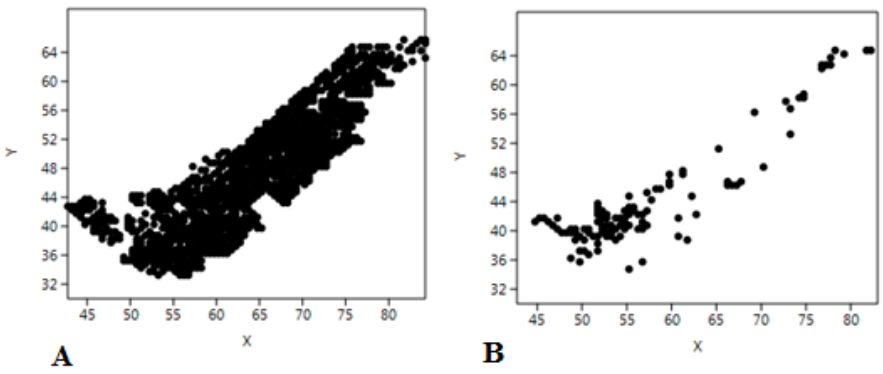

Figure 352 A)Location of sampling units with less than 42 items B) Location with more than 41 items (Zone 1, surveys 2009) (Past).

At first sight it may seem that there is some spatial patterning. Clark and Evans test gives a significant result of spatial clustering (p=0.03). Moran's I correlogram (Figure 353) of cells with more than 41 items fits with a random model between immediate sampling units, and some possible clustering between 3 and 8 meters. That is, one main concentration zone (around x=45-60 and y=35-45) and other more dispersed and less related points.

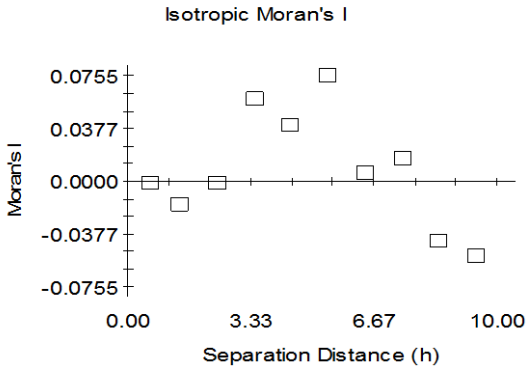

Figure 353 Moran's I Correlogram of cells with more than 41 items (Zone 1, surveys 2009) (GS+).

A Kernel density estimate model of cells with more than 41 items provides a clearer image (Figure 354).

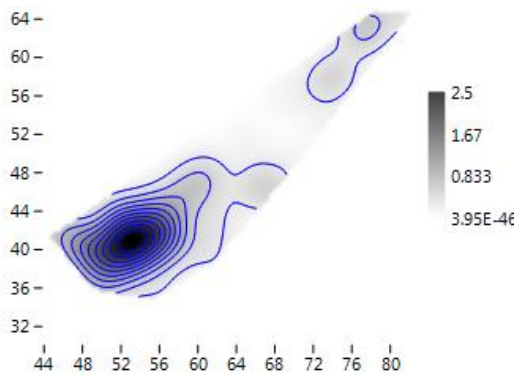

Figure 354 KDE model of cells with more than 40 items (Zone 1, surveys 2009) (Past).

It is easy to see in the South-West corner of the surveyed area an accumulation of higher density points delimiting a less dense area. Following the North-East-South-West directory there is a further area with low density of material evidence.

For Zone 2, only 34 cells show more than 16 items (Figure 355).

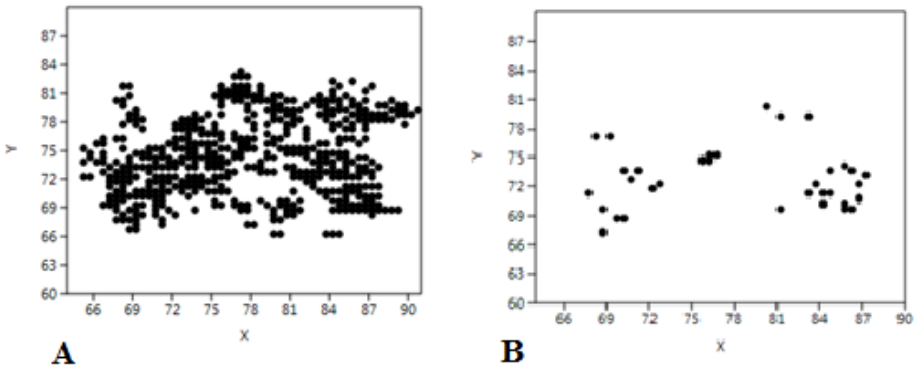

Figure 355 A)Location of sampling units with less than 17 items B) Location with more than 16 items (Zone 2, surveys 2009) (Past).

At first sight it may seem that there is some spatial patterning. Clark and Evans test gives a significant result of spatial clustering (p=0.02). Moran's I Correlogram (Figure 356) of cells with more than 16 items fits with a random model between immediate sampling units, and some possible clustering between 4 and 5 meters. That is, two main concentrations (between x=83-87 and y=69-73 and between x=75-77 and y=73-76) and further smaller concentrations and more dispersed and unrelated density points.

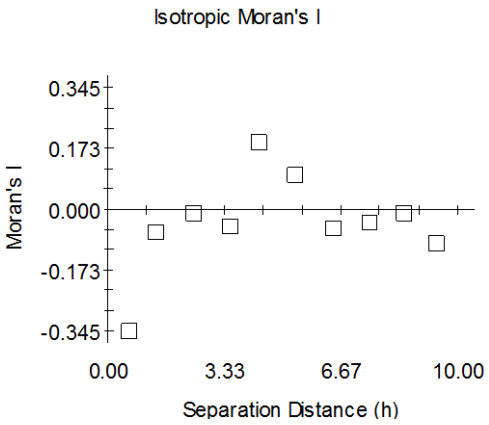

Figure 356 Moran's I Correlogram of cells with more than 16 items (Zone 2, surveys 2009) (GS+).

A Kernel density estimate model of cells with more than 16 items provides a clearer image (Figure 357)

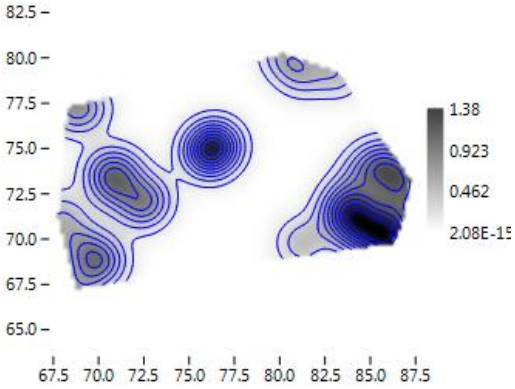

Figure 357 KDE model of cells with more than 16 items (Zone 2, surveys 2009) (Past).

It is easy to see in the East side of the surveyed area a main concentration, as well as in the centre, while other high density points are predominantly located on the West side. It is obvious that anisotropy is present in the main direction North-East-South-West, that is parallel to the estimated ancient lake shoreline. We have calculated anisotropic variograms at different directions for both zones (Figures 358 and 359).

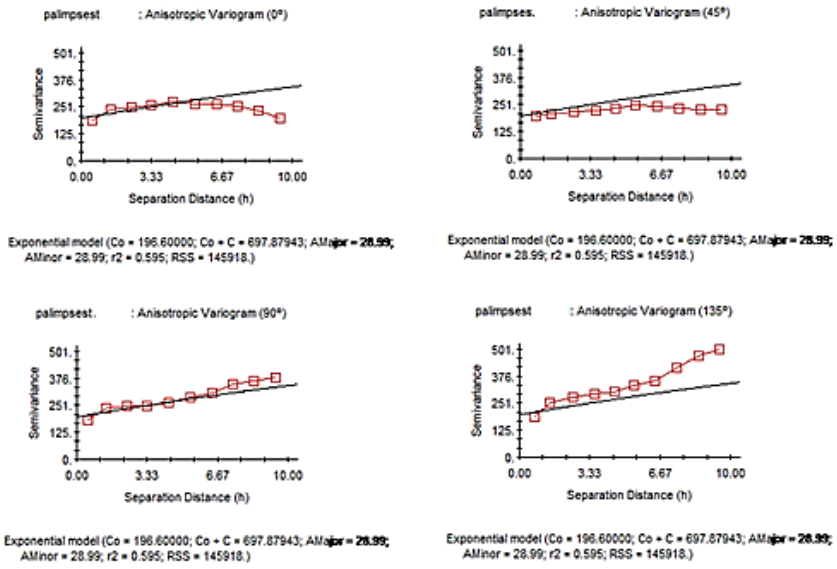

Figure 358 Anisotropic Variogram of all material evidence recovered during surveys of 2009 within Zone 1 (GS+).

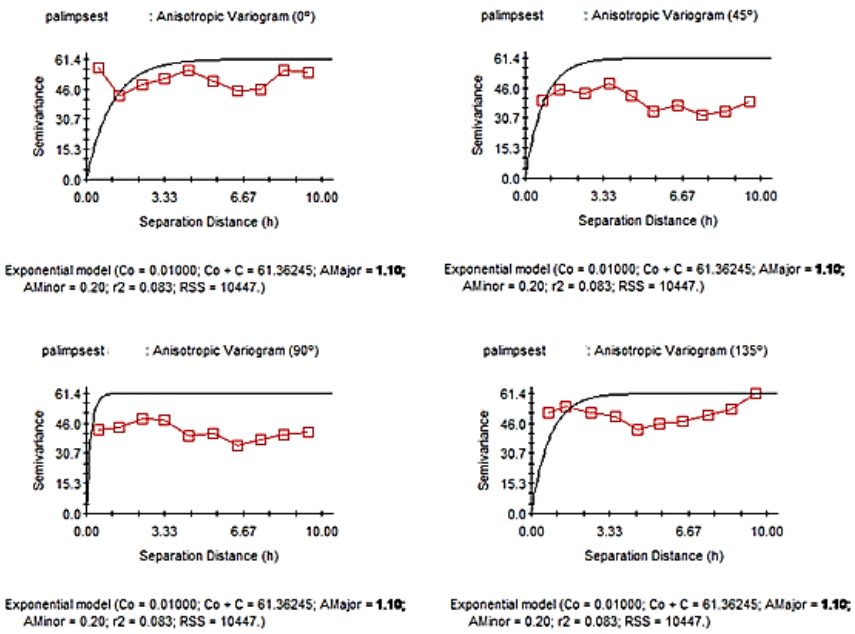

Figure 359 Anisotropic Variogram of all material evidence recovered during surveys of 2009 within Zone 2 (GS+).

For both zones, semivariance is very high in all directions. A main regular pattern characterises Zone 1, while Zone 2 is defined by an irregular discontinuity in the spatial distribution of semivariance values. Within Zone 1 semivariance varies in quite the same way in 0º and 45º (particularly between 4-10 meter), and differently in the 90º and 135º. The Semivariance Surface or Variogram Map (Figures 360 and 361) shows, for Zone 1, that the anisotropy seems to be stronger in the opposite North-West and South-East corners, the unsurveyed areas. Instead, for Zone 2 the semivariance varies in a strongly different ways at 0º, 45º, 90 º and 135º; anisotropy, less attested, is concentrated around the North-West and South-East corners.

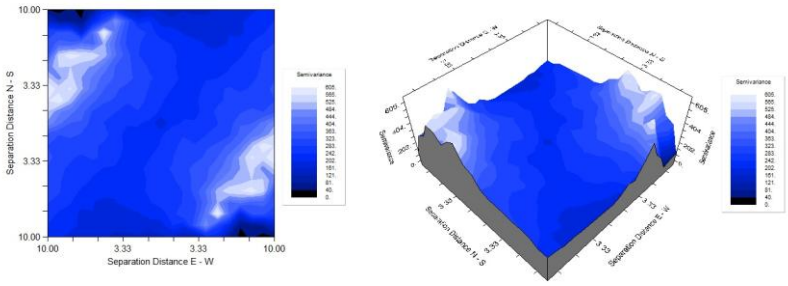

Figure 360 Variogram Map of all material evidence recovered during surveys of 2009 within Zone 1 (GS+).

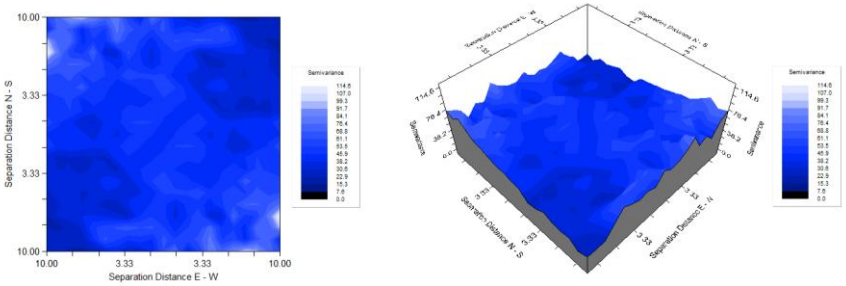

Figure 361 Variogram Map of all material evidence recovered during surveys of 2009 within Zone 2 (GS+).

An exponential isotropic variogram model has been fitted to the empirical variogram for both zones (Figure 362). For Zone 1, C_0 (nugget variance) =142.50, C_0+C (sill) = 285.10 and A_0 (Range) = 1.74, characteristic of spatial dependence at small distance. This model explains 95.2% of sample variance and offers the best possible fit for the available data.

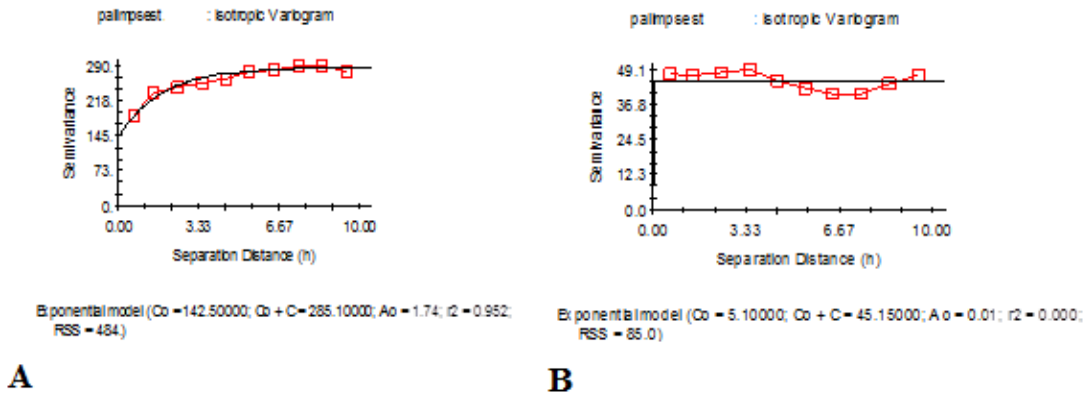

Figure 362 A) Exponential Isotropic Variogram for all material evidence recovered during surveys of 2009 within Zone 1; B) Exponential Isotropic Variogram for all material evidence recovered during surveys of 2009 within Zone 2 (GS+).

For Zone 2 the exponential variogram shows C_0 (nugget variance) =5.10, C_0+C (sill) = 45.15 and A_0 (Range) = 0.01. This model does not explain the sample variance and it does not fit conveniently the empirical data set. This condition suggests the absence of spatial autocorrelation (or, at least, low values) between near sampling units. Then, the interpolation was only performed for Zone 1, where the exponential model explains a high percentage of sample variance. In this case, the global variation of the total number of archaeological observations was estimated, using an inverse distance weighting (Figure 363).

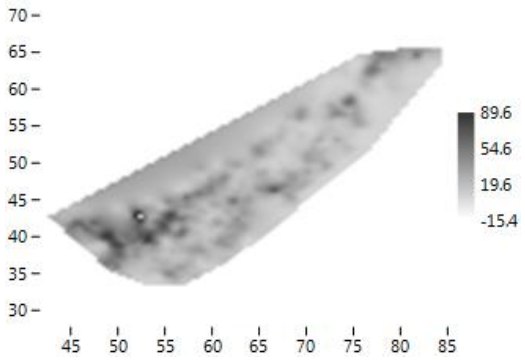

Figure 363 Graphic results of Inverse Distance Weighting calculated for all material evidence recovered during surveys of 2009 within Zone 1 (Past).

This visualization shows a spatial continuity (dependence) of cells with highest frequencies according to the main axis North-East-S outh-West in the South-West corner and in the centre of the surveyed area, with a high level of observations concentrated between x=42-56 and y=44 y. The model does not predict conveniently outliers (cells with more than 40 observations), although it gives correct estimates for all other sampling units. Such spatial pattern can be interpreted as a single quite well defined accumulation deformed for effect of post-depositional and taphonomic processes. For Zone 2 more differential concentrations of material evidence are

observed, distributed however according to a different predominant orientation, which could suggest a potential different functional use of that zone.

8.3. Vertical Posts

519 posts were identified and counted in this area. Instead of their individual *xy* coordinates, we have recorded the coordinates of the cell centroid where they have been recovered were recorded (Figure 364). There are more empty cells (1494) than cells with post, but this fact cannot be interpreted as evidence of spatial irregularity, because of the global mean of 1.16 posts per sampling unit, and a standard deviation of 0.40. Here, the lack of resolution in the spatial coordinates of posts is a problem.

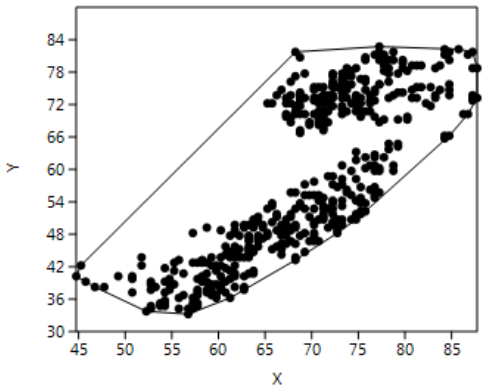

Figure 364 Spatial distribution of sampling units where posts have been recorded during surveys 2009 (Past).

Ripley's *k* analysis for all the reference area suggests the possibility of some degree of spatial clustering, at any distance (Figure 365).

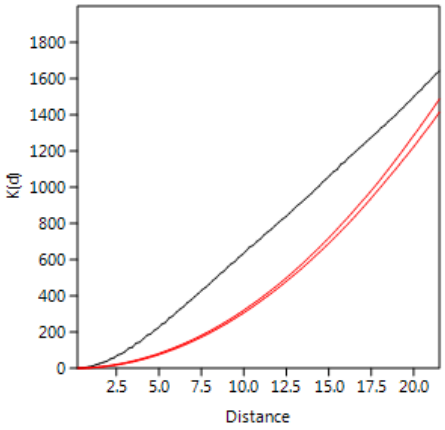

Figure 365 Ripley's *k* analysis on the distance between sampling units with posts recorded in surveys of 2009 (Past).

However, within the convex hull, non-empty sampling units are significantly clustered (Clark and Evans test of nearest neighbourhood (p<0); conversely, those cells where no evidence of post was observed, are significantly overdispersed (Clark and Evans test (p<1). Kernel Density Estimation (Figure 366) confirms the presence of two different zones. According to the Clark and Evans test, posts are statistically significantly clustered.

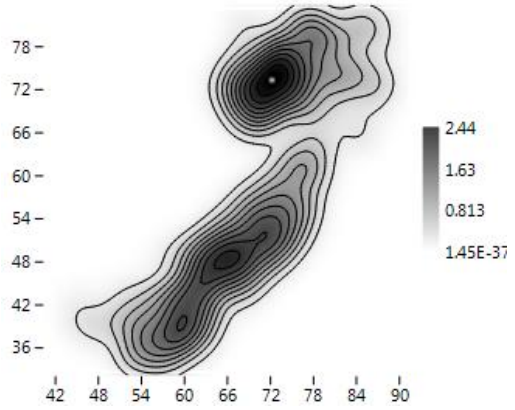

Figure 366 KDE of sampling units where posts have been recorded during surveys of 2009 (Past).

Given that the majority of cells have only one or none, we have not considered here the probability density distribution of spatial frequencies.

The spatial centroid of the area with posts, calculated using an abundance weighted mean spatial center is x= 69.252890, y= 58.282755, with 8.54 m of standard deviation along the *x* axis, and 14.90 m along the *y* axis. A standard deviation ellipse with a long axis of 46.78 m and a short one of 13.31 m delimits an area of 489.17 square meters, where most count data appears. It has been estimated an average density of 0.22 posts per square meter.

The spatial distribution of the abundance of posts per sampling unit gives a Global Moran's *I* result of –0.000452. The theoretical (expected) value assuming spatial autocorrelation (lack of spatial independence) is -0.000515 and the standard error is 0.000515. The test of significance using the normality assumption gave a *z* value of 0.123496, a low significant value. Consequently, we can accept that the probability of detecting a post at some sampling unit is independent of the observation a post in the neighbourhood. These results are comparable with those of the Geary statistics (*C*=1.000040) and Getis-Ord general G (*G*= 0.005754).

The Moran's *I* Correlogram (Figure 367) has been calculated for uniform class distance intervals of 1 meter, and taking into account a 10 meters active lag distance. *I* value between adjacent sampling units is a mere 0.084, above expected value for randomness. As the distance between sampling units increases, *I* value drops off quite gently reaching values corresponding to spatial randomness at 7 meters. From this threshold and beyond, randomness is the rule. This means that actual distribution of posts configures homogeneous areas of positive correlation of around 14 squared meters.

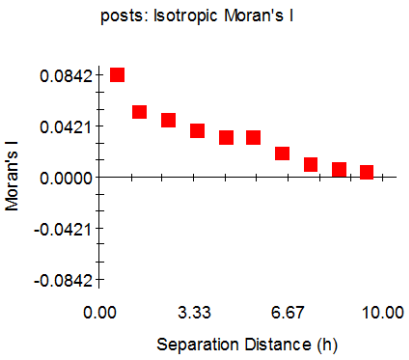

Figure 367 Moran's I Correlogram for posts recovered during surveys of 2009 (GS+).

The spatial distribution of empty cells gives no result of positive autocorrelation, what can be interpreted as the lack of significant empty areas between the main concentrations of vertical posts. Empty cells seem to be overdispersed (as showed by Clark and Evans test, $p<1$). However, those 381 cells with one post are statistically clustered (as showed by the Clark and Evans test) (Figure 368A). These constitute the 73% of all posts and are located in 85% of the effectively surveyed area. Only 66 cells show more than 1 post (Figure 368B). In this case, the Clark and Evans test suggests that the null hypothesis of a random pattern (Poisson process) cannot be rejected at $p<0.05$.

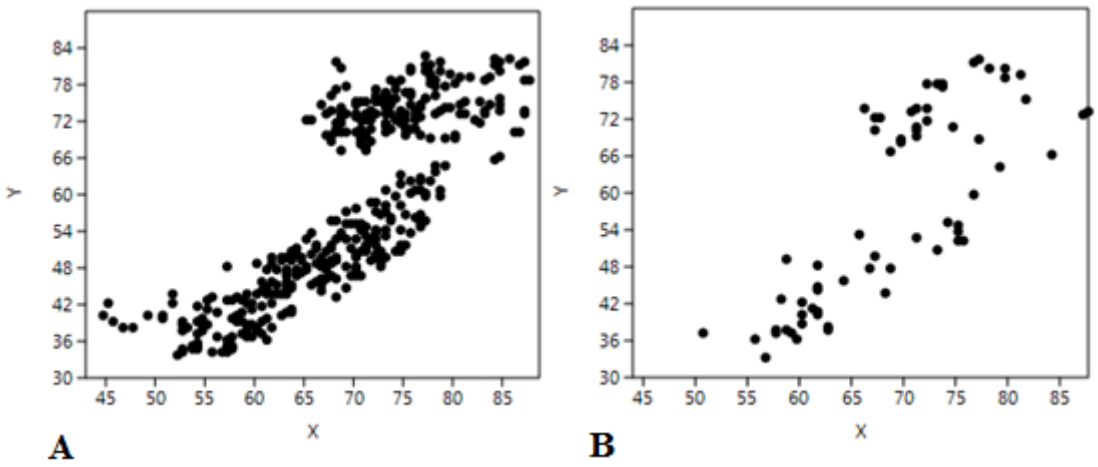

Figures 368 A)Location of sampling units with 1 post (surveys 2001) B)Location with more than 1 post (surveys 2009) (Past).

Kernel Density estimate model of cells with 1 posts provides a clearer image (Figure 369A). It is easy to see in the North-East corner of the surveyed area higher density points, delimiting a less dense sector (Zone 1). Following the South-West direction there is another concentration of high density of posts (Zone 2). The similar spatial distribution is observed for sampling units with 2 or more presences (Figure 369B), confirming a continuity and linearity in posts occurrence. However, in this case, two higher concentrations above identified are distributed in more small low density sub-zones, within the major Zone 1 and Zone 2.

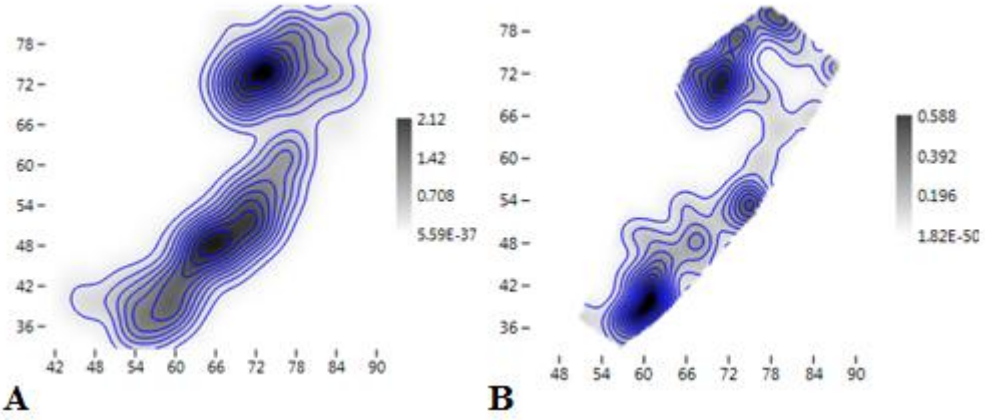

Figure 369A) KDE of cells with 1 post (surveys 2001) (Past). B)KDE of cells with more than 1 post (surveys of 2009) (Past).

The possible presence of anisotropic variation was explored, studying the empirical variogram at different directions (Figure 370).

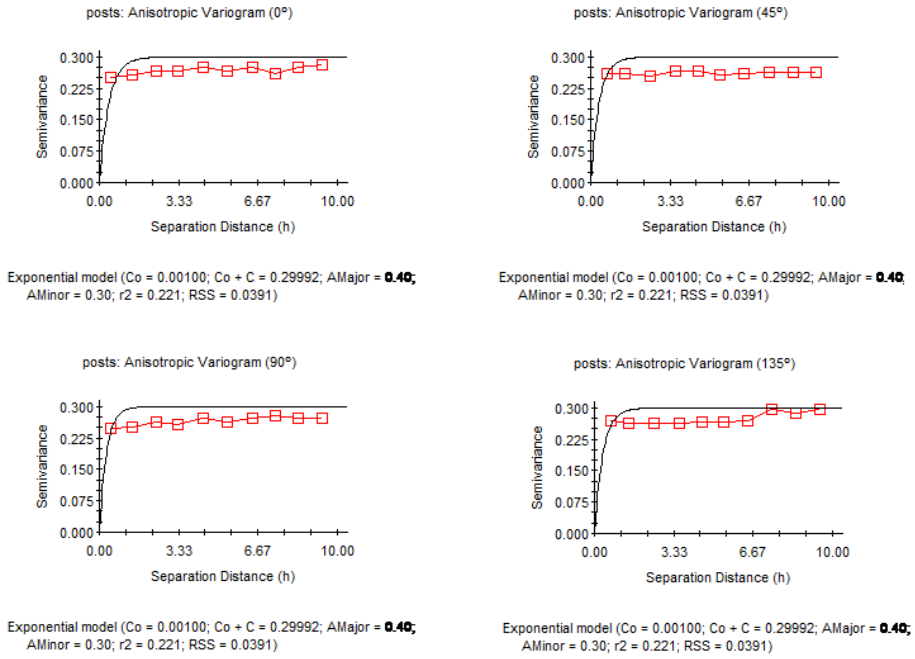

Figure 370 Anisotropic Variogram of posts recovered during surveys of 2009 (GS+).

Resulting variograms are characteristically flat, indicating that no autocorrelation seems to exist between the units, even the lowest *h*'s. We expect this pattern to appear when there is no accumulation, but a random or uniform distribution. In general, these results confirm those of Isotropic Moran Correlogram, showing statistical independence of the presence/absence of posts at any distances, with some hints of continuity in medium sized areas (below 10 meters). Results show that semivariance does not vary at 0º and 45º (particularly between 1 and 6 meters), at 90 º and 135º (that, anyway, are less similar). In the graph of anisotropic Semivariance Surface or Variogram Map (Figure 371), the centre of the map corresponds to the origin of the variogram $\gamma(h)=0$ for every direction. We can see that semivariance is only constant at a very narrow fringe following the main axis of the surveyed area (parallel to the estimated ancient lake shoreline). Anistropy seems to be stronger in the opposite North-East and South-West corners, as effect of the unsurveyed areas.

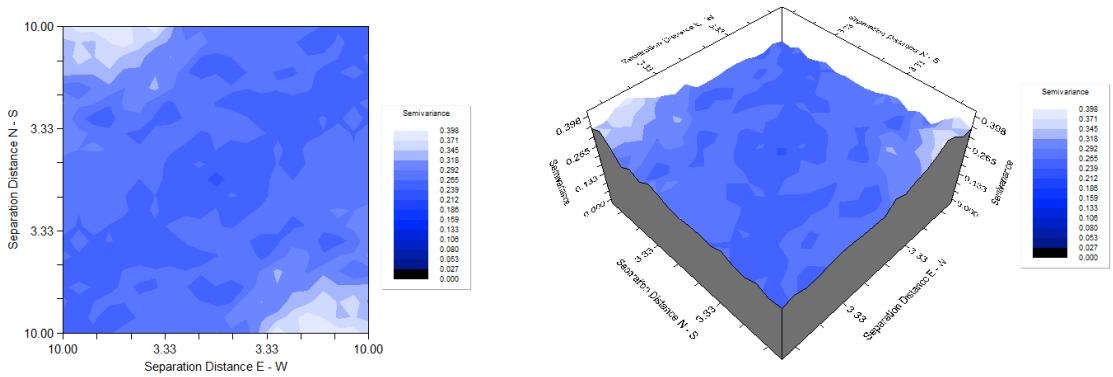

Figure 371 Variogram Map of posts recovered during surveys of 2009 (GS+).

An exponential variogram model with very low random noise (nugget variance, C_0 = 0.0218) and stressing continuity (Sill, C_0+C = 0.2676) at the level only of two related cells (Range, $A_{0=}$0.57) is the best fit for available data (Figure 372). However, it gives a very poor goodness of fit (r^2=0.272), that is, it explains just 27.2% of the spatial differences between the frequency of posts per sample unit.

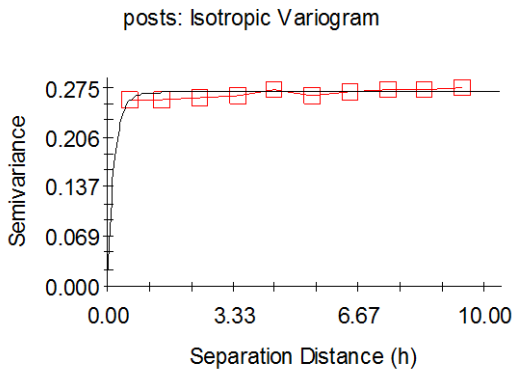

Exponential model (Co = 0.02180; Co + C = 0.26760; Ao = 0.19; **r2 = 0.272**;
RSS = 2.418E-04)

Figure 372 Exponential Isotropic Variogram for posts recovered during surveys of 2009 (GS+).

The related inverse distance weighting interpolated model (Figure 373) has very low explanatory power, but it stresses the alignment of a majority of vertical posts along the estimated ancient lake shoreline. Two differentiated areas can also be observed, separated by overdispersed empty cells.

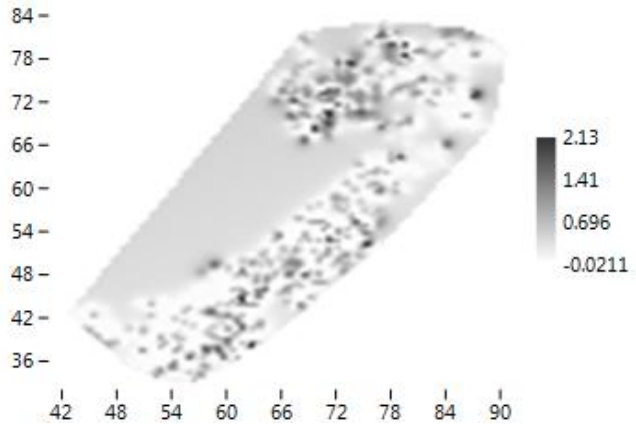

Figure 373 Graphic results of Inverse Distance Weighting calculated for posts recovered during surveys of 2009 (Past).

8.3.1 Vertical posts within Zone 1 and Zone 2

The spatial distribution of sampling units within Zone 1 and Zone 2 where posts have been identified is showed respectively in Figure 374.

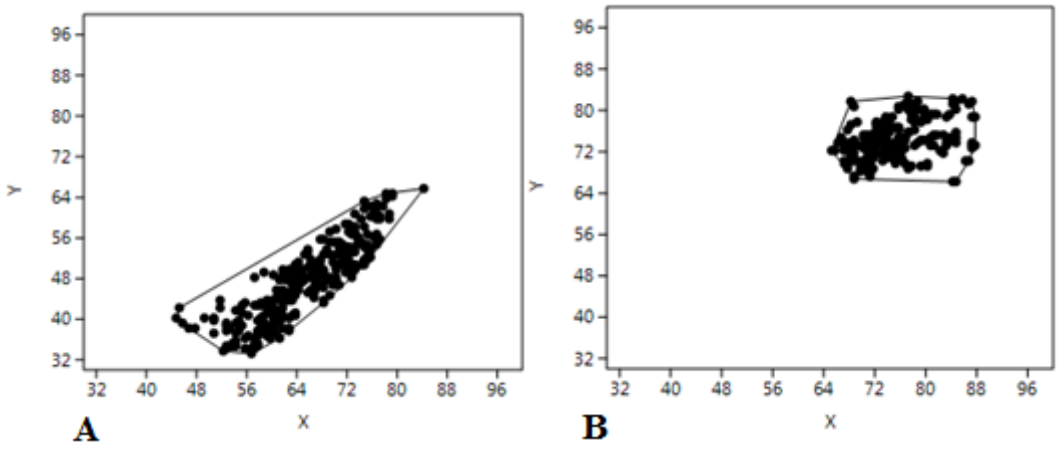

Figure 374 A)Sampling units where posts have been recovered (Zone 1, surveys 2009); B)Sampling units where posts have been recovered (Zone 2, surveys 2009) (Past).

Ripley's *k* analysis for all sampling units included in both sub-areas suggests the possibility of some degree of spatial clustering, at any distance (Figure 375).

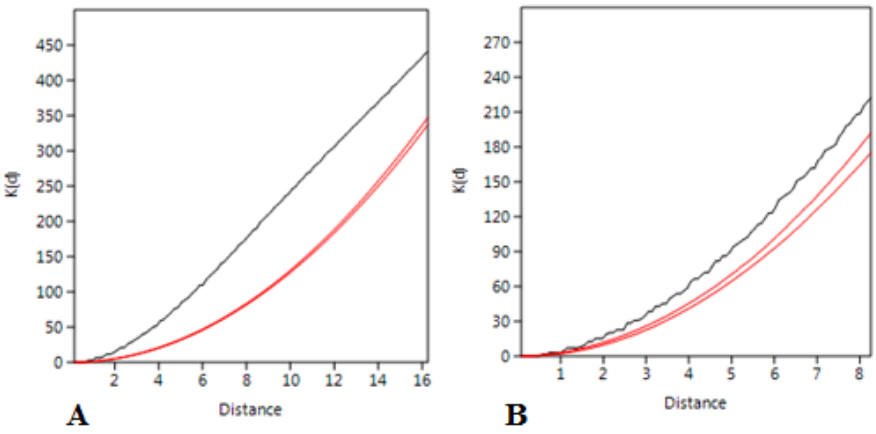

Figure 375 Ripley's *k* analyses on the distance between sampling units with posts recorded in surveys of 2009 within Zone 1 (A) and Zone 2 (B) (Past).

However, for Zone 1 and within the convex hull, the null hypothesis of a random pattern (a Poisson process) for non-empty cells cannot be rejected at $p<0.05$ (Clark and Evans test). This may indicate the possibility that if we do not take into account false zero, equidistant cells have the same probability of counting one or more posts. On the contrary, non-empty cells of Zone 2 are statistically clustered (Clark and Evans test ($p<0$). The hypothesis of randomness should be furthermore remarked when explain the results of the KDE graph (Figure 376). For Zone 1 it allows identifying a central area with two internal sub-sectors (between x=57-61 and y=36-42 and x=62-72 and y=45-53). In this case, the discrepancy between the assumption of randomness according to Clark and Evans test and the traces of clustering in KDE is based probably on the low gradient of density. Instead, within the Zone 2 one main sub-sector emerges; it is observed between x=70-75 and y=72.5 and between x=72.5-75 and y=77.5, where is attested the majority

of posts. We can conclude that the spatial distribution of posts in such zones is significantly different.

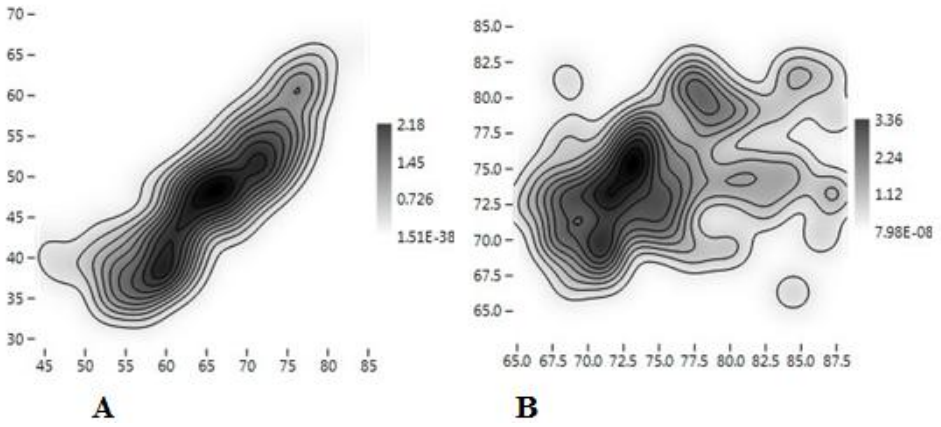

Figure 376 KDE of sampling units where posts have been recorded during surveys of 2009, particularly in Zone 1 (A) and Zone 2 (B) (Past).

Given that the majority of cells have only one or none, we have not considered here the probability density distribution of spatial frequencies.

The spatial distribution of count data per sampling unit shows, for the Zone 1, a Global Moran's *I* of -0.000729. The theoretical (expected) value assuming spatial autocorrelation (lack of spatial Independence) is -0.000756 and the standard error is 0.000756. The test of significance using the normality assumption gave a *z* value of 0.0364, a highly non-significant value. This result is comparable with those of Geary statistic (*C*=1.000315) and Getis-Ord general G (*G*=0.009150).

The spatial distribution of count data per sampling unit shows, for the Zone 2, a Global Moran's *I* of -0.013855. The theoretical (expected) value assuming spatial autocorrelation (lack of spatial Independence) is -0.014493, and the standard error of *I* is 0.014493. The test of significance using the normality assumption gave a *z* value of 0.043991, a highly non-significant value. This result is comparable with those of Geary statistic (*C*=0.999016) and Getis-Ord general G (*G*=0.012028). Consequently, we can accept that the probability of detecting a post at some sampling unit is independent of the observation of a post in the neighbourhood, for both zones.

The Moran's *I* Correlograms (Figure 377) has been calculated for uniform class distance intervals of 1 meter, and taking into account a 10 meters active lag distance. For Zone 1, *I* value between adjacent sampling units is a mere 0.0580, above expected value for randomness. As the distance between sampling units increases, *I* value drops off quite gently reaching at 1 and until 3 meters values around 0.020 (suggesting the presence of some kind of positive spatial autocorrelation). From 6 meter *I* value is located on the line (corresponding to spatial randomness) and between 7-9 meters below the expected value for randomness.

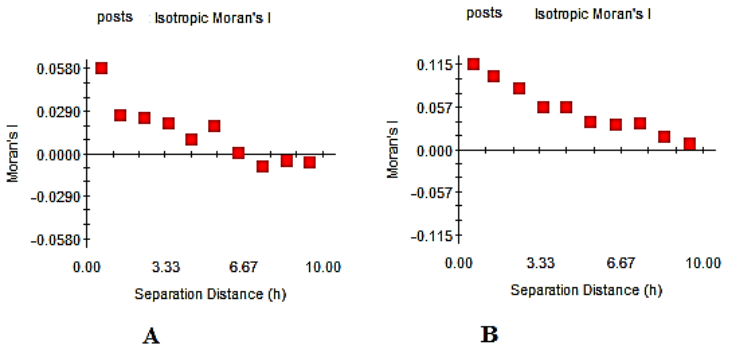

Figure 377 Moran's I Correlograms for posts recovered during surveys of 2009 within Zone 1 (A) and Zone 2 (B) (GS+).

This result gives the possibility of finding out homogeneous areas of positive correlation of around 9 squared meters. For Zone 2, a more regular spatial pattern is observed in the Moran's *I* Correlogram. Between adjacent sdampling units *I* value is a mere 0.115, above the expected for randomness. As the distance between sampling unit increases, *I* value drops off gently (positive spatial autocorrelation is attested between the starting point of the function and 8 meter) and only between 9-10 meters *I* value is nearly the line (corresponding to spatial randomness). The actual distribution of posts, within Zone 2, configures homogeneous areas of positive correlation of around 8 meters.

The spatial distribution of empty cells within both zones gives no result of positive autocorrelation, what can be interpreted as the lack of significant empty areas between the main concentrations of vertical posts. Empty cells seem to be overdispersed (as showed by the Clark and Evans test, $p<1$). For both zones, the null hypothesis of random pattern (a Poisson process) for cells with one post cannot be rejected (according to Clark and Evans test) (Figures 378 and 379). These constitute, for Zone 1, 75% of all posts and are located in 86.3% of the effectively surveyed non-empty cells, while for Zone 2 they represent 71% of all posts and are located in 84% of the surveyed non-empty cells. Furthermore, 36 cells within Zone 1 show more than 1 post; according to Clark and Evans test they are overdispersed. Within Zone 2, for such 309 cells with more than 1 post, the Clark and Evans test suggests that the null hypothesis of a random pattern (Poisson process) cannot be rejected at $p<0.05$. For both zones it is confirmed that equidistant cells have the same probability of counting one or more posts everywhere within the surveyed area.

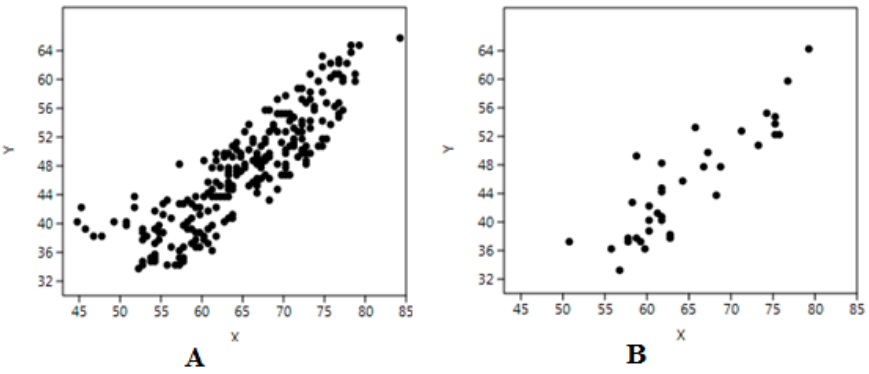

Figures 378 A)Location of sampling units with 1 post B)Location with more than 1 post (surveys 2009) within Zone 1 (Past).

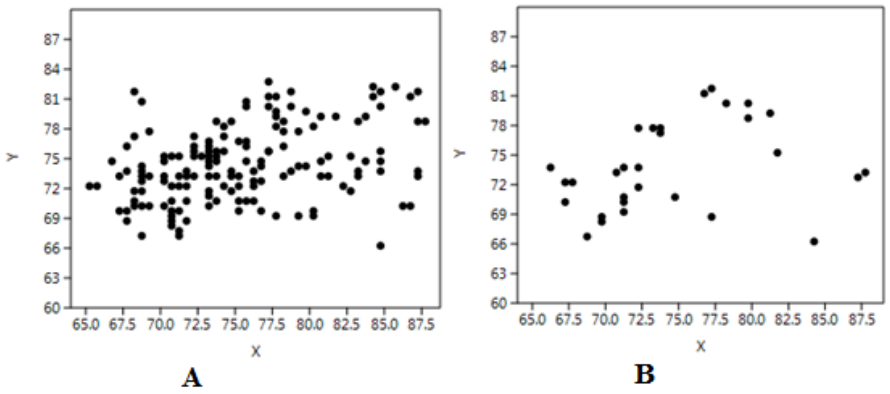

Figures 379 A)Location of sampling units with 1 post B)Location with more than 1 post (surveys 2009) within Zone 2 (Past).

Kernel Density estimate models of cells with 1 posts, for both zones, provide a clearer image (Figures 380 and 381). It is easy to see that, for Zone 1, in the center of the area is observed the higher dense concentration of posts (between x=62-72 and y=45-53); for Zone 2, they are predominantly concentrated between x=67-77 and y=67-77 and further small lower dense areas are located between x=76-78 and y=77-81 and x=82-85 and y=81-82. For Zone 1 are identified three denser concentrations and a further lower dense accumulation in the center of the area. The same occurs for Zone 2: 5 mainly concentrations of higher density are identified and two low dense accumulations.

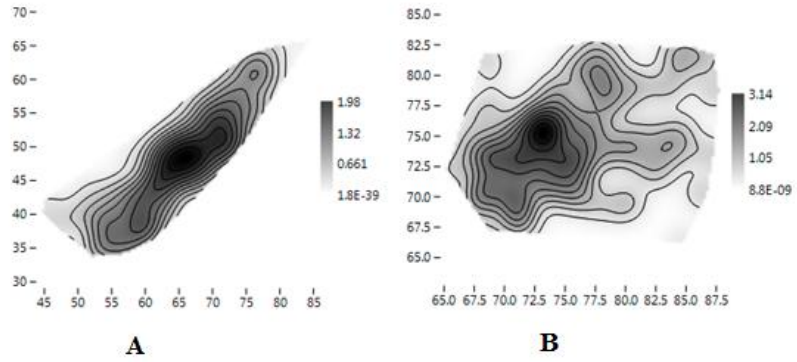

Figure 380 A) KDE of cells with 1 post B)KDE of cells with more than 1 post (surveys of 2009, Zone 1) (Past).

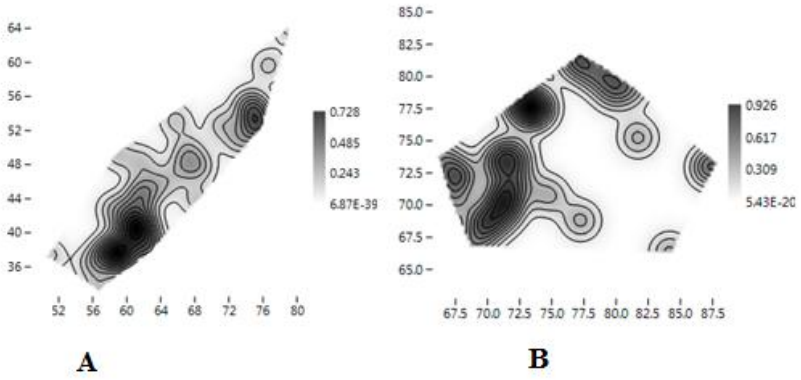

Figure 381 A) KDE of cells with 1 post B)KDE of cells with more than 1 post (surveys of 2009, Zone 2) (Past).

We have explored the possible presence of anisotropic variation, studying the empirical variogram at different directions (Figures 382 and 383).

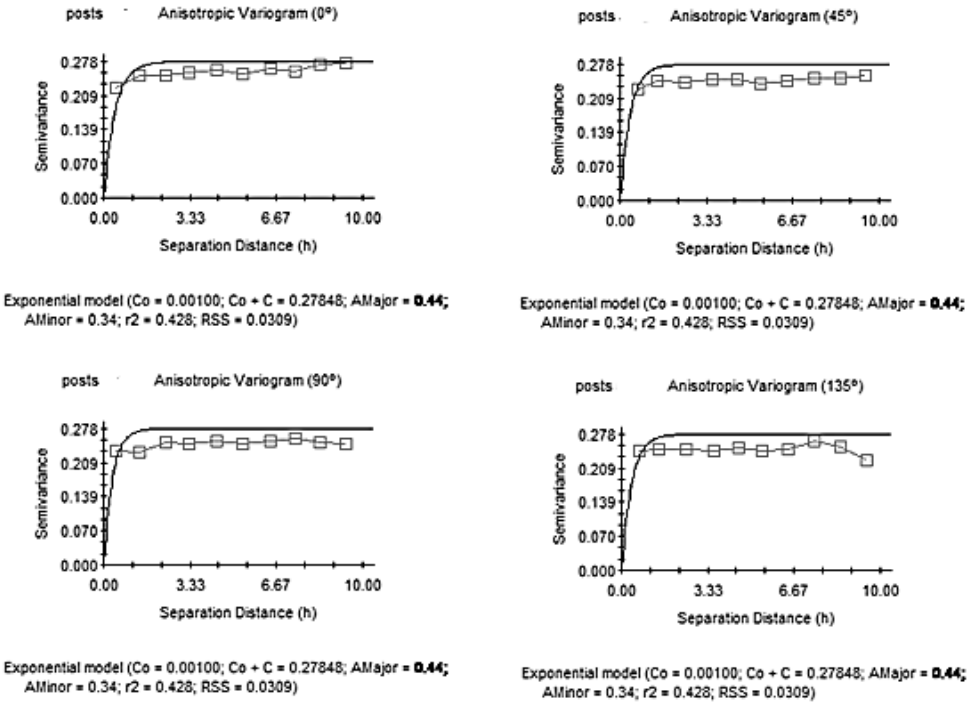

Figure 382 Anisotropic Variogram of posts recovered during surveys of 2009 within Zone 1 (GS+).

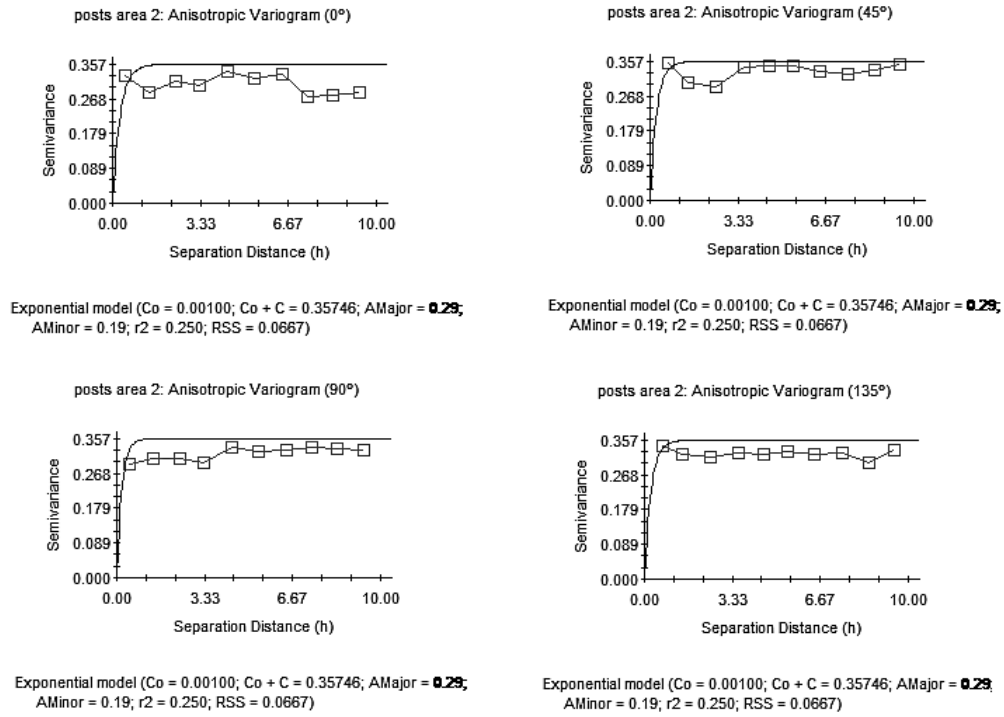

Figure 383 Anisotropic Variogram of posts recovered during surveys of 2009 within Zone 2 (GS+).

Resulting variograms are characteristically predominant flat, indicating that no autocorrelation seems to exist between the units, even at the lowest *h*'s. We expect this pattern to appear when there is no accumulation, but a random or uniform distribution. In general these results confirm those of Isotropic Moran Correlogram, showing statistical independence of the presence/absence of posts at any distances, with some hints of continuity in medium sized area (below 10 meters). Results for Zone 1 show that semivariance does not vary at 45º and 90º, as well as at 0º and 135º (particularly for the first 6 meters). For Zone 2 semivariance varies in strongly different way at any distances. In the graph of anisotropic Semivariance Surface or Variogram Map (Figures 384 and 385) the center of the map corresponds to the origin of the variogram $\gamma(h) = 0$ for every direction. We can see that semivariance, for Zone 1, is only constant in the center, following the main axis of the surveyed area (parallel to the estimated ancient lake shoreline). Anisotropy seems to be stronger in the opposite North-West and South-East corners, as effect of the unsurveyed areas, as above mentioned. For Zone 2 semivariance varies strongly in every direction and consequently higher level of anisotropy is observed, particularly concentrated around the corners.

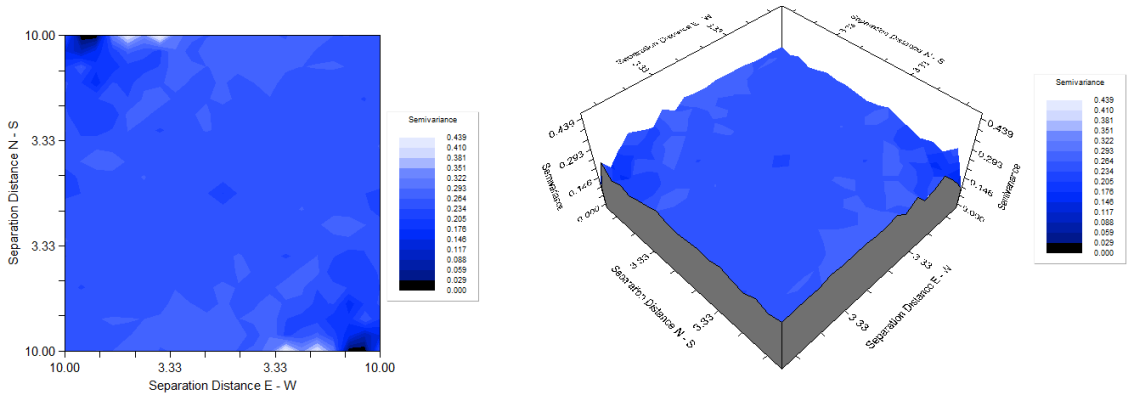

Figure 384 Variogram Map of posts recovered during surveys of 2009 within Zone 1 (GS+).

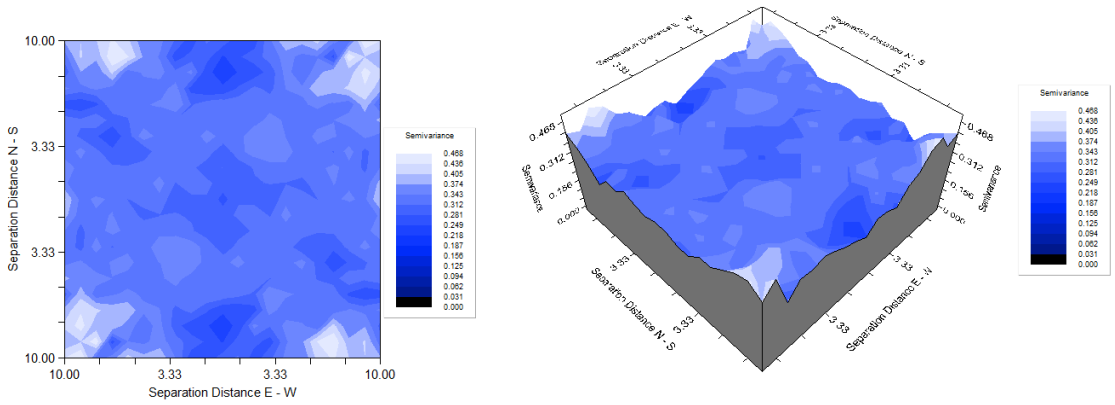

Figure 385 Variogram Map of posts recovered during surveys of 2009 within Zone 2 (GS+).

For Zone 1 an exponential variogram model with very low random noise (Nugget Variance, C_0 =0.03450) and stressing continuity (Sill, C_0+C= 0.25100) at the level only of single cells (Range, A_0 =0.25) is the best we can fit to the data (Figure 386A). However, it gives a very poor goodness of fit (r^2=0.654), that is, it explains just 65.4% of the spatial differences between the frequency of posts per sample unit.

For Zone 2 is used an exponential variogram model with Nugget Variance, C_0 =0.02190, Sill, C_0+C= 0.32080 and Range, $A_{0=}$ 0.01 (Figure 386B). However, since it does not give goodness of fit (r^2=0), it does not fit conveniently the empirical data set. This condition, as well as the strong anisotropy identified for Zone 2, confirms low values of spatial autocorrelation between near sampling units.

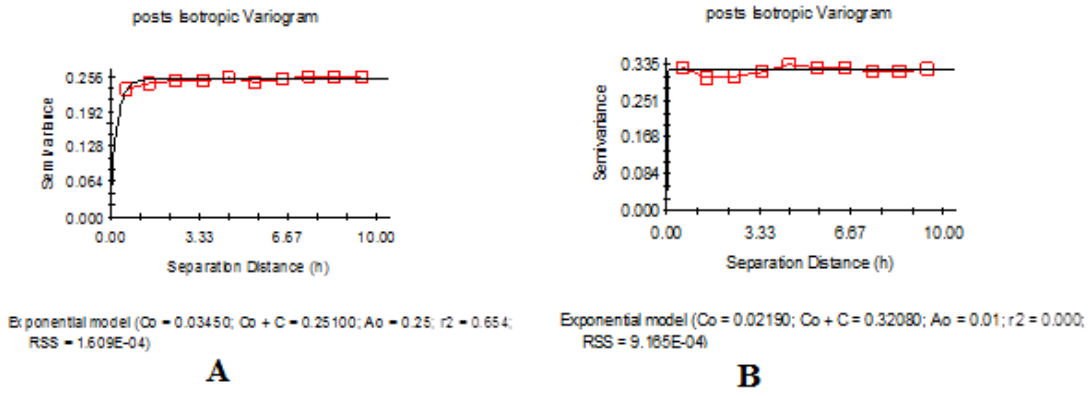

Figure 386 Exponential Isotropic Variogram for posts recovered during surveys of 2009 within Zone 1 (A) and Zone 2 (B) (GS+).

The related Inverse Distance Weighting models (Figure 387) have very low explanatory power, but they stress the alignment of a majority of vertical posts along the estimated ancient lake shoreline, especially for Zone 1. Conversely, Zone 2 shows linear-horizontally-oriented distribution of posts that would be suggesting potential different functionalities of such two zones.

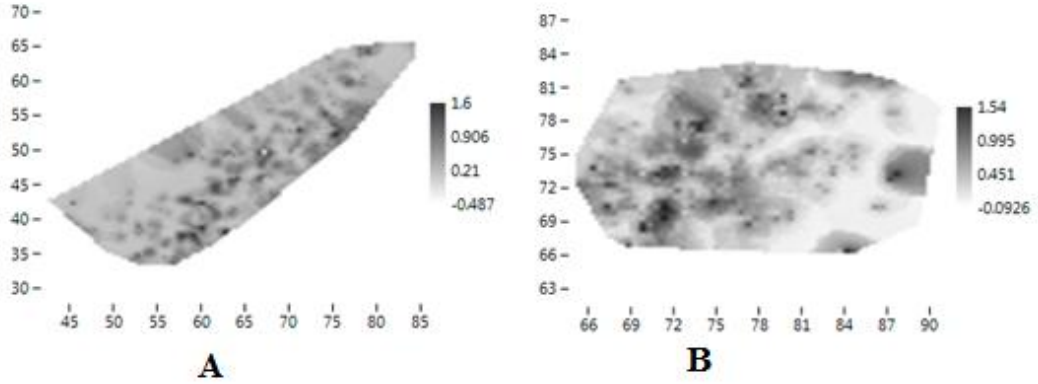

Figure 387 Graphic results of Inverse Distance Weighting calculated for posts recovered during surveys of 2009 within Zone 1 (A) and Zone 2 (B) (Past).

8.4. Saddle querns

276 saddle querns were identified and counted; they are sub-divided in 246 grindstones and 30 handstones. A lot of empty cells have been identified **(**1732), giving a frequency mean of 0.14 saddle querns per sampling unit and a standard deviation of 0.46. A single cell with 5 saddle querns should be remarked. Figure 388 shows the spatial distribution of cells with some saddle querns.

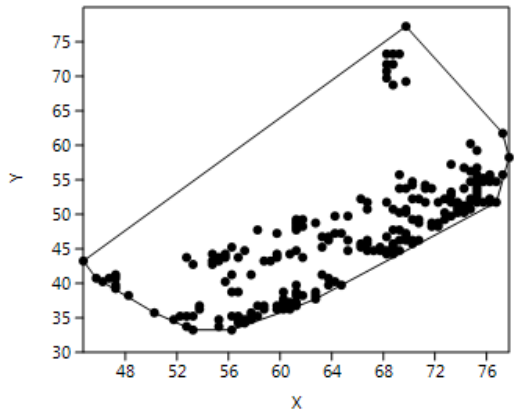

Figure 388 Spatial distribution of sampling units where saddle querns have been recorded during surveys of 2009 (Past).

Ripley's *k* analysis on the distance between sampling units with saddle querns evidence suggests the possibility of some degree of spatial clustering at the global scale of the reference area (Figure 389).

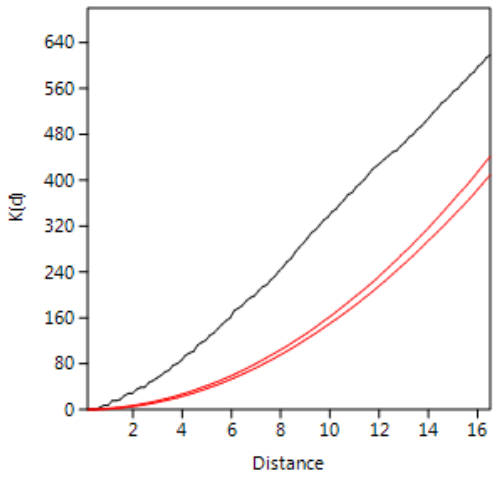

Figure 389 Ripley's *k* analyses on the distance between sampling units with saddle querns recorded in surveys of 2009 (Past).

Within the Convex hull defined by the effectively surveyed sampling units, 209 non-empty cells are statistically significantly clustered (Clark and Evans test $p<0$). A Kernel Density Estimation (Figure 390) shows a relatively regular distribution with three main sub-areas of stronger density and a further isolated presence around the South-East corner.

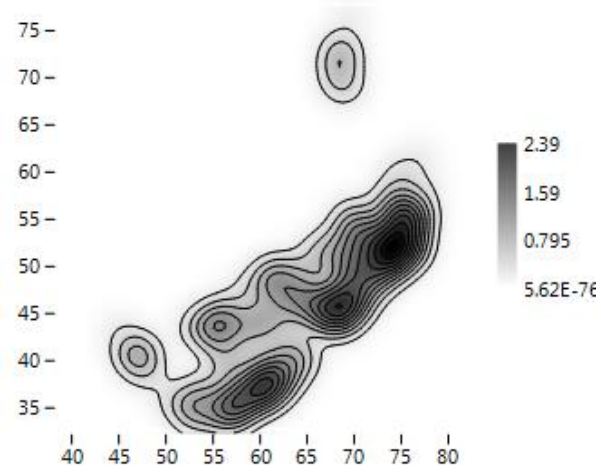

Figure 390 KDE of sampling units where saddle querns have been recorded during surveys of 2009 (Past).

When considering the raw quantity of saddle querns at each cell, the probability density distribution of spatial frequencies does not follow a J-shaped distribution. A majority of sampling units have raw counts of saddle querns of less than 1 element (global mean= 0.14 saddle querns per sampling unit) (Figure 391). Some cells are distinguished from the majority (interpretable as outliers), with 2, 3, 4 and 5 saddle querns. The low amount of such evidence per sampling unit of 0.25 sq. meters indicates the relatively high distance between individual saddle quern.

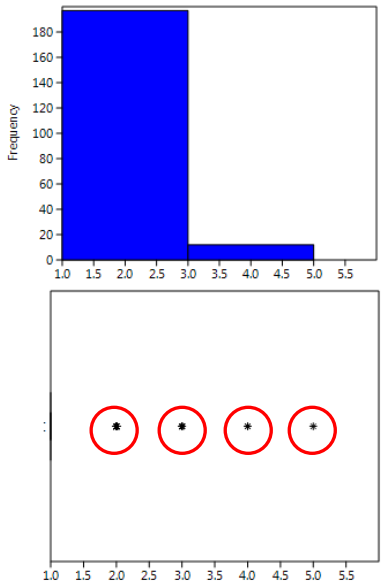

Figure 391 Histogram and box plot of frequencies observed for saddle querns recovered during 2009 (Past).

The spatial distribution of saddle querns frequencies fits with a Negative Binomial distribution with k=17.345 and p=0.977 with the Kolmogorov Smirnov Test=1.00. This condition suggests predominant randomness in the spatial distribution of the abundance of saddle querns per sampling unit (Figure 392).

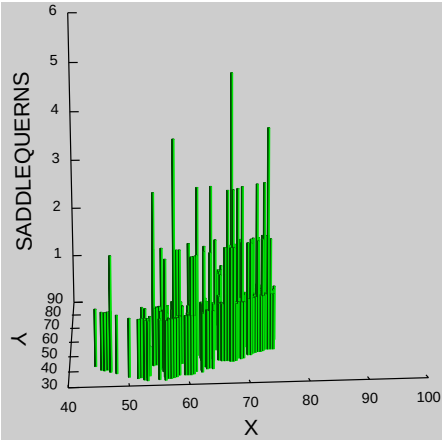

Figure 392 3D Histogram of saddle querns recovered during surveys of 2009 (Systat 13).

The spatial centroid of the area with saddle querns, calculated using an abundance weighted mean spatial center is x= 65.626812, y= 47.061594, with 7.83 m of standard deviation along the *x* axis, and 8.03 m along the *y* axis. A standard deviation ellipse with a long axis of 29.24 m and a short one of 12.48 m delimits an area of 286.72 square meters, where most count data appear. It has been estimated an average density of 0.11 saddle quern per square meter.

The spatial distribution of the abundance of saddle querns per sampling unit gives a Global Moran's *I* result of –0.000266. The theoretical (expected) value assuming spatial autocorrelation (lack of spatial independence) is -0.000515 and the standard error is 0.000515. The test of significance using the normality assumption gave a *z* value of 0.48474, a low significant value. Consequently, we can accept that the spatial distribution of saddle quern is not significantly different than the expected value under a random distribution. This is what would be expected in the case of the same frequency of saddle quern in quite every spatial location. These results are comparable with those of the Geary statistics (*C*=1.001055) and Getis-Ord general G (*G*= 0.015477).

However, as it was suggested in chapter 4, global measures of autocorrelation are misleading in the case aggregated behaviour resulting in an accumulation of things. The Moran's *I* Correlogram (Figure 393) has been calculated for uniform class distance intervals of 1 meter and taking into account a 10 meters active lag distance. *I* value at the starting point is about 0.232, above the expected value for randomness. As the distance between sampling units increases, *I* value drops off quite gently and continuously always above the expected value for randomness (suggesting the presence of positive spatial autocorrelation), although between 6-7 meter *I* value is on the line (corresponding to spatial randomness). Homogeneous areas of positive correlation of around 6 meters are observed for saddle querns.

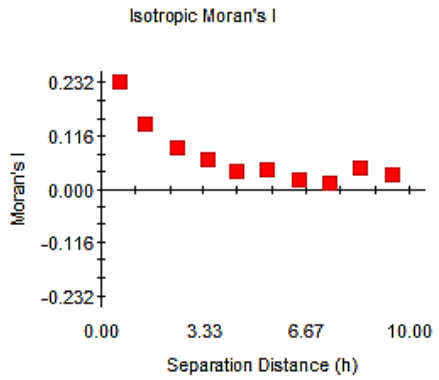

Figure 393 Moran's I Correlogram for saddle querns recovered during surveys of 2009 (GS+).

Using local indicators of spatial association (see at the end of the chapter), we have considered only those cells in which the frequency of saddle querns exceed what would be expected according to a random model, that is, the 51 cells with 2 or more items. For such sampling units, the null hypothesis of a random pattern (Poisson process) can not be rejected at $p<0.05$. Despite the absence of clustering within such data, it is interesting to note that they are predominantly distributed according to the North-East-South-West alignement, parallel to the estimated ancient lake shoreline of concentrations (Figure 394A), and more homogeneously distributed in the North-Eastern portion of the surveyed area, as showed even by the Kernel Density Estimation (Figure 394B).

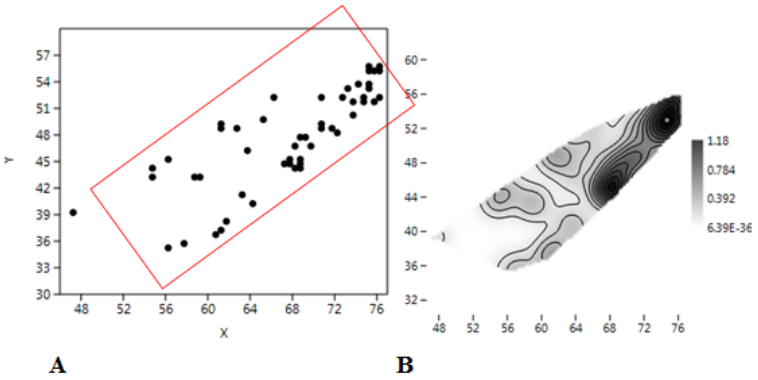

Figure 394 A)Spatial distribution of cells with more than 1 saddle quern B) KDE of such cells (surveys of 2009) (Past).

We have investigated the obvious presence of anisotropic variation exploring the empirical variogram at different directions (Figure 395).

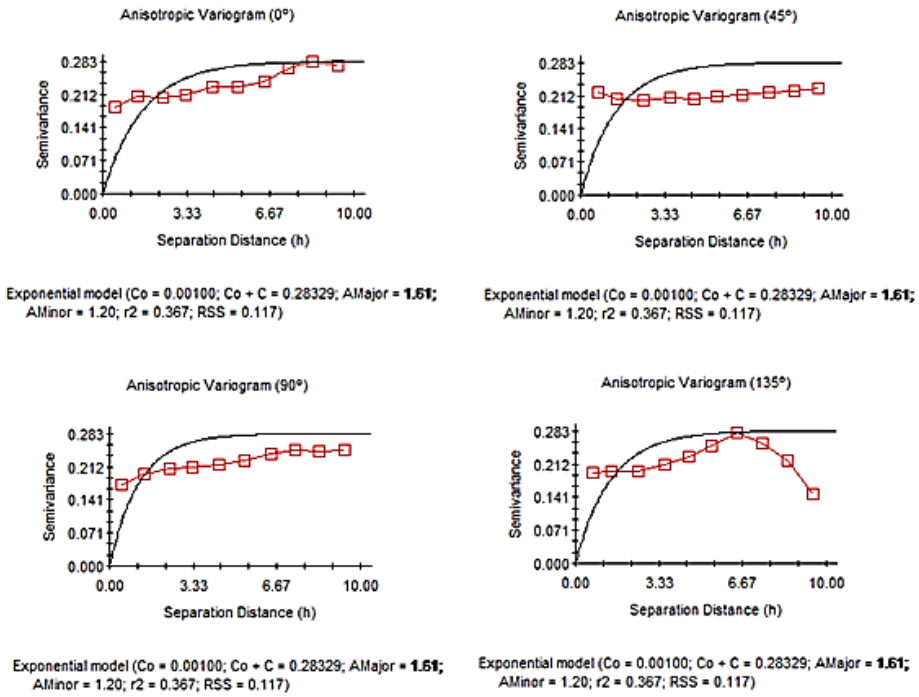

Figure 395 Anisotropic Variogram of saddle querns recovered during surveys of 2009 (GS+).

In general anisotropic variograms appeat to be comparatively flat (except for 135º), signaling the scarceness of statistical dependence even between near sampling units. The Semivariance Surface or Variogram Map (Figure 396**)** suggests that the maximum anisotropy is concentrated in the opposite North-West and South-East corner, distributed in narrow fringe, as effect of such unsurveyed corners.

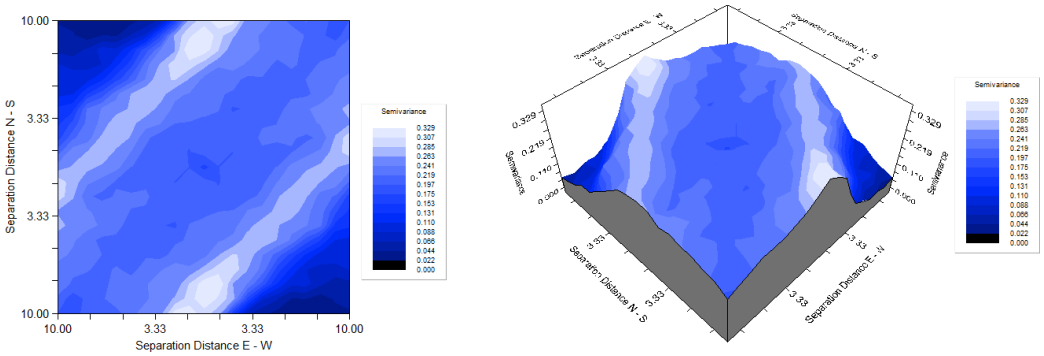

Figure 396 Variogram Map of saddle querns recovered during surveys of 2009 (GS+).

An exponential variogram model (Figure 397) with Nugget Variance, C_0 =0.04070, a Sill, C_0+C = 0.22540 and a Range, A_0 = 0.38 has been fitted to the empirical variogram. This model gives a very poor goodness of fit (r^2 = 0.349), that is, it explains just 34.9% of the spatial differences between the frequency of saddle querns per sample unit.

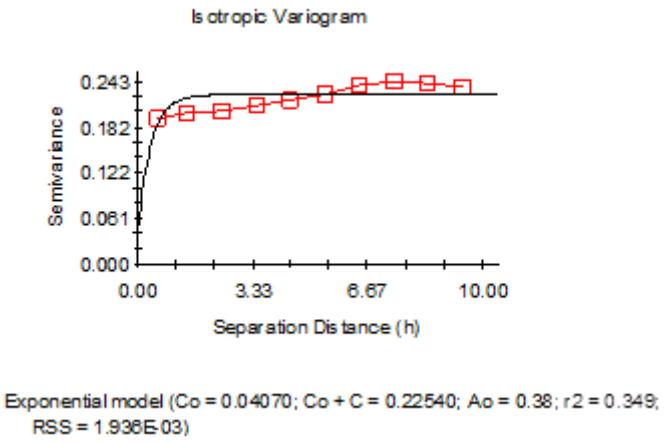

Figure 397 Exponential Isotropic Variogram for saddle querns recovered during surveys of 2009 (GS+).

Although not entiretly trustworthly because of the low non-linear fit, the corresponding inverse distance weighting to the above exponential model (Figure 398) shows some differences with the spatial distribution of posts. For instance, it is observed emptiness of saddle querns in the North-West corner, opposite to the high presences of posts there. Even the spatial continuity of saddle querns in the center of the area is differently distributed compared to posts. Then, saddle querns seem to occupy cells where posts are absent and they are predominantly observed nearby the hypothetical ancient lake shoreline.

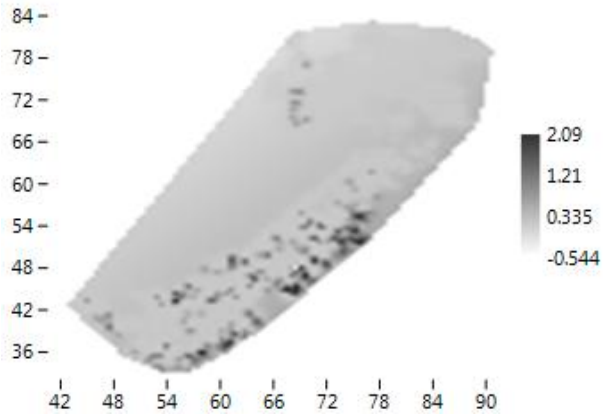

Figure 398 Graphic results of Inverse Distance Weighting calculated for saddle querns recovered during surveys of 2009 (Past).

It is important to take into account that this interpolated model has some relevant limits: it does not predict well the outliers, but gives a sufficiently good prediction of the more frequent abundance values. In general, saddle querns seem to be predominantly concentrated in the Southern side of the surveyed area and distributed according to a North-East-South-West orientation. Allignements in their distribution are observed and suggest some working hypothesis: the pattern of uniformity with quite everywhere the same number of saddle querns located in closer sampling units (attesting some kind of positive autocorrelation) seems to be the most expected result, hypothesising that such evidence was used in performing some and the same specific activities, that the comparison with the spatial distribution of other categories of observables could help to clarify.

8.4.1 Saddle querns for Zone 1 and Zone 2

Figure 399 shows the spatial distribution of sampling units where saddle querns have been identified, within both zones.

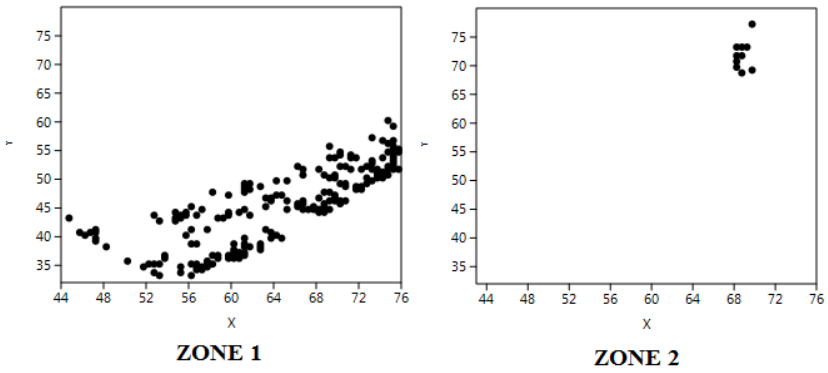

Figure 399 Spatial distribution of cells with saddle querns within Zone 1 and Zone 2 (surveys 2009) (Past).

Ripley's *k* analysis on the distance between sampling units with saddle querns suggests the possibility of some degree of spatial clustering for Zone 1 at the global scale of the reference area, while a strong random pattern characterizes Zone 2 (Figure 400).

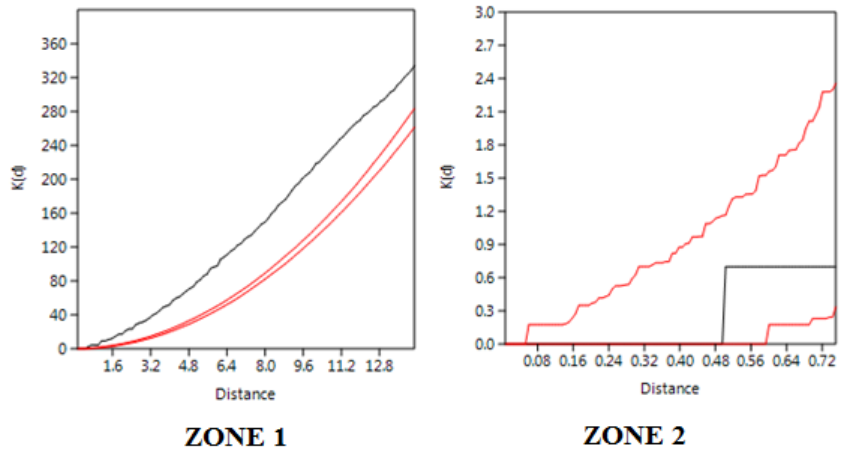

Figure 400 Ripley's *k* analyses on the distance between sampling units with saddle querns recorded in surveys of 2009 within Zone 1 and Zone 2 (Past).

However, within the convex hull defined by the effectively surveyed sampling units for each zone, the null hypothesis of a random pattern (a Poisson process) cannot be rejected at $p<0.05$ (Clark and Evans test). This indicates the possibility that equidistant cells have the same probability of counting one or more saddle querns within both areas.

The Kernel Density Estimation (Figure 401) shows, for Zone 1, the occurrence of two main concentrations (between x=56-64 and y=32-40 y and between x=64-76 and y=44-56 (internally sub-divided in two accumulations); wihin Zone 2 saddle querns are quite absent and distributed, in 1 occurrence for sampling unit, in different spatial locations.

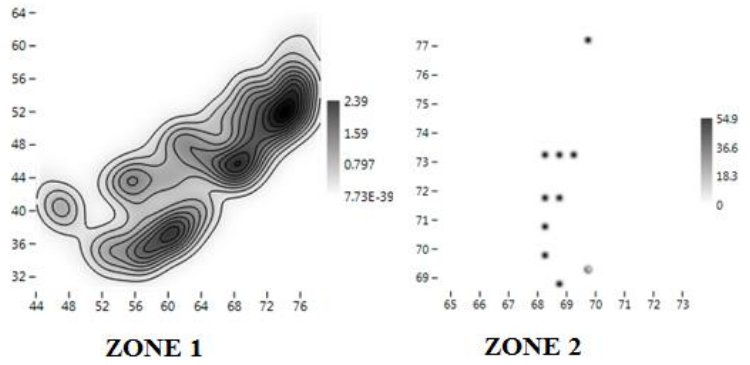

Figure 401 KDE of sampling units where saddle querns have been recorded during surveys of 2009, within Zone 1 and Zone 2 (Past).

There are relevant differences in the spatial location of sampling units with saddle querns frequencies within such zones; indeed, Zone 1 concentrates the majority of observations (n= 266), the range of frequencies is between 1 and 5, with a mean of 1.33 observations per sampling unit and the variance is 0.4365768. Both histogram and boxplot identified a break point corresponding to the value 3 and two cells are distinguished from the majority, with 4 and 5 saddle querns (interpretable, according to boxplot, as outliers) (Figure 402). Zone 2 is characterised by only 10 saddle querns, with the frequency of 1 element in each sampling unit, with a mean of 1.17 observations per sampling unit and the variance is 0.

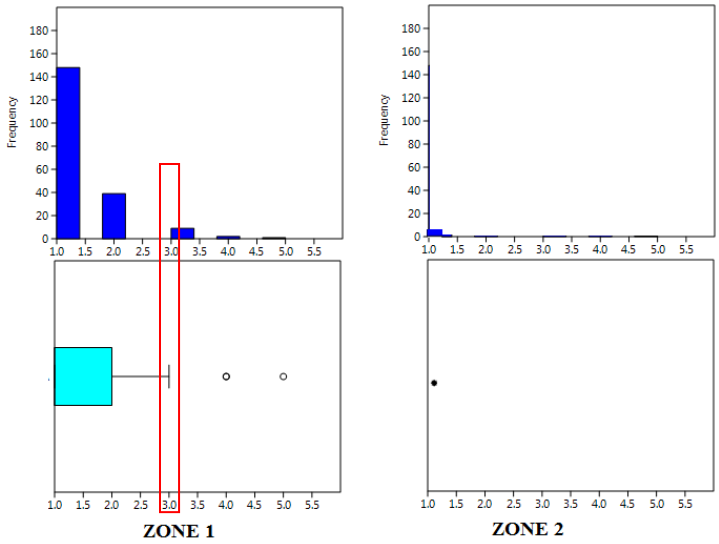

Figure 402 Histogram and box plot of frequencies observed for saddle querns recovered during 2009 within Zone 1 and Zone 2 (Past).

While the spatial distribution of saddle querns in Zone 1 is fitted with a Negative Binomial distribution (with k=0.408 and p=0.670) with K-S Test=1, spatial distribution of such scarce presences in Zone 2 is not fitted with any of standard distribution. This condition suggests randomness in the spatial distribution of saddle querns per sampling unit within Zone 1 and highlights their scarceness for Zone 2 (Figure 403).

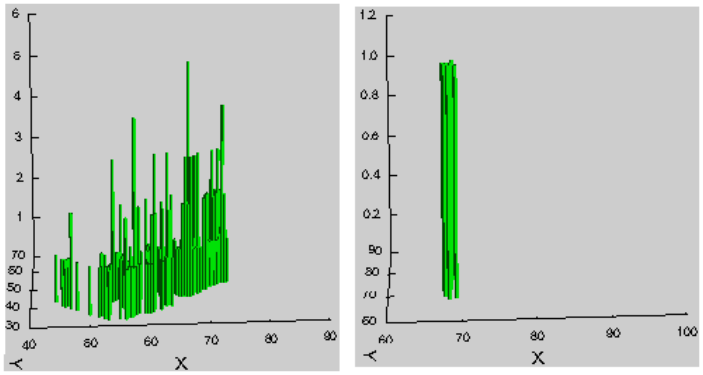

Figure 403 3D Histogram of saddle querns recovered during surveys of 2009 within Zone 1 and Zone 2 (Systat 13).

Within Zone 1 the spatial distribution of count data per sampling unit shows a Global Moran's *I* of -0.000705. The theoretical (expected) value assuming spatial autocorrelation (lack of spatial Independence) is -0.000756 and the standard error of *I* is 0.000756. The test of significance using the normality assumption gave a *z* value undefined. These results are comparable with those of the Geary statistics (*C*=1.000485) and Getis-Ord general G (*G*=0.016497).

The spatial distribution of count data per sampling unit shows, for Zone 2, a Global Moran's *I* of -0.001535. The theoretical (expected) value assuming spatial autocorrelation (lack of spatial Independence) is -0.001621, and the standard error of *I* is 0.001621. The test of significance using the normality assumption gave a *z* value of 0.052647, a highly non-significant value. This result is comparable with those of Geary statistic (*C*=0.999193) and Getis-Ord general G (*G*=0.133333).

Consequently, we can accept that the spatial distribution of saddle querns within both zones is not significantly different than the expected value under a random distribution, as expected in the case of the general same frequency of grindstones in every spatial location.

The Moran's *I* Correlogram (Figure 404) has been calculated for uniform class distance intervals of 1 meter, and taking into account a 10 meters active lag distance. For Zone 1, *I* value at the starting point of the function is about 0.190, above expected value for randomness. As the distance between sampling units increases, *I* value drops off quite gently reaching at 1 meter and until 3 meter around 0.020. From 4 meter *I* value is located on the line (corresponding to spatial randomness) and between 7 and 9 meter below the expected value for randomness. From 6 meter I value is twice located on the line, and between 7-9 meters I values are below the expected value for randomness.

For Zone 2 Moran's *I* Correlogram shows a more irregular spatial pattern (Figure 404). At the starting point of the function *I* value is about 0.123, above the expected value for randomness. As the distance between sampling unit increases (after the 1 meter where *I* value is 0.125) *I* value drops off abruptly above the expected value for randomness only between 2 and 4 meters. From 5 meters *I* values are distributed on the line (corresponding to spatial randomness).

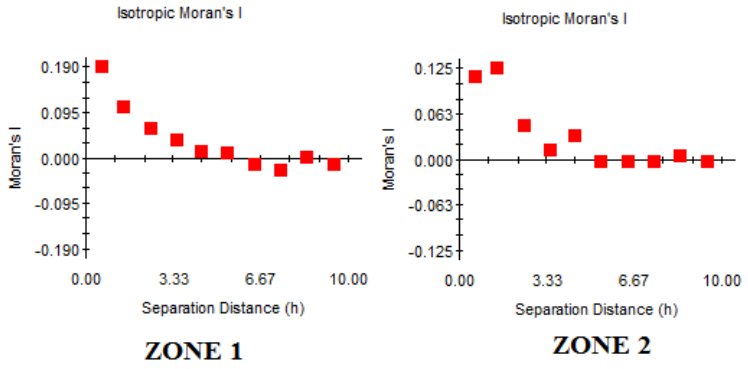

Figure 404 Moran's I Correlograms for saddle querns recovered during surveys of 2009 within Zone 1 and Zone 2 (GS+).

Then, for both zones such results give the possibility of finding spatially dependent area (positively autocorrelated) of 3 meters of radius.

Taking into consideration what is suggested both by box plot and histogram, that is the occurrence of a break point in the frequencies of saddle querns in correspondence with a value of 3 items for Zone 1 (where the majority of saddle querns are observed), 95% of them are located in 74% of the effectively surveyed area, in such a way that only 3 cells show more than 3 items.

We have investigated the obvious presence of anisotropic variation exploring the empirical variogram at different directions, for both zones (Figure 405). In general, results for Zone 1 show that semivariance partially varies in the same way in 0º and 90º and in 45º and 135º, only in the first distances, because from 3-4 meter they change abruptly. The Semivariance Surface or Variogram Map (Figure 406) suggests that the maximum anisotropy is concentrated in the centre of the Southern and Northern side of the considered area.

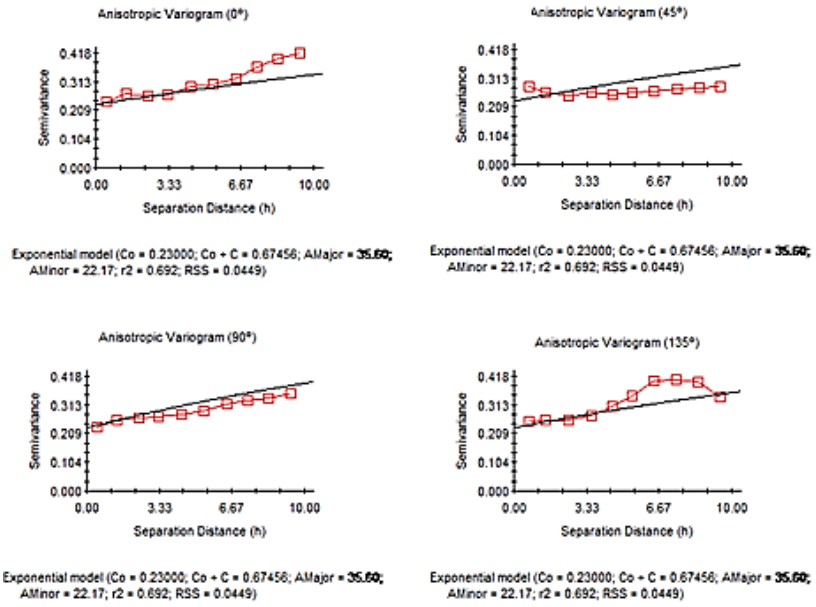

Figure 405 Anisotropic Variogram of saddle querns recovered during surveys of 2009 within Zone 1 (GS+).

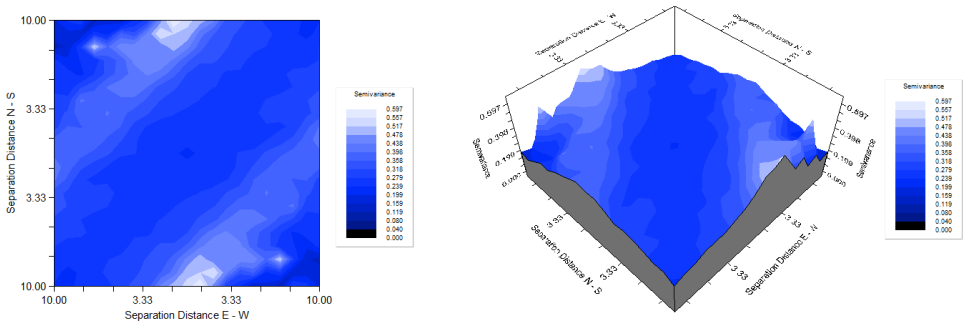

Figure 406 Variogram Map of saddle querns recovered during surveys of 2009 within Zone 1 (GS+).

For Zone 2 (Figure 407) a stronger spatial anisotropy is observed, showing that the semivariance varies in different ways in each degree. As proved by the graph of anisotropic Semivariance Surface or Variogram Map (Figure 408), anisotropy is predominantly concentrated in the centre middle of the distribution with two peaks corresponding to South-West and North-East corners.

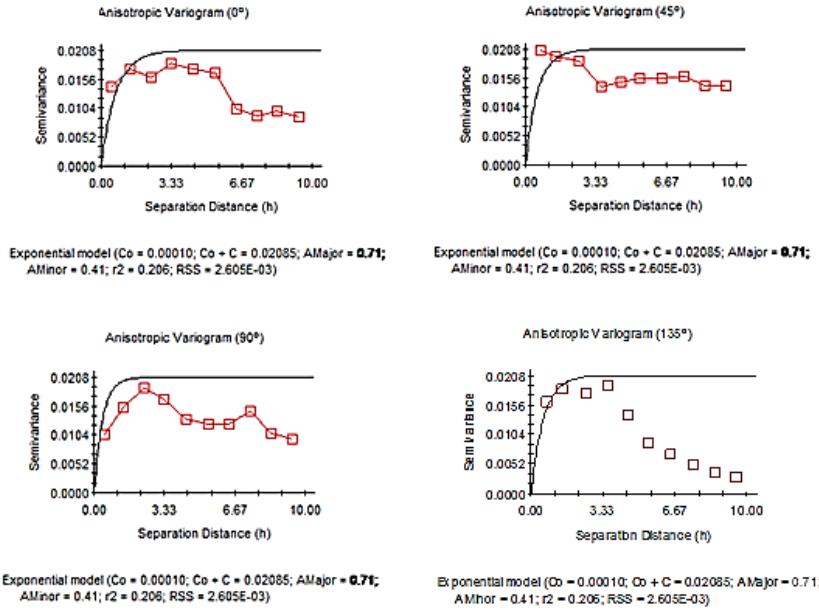

Figure 407 Anisotropic Variogram of saddle querns recovered during surveys of 2009 within Zone 2 (GS+).

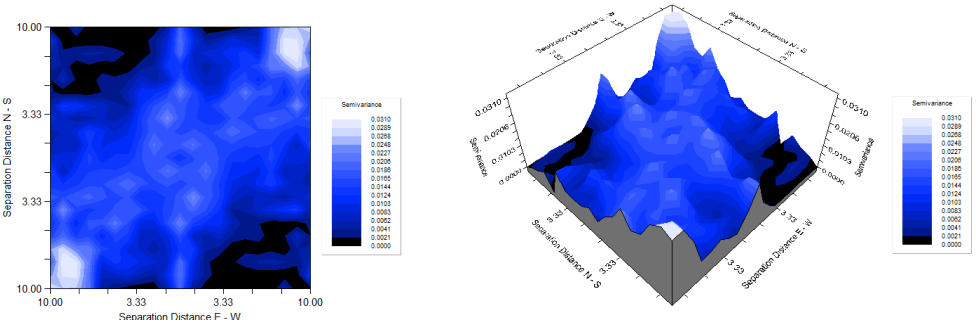

Figure 408 Variogram Map of saddle querns recovered during surveys of 2009 within Zone 2 (GS+).

An exponential isotropic variogram model (Figure 409) has been fitted to the empirical variogram, using, for Zone 1, Nugget Variance, C_0 =0.05270, Sill, C_0+C = 0.29740 and Range, A_0 = 0.41. This model gives a very poor goodness of fit (r^2 = 0.231), that is, it explains just 23.1% of the spatial differences between the frequency of saddle querns per sample unit.

For Zone 2 the exponential variogram shows Nugget Variance, C_0 =0.000057, Sill, C_0+C = 0.01394 and Range, A_0= 0.01. This model does not explain the sample variance because of the strong spatial independence proved by the sample (Figure 409).

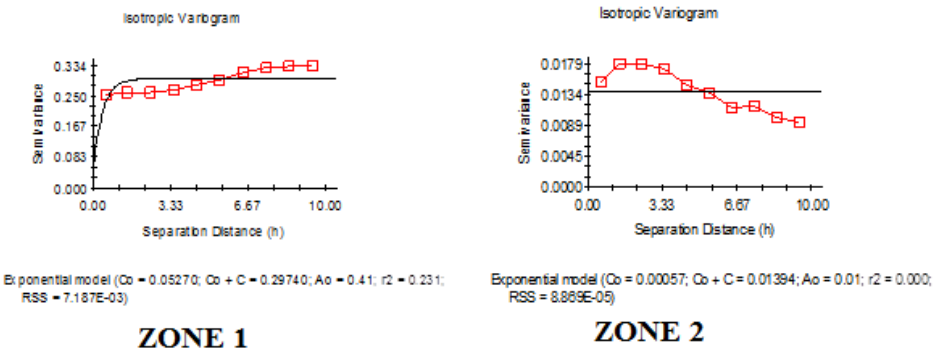

Figure 409 Exponential Isotropic Variogram for saddle querns recovered during surveys of 2009, within Zone 1 and Zone 2 (GS+).

Although not entirety trustworthly because of the low non-linear fit, the inverse distance weighting corresponding to the above exponential models shows, for Zone 1, the maintained North-East-South-West general alignement of saddle querns and they are predominantly concentrated in the center of the distribution (Figure 410). For Zone 2 saddle querns are predominantly concentrated between x=65-70 and y=66-75 and oriented according to a North-South directory, which is distinguished from the widespread North-East-South-West orientation followed in Zone 1 by the most archaeological evidence.

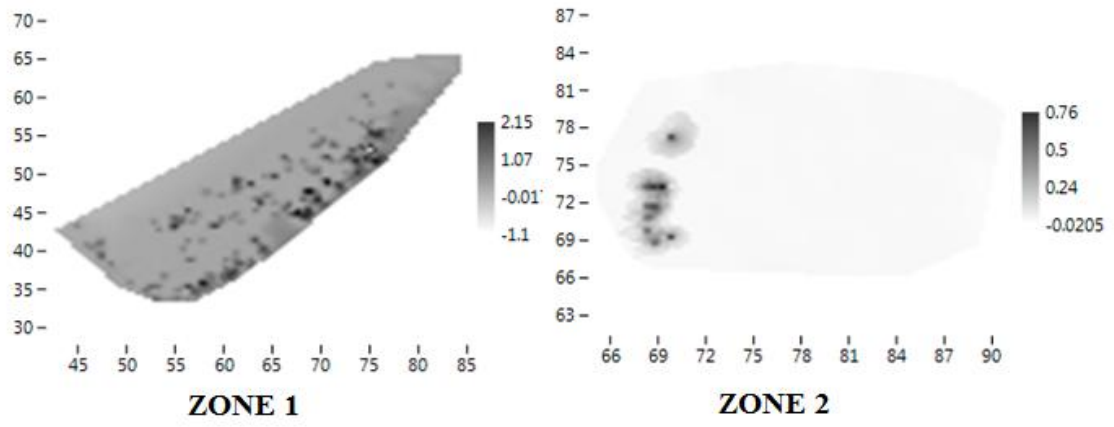

Figure 410 Graphic results of Inverse Distance Weighting calculated for saddle querns recovered during surveys of 2009 within Zone 1 and Zone 2 (Past).

8.4.2 Sub-categories of saddle querns: grindstones and handstones

Within the general category of saddle querns the sub-categories of grindstones and handstones have been identified during surveys of 2009.

8.4.2.1 Grindstones and handstones

Within the two identified zones, spatial distribution of sampling units where grindstones have been identified is showed in Figure 411.

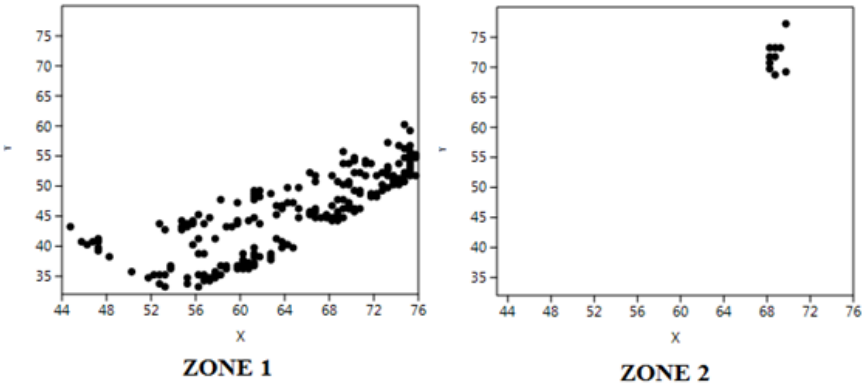

Figure 411 Spatial distribution of cells where grindstones have been recovered during surveys of 2009, within Zone 1 and Zone 2 (Past).

Since grindstones distributed in Zone 2 are those analysed in the previous section and the handstones are absent in such sub-sector, the spatial analysis will be here focused on comparing the spatial distribution of sampling units containing grindstones and handstones in Zone 1, as showed in Figure 412.

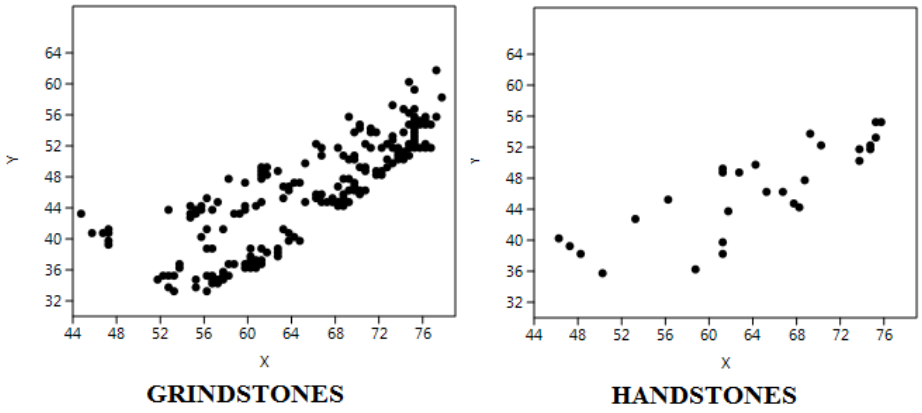

Figure 412 Spatial distribution of sampling units with grindstones and handstones within Zone 1 (Past).

Ripley's *k* analysis on the distance between sampling units with respectively grindstones and handstones evidence suggest the possibility of some degree of spatial clustering at the global scale of the reference area (Figure 413). Particularly for handstones, potential spatial clustering may be located between 1.50 and 9 metres with a spatial pattern that in some distances (as between the starting point of the function and 1.5 metre, at 3 metre and between 7 and 8 metre) tends to the randomness.

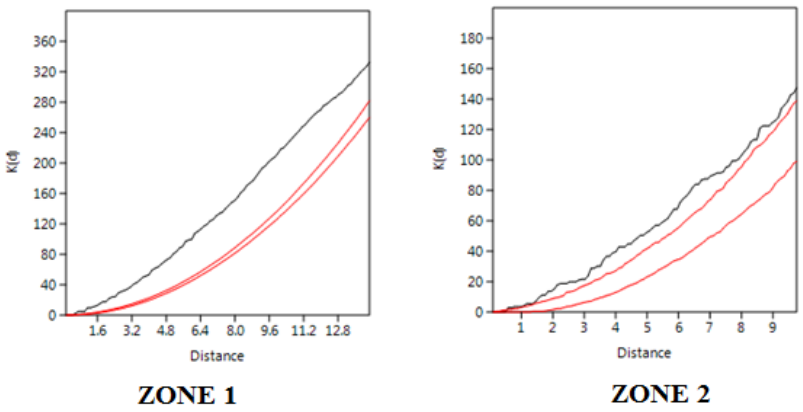

Figure 413 Ripley's *k* analyses on the distance between sampling units with grindstones and handstones recorded in surveys of 2009 within Zone 1 (Past).

Within the convex hull defined by the effectively surveyed sampling units, grindstones seem to be clustered (Clark and Evans test, $p<0$), while for handstones the null hypothesis of a random pattern (Poisson process) for them cannot be rejected at $p<0.05$, confirming the scarce potentiality of clustering suggested by Ripley's k analysis. This pattern is expected, considering handstones as "portable" objects, for their small dimensions (compared to those of grindstones).

The Kernel Density Estimation (Figure 414) shows that grindstones are concentrated in two main sub-areas located between x=52-64 and y=32-40 y and between x=64-76 and y=44-56 (internally sub-divided in two concentrations), while handstones seem to be more dispersed in smaller lower dense concentrations, located between x=45-50 and y=36-40, between x=60-64 and y=36-42, between x=60-70 and y=42-50 (internally sub-divided in two main concentrations) and between x=72-76 and y=50-56 (where the higher density is concentrated).

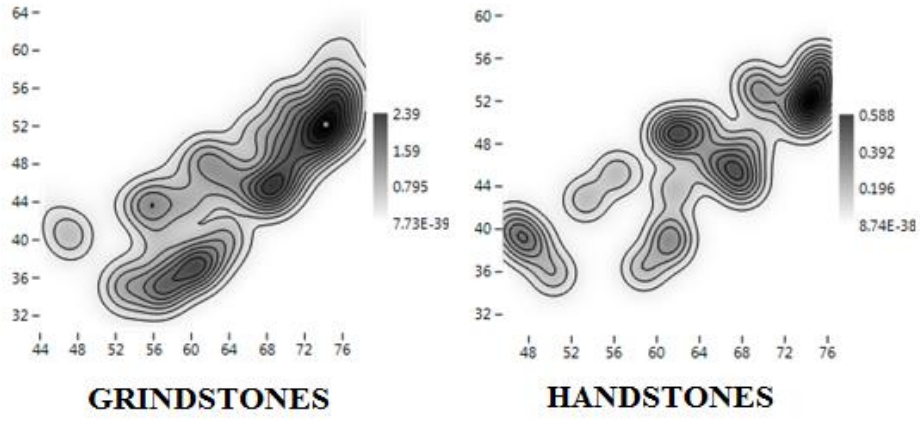

Figure 414 KDE of sampling units where grindstones and handstones have been recorded during surveys of 2009, within Zone 1 (Past).

Within Zone 1 are concentrated the majority of grindstones (n=236) and all handstones (n=30). For grindstones the range of frequencies is between 1 and 4, with a mean of 1.26 observations per sampling unit and the variance is 0.32. Box plot identifies three values distinguishing from the majority, 2, 3 and 4 (interpretable as outliers) (Figure 415). For handstones the range of frequencies is between 1 and 2, with a mean of 1.07 observations per sampling unit and the variance is 0.06. Box plot identifies the value 2 as an outlier (Figure 415).

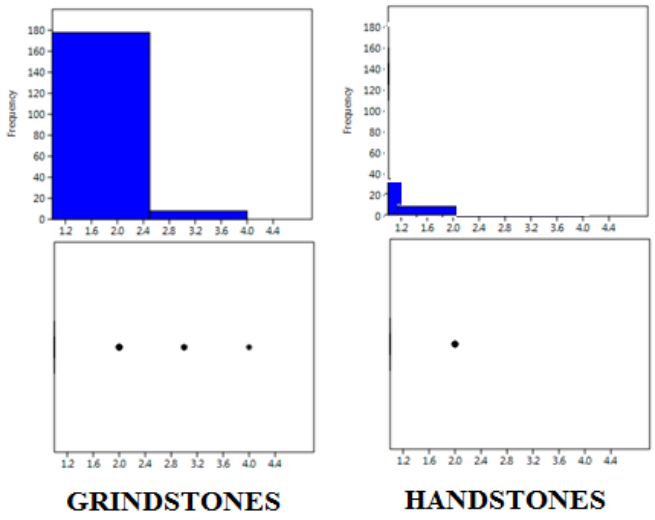

Figure 415 Histogram and box plot of frequencies observed for grindstones and handstones recovered during 2009 within Zone 1 (Past).

While the spatial distribution of grindstones is fitted with a Negative Binomial distribution (with k=0.483 and p=0.730) with Kolmogorov Smirnov Test=1, the spatial distribution of handstones is fitted both with a Negative Binomial distribution (with k=0.187 and p=0.892) as well as with a Poisson (with λ=0.023) with Kolmogorov Smirnov Test=1. For both categories such conditions suggest randomness in the spatial distribution of the abundance of grindstones and handstones per sampling unit, within Zone 1 (Figure 416).

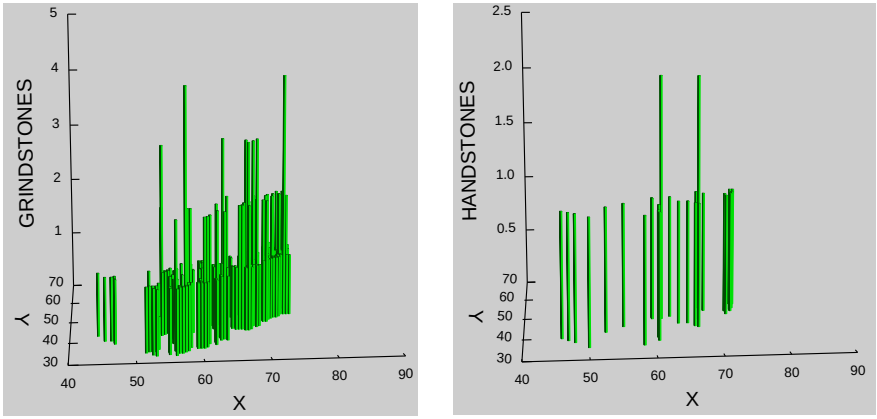

Figure 416 3D Histogram of grindstones and handstones recovered during surveys of 2009 within Zone 1 (Systat 13).

The spatial distribution of count data per sampling unit shows, for grindstones, a Global Moran's *I* of -0.000702. The theoretical (expected) value assuming spatial autocorrelation (lack of spatial Independence) is -0.000756 and the standard error of I is 0.000756. The test of significance using the normality assumption gave a low representative z value 0.071513. Those results are comparable with those of the Geary statistics (C=1.000439) and Getis-Ord general G (=0.017312).

The spatial distribution of count data per sampling unit shows, for handstones, a Global Moran's *I* of -0.000756, corresponding to the theoretical (expected) value assuming spatial autocorrelation (lack of spatial Independence) is -0.001621, and the standard error of *I* is 0.000756. The test of significance using the normality assumption gave a *z* value of 0.0000625,

a highly non-significant value. This result is comparable with those of Geary statistic (*C*=1.000701) and Getis-Ord general G (*G*=0.011547).

Consequently, we can accept that the spatial distribution of both grindstones and handstones is not significantly different than the expected value under a random distribution. This is what would be expected in the case of the general same frequency of items in every spatial location.

The Moran's *I* Correlograms (Figure 417) have been calculated for uniform class distance intervals of 1 metre, and taking into account a 10 metres active lag distance. For grinstones, at the starting point of the function *I* value is 0.201, above expected value for randomness. As the distance between sampling units increases, *I* value drops off quite gently reaching, until 3 metre, values above those expected for randomness (positive spatial autocorrelation). Between 4 and 5 metre *I* value is attested on the line (corresponding to spatial randomness) and between 6 and 7 metre and also at 9 metre *I* value is located below the expected value for randomness.

For handstones (Figure 417), a more irregular pattern is attested; at the starting point of the function I value is ca.0.0170 (value tending to randomness) as well as at 1 metre (0.0182). As the distance between sampling units increases, *I* value drops off quite abruptly reaching predominantly values below or around those expected for randomness.

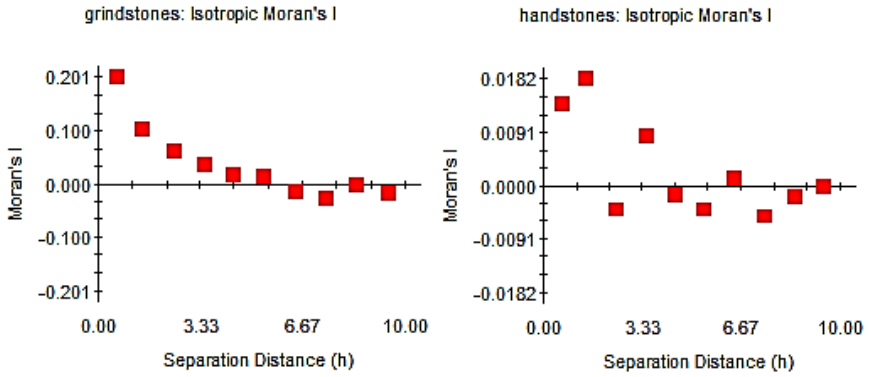

Figure 417 Moran's I Correlograms for grindstones and handstones recovered during surveys of 2009 within Zone 1 (GS+).

For grindstones such result gives the possibility of finding spatially dependent area (positively autocorrelated) of 3 metres of radius. For handstones, a low significant positive spatial autocorrelation is only attested in the first 2 metres of the function and it does not allow us to identify particular spatially dependent area.

Using local indicators of spatial association, we have considered only those cells in which the frequency of gridnstones exceed what would be expected according to a random model, that is cells with more than 1 item. For these sampling units, however, the null hypothesis of a random pattern (Poisson process) cannot be rejected at $p<0.05$. Despite the absence of spatial clustering within such data, it is interesting to note that they are predominantly distributed according to the North-East-South-West alignement, parallel to the estimated ancient lake shoreline and more homogeneously distributed in the North-East corner than in its opposite South-West one, within Zone 1 **(**Figure 418).

Furthermore, 86.66% of handstones are located in 92.85% of the effectively surveyed area, in such a way that only 2 sampling units show more than 1 handstones.

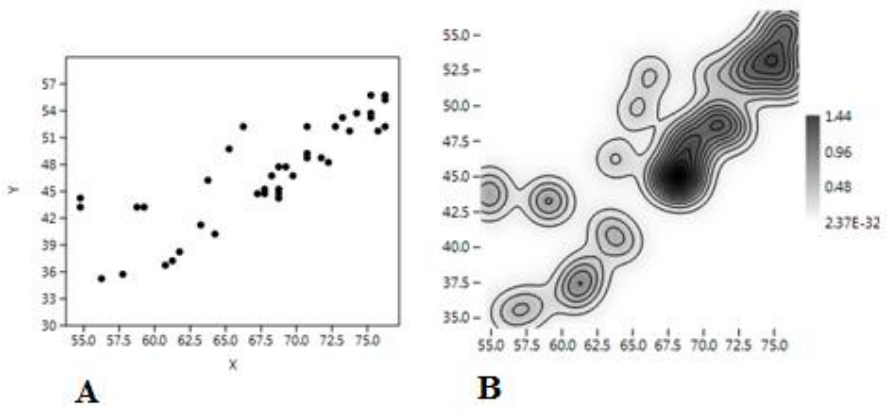

Figure 418 A) Spatial distribution of cells with more than 1 grindstones. B) KDE of such cells within Zone 1 (surveys 2009) (Past).

We have investigated the obvious presence of anisotropic variation exploring the empirical variogram at different directions (Figures 419 and 420).

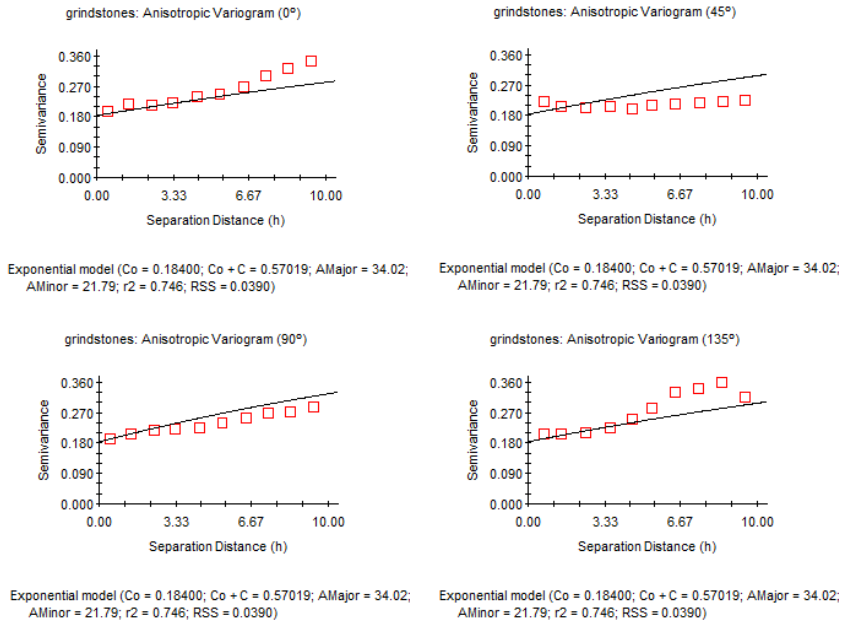

Figure 419 Anisotropic Variogram of grindstones recovered during surveys of 2009 within Zone 1 (GS+).

In general, results for grindstones confirm those of Isotropic Moran Correlogram, showing that semivariance partially varies in the same way at 0 ° and 45º, and at 90º and 135º, only in the first distances, since from 3-4 metre they change abruptly. This condition suggests the presence of low anisotropy, which, according to what is suggested by Semivariance Surface or Variogram Map, is particularly concentrated around the North-West and South-East corner (Figure 420).

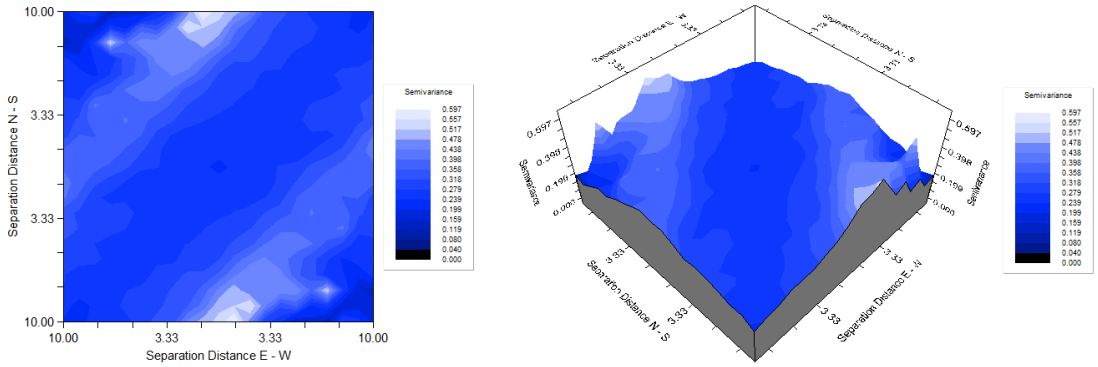

Figure 420 Variogram Map of grindstones recovered during surveys of 2009 within Zone 1 (GS+).

For handstones, semivariance varies in the same way at 0 º and 135º, and at 45º and 90º, only in the first distances, since from 3-4 metre they change abruptly (Figure 421).

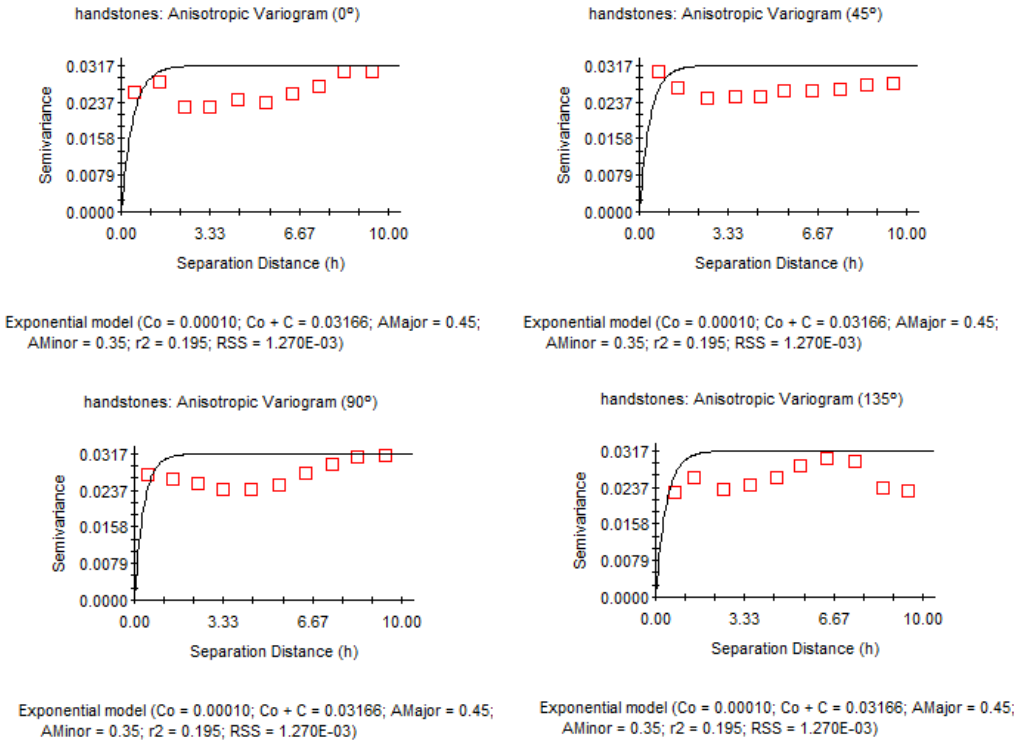

Figure 421 Anisotropic Variogram of handstones recovered during surveys of 2009 within Zone 1 (GS+).

This condition suggests the presence of anisotropy, which, according to what is suggested by the Semivariance Surface or Variogram Map (Figure 422) is predominantly distributed in narrow fringe around the North-West and South-East corners. Compared with the Variogram Map of grindstones, in this case higher values of anisotropy are observed.

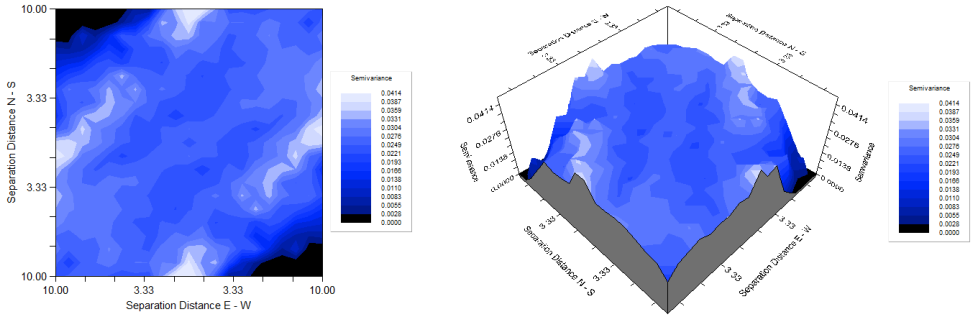

Figure 422 Variogram Map of handstones recovered during surveys of 2009 within Zone 1 (GS+).

An exponential isotropic variogram model (Figure 423) has been fitted to the empirical variogram for both categories. For grindstones, the exponential variogram shows Nugget Variance, C_0 =0.04340, Sill, C_0+C = 0.24380 and Range, A_0 () = 0.44. This model explains only 25.3% of spatial variance.

For handstones, the exponential variogram shows Nugget Variance, C_0 =0.000 370, Sill, C_0+C = 0.002640 and Range, A_0 = 0.01. This model, however, does not explain the spatial variance (Figure 423).

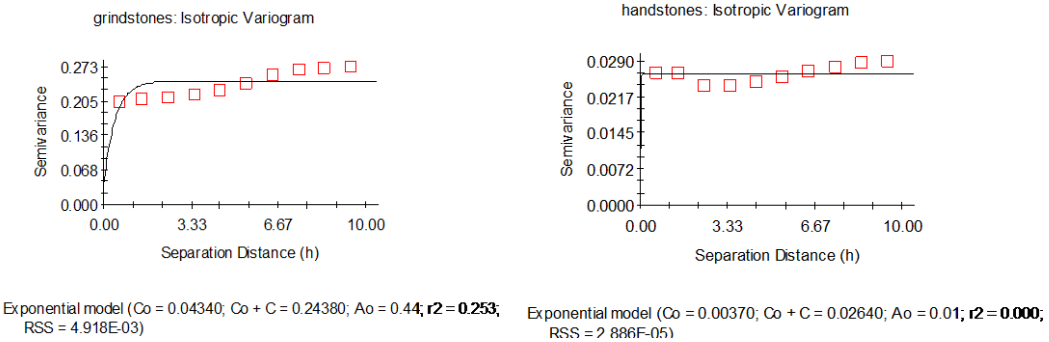

Figure 423 Exponential Isotropic Variogram for grindstones and handstones recovered during surveys of 2009, within Zone 1 (GS+).

Although not entirely trustworthy because of the low (or absent) non-linear fit, the inverse distance weightings corresponding to the above exponential models (Figure 424) show a general alignement North-East-South-West of grindstones and they are predominantly concentrated around the expected ancient lake shoreline. In the same way seems to be distributed handstones.

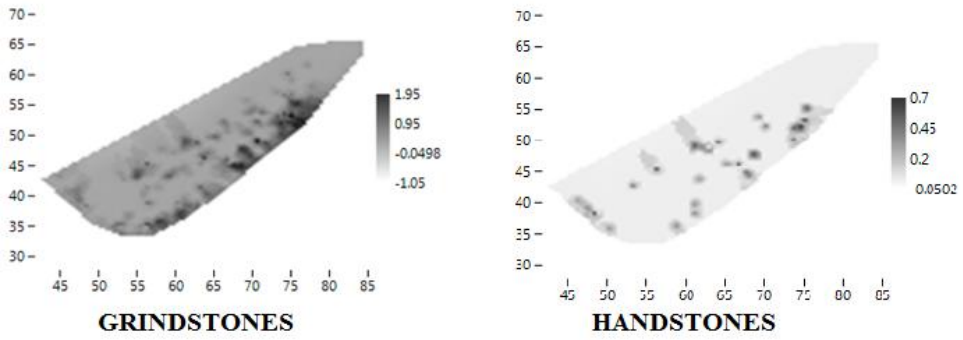

Figure 424 Graphic results of Inverse Distance Weighting calculated for grindstones and handstones recovered during surveys of 2009 within Zone 1 (Past).

8.5. Faunal remains (all taxa and all skeletal parts mixed together)

2164 faunal remains were identified and counted; 1163 were the surveyed empty cells, while the sampling unit with more presence gave 23 items. The spatial distribution of sampling units where faunal remains have been identified is showed in Figure 425.

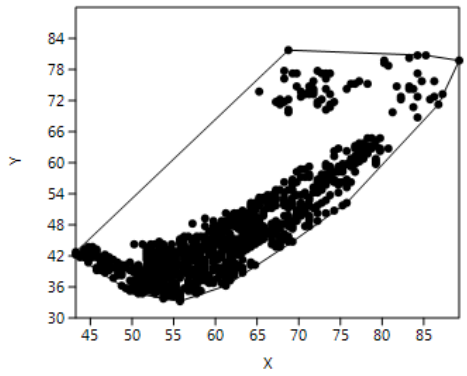

Figure 425 Spatial distribution of cells where faunal remains have been recovered during surveys of 2009 (Past).

Ripley's *k* analysis on the distance between sampling units with faunal remains evidence suggests the possibility of some degree of spatial clustering, at the scale of the total reference area (Figure 426).

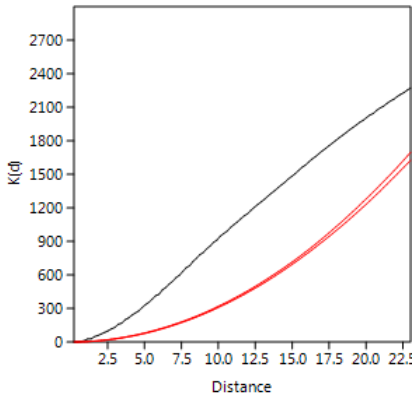

Figure 426 Ripley's *k* analysis on the distance between sampling units with faunal remains, recorded in surveys of 2009 (Past).

Within the convex hull defined by the effectively surveyed sampling units the non-empty cells are significantly clustered, according to Clark and Evans test, while the empty sampling units are overdispersed. KDE (Figure 427) confirms the presence of above mentioned zones, although the absolute majority of faunal remains are accumulated in the Zone 1.

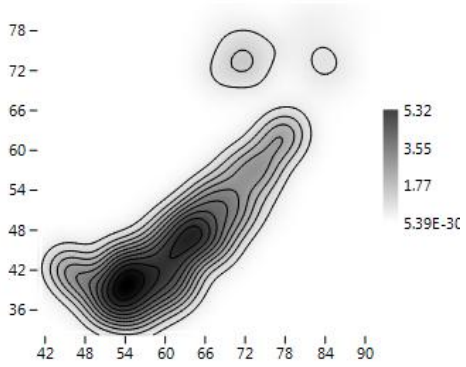

Figure 427 KDE of sampling units where faunal remains have been recorded during surveys of 2009 (Past).

When considering the raw quantity of faunal remains at each cell, the probability density distribution of spatial frequencies follows a *J*-shaped distribution. A majority of sampling units have raw counts of faunal remains of less than 3 elements (global mean=2.78 observations per sampling unit). Three cells distinguish from the majority (interpretable as outliers), with 18, 21 and 24 faunal remains. According to both histogram and box plot is evident a break point in the frequency of faunal remains in relation to the value 6 (as showed in Figure 428).

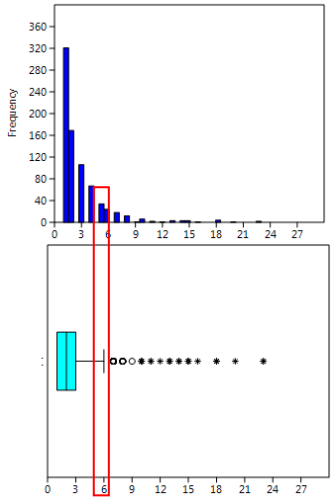

Figure 428 Histogram and box plot of frequencies observed for faunal remains recovered during 2009 (Past).

The Negative Binomial distribution with k=17.345 and p=0.977 fits with the observed frequencies of fauna, according to the Kolmogorov Smirnov Test=0.998. This condition suggests quite scarce differences in the spatial frequencies between sampling units. It is noted, however, a strong effect of outliers (Figure 429).

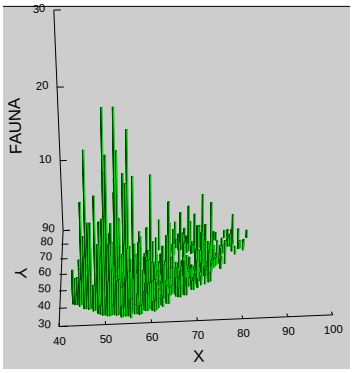

Figure 429 3D Histogram of faunal remains recovered during surveys of 2009 (Systat 13).

The spatial centroid of the area with faunal remains, calculated using an abundance weighted mean spatial center is x=58.798521 and y=45.153882 with 8.96 m of standard deviation along the x axis and 9.29 m along the y axis. A standard deviation ellipse with a long axis of 34.75 m and a short one of 11.28 m delimits an area of 307.82 square meters, where most data count appears. It has been estimated an average density of 0.90 faunal remains per square meter.

The spatial distribution of the abundance of faunal remains per sampling unit gives a Global Moran's *I* result of 0.000700. The theoretical (expected) value assuming spatial autocorrelation (lack of spatial independence) is -0.000515 and the standard error is 0.000515. The test of significance using the normality assumption gave a *z* value of 2.357726, a highly significant value. Consequently, we can accept that the spatial distribution of faunal remains could be in some way different than the expected value under a random distribution. This is what would be expected when not all spatial location have the same frequency of items. These results are comparable with those of the Geary statistics (*C*=0.997654) and Getis-Ord general G (*G*= 0.012033).

The Moran's *I* Correlogram (Figure 430) has been calculated for uniform class distance intervals of 1 metre, and taking into account a 10 metres active lag distance. At the starting point of the function *I* value is about 0.374, above the expected value for randomness. As the distance between sampling units increases, *I* value drops off quite gently and continuously always above the expected value for randomness, proving the existence of positive spatial autocorrelation in a spatial interval of around 10 metres.

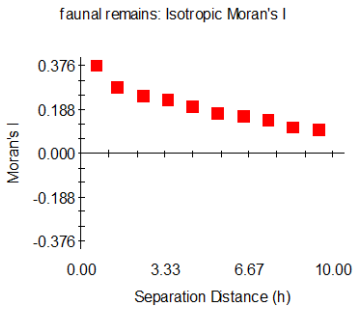

Figure 430 Moran's I Correlogram for faunal remains recovered during surveys of 2009 (GS+).

In light of these results, spatially continuous areas of at least 10 metres of radius are attested; they may coincide with ancient activity areas.

Local indicator of spatial association suggest that 57 cells with more than 6 fragments of animal bone distinguish from their neighbours items. These differentiated sampling units show a clustered pattern (according to Clark and Evan Test *p*=0.009). Such faunal remains (28%) are distributed in 3% of the effectively surveyed area and are predominantly concentrated between x=44-60 and y=35-44, between x=60-65 and y=45-50 and two isolated points are located respectively between Zone 1 and Zone 2 and within Zone 2 (Figure 431).

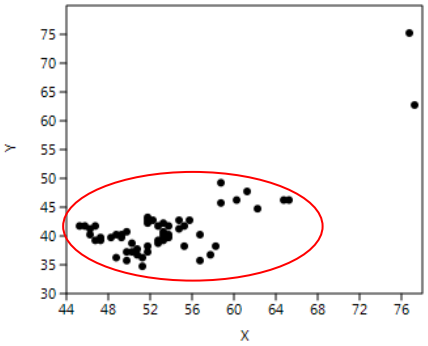

Figure 431 Spatial distribution of cells with more than 6 faunal remains (surveys of 2009) (Past).

Moran's *I* correlogram (Figure 432) of cells with more than 6 faunal remains fits with a random model between immediate sampling units, and some possible clustering between the starting point of the function and the first 3 meters. That is, one main concentration zone (around x=45-57 and y=35-45) and other dispersed and unrelated sub-areas. A Kernel density estimate model of cells with more than 10 items provides a clearer image (Figure 433).

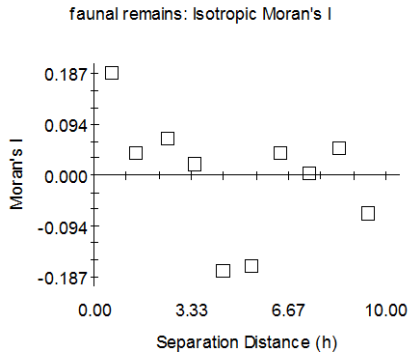

Figure 432 Moran's I Correlogram for faunal remains with more than 6 fragments recovered during surveys of 2009 (GS+).

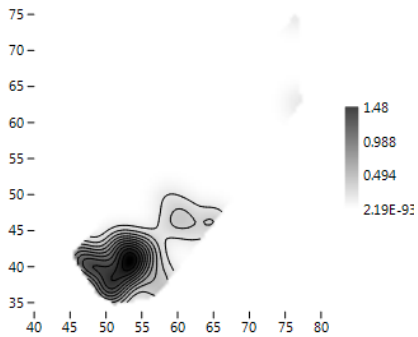

Figure 433 KDE of sampling units where more than 6 fragments of faunal remains have been recorded during surveys of 2009 (Past).

It is easy to see in the South portion of the surveyed area a main accumulation of faunal remains delimiting a less dense area, spatially distributed according to a South-West orientation.

We have explored the possible presence of anisotropic variation fitting a theoretical variogram at different directions (Figure 434).

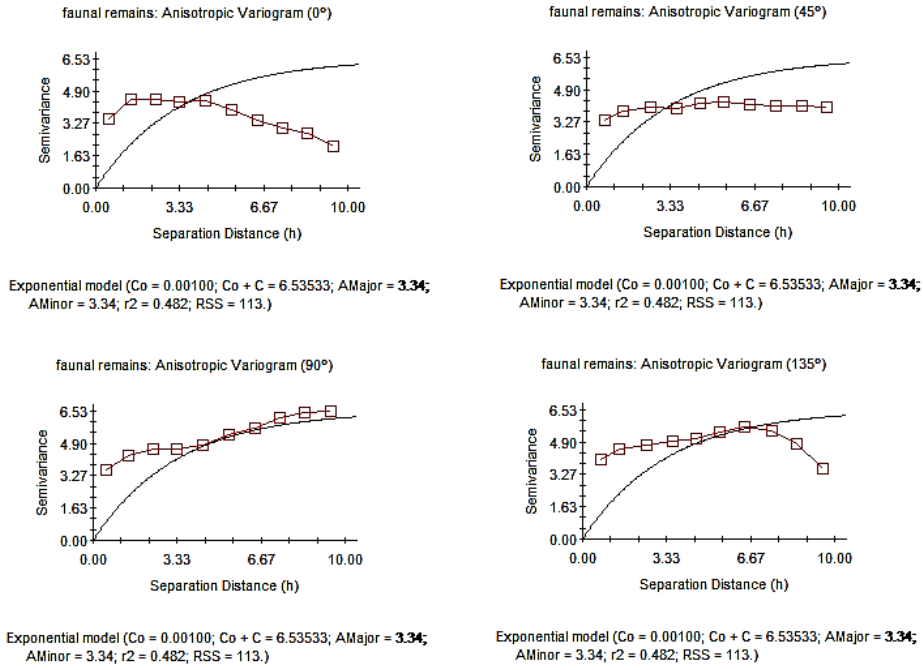

Figure 434 Anisotropic Variogram of faunal remains recovered during surveys of 2009 (GS+).

Semivariance is very high and it increases with distance, suggesting that spatial continuity diminuishes with distance. This can be explained in terms of an intentional pattern at small-medium scale, probably configuring a main activity area. Semivariance varies in the same way at 0º and 90º for the first distances (between the starting point of the function and until 4 metre), and at 45º and 135º (such last degrees are, anyway, less similar), indicating quite regular spatial pattern, with continuity in medium areas. The graph of anisotropic Semivariance Surface or Variogram Map (Figure 435) reveals strong anisotropy in the Western and Eastern side of the 3D diagram, while in the centre is observed continuity at small and medium distances.

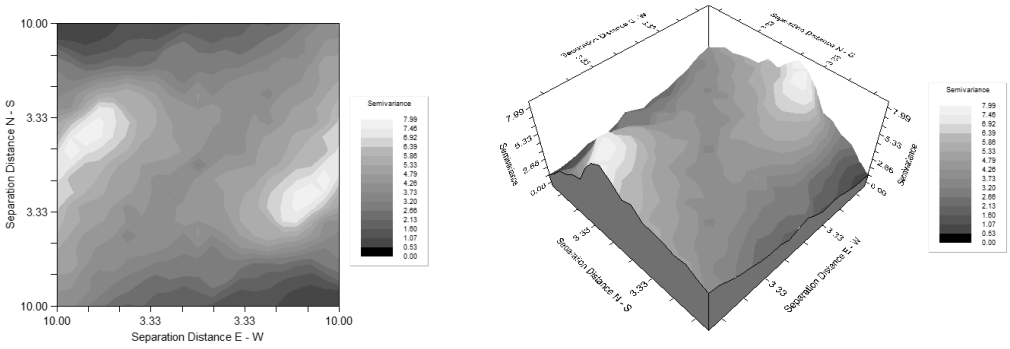

Figure 435 Variogram Map of faunal remains recovered during surveys of 2009 (GS+).

An exponential variogram model (Figure 436) has been fitted to the empirical variogram, using Nugget Variance, C_0=0.0100, Sill, C_0+C= 4.510 and Range, A_0= 0.39. Isotropic variogram

confirms a predominant regularity in the spatial pattern in a medium-large scale, in such a way that some neighbouring sample units could have the same spatial frequencies. This model explains 80.6% of spatial variance.

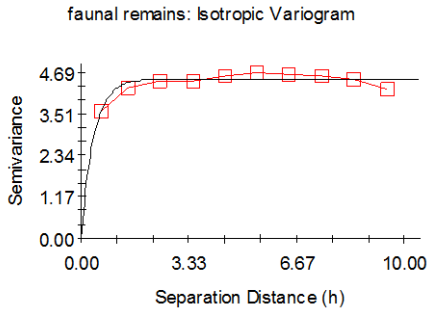

Exponential model (Co = 0.01000; Co + C = 4.51000; Ao = 0.39; **r2 = 0.806**; RSS = 0.183)

Figure 436 Exponential Isotropic Variogram for faunal remains recovered during surveys of 2009 (GS+).

The related inverse distance weighting interpolated model (Figure 437) stresses the alignment of a majority of faunal remains along the estimated ancient lake shoreline and their higher concentration in the South-West corner, with scarce high presences in the opposite North-East corner.

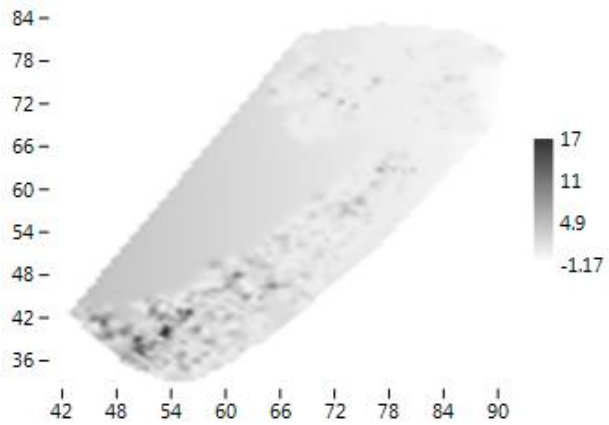

Figure 437 Graphic results of Inverse Distance Weighting calculated for faunal remains recovered during surveys of 2009 (Past).

It is important to take into account that this interpolated model has some relevant limits: it does not predict well the outliers, but gives a sufficiently good prediction of more frequent abundance values.

8.5.1 Faunal remains in Zone 1 and Zone 2

The spatial distribution of sampling units where faunal remains have been identified within Zone 1 and Zone 2 is showed in Figure 438.

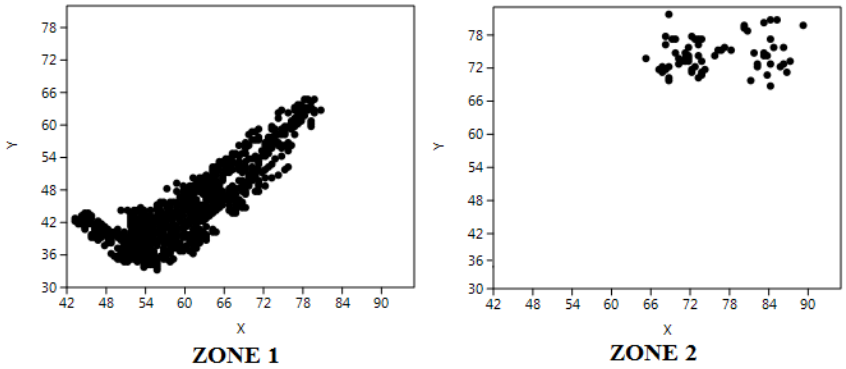

Figure 438 Spatial distribution of faunal remains within Zone 1 and Zone 2 (surveys 2009) (Past).

Ripley's *k* analysis on the distance between sampling units with faunal remains suggests the possibility of some degree of spatial clustering for Zone 1; conversely, a more irregular pattern is observed for Zone 2, where tendency to randomness is attested between the starting point to the function and 3.8 metre, while from 4 to 6.4 metres it is attested a pattern more oriented to clustering (Figure 439).

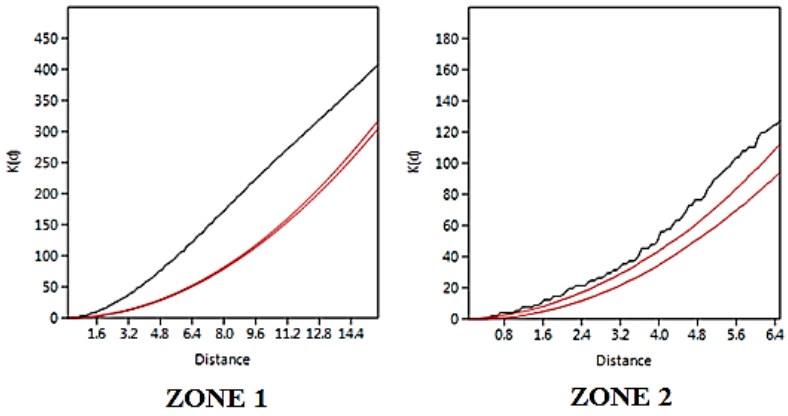

Figure 439 Ripley's *k* analysis on the distance between sampling units with faunal remains, recorded in surveys of 2009, within Zone 1 and Zone 2 (Past).

Kernel Density Estimation of cells with faunal evidence shows for Zone 1 the occurrence of a wider central area, sub-divided in two sectors which are extended between x=50-57 and y=36-43 and x=61-67 and y=44-48 y, while within Zone 2 three sub-concentrations emerge (one between x=69-75 and y=72-76 and x=81-87 and y=72-76 y and the other between x=79-80 and y=79-80) (Figure 440). Within Zone 1 are attested 711 surveyed non-empty cells that were overdispersed (Clark and Evans test, $p<1$). Within Zone 2, 67 surveyed non-empty cells are observed, for which the null hypothesis of a random pattern (Poisson process) cannot be rejected at $p<0.05$ (Clark and Evans test). Thus, for this last area it is possible that equidistant cells have the same probability of counting one or more faunal remains.

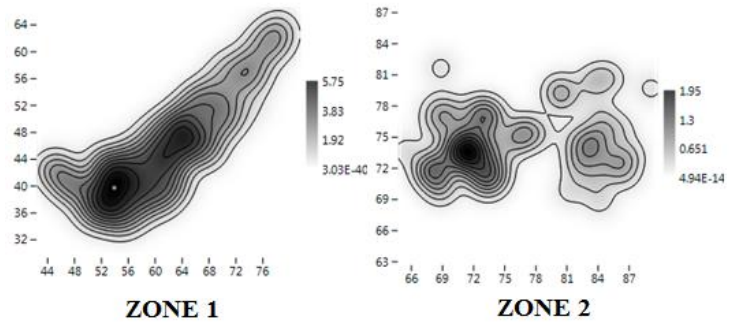

Figure 440 KDE of sampling units where faunal remains have been recorded during surveys of 2009, within Zone 1 and Zone 2 (Past).

When considering the raw quantity of faunal remains at each cell, the probability density distribution of spatial frequencies follows, for both zones, a *J*-shaped distribution. There are, however, relevant differences in the spatial location of sampling units with faunal frequencies within both zones; Zone 1 concentrates the majority of observations (n= 2054), the range of frequencies is between 1 and 23, with a mean of 2.88 observations per sampling unit and variance = 8.4622. Three values are distinguished from the majority, with 18, 20 and 23 faunal fragments (interpretable as outliers). According to both histogram and box plot is evident a break point in the frequency of occurrence of faunal remains in relation to the value 6 (as showed in Figure 441).

Zone 2 concentrates 110 faunal remains, the range of frequencies is between 1 and 7, with a mean of 1.64 observations per sampling unit and variance = 1.6879. Four values are distinguished from the majority, with 4, 5, 6 and 7 faunal fragments (interpretable as outliers). According to both histogram and box plot is evident a break point in the frequency of occurrence of faunal remains in relation to the value 3 (as showed in Figure 441).

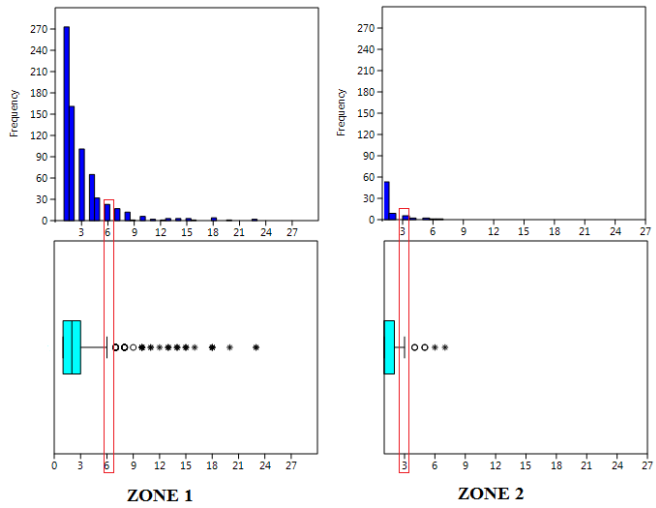

Figure 441 Histograms and box plots of frequencies observed for faunal remains recovered during 2009 within Zone 1 and Zone 2 (Past).

The spatial distribution of faunal remains in both zones is fitted with a Negative Binomial distribution, with k=0.585 and p=0.274 and a Kolmogorov Smirnov Test=0.912 for Zone 1 and with k=0.137 and p=0.435 and Kolmogorov Smirnov Test=1.000 for Zone 2. For both zones

this condition suggests a scarce difference in the spatial frequencies between sampling units; it is noted, however, a strong effect of outliers (Figure 442).

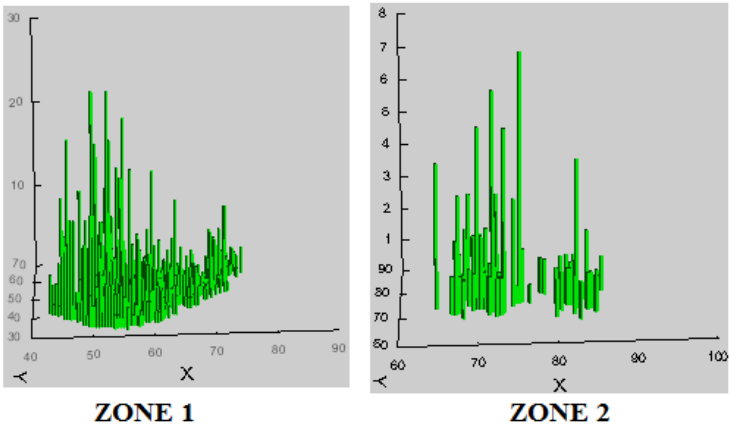

Figure 442 3D Histogram of faunal remains recovered during surveys of 2009, within Zone 1 and Zone 2 (Systat 13).

The spatial distribution of count data per sampling unit shows, for Zone 1, a Global Moran's *I* of -0.000153. The theoretical (expected) value assuming spatial autocorrelation (lack of spatial Independence) is -0.000756 and the standard error is 0.000756. The test of significance using the normality assumption gave a *z* value of 0.797087, a quite significant value. This result is comparable with those of Geary statistic (*C*=0.998919) and Getis-Ord general G (*G*=0.013289).

The spatial distribution of count data per sampling unit shows, for Zone 2, a Global Moran's *I* of -0.001588. The theoretical (expected) value assuming spatial autocorrelation (lack of spatial Independence) is -0.001621, and the standard error of I, is 0.001621. The test of significance using the normality assumption gave a *z* value of 0.020074, a highly non-significant value. This result is comparable with those of Geary statistic (*C*=1.000441) and Getis-Ord general G (*G*=1.000000).

Consequently, we can accept that the spatial distribution of faunal remains for Zone 1 could be quite significantly different than the expected value under a random distribution, compared to Zone 2. For both zones, however, this is what would be expected in the case of the same frequency of fauna in quite every spatial location (particularly for Zone 2).

The Moran's *I* Correlogram (Figure 443) has been calculated for uniform class distance intervals of 1 metre, and taking into account a 10 metres active lag distance. For Zone 1, *I* value at the starting point of the function is about 0.303, above expected value for randomness. As the distance between sampling units increases, *I* value drops off quite gently reaching always *I* values above the expected value for randomness, proving the presence of positive spatial autocorrelation between the starting point of the function and 10 metre. For Zone 2, a more irregular spatial pattern is attested in the Moran's *I* Correlogram. At the starting point of the function *I* value is about 0.0867 (lower than *I* value showed at the same distance for Zone 1), above the expected value for randomness. As the distance between sampling unit increases, *I* value drops off quite abruptly, reaching value around the line, on the line (corresponding to spatial randomness) and below the expected value for randomness at 3 metre and from 5 metre.

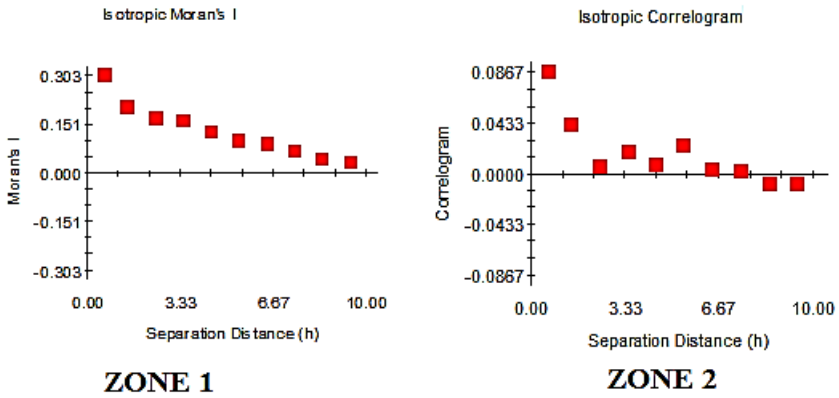

Figure 443 Moran's I Correlograms for faunal remains recovered during surveys of 2009, within Zone 1 and Zone 2 (GS+).

For Zone 1 is observed spatial continuity which reaches at least 10 metres of radius, probably coinciding with ancient activity areas. For Zone 2 a more irregular pattern is observed and potential spatially dependent areas of 2-3 metres.

Local indicator of spatial association suggests that 56 cells with more than 6 items within Zone 1 dinstinguish from their neighbours items. For these differentiated sampling units the null hypothesis of a random pattern (Poisson process) can not be rejected at $p<0.05$ (Clark and Evans test). Despite the absence of spatial clustering within such data it is interesting to note that they are predominantly distributed according to the North-East-South-West line of concentrations (particularly between x=45-60 and y=32-43), as showed by Kernel Density Estimation (Figure 444).

Taking into consideration what is suggested both by boxplot and histogram, that is the occurrence of a breaking point in the frequencies faunal remains in correspondence with a value of 6 items (for Zone 1) and of 3 item (for Zone 2), sampling units with respectively more than 6 and 3 frequencies of fragments are analysed separately. For Zone 1, 71% of faunal remains are located in 92% of the effectively surveyed area, in such a way that 56 cells show more than 6 items (representing, this limit, the breaking point highlighted by both histogram and boxplot). However for the spatial distribution of these sampling units the null hypothesis of a random pattern (Poisson process) can not be rejected at $p<0.05$.

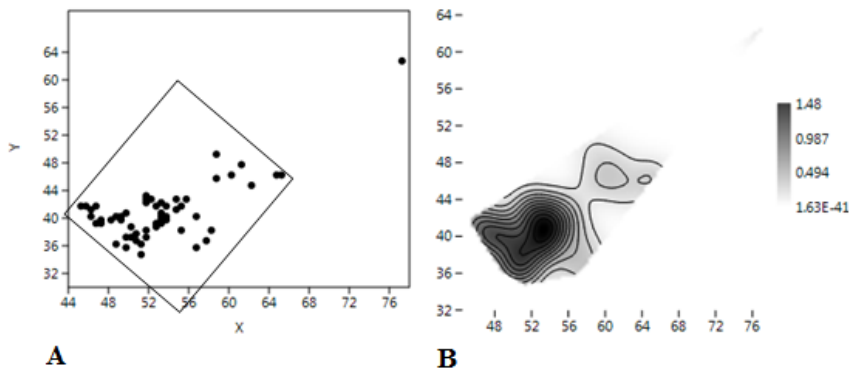

Figure 444 A) Spatial distribution of cells where more than 6 fragments faunal remains have been recovered during surveys of 2009, within Zone 1 (Past). B) KDE of such cells.

We have explored the possible presence of anisotropic variation, fitting a thereotical variogram at different directions (Figure 445). For Zone 1 homogeneous variations of semivariance, predominantly at 0º and 90º and lower similarity at 135º (45º is totally different), are observed; such homogeneity is particularly concentrated in the first portion of the function, before 4 metre, since from this spatial distance there are evident variations between different degrees. Semivariance is high, and diminishes with distance in correspondence to 0º and 45º, while increases with distance at 90º and 135º, proving different patterns corresponding to distinct orientations. The graph of anisotropic Semivariance Surface or Variogram Map (Figure 446) reveals strong anisotropy concentrated in the Western and Eastern side of the 3D diagram.

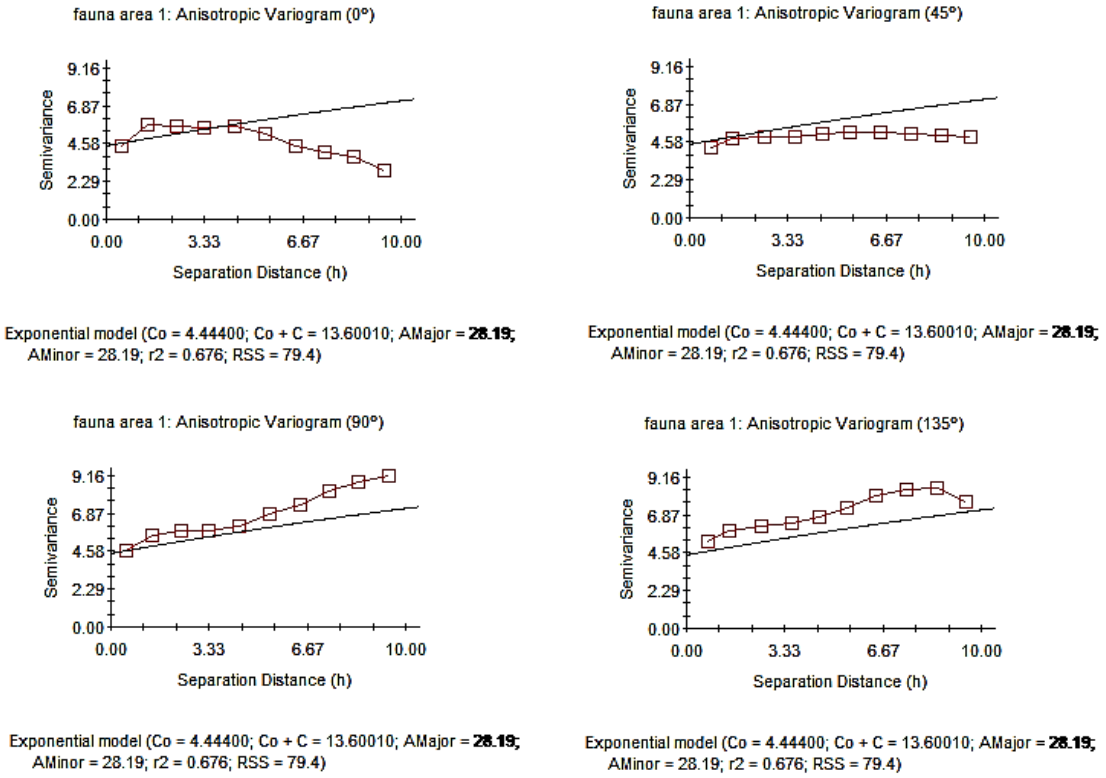

Figure 445 Anisotropic Variogram of faunal remains recovered during surveys of 2009, within Zone 1 (GS+).

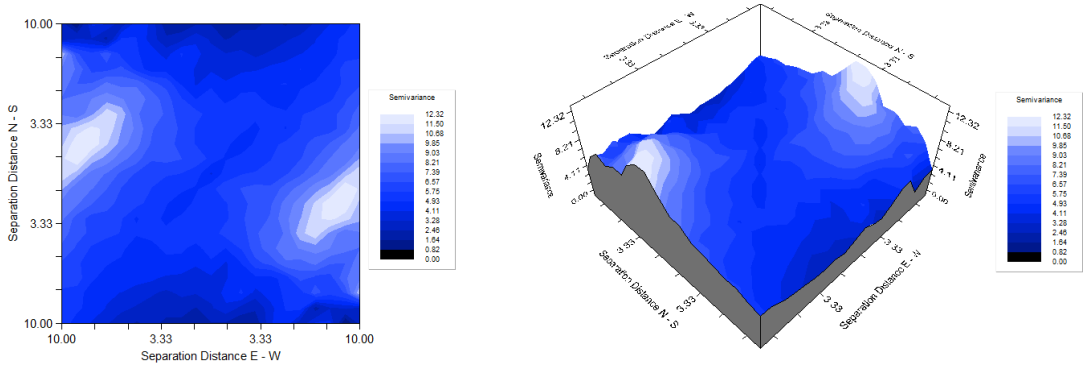

Figure 446 Variogram Map of faunal remains recovered during surveys of 2009, within Zone 1 (GS+).

Results for Zone 2 show similar variation of semivariance at 0º and 90º, particularly in the first portion of the function (between the starting point of the function and 3 metre), while

semivariance varies in different way at 45º and 135º (Figure 447). The graph of anisotropic Semivariance Surface or Variogram Map (Figure 448) reveals a stronger spatial anisotropy, widespread within the centre of the 3D diagram. Then, spatial continuity is quite absent. The strong North-East-South-West trend in this anisotropy map reinforces the working hypothesis of a main concentration of faunal remains at the South-West corner, and a probably post-depositional deformation, parallel to the estimated ancient lake shoreline.

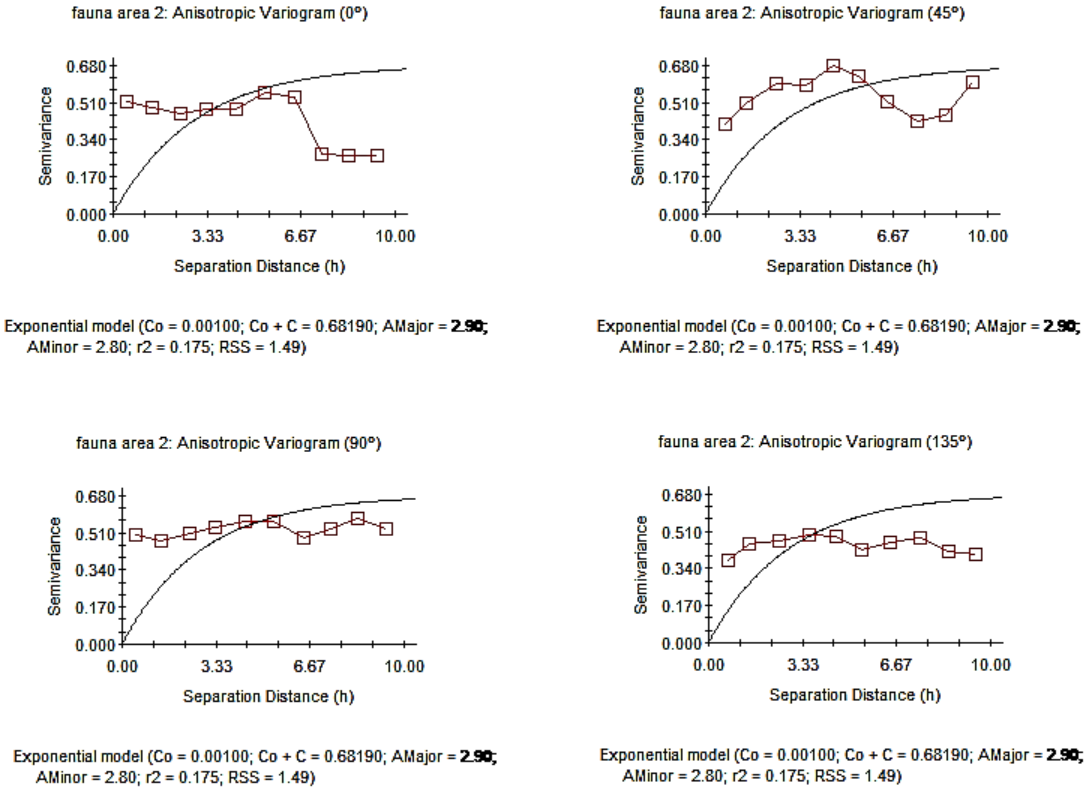

Figure 447 Anisotropic Variogram of faunal remains recovered during surveys of 2009, within Zone 2 (GS+).

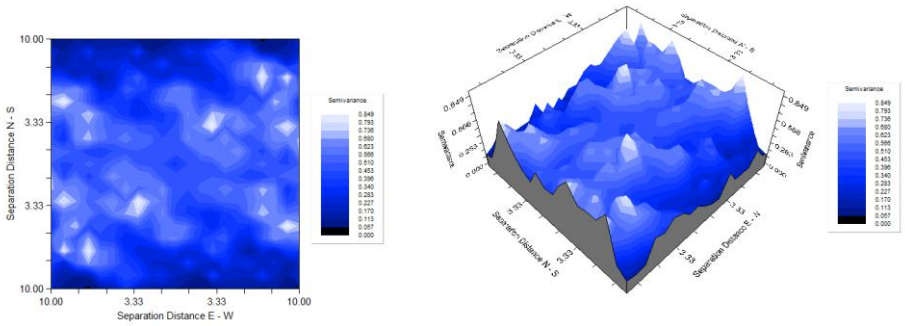

Figure 448 Variogram Map of faunal remains recovered during surveys of 2009, within Zone 2 (GS+).

An exponential isotropic variogram model for both zones has best fitted to the empirical data. For Zone 1 an isotropic variogram with Nugget Variance, C_0 =0.02000, Sill, C_0+C = 5.85700 and Range, A_0 = 0.40 explains 82.1% of spatial variance and it fits conveniently the empirical data set (Figure 449). For Zone 2 an exponential variogram with Nugget Variance, C_0 =0.10800, Sill, C_0+C = 0.49800 and Range, A_0 = 0.28 explains only 11.3% of spatial variance (Figure 449).

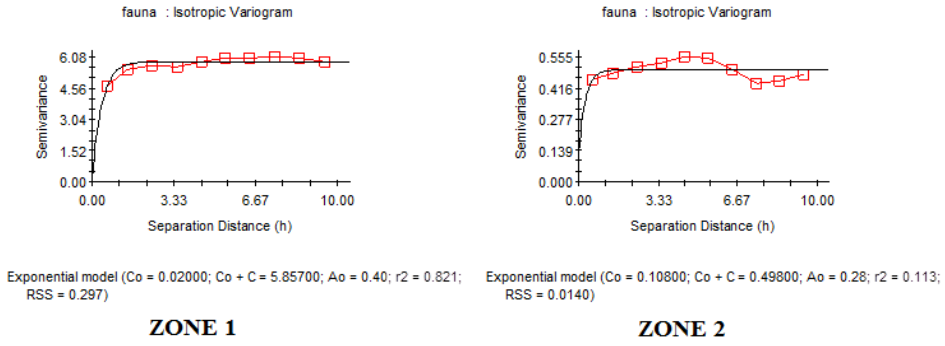

Figure 449 Exponential Isotropic VariogramS for faunal remains recovered during surveys of 2009, within Zone 1 and Zone 2 (GS+).

The inverse distance weighting corresponding to the above exponential model shows, for Zone 1, a predominant concentration of faunal remains within the South-West corner and in the centre of the surveyed area, with further small high dense points observed around the North-East corner (Figure 450). For Zone 2 predominant high concentrations of faunal remains are observed in the Western and Eastern side of the surveyed area (Figure 450).

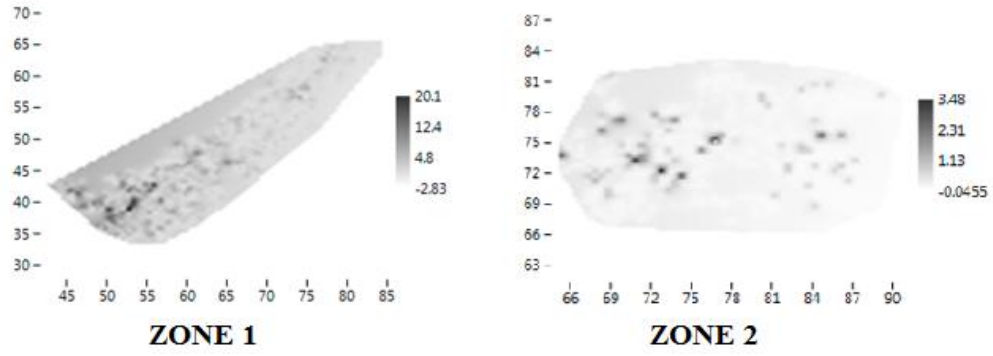

Figure 450 Graphic results of Inverse Distance Weightings calculated for faunal remains recovered during surveys of 2009, within Zone 1 and Zone 2 (Past).

It is important to take into account that this interpolated model has some relevant limits: it does not predict well the outliers, but gives a sufficiently good prediction of more frequent abundance values.

8.5.2 Sub-categories of faunal remains

We have explored the spatial distribution of different skeletal parts. Nevertheless, frequencies are low in quantitative terms, and we have limited the analysis to an exploration of presence/absence in the surveyed area.

8.5.2.1. Cranial faunal remains

171 cranial remains from all taxa have been identified and counted; they are spatially distributed in 128 sampling units, while 1813 squares were empty (Figure 451).

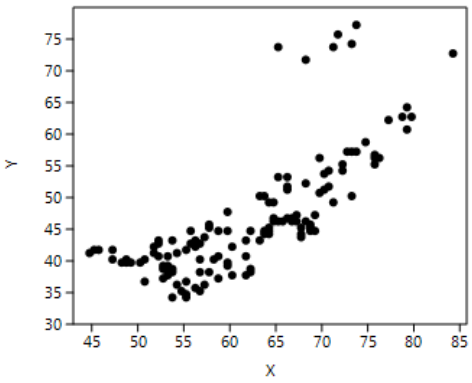

Figure 451 Spatial distribution of sampling units where cranial faunal remains have been recorded in surveys of 2009 (Past).

Ripley's *k* analysis on the distance between sampling units with cranial remains suggests, as proved by the KDE, the possibility of some degree of spatial clustering (Figure 452).

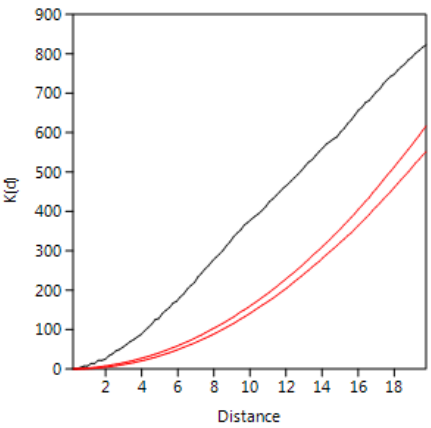

Figure 452 Ripley's *k* analysis on the distance between sampling units with cranial faunal remains, recorded in surveys of 2009 (Past).

Within the convex hull defined by the effectively explored sampling units, a cluster pattern is observed (as confirmed by Clark and Evans test). KDE shows the occurrence of two possible concentrations located between x=44-60 and y=33-44 and between x=67-74 and y=45-52. Three further lower dense concentrations are located between x=70-75 and y=55-57, between x=75-77 and y=60-65 and between x=65-75 and y=70-75 (Figure 453).

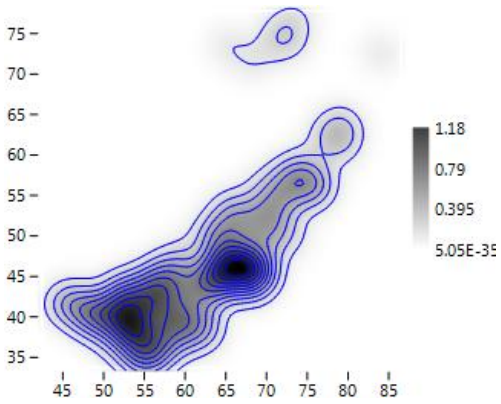

Figure 453 KDE of sampling units where cranial faunal remains have been recorded during surveys of 2009 (Past).

When considering the raw quantity of cranial remain at each cell, the probability density distribution of spatial frequencies follows a *J*-shaped distribution. A majority of sampling units have raw counts of such faunal remains of less than 2 elements (global mean = 1.625 observables per sampling unit). Both histogram and boxplot identified a break point in the distribution of frequencies in correspondence to the value 3. Furthermore, three cells are distinguished from the majority (interpretable as outliers), with 4, 5 and 15 cranial fragments (Figure 454).

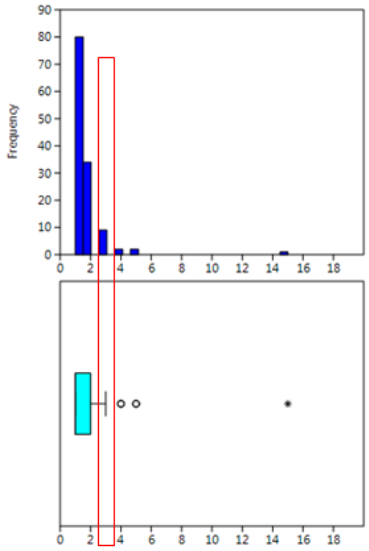

Figure 454 Histogram and box plot of frequencies observed for cranial faunal remains recovered during 2009 (Past).

84% of cranial fragments are located in 96% of the effectively surveyed area, in such a way that only 5 cells show more than 3 items.

The spatial distribution of cranial fragments is fitted with a Negative Binomial distribution (with k=0.081 and p=0.430) and Kolmogorov Smirnov Test=1. This condition suggests a predominant uniformity in the spatial distribution of the abundance of cranial fragments per sampling unit (Figure 455).

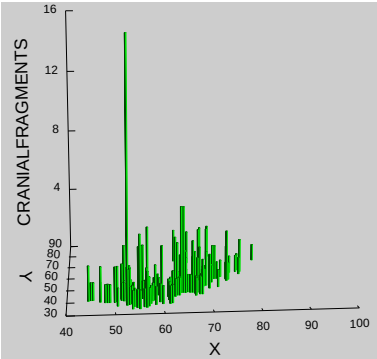

Figure 455 3D Histogram of cranial faunal remains recovered during surveys of 2009 (Systat 13).

The spatial distribution of count data per sampling unit for cranial fragments shows a Global Moran's *I* of -0.000397. The theoretical (expected) value assuming spatial autocorrelation (lack of spatial Independence) is -0.000515 and the standard error of I is 0.000515. The test of significance using the normality assumption gave a *z* value of 0.230379, low significant value. These results are comparable with those of the Geary statistics (*C*=10.999683) and Getis-Ord general G (*G*=0.015518). Consequently, it is evident that the spatial distribution of cranial fragments is not significantly different than the expected value under a random distribution. This is what would be expected in the case of predominant similar frequency of occurrence within every spatial location.

Moran's *I* Correlogram (Figure 456) has been calculated for uniform class distance interval of 1 metre, and taking into account a 10 metres active lag distance. *I* value at the starting point of the function is about 0.0965, a bit above the expected value for randomness. As the distance between sampling units increases, *I* value drops off abruptly. It reaches values less above the expected for randomness until 6 metre, where they are located predominantly on the line (corresponding to spatial randomness).

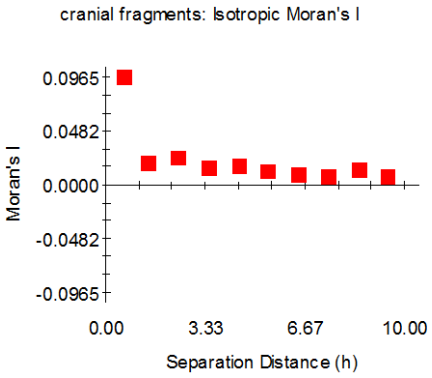

Figure 456 Moran's I Correlograms for cranial faunal remains recovered during surveys of 2009 (GS+).

We have explored the possible presence of anisotropic variation fitting a theoretical variogram at different directions (Figure 457). Anisotropy is higher at 45º and 135º, concentrated in the centre of the 3D diagram and particularly in the Western and Eastern sides (Figure 458).

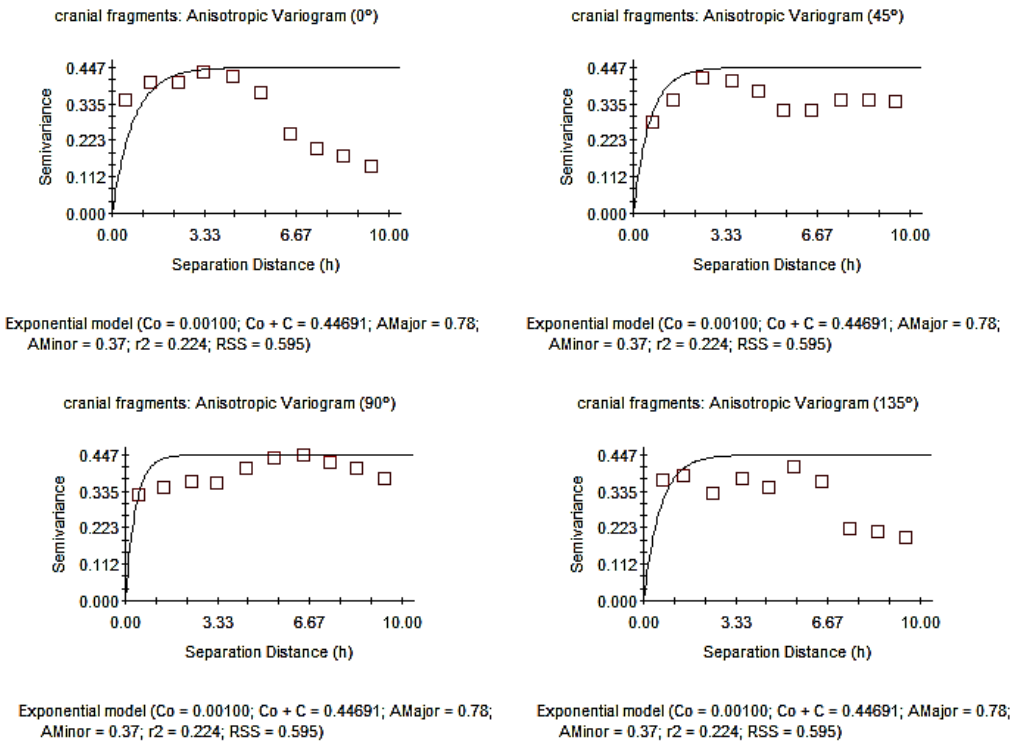

Figure 457 Anisotropic Variogram of cranial faunal remains recovered during surveys of 2009 (GS+).

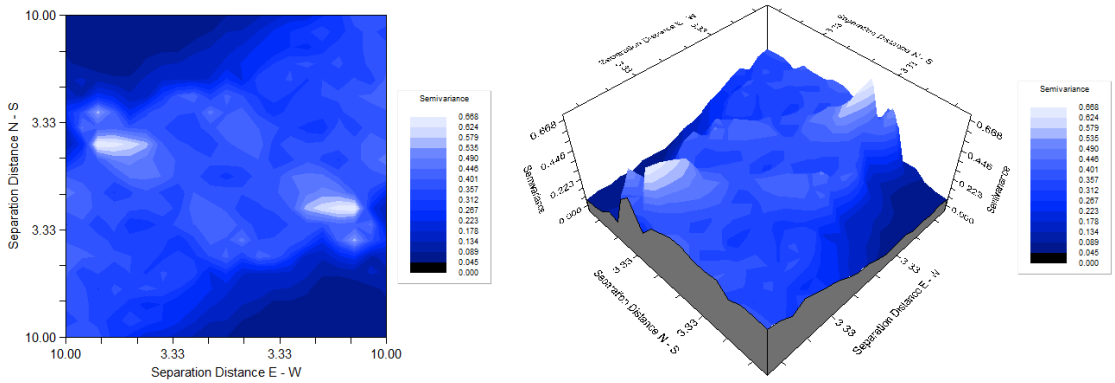

Figure 458 Variogram Map of cranial faunal remains recovered during surveys of 2009 (GS+).

Spatial semivariance is not quite relevant to calculate a reliable interpolated model of spatial frequencies. An isotropic model would explain a tiny 22.4% of global variance.

8.5.2.2 Axial faunal remains

20 axial remains were identified and counted; they were distributed in 19 sampling units, all located within Zone 1, while 1922 squares were empty. The spatial distribution of sampling units where axial remains have been identified is showed in Figure 459.

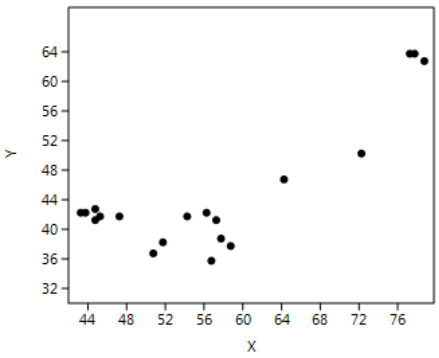

Figure 459 Spatial distribution of sampling units where axial faunal remains have been recorded in surveys of 2009 (Past).

Ripley's *k* analysis on the distance between sampling units with axial remains suggests the possibility of low degree of spatial clustering, particularly for distances higher than 1.6 metre, as (Figure 460).

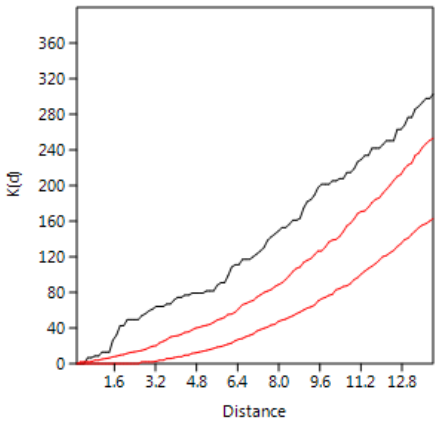

Figure 460 Ripley's *k* analysis on the distance between sampling units with axial faunal remains, recorded in surveys of 2009 (Past).

Within the convex hull defined by the 19 sampling units where axial fragments have been recovered, the null hypothesis of random pattern (Poisson process) cannot be rejected at $p<0.05$. A Kernel Density Estimation (Figure 461) suggests the occurrence of three predominant concentrations between x=44-48 and y=40-45, between x=48-60 and y= 32-44 and between x=73-78 and y=60-64.

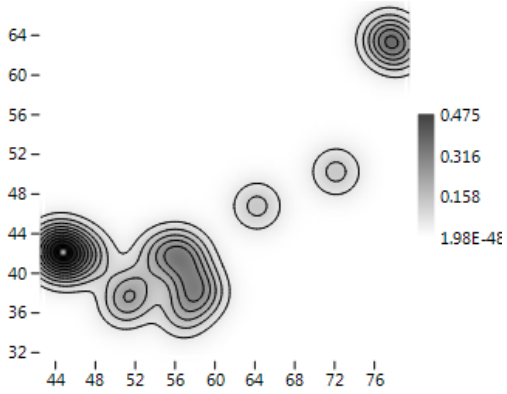

Figure 461 KDE of sampling units where axial faunal remains have been recorded during surveys of 2009 (Past).

When considering the raw quantity of axial remain at each cell, the probability density distribution of spatial frequencies does not follow a *J*-shaped distribution. A majority of sampling units have raw counts of such faunal remains of less than 2 elements (global mean = 1.263 observables per sampling unit) and that only range between 1 and 2 items.

The spatial distribution of cranial fragments is fitted with a Geometric distribution (with p=0.988) Negative Binomial distribution (with k=0.022 and p=0.643) and a Poisson distribution (with λ=0.012) and Kolmogorov Smirnov Test=1. This is what is expected when, as in this case, the sample consists in predominant empty sampling units and similar frequencies values in all non-empty cells, obtaining randomness (as also showed in Figure 462).

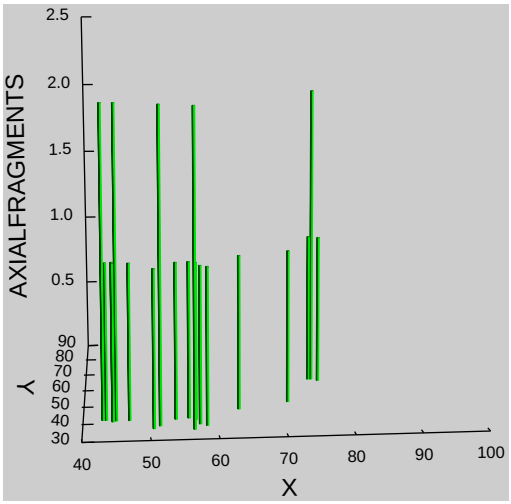

Figure 462 3D Histogram of axial faunal remains recovered during surveys of 2009 (Systat 13).

The spatial distribution of count data per sampling unit for axial fragments shows a Global Moran's *I* of -0.000466. The theoretical (expected) value assuming spatial autocorrelation (lack of spatial Independence) is -0.000515 and the standard error of *I* is 0.000515. The test of significance using the normality assumption gave a quite non-significant *z* value of 0.095646. These results are comparable with those of the Geary statistics (C=0.998152) and Getis-Ord general G (=0.022140). Consequently, we can accept that the spatial distribution of axial fragments could not be significantly different than the expected value under a random distribution. This is what would be expected in the case of similar frequency of occurrence within every spatial location.

Moran's *I* Correlogram (Figure 463) has been calculated for uniform class distance interval of 1 metre, and taking into account a 10 metres active lag distance. *I* value at the starting point of the function is about 0.0509, a bit above the expected value for randomness. As the distance between sampling units increases, *I* value drops off quite gently and reaches values less above the expected value for randomness until 2 metre, where they are located predominantly on the line (corresponding to spatial randomness) between 3 and 5 metre and later between 8 and 9 metre. Between 6 and 7 metre *I* value is located a bit above the line.

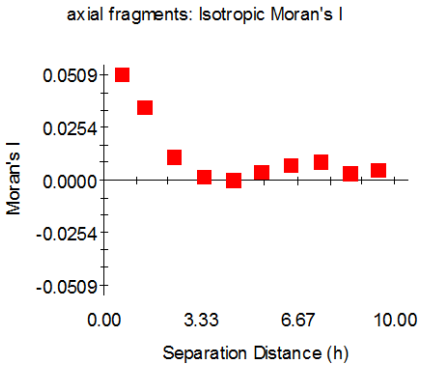

Figure 463 Moran's I Correlograms for axial faunal remains recovered during surveys of 2009 (GS+).

This result shows that scarce positive spatial autocorrelation is attested in the first 2 metres of the function, giving the possibility of finding spatially dependent area of 2 metres of radius, what is suggestive working hypothesis for locating individual activity area; however, it is interesting to remark that all *I* values are around 0.

Taking into consideration the scarce frequencies of axial fragments within the surveyed area (ranging from 1 to 2) it is interesting to verify if are attested differential spatial distributions between sampling units with more frequencies. However, 58% of axial fragments are located in 74% of the effectively surveyed area, in such a way that only 5 cells show 2 items.

We have explored the possible presence of anisotropic variation, fitting a theoretical variogram at different directions (Figure 464). In general, semivariance varies in quite the same way at 0º, 45º and 90º for the first distances (between the starting point of the function and 3 metres), while at 135º semivariance varies in a strongly different way. It is strongest in the 135º degrees, that is, in the general North-West-South-East direction, perpendicular to the ancient estimated shoreline of the lake.

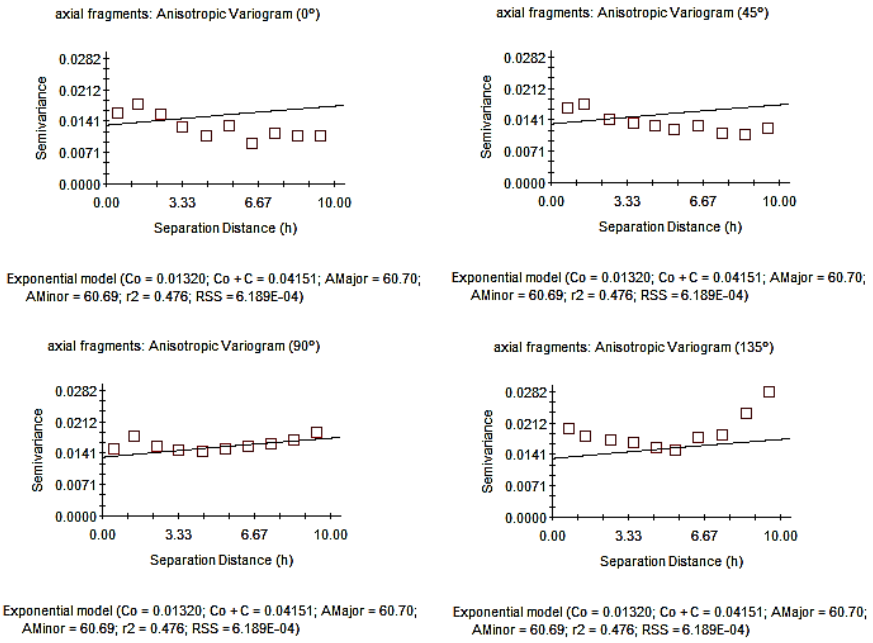

Figure 464 Anisotropic Variogram of axial faunal remains recovered during surveys of 2009 (GS+).

The graph of anisotropic Semivariance Surface or Variogram Map is particularly concentrated around the North-West and South-East corners, probably related to the unsurveyed surrounding areas (Figure 465).

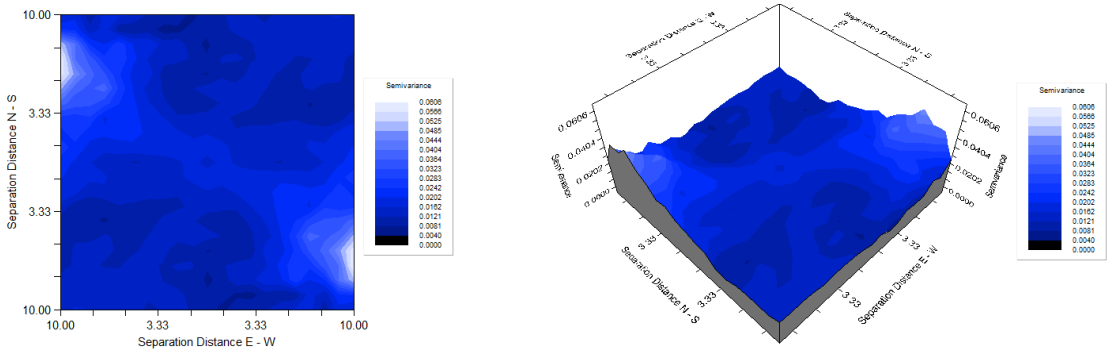

Figure 465 Variogram Map of axial faunal remains recovered during surveys of 2009 (GS+).

Spatial semivariance is not quite relevant to calculate a reliable interpolated model of spatial frequencies. An isotropic model would explain a tiny 22.4% of global variance.

8.5.2.3 Appendicular faunal remains

165 appendicular remains were identified and counted; they are spatially distributed in 120 sampling units, predominantly distributed in Zone 1 (only three points are located in Zone 2) and 1822 squares were empty. The spatial distribution of sampling units where appendicular remains have been identified is showed in Figure 466.

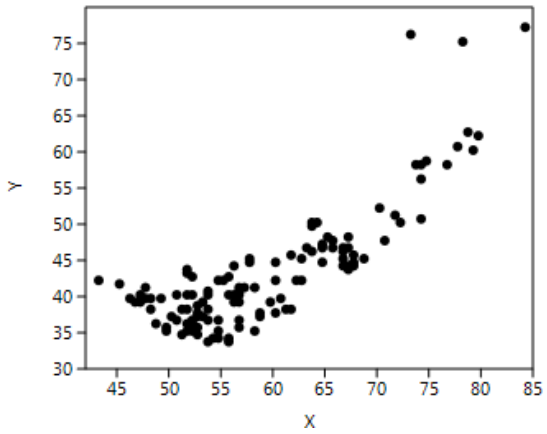

Figure 466 Spatial distribution of sampling units where appendicular faunal remains have been recovered during surveys of 2009 (Past).

Ripley's *k* analysis on the distance between sampling units with appendicular remains suggests the possibility of some degree of spatial clustering, for all the reference area (Figure 467).

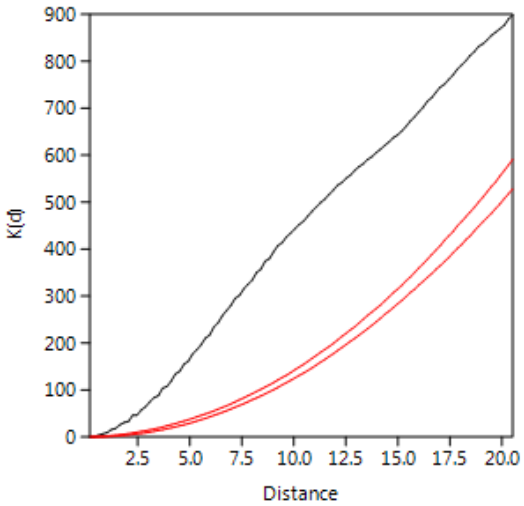

Figure 467 Ripley's *k* analysis on the distance between sampling units with appendicular faunal remains, recorded in surveys of 2009 (Past).

Within the convex hull, configured by sampling units with appendicular faunal remains are statistically significant clustered (according to Clark and Evans test). Kernel Density estimation (Figure 468) shows the presence of two predominant concentrations between x=44-60 and y=33-44 and between x=61-70 and y=42-50. A further lower dense concentration is observed between x=72-80 and y=55-64.

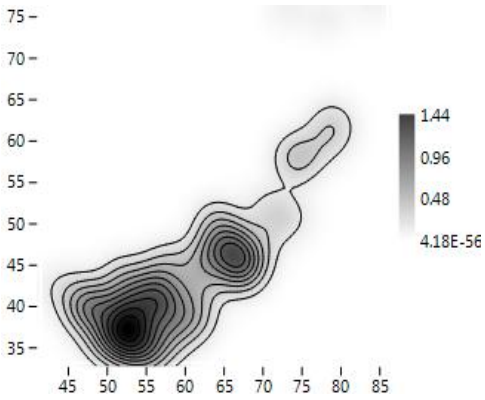

Figure 468 KDE of sampling units where appendicular faunal remains have been recorded during surveys of 2009 (Past).

When considering the raw quantity of appendicular remain at each cell, the probability density distribution of spatial frequencies does not follow a *J*-shaped distribution. A majority of sampling units have raw counts of such faunal remains of less than 2 elements (global mean = 1.38 observables per sampling unit). Both histogram and box plot distinguish four cells from the majority (interpretable as outliers), with 2, 3, 4 and 6 appendicular fragments (Figure 469).

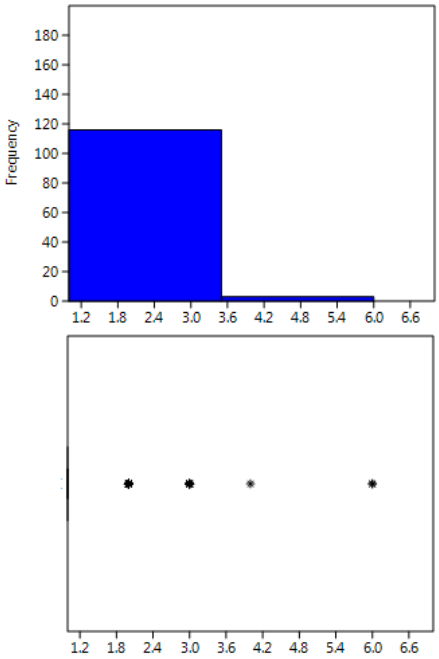

Figure 469 Histogram and box plot of frequencies observed for appendicular faunal remains recovered during 2009 (Past).

The spatial distribution of appendicular fragments is fitted with a Negative Binomial distribution (with k=0.112 and p=0.567) and Kolmogorov Smirnov Test=1. This condition suggests randomness in the spatial distribution of the abundance of appendicular fragments per sampling unit (Figure 470).

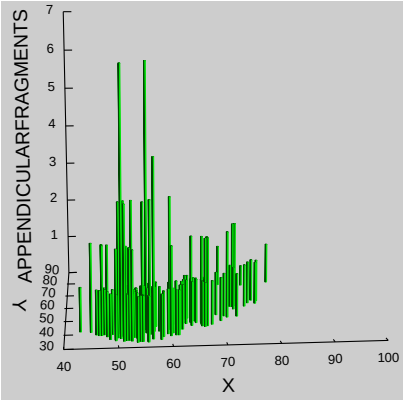

Figure 470 3D Histogram of appendicular faunal remains recovered during surveys of 2009 (Systat 13).

The spatial distribution of count data per sampling unit for cranial fragments shows a Global Moran's *I* of -0.000221. The theoretical (expected) value assuming spatial autocorrelation (lack of spatial Independence) is -0.000515 and the standard error of *I* is 0.000515. The test of significance using the normality assumption gave a quite significant *z* value of 0.571473. These results are comparable with those of the Geary statistics (*C*=0.998766) and Getis-Ord general G (*G*=0.012636). Consequently, we can accept that the spatial distribution of appendicular fragments could not be significantly different than the expected value under a random distribution. This is what would be expected in the case of similar frequency of occurrence within every spatial location.

Moran's *I* Correlogram (Figure 471) has been calculated for uniform class distance interval of 1 metre, and taking into account a 10 metres active lag distance. *I* value at the starting point of the function is about 0.0844, a bit above the expected value for randomness. As the distance between sampling units increases, *I* value drops off gently reaching, within 10 metres, all *I* values below the expected value for randomness.

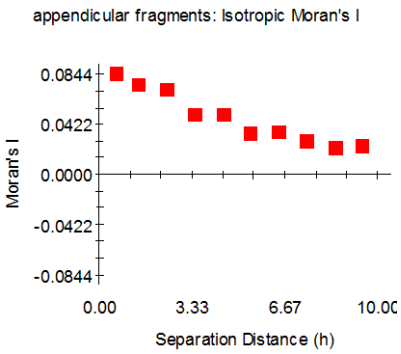

Figure 471 Moran's I Correlograms for appendicular faunal remains recovered during surveys of 2009 (GS+).

This result shows that scarce positive spatial autocorrelation is attested in the 10 metres of the function, giving the possibility of finding spatially dependent area of such radius, what is suggestive working hypothesis for locating homogeneous activity area; however, it is interesting to remark that all *I* values are all around 0, particularly those corresponding to distances included between 6 to 9 metres.

Taking into consideration the low frequencies of appendicular fragments within the surveyed area (ranging from 1 to 6) it is interesting to verify if there are attested differential spatial distributions between sampling units with more frequencies. 55% of appendicular fragments is

located in 76% of the effectively surveyed area, in such a way that 45% of cells show more than 1 fragment, distributed within 24% of the effectively surveyed area (as showed in Figure 472). However, for this distribution the null hypothesis of a random pattern (Poisson process) cannot be rejected at $p<0.05$. Kernel Density Estimation for such cells shows two main higher dense concentrations located between x=46-58 and y=32-42 and between x=63-70 and y=42-48 and two further lower dense areas are observed between x=68-70 and y=48-50 and between x=72-74 and y=54-58.

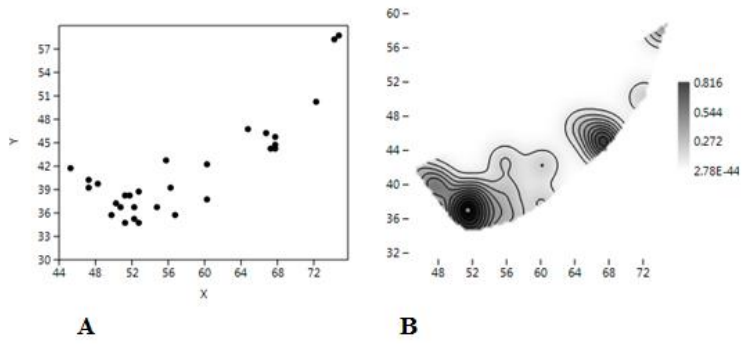

Figure 472 A)Spatial distribution of sampling units where more than 1 fragment of appendicular faunal remains have been recovered during surveys of 2009. B)KDE of such cells (Past).

We have explored the possible presence of anisotropic variation, fitting a theoretical variogram at different directions (Figure 473). Semivariance varies in quite the same way at 0º, 45º and 90º for the first distances (between the starting point of the function to 3-4 metres) while at 135º semivariance varies in a quite different way. This condition suggests the presence of anisotropy.

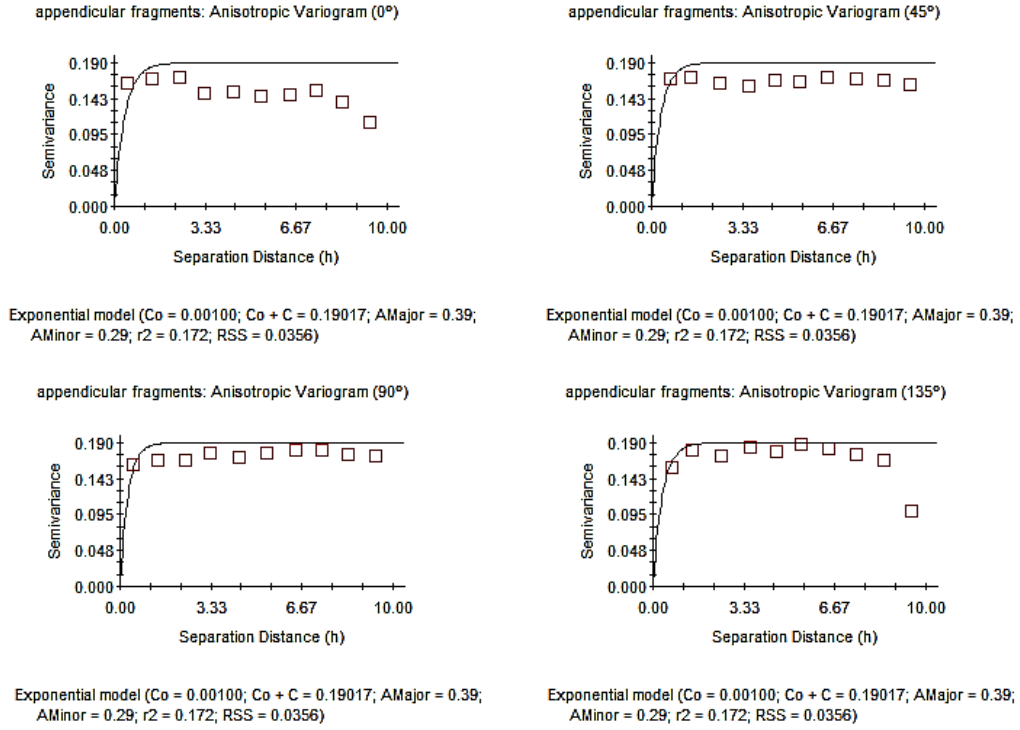

Figure 473 Anisotropic Variogram of appendicular faunal remains recovered during surveys of 2009 (GS+).

As suggested by the graph of anisotropic Semivariance Surface or Variogram Map (Figure 474), anisotropy and the lack of spatial contiguity is a very remarkable effect, as observed for other categories of faunal remains. However, an exponential model could not be fitted to the empirical variogram.

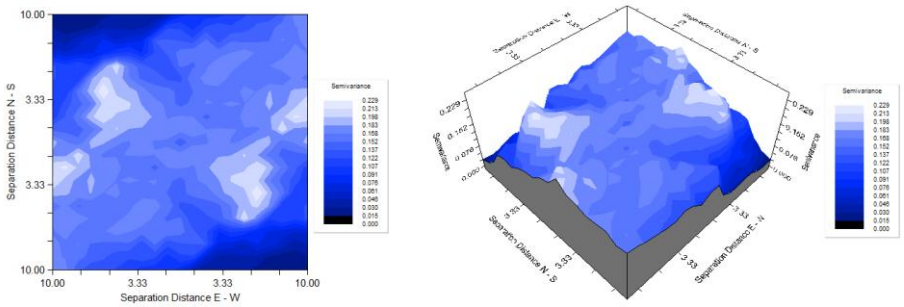

Figure 474 Anisotropic Variogram of appendicular faunal remains recovered during surveys of 2009 (GS+).

8.5.2.4 Faunal Remains ascribable to Ovis Vel Capra

44 faunal remains of *ovis vel capra* were identified and counted; they were spatially distributed in 34 sampling units (all within Zone 1), while 1907 squares were empty. Sampling units where *ovis vel capra* remains have been identified are spatially distributed as showed in Figure 475**.**

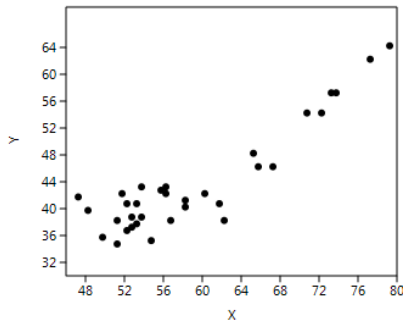

Figure 475 spatial distribution of cells with *ovis vel capra* faunal remains (surveys of 2009) (Past).

Ripley's k analysis on the distance between sampling units with *ovis vel capra* remains suggests the possibility of some degree of spatial clustering at the scale of the reference area (Figure 476).

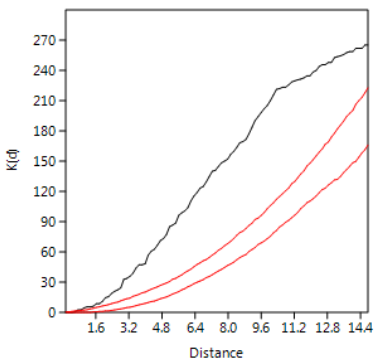

Figure 476 Ripley's k analysis on the distance between sampling units with *ovis vel capra* remains, recorded in surveys of 2009 (Past).

Within the convex hull configured by those sampling units with some positive frequency of these remains, the null hypothesis of a random pattern (Poisson process) cannot be rejected at $p<0.05$ (Clark and Evans test). A Kernel Density estimation (Figure 477) however shows linearity in the distribution of data; there is a wider accumulation of remains between x=48-60 and y=33-44 and three smaller concentrations located between x=64-68 and y=44-48 y, between x=68-75 and y=52-60 and between x=74-80 and y=60-64. They are all observed along the main axis of the surveyed area, parallel to the ancient estimated lake shoreline.

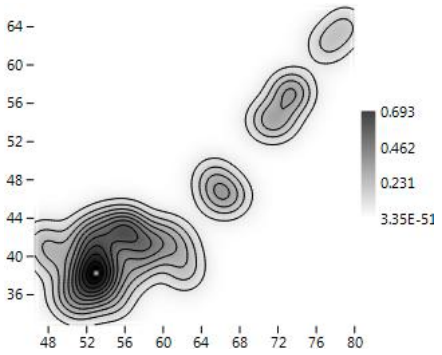

Figure 477 KDE of sampling units where *ovis vel capra* remains have been recovered during surveys of 2009 (Past).

When considering the raw quantity of *ovis vel capra* fragments at each cell, the probability density distribution of spatial frequencies does not follow a *J*-shaped distribution. A majority of sampling units have raw counts of such faunal remains of less then 2 elements (global mean=1.45 observables per sampling unit). Three cells are distinguished from the majority (interpretable as outliers) with 2, 3 and 12 *ovis vel capra* remains (Figure 478).

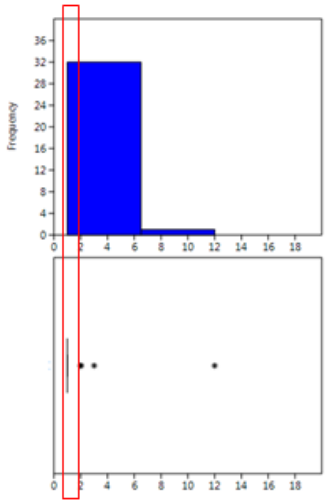

Figure 478 Histogram and box plot of frequencies observed for *ovis vel capra* remains, surveys 2009 (Past).

The spatial distribution of *sus ovis vel capra* remains is fitted with both a Geometric distribution (with $p=0.976$) a Negative Binomial distribution (with $k=0.024$ and $p=0.497$) and Kolmogorov Smirnov Test=1. This is what is expected when, as in this case, the sample consists in predominant empty sampling units and similar frequencies values in all non-empty cells, obtaining randomness (as also showed in Figure 479).

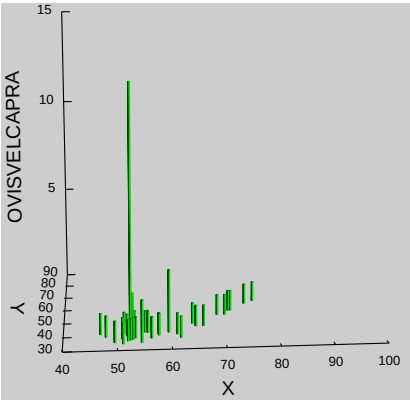

Figure 479 3D Histogram of *ovis vel capra* remains recovered during surveys of 2009 (Systat 13).

The spatial distribution of count data per sampling unit for *ovis vel capra* remains shows a Global Moran's *I* of -0.000473. The theoretical (expected) value assuming spatial autocorrelation (lack of spatial Independence) is -0.000515 and the standard error of *I* is 0.000515. The test of significance using the normality assumption gave a z value of 0.083122, highly non-significant value. These results are comparable with those of the Geary statistics (*C*=0.998601) and Getis-Ord general G (*G*=0.019868). Consequently, we can accept that the spatial distribution of *ovis vel capra* fragments could not be significantly different than the expected value under a random distribution. This is what would be expected in the case of similar frequency of occurrence within quite every spatial location.

Moran's *I* Correlogram (Figure 480) has been calculated for uniform class distance interval of 1 metre, and taking into account a 10 metres active lag distance. *I* values show a strongly irregular pattern; at the starting point of the function it is on the line (corresponding to randomness) while at 1 metre reaches a value of about 0.0184, very few above the expected value for randomness. As the distance between sampling units increases, *I* value drops off quite gently at 2 metre and abruptly at 3 metre, where it is located on the line. This same oscillation between value, above those expected for randomness and corresponding to randomness, characterizes the function.

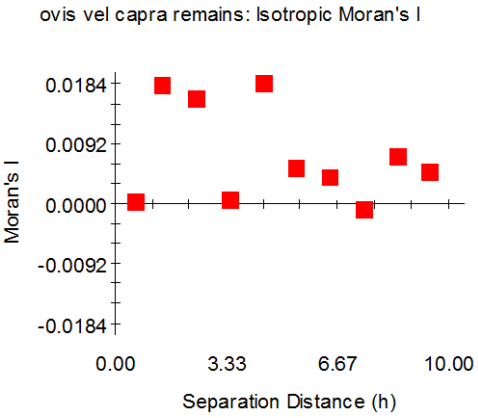

Figure 480 Moran's I Correlogram for *ovis vel capra* remains recovered during surveys of 2009 (GS+).

According to such result for *ovis vel capra* remains is attested scarce spatial dependence, limited to 2-3 metres. Furthermore, it is relevant to remark that all *I* values are around 0.

Taking into account what is suggested both by box plot and histogram, that is the occurrence of a breaking point in the frequencies of such faunal remains in correspondence with a value of 1

item, sampling units with more than 1 fragment are analysed separately. However, 60% of *ovis vel capra* fragments are located in 88% of the effectively surveyed area, in such a way that only 4 cells show more than 1 item.

We have explored the presence of anisotropic variation comparing the anisotropic variogram for different directions (Figure 481). Semivariance varies in strongly different ways at each degree. This condition suggests the presence of anisotropy.

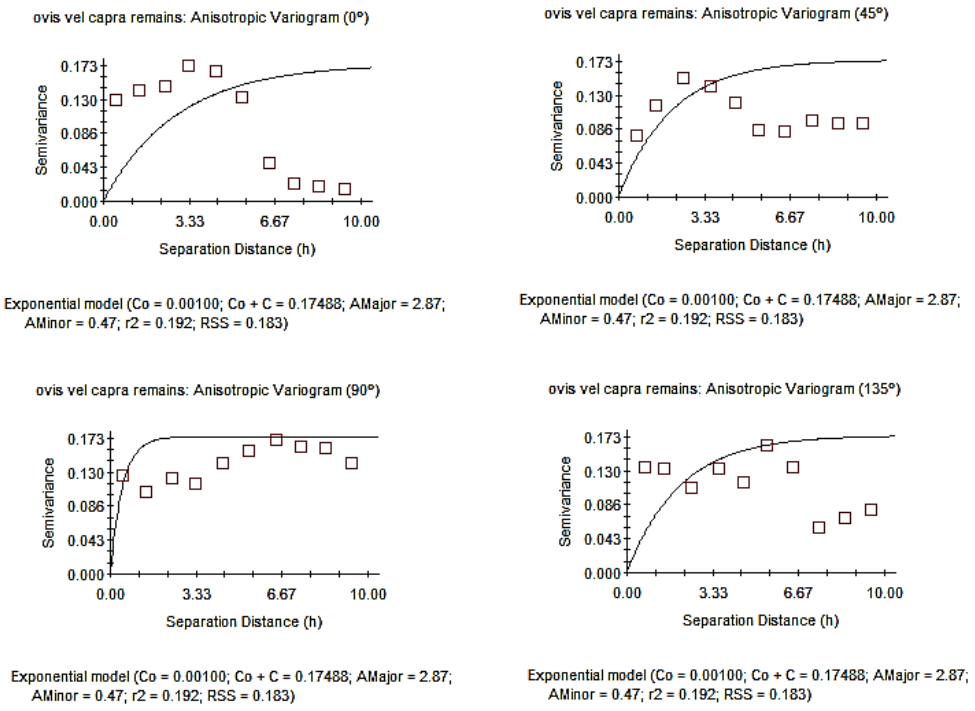

Figure 481 Anisotropic Variogram of *ovis vel capra* remains recovered during surveys of 2009 (GS+).

The graph of anisotropic Semivariance Surface or Variogram Map suggests that anisotropy is particularly concentrated in the centre of the 3D diagram and, with peaks, around the North-West and South-West corners (Figure 482).

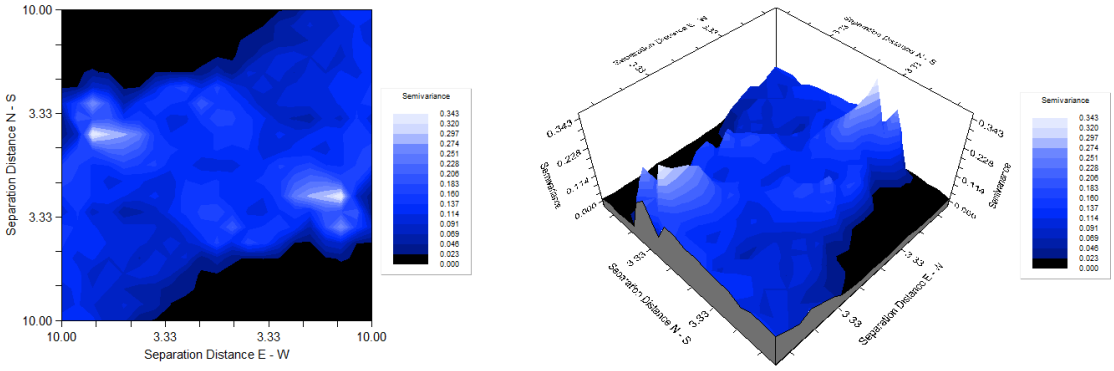

Figure 482 Variogram Map of *ovis vel capra* remains recovered during surveys of 2009 (GS+).

An exponential isotropic variogram model fitted to the empirical variogram Nugget Variance, C_0 =0.03280, Sill, C_0+C = 0.11560 and Range, A_0 = 0.01, does not explain the sample variance.

8.5.2.5 *Faunal remains ascribable to* <u>*Sus Domesticus*</u>

35 faunal remains of *sus domesticus* species were identified and counted; they were spatially distributed in 29 sampling units, while 1912 squares were empty. Cells where faunal remains ascribable to *sus domesticus* have been identified are spatially distributed as showed in Figure 483.

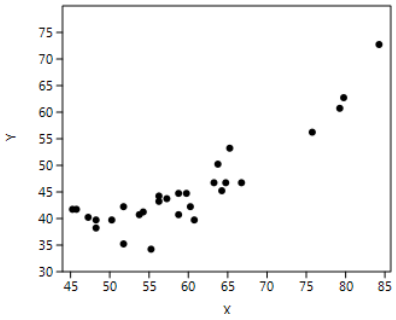

Figure 483 Spatial distribution of sampling units where *sus domesticus* remains have been recovered (surveys 2009) (Past).

Ripley's *k* analysis on the distance between sampling units with *sus domesticus* fragments suggests the possibility of some degree of spatial clustering, at the scale of the reference area (Figure 484).

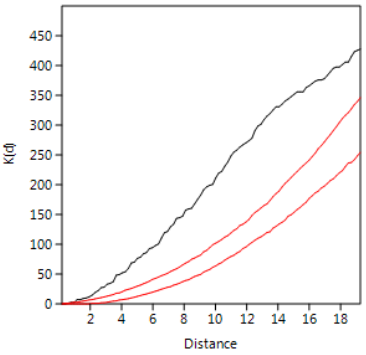

Figure 484 Ripley's *k* analysis on the distance between sampling units with *sus domesticus* remains, recorded in surveys of 2009 (Past).

Within the convex hull configured by those sampling units where *sus domesticus* have been identified, the null hypothesis of a random pattern (Poisson process) cannot be rejected at $p<0.05$. This result suggests that randomness characterizes the spatial distribution of *sus domesticus* fragments; this is what would be expected when the majority of the scarce sampling units show the same frequency of remains. A Kernel Density Estimation (Figure 485) shows the occurrence of a concentration locates between x=45-70 and y=38-50 (internally sub-divided in three main sub.concentrations) and a further small concentration is identified between x=72-80 and y=55-63. Even in this case quite total amount of remains (only 1 cell belonging to Area 2 shows one fragment of *sus domesticus*) are ascribable to Zone 1.

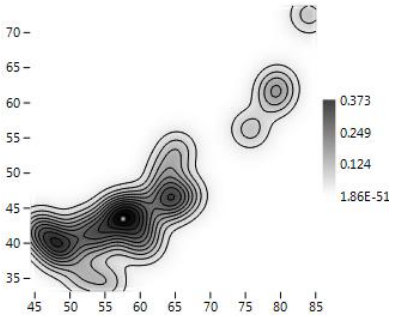

Figure 485 KDE of sampling units where *sus domesticus* remains have been recovered during surveys of 2009 (Past).

When considering the raw quantity of *sus domesticus* remains at each cell, the probability density distribution of spatial frequencies does not follow a *J*-shaped distribution. A majority of sampling units have raw counts of such faunal remains of less than 2 elements (global mean = 1.20 observables per sampling unit). Cells with 2 *sus domesticus* remains are distinguished from the majority (interpretable as outliers) (Figure 486).

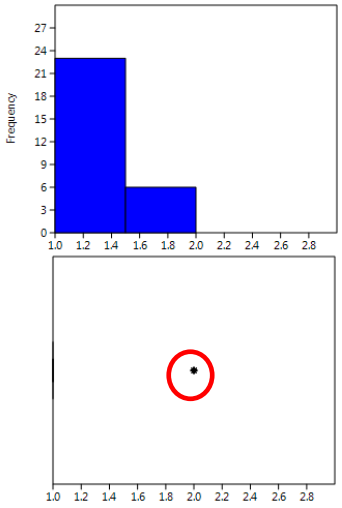

Figure 486 Histogram and box plot of frequencies observed for *sus domesticus* remains, surveys 2009 (Past).

66% of *sus domesticus* fragments are located in 79% of the effectively surveyed area, in such a way that only 6 cells show more than 1 item (the outlier which has showed 2 fragments).

The spatial distribution of *sus domesticus* fragments is fitted with a Geometric distribution (with p=0.982), a Negative Binomial distribution (with k=0.043 and p=0.705) and a Poisson distribution (with λ=0.018) with Kolmogorov Smirnov Test=1. This condition suggests randomness in the spatial distribution of the abundance of *sus domesticus* fragments per sampling unit (Figure 487).

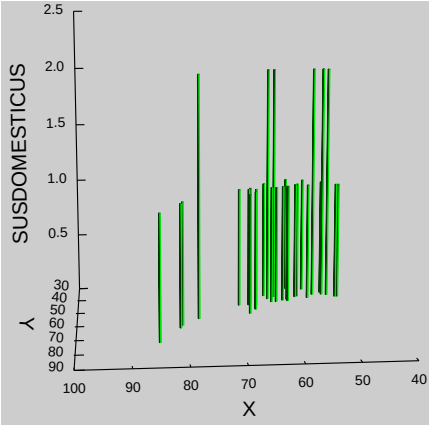

Figure 487 3D Histogram of *sus domesticus* remains recovered during surveys of 2009 (Systat 13).

The spatial distribution of count data per sampling unit for *sus domesticus* fragments shows a Global Moran's *I* of -0.000458. The theoretical (expected) value assuming spatial autocorrelation (lack of spatial Independence) is -0.000515 and the standard error of *I* is 0.000515. The test of significance using the normality assumption gave a quite significant z value of 0.111365. These results are comparable with those of the Geary statistics (*C*=0.999515) and Getis-Ord general G (*G*=0.006791). Consequently, we can accept that the spatial distribution of *sus domesticus* fragments could not be significantly different than the expected value under a random distribution. This is what would be expected in the case of predominant similar frequency of occurrence within quite every spatial location.

Moran's *I* Correlogram (Figure 488) has been calculated for uniform class distance interval of 1 metre, and taking into account a 10 metres active lag distance. *I* values are distributed according to an irregular pattern. At the starting point of the function I value is below the expected value for randomness, while at 1 metre is very few above the expected value for randomness and at 2 metre reaches 0.0235. As the distance between sampling units increases, *I* value drops off abruptly and reaches values less above the expected value for randomness until 6 metre, where they are located predominantly on the line (corresponding to spatial randomness).

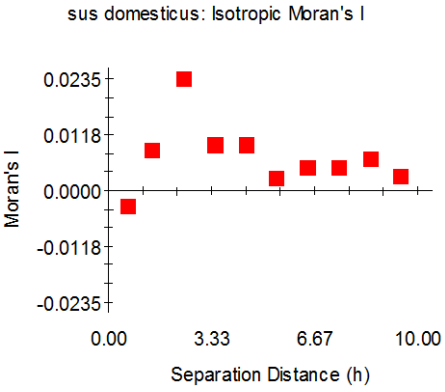

Figure 488 Moran's I Correlogram for *sus domesticus* remains recovered during surveys of 2009 (GS+).

As proved by such result, scarce positive spatial autocorrelation is attested between 2 and 4 metres, giving the possibility of finding spatially dependent area of 2 meters of radius, what is suggestive working hypothesis for locating individual activity area; however it is interesting to remark that all *I* values are around 0.

We have explored the possible presence of anisotropic variation fitting a theoretical variogram at different directions (Figure 489). Semivariance varies, for the first meters of the function (between the starting point and 3-4 metres) in similar way at 0º and 45º and at 90º and 135º.

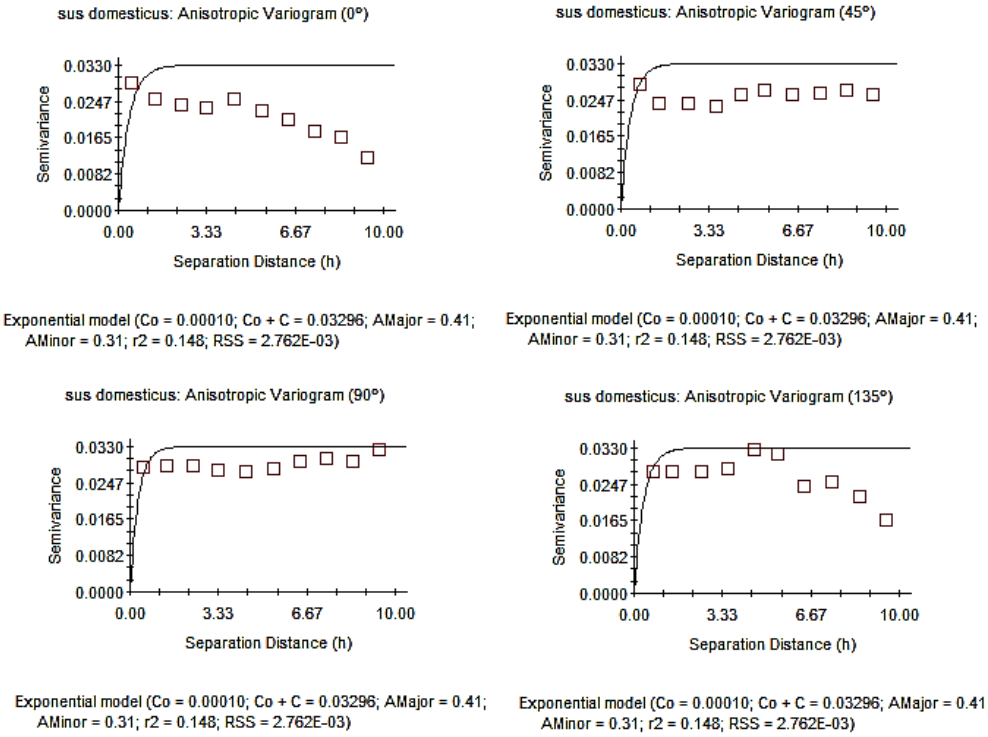

Figure 489 Anisotropic Variogram of *sus domesticus* remains recovered during surveys of 2009 (GS+).

The graph of anisotropic Semivariance Surface or Variogram Map shows that anisotropy is particularly concentrated in the Western and Eastern side of the 3D diagram which a tendency to the centre (Figure 490).

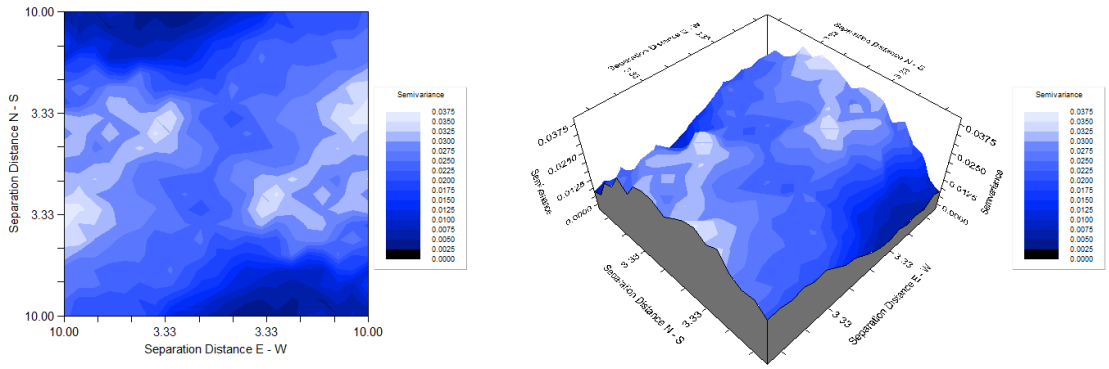

Figure 490 Variogram Map of *sus domesticus* remains recovered during surveys of 2009 (GS+).

An exponential isotropic variogram fitted to the empirical variogram –Nugget Variance, C_0 =0.00494, Sill, C_0+C = 0.02598 and Range, A_0 = 0.01. This model does not explain the sample variance.

8.5.2.6 Faunal Remains ascribable to Bos Taurus

68 *bos taurus* faunal remains were identified and counted; they are spatially distributed in 58 sampling units (all within Zone 1), while 1883 squares were empty. Cells where *bos taurus* remains have been identified are spatially distributed as showed in Figure 491.

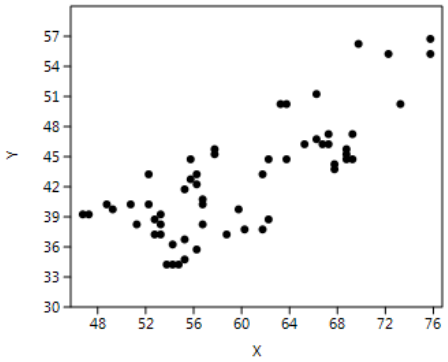

Figure 491 spatial distribution of sampling units where *bos taurus* faunal remains have identified (surveys 2009) (Past).

Ripley's *k* analysis on the distance between sampling units with *bos taurus* remains suggests the possibility of some degree of spatial clustering, at the scale of the global reference area (Figure 492).

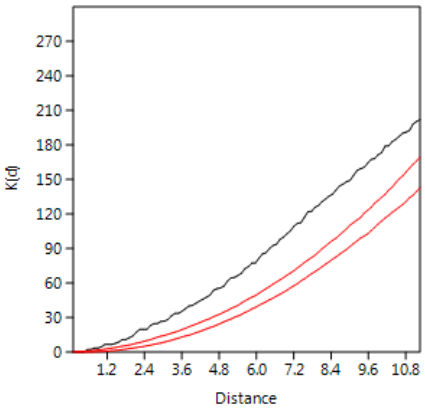

Figure 492 Ripley's *k* analysis on the distance between sampling units with *bos taurus* remains, recorded in surveys of 2009 (Past).

Within the convex hull configured by 58 sampling units where *bos taurus* remains have been identified, the null hypothesis of a random pattern (Poisson process) cannot be rejected at $p<0.05$, according to Clark and Evans Test. Thus, randomness characterizes the spatial distribution of *bos taurus* fragments; this is what would be expected when the majority of the scarce sampling units show the same frequency of remains. However, as in the case of other faunal categories, Kernel Density Estimation (Figure 493) shows some degree of irregularity,

By detecting two predominant concentrations, respectively observed between x=45-65 and y=32-46 as well as between x=65-72 and y=42-46. A further smaller aggrupation is located between x=68-76 and y=53-56.

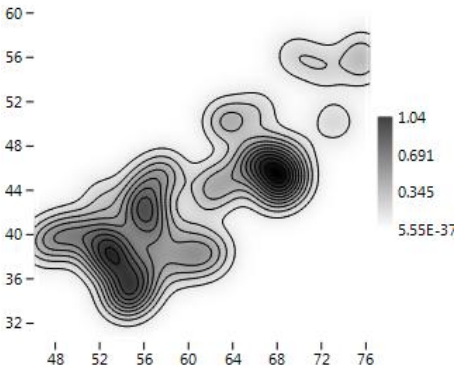

Figure 493 KDE of sampling units where *bos taurus* remains have been recovered during surveys of 2009 (Past).

When considering the raw quantity of *bos taurus* remains at each cell, the probability density distribution of spatial frequencies does not follow a J-shaped distribution. A majority of sampling units have raw counts, of such fauna, of less than 2 elements (global mean = 1.17 observables per sampling unit). Cells with two and three remains are distinguished from the majority (interpretable as outliers) (Figure 494).

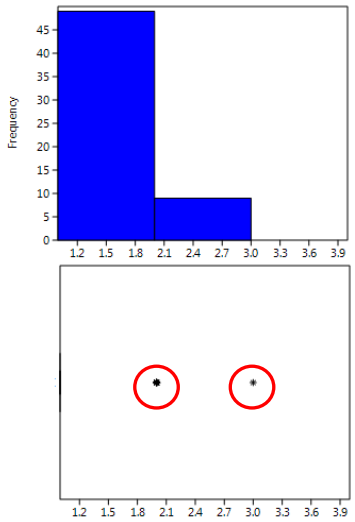

Figure 494 Histogram and box plot of frequencies observed for *bos taurus* remains (Past).

72% of *bos taurus* fragments is located in 84% of the effectively surveyed area, in such a way that only 9 cells show more than 1 item (representing, higher values, outliers, as showed by both histogram and box plot).

The spatial distribution of cranial fragments is fitted with a Geometric distribution (with p=0.966), a Negative Binomial distribution (with k=0.109 and p=0.756) and a Poisson distribution (with λ=0.035) Kolmogorov Smirnov Test=1. This condition suggests randomness in the spatial distribution of the abundance of *bos taurus* fragments per sampling unit (Figure 495).

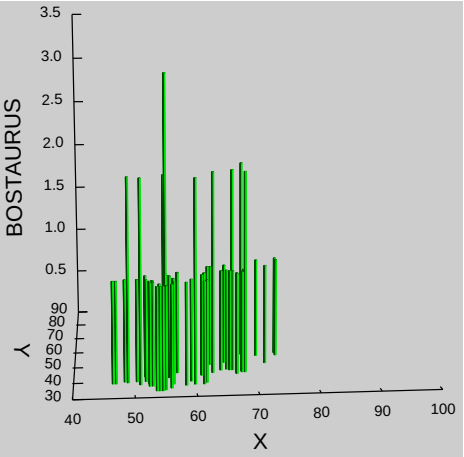

Figure 495 3D Histogram of *bos taurus* remains recovered during surveys of 2009 (Systat 13).

The spatial distribution of count data per sampling unit for *bos taurus* fragments shows a Global Moran's *I* of -0.000366. The theoretical (expected) value assuming spatial autocorrelation (lack of spatial Independence) is -0.000515 and the standard error of *I* is 0.000515. The test of significance using the normality assumption gave a quite significant *z* value of 0.290318. Those results are comparable with those of the Geary statistics (*C*=0.999934) and Getis-Ord general G (*G*=0.013233). Consequently, we can accept that the spatial distribution of *bos taurus* fragments could not be significantly different than the expected value under a random distribution. This is what would be expected in the case of predominant similar frequency of occurrence within quite every spatial location.

Moran's *I* Correlogram (Figure 496) has been calculated for uniform class distance interval of 1 metre, and taking into account a 10 metres active lag distance. *I* value at the starting point of the function is about 0.0552, a very few above the expected value for randomness. As the distance between sampling units increases, *I* value drops off quite gently and reaches values less above the expected value for randomness until 8 metre, where it is located quite on the line (corresponding to spatial randomness).

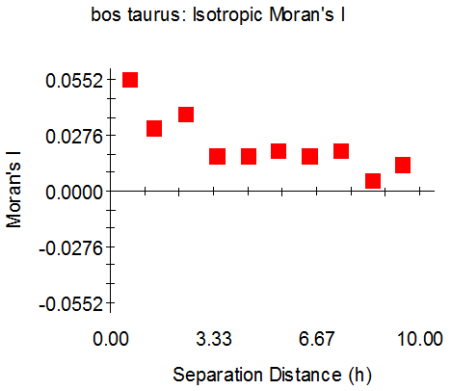

Figure 496 Moran's I Correlogram for*bos taurus* remains recovered during surveys of 2009 (GS+).

As such result proved, positive spatial autocorrelation is attested in the first 4 meters of the function, giving the possibility of finding spatially dependent area of at least such radius, what is suggestive working hypothesis for locating individual activity area; however it is remarkable that all *I* values are around 0.

We have explored the possible presence of anisotropic variation, fitting a theoretical variogram at different directions (Figure 497). Semivariance varies in quite different ways at each degree. This condition suggests the presence of anisotropy.

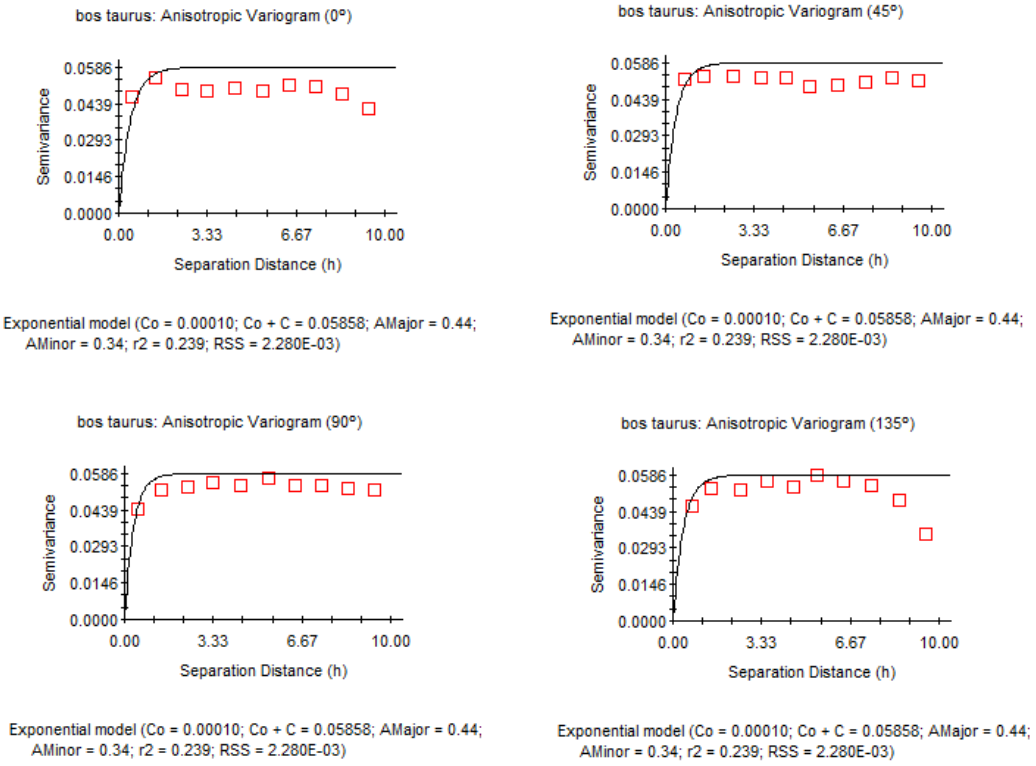

Figure 497 Anisotropic Variogram of *bos taurus* remains recovered during surveys of 2009 (GS+).

The graph of anisotropic Semivariance Surface or Variogram Map insists on the lack of spatial continuity, even at very small distances, with highest values of anisotropy concentrated around the North-West and South-East corners (Figure 498).

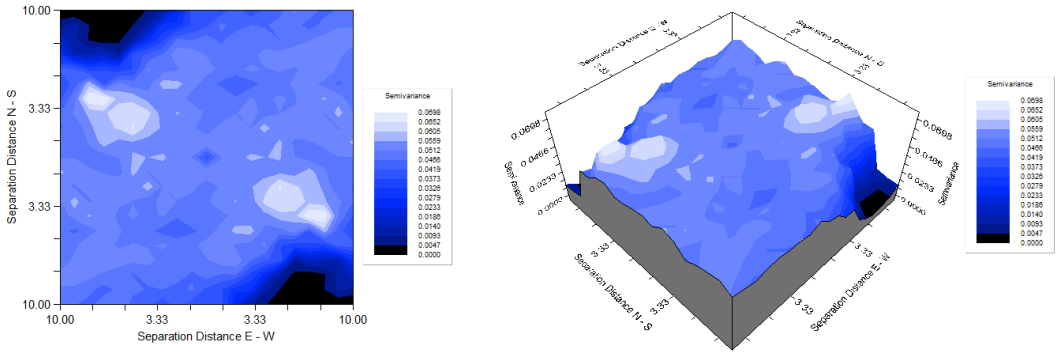

Figure 498 Variogram Map of *bos taurus* remains recovered during surveys of 2009 (GS+).

An exponential isotropic variogram model has been fitted to the empirical variogram. In this case Nugget Variance, C_0=0.01180, Sill, C_0+C= 0.05190 and Range, A_0= 0.27. This model explains 40.9% of sample variance and it fits conveniently the empirical data set (Figure 499).

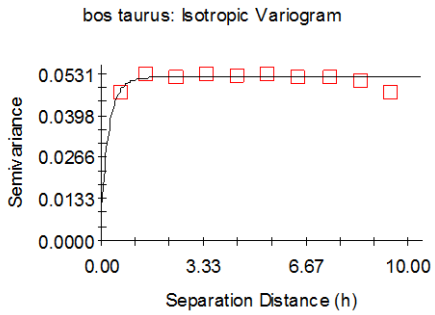

Exponential model (Co = 0.01180; Co + C = 0.05190; Ao = 0.27; **r2 = 0.409;** RSS = 2.582E-05)

Figure 499 Exponential Isotropic Variogram for *bos taurus* remains recovered during surveys of 2009 (GS+).

An inverse distance weighting (Figure 500) coincides with the other faunal categories, signaling the total concentration of *bos taurus* remains within Zone 1, distributed according to a predominant North-East-South-West orientation.

Figure 500 Graphic results of inverse distance weighting calculated for *bos tuarus* remains recovered during surveys of 2009 (Past).

8.5.2.7 Faunal Remains ascribable to Cervus Elaphus

90 *cervus elaphus* faunal remains were identified and counted; they are spatially distributed in 76 sampling units, while 1865 squares were empty. Cells where *cervus elaphus* fragments have been identified are spatially distributed as showed in Figure 501.

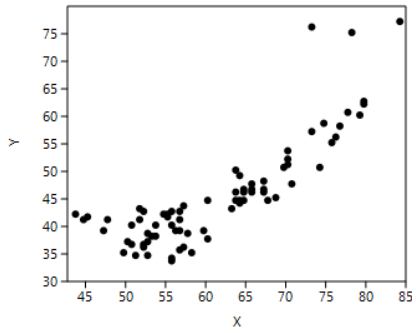

Figure 501 spatial distribution of cells with *cervus elaphus* remains, surveys 2009 (Past).

Ripley's *k* analysis on the distance between sampling units with *cervus elaphus* remains suggests the possibility of some degree of spatial clustering, at the scale of the global reference area (Figure 502).

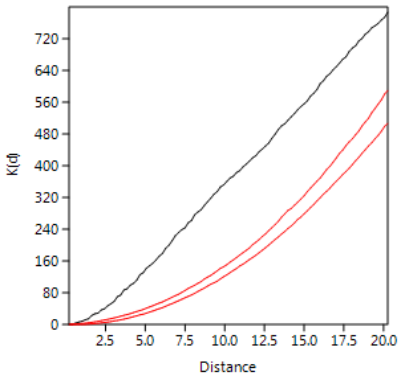

Figure 502 Ripley's *k* analysis on the distance between sampling units with *cervus elaphus* remains, recorded in surveys of 2009 (Past).

Within the convex hull configured by 76 sampling units where *cervus elaphus* remains have been identified, a statistically significant clustering is observed. A Kernel Density estimation (Figure 503) shows two main concentrations of evidence located between x=50-60 and y=33-45 and between x=62-70 and y=42-50. Another lower dense concentration is observed between x=72-80 and y=55-65 (the only three points located in Zone 2).

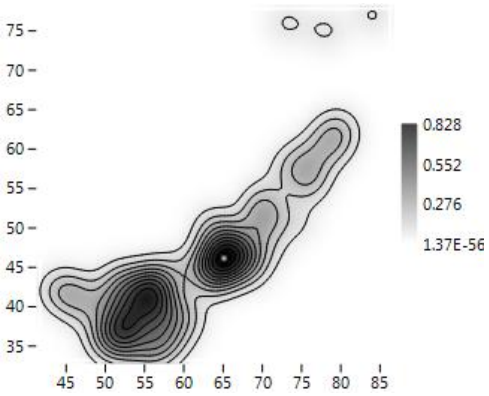

Figure 503 KDE of sampling units where *cervus elaphus* remains have been recovered during surveys of 2009 (Past).

When considering the raw quantity of *cervus elaphus* remain at each cell, the probability density distribution of spatial frequencies does not follow a *J*-shaped distribution. A majority of sampling units have raw counts, of such fauna, of less than 2 elements (global mean = 1.18 observables per sampling unit). Three values (2, 3 and 4) are distinguished from the majority (interpretable as outliers) (Figure 504).

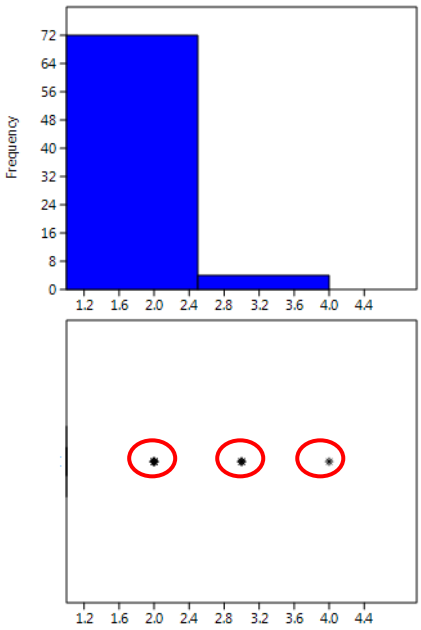

Figure 504 Histogram and box plot of frequencies observed for *cervus elaphus* remains (Past).

74% of *cervus elaphus* fragments are located in 88% of the effectively surveyed area, in such a way that only 9 cells show more than 1 item (representing, higher values, outliers as showed by both histogram and box plot). Such cells are overdispersed, according to Clark and Evans test ($p<1$).

The spatial distribution of cells with *cervus elaphus* fragments is fitted both with a Negative Binomial distribution (with $k=0.135$ and $p=0.744$) and a Poisson distribution (with $\lambda=0.046$) with Kolmogorov Smirnov Test=1. This condition suggests randomness in the spatial distribution of the abundance of *cervus elaphus* fragments per sampling unit (Figure 505).

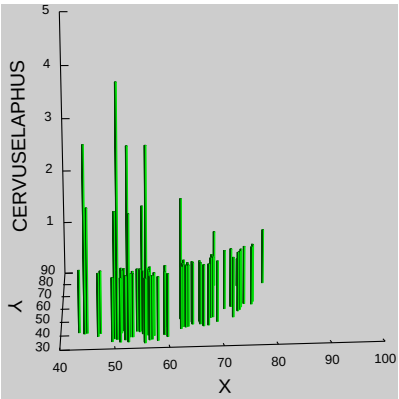

Figure 505 3D Histogram of *cervus elaphus* remains recovered during surveys of 2009 (Systat 13).

The spatial distribution of count data per sampling unit for *cervus elaphus* fragments shows a Global Moran's *I* of -0.000397. The theoretical (expected) value assuming spatial autocorrelation (lack of spatial Independence) is -0.000515 and the standard error of *I* is 0.000515. The test of significance using the normality assumption gave a low significant *z* value of 0.230379. These results are comparable with those of the Geary statistics (*C*=10.999683) and Getis-Ord general G (*G*=0.015518). Consequently, we can accept that the spatial distribution of *cervus elaphus* fragments could not be significantly different than the expected value under a random distribution. This is what would be expected in the case of predominant similar frequency of occurrence within quite every spatial location.

Moran's *I* Correlogram (Figure 506) has been calculated for uniform class distance interval of 1 metre, and taking into account a 10 metres active lag distance. *I* value at the starting point of the function is about 0.0681, a bit above the expected value for randomness. As the distance between sampling units increases, *I* value drops off quite abruptly and reaches values few above the expected value for randomness until 10 metre (with I value around 0 at 5 metre).

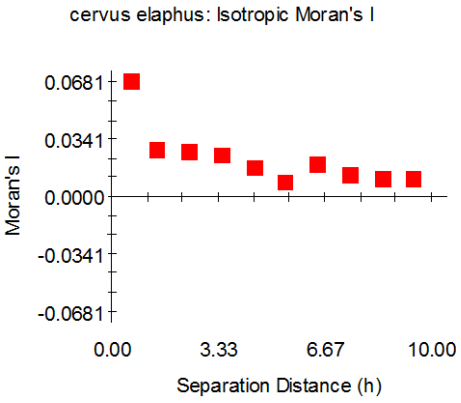

Figure 506 Moran's I Correlogram for *cervus elaphus* remains recovered during surveys of 2009 (GS+).

Such result proves that scarce positive spatial autocorrelation is attested in the first 5 metres of the function, giving the possibility of finding spatially dependent area of such radius, what is suggestive working hypothesis for locating individual activity area; however it is interesting that all *I* values are around 0.

We have explored the possible presernce of anisotropic variation, fitting a theoretical variogram at different directions (Figure 507). Anisotropy is clearly present, most notably at 0º and 135º.

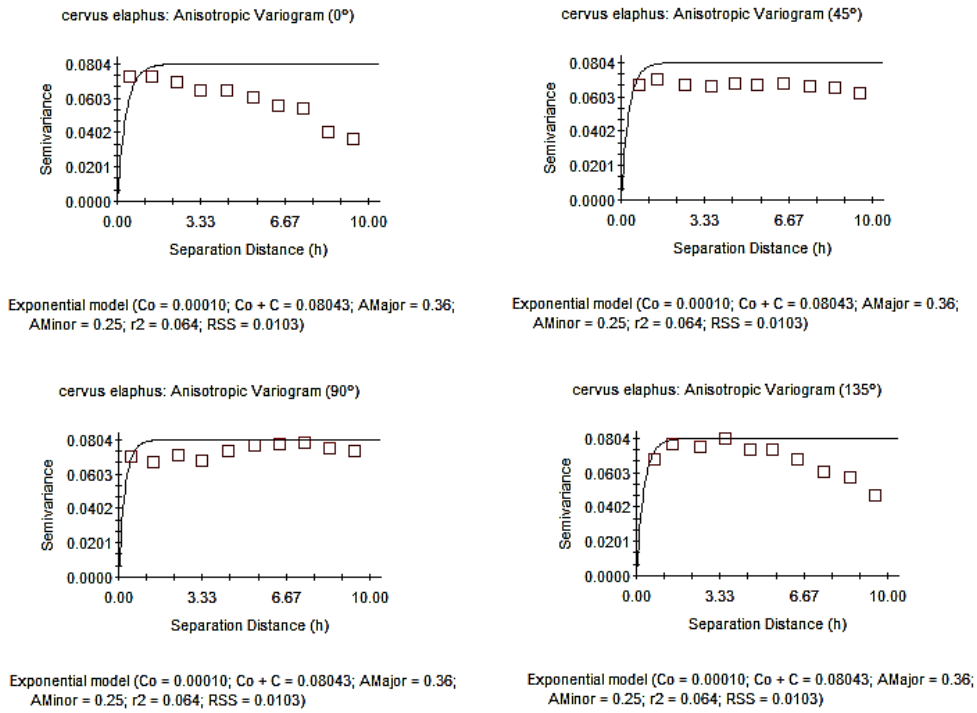

Figure 507 Anisotropic Variogram of *cervus elaphus* remains recovered during surveys of 2009 (GS+).

The graph of anisotropic Semivariance Surface or Variogram Map insists on the lack of spatial continuity, even at very small distances; anisotropy is predominantly concentrated in the centre of the area and some peaks are identified near the North-West and South-East corners with higher values than the previous categories (Figure 508).

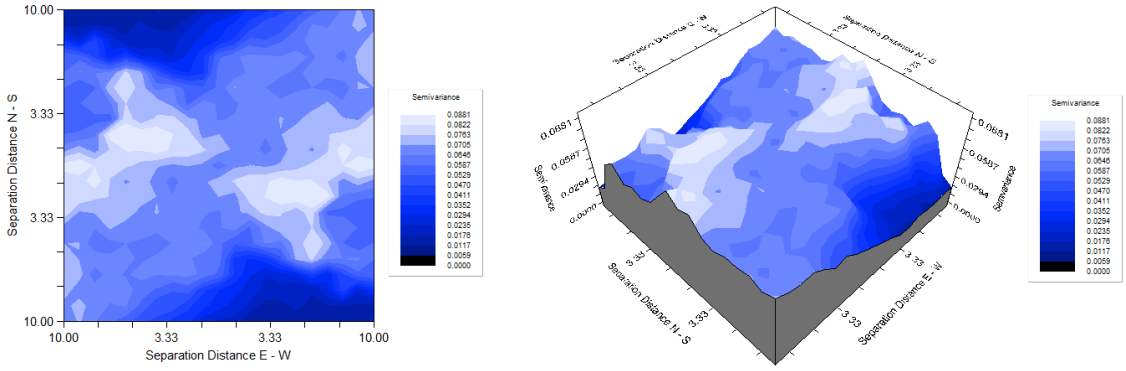

Figure 508 Variogram Map of *cervus elaphus* remains recovered during surveys of 2001 (GS+).

An exponential variogram model, fitted to the empirical variogram, has too low values of goodness of fit, and therefore cannot be used to obtain an interpolated model.

8.5.2.8 Faunal remains ascribable to Turtle

16 turtle remains were identified and counted; they are spatially distributed in 14 sampling units, while 1927 squares were empty. The spatial distribution of sampling units where turtle remains have been identified is showed in **Figure 509.**

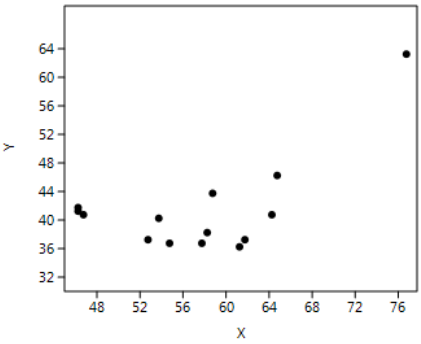

Figure 509 spatial distribution of sampling units where fragments of turtles have identified (surveys 2009) (Past).

Ripley's *k* analysis on the distance between sampling units with turtle remains suggests the possibility of some degree of spatial clustering, particularly from 3.2 metre, since in the first portion of function a more irregular and tending to random function is observed (Figure 510).

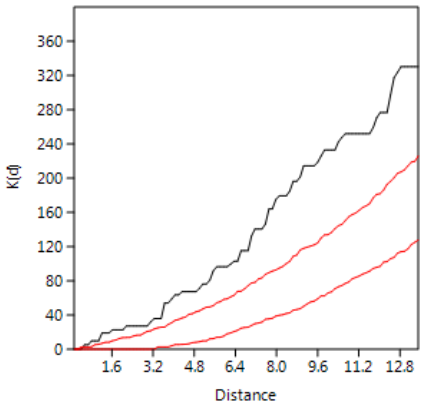

Figure 510 Ripley's *k* analysis on the distance between sampling units with fragments of turtle recorded in surveys of 2009 (Past).

Within the convex hull configured by 14 sampling units where turtle's fragments have been identified, the null hypothesis of random pattern (Poisson process) cannot be rejected with a $p<0.05$. Thus, randomness characterizes the spatial distribution of such remains; this is what would be expected when the majority of the scarce sampling units show the same frequency of remains. However, as in the case of other faunal categories, Kernel Density Estimation (Figure 511) shows some degree of irregularity, by detecting two predominant concentrations between x=46-48 and y=38-44y and between x=50-64 and y=35-42. Three further lower dense concentrations are located between x=57-60 and y=42-44, between x=63-65 and y=46-48 and between x=76-78 and y=60-64.

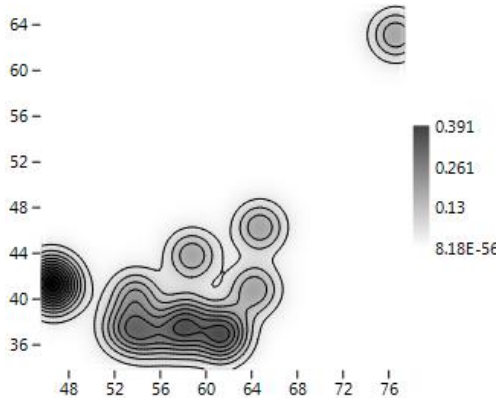

Figure 511 KDE of sampling units where turtle's remains have been recovered during surveys of 2009 (Past).

When considering the raw quantity of turtle's remains at each cell, the probability density distribution of spatial frequencies does not follow a *J*-shaped distribution. A majority of sampling units have raw counts of such faunal remains of less than 2 elements (global mean =1.14 observables per sampling unit). Both histogram and box plot identified, as outlier, the value 2 (Figure 512).

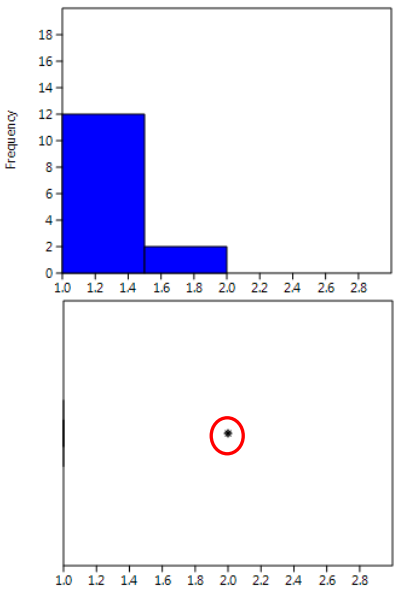

Figure 512 Histogram and box plot of frequencies observed for turtle's remains (Past).

75% of turtle fragments are located in 86% of the effectively surveyed area, in such a way that only 2 cells show more than 1 item.

The spatial distribution of turtle fragments is fitted with both a Negative Binomial distribution (with k=0.029 and p=0.776) and a Poisson distribution (with λ=0.08) with Kolmogorov Smirnov Test=1. This condition suggests predominant uniformity in the spatial distribution of the abundance of turtle fragments per sampling unit (Figure 513).

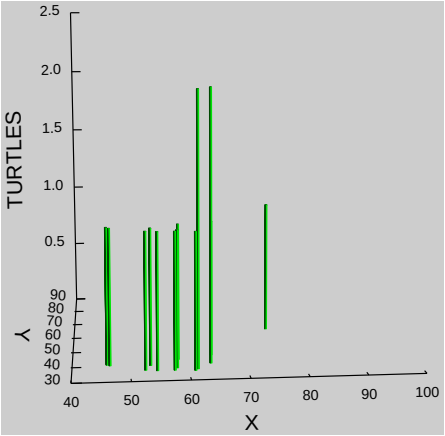

Figure 513 3D Histogram of turtle's fragments recovered during surveys of 2009 (Systat 13).

The spatial distribution of count data per sampling unit for cranial fragments shows a Global Moran's *I* of -0.000468. The theoretical (expected) value assuming spatial autocorrelation (lack of spatial Independence) is -0.000515 and the standard error of I is 0.000515. The test of significance using the normality assumption gave a non significant *z* value of 0.091202. These results are comparable with those of the Geary statistics (*C*=0.999351) and Getis-Ord general G (*G*=0.016949). Consequently, we can accept that the spatial distribution of cells with turtle fragments could not be significantly different than the expected value under a random distribution. This is what would be expected in the case of predominant similar frequency of occurrence within quite every spatial location.

Moran's *I* Correlogram (Figure 514) has been calculated for uniform class distance interval of 1 metre, and taking into account a 10 metres active lag distance. *I* value at the starting point of the function is about 0.0262, a very few above the expected value for randomness. As the distance between sampling units increases, *I* value drops off abruptly and irregularly reachs values less above the expected value for randomness until 10 meter (although at 2 meter*I* value is located below the expected for randomness).

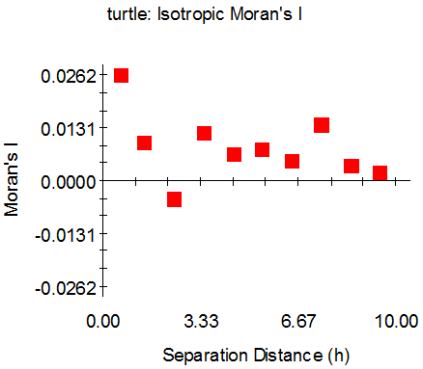

Figure 514 Moran's I Correlogram for turtle fragments recovered during surveys of 2009 (GS+).

Such result proved that scarce positive spatial autocorrelation is attested for 2-3 metres of the function, giving the possibility of finding spatially dependent area of such radius, what is suggestive working hypothesis for locating individual activity area; however it is notable that all *I* values are around 0.

We have explored the possible presence of anisotropic variation, fitting a theoretical variogram at different directions (Figure 515). Semivariance varies in strongly different ways at each degree.

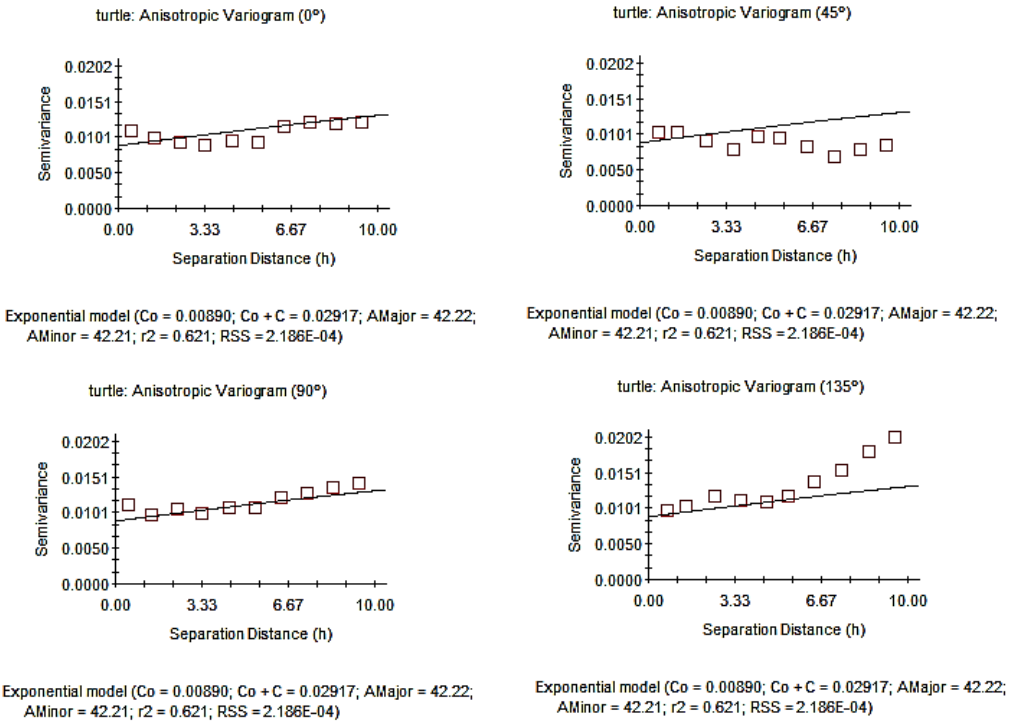

Figure 515 Anisotropic Variogram of turtle remains recovered during surveys of 2009 (GS+).

The graph of anisotropic Semivariance Surface or Variogram Map shows a particular concentration of anisotropy around North-West and South-East corners (Figure 516).

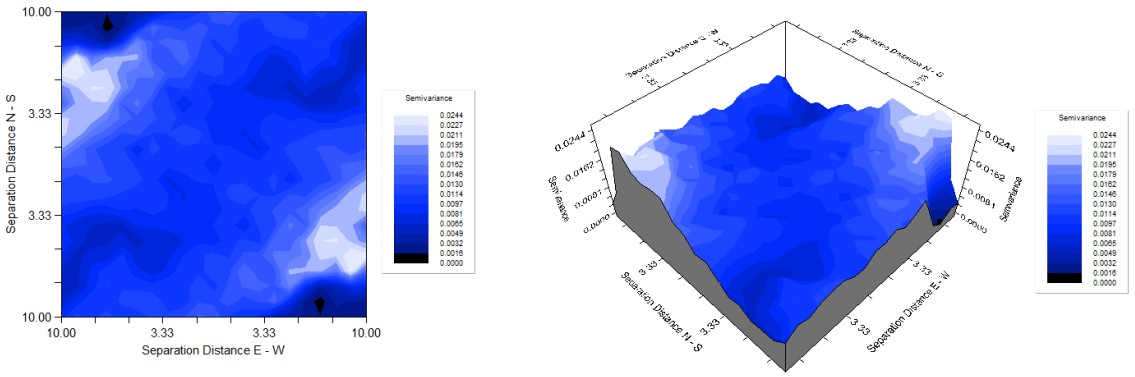

Figure 516 Variogram Map of turtle remains recovered during surveys of 2009 (GS+).

An exponential variogram model, fitted to the empirical variogram, has too low values of goodness of fit, and therefore cannot be used to obtain an interpolated model.

8.6. Pottery

22599 fragments were identified and counted. 310 were the surveyed empty cells, while the cell with more presence gave 186 items. The spatial distribution of sampling units where pottery has been identified is showed in Figure 517.

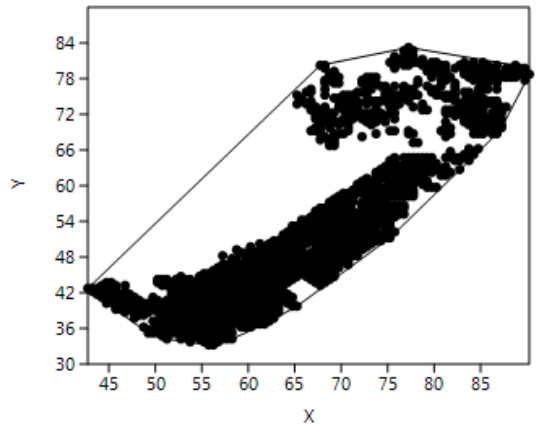

Figure 517 Spatial distribution of sampling units where pottery has been recorded in surveys of 2009 (Past).

Ripley's *k* analysis on the distance between sampling units with pottery evidence suggests the possibility of some degree of spatial clustering, at the scale of the reference area (Figure 518).

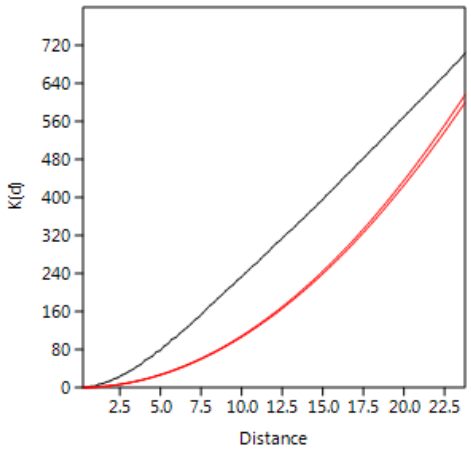

Figure 518 Ripley's *k* analysis on the distance between sampling units with pottery, recorded in surveys of 2009 (Past).

Within the convex hull configured by those sampling units with some positive frequency of pottery, Clark and Evans test suggests overdispersion. KDE of such cells (Figure 519) the presence of two different concentration areas (between x=48-76 and y=33-66 and between x=65-85 and y=66-82. These two higher dense concentrations correspond to the above mentioned Zone 1 and Zone 2.

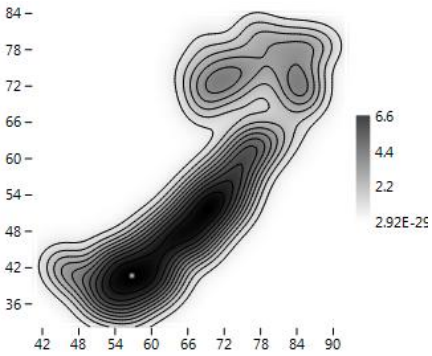

Figure 519 KDE of sampling units where pottery has been recovered during surveys of 2009 (Past).

When considering the raw quantity of pottery at each cell, the probability density distribution of spatial frequencies clearly follows a *J*-shaped distribution. Where pottery is present, it appears in relatively high frequency (global mean= 13.85 potsherds per sampling unit). Furthermore, one cell distinguishes from the majority with 186 observations (interpretable as outlier). Histogram as well as box plot identifies a break point in the distribution of frequencies corresponding to the value 40 (Figure 520).

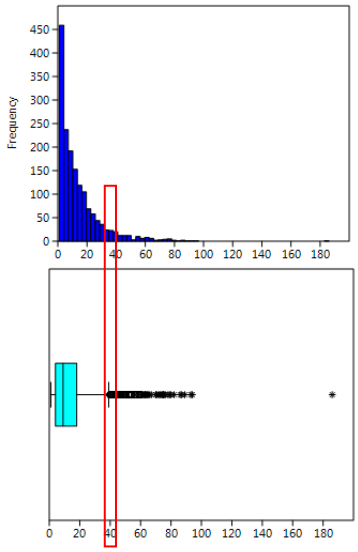

Figure 520 Histogram and box plot of frequencies observed for pottery (Past).

The spatial distribution of pottery frequencies does not fit with any of the standard distribution. 75% of pottery are located in the 94% of the effectively surveyed area, in such a way that 25% of pottery show more than 40 items located in 6% of the effectively surveyed area (Figure 521).

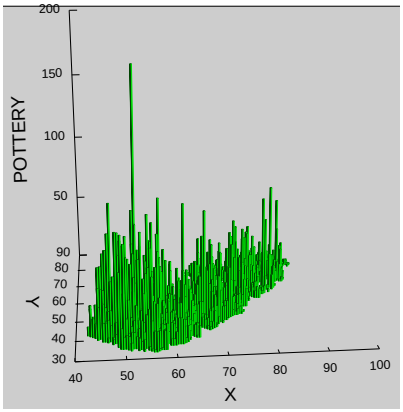

Figure 521 3D Histogram of pottery recovered during surveys of 2009 (Systat 13).

The spatial centroid of the area with pottery, calculated using an abundance weighted mean spatial center is x= 62.932729, y= 48.804671, with 10.48 m of standard deviation along the *x* axis, and 11.24 m along the *y* axis. A standard deviation ellipse with a long axis of 41.82 m and a short one of 11.88 m delimits an area of 390.25 square meters, where most count data appear. It has been estimated an average density of 9.42 objects per square metre.

The spatial distribution of the abundance of pottery per sampling unit gives a Global Moran's *I* result of 0.0000557. The theoretical (expected) value assuming spatial autocorrelation (lack of spatial independence) is -0-000515 and the standard error is 0.000515. The test of significance using the normality assumption gave a highly significant *z* value of 2.080850. Consequently, we can accept that the spatial distribution of pottery is significantly different than the expected value under a random distribution. This is what would be expected when not all spatial location have the same frequency of items. These results are comparable with those of the Geary statistics (*C*=0.998287) and Getis-Ord general G (*G*= 0.008374).

The Moran's *I* Correlogram (Figure 522) has been calculated for uniform class distance intervals of 1 metre, and taking into account a 10 metres active lag distance. *I* value at the starting point is about 0.451, above the expected value for randomness. As the distance between sampling units increases, *I* value drops off quite gently and continuously always above the expected value for randomness. It is easy to see the presence of positive spatial autocorrelation for 10 metres.

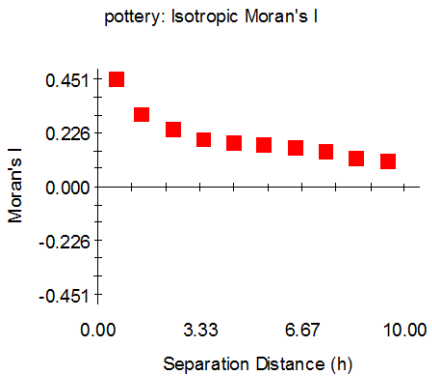

Figure 522 Moran's I Correlogram for pottery recovered during surveys of 2009 (GS+).

This result gives the possibility of finding spatially dependent areas of 10 metres of radius, what is a suggestive working hypothesis for locating homogeneous activity areas.

Using sampling units selected by local indicators of spatial association, as overabundant in respect to others, we obtain a spatial distribution of concentrations (more than 40 fragments of pottery). Within the convex hull defined by this selected locations, there is statistically significant degree of clustering. KDE shows predominant concentrations at the South-West corner, where it is generates spatial continuity, and along a North-East-South-West orientation within the centre of the surveyed area and around the North-East corner in lower presences (Figure 523).

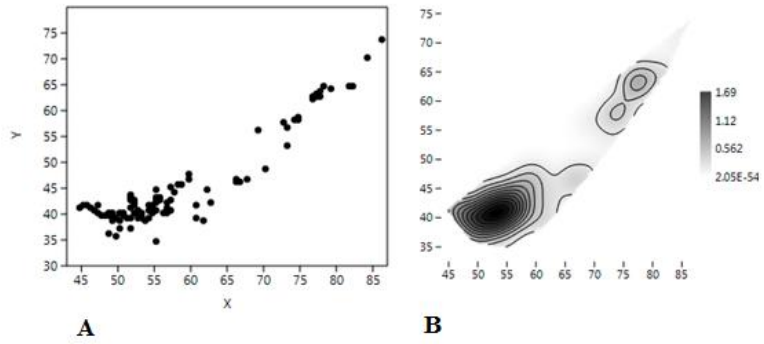

Figure 523 A)Spatial distribution of cells with more than 40 fragments of pottery (surveys 2009) (Past). B)KDE of such cells (surveys of 2009) (Past).

Moran's *I* correlogram (Figure 524) of cells with more than 40 items fits with an irregular model between immediate sampling units, and some possible clustering between 0 to 1 metres and between 5 and 8 metres (in this last case as negative spatial autocorrelation). That is, two main concentration zone, as showed above by KDE.

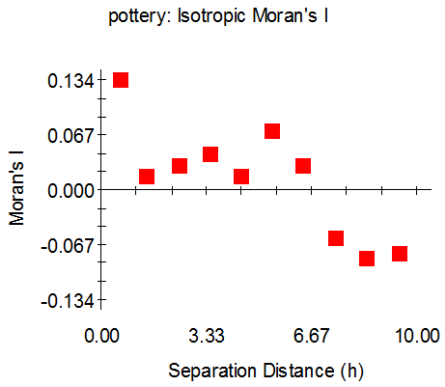

Figure 524 Moran's I Correlogram for sampling units with more than 40 potsherds recovered during surveys of 2009 (GS+).

We have explored the possible presence of anisotropic variation (Figure 525). A quite fast change of average semivariance at short distances is observed; the slope of the curve suggests a quite regular spatial pattern, with continuity in medium-large areas; indeed, semivariance varies in quite similar way in the 0º and 45º as well as in 90º and 135º, only in the first meters, suggesting the presence of anisotropy.

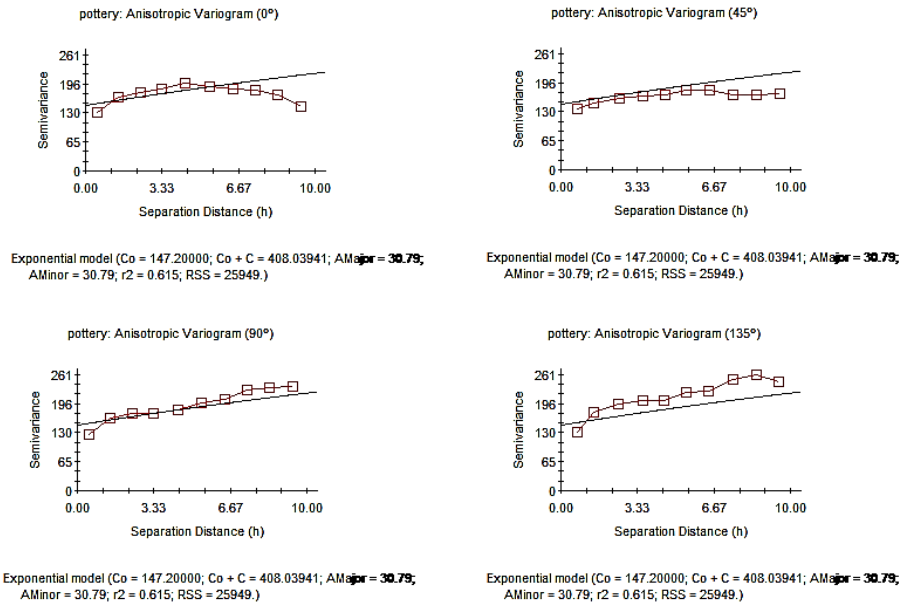

Figure 525 Anisotropic Variogram of pottery recovered during surveys of 2009 (GS+).

The graph of anisotropic Semivariance Surface or Variogram Map (Figure 526) shows that anisotropy is predominantly concentrated around the North-West and South-East side of the surveyed area, with some kind of continuity in the centre of the 3D diagram.

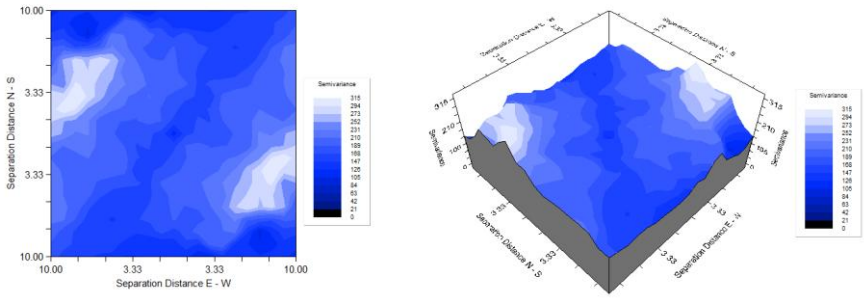

Figure 526 Variogram Map of pottery recovered during surveys of 2009 (GS+).

An exponential variogram model (Figure 527) has been fitted to the empirical variogram; in this case Nugget Variance, C_0 =59.60, Sill, C_0+C =191.80 and Range, A_0= 0.88, showing a global fit of 91.7%.

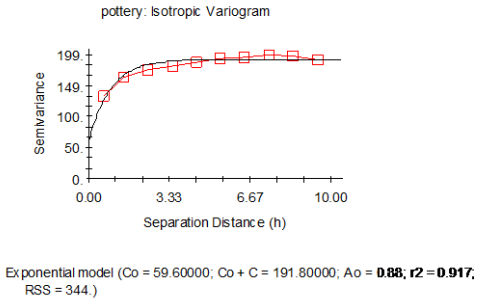

Figure 527 Exponential Isotropic Variogram for pottery recovered during surveys of 2009 (GS+).

Using this model, an inverse distance weighting algorithm has allowed building a spatial predictive model of pottery in this reference area (Figure 381). Such category seems to be distributed with spatial continuity within the South-West corner and in the centre of the surveyed area (Figure 528). Such kriging results are in accordance with what obtained throughout the Kernel Density estimation (see above).

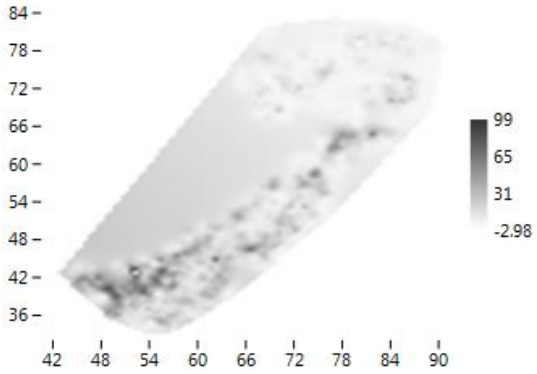

Figure 528 Graphic results of Inverse Distance Weighting calculated for pottery recovered during surveys of 2009 (Past).

It is important to take into account that this interpolated model has some relevant limits: it does not predict well the outliers, but gives a sufficiently good prediction of more frequent abundance values.

8.6.1 Pottery within Zone 1 and Zone 2

The spatial distribution of sampling units where pottery has been identified within both zones is showed in Figure 529.

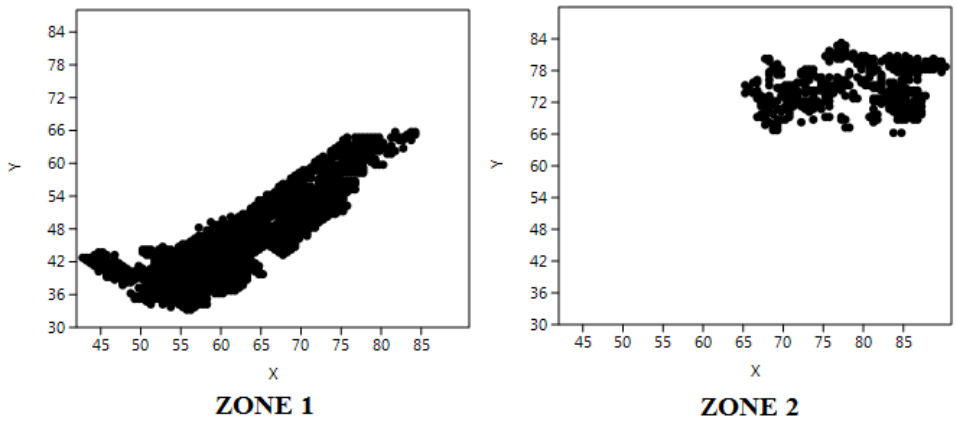

Figure 529 Spatial distribution of sampling units where pottery has been recorded in surveys of 2009, within Zone 1 and Zone 2 (Past).

Ripley's *k* analysis on the distance between sampling units with pottery suggests the possibility of some degree of spatial clustering for both zones, within the reference area. However, for Zone 2 such potential lower spatial clustering is particularly limited to the distances included between 1.10 to 8 metres (Figure 530).

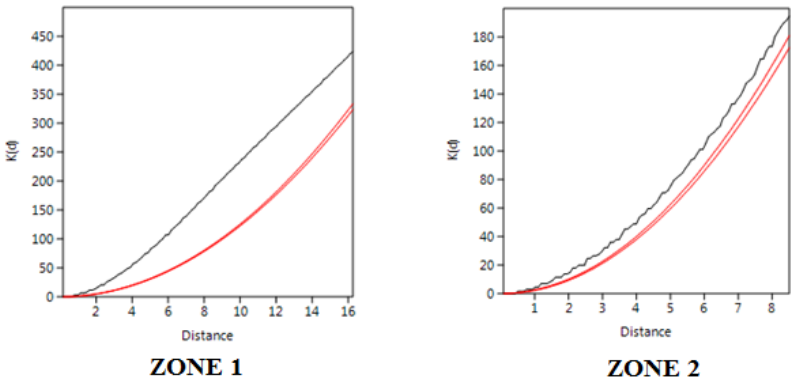

Figure 530 Ripley's *k* analysis on the distance between sampling units with pottery, recorded in surveys of 2009 within Zone 1 and Zone 2 (Past).

Within the convex hull configured by those sampling units with some positive frequency of pottery, Clark and Evans test suggests overdispersion, for both zones. Kernel Density Estimation of such cells (Figure 531) shows for Zone 1 the occurrence of a single concentration extended between x=50-80 and y=32-65. Within Zone 2 pottery is distributed in three different sub-concentrations, located respectively between x=67-76 and y=69-75.

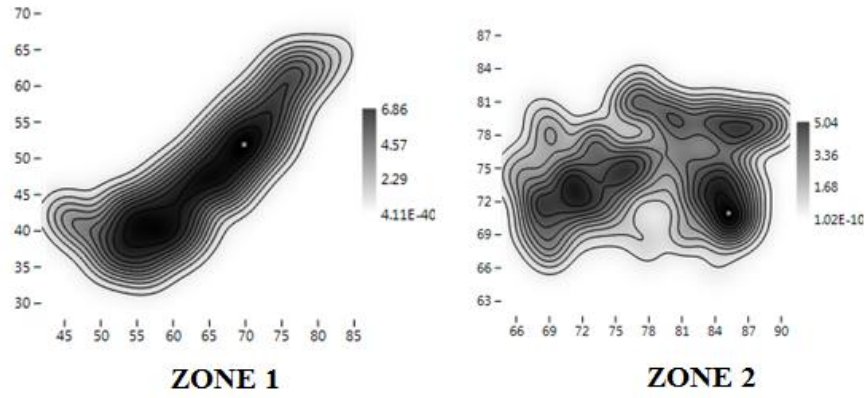

Figure 531 KDE of sampling units where pottery has been recovered during surveys of 2009 within Zone 1 and Zone 2 (Past).

There are relevant differences in the spatial location of sampling units with pottery frequencies within both zones; Zone 1 concentrates the majority of observations (n= 20243), the range of frequencies is between 1 and 186, with a mean of 16.55 observations per sampling unit and the variance is 254.1002. The probability density distribution of pottery within Zone 1 follows a *J*-shaped distribution. Both histogram and box plot identified a break point corresponding to the value 40 and one cell is distinguished from the majority, with 186 pottery fragments (interpretable as outlier) (Figure 532). Zone 2 is characterised by 2356 pottery fragments, the range of frequencies is between 1 and 73, with a mean of 5.77 observations per sampling unit and variance is 51.23. The probability density distribution clearly follows a *J*-shaped distribution. A majority of sampling units have raw counts of pottery of less than 5 elements (as mean showed). Both histogram and box plot identified a break point corresponding to the value 15 and three cells are distinguished from the majority, with 40, 59 and 73 pottery fragments (Figure 532).

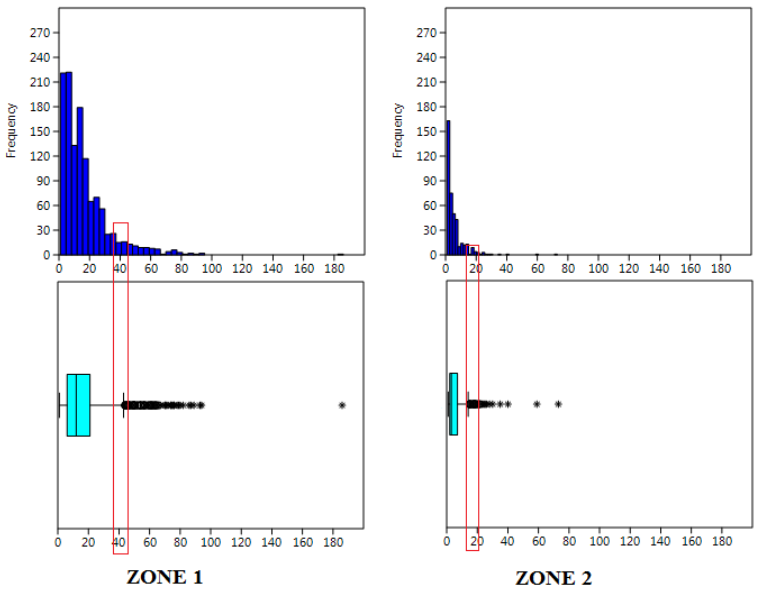

Figure 532 Histograms and box plots of frequencies observed for pottery within Zone 1 and Zone 2 (surveys 2009) (Past).

The spatial distribution of cells with pottery in Zone 1 is not fitted by any of the standards distributions, while in Zone 2 sampling units where pottery has been identified are distributed according to a Negative Binomial distribution (with k=0.484, p=0.113) and Kolmogorov Smirnov Test=1. For Zone 1 the spatial distribution of cells with pottery seems to show a pattern of accumulation, while for Zone 2 it is observed a predominant randomness in the spatial distribution of abundance of pottery per sampling unit (Figure 533).

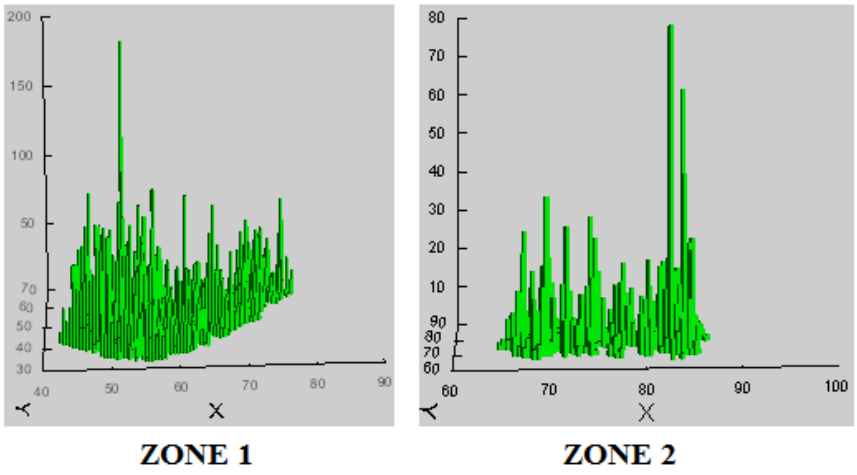

Figure 533 3D Histogram of pottery recovered during surveys of 2009 within Zone 1 and Zone 2 (Systat 13).

For Zone 1, 73% of pottery is located in 92% of the effectively surveyed area, in such a way that 27% of pottery show more than 40 items and such cells are distributed in 8% of the effectively surveyed area. For Zone 2, 70% of pottery is located in 93% of the effectively surveyed area, in such a way that 30% of pottery show more than 15 items and such cells are distributed in 7% of the effectively surveyed area.

In Zone 1 the spatial distribution of count data per sampling unit shows a Global Moran's I of -0.000430. The theoretical (expected) value assuming spatial autocorrelation (lack of spatial

Independence) is -0.000756 and the standard error of *I* is 0.000756. The test of significance using the normality assumption gave a quite significant *z* value of 0.430954. These results are comparable with those of the Geary statistics (*C*=0.999317) and Getis-Ord general G (*G*=0.010175).

The spatial distribution of count data per sampling unit shows, for Zone 2, a Global Moran's *I* of -0.001600. The theoretical (expected) value assuming spatial autocorrelation (lack of spatial Independence) is -0.001621, and the standard error of *I*, is 0.001609. The test of significance using the normality assumption gave a highly non significant *z* value of 0.012668. This result is comparable with those of Geary statistic (*C*=0.999964) and Getis-Ord general G (*G*=0.019544).

Consequently, we can accept that the spatial distribution of pottery for Zone 1 could be partially different than the expected value under a random distribution; conversely, for Zone 2 the spatial distribution of sampling units with pottery is not significantly different than the expected value under a random distribution. This is what would be expected in the case of predominant same frequency of pottery in quite every spatial location.

The Moran's *I* Correlogram has been calculated for uniform class distance intervals of 1 metre, and taking into account a 10 metres active lag distance. For Zone 1, *I* value at the starting point is about 0.368, above expected value for randomness. As the distance between sampling units increases, *I* value drops off quite gently reaching, until 6 metres, values above the expected value for randomness; from this distance they are located on the line (corresponding to spatial randomness). Positive spatial autocorrelation is thus identified between the starting point to the function and 6 metres. This result gives the possibility of finding spatially dependent area of 6 metres of radius, what is suggestive working hypothesis for locating the activity areas (Figure 534).

For Zone 2, Moran's *I* Correlogram (Figure 534) shows that at the starting point of the function *I* value is about 0.149 and at 1 metre it is around 0.100, above the expected value for randomness. As the distance between sampling unit increases, *I* value drops off quite abruptly, reaching value around, on and below the line from 3 metres. For the first 3 metres of the function positive spatial autocorrelation is thus observed, while between 4 and 6 it is attested few negative spatial autocorrelation. This result gives the possibility of finding spatially dependent areas of 3-4 metres, what is suggesting working hypothesis for locating homogeneous individual activity.

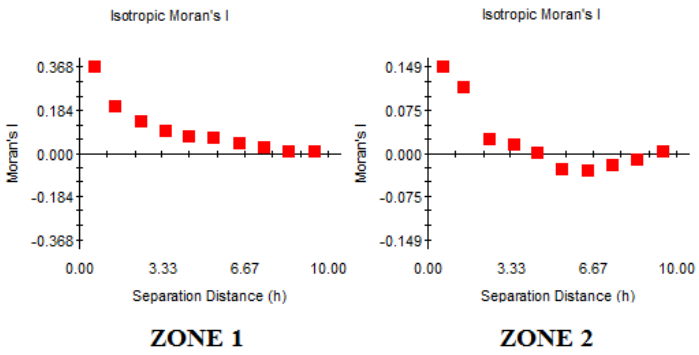

Figure 534 Moran's I Correlogram for pottery recovered during surveys of 2009, within Zone 1 and Zone 2 (GS+).

Using sampling units selected by local indicators of association, as overabundant in respect to others, we obtain a spatial distribution of concentrations (more than 40 fragments of pottery for Zone 1 and more than 16 for Zone 2). Within the convex hull defined by this selected locations, there is statistically significant degree of clustering, within Zone 1 (Figure 535). Moran's I Correlogram (Figure 536) of cells with more than 40 items fits an irregular model between sampling units, with some possible clustering between 0 and 1 metre and between 7 and 8 metres (in this last case as negative spatial autocorrelation). That is, two concentration zones, as showed in KDE (Figure 535B).

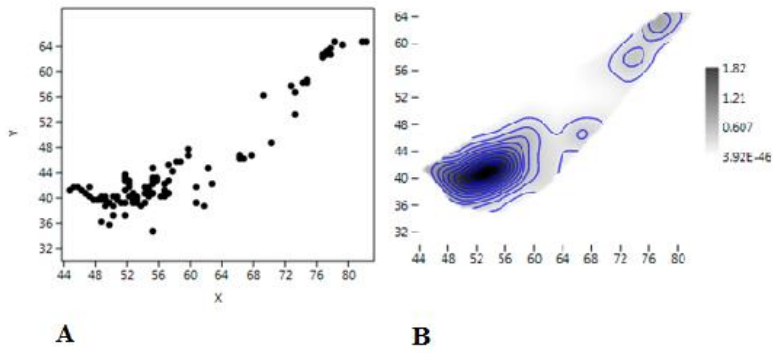

Figure 535 A) spatial distribution of cells with more than 40 items; B) KDE of such cells (surveys 2009), Zone 1 (Past).

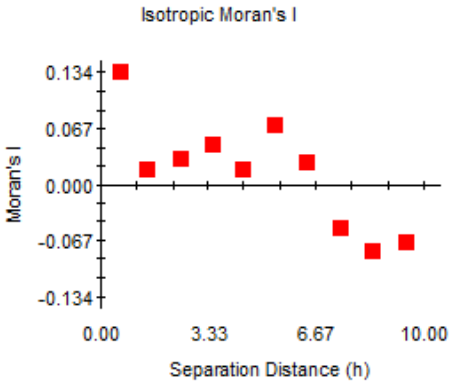

Figure 536 Moran's I Correlogram of sampling units with more than 40 potsherds, surveys 2009, Zone 1 (GS+).

It is easy to see in the South-West corner of the surveyed area a higher density concentration, delimiting a less dense area. Following the North-East direction there is a small accumulation of material evidence with lower frequencies.

For Zone 2, according to Clark and Evans test, for sampling units with more than 15 potsherds the null hypothesis of a random pattern (Poisson process) can not be rejected at $p<0.05$. However, according to Kernel Density Estimation two main concentrations of pottery can be identified, located respectively between x=75-78 and y=72-76 and between x=82-88 and y=70-76 (Figure 537).

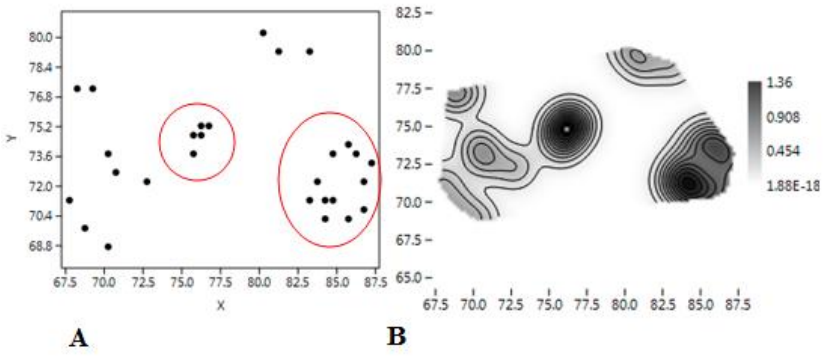

Figure 537 A) Spatial distribution of sampling units with more than 15 potsherds; B)KDE of such cells (surveys 2009), Zone 2.

We have explored the possible presence of anisotropic variation (Figures 538 and 540). For Zone 1, semivariance varies in quite similar way in the 0º and 45º as well as in 90º and 135º, only in the first metres, suggesting the presence of anisotropy.

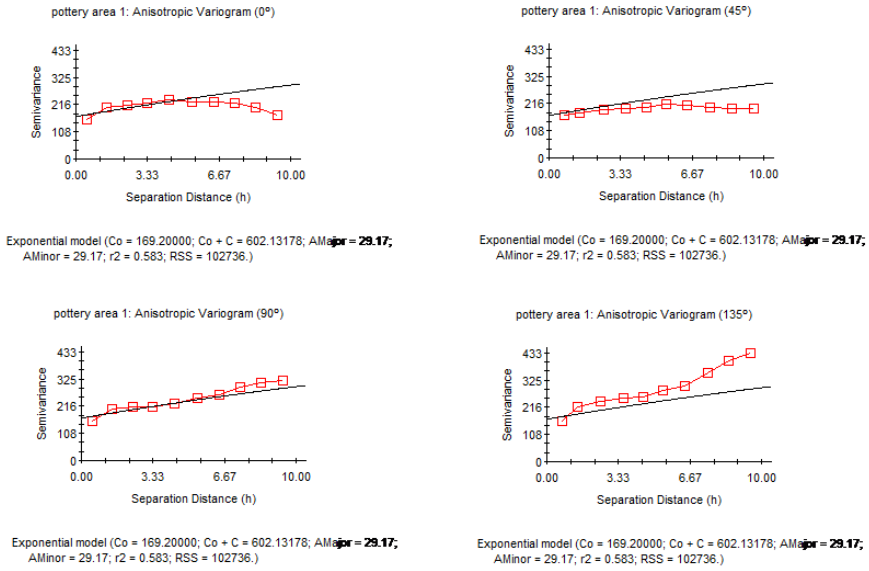

Figure 538 Anisotropic Variogram of pottery recovered during surveys of 2009, within Zone 1 (GS+).

The graph of anisotropic Semivariance Surface or Variogram Map for Zone 1 (Figure 539) shows that anisotropy is predominantly concentrated around North-West and South-East corners.

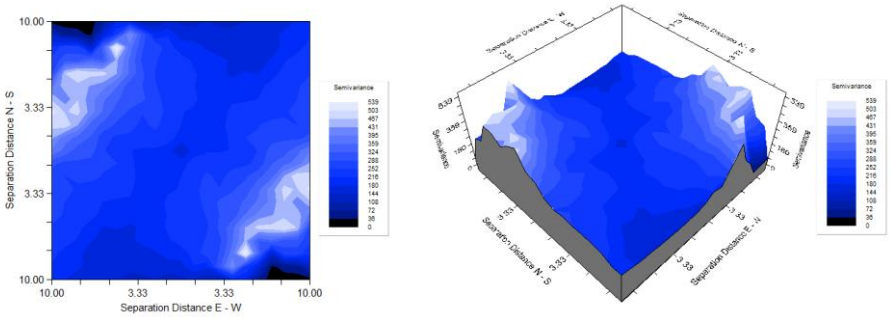

Figure 539 Variogram Map of pottery recovered during surveys of 2009, within Zone 1 (GS+).

For Zone 2 the semivariance varies in strongly different ways at each degree (Figure 540).

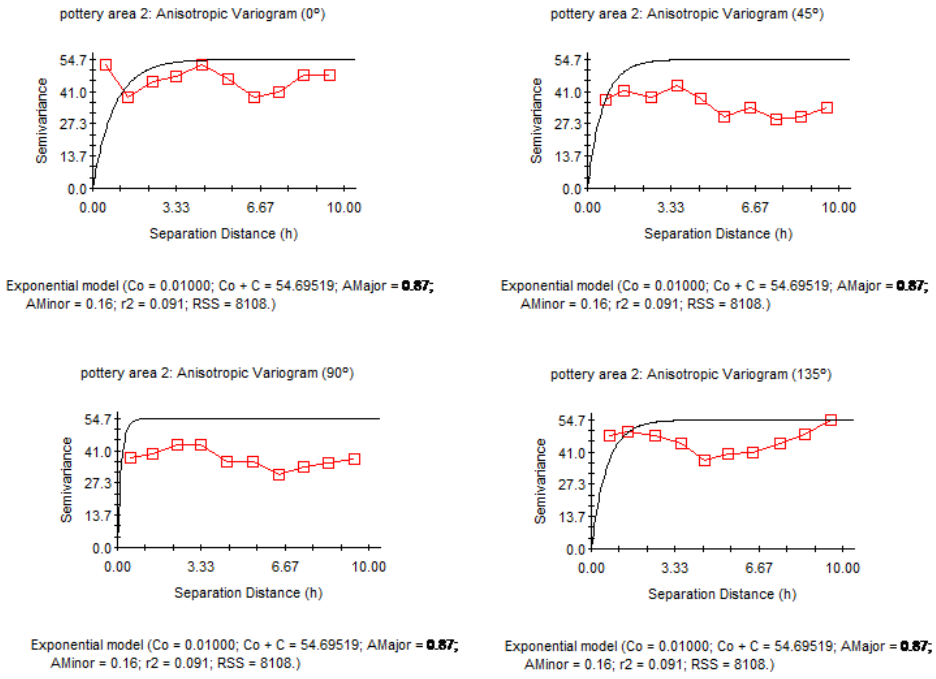

Figure 540 Anisotropic Variogram of pottery recovered during surveys of 2009, within Zone 2 (GS+).

The graph of Semivariance Surface or Variogram Map (Figure 541) shows lower anisotropy with higher values distributed around the South-East and North-West corners.

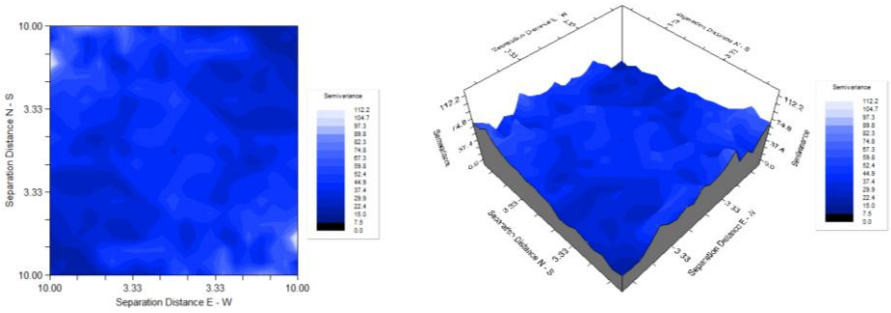

Figure 541 Variogram Map of pottery recovered during surveys of 2009, within Zone 2 (GS+).

An exponential model for both zones has been fitted to the empirical variogram; for Zone 1, C_0 (nugget variance) =122.50, C_0+C (sill) = 245.10 and A_0 (Range) = 1.73; this model explains 95.3% of spatial variance (Figure 542). For Zone 2 the exponential variogram shows C_0 (nugget variance) =5.0000, C_0+C (sill) = 40.81000 and A_0 (Range) = 0.01; it does not explain sample variance.

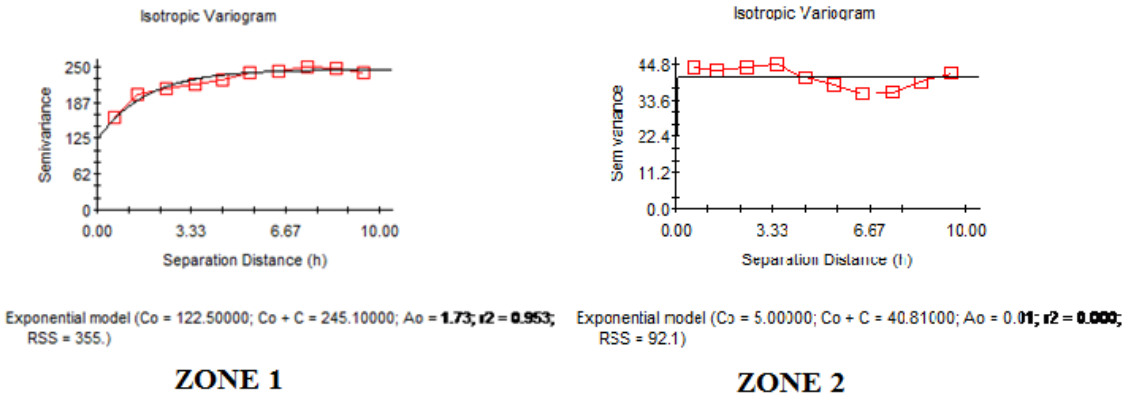

Figure 542 Exponential Isotropic Variograms for pottery recovered during surveys of 2009, within Zone 1 and Zone 2 (GS+).

Then, using this model for Zone 1, an inverse distance weightin algorithm has allowed building a spatial predictive model of pottery in this reference area (Figure 543). Such category seem to be distributed regularly within Zone 1 with a significant concentration in the South-West corner, as already highlighted by KDE.

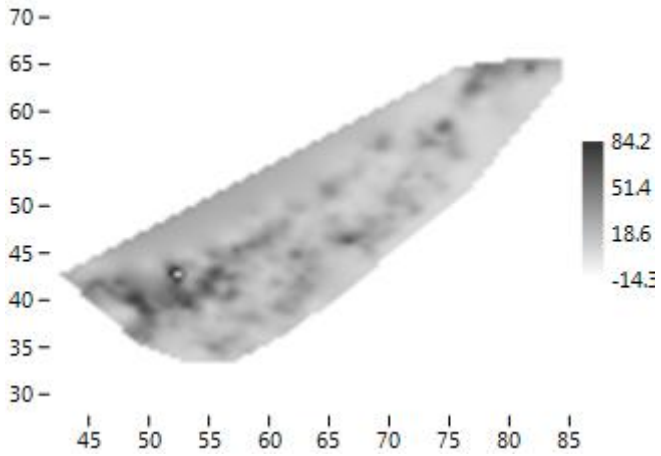

Figure 543 Graphic results of Inverse Distance Weighting calculated for pottery recovered during surveys of 2009, within Zone 1 (Past).

It is important to take into account that this interpolated model has some relevant limits: it does not predict well the outliers, but gives a sufficiently good prediction of more frequent abundance values.

8.6.2 Sub-categories of pottery

We have explored the spatial distribution of different pottery functional categories. Nevertheless, frequencies are low in quantitative terms, and we have limited the analysis to an exploration of presence/absence in the surveyed area.

8.6.2.1 Jars

38 fragments ascribable to this category were identified and counted; they are spatially distributed in 37 sampling units, while 1904 cells were empty. Sampling units with jars are spatially distributed according to Figure 544.

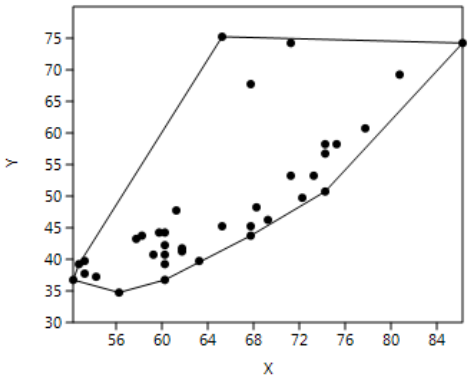

Figure 544 Spatial distribution of sampling units where jars fragments have been recovered during surveys of 2009 (Past).

Ripley's *k* analysis on the distance between sampling units with jars evidence suggests the possibility of some degree of spatial clustering, at the scale of all the reference area. Nevertheless, between 0 and 1 meter the distribution shows tendency to randomness (Figure 545)

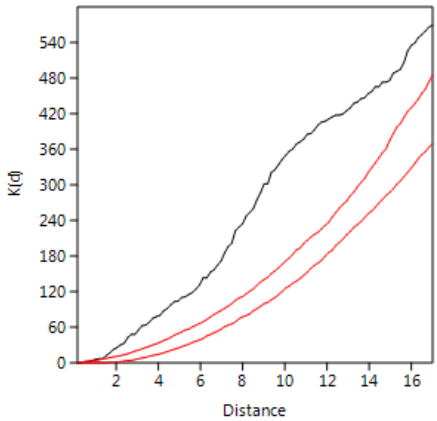

.

Figure 545 Ripley's *k* analysis on the distance between sampling units with jars, recorded in surveys of 2009 (Past).

For the non-empty cells, however, Clark and Evans test suggests that the null hypothesis of random pattern (Poisson process) cannot be rejected at $p<0.05$. Then, it is possible that equidistant cells have the same probability of counting one or more jars fragments. A KDE (Figure 546) shows the relevant presence of small concentrations (between x=50-55 and y=35-40, between x=60-65 and y=37-45, between x=67-70 and y=42-47, between x=72-75 and y=50-60 (Zone 1); few isolated lower dense points are observed within Zone 2.

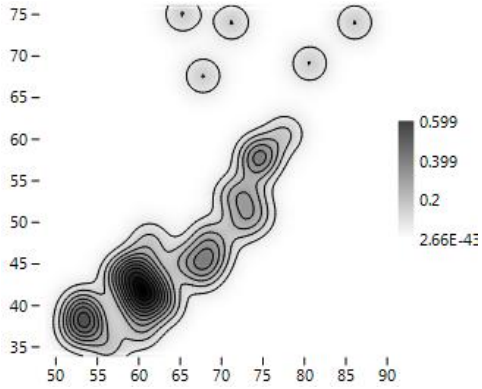

Figure 546 KDE of sampling units where jars have been recovered during surveys of 2009 (Past).

The majority of jars are attested in one item for sampling units and for this reason boxplot distinguishes the higher frequency value 2 as outlier. Only 2% of spatial sampling units have given evidence of jars (as showed in Figure 547).

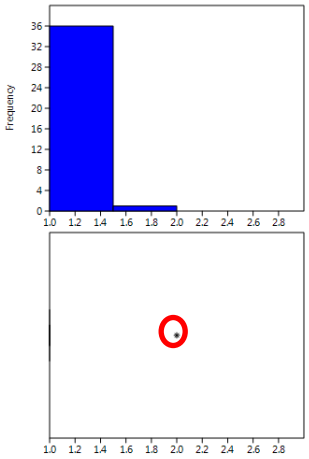

Figure 547 Histogram and box plot of frequencies observed for jars (Past).

The spatial distribution of jars fragments is fitted with a Geometric distribution (with p=0.981), a Negative Binomial distribution (with k=0.572 and p=0.967) and a Poisson distribution (with λ=0.020) and Kolmogorov Smirnov Test=1**.** This is what is expected when, as in this case, the sample consists in predominant empty sampling units and similar frequencies values in all non-empty cells (Figure 548).

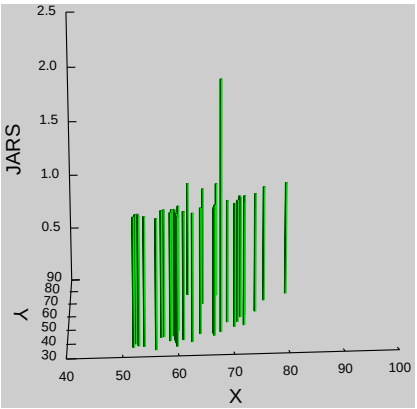

Figure 548 3D Histogram of jars recovered during surveys of 2009 (Systat 13).

The spatial distribution of the abundance of jars per sampling unit gives a Global Moran's *I* result of –0.000487. The theoretical (expected) value assuming spatial autocorrelation (lack of spatial independence) is -0.000515 and the standard error of *I* is 0.000515. The test of significance using the normality assumption gave a highly non-significant *z* value of 0.054521. Consequently, we can accept that the spatial distribution of jars could not be significantly different than the expected value under a random distribution.These results are comparable with those of the Geary statistics (*C*=1.000814) and Getis-Ord general G (*G*= 0.0008547).

The Moran's *I* Correlogram (Figure 549) shows a predominant irregular and random pattern. The scarce positive spatial autocorrelation is observed between 2 and 3 metres, while negative spatial autocorrelation is attested between 3 and 5 metres. The quantity of jar fragments per sampling unit is, however, very low, and therefore spatial continuity is more a question of the number of non-empty cells than a question of relevant peaks in spatial frequency.

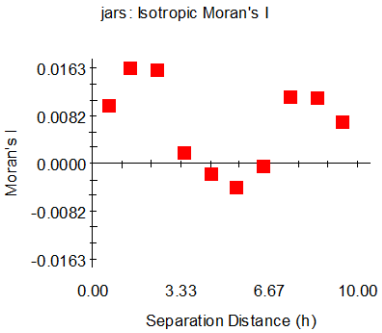

Figure 549 Moran's I Correlogram for jars recovered during surveys of 2009 (GS+).

We have explored the possible presence of anisotropic variation in the spatial distribution of jars (Figure 550). Semivariograms are predominantly flat, with generally extremely reduces changes (only between 5-6 and 10 metres at 0º and 135º some changes in semivariance are observed), insisting on the general idea of randomness in spatial frequency differences.

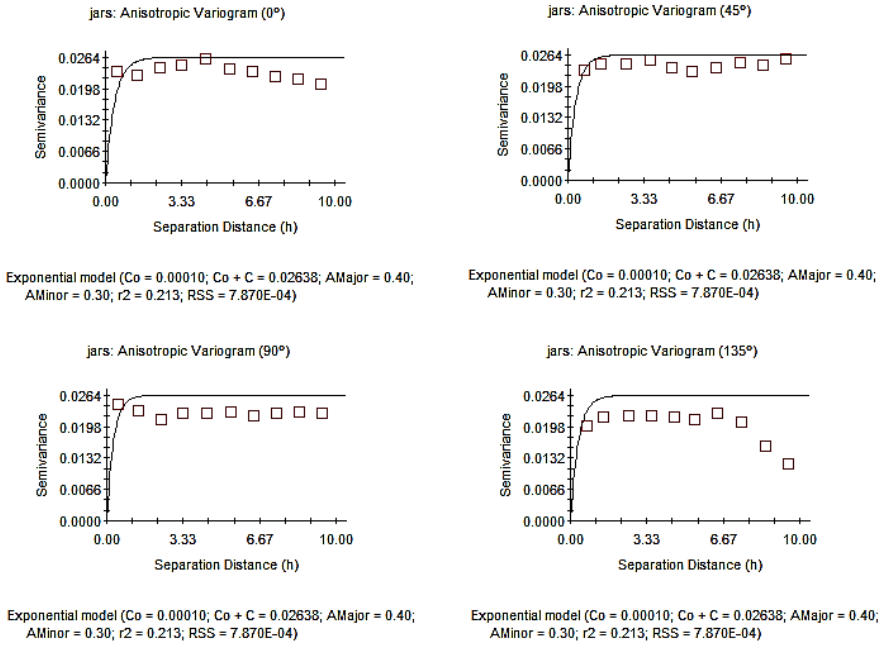

Figure 550 Anisotropic Variogram of jars recovered during surveys of 2009 (GS+).

The graph of anisotropic Semivariance Surface or Variogram Map (Figure 551**)** shows extreme anisotropy and the lacks of spatial continuity in frequency, even at small distances.

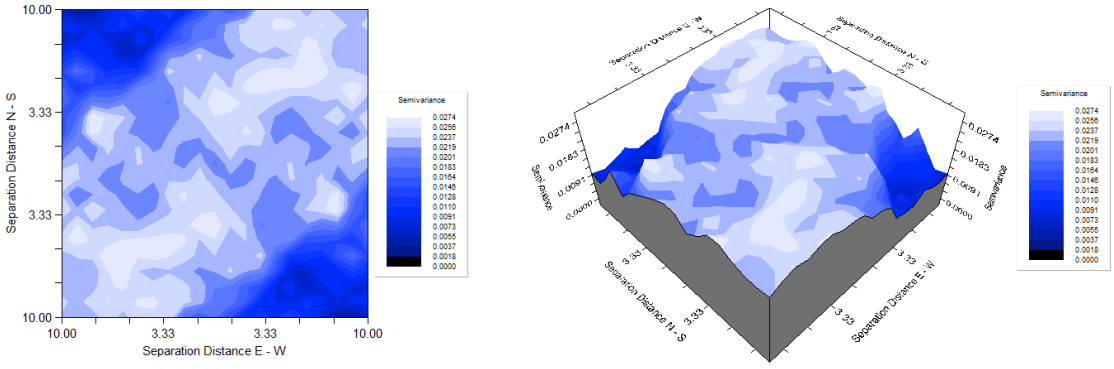

Figure 551 Variogram Map of jars recovered during surveys of 2009 (GS+).

The exponential variogram model (Figure 552) that best fits the data - C_0 (nugget variance) =0.00513, C_0+C (sill) = 0.02296 and A_0 (Range) = 0.13- does not explain the spatial variance; therefore it cannot be used to obtain an interpolated model.

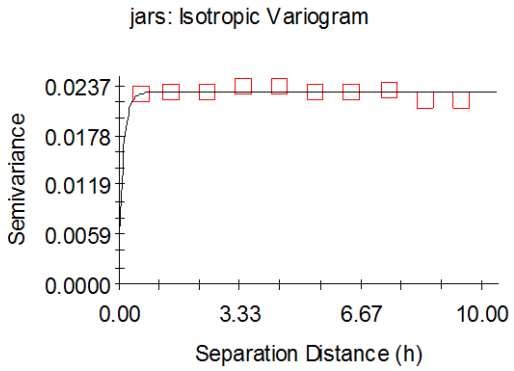

Exponential model (Co = 0.00513; Co + C = 0.02296; Ao = 0.13**; r2 = 0.010;**
RSS = 2.750E-06)

Figure 552 Exponential Isotropic Variogram for jars recovered during surveys of 2009 (GS+).

8.6.2.2 Closed forms

Taking into account the above results for jars –a typical example of closed form-, we have added all other evidence for this category (jars, dolia and mugs). We have identified 113 pottery fragments ascribable to closed forms; they are spatially distributed in 95 sampling units. Cells where fragments of ceramic closed forms have been identified are spatially distributed according to Figure 553.

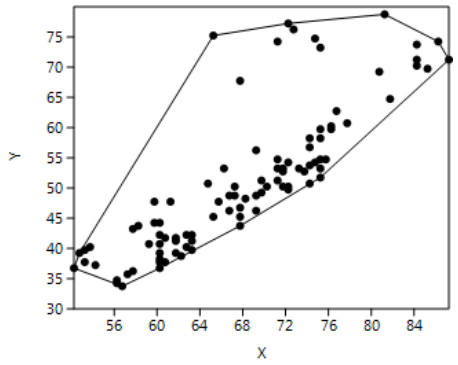

Figure 553 Spatial distribution of sampling units where ceramic closed forms have been recovered during surveys of 2009 (Past).

Ripley's *k* analysis on the distance between sampling units with fragments of ceramic closed forms suggests the possibility of some degree of spatial clustering, as showed by from 2 metre. Indeed, between the starting point of the function until such distance the distribution seems to tend to randomness (Figure 554).

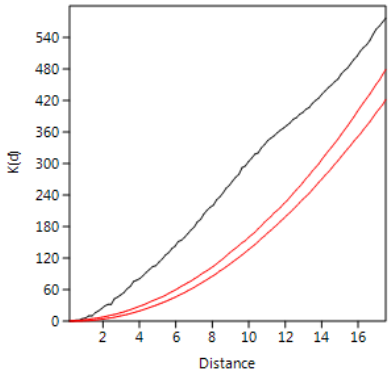

Figure 554 Ripley's *k* analysis on the distance between sampling units with closed forms, recorded in surveys of 2009 (Past).

Within the convex hull defined by those sampling units where closed forms have been recovered, null hypothesis of a random pattern (Poisson process), for non–empty cells, cannot be rejected at $p<0.05$, as proved by the Clark and Evans Test; this indicates the possibility that equidistant cells have the same probability of counting one or more fragments of closed forms. A KDE (Figure 555), however, shows two predominant concentrations located respectively between x=50-65 and y=33-42 and between x=67-78 and y=45-65. Two lower dense aggrupations, observed between x=70-75 and y=72-75 y and x=80-85 and y=67-72 belong to the Zone 2.

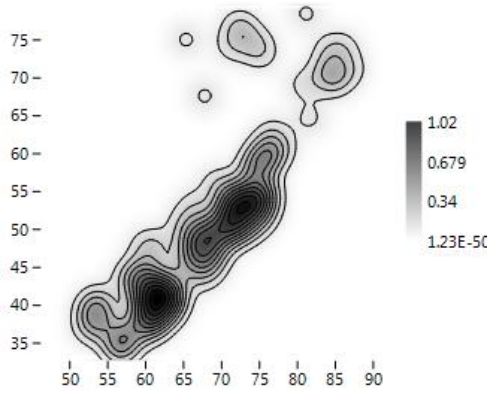

Figure 555 KDE of sampling units where closed forms have been recovered during surveys of 2009 (Past).

The majority of ceramic closed forms are predominantly attested in one item for sampling units and, for this reason, box plot distinguishes higher frequency values (as 2, 3 and 4) as outliers (Figure 556).

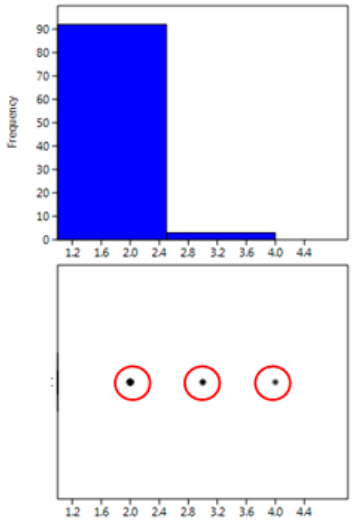

Figure 556 Histogram and box plot of frequencies observed for closed forms (Past).

The spatial distribution of ceramic closed forms is fitted with a Geometric distribution (with p=0.945), a Negative Binomial distribution (with k=0.172 and p=0.747) and a Poisson distribution (with p=0.058) and a Kolmogorov Smirnov Test=1. This is what is expected when, as in this case, the sample consists in predominant empty sampling units and similar frequencies values in all non-empty cells (as also showed in Figure 557).

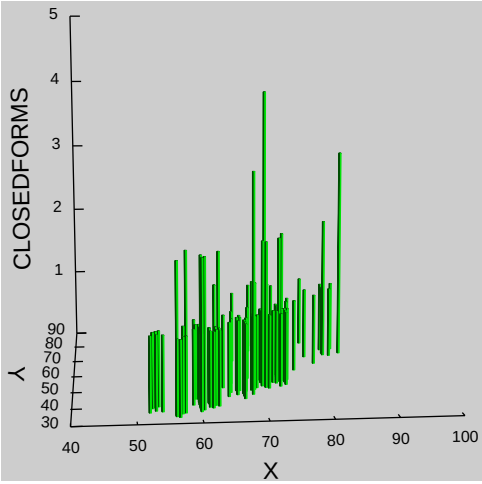

Figure 557 3D Histogram of closed forms recovered during surveys of 2009 (Systat 13).

75% of closed forms fragments are located in 85% of the effectively surveyed area, in such a way that 28% of cells show more than 1 item and they are distributed in 15% of the effectively surveyed area.

The spatial distribution of count data per sampling unit for ceramic closed forms shows a Global Moran's *I* of 0.009177. The theoretical (expected) value assuming spatial autocorrelation (lack of spatial Independence) is -0.000515 and the standard error of *I* is 0.001667. The test of significance using the normality assumption gave a highly significant *z* value of 5.814226. Those results are comparable with those of the Geary statistics (*C*=1.000950) and Getis-Ord general G (*G*=0.000000). Consequently, we can accept that the spatial distribution of ceramic closed forms is significantly different than the expected value under a random distribution.

Moran's *I* Correlogram (Figure 558) shows very low values of positive spatial autocorrelation in the first 3 metres of the function. The quantity of closed forms fragments per sampling unit is very low, and therefore spatial continuity is more a question of the number of non-empty cells, than a question of relevant peaks in spatial frequency.

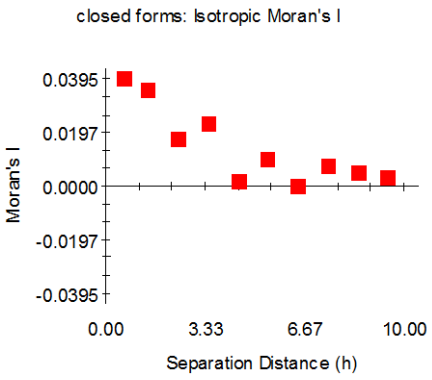

Figure 558 Moran's I Correlogram for closed forms recovered during surveys of 2009 (GS+).

We have explored the possible presence of anisotropy at different directions (Figure 559). Differences in the range are very scarce in the four variograms, and therefore we can conclude lack of anisotropy.

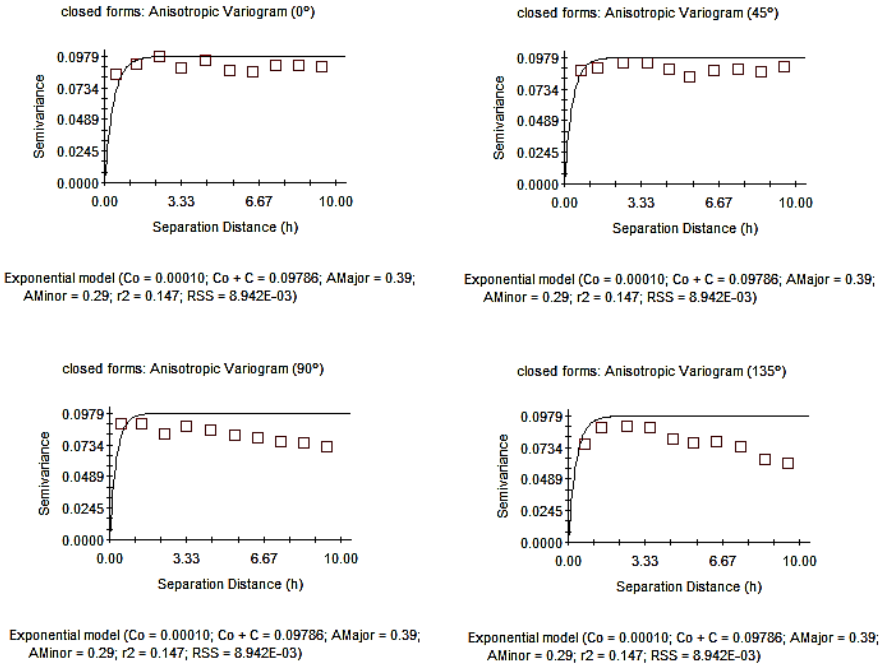

Figure 559 Anisotropic Variogram of closed forms recovered during surveys of 2009 (GS+).

The graph of anisotropic Semivariance Surface or Variogram Map, confirms a more concentrated anisotropy, predominant observed in a centeral narrow fringe with highest value around the South-West and North-East corners (Figure 560).

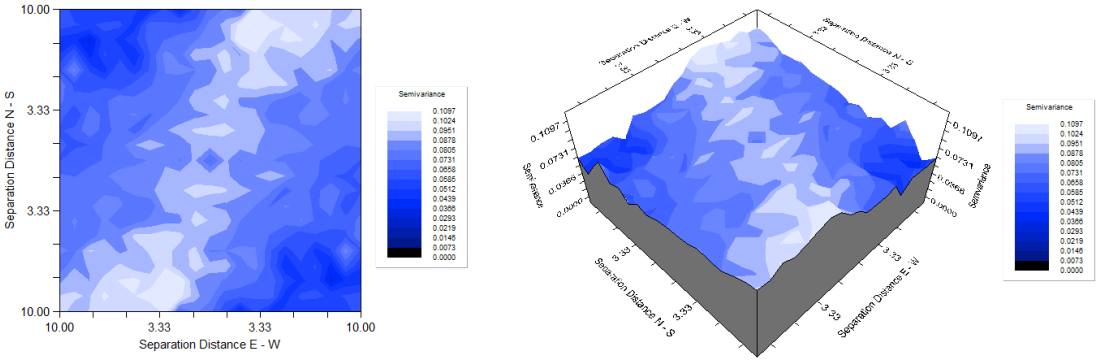

Figure 560 Variogram Map of closed forms recovered during surveys of 2009 (GS+).

The best fitted exponential model - C_0 (nugget variance) =0.01650, C_0+C (sill) = 0.08570 and A_0 (Range) = 0.15- (Figure 561) does not explain the spatial variance; therefore it cannot be used to obtain an interpolated model.

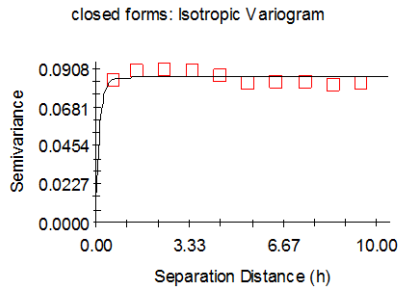

Exponential model (Co = 0.01650; Co + C = 0.08570; Ao = 0.15; **r2 = 0.013**; RSS = 1.112E-04)

Figure 561 Exponential Isotropic Variogram for closed forms recovered during surveys of 2009 (GS+).

8.6.2.3 Bowls

87 fragments ascribable to bowls were identified and counted; they are spatially distributed in 77 sampling units. Sampling units where bowls have been identified are spatially distributed according to Figure 562.

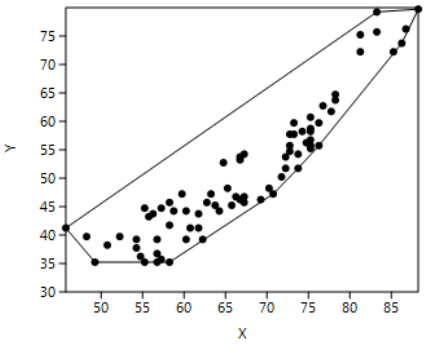

Figure 562 Spatial distribution of sampling units where bowls have been recovered during surveys of 2009 (Past).

Ripley's *k* analysis on the distance between sampling units with bowls evidence suggests the possibility of some degree of spatial clustering, at the scale of the global reference area (Figure 563).

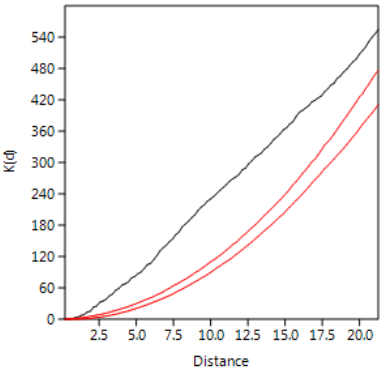

Figure 563 Ripley's *k* analysis on the distance between sampling units with bowls, recorded in surveys of 2009 (Past).

Within the convex hull defined by those sample units with a presence of shalow bowls, the null hypothesis of a random pattern cannot be rejected (according to Clark and Evans Test), what indicates the possibility that equidistant cells have the same probability of counting one or more fragments of bowls. A KDE (Figure 564) shows a concentration area (internally sub-divided in 3 sub-areas) located between x=45-60 and y=35 and between x=70-75 and y=65. Even in this case quite the entirety of sample belongs to the above mentioned Zone 1; only one small concentration is located between x=80-85 and y=70-75, within Zone 2.

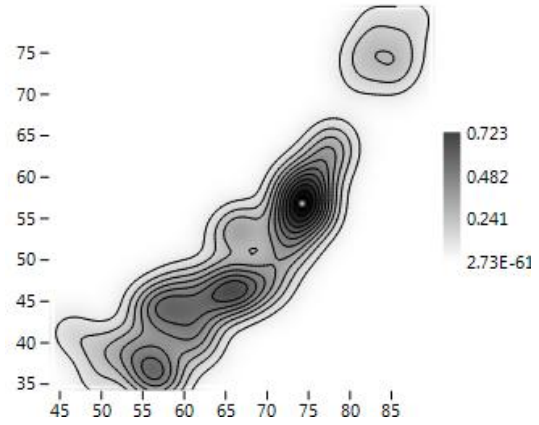

Figure 564 KDE of sampling units where bowls have been recovered during surveys of 2009 (Past).

When considering the raw quantity of bowls fragments at each cell, the probability density distribution of spatial frequencies does not follow a J-shaped distribution. A majority of sampling units have raw counts of such pottery of less than 2 elements (global mean = 1.12 bowl fragment per sampling unit). 7 cells are distinguished from the majority (interpretable as outliers), with 2, 3 and 4 observables (Figure 565).

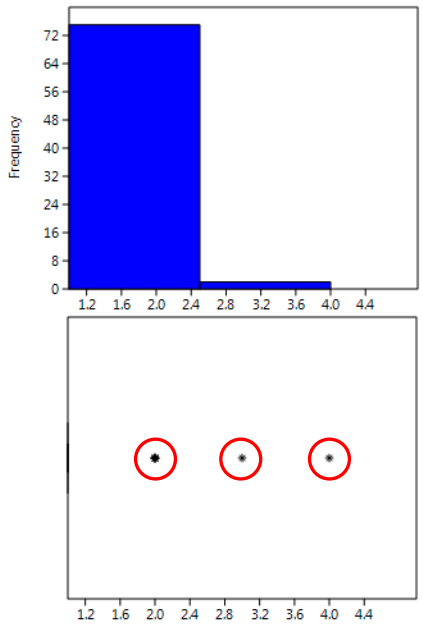

Figure 565 Histogram and box plot of frequencies observed for bowls (Past).

The spatial distribution of bowls fragments is fitted both with a Negative Binomial distribution (with k=0.197 and p=0.815) and a Geometric distribution (with p=0.957) and Kolmogorov Smirnov Test=1. This is what is expected when, as in this case, the sample consists in

predominant empty sampling units and similar frequencies values in all non-empty cells (as also showed in Figure 566).

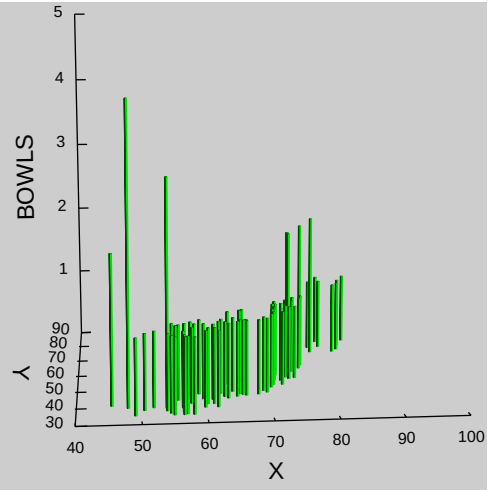

Figure 566 3D Histogram of bowls recovered during surveys of 2009 (Systat 13).

80% of bowls fragments are located in 90% of the effectively surveyed area, in such a way that only 7 cells show more than 1 item.

The spatial distribution of count data per sampling unit for bowls fragments shows a Global Moran's *I* of -0.000492. The theoretical (expected) value assuming spatial autocorrelation (lack of spatial Independence) is -0.000515 and the standard error of *I* is 0.000515. The test of significance using the normality assumption gave a highly non-significant *z* value of 0.045708. These results are comparable with those of the Geary statistics (*C*=0.999974) and Getis-Ord general G (*G*=0.006708). Consequently, we can accept that the spatial distribution of bowls fragments could not be significantly different than the expected value under a random distribution. This is what would be expected in the case of predominant similar frequency of occurrence within quite every spatial location.

Moran's *I* Correlogram (Figure 567) shows extremely low values at the starting point of the function (0.0199), what gives a signal of randomness. The changes in positive and negative autocorrelation are not significant at such low values.

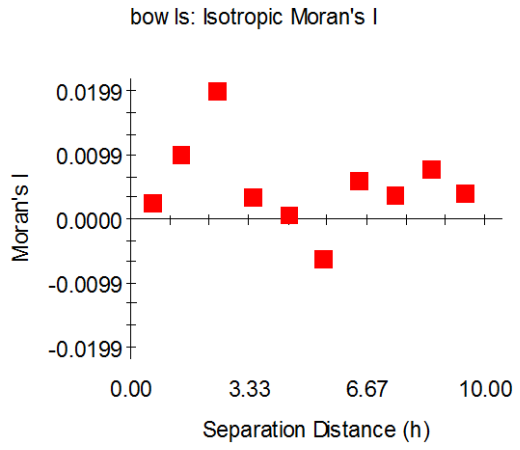

Figure 567 Moran's I Correlogram for bowls recovered during surveys of 2009 (GS+).

Using sampling units selected by local indicators of spatial association as overabundant in respect to others, we obtain a spatial distribution of concentrations of more than 2 fragments of bowls. Within the convex hull defined by this selected locations, a null hypothesis of a random pattern (Poisson process) cannot be rejected at $p<0.05$, according to the Clark Evans test (p<1).

We have explored the possible presence of anisotropic variation (Figure 568). As showed also in the graph of anisotropic Semivariance Surface or Variogram Map (Figure 569) anisotropy is predominantly concentrated in the centre of 3D diagram, with peaks around North-West and South-East corners.

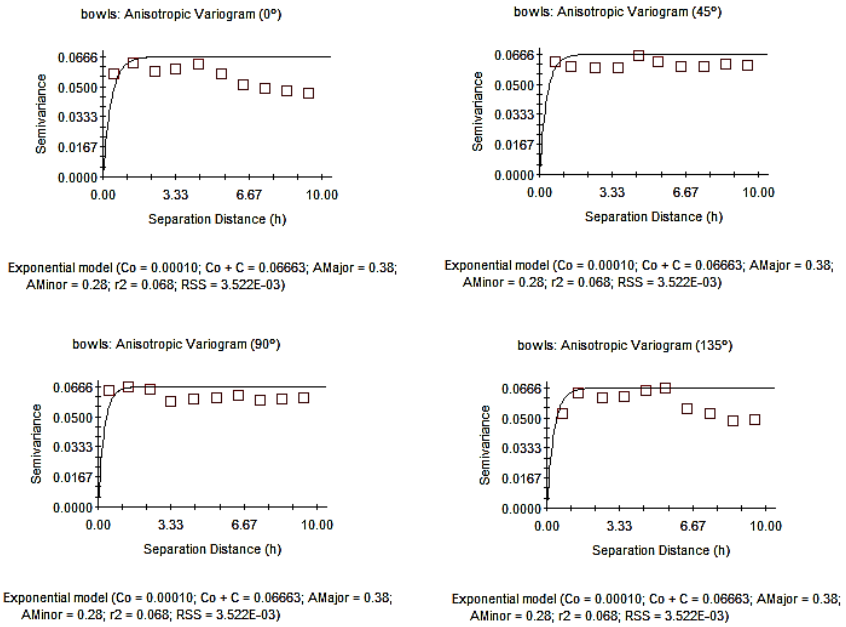

Figure 568 Anisotropic Variogram of bowls recovered during surveys of 2009 (GS+).

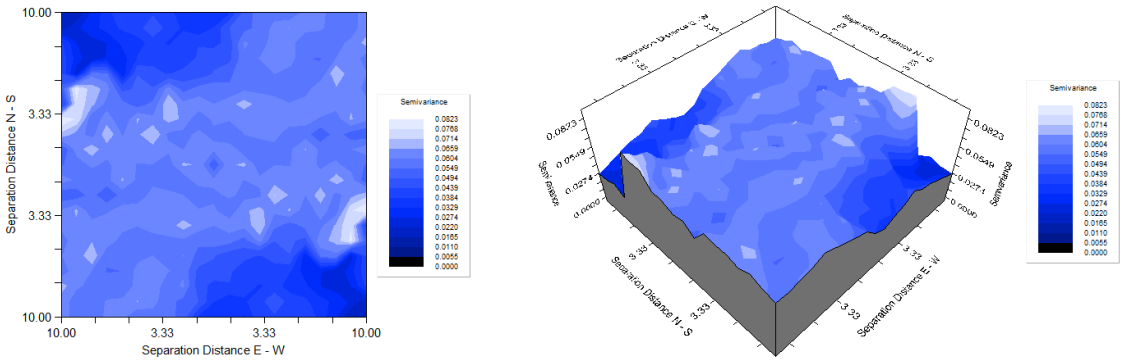

Figure 569 Exponential Isotropic Variogram for bowls recovered during surveys of 2009 (GS+).

The best exponential model - C_0 (nugget variance) =0.00910, C_0+C (sill) = 0.05940 and A_0 (Range) = 0.12- (Figure 570) does not explain the spatial variance; therefore it cannot be used to obtain an interpolated model.

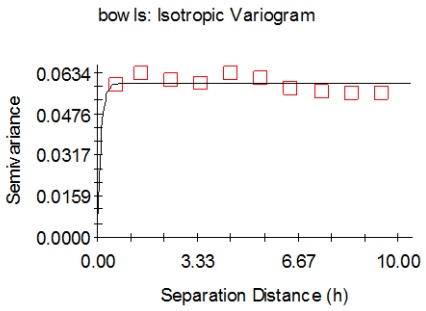

Exponential model (Co = 0.00910; Co + C = 0.05940; Ao = 0.12; r2 = 0.002; RSS = 7.394E-05)

Figure 570 Exponential Isotropic Variogram for bowls recovered during surveys of 2009 (GS+).

8.6.2.4 Open forms

Taking into account the above results for bowls –a typical example of open form-, we have added all other evidence for this category (shallow bowls, cups and the mixture category of bowls/shallow bowls and cups). 151 fragments ascribable to open forms were identified and counted; they are spatially distributed in 129 sampling units. Sampling units where ceramic open forms have been identified are spatially distributed according to Figure 571**.**

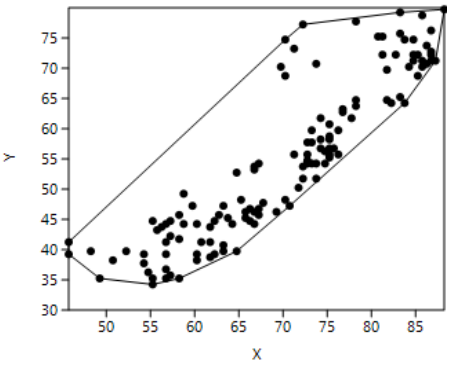

Figure 571 Spatial distribution of cells where ceramic open forms fragments have been recovered (Past).

Ripley's k analysis on the distance between sampling units with fragments ascribable to open forms suggests the possibility of some degree of spatial clustering, at the scale of all the reference area (Figure 572).

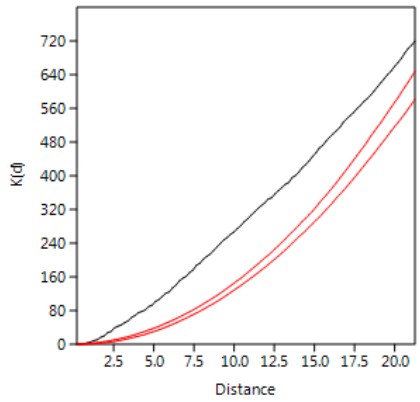

Figure 572 Ripley's K analysis on the distance between sampling units with open forms, recorded in surveys of 2009 (Past).

Within the convex hull defined by those sampling units with a presence of open forms, the null hypothesis of a random pattern (Poisson process) cannot be rejected at $p<0.05$ (Clark and Evans test); this indicates the possibility that equidistant cells have the same probability of counting one or more fragments of open forms. A Kernel Density Estimation (Figure 573) shows three accumulations of open forms, two located within the Zone 1 (between x=50-70 and y=33-50 and between x=70-77 and y=50-65) and one within the Zone 2 (located between x=77-85 and y=68-77).

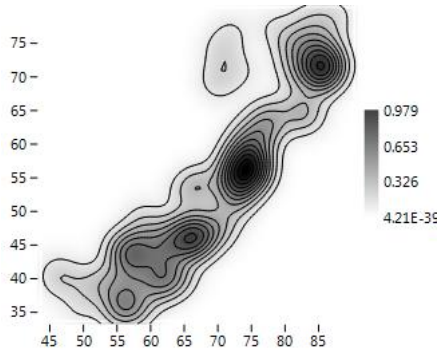

Figure 573 KDE of sampling units where open forms have been recovered during surveys of 2009 (Past).

When considering the raw quantity of open forms fragments at each cell, the probability density distribution of spatial frequencies does not follow a J-shaped distribution. A majority of sampling units have raw counts of such pottery of less than 2 elements (global mean = 1.17 open form fragment per sampling unit). 16 cells are distinguished from the majority (interpretable as outliers), with 2, 3 and 4 observables (Figure 574).

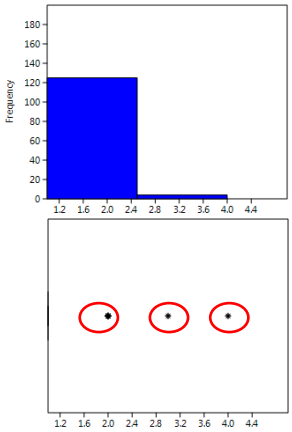

Figure 574 Histogram and box plot of frequencies observed for open forms (Past).

The spatial distribution of open forms fragments is fitted both with a Geometric distribution (with p=0.928) and a Negative Binomial distribution (with k=0.278 and p=0.781) with Kolmogorov Smirnov Test=1. This is what is expected when, as in this case, the sample consists in predominant empty sampling units and similar frequencies values in all non-empty cells, obtaining randomness (as also showed in Figure 575).

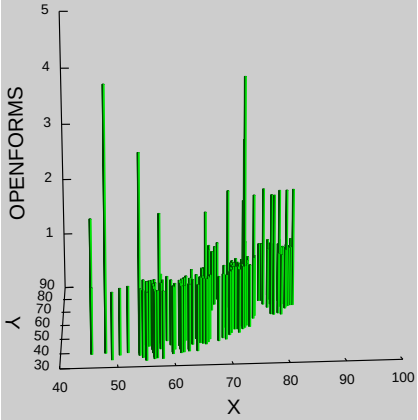

Figure 575 3D Histogram of open forms recovered during surveys of 2009 (Systat 13).

75% of open forms fragments are located in 88% of the effectively surveyed area, in such a way that only 16 cells show more than 1 item.

The spatial distribution of count data per sampling unit for open forms fragments shows a Global Moran's I of -0.000508. The theoretical (expected) value assuming spatial autocorrelation (lack of spatial Independence) is -0.000515 and the standard error of I is 0.000515. The test of significance using the normality assumption gave a z value of 0.014944 highly non-significant value. Those results are comparable with those of the Geary statistics (C=1.000113) and Getis-Ord general G (G=0.008411). Consequently, we can accept that the spatial distribution of open forms fragments could not be significantly different than the expected value under a random distribution. This is what would be expected in the case of predominant similar frequency of occurrence within quite every spatial location.

Moran's I Correlogram (Figure 576) shows extremely low values at the starting point of the function (0.0233), what gives a signal of randomness. The changes in positive and negative autocorrelation are not significant at such low values.

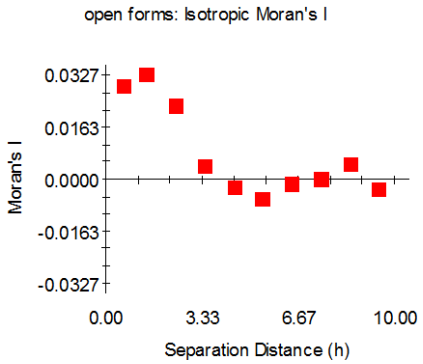

Figure 576 Moran's I Correlogram for open forms recovered during surveys of 2009 (GS+).

Using sampling units selected by local indicators of spatial association, as overabundant in respect to others, we obtain a spatial distribution of concentrations of more than 1 fragment of open forms. Within the convex hull defined by this selected locations and for such cells the null hypothesis of a random pattern (Poisson process) can not be rejected at $p<0.05$, according to the Clark and Evans test (Figure 577).

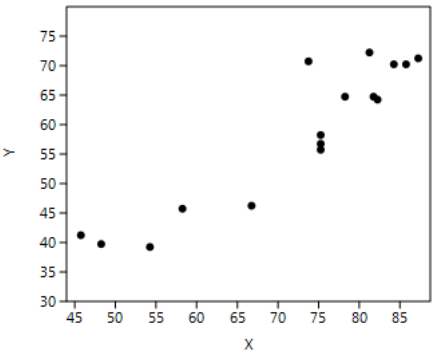

Figure 577 Spatial distribution of sampling units with more than 1 fragment of open forms (surveys of 2009) (Past).

We have explored the possible presence of anisotropic variation (Figure 578). The North-East-South-West direction (45º) seems to have less anisotropy than all other directions.

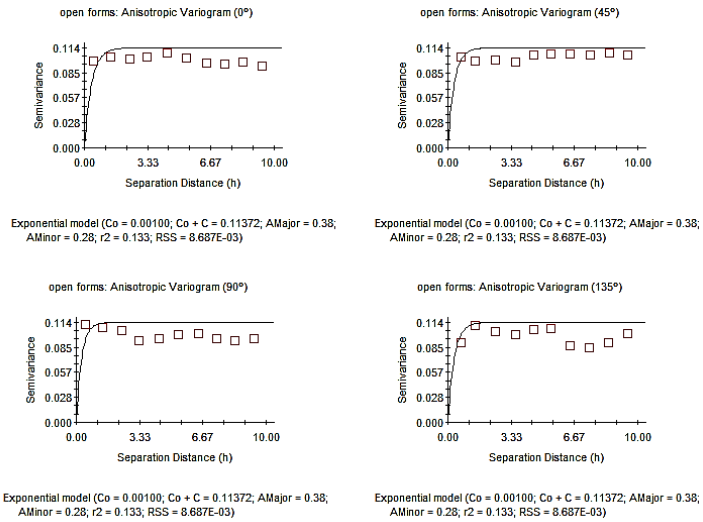

Figure 578 Anisotropic Variogram of open forms recovered during surveys of 2009 (GS+).

The graph of anisotropic Semivariance Surface or Variogram Map (Figure 579) is quite widespread in all surveyed area, with some concentrations around all four corners, in such a way that spatial continuity is scarce.

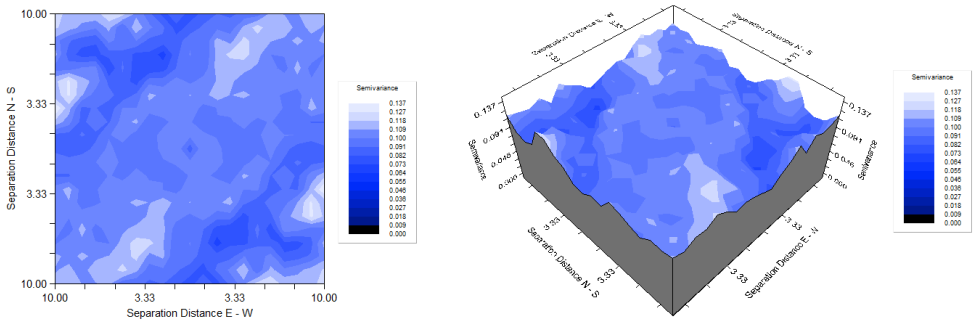

Figure 579 Variogram Map of open forms recovered during surveys of 2009 (GS+).

The best fitted exponential model - C_0 (nugget variance) =0.00980, C_0+C (sill) = 0.10060 and A_0 (Range) = 0.01- (Figure 580) does not explain the spatial variance; therefore it cannot be used to obtain an interpolated model.

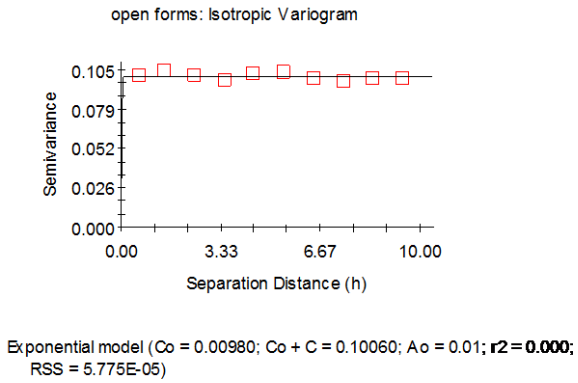

Figure 580 Exponential Isotropic Variogram for open forms recovered during surveys of 2009 (GS+).

8.7. Lithic industry

96 fragments of lithic industry were identified and counted. 1850 were the surveyed empty cells, while the sampling unit with more presence gave 2 items. Cells where lithic industry has been recorded are spatially distributed according to Figure 581.

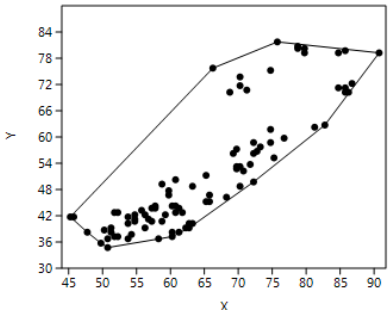

Figure 581 spatial distribution of sampling units where lithic industry has been recorded during surveys of 2009 (Past).

Ripley's *k* analysis (Figure 582) on the distance between sampling units with lithic evidence, suggest the possibility of some degree of spatial clustering, at the scale of all the reference area.

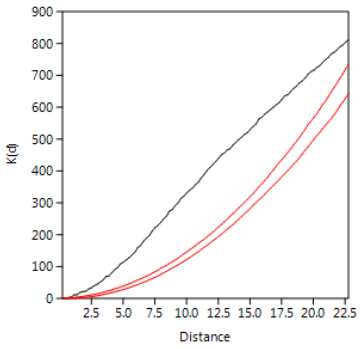

Figure 582 Ripley's *k* analysis on the distance between sampling units with lithic industry, recorded in surveys of 2009 (Past).

Within the convex hull defined by those sample units with a presence of lithic industry, a statistically significant clustered pattern is observed, as confirmed by Clark and Evans test. A Kernel density Estimation (Figure 583) confirm the presence of two different zones (Zone 1 between x=47-75 and y=35-65 (internally sub-divided in two main areas) and another smaller one smaller with low presence and divided into three sub-groups between x=65-90 and y=68-80 (corresponding to Zone 2).

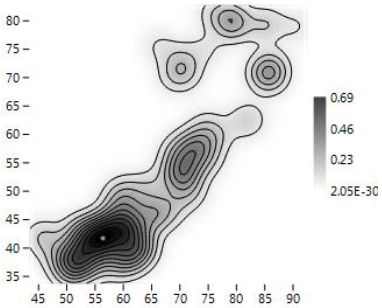

Figure 583 KDE of sampling units where lithic industry has been recovered during surveys of 2009 (Past).

A majority of sampling units have raw counts of 1 lithic fragment (global mean=1.05 observations per sampling unit). Frequency values of 2 are considered as outliers (Figure 584).

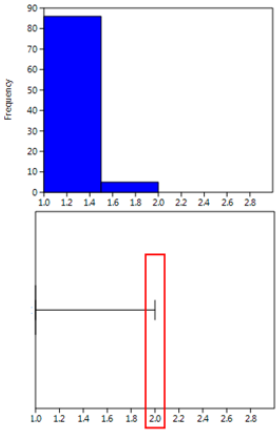

Figure 584 Histogram and box plot of frequencies observed for lithic industry (Past).

The spatial distribution of lithic industry frequencies fits with a Negative Binomial distribution with k=0.842 and p=0.944, a Geometric distribution (with p=0.953) and a Poisson distribution (with λ=0.049) with a Kolmogorov Smirnos Test=1. This is what is expected when, as in this case, the sample consists in predominant empty sampling units and similar frequencies values in all non-empty cells, obtaining randomness (as also showed in Figure 585).

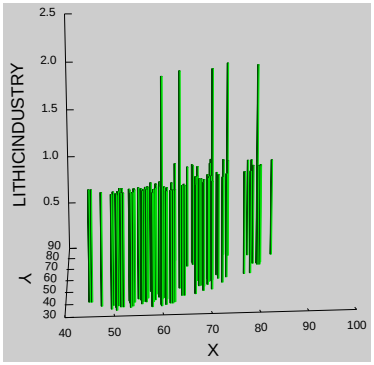

Figure 585 3D Histogram of lithic industry recovered during surveys of 2009 (Systat 13).

89% of lithic industry fragments are located in 94% of the effectively surveyed area, in such a way that only 5 cells show 10 items (representing, this value, the outlier highlighted by both histogram and box plot).

The spatial centroid of the area with lithic industry, calculated using an abundance weighted mean spatial center is x=65.526042 and y=52.192708 with 11.11 m of standard deviation along the x axis and 14.19 m along the y axis. A standard deviation ellipse with a long axis of 49.62 m and a short one of 12.93 m delimits an area of 504.03 square meters, where most data count appears. It has been estimated an average density of 0.04 lithic remains per square meter.

The spatial distribution of the abundance of lithic industry per sampling unit gives a Global Moran's I result of -0.000492. The theoretical (expected) value assuming spatial autocorrelation (lack of spatial independence) is -0.000515 and the standard error is 0.000515. The test of significance using the normality assumption gave a highly non-significant z value of 0.0455551. These results are comparable with those of the Geary statistics (C=0.998858) and Getis-Ord

general G (*G*= 0.007684). Consequently, we can accept that the spatial distribution of lithic industry is not different than the expected value under a random distribution. This is what would be expected in the case of the same frequency of lithic industry in every spatial location.

The Moran's *I* Correlogram (Figure 586) shows extremely low values at the starting point of the function (0.0233), what gives a signal of randomness. The changes in positive and negative autocorrelation are not significant at such low values.

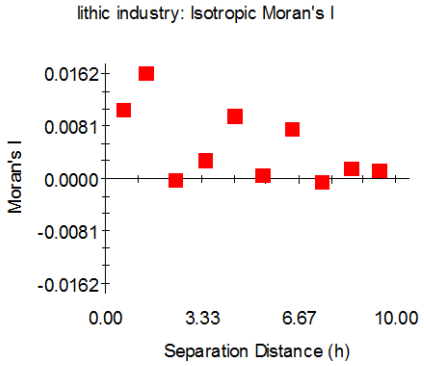

Figure 586 Moran's I Correlogram for lithic industry recovered during surveys of 2009 (GS+).

We have explored the possible presence of anisotropic variation fitting a theoretical variogram at different directions (Figure 587). No homogeneous variations of semivariance are observed, indicating quite irregular spatial pattern, without continuity in medium-large areas.

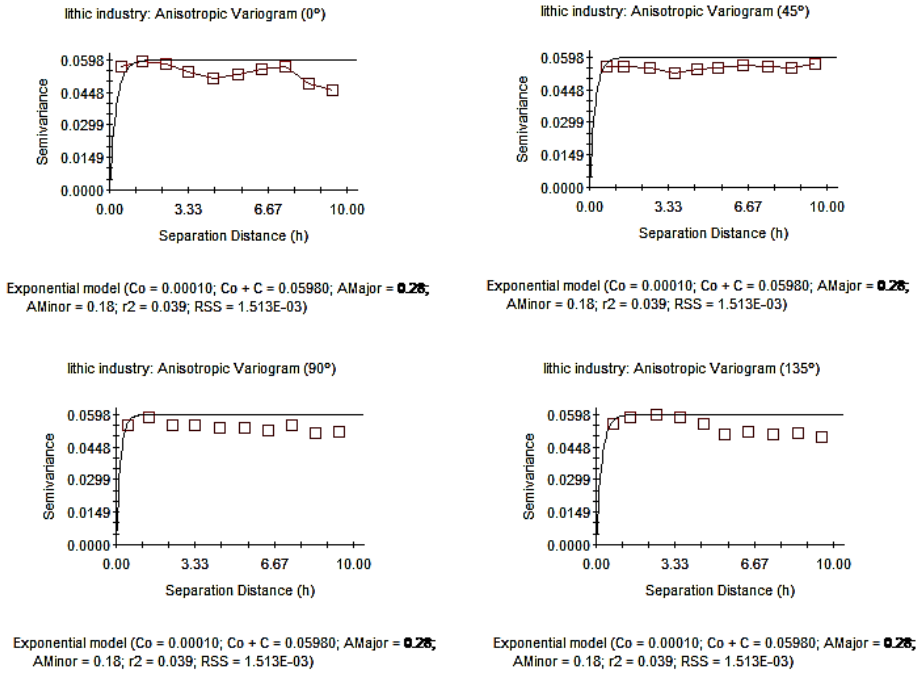

Figure 587 Anisotropic Variogram of lithic industry recovered during surveys of 2009 (GS+).

The graph of anisotropic Semivariance Surface or Variogram Map suggests a high impact of anisotropy, even at small distances, with absence of continuity. Anisotropy seems to be predominantly distributed in the centre of 3D diagram (Figure 588).

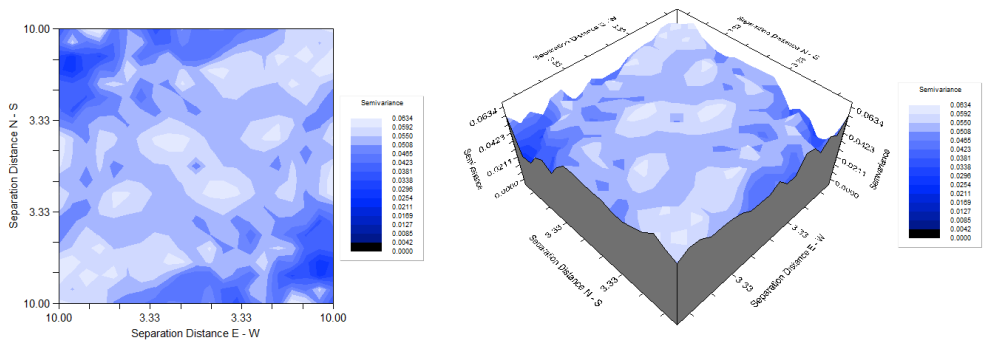

Figure 588 Variogram Map of lithic industry recovered during surveys of 2009 (GS+).

The best fitted exponential model - C_0 (nugget variance) =0.00870, C_0+C (sill) = 0.05460 and A_0 (Range) = 0.01 – (Figure 589) does not explain spatial variance; therefore, it cannot be used to obtain an interpolated model.

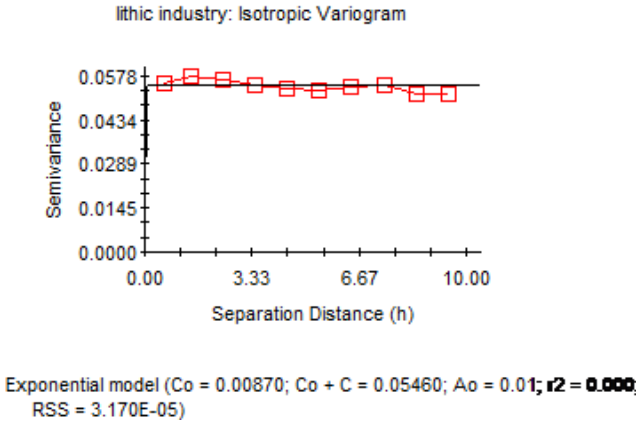

Figure 589 Exponential Isotropic Variogram for lithic industry recovered during surveys of 2009 (GS+).

8.7.1 Lithic industry within Zone 1 and Zone 2

The spatial distribution of sampling units with lithic industry within the Zone 1 and 2 is showed in the Figure 590.

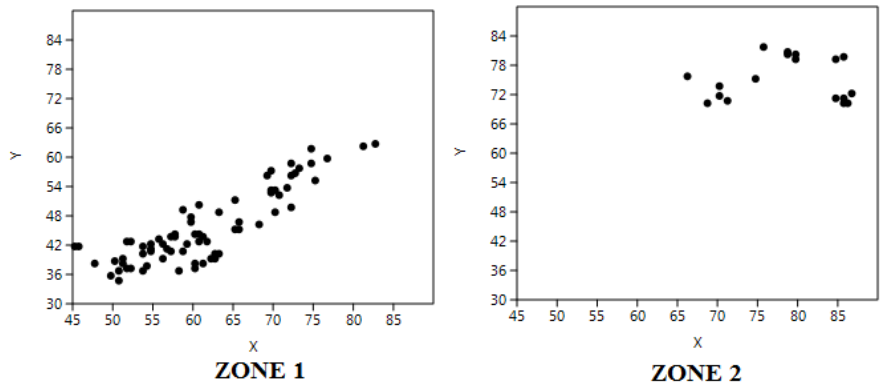

Figure 590 Spatial distribution of sampling units where lithic industry has been recovered during surveys of 2009 within Zone 1 and Zone 2 (Past).

Ripley's *k* analysis on the distance between sampling units with lithic industry evidence suggests the possibility of some degree of spatial clustering within Zone 1, while a predominant random pattern is observed for Zone 2, at the scale of all the reference area (Figure 591).

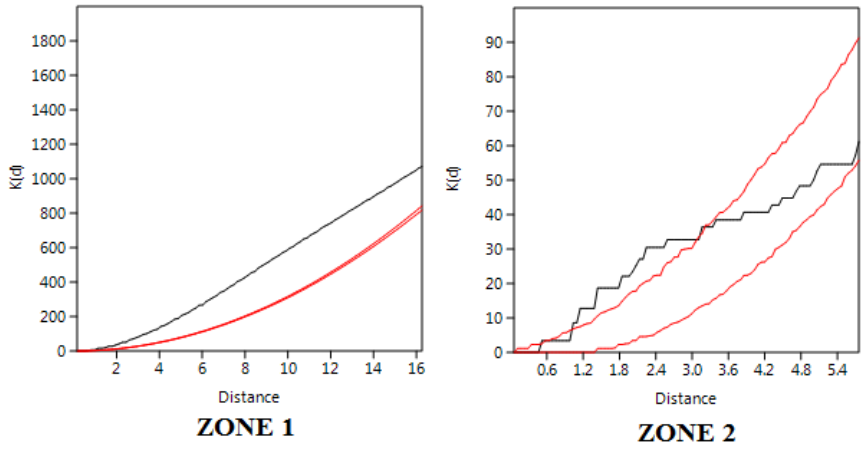

Figure 591 Ripley's *k* analysis on the distance between sampling units with lithic industry, recorded in surveys of 2009, within Zone 1 and Zone 2 (Past).

Within the convex hulls defined by those sampling units with presence of lithic industry within Zone 1 and Zone 2, the null hypothesis of a random pattern (Poisson process) cannot be rejected at $p<0.05$ (for both zones). A KDE (Figure 592**)** shows for Zone 1 the occurrence of a wider central area, sub-divided in two concentrations which are extended between x=48-64 and y=32-45 and between x=67-77 and y=49-62, while within Zone 2 three sub-concentrations emerge (one between x=67-73 and y=69-75, another between x=83-89 and y=68-73 and the last between x=75-87 and y=78-84 (internally sub-divided in two sectors).

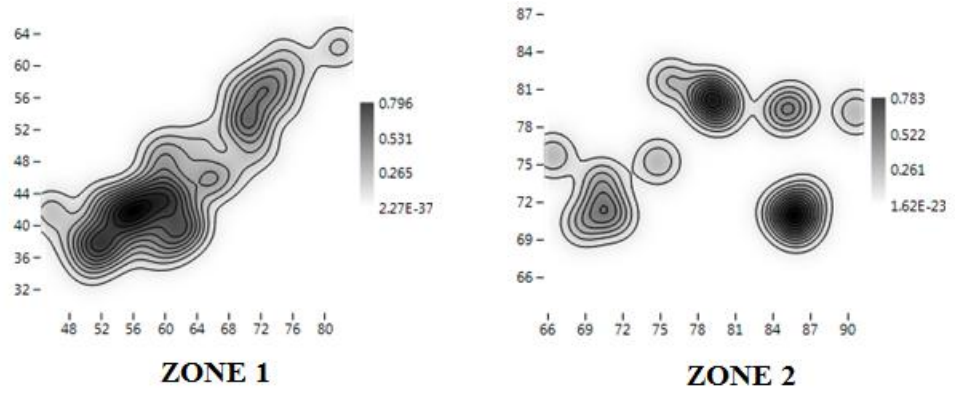

Figure 592 KDEs of sampling units where lithic industry has been recovered during surveys of 2009, within Zone 1 and Zone 2 (Past).

There are not relevant differences in the spatial location of lithic industry frequencies; Zone 1 concentrates the majority of observations (n= 75), the range of frequencies is between 1 and 2, with a mean of 2.88 observations per sampling unit and variance = 8.4622. The spatial distribution of lithic industry in Zone 1 is fitted with both a Negative Binomial distribution (with k=2.302 and p=0.976) and a Poisson distribution (with λ=0.057) with a Kolmogorov Smirnov Test=1 **(**Figure 593**)**. Zone 2 concentrates 19 lithic industry remains, the range of frequencies is between 1 and 2, with a mean of 1.10 observations per sampling unit and a variance = 0.0994152 (Figure 593). In both cases a break point is identified corresponding to the frequency value of 2 (both in histogram and box plot). The spatial distribution of lithic remains in Zone 2 is fitted with both the Negative Binomial distribution (with k=0.190 and p=0.848) and a Poisson distribution (with λ=0.034) with a Kolmogorov Smirnov Test=1.

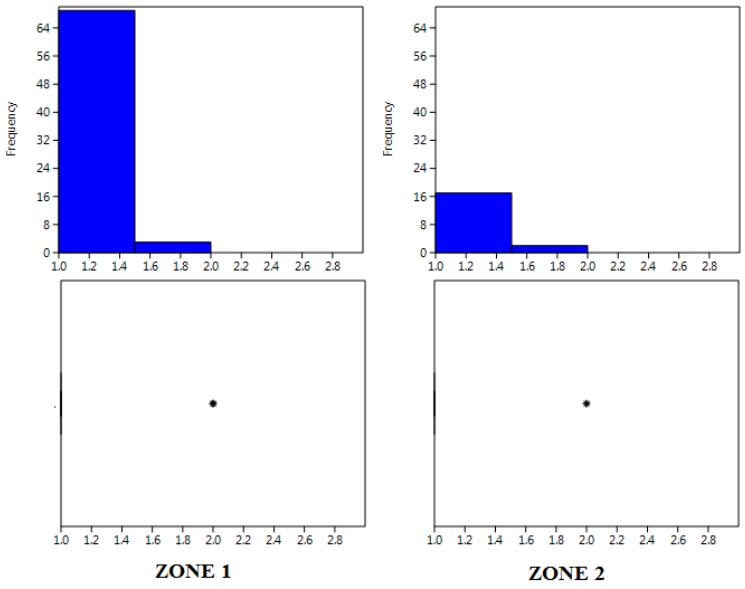

Figure 593 Histogram and box plot of frequencies observed for lithic industry within Zone 1 and Zone 2 (Past).

The spatial distribution of count data per sampling unit shows, for Zone 1, a Global Moran's I of -0.000746. The theoretical (expected) value assuming spatial autocorrelation (lack of spatial Independence) is -0.000756 and the standard error I is 0.000756. The test of significance using the normality assumption gave a z value of 0.013929, a quite non-significant value. This result

is comparable with those of Geary statistic (*C*=1.000202) and Getis-Ord general G (*G*=0.009019).

The spatial distribution of count data per sampling unit shows, for Zone 2, a Moran's *I* of -0.001618. The theoretical (expected) value assuming spatial autocorrelation (lack of spatial Independence) is -0-001621, and the standard error of *I* is 0.001621. The test of significance using the normality assumption gave a *z* value of 0.0001477, a highly non-significant value. This result is comparable with those of Geary statistic (*C*=0.999791) and Getis-Ord general G (*G*=0.048077).

Consequently, we can accept that the spatial distribution of lithic industry for both areas is not significantly different than the expected value under a random distribution. This is what would be expected in the case of the same frequency of lithic industry in quite every spatial location.

The Moran's *I* Correlogram (Figure 594) shows for both zones extremely low values at the starting point of the function (0.0102 for Zone 1 and 0.0498 for Zone 2), what gives a signal of randomness. The changes in positive and negative autocorrelation are not significant at such low values.

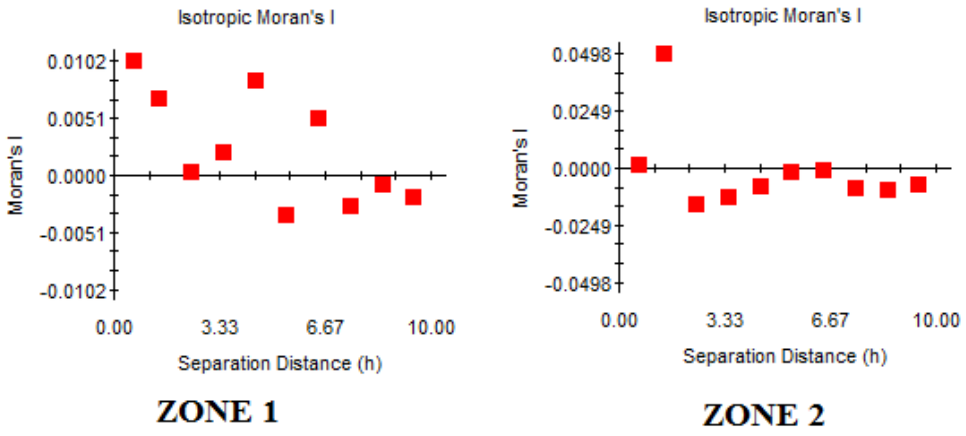

Figure 594 Moran's I Correlograms for lithic industry recovered during surveys of 2009, within Zone 1 and Zone 2 (GS+).

We have explored the possible presence of anisotropic variation (Figures 595 and 597). For Zone 1, no homogeneous variations of semivariance at any distances are observed (Figure 595).

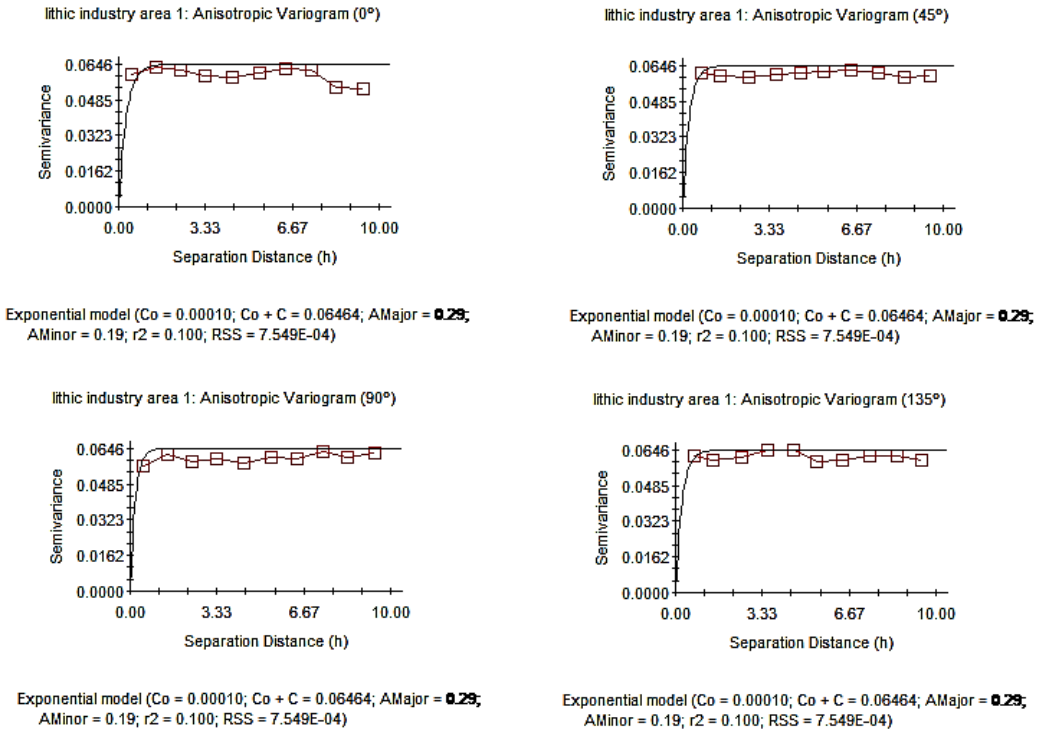

Figure 595 Anisotropic Variogram of lithic industry recovered during surveys of 2009 within Zone 1 (GS+).

Anisotropy is widespread in the centre of 3D diagram, preventing any kind of spatial continuity (Figure 596).

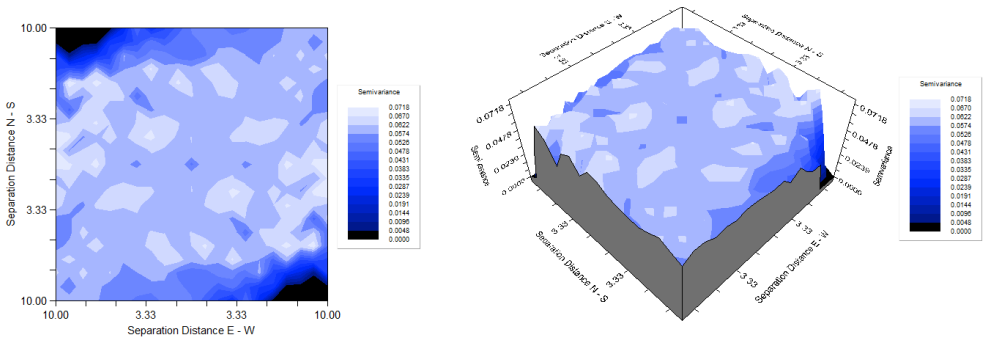

Figure 596 Variogram Map of lithic industry recovered during surveys of 2009, within Zone 1 (GS+).

For Zone 2 the same absence of homogeneous variation of semivariance at any distance is observed (Figure 597).

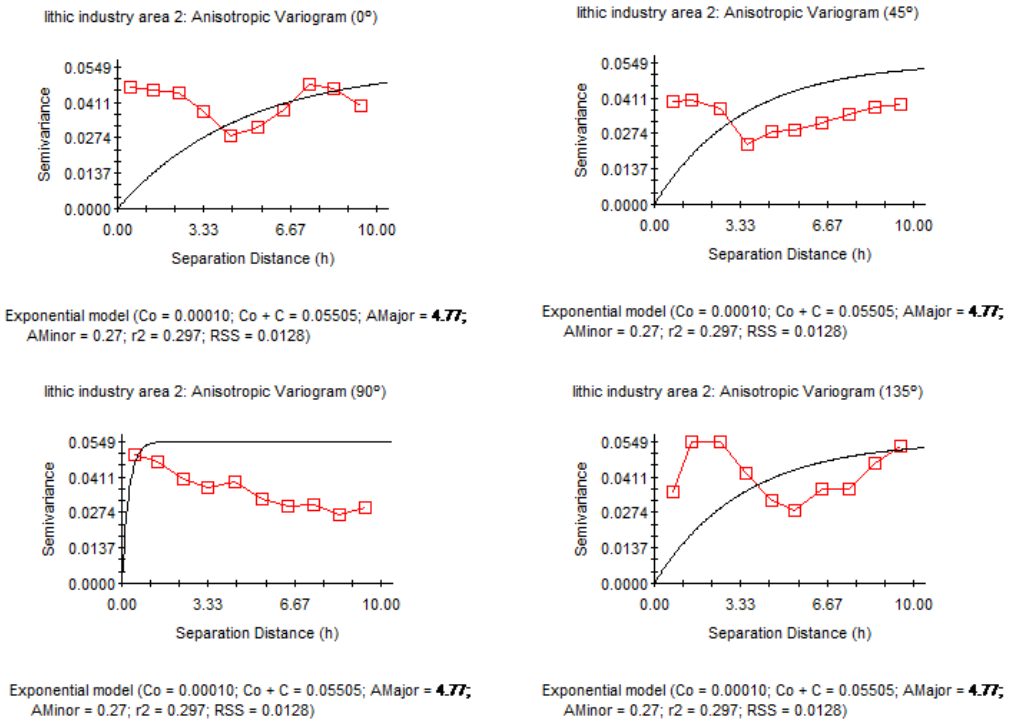

Figure 597 Anisotropic Variogram of lithic industry recovered during surveys of 2009 within Zone 2 (GS+).

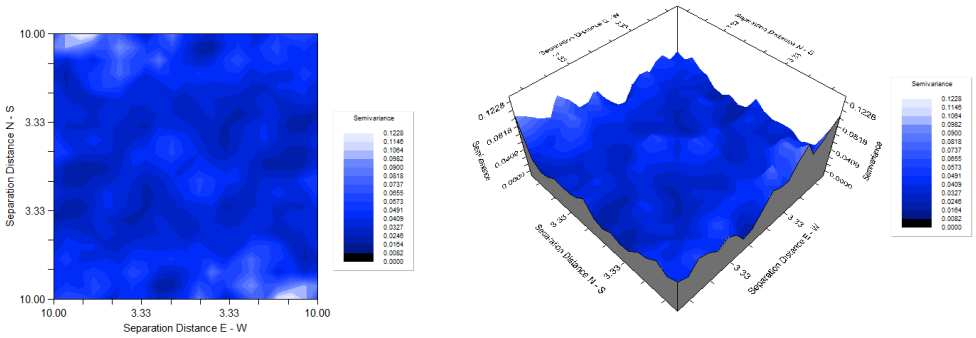

Figure 598 Variogram Map of lithic industry recovered during surveys of 2009, within Zone 2 (GS+).

The best fitted exponential model, for Zone 1, - C_0 (nugget variance) =0.00940, C_0+C (sill) = 0.06070 and A_0 (Range) = 0.15 - explains only 7.1% of sample variance (Figure 599). For Zone 2, the best fitted exponential model - C_0 (nugget variance) =0.00420, C_0+C (sill) = 0.03790 and A_0 (Range) = 0.01- does not explain the spatial variance.

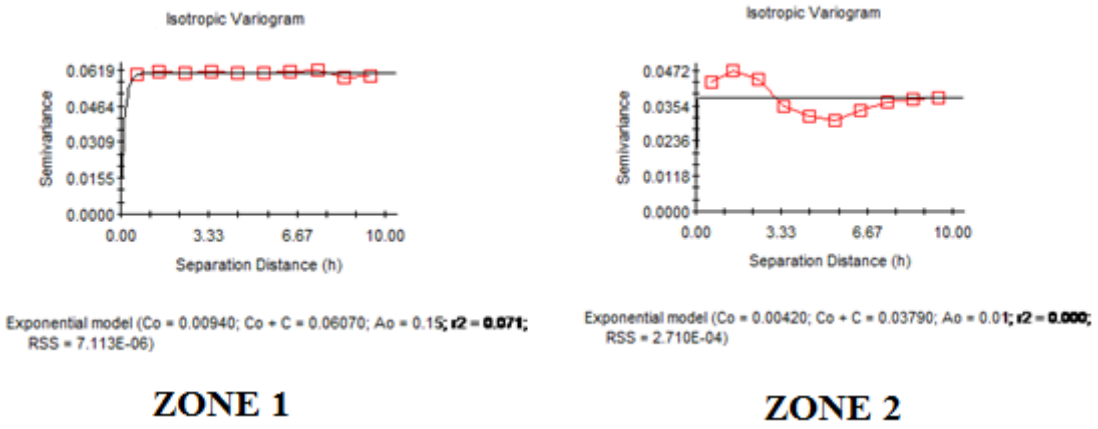

Figure 599 Exponential Isotropic Variogram for lithic industry recovered during surveys of 2009, within Zone 1 and Zone 2 (GS+).

Although not entirely reliable, a predictive model for the frequency of lithic industry distribution within Zone 1 (Figure 600) shows a predominant accumulation of lithic industry around the South-West corner and in the middle of the surveyed area, according to the widespread North-East-South-West orientation. Such interpolated results predominantly mirrors the above mentioned KDE.

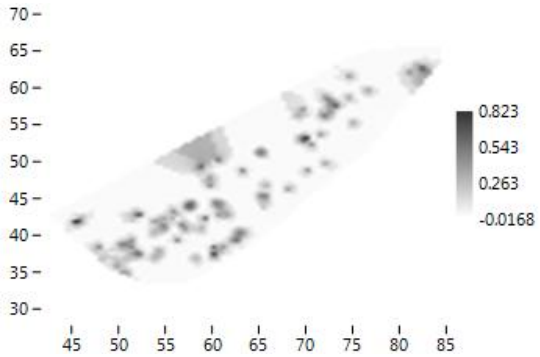

Figure 600 Graphic results of Inverse Distance Weighting calculated for lithic industry recovered during surveys of 2009 within Zone 1 (Past).

8.7.1.1 Sub-categories of lithic industry

We have explored the spatial distribution of different lithic industry categories. Nevertheless, frequencies are low in quantitative terms, and we have limited the analysis to an exploration of presence/absence in the surveyed area.

8.7.1.2 Pebbles and choppers

20 among pebbles and choppers were identified and counted; they are spatially distributed in 17 sampling units, while 1924 cells were empty. Cells with pebbles and choppers are spatially distributed according to Figure 601**.**

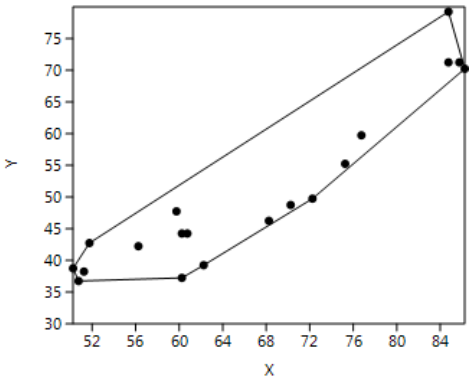

Figure 601 Spatial distribution of sampling units where pebbles and choppers have been recovered during surveys of 2009 (Past).

Ripley's *k* analysis on the distance between sampling units with such lithic industry evidence suggests the possibility of some degree of spatial clustering, at the scale of all the reference area (Figure 602).

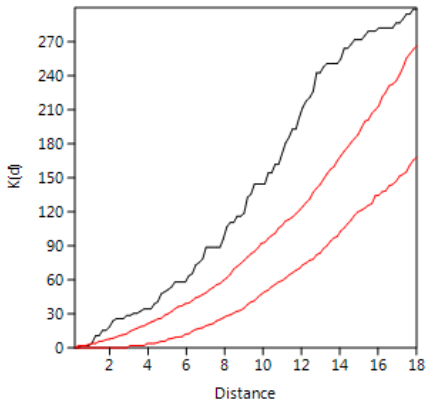

Figure 602 Ripley's k analysis on the distance between sampling units with pebbles and choppers, recorded in surveys of 2009 (Past).

Within the convex hull defined by those sampling units where pebbles and choppers have been recovered, the null hypothesis of random pattern (Poisson process) cannot be rejected at $p<0.05$ (Clark and Evans test). A Kernel Density Estimation (Figure 603) shows concentrations located respectively between x=49-65 and y=30-50, between x=65-75 and y=45-52 and two small aggrupations located respectively between x=80-87 and y=67-80. These latter are observed on the Zone 2.

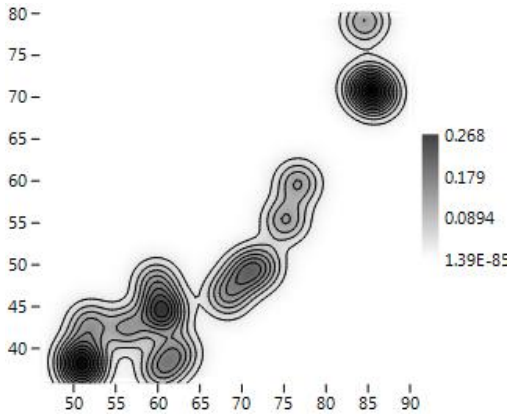

Figure 603 KDE of sampling units where pebbles and choppers have been recovered during surveys of 2009 (Past).

The scarce presence of pebbles and choppers cause the interpretation of frequency value of 1 and 2 as outliers in box plot (global mean= 0.010 pebble/chopper per sampling unit) (Figure 604).

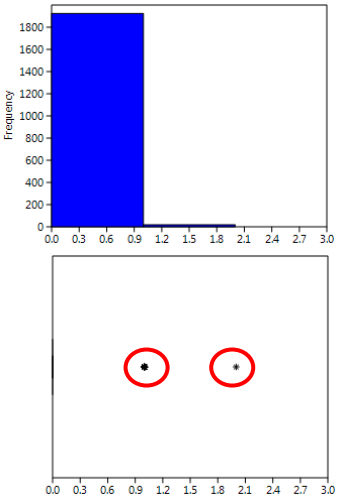

Figure 604 Histogram and box plot of frequencies observed for pebbles and choppers (Past).

The spatial distribution of pebbles and choppers frequencies fits with a Geometric distribution (with p=0.989), a Negative Binomial distribution (with a k=0.144 and p=0.929) and a Poisson distribution (with λ=0.011), with Kolmogorov Smirnov Test=1. This is what is expected when, as in this case, the sample consists in predominant empty sampling units and similar frequencies values in all non-empty cells (as also showed in Figure 605).

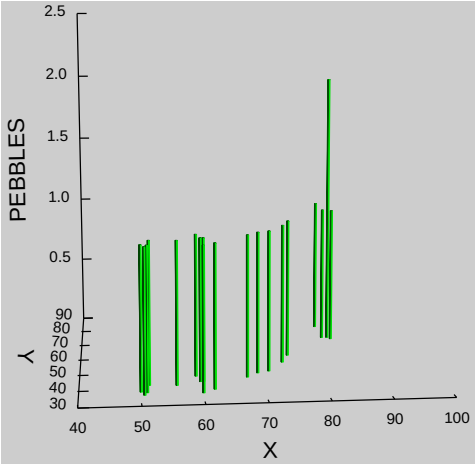

Figure 605 3D Histogram of pebbles and choppers recovered during surveys of 2009 (Systat 13).

90% of pebbles and choppers are located in 95% of the effectively surveyed area, in such a way that only 1 cell shows more than 1 item.

The spatial distribution of count data per sampling unit for pebbles and choppers shows a Global Moran's *I* of -0.000514. The theoretical (expected) value assuming spatial autocorrelation (lack of spatial Independence) is -0.000515 and the standard error of *I* is 0.000515. The test of significance using the normality assumption gave a z value of 0.002361, highly non-significant value. Those results are comparable with those of the Geary statistics (*C*=0.999505) and Getis-Ord general G (*G*=0.015873). Consequently, we can accept that the spatial distribution of pebbles and choppers is the same than the expected value under a random distribution. This is what would be expected in the case of similar frequency of occurrence within every spatial location.

Moran's *I* Correlogram (Figure 606) shows for both zones extremely low values at the starting point of the function (0.0136), what gives a signal of randomness. The changes in positive and negative autocorrelation are not significant at such low values.A strong irregular spatial pattern in observed, with a quite total absence of spatial dependence at any distance.

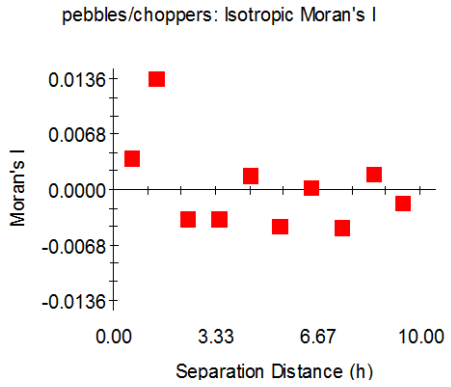

Figure 606 Moran's I Correlogram for pebbles and choppers recovered during surveys of 2009 (GS+).

We have explored the possible presence of anisotropic variation in the spatial distribution of pebbles and choppers (Figure 607) and it is highlitghts the absence of homogeneous variation of semivariance at any distance.

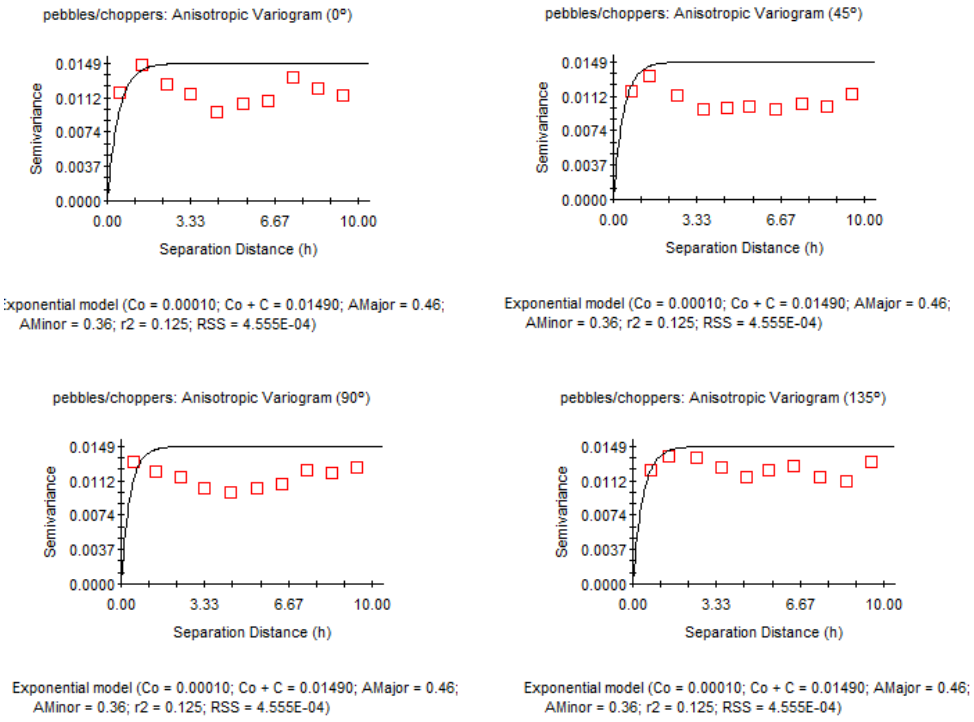

Figure 607 Anisotropic Variogram of pebbles/choppers recovered during surveys of 2009 (GS+).

The graph of anisotropic Semivariance Surface or Variogram Map shows that anisotropy is particularly observed in the centre of the surveyed area and with higher values around the North-West and South-East corners (Figure 608).

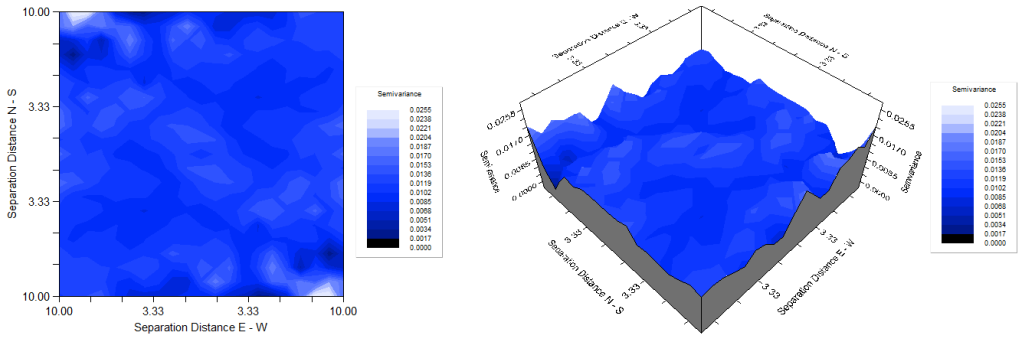

Figure 608 Variogram Map of pebbles/choppers recovered during surveys of 2009 (GS+).

The exponential model that best fits the data - C_0 (nugget variance) =0.00182, C_0+C (sill) = 0.01154 and A_0 (Range) = 0.01 (Figure 609) - does not explain the sample variance; therefore, it cannot be used to obtain an interpolated model.

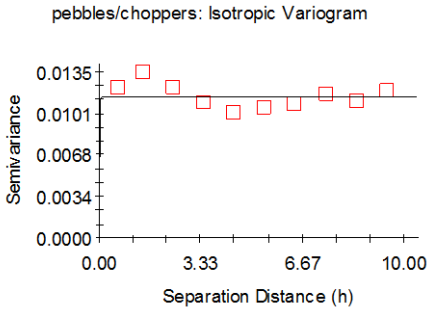

Exponential model (Co = 0.00182; Co + C = 0.01154; Ao = 0.01; **r2 = 0.000**; RSS = 8.737E-06)

Figure 609 Exponential Isotropic Variogram for pebbles/choppers recovered during surveys of 2009 (GS+).

8.7.1.3 Debitage

60 fragments ascribable to debitage were identified and counted; they are spatially distributed in 55 sampling units. The spatial distribution of cells where debitage has been recovered is showed in Figure 610**.**

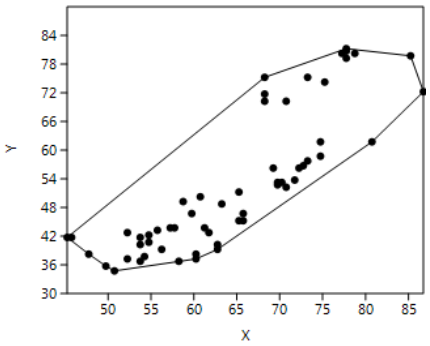

Figure 610 Spatial distribution of sampling units where debitage has been recovered during surveys of 2009 (Past).

Ripley's *k* analysis on the distance between sampling units with debitage suggests the possibility of some degree of spatial clustering, at the scale of the global reference area (Figure 611).

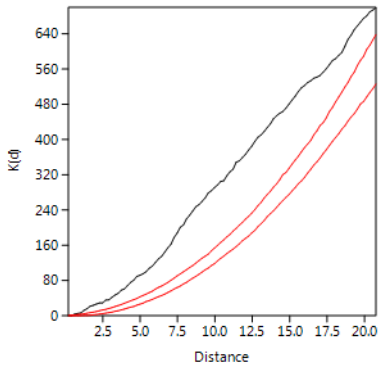

Figure 611 Ripley's *k* analysis on the distance between sampling units with debitage, recorded in surveys of 2009 (Past).

Within the convex hull defined with presence of debitage the null hypothesis of random pattern (Poisson process) cannot be rejected at $p<0.05$, what indicates the possibility that equidistant cells have the same probability of counting one or more debitage. However, a Kernel Density Estimation (Figure 612) shows concentrations between x=45-65 and y=33-50, between x=68-72 and y=50-64 and two small aggruppations respectively between x=62-80 x and 67-77 y and between x=72-80 and y=75-80 (these latter are part of Zone 2).

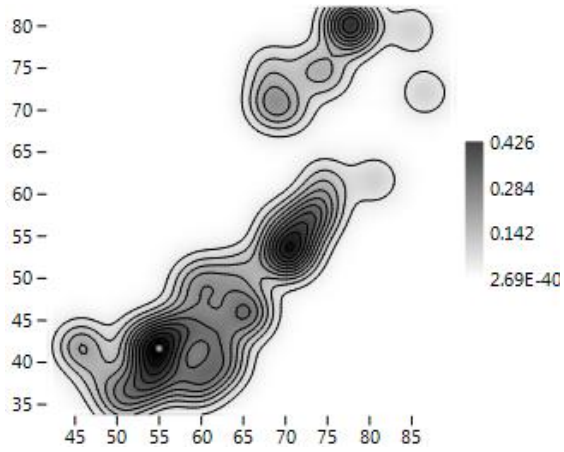

Figure 612 KDE of sampling units where debitage has been recovered during surveys of 2009 (Past).

A majority of sampling units have raw counts of 1 debitage (global mean=0.02 observations per sampling unit). Frequency values of 2 are considered as outliers[40] (Figure 613).

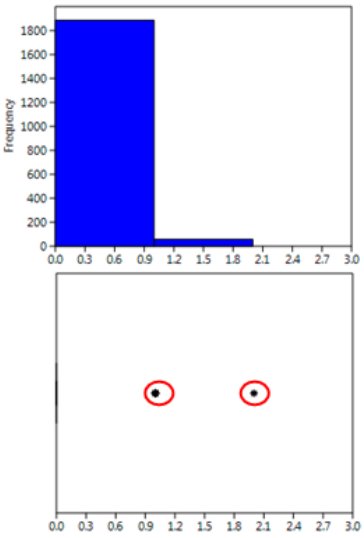

Figure 613 Histogram and box plot of frequencies observed for debitage (Past).

The spatial distribution of debitage frequencies fits with a Negative Binomial distribution (with k=0.417 and p=0.931), a Geometric distribution (with p=0.970) and a Poisson distribution (with λ=0.031) with a Kolmogorov Smirnov Test=1. This is what is expected when, as in this case, the sample consists in predominant empty sampling units and similar frequencies values in all non-empty cells (Figure 614).

[40] in this case even the value 1 is considered as outlier due to the scarce presences of debitage fragments

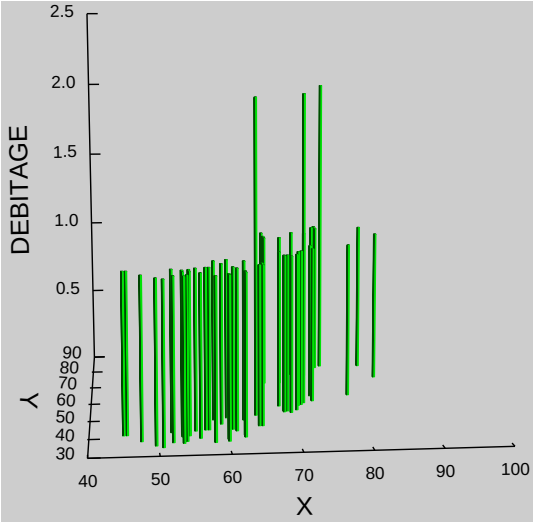

Figure 614 3D Histogram of debitage recovered during surveys of 2009 (Systat 13).

90% of debitage is located in 95% of the effectively surveyed area, in such a way that only 3 cells show 2 items.

The spatial distribution of the abundance of debitage per sampling unit gives a Global Moran's *I* result of -0.000507. The theoretical (expected) value assuming spatial autocorrelation (lack of spatial independence) is -0.000515 and the standard error *I* is 0.000515. The test of significance using the normality assumption gave a highly non significant *z* value of 0.014937. These results are comparable with those of the Geary statistics (*C*=1.000069) and Getis-Ord general G (*G*= 0.006225). Consequently, we can accept that the spatial distribution of debitage is not different than the expected value under a random distribution. This is what would be expected in the case of the same frequency of debitage in every spatial location.

The Moran's *I* Correlogram (Figure 615) hows for both zones extremely low values at the starting point of the function (0.0169), what gives a signal of randomness. The changes in positive and negative autocorrelation are not significant at such low values.

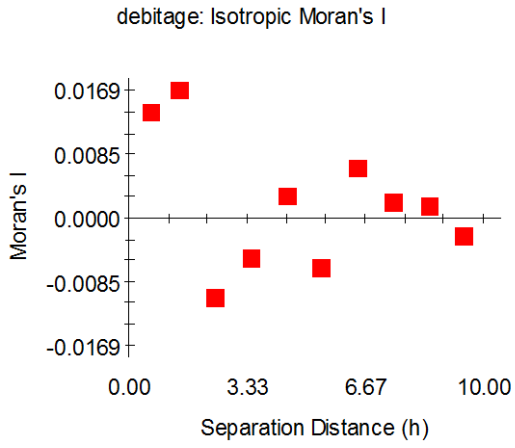

Figure 615 Moran's I Correlogram for debitage recovered during surveys of 2009 (GS+).

We have explored the possible presence of anisotropic variation (Figure 616). Semivariance seems to vary in different way at each distance, without homogeneity.

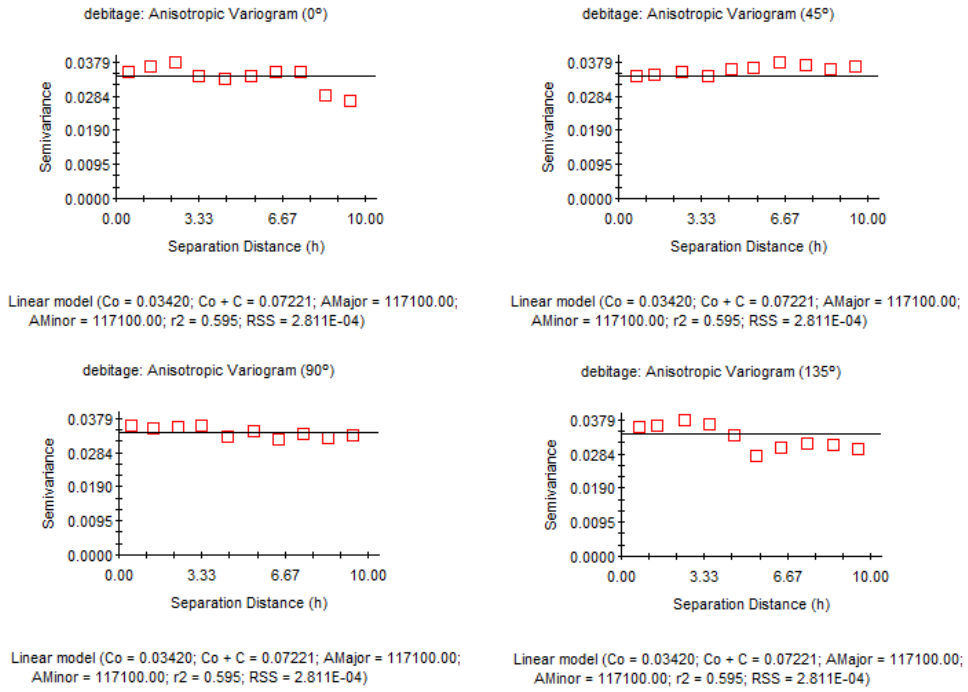

Figure 616 Anisotropic Variogram of debitage recovered during surveys of 2009 (GS+).

The graph of anisotropic Semivariance Surface or Variogram Map (2D-3D) (Figure 617) shows the widespread presence of anisotropy, predominantly concentrated in the centre of the 3D diagram and around the North-East and South-West corners.

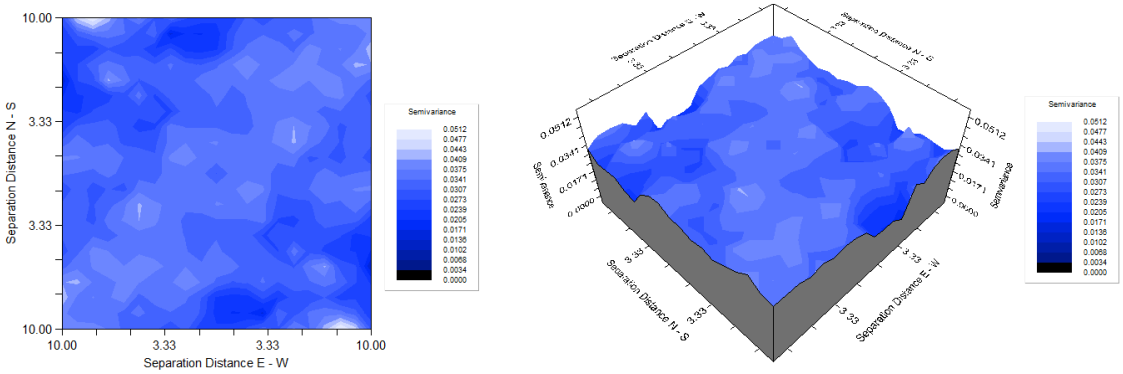

Figure 617 Exponential Isotropic Variogram for debitage recovered during surveys of 2009 (GS+).

The best exponential model - C_0 (nugget variance) =0.03456, C_0+C (sill) = 0.03456 and A_0 (Range) = 9.45 – (Figure 618) does not explain the sample variance; therefore, it cannot be used to obtain an interpolated model.

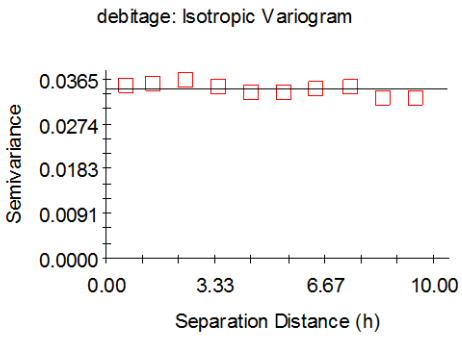

Linear model (Co = 0.03456; Co + C = 0.03456; Ao = 9.45; r2 = **0.000;**
RSS = 1.363E-05)

Figure 618 Exponential Isotropic Variogram for debitage recovered during surveys of 2009 (GS+).

8.8 Wooden remains

As above mentioned in chapter 5 this more general category includes two sub-classes (wood fragments and wood horizontal posts) and the intra-site spatial analysis was performed separately for each one of them.

8.8.1 General wooden remains (excluding vertical posts)

316 wooden fragments were identified and counted; they are spatially distributed in 149 sampling units. Cells where wooden fragments have been recovered are spatially distributed as showed in Figure 619.

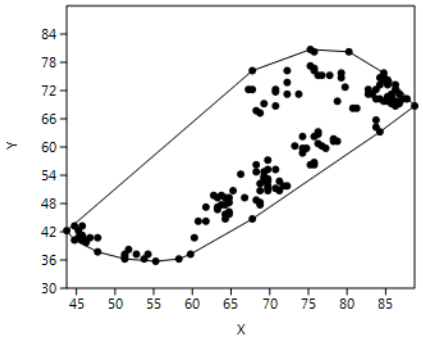

Figure 619 spatial distribution of sampling units where wooden remains have been recorded during surveys of 2009 (Past).

Ripley's *k* analysis on the distance between sampling units with wooden fragments evidence, suggest the possibility of some degree of spatial clustering, at the scale of global reference area (Figure 620).

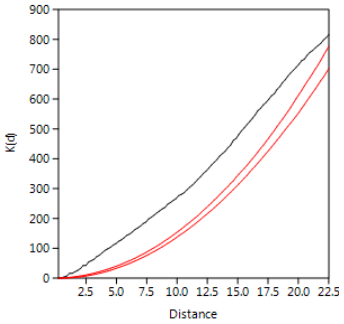

Figure 620 Ripley's *k* analysis on the distance between sampling units with wooden fragments, recorded in surveys of 2009 (Past).

Within the convex hull defined by those sampling units with presence of wooden fragments, these non-empty cells are clustered, according to Clark and Evans test. A Kernel density estimation (Figure 621) shows the presence of wooden fragments in both different zones, particularly, within Zone 1, between x=44-55 and y=33-45, between x=60-75 and y=43-57 and between x=72-77 and y=57-65 y, while within Zone 2 they are observed between x=80-85 and y=65-77).

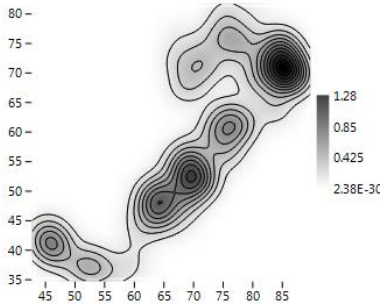

Figure 621 KDE of sampling units where wooden fragments have been recovered during surveys of 2009 (Past).

A majority of sampling units have raw counts of wooden fragments of less than 3 elements (global mean=2.12 observations per sampling unit). Three cells are distinguished from the majority (representing outliers), with 7, 8 and 11 wooden remains. A break point in the frequencies of wooden fragments is attested in correspondence with the value of 5 items as highlighted by both histogram and box plot (Figure 622).

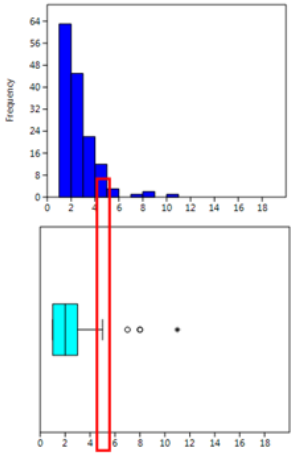

Figure 622 Histogram and box plot of frequencies observed for wooden fragments (Past).

The Negative Binomial distribution with k=17.345 and p=0.977 fits with the observed frequencies of wood fragments, according to the Kolmogorov Smirnov Test=0.998. This condition suggests randomness in the spatial distribution of the abundance of wood fragments per sampling unit (Figure 623).

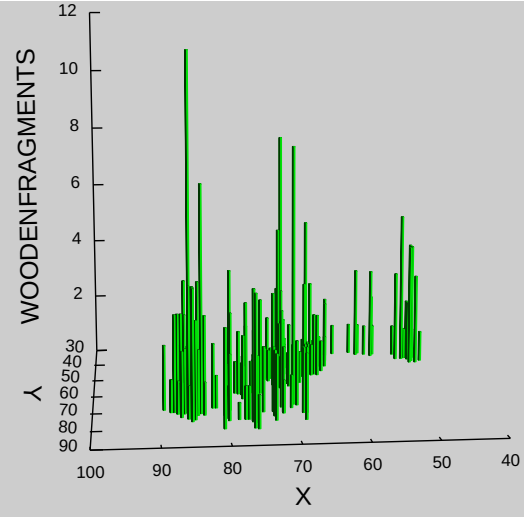

Figure 623 3D Histogram of wooden fragments recovered during surveys of 2009 (Systat 13).

89% of wood fragments are located in 97% of the effectively surveyed area, in such a way that only 4 cells show more than 5 items (representing, this limit, the break point above mentioned).

The spatial centroid of the area with wooden remains, calculated using an abundance weighted mean spatial center is is x= 71.613924, y= 60.224684, with 12.33 m of standard deviation along the *x* axis, and 13.02 m along the *y* axis. A standard deviation ellipse with a long axis of 48.83 m and and a short one of 14.03 m delimits an area of 537.94 square meters, where most count data appears. It has been estimated an average density of 0.13 items per square meter.

The spatial distribution of the abundance of wooden fragments per sampling unit gives a Global Moran's *I* result of -0.000463. The theoretical (expected) value assuming spatial autocorrelation (lack of spatial independence) is -0.000515 and the standard error is 0.000515. The test of significance using the normality assumption gave ahighly non-significant *z* value of 0.101850. These results are comparable with those of the Geary statistics (*C*=1.000000) and Getis-Ord general G (*G*= 0.016024). Consequently, we can accept that the spatial distribution of wood fragments is not different than the expected value under a random distribution. This is what would be expected in the case of the same frequency of wood fragments in every spatial location.

The Moran's *I* Correlogram (Figure 624) has been calculated for uniform class distance intervals of 1 meter, and taking into account a 10 meters active lag distance. *I* value at 0.50 distance is 0.147, above the expected value for randomness. As the distance between sampling units increases, *I* value drops off quite gently and continuously above the expected value for randomness and in some cases reaching such value.

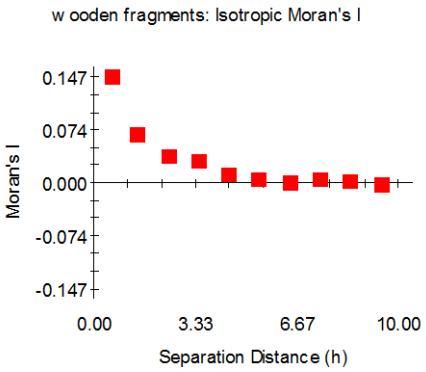

Figure 624 Moran's I Correlogram for wooden fragments recovered during surveys of 2009 (GS+).

This result gives the possibility of finding spatially dependent areas of 5 meters of radius, what is a suggestive working hypothesis for locating homogeneous areas. Although, it is important to remark that all I values are strictly around 0.

We have explored the possible presence of anisotropic variation at different directions (Figure 625). Semivariance varies strongly, particularly at 0º and 135º.

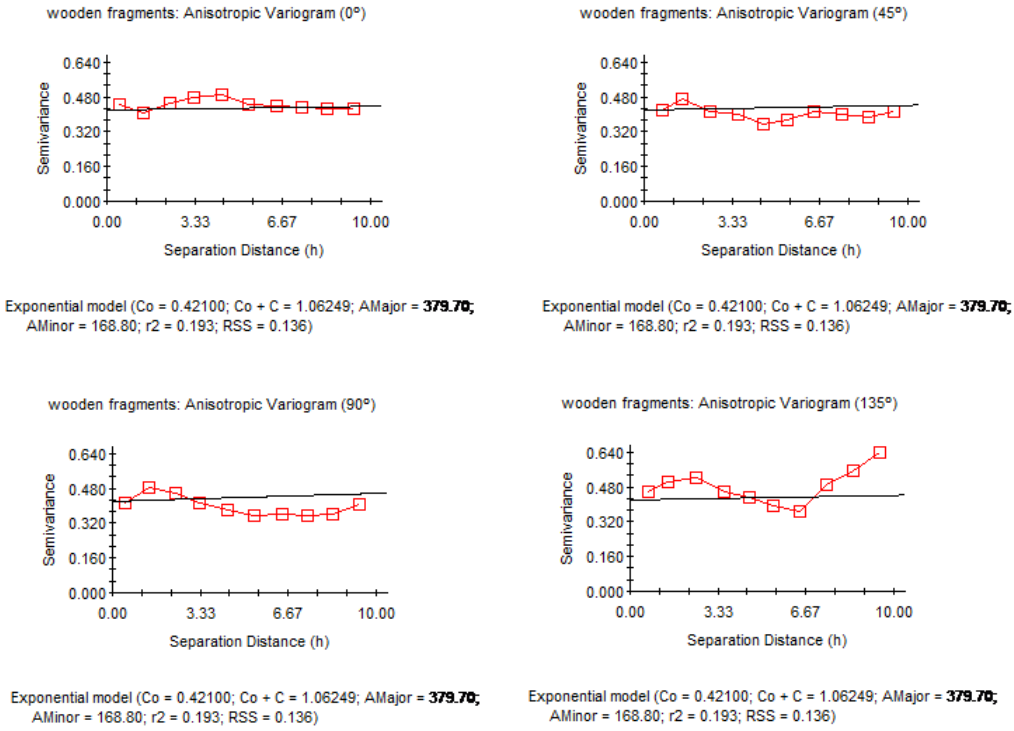

Figure 625 Anisotropic Variogram of wooden fragments recovered during surveys of 2009 (GS+).

The graph of anisotropic Semivariance Surface or Variogram Map (Figure 626) suggests a high impact of anisotropy, which, however, allows the presence of some kind of spatial continuity. Higher values of anisotropy are observed around the North-West and South-East corners.

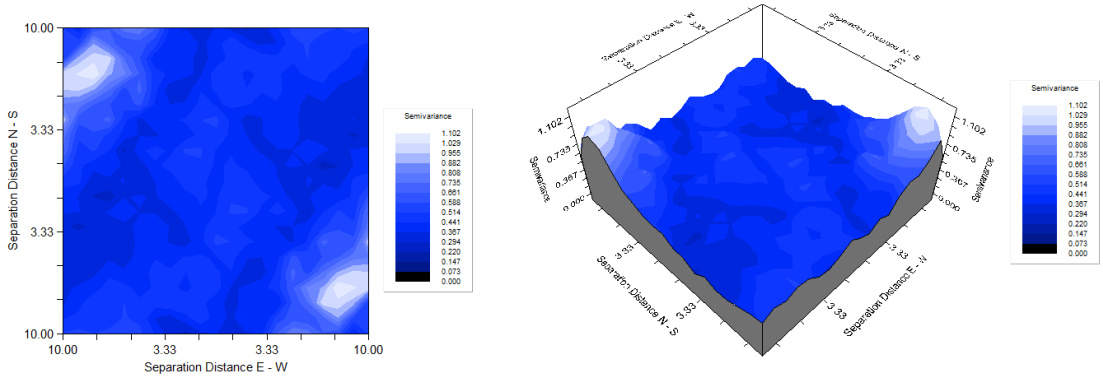

Figure 626 Variogram Map of wooden fragments recovered during surveys of 2009 (GS+).

The best fitted exponential model - C_0 (nugget variance) =0.0100, C_0+C (sill) = 4.270 and A_0 (Range) = 0.01 (Figure 627) does not explain sample variance; therefore, it cannot be used to obtain an interpolated model.

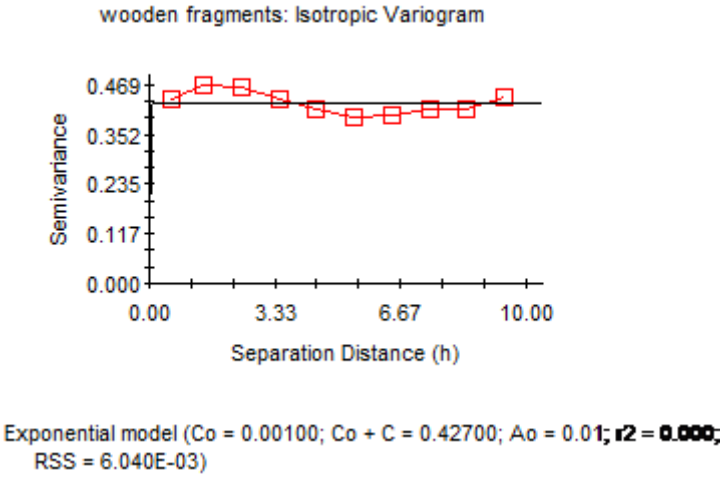

Figure 627 Exponential Isotropic Variogram for wooden fragments recovered during surveys of 2009 (GS+).

8.8.1.1 Wooden fragments within Zone 1 and Zone 2

Within Zone 1 in 89 sampling units have been recovered 167 wooden fragments, while 149 wooden remains belong to 60 cells, located within Zone 2. Such cells were spatially distributed as is showed in Figure 628.

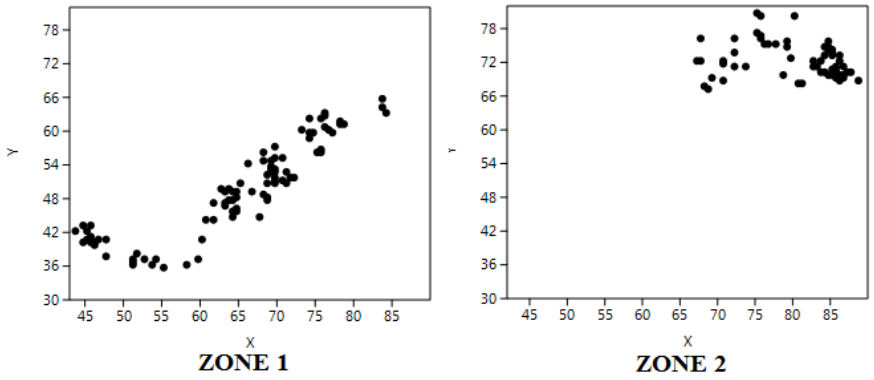

Figure 628 spatial distribution of sampling units where wooden remains have been recorded during surveys of 2009, within Zone 1 and Zone 2 (Past).

Ripley's *k* analysis on the distance between sampling units with wooden fragments evidence suggests the possibility of some degree of spatial clustering for both zones, at the scale of global reference area (Figure 629).

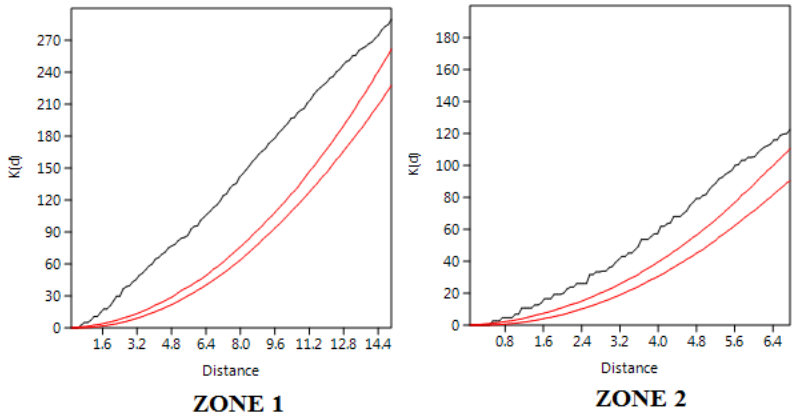

Figure 629 Ripley's *k* analysis on the distance between sampling units with wooden fragments, recorded in surveys of 2009, within Zone 1 and Zone 2 (Past).

Within the convex hull defined by those sampling units with presence of wooden fragments within Zone 1 a clustered spatial pattern is statistically significantly observed (according to Clark and Evans test). Conversely, for Zone 2 and within the convex hull defined by cells where wooden remains have been recorded, the null hypothesis of a random pattern (Poisson process) cannot be rejected at $p<0.05$, according to Clark and Evans test. KDE shows, for Zone 1, the occurrence of a wider central concentration and two further smaller aggruppation located around the South-West corner (between x=42-55 and y=33-45) and around the North-East corner (between x=73-78 and y=57-65); within Zone 2 one sub-sector emerges (located between x=82.5-88 and y=67.5-77) and smaller groups between x=75-80 and y=74-77 and between x=67.5-73 and y=67.5-74 (Figure 630).

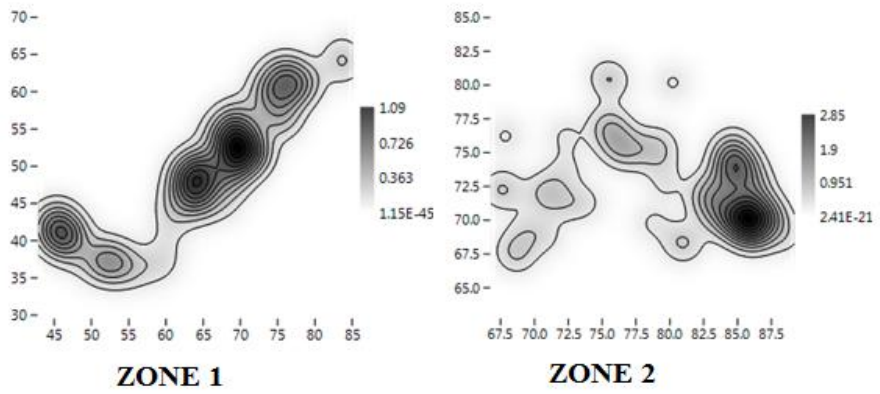

Figure 630 KDEs of sampling units where wooden fragments have been recovered during surveys of 2009, within Zone 1 and Zone 2 (Past).

There are not relevant differences in the spatial location of wooden remains frequencies among both sectors; Zone 1 concentrates more observations (n=167), the range of frequencies is between 1 and 8, with a mean of 1.87 observations per sampling unit and variance = 1.564096. The spatial distribution of wooden fragments in Zone 1 is fitted with a Negative Binomial distribution (with k=0.064 and p=0.338) and a Kolmogorov Smirnov Test=1 (Figure 631). The probability density distribution clearly follows a J-shaped distribution. A break point within the frequencies is observed, both in histogram and box plot, in correspondence with the value of 3 items; furthermore, 3 outliers have been identified (4, 5 and 8).

The Zone 2 concentrates 149 wood remains, the range of frequencies is between 1 and 11, with a mean of 2.48 observations per sampling unit, variance =3.135311 (Figure 631). The spatial distribution of wooden remains in Zone 2 is fitted with a Negative Binomial distribution with k=0.069 and p=0.221 and Kolmogorov Smirnov Test=0.946. The probability density distribution follows a J-shaped distribution. A break point within the frequencies is observed, both in histogram and box plot, in correspondence with the value of 4 items; furthermore, 3 outliers have been identified (7, 8 and 11).

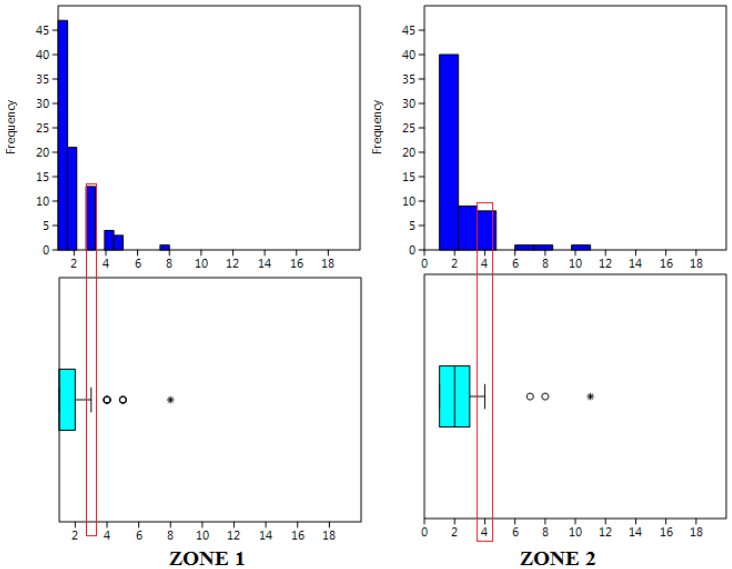

Figure 631 Histograms and box plots of frequencies observed for wooden fragments within Zone 1 and Zone 2 (Past).

The spatial distribution of count data per sampling unit shows, for Zone 1, a Global Moran's *I* of -0.000738. The theoretical (expected) value assuming spatial autocorrelation (lack of spatial Independence) is -0.000756 and the standard error *I* is 0.000756. The test of significance using the normality assumption gave a z value of 0.023703, a quite non-significant value. This result is comparable with those of Geary statistic (*C*=0.999519) and Getis-Ord general G (*G*=0.026605).

The spatial distribution of count data per sampling unit shows, for Zone 2, a Global Moran's *I* of -0.001581. The theoretical (expected) value assuming spatial autocorrelation (lack of spatial Independence) is -0.001621, and the standard error of *I* is 0.001620. The test of significance using the normality assumption gave a *z* value of 0.024453, a highly non-significant value. This result is comparable with those of Geary statistic (*C*=0.999837) and Getis-Ord general G (*G*=0.039453).

Consequently, we can accept that the spatial distribution of wooden fragments for both zones is not significantly different than the expected value under a random distribution. This is what would be expected in the case of the same frequency of wooden fragments in quite every spatial location.

The Moran's *I* Correlogram has been calculated for uniform class distance intervals of 1 metre, and taking into account a 10 meters active lag distance. For Zone 1, *I* value at the starting point is about 0.145, above expected value for randomness, as well as at 1 and 2 metre. As the distance between sampling units increases, *I* value drops off gently reaching *I* values that range on the line (corresponding to spatial randomness) and below the value expected for randomness, according to an irregular pattern (Figure 632). For Zone 2, a quite more regular spatial pattern is attested in the Moran's *I* Correlogram (Figure 632). At the starting point *I* value is about 0.159, above the expected value for randomness. As the distance between sampling unit increases, *I* value drops off quite gently for the first metres (until 5 metres), above the expected value for randomness. From 6 metres values are around and below the expected value for randomness.

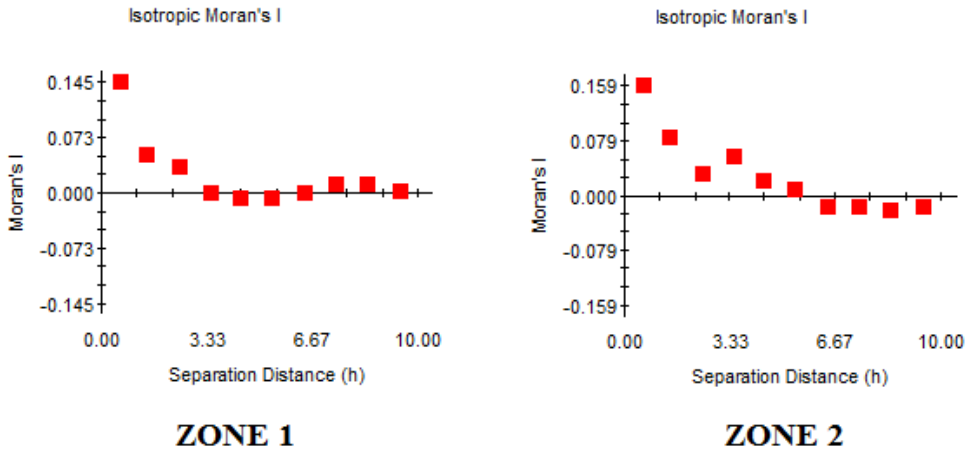

Figure 632 Moran's I Correlograms for wooden fragments recovered during surveys of 2009, within Zone 1 and Zone 3 (GS+).

Such results give the possibility of finding spatially dependent area of 2-3 metres of radius for both zones.

We have explored the possible presence of anisotropic variation at different directions (Figure 633 and 635). The North-East-South-West (45º) direction seems to have less anisotropy than all other directions.

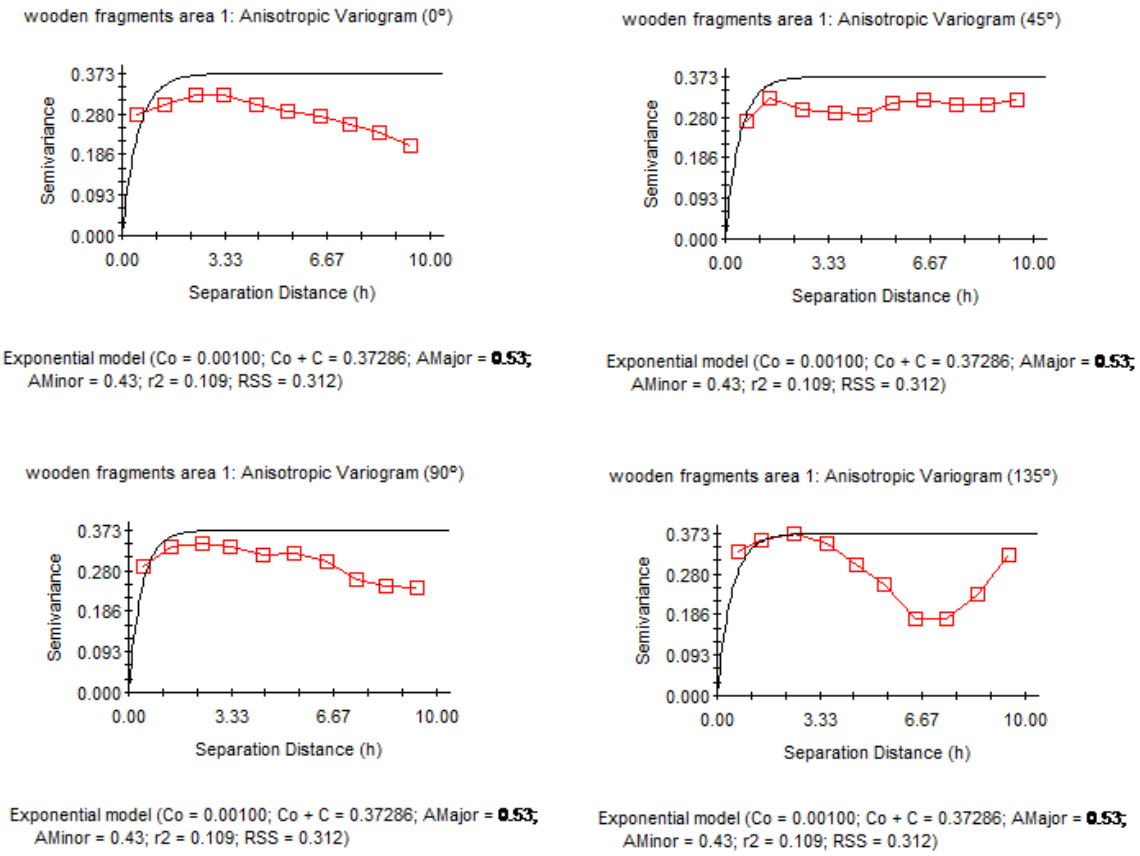

Figure 633 Anisotropic Variogram of wooden fragments recovered during surveys of 2009, within Zone 1 (GS+).

The graph of anisotropic Semivariance Surface or Variogram Map (Figure 634) for Zone 1 does not show high values of anisotropy and it is predominantly concentrated in the North-West and South-East corners.

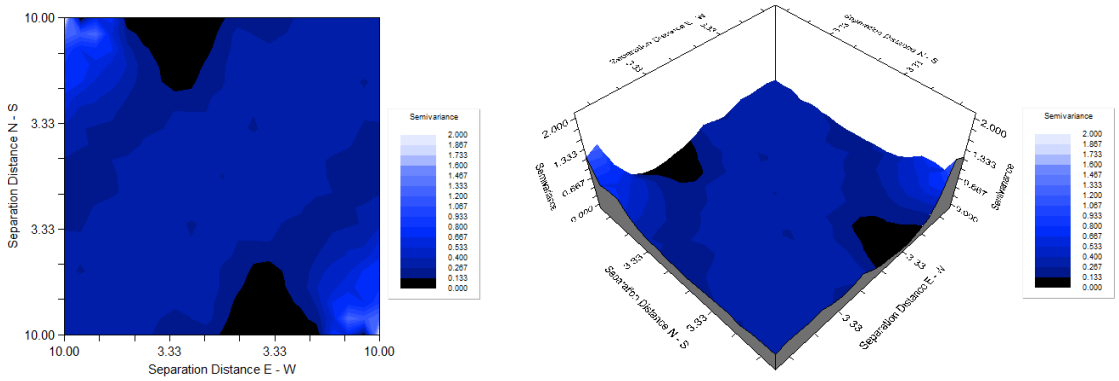

Figure 634 Variogram Map of wooden fragments recovered during surveys of 2009, within Zone 1 (GS+).

Semivariance, related to Zone 2, seems to vary strongly at any distance (Figure 635).

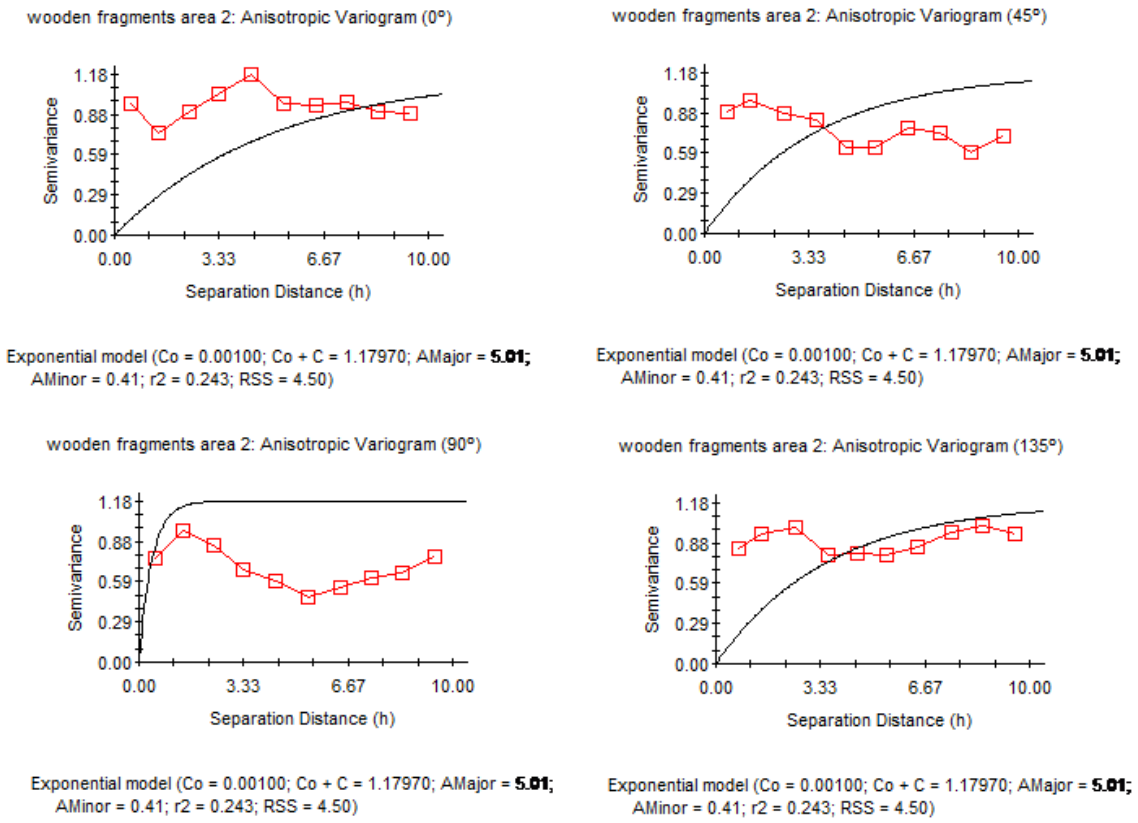

Figure 635 Anisotropic Variogram of wooden fragments recovered during surveys of 2009, within Zone 2 (GS+).

For Zone 2 higher values of anisotropy are observed, with peaks particularly concentrated in the North-West and South-East corners (Figure 636).

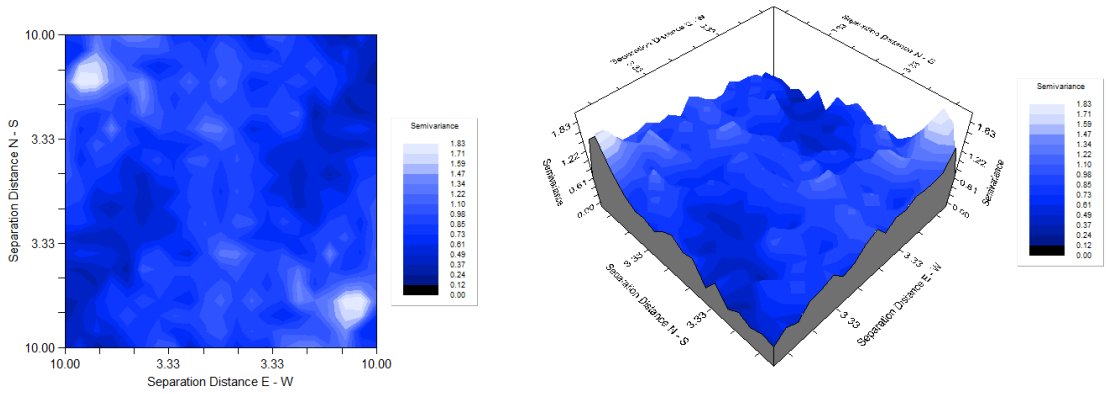

Figure 636 Variogram Map of wooden fragments recovered during surveys of 2009, within Zone 2 (GS+).

The best fitted exponential model for Zone 1 - C_0 (nugget variance) =0.1720, C_0+C (sill) = 0.29740 and A_0 (Range) = 0.15- explains only 0.004% of sample variance (Figure 637). In the same way, for Zone 2 the best fitted exponential model shows C_0 (nugget variance) =0.08200, C_0+C (sill) = 0.81700 and A_0 (Range) = 0.01. It does not explain the sample variance (Figure 637).

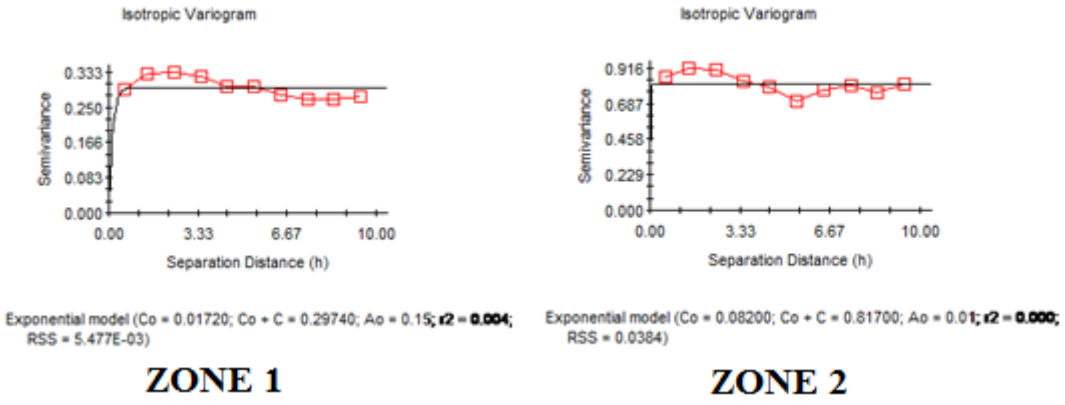

Figure 637 Exponential Isotropic Variograms for wooden fragments recovered during surveys of 2009, within Zone 1 and Zone 2 (GS+).

Although not entirely reliable, a predictive model for the frequency of wooden fragments distribution within Zone 1 (Figure 638) shows main concentrations located around the South-West corner and in the centre of the surveyed area, with a further aggruppation around the North-East corner. Such interpolated result is predominantly in agreement with what obtained throughout the Kernel Density estimation (see above).

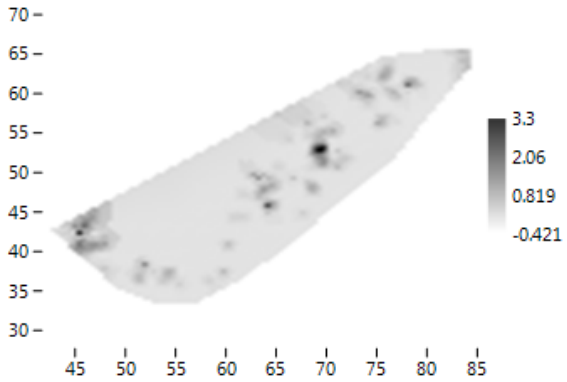

Figure 638 Graphic results of Inverse distance weighting calculated for wooden fragments recovered during surveys of 2009 within Zone 1 (Past).

8.8.2 Remains of horizontal posts

316 fragments related to horizontal posts were identified and counted; they are spatially distributed in 67 sampling units. Cells where horizontal posts remains have been recovered are spatially distributed as showed in Figure 639.

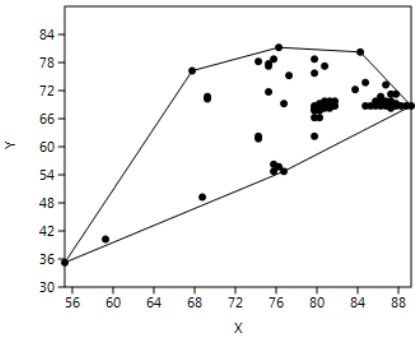

Figure 639 spatial distribution of sampling units where horizontal posts remains have been recorded during surveys of 2009 (Past).

Ripley's *k* analysis (Figure 640) on the distance between sampling units with horizontal posts remains, suggests the possibility of some degree of spatial clustering, at the scale of global reference area.

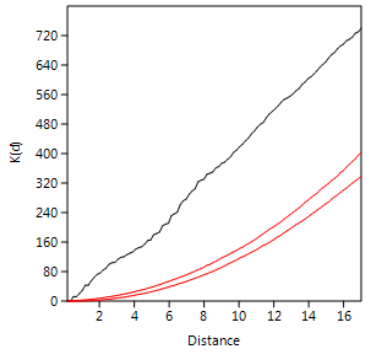

Figure 640 Ripley's *k* analysis on the distance between sampling units with horizontal posts remains, recorded in surveys of 2009 (Past).

Within the convex hull defined by the sampling units where horizontal posts have been recovered, such cells are statistically significantly clustered, according to Clark and Evans test. A Kernel density Estimation (Figure 641) shows the presence of horizontal posts remains particularly concentrated in Zone 2 (between x=76-88 and y=64-74 and between x=70-80 and y=74-80), while within Zone 1 there is a only one small aggrupation of remains between x=74-76 and y=54-56.

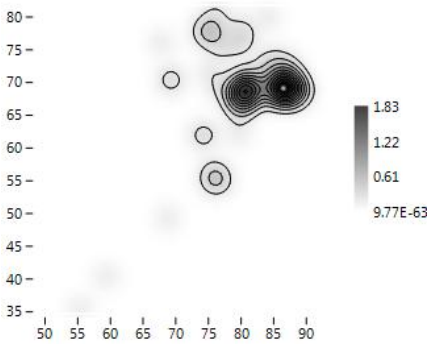

Figure 641 KDE of sampling units where horizontal posts remains have been recovered during surveys of 2009 (Past).

When considering the raw quantity of horizontal posts at each cell, the probability density distribution of spatial frequencies does not follow a J-shaped distribution. A majority of sampling units have raw counts of horizontal posts remains of less than 3 elements (global mean=2.10 observations per sampling unit). Two cells are distinguished from the majority (representing outliers), with 7 and 8 remains of horizontal posts. A break point in frequencies of such remains was observed, both in histogram and box plot, in correspondence with the value of 5 items (Figure 642).

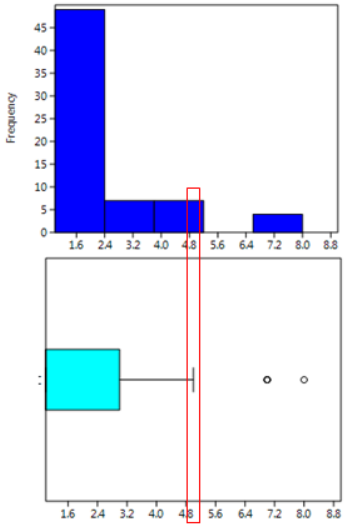

Figure 642 Histogram and box plot of frequencies observed for horizontal posts remains (Past).

The Negative Binomial distribution with k=0.027 and p=0.269 fits with the observed frequencies of horizontal posts, according to the Kolmogorov Smirnov Test=1.00. This condition suggests randomness in the spatial distribution of the abundance of horizontal posts fragments per sampling unit (Figure 643).

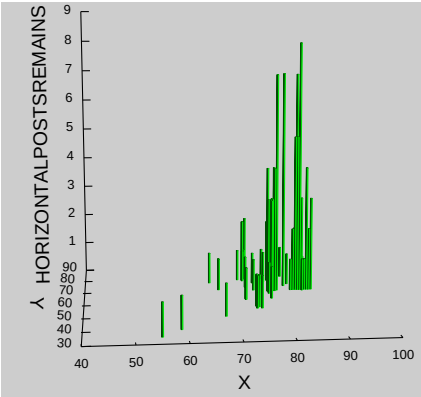

Figure 643 3D Histogram of horizontal posts remains recovered during surveys of 2009 (Systat 13).

79% of horizontal posts remains are located in 94% of the effectively surveyed area, in such a way that only 4 cells show more than 5 items (representing, this value, the break point highlighted by both box plot and histogram).

The spatial centroid of the area with horizontal posts remains, calculated using an abundance weighted mean spatial center is is x= 82.267730, y= 68.998227, with 5.45 m of standard deviation along the *x* axis, and 5.76 m along the *y* axis. A standard deviation ellipse, with a long axis of 18.90 m and a short one of 12.30 m, delimits an area of 182.49 square meters, where most count data appear. It has been estimated an average density of 0.05 objects per square meter.

The spatial distribution of the abundance of horizontal posts remains per sampling unit gives a Global Moran's *I* of -0.000283. The theoretical (expected) value assuming spatial autocorrelation (lack of spatial independence) is -0.000515 and the standard error is 0.000515. The test of significance using the normality assumption gave a highly non significant *z* value of 0.450220. Consequently, we can accept that the spatial distribution of horizontal posts fragments is not different than the expected value under a random distribution. This is what would be expected in the case of the same frequency of items in quite every spatial location. Those results are comparable with those of the Gear statistic (*C*=0.998202) and Getis-Ord general G (*G*= 0.082818).

The Moran's *I* Correlogram (Figure 644) has been calculated for uniform class distance intervals of 1 meter, and taking into account a 10 metres active lag distance. *I* value at 0.50 distance is 0.367, above the expected value for randomness. As the distance between sampling units increases, *I* value drops off quite gently and continuously above the expected value for randomness and in some cases reaching such value. This result gives the possibility of finding spatially dependent areas of 3-4 metres of radius.

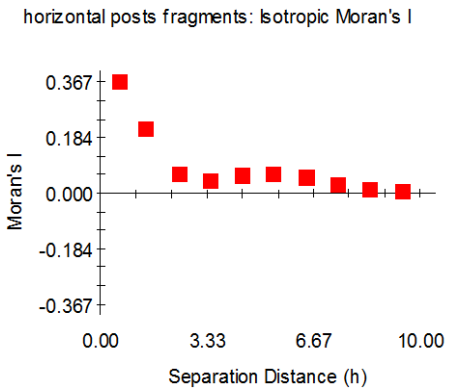

Figure 644 Moran's I Correlogram for horizontal posts remains recovered during surveys of 2009 (GS+).

We have explored the possible presence of anisotropic variation at different directions (Figure 645). No homogeneous variation of semivariance at 0 º, 45º, 90º and 135º are observed, suggesting the presence of anisotropy.

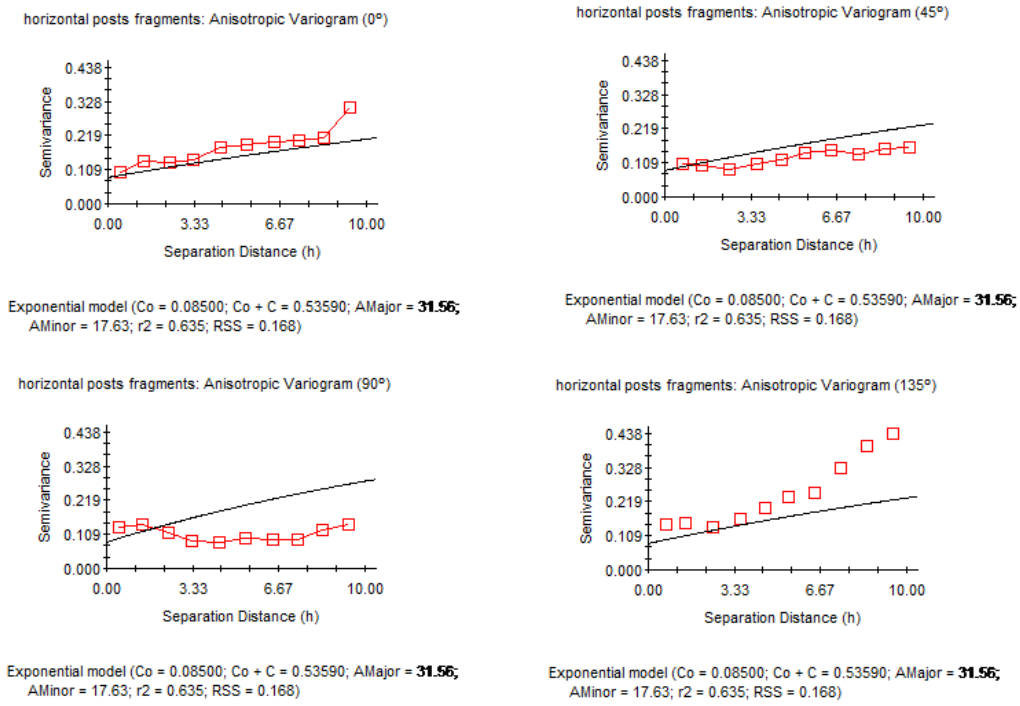

Figure 645 Anisotropic Variogram horizontal posts remains recovered during surveys of 2009 (GS+).

The graph of anisotropic Semivariance Surface or Variogram Map suggests a particular concentration of anisotropy in the centre of 3D diagram and around the opposite North-West and South-East corners, with peaks near the corner (Figure 646).

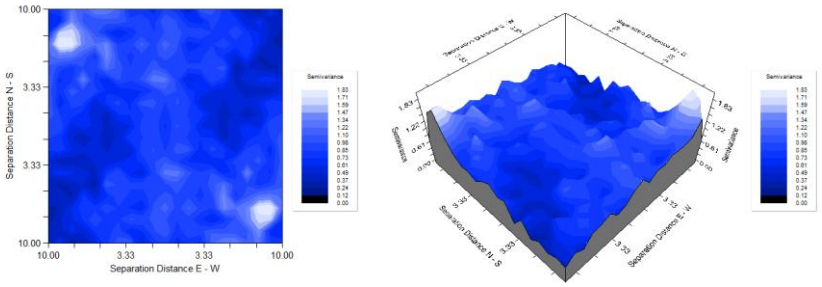

Figure 646 Variogram Map of horizontal posts remains recovered during surveys of 2009 (GS+).

The best fitted exponential model - C_0 (nugget variance) =0.010000, C_0+C (sill) = 4.8300 and A_0 (Range) = 30.99 - explains 86.7% of sample variance (Figure 647).

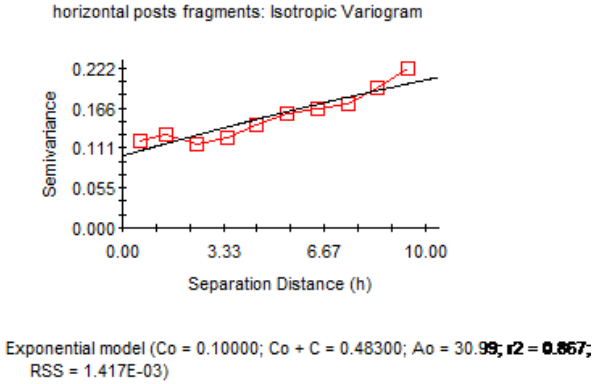

Figure 647 Exponential Isotropic Variogram for horizontal posts remains recovered during surveys of 2009 (GS+).

Using this variogram model, we have obtained a representation of the scalar field of the horizontal posts remains distribution using a kriging algorithm (Figure 648). It is easy to see a spatial continuity in the North-East side where the horizontal posts remains seem to be aggrupated, in contrast with the emptiness which characterizes the remaining zones. It is also important to remark that the interpolation is performed taking into account as highest value 3.80. This means that both higher values and outliers have not been considered.

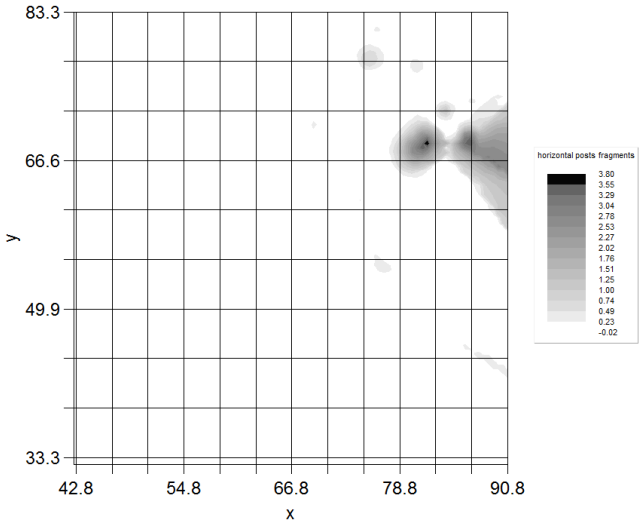

Figure 648 Graphic results of kriging calculated for horizontal posts remains recovered during surveys of 2009 (GS+).

8.8.2.1 Remains of horizontal posts within Zone 1 and Zone 2

Within Zone 1, in 10 sampling units cells have been recovered 10 horizontal posts remains, while 131 fragments belong to 57 cells located within Zone 2. Such cells were spatially distributed as is showed in Figure 649.

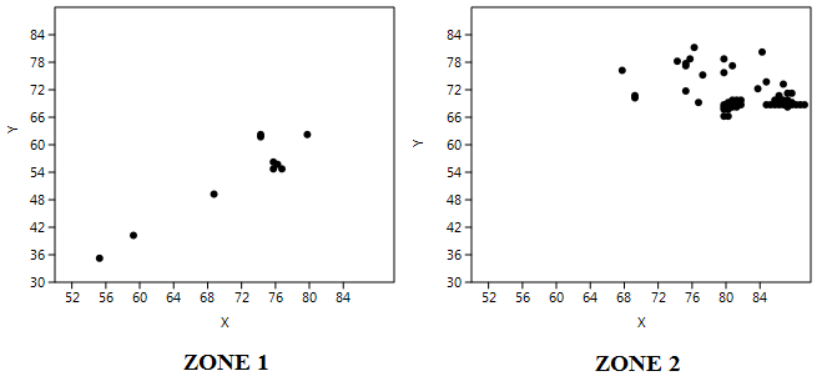

Figure 649 spatial distribution of sampling units where horizontal posts remains have been recorded during surveys of 2009, within Zone 1 and Zone 2 (Past).

Ripley's *k* analysis on the distance between sampling units with horizontal posts, at the scale of global reference area, suggests the possibility of some degree of spatial clustering only between 6 and 12 metres for Zone 1. Conversely, between 0.8 and 7.5 there is possibility of some degree of spatial clustering for Zone 2 (Figure 650).

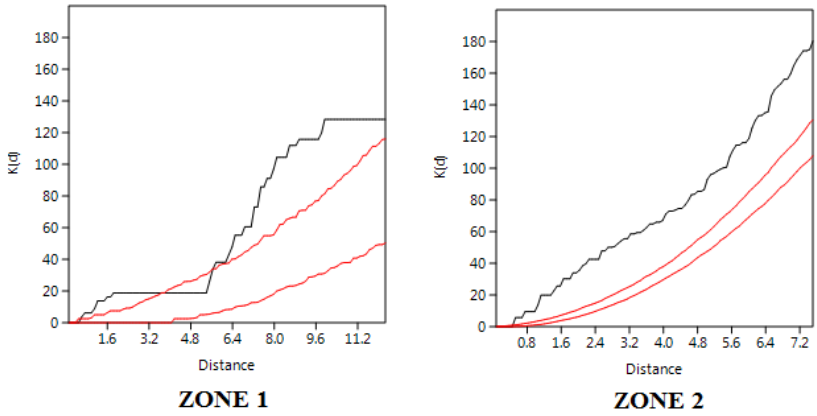

Figure 650 Ripley's *k* analyses on the distance between sampling units with horizontal posts remains, recorded in surveys of 2009, within Zone 1 and Zone 2 (Past).

Within the convex hull defined by the sampling units where horizontal posts have been recovered, for such cells are, within both zones, the null hypothesis of a random pattern (Poisson process) cannot be rejected at $p<0.05$, according to Clark and Evans test. KDEs (Figure 651) show, for Zone 1, the occurrence of a wider concentration, sub-divided in two main aggrupations around the North-East corner and further smaller concentrations located in the centre of the surveyed area and around the South-West corner. Within Zone 2 two main close concentrations are observed, located between x=82.5-88 and y=67.5-77, and smaller concentrations between x=75-80 and y=74-77 and between x=67.5-73 and y=67.5-74.

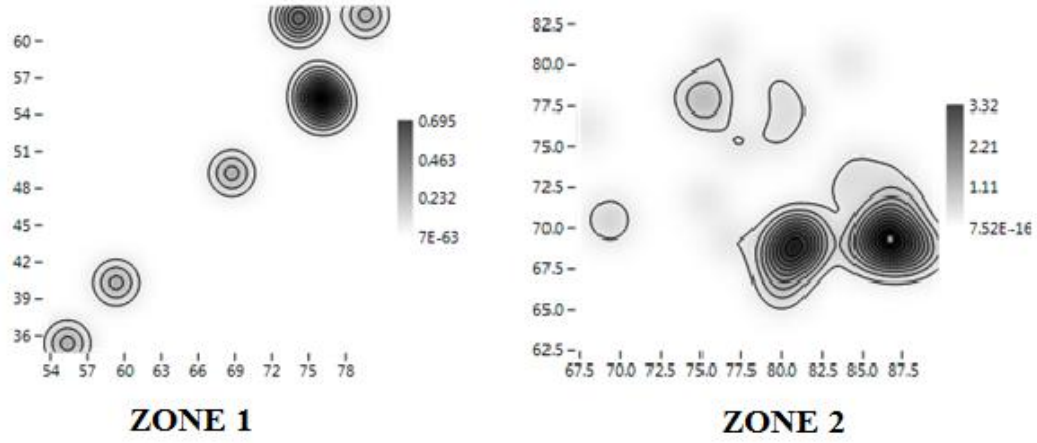

Figure 651 KDEs of sampling units where horizontal posts remains have been recovered during surveys of 2009 within Zone 1 and Zone 2 (Past).

There are relevant differences in the spatial location of frequencies in which horizontal posts remains are observed; Zone 1 concentrates low observations (n=10), with only 1 presence in each cell[41]. The spatial distribution of horizontal posts remains within Zone 1 is fitted with a Poisson distribution (with λ=0.008) and a Kolmogorov Smirnov Test=1.000. The probability density distribution does not follow a J-shaped distribution. Zone 2 concentrates majority of observations (n=131), the range of frequencies is between 1 and 8, with a mean of 2.29 observations per sampling unit and a variance =3.177318 (Figure 652). The spatial distribution of horizontal posts remains within Zone 2 is fitted with a Negative Binomial distribution with k=0.069 and p=0.246 and Kolmogorov Smirnov Test=1.000. The probability density distribution clearly does not completely follow a J-shaped distribution. A break point in the frequencies of horizontal posts remains within Zone 2 is observed in correspondence with 5 items; furthermore, two outliers are identified (corresponding to 7 and 8 items).

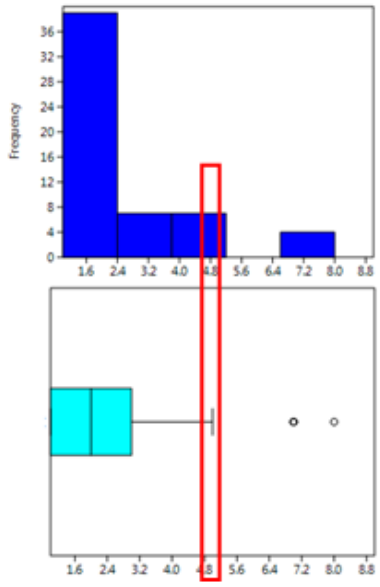

Figure 652 Histogram and box plot of frequencies observed for horizontal posts remains within Zone 2 (Past).

[41] the scarce presence of such remains within Zone 1 does not allow to produce histogram and box plot

The spatial distribution of count data per sampling unit shows, for Zone 1, a Global Moran's *I* of -0.000732. The theoretical (expected) value assuming spatial autocorrelation (lack of spatial Independence) is -0.000756 and the standard error *I* is 0.000756. The test of significance using the normality assumption gave a highly non-significant z value of 0.031763. This result is comparable with those of Geary statistic (*C*=0.998626) and Getis-Ord general G (*G*=0.066667).

The spatial distribution of count data per sampling unit shows, for Zone 2, a Global Moran's *I* of -0.001432. The theoretical (expected) value assuming spatial autocorrelation (lack of spatial Independence) is -0.001621, and the standard error of *I* is 0.001621. The test of significance using the normality assumption gave a highly non significant *z* value of 0.116596. This result is comparable with those of Geary statistic (*C*=0.999315) and Getis-Ord general G (*G*=0.095912).

Consequently, we can accept that the spatial distribution of horizontal posts fragments for both areas is not significantly different than the expected value under a random distribution. This is what would be expected in the case of the same frequency of remains in quite every spatial location.

The Moran's *I* Correlograms (Figure 653) have been calculated for uniform class distance intervals of 1 metre, and taking into account a 10 metres active lag distance. For Zone 1, a very irregular pattern is observed, with scarce relevant *I* values (all around zero). For Zone 2, a quite more regular spatial pattern is attested. At the starting point *I* value is about 0.447, above the expected value for randomness. As the distance between sampling unit increases, *I* value drops off quite gently for the first metres (until 6 metres), above the expected value for randomness. From 6 metres, the values are around and below the expected value for randomness. For Zone 2 such result gives the possibility of finding spatially dependent area of 2-3 metres of radius.

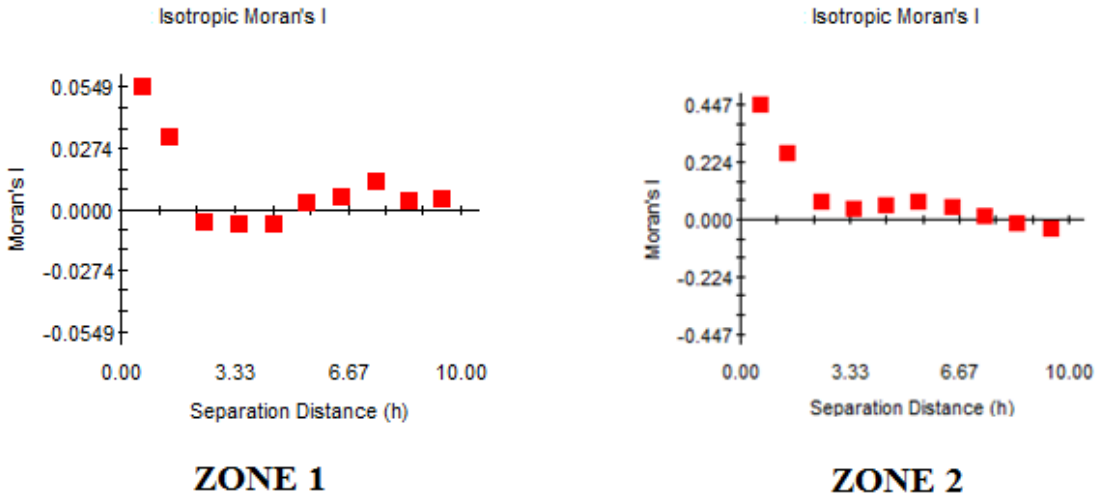

Figure 653 Moran's I Correlograms for horizontal posts remains recovered during surveys of 2009, within Zone 1 and Zone 2 (GS+).

We have explored the possible presence of anisotropic variation at different directions (Figures 654 and 656); for Zone 1 no homogeneous variations of semivariance are observed at any distance.

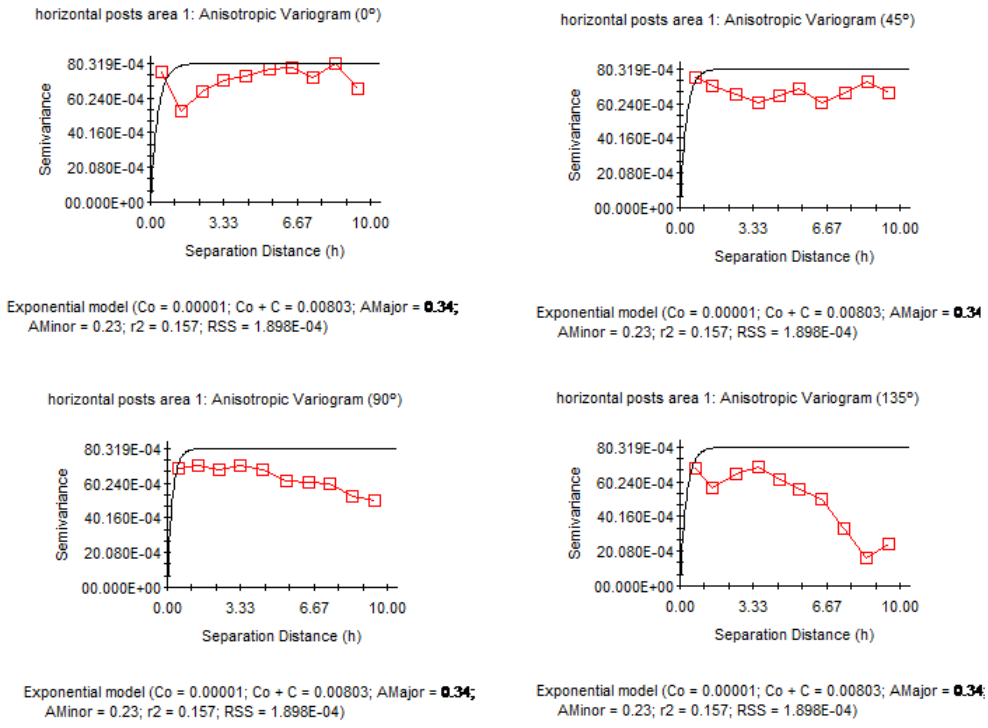

Figure 654 Anisotropic Variogram horizontal posts remains recovered during surveys of 2009, within Zone 1 (GS+).

The graph of anisotropic Semivariance Surface for Zone 1 (Figure 655) shows that anisotropy is particularly attested in the centre of the surveyed area and, in some way, also in the North-West and South-East corners.

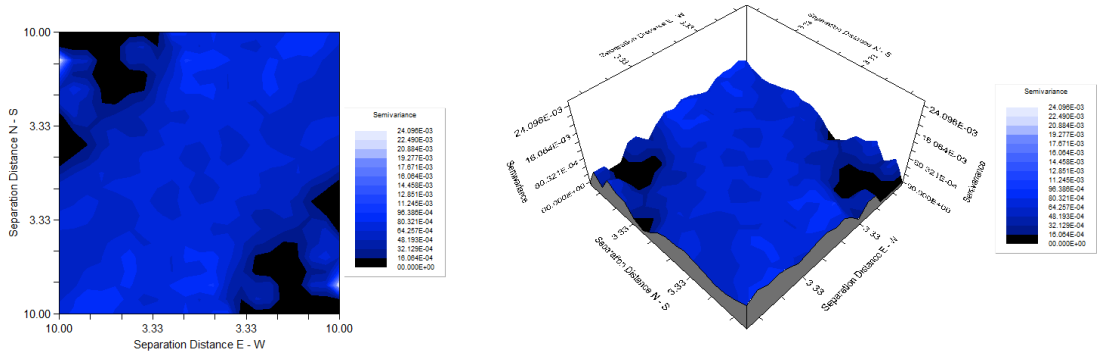

Figure 655 Variogram Map of horizontal posts remains recovered during surveys of 2009, within Zone 1 (GS+).

For Zone 2 (Figure 656) an irregular variation of semivariance at different degrees is attested, confirming the presence of anisotropy.

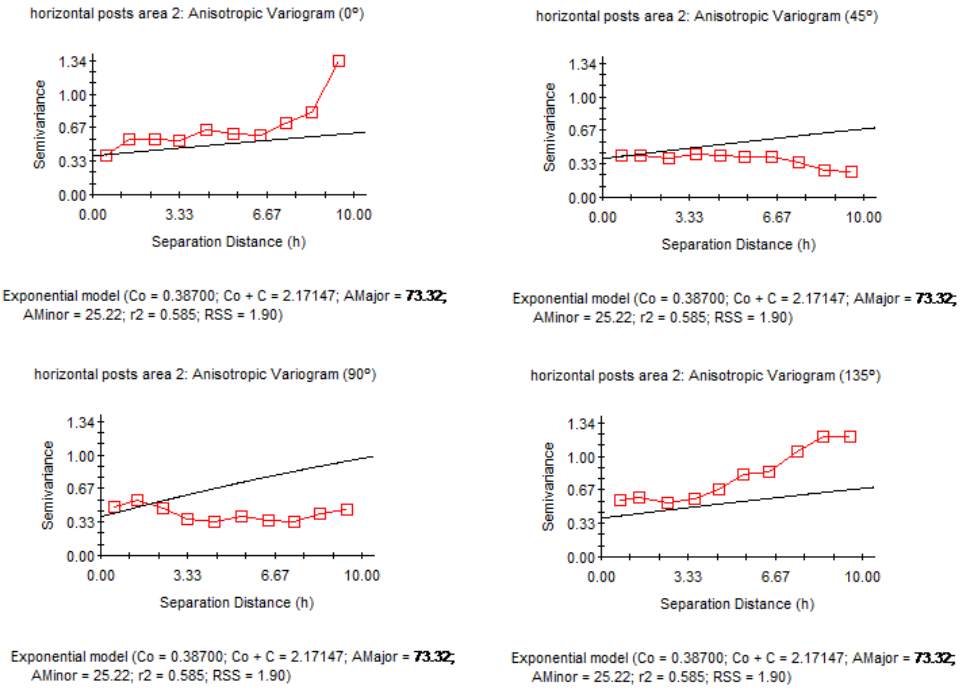

Figure 656 Anisotropic Variogram horizontal posts remains recovered during surveys of 2009, within Zone 2 (GS+).

The graph of anisotropic Semivariance Surface for Zone 2 (Figure 657) shows that, however, compared with Zone 1,such sector is lower affected by anisotropy that is observed, with higher values, in the Northest and Southest side of the 3D diagram, particularly around the North-West and South-East corners.

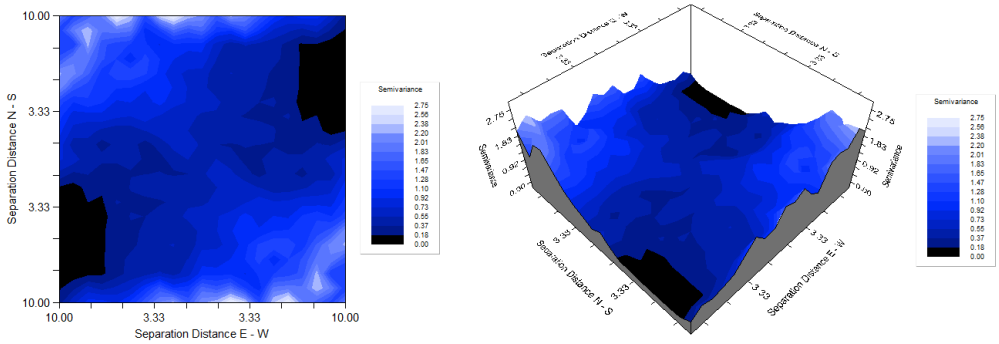

Figure 657 Variogram Map of horizontal posts remains recovered during surveys of 2009, within Zone 2 (GS+).

The best fitted exponential model for Zone 1 - C_0 (nugget variance) =0.00001, C_0+C (sill) = 0.00648 and A_0 (Range) = 0.01- does not explain the sample variance (Figure 658); for such zone it cannot be used to obtain an interpolated model. Conversely, for Zone 2, the best fitted model -C_0 (nugget variance) =0.00100, C_0+C (sill) = 0.55700 and A_0 (Range) = 0.34 - explains 14.9% of sample variance.

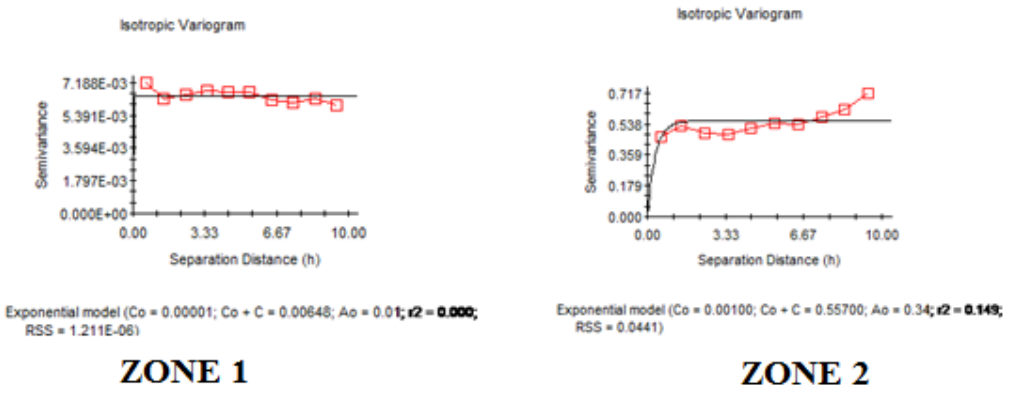

Figure 658 Exponential Isotropic Variograms for horizontal posts remains recovered during surveys of 2009, within Zone 1 and Zone 2 (GS+).

Using this variogram model for Zone 2, a representation of the scalar field of the horizontal posts remains distribution was obtained using a kriging algorithm (Figure 659). It is evident a spatial discontinuity in the centre of the surveyed area, where observations seem to be predominatly absent. They are mainly concentrated in the South-West corner (between x=75-90 and y=66-70 and between x=82-84 and y=70-72). However, it is also important to remark that the interpolation is performed taking into account as highest value 3.80. This means that both higher values and outliers have not been considered.

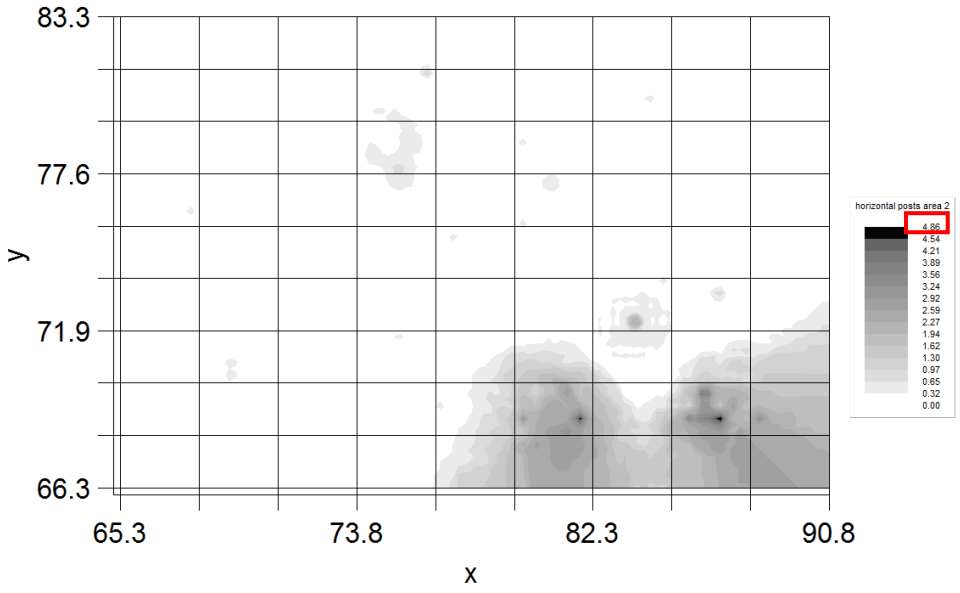

Figure 659 Graphic results of Kriging calculated for horizontal posts remains recovered during surveys of 2009 within Zone 2 (GS+).

8.9 Concotto remains

This category includes both concotto fragments as well as remains of concotto slabs (for more details see Chapter 5). 21 fragments were identified and counted; they were spatially distributed in 40 cells. 1921 were the surveyed empty cells, while the sampling unit with more presence gave 2 items. A frequency mean of 0.10 and a standard deviation of 0.10 were counted. Sampling units where concotto remains have been recovered are spatially distributed as showed in Figure 660.

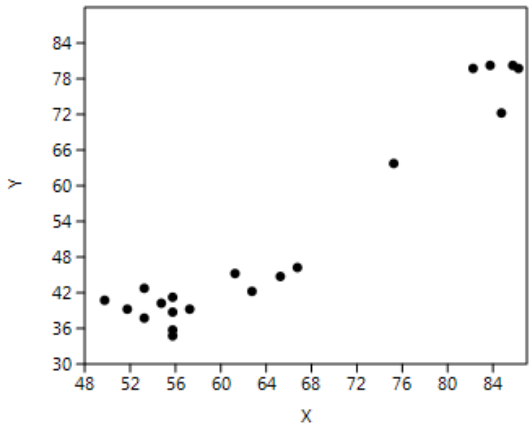

Figure 660 spatial distribution of sampling units where concotto remains have been recorded during surveys of 2009 (Past).

Ripley's *k* analysis (Figure 661) on the distance between sampling units with concotto evidence suggests the possibility of some degree of spatial clustering, at the scale of global reference area.

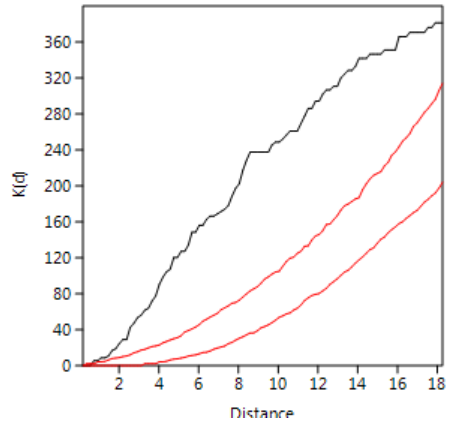

Figure 661 Ripley's *k* analysis on the distance between sampling units with concotto remains, recorded in surveys of 2009 (Past).

Within the convex hull defined by sampling units where concotto remains have been recovered, for such cells the null hypothesis of a random pattern (Poisson process) cannot be rejected at $p<0.05$, according to Clark and Evans test. A Kernel density estimation (Figure 662) shows the presence of concotto fragments in both different zones: within Zone 1, they are located particularly between x=47-70 and y=33-48 (sub-divided in two predominant concentrations). Within Zone 2 they are instead observed between x=80-90 and y=70-80 and single presences are attested between x=72-75 and y=60-65 and between x=82-87 and y=70-75.

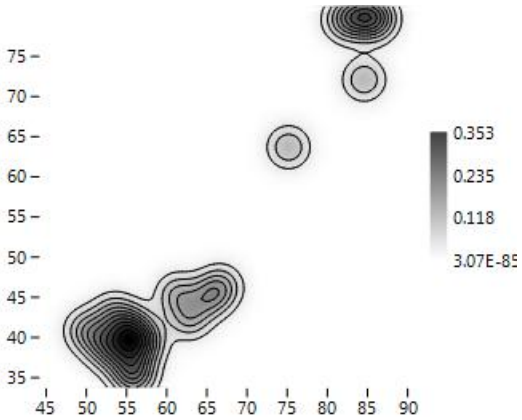

Figure 662 KDE of sampling units where concotto remains have been recovered during surveys of 2009, within Zone 1 and Zone 2 (Past).

A majority of sampling units have raw counts of concotto remains of less than 2 elements (global mean=1.05 observations per sampling unit). One cell distinguishes from the majority (representing outlier), with 2 concotto remains (Figure 663).

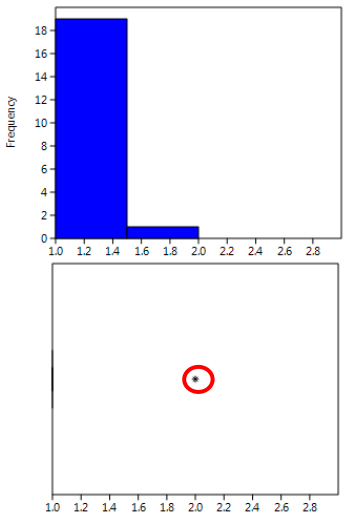

Figure 663 Histogram and box plot of frequencies observed for concotto remains (Past).

The spatial distribution of concotto fragments is fitted with a Geometric distribution (with p=0.989) Negative Binomial distribution (with k=0.120 and p=0.917) and a Poisson distribution (with λ=0.011) and Kolmogorov Smirnov Test=1. This is what is expected when, as in this case, the sample consists in predominant empty sampling units and similar frequencies values in all non-empty cells, obtaining randomness (as also showed in Figure 664).

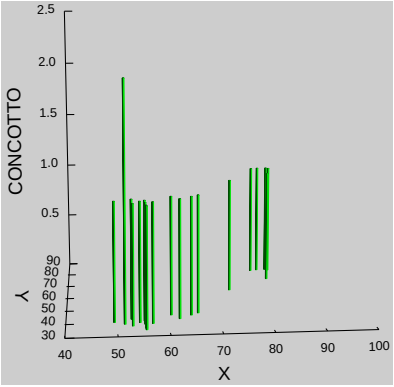

Figure 664 3D Histogram of concotto fragments recovered during surveys of 2009 (Systat 13).

95% of concotto fragments are located in 95% of the effectively surveyed area, in such a way that only 1 cell shows more than 1 item.

The spatial centroid of the area with concotto remains, calculated using an abundance weighted mean spatial center is is x= 64.226190, y= 50.678571, with 13.04 m of standard deviation along the *x* axis, and 16.98 m along the *y* axis. A standard deviation ellipse with a long axis of 30.78 m and and a short one of 4.22 m delimits an area of 407.95 square meters, where most count data appears. It has been estimated an average density of 0.008 items per square meter.

The spatial distribution of the abundance of concotto fragments per sampling unit gives a Global Moran's *I* result of -0.000522. The theoretical (expected) value assuming spatial autocorrelation (lack of spatial independence) is -0.000515 and the standard error is 0.000515. The test of significance using the normality assumption gave a highly non-significant *z* value of 0.011795. These results are comparable with those of the Geary statistics (*C*=0.998612) and Getis-Ord general G (*G*= 0.009569). Consequently, we can accept that the spatial distribution of concotto fragments is not different than the expected value under a random distribution. This is what would be expected in the case of the same frequency of concotto remains in every spatial location.

The Moran's *I* Correlogram (Figure 665) has been calculated for uniform class distance intervals of 1 metre, and taking into account a 10 metres active lag distance. *I* value are in all cases below the expected value for randomness indicating a quite predominant random pattern.

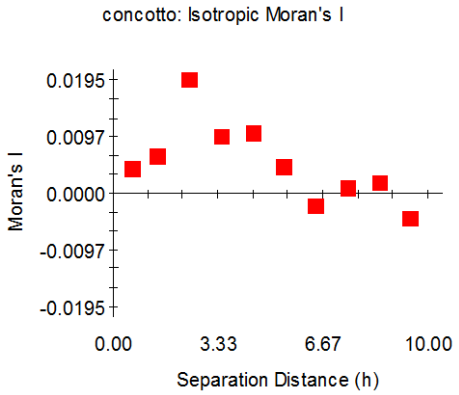

Figure 665 Moran's I Correlogram for concotto fragments recovered during surveys of 2009 (GS+).

We have explored the possible presence of anisotropic variation fitting a theoretical variogram at different directions (Figure 666). Homogeneous variations of semivariance are only observed at the first distances only in the 45 º and 90 º. Indeed, semivariance varies strongly particularly at 0º and 135º.

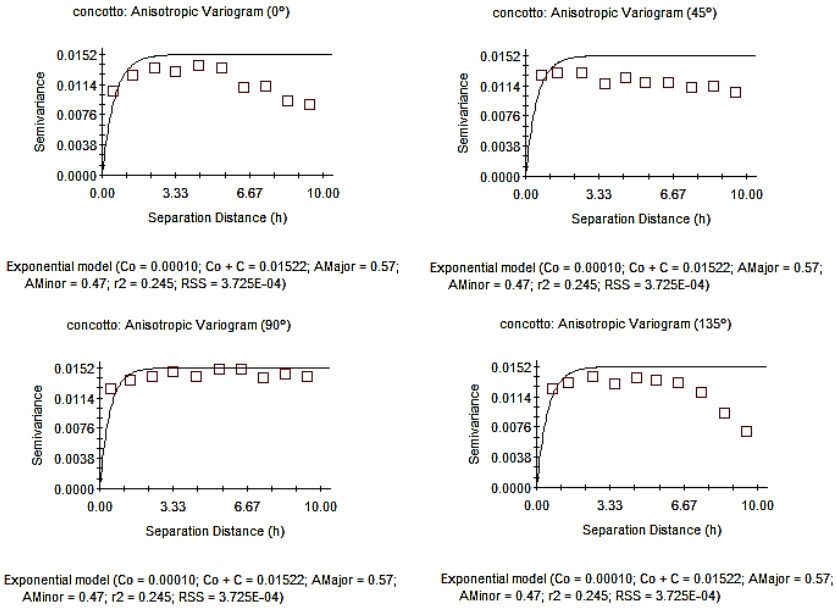

Figure 666 Anisotropic Variogram of concotto remains recovered during surveys of 2009 (GS+).

The graph of anisotropic Semivariance Surface or Variogram Map (Figure 667) shows that anisotropy seems to be particularly concentrated in the centre of the surveyed area with some peaks particularly around the Western and Eastern side of the 3D diagram.

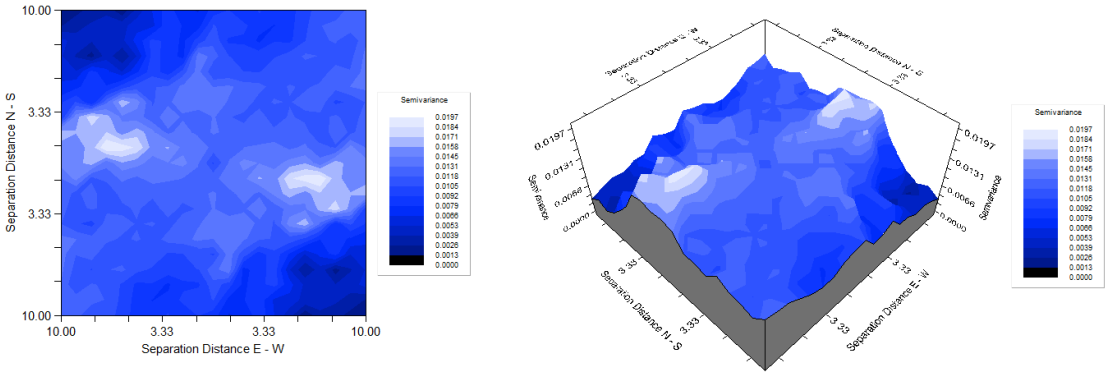

Figure 667 Variogram Map of concotto remains recovered during surveys of 2009 (GS+).

The best fitted exponential model (Figure 668) - C_0 (nugget variance) =0.00231, C_0+C (sill) = 0.01262 and A_0 (Range) = 0.20- does not explain the spatial variance; for this condition it cannot be used to obtain an interpolated model.

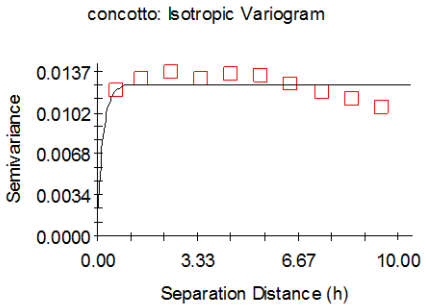

Exponential model (Co = 0.00231; Co + C = 0.01262; Ao = 0.20; r2 = 0.028; RSS = 8.368E-06)

Figure 668 Exponential Isotropic Variogram for concotto remains recovered during surveys of 2009 (GS+).

8.10 MULTIDIMENSIONALITY OF SPATIAL RELATIONSHIPS

8.10.1 Introduction

The results of geostatistical intra-site spatial analyses suggest the existence of two differentiated zones. To know better the spatial organization of these two zones, the spatial correlation of main variables is analysed.

8.10.2 Selecting the most relevant areas (cells with the highest frequencies)

As it has been already mentioned in this chapter, the high amount of sampling units with very low counts of data may alter the correlation structure. Therefore, we have selected cells with the highest counts of each archaeological functional category. "Highest" means here what has been considered "outlier" in preceding analysis, that is those sampling units clearly beyond the interquartile range. Local indicators of spatial association have also been taken into account to select locations with higher relevance.

The following figures (Figure 669) depict the localization of cells with higher measures of positive autocorrelation using Local Moran one dimensional analysis. The Local Moran statistic $I_{i,t}$ is positive when values at neighbouring locations are similar, and negative if they are dissimilar. Given a Null Hypothesis of no association between the value observed at a location and values observed at nearby sites, that is, where values of Moran *I* are close to zero, we have selected those cells for which this hypothesis was below the 0.05 threshold of statistical relevance. Monte Carlo randomizations, using conditional randomization, have been used for evaluating the significance of Local Moran statistic values (Jacquez et al. 2014).

Figure 669 Localization of cells with higher measures of positive autocorrelation for each category of evidence, using Local Moran one dimensional analysis (SpaceStat 4).

In all cases, zones with significant positive autocorrelation are very small (3-4 metres at the maximum).

VERTICAL POSTS: cells with significant higher frequency, surrounded by neighbour sampling units with also high frequencies (Positive Correlation), are concentrated in Nort-Eastern extreme of the distribution, in front of the significant concentrations of horizontal posts. There is not any significant area of spatial continuity of low frequency, but overdispersed outliers with significant higher than expected, or lower than expected, frequencies. The higher than expected seem to be concentrated on the Southern part of the surveyed area, whereas lower frequency than expected appears at the North-Eastern corner, just in front of the positive autocorrelation areas.

SADDLE QUERNS: cells with significant higher frequency, surrounded by neighbour sampling units with also high frequencies (Positive Correlation), are aligned in the Southern part of the distribution, along the edge nearer to the estimated shoreline. Overdispersed outliers of higher and lower than expected frequencies are observed in front of this alignment. Not significant values (lack of spatial correlation) are attested in North-Eastern corner.

FAUNA: cells with significant higher frequency, surrounded by neighbour sampling units with also high frequencies (Positive Correlation), are concentrated in South-Western extreme of the distribution. Low frequency cells surrounded by equally low frequency are concentrated on the opposite North-Eastern corner. Spatial continuity is statistically significant at both extremes of the surveyed area, but with opposite sign at both extremes. Negative autocorrelation (high frequency, surrounded by cells of low frequency) are very scarce and notoriously overdispersed.

POTTERY: cells with significant higher frequency, surrounded by neighbour sampling units with also high frequencies (Positive Correlation), are concentrated in South-Western extreme of the distribution. Low frequency cells surrounded by equally low frequency are concentrated on the opposite North-Eastern corner. Spatial continuity is statistically significant at both extremes of the surveyed area, but with opposite sign at both extremes. Negative autocorrelation (high frequency, surrounded by cells of low frequency) are very scarce and notoriously overdispersed.

LITHIC INDSTRY: overdispersed outliers of higher and lower than expected frequencies. A random distribution is observed.

WOODEN FRAGMENTS*:* cells with significant higher frequency, surrounded by neighbour sampling units with also high frequencies (Positive Correlation), are concentrated in North-Eastern extreme of the distribution, probably in connection with horizontal and vertical posts, but not eactly in the same locations. There is a secondary concentration of positive autocorrelation in the center of the surveyed area. There is not any significant area of spatial continuity of low frequency, but overdispersed outliers with significant lower than expected seem to be concentrated on the North-Eastern part of the surveyed area.

HORIZONTAL POSTS: Cells with significant higher frequency, surrounded by neighbour sampling units with also high frequencies (Positive Correlation), are concentrated in North-Eastern extreme of the distribution, in front of the significant concentrations of vertical posts. There is not any significant area of spatial continuity of low frequency, but overdispersed outliers with significant higher than expected or lower than expected frequencies. Higher than expected seem to be concentrated also on the North-Eastern corner.

CONCOTTO: There are no areas of significant higher concentration. Positive autocorrelation is manifested in the spatial continuity of low or very low frequencies. Some overdispersed outliers showing overabundance in North-Eastern corner.

8.10.3 Looking for correlations

8.10.3.1 Correlation between general categories within the entire dataset

The entire database (1941 entries) has been used to calculate potential ordinal correlations between general categories (that is posts, saddle querns, faunal remains, pottery, concotto, wood fragments, horizontal posts remains and lithic industry). Spearman's Correlation Coefficient of the ranks has positive values in very few cases. In the majority of crossing pairs, the rank correlation adopts negative values. For instance, faunal remains are negatively correlated with horizontal posts remains, posts (both negatively correlated to pottery) and concotto, as well as saddle querns and horizontal posts remains. Positive correlation relates instead faunal remains, lithic industry and pottery, as well as wooden fragments and horizontal posts remains.

	lithic industry	pottery	horizontal posts	posts	fauna	
fauna	0.0003	2.77E-132	1.94E-07	0.010335		
pottery	5.45E-10		4.98E-11	5.04E-09		
saddle querns			0.089647			
wooden fragments			0.00118			
horizontal posts				0.026167		
concotto remains				0.05302	0.024465	
	lithic industry	pottery	horizontal posts	posts	fauna	pottery
fauna	0.081971	5.16E-01	-0.11781	-0.0582		
pottery	1.40E-01		-1.48E-01	-0.13219		
saddle querns			-0.038535			
wooden fragments			0.00118			
horizontal posts				0.026167		
concotto remains				0.05302	0.024465	
	lithic industry	pottery	horizontal posts	posts	fauna	pottery
fauna	0.081971	5.16E-01	-0.11781	-0.0582		
pottery	1.40E-01		-1.48E-01	-0.13219		
saddle querns			-0.038535			
wooden fragments			0.073574			
horizontal posts				-0.05047		-0.14849
concotto remains				-0.04392	0.051064	

Table 12 Spearman's Correlation Coefficient of the ranks for general categories (values of p(uncorrect) (above) and p(uncorrect)-statistic (below).

8.10.3.2 Correlation between salient locations (local Moran significant cells)

We have selected those cells that are beyond the 0.05 level in the local Moran analysis. Rank order correlation between dependent variables has been recalculated for those 251 sampling units. To the confirmed positive correlations above mentioned, is added the positive relation between pottery and concotto remains. Further negative correlation relates saddle querns to lithic industry, faunal remains and pottery.

	fauna	lithic industry	saddle querns	pottery	horizontal posts
saddle querns	0.000102	0.02075			
pottery	2.96E-18	0.011981	7.29E-07		
horizontal posts	0.006136			-0.13083	
posts	5.30E-08	0.012196	0.000259	8.39E-14	
wooden fragments				0.023199	0.027995
concotto remains				0.032247	
	fauna	lithic industry	saddle querns	pottery	horizontal posts
saddle querns	-0.2428	-0.14591			
pottery	0.51306	0.15839	-0.30662		
horizontal posts	-0.17254			-0.13083	
posts	-0.33513	-0.158	-0.22865	-0.44815	
wooden fragments				-0.14327	0.13872
concotto remains				0.13521	

Table 13 Spearman's Correlation Coefficient of the ranks for higher frequencies of general categories (values of p(uncorrect) (above) and p(uncorrect)-statistic (below).

8.10.3.3 Correlation between sub-categories: wild and domestic fauna versus ceramic open and closed forms

In some cases, global categories like "fauna" or "pottery" can be subdivided into more coherent functional categories, like wild and domestic fauna on one hand, and open and closed pottery forms. Using the results of the above Local indicators of spatial association, 284 cells have been selected, according to the frequency of those subcategories at those locations, higher than expected assuming the hull hypothesis. Rank order correlations are predominantly positive, relating subcategories within the same global category. Positive correlation relates lithic industry and wild fauna, as well as closed pottery forms with concotto remains. Negative correlation is observed between posts and open pottery forms.

	domestic fauna	lithic industry	posts	horizontal posts	concotto remains	open forms
wild fauna	1,28E-06	0.071286	0,029422			
saddle querns	0.080804	0,014864	0.002556			
posts	0.008196	0.007748				
wooden fragments				0.004027		
open forms			0.026637			
closed forms					0.065265	0.001643
	domestic fauna	lithic industry	posts	horizontal posts	concotto remains	open forms
wild fauna	0,28274	0,10719	-0,12926			
saddle querns	-0,10379	-0,14441	-0,17835			
posts	-0,15661	-0,15772				
wooden fragments				0,17017		
open forms			-0,13155			
closed forms					0,10954	0,186

Table 14 Spearman's Correlation Coefficient of the ranks for sub-categories (wild and domestic fauna as well as open and closed ceramic forms) (values of p(uncorrect) (above) and p(uncorrect)-statistic (below).

8.10.3.4 Correlation between sub-categories: skeletal faunal anatomical parts versus ceramic open and closed forms

When specifying taxa and skeletal part, instead of a global and undifferentiated "faunal remains" category, and restricting rank order correlation to salient points in Local Moran analysis, it is again obtained a pattern of positive relationship between subcategories of the same global category. Neither different skeletal parts, nor distinct remains from different taxa, are distributed at different locations, but a similar frequency of each subcategory appears at the same locations. Negative correlation can be detected between wooden fragments and cranial faunal remains, as well as between saddle querns and axial faunal fragments.

	cranial fragments	axial fragments	posts	lithic industry	horizontal posts	open forms
axial fragments	0,048235					
appendicular fragments	1,54E-06	2,34E-05	0,002408			
wooden fragments	0,0386				0,043758	
saddle querns		0,048891	0,001593	0,012794		
posts				0,008434		0,028885
closed forms						0,003725
	cranial fragments	axial fragments	posts	lithic industry	horizontal posts	open forms
axial fragments	0,11837					
appendicular fragments	0,28307	0,25029	-0,18099			
wooden fragments	-0,12391				0,12082	
saddle querns		-0,11803	-0,18817	-0,14888		
posts				-0,15743		-0,13084
closed forms						0,17312

Table 15 Spearman's Correlation Coefficient of the ranks for sub-categories (cranial, axial and appendicular faunal remains as well as open and closed ceramic forms) values of p(uncorrect) (above) and p(uncorrect)-statistic (below).

8.10.4 Correspondence Analysis between general categories: higher frequencies

Considering the low value of correlation observed between subcategories of pottery and faunal remains with other categories, Detrended Correspondence Analysis (Figure 670) is only performed for higher frequencies of general categories. Posts are excluded because of their frequency uniformity. First two axes explain a cumulative 82%. The first one explains the 53%, proving the negative correspondence between wooden fragments (associated to horizontal posts) and fauna (associated to concotto remains).

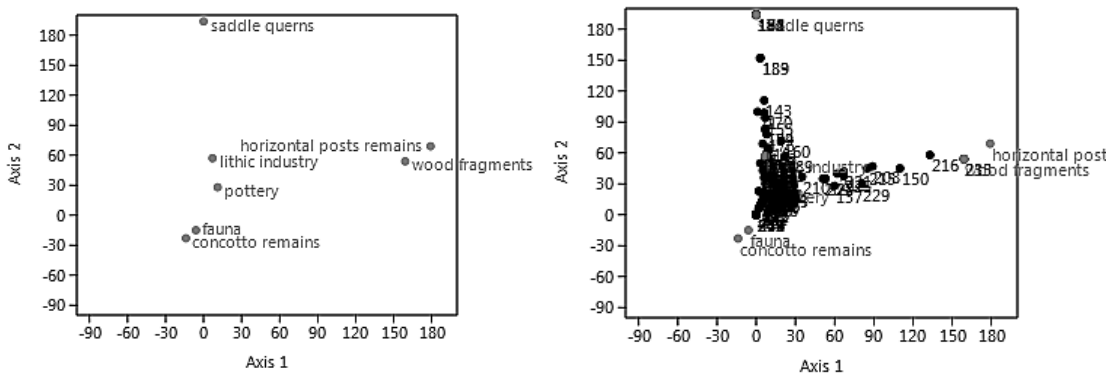

Figure 670 Graphic results of Correspondence Analysis calculated using higher frequencies of general categories (Detrended Correspondence Analysis) (surveys 2009) (Past).

The graphic result of the inverse distance weighting for Axis 1 (Figure 671) shows the spatial distribution of cells with horizontal posts remains and wooden fragments (corresponding to darkest gray values) negatively correlated to fauna and concotto remains (corresponding to clearest values). Wooden fragments (associated to horizontal posts) are predominantly observed in isolated high density points, along all surveyed area (particularly concentrated in the Northern zone and in the middle). Fauna (and concotto) is predominantly concentrated in the South-West corner and in the middle of the surveyed area, with some isolated presences in the NorthWest corner. As proved by Figure 670, where faunal remains and associated concotto are observed, horizontal posts remains as well as wooden fragments are predominantly absent.

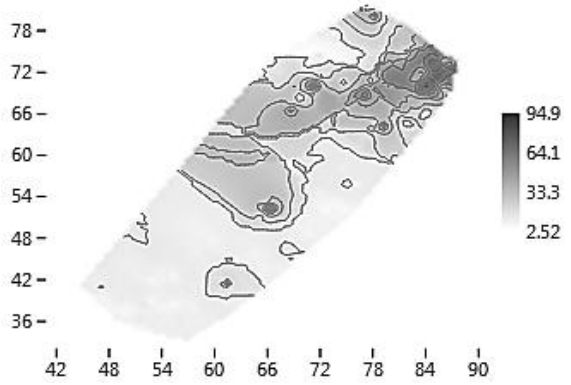

Figure 671 Graphic result of inverse distance weighting for Axis 1 (higher frequencies of general categories) (surveys 2001) (Detrended Correspondence Analysis) (Past).

The second axis explains 29%, proving the negative correspondence between saddle querns and faunal remains (associated to concotto fragments). The graphic result of the inverse distance weighting shows a spatial distribution of saddle querns (corresponding to darkest gray values) predominantly accumulated in the Eastern side of the surveyed area, while faunal remains (associated to concotto fragments) are particularly concentrated in the middle of the distribution and in the South-West corner (Figure 672). Then, where saddle querns are observed, faunal remains and concotto fragments are quite absent.

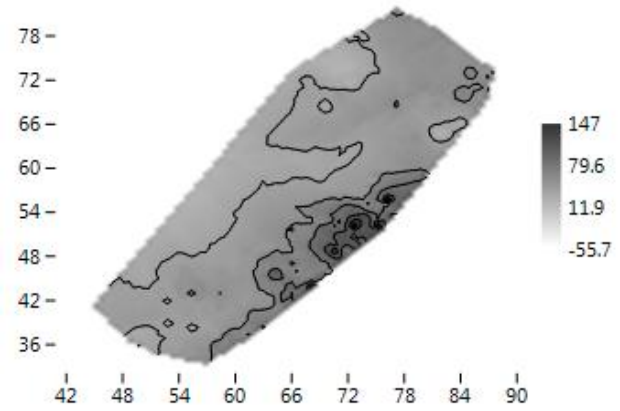

Figure 672 Graphic result of inverse distance weighting for Axis 2 (higher frequencies of general categories) (surveys 2009) (Detrended Correspondence Analysis) (Past).

Instead of analysing the second axis in depth, which can be affected by the classical "horse-shoe" deformation effect (it is partially correlated with the first axis) the analysis has been repeated without the scarcest categories, that is those observations that appear in very low frequencies in the studied area: horizontal posts and concotto remains. The first axis of the resulting analysis explains 46%, what suggests that, by deleting these categories, spatial variation does not change significatively. The analysis shows the high contribution of pottery (darkest values) and saddle querns (clearer values) as the leading opposition: where there is more pottery there are less saddle querns. A spatial view of first axis row scores appears in Figure 673.

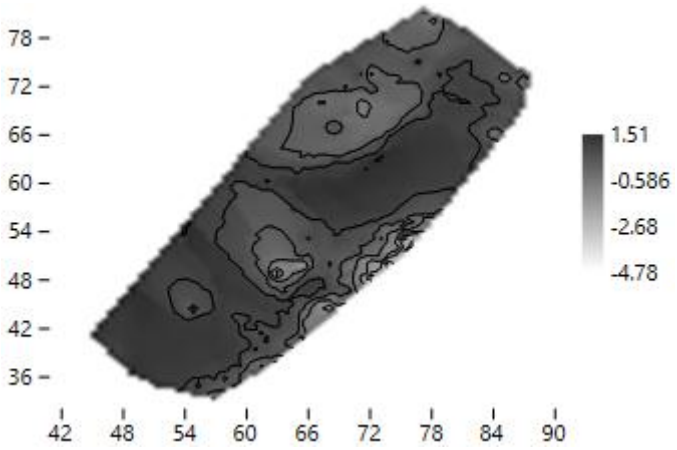

Figure 673 Graphic result of inverse distance weighting for Axis 1 (higher frequencies of general categories, excluding those variables attested in scarce presences (in this case horizontal posts and concotto remains) (surveys 2009) (Detrended Correspondence Analysis) (Past).

8.10.5 Looking for correlations within Zone 1 and Zone 2

As above mentioned, two zones are identified within the area surveyed in 2009, Zone 1 (with y<65) and Zone 2 (with y>65) (Figure 674). Empty cells which separate such sub-sectors are

spatially significant clustered, suggesting to perform Correlation as well as Correspondence Analysis separately for each sector.

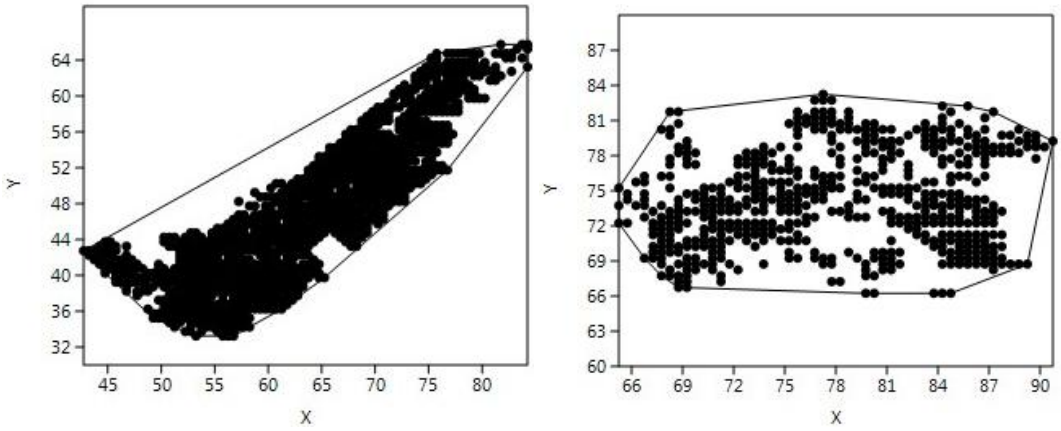

Figure 674 1)spatial distribution of non-empty sampling units in Zone 1 2)spatial distribution of non-empty sampling units in Zone 2.

8.10.5.1 Correlation between general categories within the entire dataset of Zone 1

The entire database (1323 entries) has been used to calculate potential ordinal correlation between general categories (that is posts, saddle querns, faunal remains, pottery, concotto, wood fragments, horizontal posts remains and lithic industry). Spearman's Correlation Coefficient has significant negative values in very few cases. In the majority of crossing pairs, the rank correlation adopts positive values. For instance, negative correlations relate saddle querns to faunal remains and pottery. Pottery is positively correlated with fauna and lithic industry, as well as concotto remains with fauna.

	lithic industry	saddle querns	pottery	concotto remains
fauna	0,0020669	0,00066899	1,13E-67	0,012593
pottery	4,68E-07	0,0015205		
	lithic industry	saddle querns	pottery	concotto remains
fauna	0,084619	-0,093414	0,45223	0,068581
pottery	0,13801	-0,087089		

Table 16 Spearman's Correlation Coefficient of the ranks for general categories within Zone 1 (values of p(uncorrect) (above) and p(uncorrect)-statistic (below).

8.10.5.2 Correlation between general categories within the entire dataset of Zone 2

The entire database (619 entries) has been used to calculate potential ordinal correlations between general categories (that is posts, saddle querns, faunal remains, pottery, concotto, wood fragments, horizontal posts remains and lithic industry). Spearman's Correlation Coefficient has significant positive values in very few cases. In the majority of crossing pairs, the rank correlation adopts negative values. For instance, positive correlation relates horizontal posts remains and wooden fragments, as well as lithic industry and pottery. Horizontal posts remains are negatively correlated with faunal remains, pottery and posts, as well as posts with pottery.

	fauna	pottery	wooden fragments	posts
horizontal posts	0,021695	0,0085537	0,0285	0,002027
lithic industry		0,0087461		
posts		1,71E-08		
	fauna	pottery	wooden fragments	posts
horizontal posts	-0,092335	-0,10569	0,088115	-0,12392
lithic industry		0,10538		
posts		-0,22439		

Table 17 Spearman's Correlation Coefficient of the ranks for general categories within Zone 2 (values of p(uncorrect) (above) and p(uncorrect)-statistic (below).

8.10.5.3 Correlation between salient locations within Zone 1 (Local Moran significant cells)

We have selected those cells that are beyond the 0.05 level in the local Moran analysis. Rank order correlation between dependent variables has been recalculated for those 90 sampling units. Results are different from what obtained in the case of all surveyed sampling units, with a significant zero inflation. Previously observed negative and positive correlations are confirmed, and also are added some negative correlations. For instance, posts are negatively correlated with pottery, concotto, lithic industry and faunal remains. In the same way, negative correlations related horizontal posts remains to faunal remains and pottery (and this latter as also negatively related to wooden fragments).

	fauna	lithic industry	saddle querns	wooden fragments	horizontal posts	posts
saddle querns	0,0258					
pottery	2,82E-07	0,043659	0,00065836	0,0018944	6,57E-05	3,24E-07
fauna					0,0066495	4,76E-06
posts		0,011489				
concotto remains						0,021494
	fauna	lithic industry	saddle querns	wooden fragments	horizontal posts	posts
saddle querns	-0,16172					
pottery	0,36219	0,14653	-0,24496	-0,22396	-0,2854	-0,36047
fauna					-0,19626	-0,32499
posts		-0,18302				
concotto remains						-0,16673

Table 18 Spearman's Correlation Coefficient of the ranks for higher frequencies of general categories within Zone 1 (values of p(uncorrect) (above) and p(uncorrect)-statistic (below).

8.10.5.4 Correlation between salient locations within Zone 2 (Local Moran significant cells)

We have selected those cells that are beyond the 0.05 level in the local Moran analysis. Rank order correlation between dependent variables has been recalculated for those 94 sampling units. Results are different from what obtained in the case of all surveyed sampling units, with a significant zero inflation. Only negative correlations are observed. The previously observed are confirmed and it is added the negative correlation between lithic industry and pottery with saddle querns.

	lithic industry	pottery	concotto remains
saddle querns	0,094948	0,010171	
posts	0,028913	0,0011155	0,040005
	lithic industry	pottery	concotto remains
saddle querns	-0,17325	-0,26389	
posts	-0,22544	-0,3311	-0,21224

Table 19 Spearman's Correlation Coefficient of the ranks for higher frequencies of general categories within Zone 2 (values of p(uncorrect) (above) and p(uncorrect)-statistic (below).

8.10.5.5 Correlation between sub-categories: wild and domestic fauna versus ceramic open and closed forms within Zone 1

In some cases, global categories like "fauna" or "pottery" can be subdivided into more coherent functional categories, like wild and domestic fauna on one hand, and open and closed pottery forms. Using the result of the above Local indicators of spatial association, 185 cells have been selected, according to the frequency of those subcategories at those locations, higher than expected assuming the null hypothesis. Only two positive correlations are observed, relating subcategories within the same global category, as well as horizontal posts remains and concotto. Rank order correlations are instead predominantly negative and relate domestic faunal remains with lithic industry, concotto and posts and lithic industry with remains of horizontal posts.

	domestic fauna	horizontal posts	posts	concotto remains	open forms	wooden fragments
wild fauna	0,000115					
lithic industry	0,012225	0,009635	0	0,001227		
closed forms					0,03181	0,055911
horizontal posts			0,07			
posts				0,012492		
	domestic fauna	horizontal posts	posts	concotto remains	open forms	wooden fragments
wild fauna	0,27976					
lithic industry	-0,18389	-0,18988	-0,3	-0,23589		
closed forms					0,15791	0,055911
horizontal posts			-0,1			

Table 20 Spearman's Correlation Coefficient of the ranks for sub-categories (wild and domestic fauna as well as open and closed ceramic forms) within Zone 1 (values of p(uncorrect) (above) and p(uncorrect)-statistic (below).

8.10.5.6 Correlation between sub-categories: faunal fragments versus ceramic open and closed forms within Zone 2

In this case only general category of "pottery" can be subdivided into more coherent functional categories (open and closed pottery forms). Using the results of the above Local indicators of spatial association, 80 cells have been selected, according to the frequency of those subcategories at those locations, higher than expected assuming the null hypothesis. Rank order correlations are predominantly negative, relating posts with lithic industry, open ceramic forms, remains of horizontal posts and concotto fragments. Positive correlation relate subcategories of pottery within the same global category.

	lithic industry	open forms	horizontal posts	concotto remains
posts	0,0062669	0,0077902	0,077585	0,025152
closed forms		8,85E-06		
	lithic industry	open forms	horizontal posts	concotto remains
posts	-0,30316	-0,29549	-0,19847	-0,25028
closed forms		0,47422		

Table 21 Spearman's Correlation Coefficient of the ranks for sub-categories (open and closed ceramic forms) within Zone 2 (values of p(uncorrect) (above) and p(uncorrect)-statistic (below).

8.10.5.7 Correlation between sub-categories: skeletal faunal anatomical parts versus ceramic open and closed forms within Zone 1

When specifying taxa and skeletal part, instead of a global undifferentiated "faunal remains" category, and restricting rank order correlation to salient points in Local Moran analysis, it is again obtained a pattern of positive relationship between subcategories of the same global category. Specific subcategories-skeletal and taxonomic-of fauna are also positively correlated with specific functional subcategories of pottery. Negative correlation can be detected between posts and appendicular fragments, lithic industry and concotto remains. Lithic industry is negatively correlated to concotto and horizontal posts remains, as well as closed pottery forms with wooden fragments.

	domestic fauna	horizontal posts	posts	concotto remains	closed forms
wild fauna	0,00011497				
lithic industry	0,012225	0,0096347	1E-04	0,0012273	
open forms					0,055911
horizontal posts			0,068		
posts				0,012492	
	domestic fauna	horizontal posts	posts	concotto remains	closed forms
wild fauna	0,27976				
lithic industry	-0,18389	-0,18988	-0,28	-0,23589	
open forms					0,15791
horizontal posts			-0,19		
posts				-0,18333	

Table 22 Spearman's Correlation Coefficient of the ranks for sub-categories (wild and domestic fauna as well as open and closed ceramic forms) within Zone 1 (values of p(uncorrect) (above) and p(uncorrect)-statistic (below).

8.10.5.8 Correspondence Analysis between general categories within Zone 1: higher frequencies

Considering the scarce correlations observed between subcategories of pottery and faunal remains with other categories, Detrended Correspondence Analysis (Figure 675) is only performed for higher frequencies of general categories. Posts are excluded because of their frequency uniformity. First two axes explain a cumulative 77%. The first one explains 48%, proving a predominant positive correspondence between concotto fragments, pottery, fauna and lithic industry.

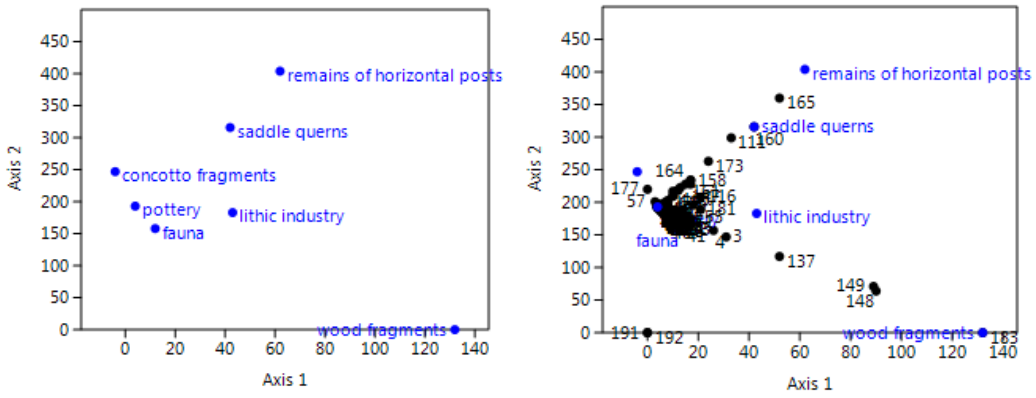

Figure 675 Correspondence analysis between higher frequencies of general categories within Zone 1 (surveys 2009) (Past).

The second axis explains 29%, proving the negative correspondence between wooden fragments and remains of horizontal posts. The graphical result of the inverse distance weighting shows a spatial distribution of horizontal posts remains (corresponding to black values) and wooden fragments (corresponding to clearest values). While the former are distributed around the North-East corner as well as in the South-East corner. In contrast wooden fragments are accumulated in the North-West side, in the middle of the surveyed area and around the South-West corner (Figure 676).

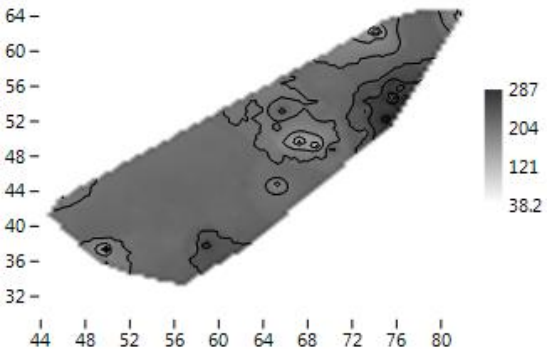

Figure 676 Graph results of inverse distance weighting for Axis 2 (higher frequencies of general categories within Zone 1 (surveys 2009) (Detrended Correspondence Analysis) (Past).

8.10.5.9 Correspondence Analysis between general categories within Zone 2: higher frequencies

Considering the scarce correlations observed between subcategories of pottery and faunal remains with other categories, Detrended Correspondence Analysis (Figure 677) is only performed for higher frequencies of general categories. Posts are excluded because of their frequency uniformity. First two axes explain a cumulative 71%. The first one explains the 39%, proving the negative correspondence between saddle querns and pottery (associated to fauna and lithic industry).

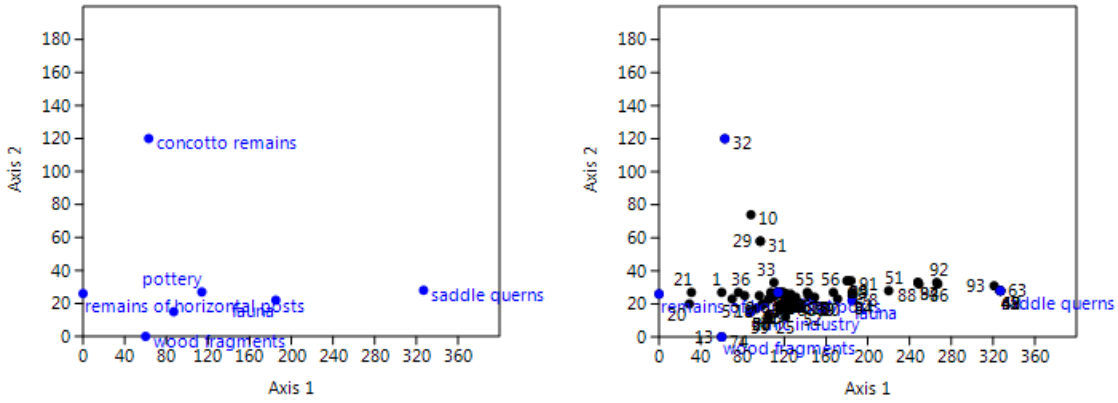

Figure 677 Correspondence analysis between higher frequencies of general categories within Zone 2 (surveys 2009) (Past).

The graphic result of the inverse distance weighting for Axis 1 (Figure 678) shows the spatial distribution of cells with saddle querns (corresponding to black values) negatively correlated to sampling units with pottery and faunal remains (corresponding to clear gray values). Within Sector 2 saddle querns are linearly distributed in isolated points in the Western side of the surveyed area. Pottery, faunal remains and lithic industry are particularly accumulated in the Western side as well as in the North-East and South-East corners.

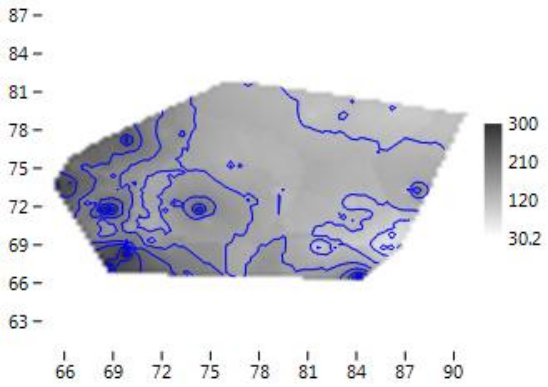

Figure 678 Graph results of inverse distance weighting for Axis 1 (higher frequencies of general categories within Zone 2 (surveys 2009) (Detrended Correspondence Analysis) (Past).

The second axis explains 32%, proving the negative correspondence between concotto remains and pottery (associated to faunal remains and lithic industry). The graphic result of the inverse distance weighting shows a spatial distribution of concotto remains (corresponding to black

values) particularly concentrated in the North-East corner. In contrast, pottery (associated to faunal remains and lithic industry) is particularly accumulated around both the South-West and the North-East corners (Figure 679).

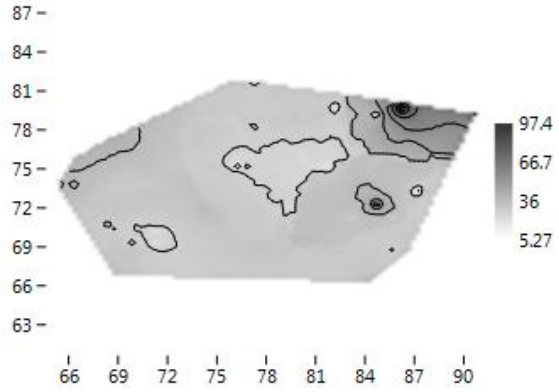

Figure 679 Graph results of inverse distance weighting for Axis 2 (higher frequencies of general categories within Zone 2 (surveys 2009) (Detrended Correspondence Analysis) (Past).